IMPROVE

Interagency Monitoring of Protected Visual Environments

Spatial and Seasonal Patterns and Temporal Variability of Haze and its Constituents in the United States: Report III

May 2000

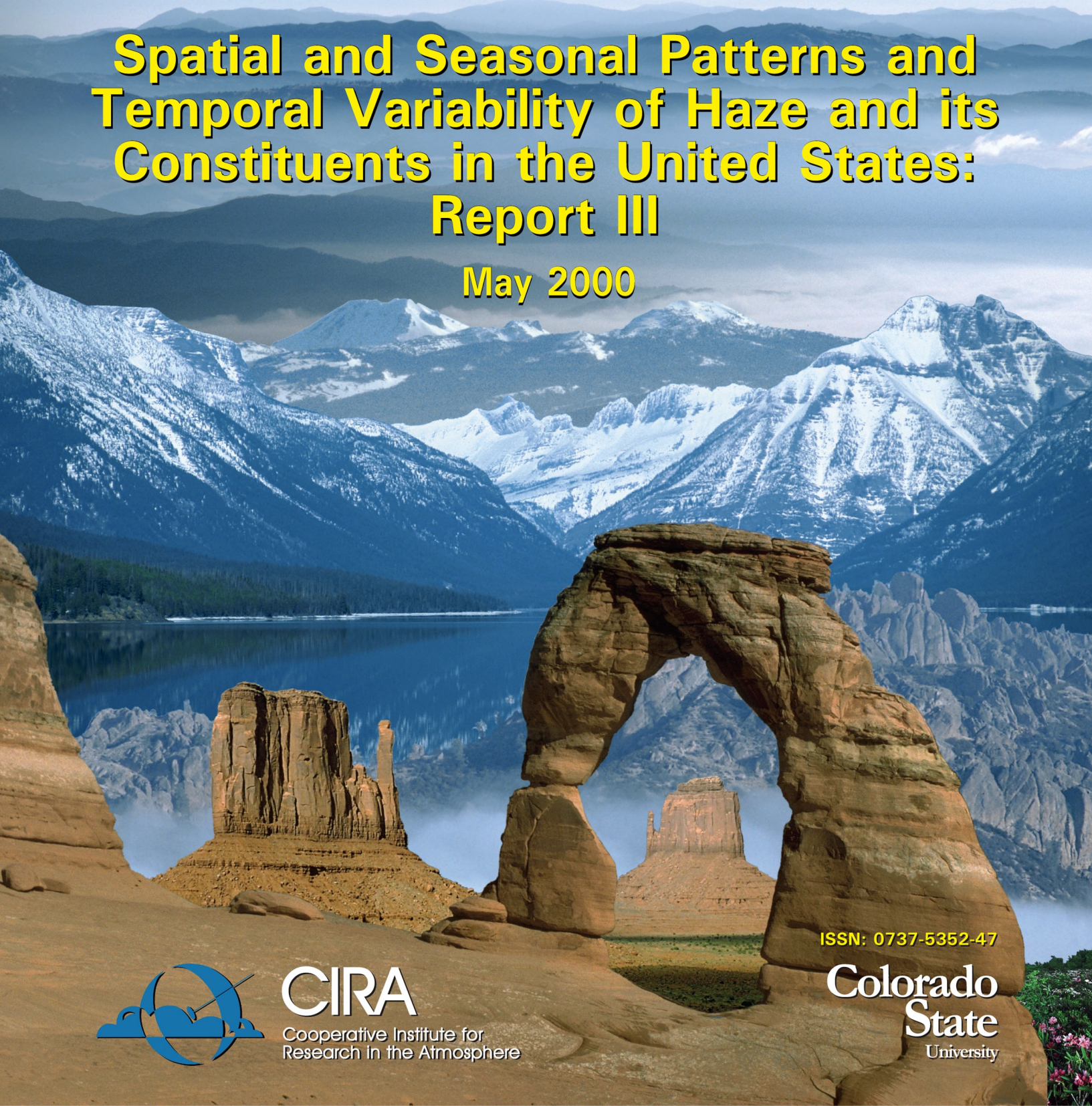

ISSN: 0737-5352-47

CIRA
Cooperative Institute for Research in the Atmosphere

Colorado State University

ISSN: 0737-5352-47

SPATIAL AND SEASONAL PATTERNS AND TEMPORAL VARIABILITY OF HAZE AND ITS CONSTITUENTS IN THE UNITED STATES

REPORT III

Principal Author: William C. Malm[1]

Authors by Chapter

Overview and Summary: William C. Malm[1]

Chapter 1: Marc L. Pitchford[2] and Mark Scruggs[1]

Chapter 2: James F. Sisler[3]

Chapter 3: James F. Sisler[3] and William C. Malm[1]

Chapter 4: Rodger Ames[3]

Chapter 5: James F. Sisler[3], William C. Malm[1], Scott Copeland[3] and Kristi A. Gebhart[1]

Chapter 6: William C. Malm[1] and Derek E. Day[3]

[1]National Park Service
[2]National Oceanic and Atmospheric Administration
[3]CIRA

Cooperative Institute for Research in the Atmosphere
Colorado State University
Fort Collins, CO 80523

May 2000

ISSN: 0737-5352-47

ACKNOWLEDGEMENTS

This report is the result of a collaborative effort involving the authors and a number of other individuals. We thank Dr. Lowell Ashbaugh and his staff at the University of California at Davis for their efforts in managing the IMPROVE aerosol monitoring network, managing the aerosol database, and providing input to the report concerning aerosol sampling and analysis. We thank Mr. John Molenar and Dr. David Dietrich of Air Resource Specialists in Fort Collins, Colorado for management of the IMPROVE visibility monitoring network, supplying the optical and relative humidity data, and for their input to this report. We also wish to thank Ms. Becky Burke for editing and formatting and Mr. Jeff Lemke for graphical presentation. In addition, we thank the reviewers: Dr. Marc Pitchford, Chief of Applied Sciences Branch, National Oceanic and Atmospheric Administration; Dr. Mark Scruggs, Chief Research Branch, National Park Service; Ms. Kristi Heuer, Fish and Wildlife Branch, Air Resources Division, National Park Service; Mr. Dan Ely, Air Pollution Control Division, State of Colorado; and Drs. Lowell Ashbaugh and Robert Eldred, Crocker Nuclear Laboratory, University of California at Davis.

DISCLAIMER

The assumptions, findings, conclusions, judgements, and views presented herein are those of the authors and should not be interpreted as necessarily representing official National Park Service policies.

ISSN: 0737-5352-47

TABLE OF CONTENTS

ISSN: 0737-5352-47

ISSN: 0737-5352-47

ISSN: 0737-5352-47

LIST OF FIGURES

ISSN: 0737-5352-47

LIST OF TABLES

OVERVIEW AND SUMMARY

This report describes data collected by the Interagency Monitoring of Protected Visual Environments (IMPROVE) measurement program. IMPROVE is a cooperative visibility monitoring effort between the U.S. Environmental Protection Agency (EPA), federal land management agencies, and state air agencies.

The objectives of IMPROVE are:

(1) to establish current visibility and aerosol conditions in mandatory Class I areas (CIAs);

(2) to identify chemical species and emission sources responsible for existing man-made visibility impairment;

(3) to document long-term trends for assessing progress towards the national visibility goal; and

(4) with the enactment of the Regional Haze Rule, to provide regional haze monitoring representing all visibility-protected federal CIAs where practical.

When the IMPROVE monitoring program was initiated it was resource and funding limited so that it was not practical to place monitoring stations at all 156 mandatory Class I areas where visibility is an important attribute. Therefore, the first IMPROVE report [Sisler et al., 1993] reflected data that was collected at only 36 sites for the time period March 1988 through February 1991. Over subsequent years the IMPROVE Network evolved and a second IMPROVE report [Sisler, 1996] was published that covered data gathered between March 1992 and February 1995 at 43 sites. Currently, there are a number of sites that use IMPROVE monitoring equipment and operate under IMPROVE protocol, however, for this report, the spatial trend analysis, which covers the time period from March 1996 to February 1999, will use 49 sites. An analysis of species contributions to the extreme (high and low) fine mass concentrations will utilize 51 sites, while an 11-year trend analysis will use 29 sites. Thirty-one of the 49 sites have optical monitoring and these data will be used to explore diurnal variability in the extinction or scattering coefficient. Figure S.1 shows a map of the United States indicating the locations of the monitoring sites along with those sites that have optical monitoring, those sites used in the spatial and temporal trend analyses, and those sites used in the extreme fine mass analysis. Finally, on the basis of regional similarities, the sites are grouped into 21 regions, listed in Table S.1.

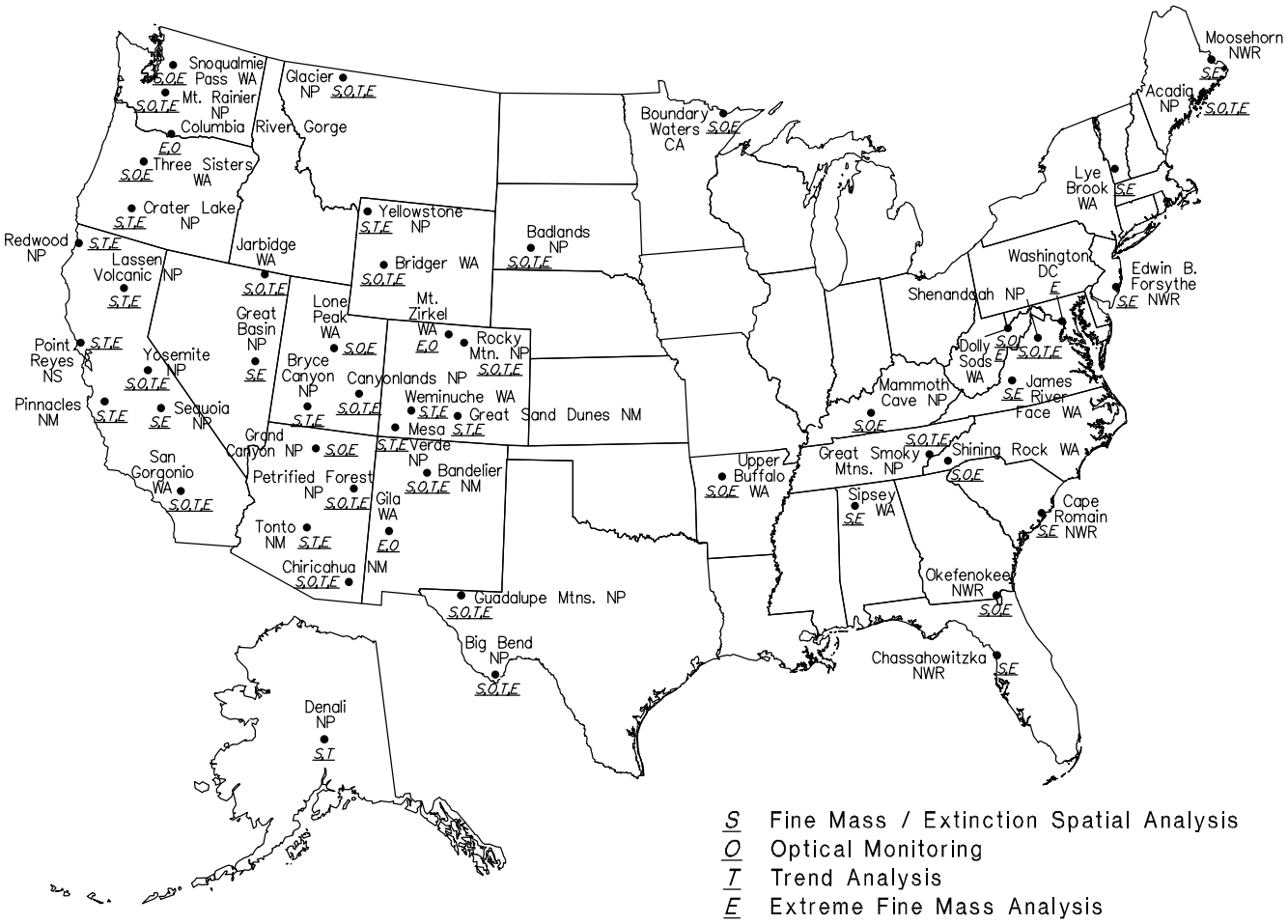

Figure S.1 *Map of the IMPROVE sites included in this report.*

S.1 OPTICAL AND AEROSOL DATA

Aerosol monitoring in the IMPROVE Network is accomplished by a combination of particle sampling and sample analysis. The sampler was designed specifically for IMPROVE. It collects four simultaneous samples: one PM_{10} sample (particles less than 10 μm in diameter) on a Teflon filter and three $PM_{2.5}$ samples on Teflon, nylon, and quartz filters. The IMPROVE sampler is programmed to collect two 24-hour duration samples per week (i.e., 26 per season, 104 per year). The PM_{10} filter is used to determine total gravimetric PM_{10} mass concentration, while the $PM_{2.5}$ Teflon filter is analyzed to determine gravimetric mass concentrations and concentrations of selected elements using particle-induced x-ray emission (PIXE), x-ray fluorescence (XRF), and Proton Elastic Scattering Analysis (PESA). The nylon filter is analyzed to determine nitrate and sulfate aerosol concentrations using Ion Chromatography (IC). Finally, the quartz filters are analyzed for organic and elemental carbon using the Thermal Optical Reflectance (TOR) method.

Table S.1 *IMPROVE monitoring sites listed according to region.*

Alaska (AKA)
•Denali NP&P (DENA)

Appalachian Mountains (APP)
•Great Smoky Mountains NP (GRSM)
•Shenandoah NP (SHEN)
•Dolly Sods WA (DOSO)
•James River Face WA (JARI)
•Shining Rock WA (SHRO)

Boundary Waters (BWA)
•Boundary Waters Canoe Area (BOWA)

Cascade Mountains (CAS)
•Columbia River NSA (CORI)
•Mount Rainier NP (MORA)
•Snoqualmie Pass WA (SNPA)
•Three Sisters WA (THIS)

Central Rocky Mountains (CRK)
•Bridger WA (BRID)
•Great Sand Dunes NM (GRSA)
•Mount Zirkel WA (MOZI)
•Rocky Mountain NP (ROMO)
•Weminuche WA (WEMI)
•Yellowstone NP (YELL)

Colorado Plateau (CPL)
•Bandelier NM (BAND)
•Bryce Canyon NP (BRCA)
•Canyonlands NP (CANY)
•Grand Canyon NP (GRCA)
•Mesa Verde NP (MEVE)
•Petrified Forest NP (PEFO)

Great Basin (GBA)
•Jarbidge WA (JARB)
•Great Basin NP (GRBA)

Mid Atlantic (MAT)
•Edwin B. Forsythe NWR (EBFO)

Mid South (MDS)
•Upper Buffalo WA (UPBU)
•Sipsey WA (SIPS)
•Mammoth Cave NP (MACA)

Northeast (NEA)
•Acadia NP (ACAD)
•Lye Brook WA (LYBR)
•Moosehorn NWR (MOOS)

Northern Great Plains (NGP)
•Badlands NP (BADL)

Northern Rocky Mountains (NRK)
•Glacier NP (GLAC)

Pacific Coastal Mountains (PCM)
•Pinnacles NM (PINN)
•Point Reyes NS (PORE)
•Redwood NP (REDW)

Sierra Nevada (SRA)
•Yosemite NP (YOSE)
•Sequoia NP (SEQU)

Sierra-Humboldt (SRH)
•Crater Lake NP (CRLA)
•Lassen Volcanic NP (LAVO)

Sonoran Desert (SON)
•Chiricahua NM (CHIR)
•Gila WA (GILA)
•Tonto NM (TONT)

Southeast (SOE)
•Chassahowitzka NWR (CHAS)
•Okefenokee NWR (OKEF)
•Cape Romain NWR (CARO)

Southern California (SCA)
•San Gorgonio WA (SAGO)

Wasatch (WAS)
•Lone Peak WA (LOPE)

Washington, D.C. (WDC)
•Washington, D.C. (WASH)

West Texas (WTX)
•Big Bend NP (BIBE)
•Guadalupe Mountains NM (GUMO)

NP&P = National Park and Preserve NM =National Monument NSA = National Scenic Area
NP = National Park NWR =National Wildlife Refuge WA = Wilderness Area
NS = National Seashore

Transmissometers are employed to measure the light-extinction coefficient at 15 of the IMPROVE sites, and 16 sites have integrating nephelometers, which measure the scattering coefficient. Transmissometers measure the light transmitted through the atmosphere over a distance of 1 to 15 kilometers. The light transmitted between the light source (transmitter) and the light-monitoring component (receiver) is converted to the path-averaged light extinction coefficient (b_{ext}), which is the sum of scattering (b_{scat}) and absorption (b_{abs}). An integrating nephelometer measures the scattering of light from a small volume of air and thus it is a point measurement of scattering. By combining an estimate of the absorption coefficient from the particle data with the scattering coefficient from the nephelometer the extinction coefficient can be estimated at the 16 nephelometer sites. Relative humidity is measured continuously at the transmissometer and nephelometer sites.

In the next sections the spatial and temporal trends of fine and coarse mass concentrations along with their associated optical extinction and/or scattering characteristics will be summarized.

S.2 SPATIAL DISTRIBUTION OF AEROSOL CONCENTRATION AND CHEMICAL COMPOSITION

Coarse mass, the difference between PM_{10} and $PM_{2.5}$, concentrations are highest along the Southeast, Pacific Coastal Mountains, West Texas, and Sonoran Desert regions, while it is lowest in the Sierra-Humboldt and Cascade Mountains regions.

Fine aerosol concentrations are highest in the eastern United States (in the Appalachian Mountains, Mid-South, Mid-Atlantic, and Washington, D.C. regions). Concentrations are also relatively high in the Southern California region. The lowest concentrations occur in the Great Basin in Nevada, the Colorado Plateau in the Four Corners states, Wyoming, and Alaska.

The largest single component of the fine aerosol in the East is sulfate at 60-65% of the mass, while in the Pacific Northwest it is organics, and in southern California it is nitrates. In general, the largest mass fractions of the fine aerosol are sulfates, organics and soil/dust. Of the 21 regions in the IMPROVE Network, carbon (organic plus light-absorbing carbon) is the largest single component in ten regions (Alaska, Cascade Mountains, Central Rocky Mountains, Colorado Plateau, Great Basin, Northern Rocky Mountains, Pacific Coastal Mountains, Sierra-Nevada, Sierra-Humboldt, and Wasatch regions). Sulfate is the largest single component of fine aerosol in ten regions, primarily in the East (Appalachian Mountains, Boundary Waters, Mid-Atlantic, Mid-South, Northeast, Northern Great Plains, Sonoran Desert, Southeast, Washington, D.C., and West Texas regions), while nitrates are slightly greater than carbon in the Southern California region. Sulfates and carbon are approximately the same on the Colorado Plateau and Sonoran Desert.

With few exceptions, average fine mass concentrations, as well as the sulfate, organic carbon, and light-absorbing carbon components of fine mass, are highest in summer. Soil concentrations are highest in spring or summer. Nitrate concentrations are generally highest in winter or spring.

S.3 SPATIAL DISTRIBUTION OF RECONSTRUCTED LIGHT EXTINCTION AND SPECIES CONTRIBUTIONS

The light-extinction coefficient (b_{ext}) is calculated from the measured aerosol species' concentrations by multiplying the concentration of a given species by its light-extinction efficiency, and summing over all species. Since sulfates and nitrates are assumed to be hygroscopic, their light-extinction efficiencies increase with relative humidity; therefore, extinction efficiencies for soluble species must be adjusted according to average relative humidity at each site.

There are two ways reconstructed extinction is calculated in this report that are different from the 1996 IMPROVE report. First, the factor *f*(RH) that accounts for the relative humidity effects on hygroscopic aerosols has been upgraded with new relative humidity data from additional relative humidity monitoring sites and second, absorption is estimated from measurements of light-absorbing carbon rather than from transmission measurements of filter media. Therefore, some differences in aerosol extinction between this and the 1996 report are due to changes other than levels of aerosol mass concentration.

To show the effect on visibility of aerosol extinction, the deciview (dv) scale is applied to the total (Rayleigh included) reconstructed aerosol extinction (see Chapter 2). By utilizing the dv scale, the effect of light extinction on visibility is portrayed in a way that is approximately linear with respect to perceived visual air quality. Because higher extinction coefficients lead to higher dv numbers, the geographic trends in visibility follow the trends in reconstructed extinction. Pristine or Rayleigh conditions correspond to a dv of zero.

Figures S.2 and S.3 are the spatial deciview maps using just the IMPROVE data and IMPROVE plus the EPA's Clean Air Status and Trends Network (CASTNet) data, respectively. Figure S.2 incorporates data for the time period March 1996 through February 1999, and Figure S.3 uses data for the time period December 1995 through November 1998. Therefore, the estimates of deciview and extinction are slightly different for the two time periods. These different time periods are used for the respective maps because at the time of this writing the CASTNet data were available only through the end of 1998. The discussion of how the two data sets are combined is presented in Appendix A. The maps of the combined data sets are presented here because of the higher density of deposition sites in the eastern United States. Figures S.4 and S.5 are the corresponding extinction maps for the time periods analogous to Figures S.2 and S.3. Figures S.6a through S.6e show the fractional contribution of sulfates, nitrates, organics, light-absorbing carbon, and dust to total aerosol extinction.

Deciview and reconstructed light extinction varies throughout the United States in a way analogous to fine aerosol concentrations. The greatest light extinction occurs in the eastern United States and in southern California, while the least light extinction occurs in the nonurban west (e.g., the Great Basin and the Colorado Plateau) and in Alaska. However, because relative humidity (and therefore the light-scattering efficiency of sulfate and nitrate) is higher in the East than in the West, the difference between eastern and western light extinction is even more pronounced than the difference in aerosol concentrations.

Figures S.2 and S.3 show isopleths of deciviews averaged over the respective time periods previously described. The smallest dv value or best visibility is reported at Denali National Park with 7 dv. A broad region, which includes the Great Basin, most of the Colorado Plateau, and portions of the Central Rockies, has visibility impairment of less than 10 dv. Moving in any direction from this region generally results in increasing dv values. West of the Sierra Mountain Range and including southern California one finds dv values in excess of 15, with a maximum value of 18 dv at Sequoia National Park. The northwest United States and the entire eastern half of the United States have an excess of 14 dv of impaired visibility. The region east of the Mississippi and south of the Great Lakes has impairment in excess of 20 dv, with the Appalachian, Mid-South and Southeast regions exceeding 24 dv. Figure S.3 shows the highest annual dv values, greater than or equal to 26 dv, occurring in the eastern United States in the general region of the Ohio River and Tennessee Valleys. Total aerosol extinction, shown in Figures S.4 and S.5, show the same general spatial trend as deciviews.

Fine aerosols are the most effective in scattered light and are the major contributors to light extinction. Referring to Figure S.6a, in most cases the sulfate component of fine aerosol is the largest single contributor to total aerosol light extinction. This is because sulfate, being hygroscopic, generally has a higher light extinction efficiency than other species due to associated liquid water. This is especially true in the eastern United States, where relative humidity is high. In the Appalachian Mountains (Shenandoah and Great Smoky Mountains National Parks), sulfate accounts for nearly 80% of the total aerosol light extinction on an annual basis, and more during the summer months. Sulfates contribute the least in the Great Basin region at about 25%, while along the Rocky Mountains the contribution is about 30-40%. In the Cascade Mountains region, sulfates contribute significantly at 50-60%. Sulfates are the largest single contributor to light extinction in 17 of the 21 regions and are about comparable to organics in two of these regions, Northern Rocky Mountains and Wasatch.

Figure S.6b shows the fractional contribution of nitrates to total aerosol extinction. Nitrates are not only the single largest contributor to extinction in the Southern California region at 39% but also contribute significantly along the coastal areas of California at about 20-25%. Nitrates are 16% of extinction at Lone Peak Wilderness Area, which is near Salt Lake City, while in the rest of the United States it is less than 10%.

Figure S.6c shows the fractional contribution of organics to extinction. Organics are, in general, the second largest contributor to total aerosol extinction. It is the largest contributor in the Great Basin, Sierra-Humboldt, and Sierra-Nevada regions at 33%, 36%, and 32% respectively. It is the largest contributor at Yosemite National Park at 40% and on the order of about 10% in most of the eastern United States. In the Central Rockies and on the Colorado Plateau, its contribution to extinction is about 20-25%.

Figure S.6d shows the fractional contribution of light-absorbing carbon to total aerosol extinction. It is on the order of about 10% in much of the western United States and on the order of 5% east of the Mississippi. In the three regions where organics are the largest contributors to extinction, the sum of organic and light-absorbing carbon, or the contribution of carbon in general, to extinction is 40-50%.

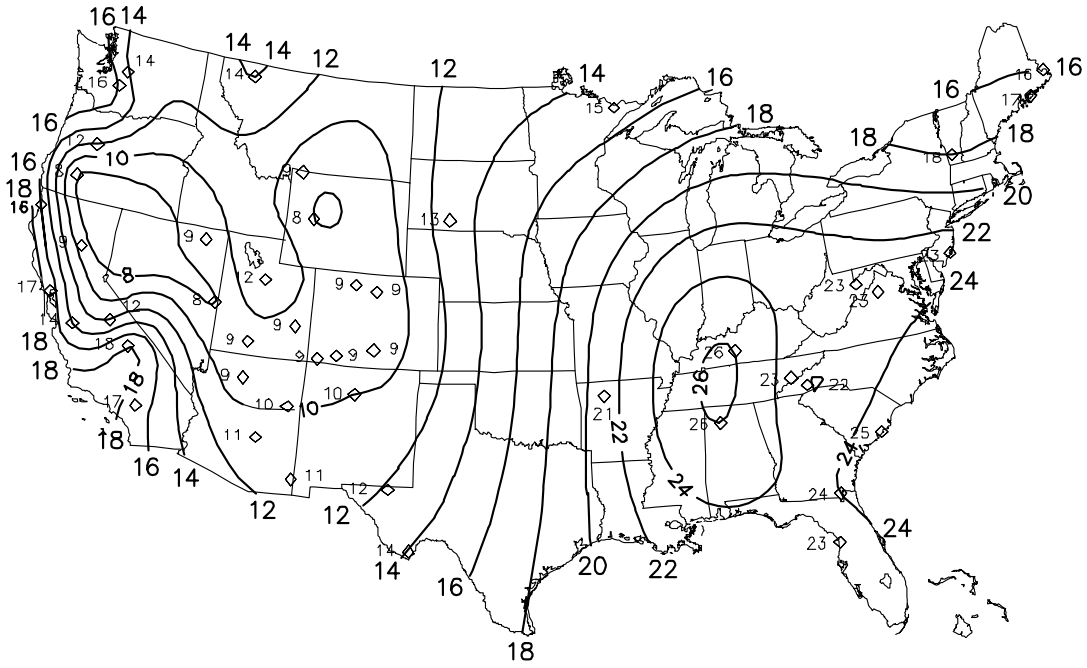

Figure S.2 *Three-year averages of deciview values using only data collected in the IMPROVE Network.*

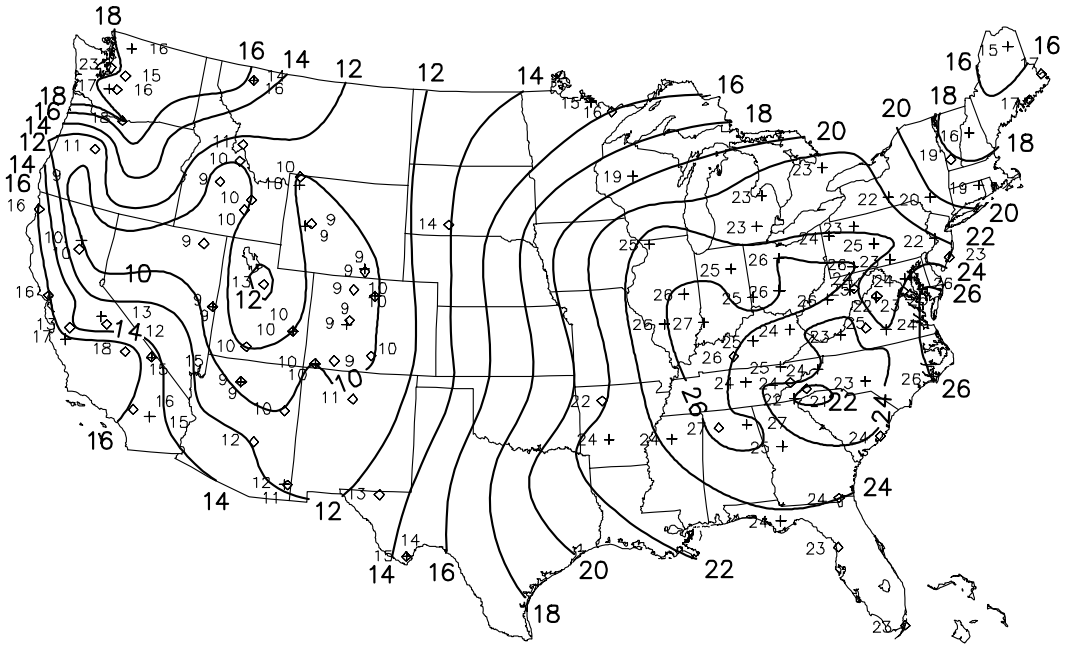

Figure S.3 *Three-year averages of deciview values using data collected in the IMPROVE Network and CASTNet.*

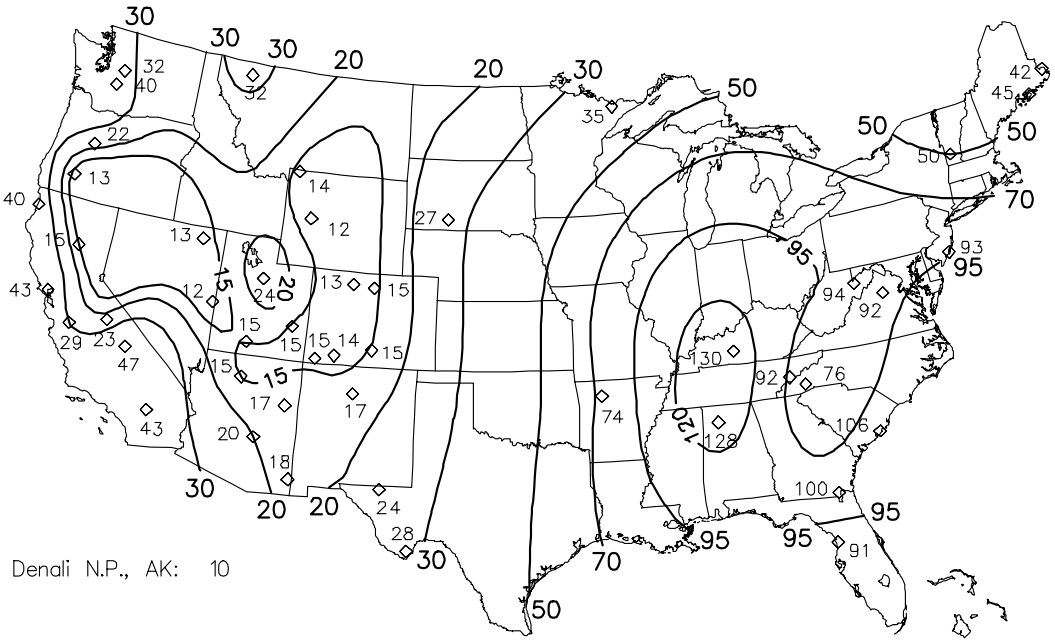

Figure S.4 *Three-year averages of total reconstructed aerosol light-extinction coefficient (1/Mm) using only data collected in the IMPROVE Network.*

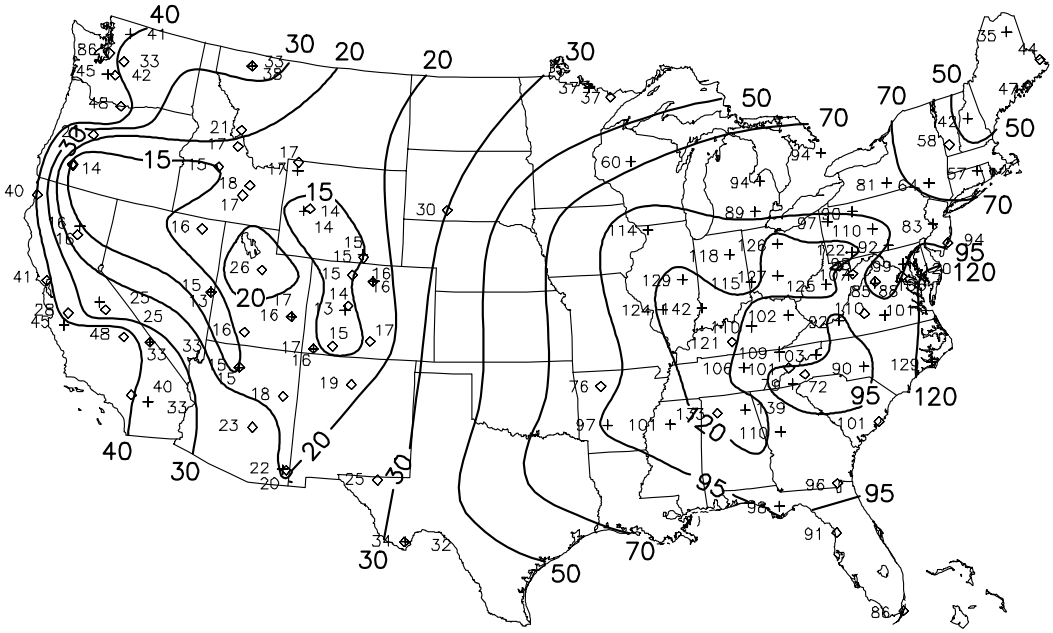

Figure S.5 *Three-year averages of total reconstructed aerosol light-extinction coefficient (1/Mm) using data collected in the IMPROVE and CASTNet.*

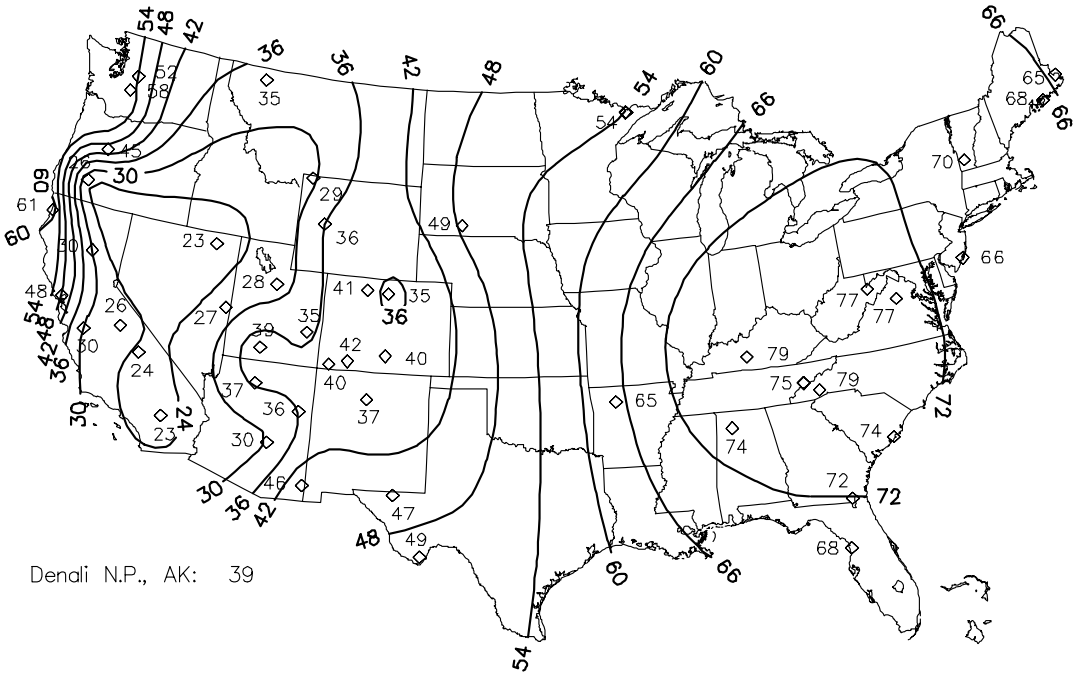

Figure S.6a *Fractional contribution of sulfates to total aerosol reconstructed light extinction (%).*

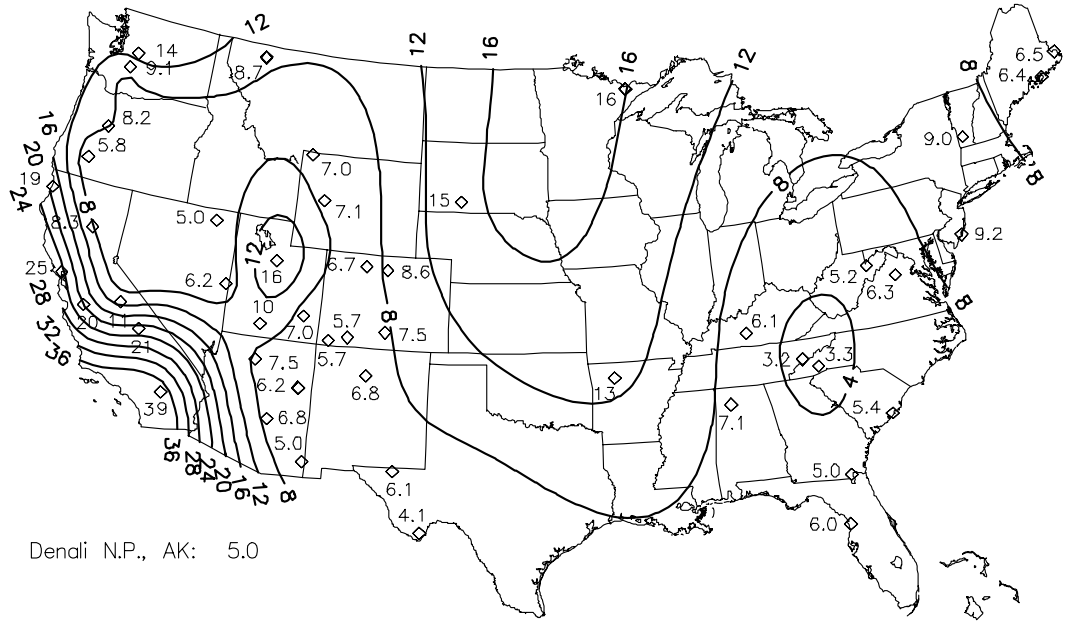

Figure S.6b *Fractional contribution of nitrates to total aerosol reconstructed light extinction (%).*

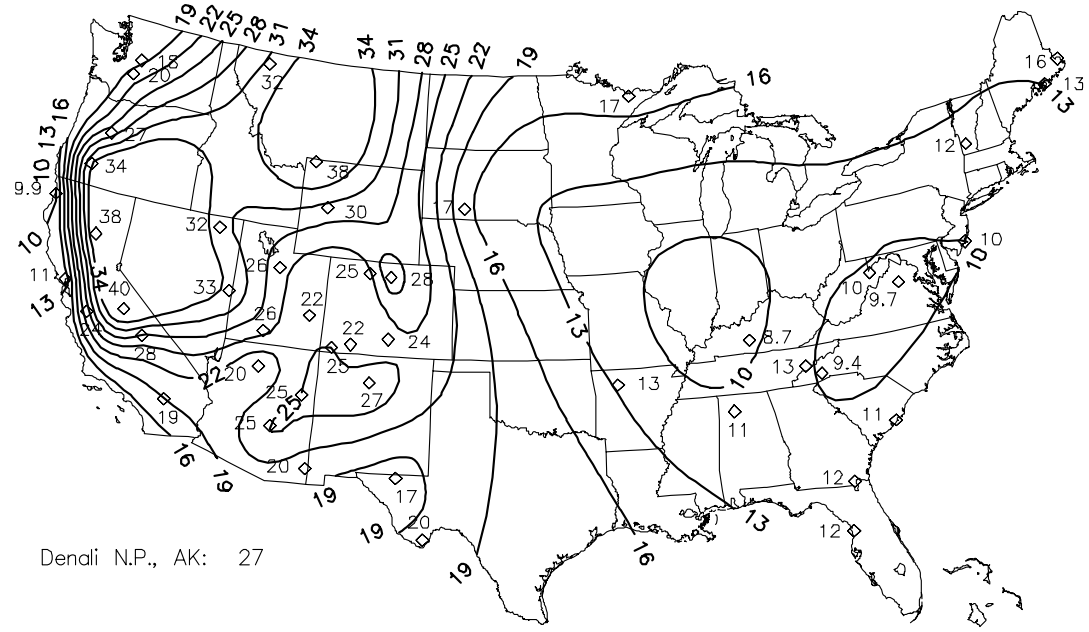

Figure S.6c *Fractional contribution of organics to total aerosol reconstructed light extinction (%).*

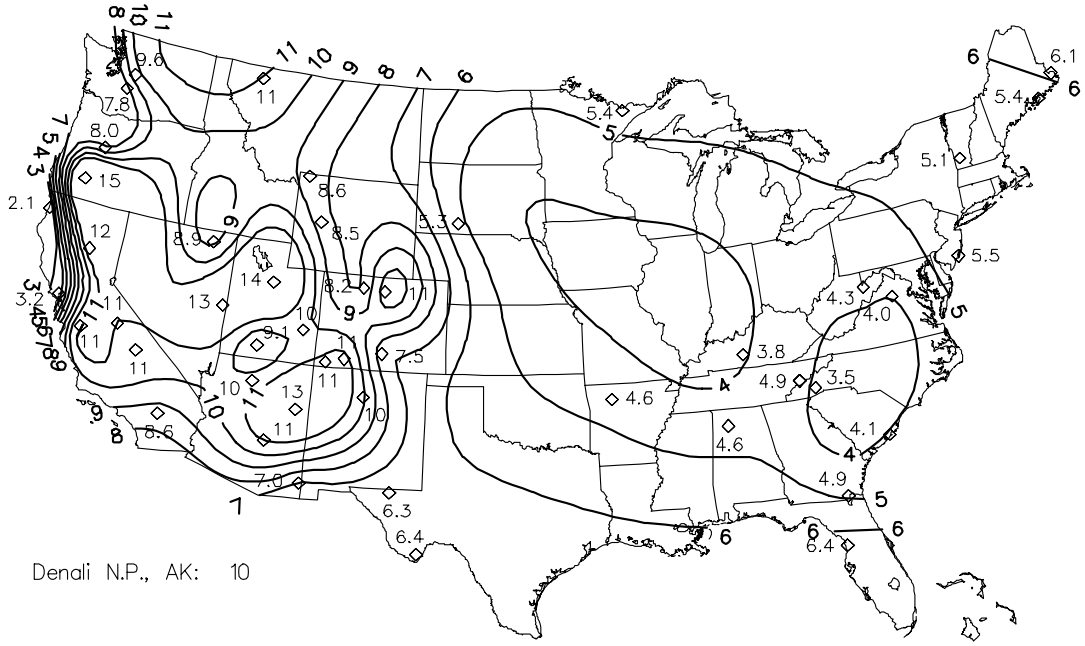

Figure S.6d *Fractional contribution of light-absorbing carbon to total aerosol reconstructed light extinction (%).*

Finally, the fractional contribution of fine and coarse soil/dust is shown in Figure S.6e. In the eastern United States, it is generally less than 5%, while in the Sonoran Desert, West Texas, and Great Basin regions its contribution to extinction is on the order of 20-30%. In the Cascade Mountains region, it is about 5%. In the rest of the United States, soil/dust contributes between about 10 and 20% of extinction.

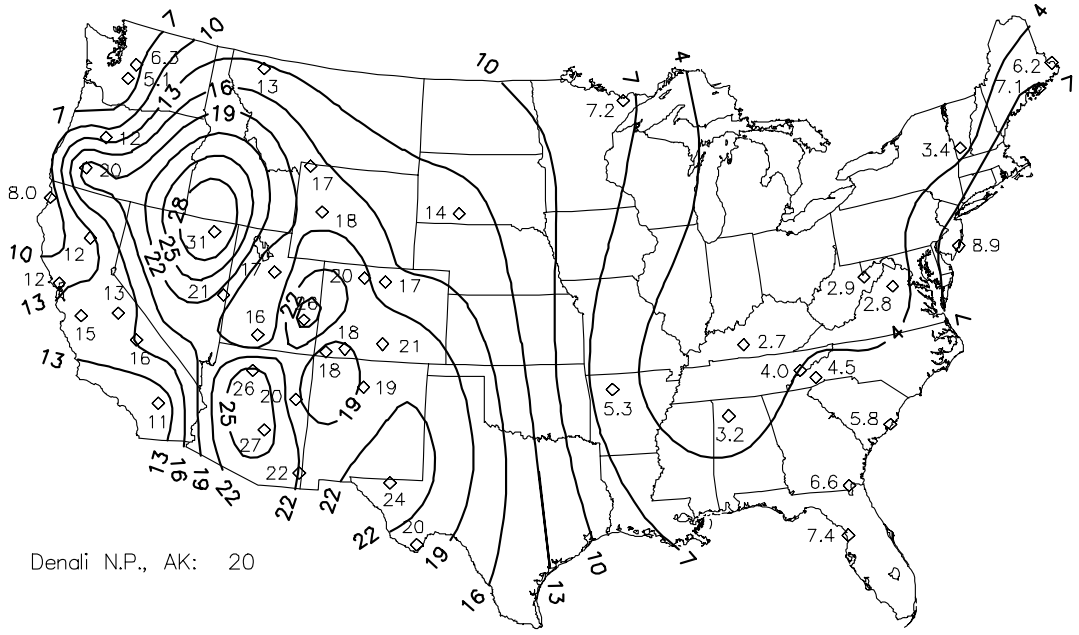

Figure S.6e *Fractional contribution of soil/dust to total aerosol reconstructed light extinction (%).*

S.4 SEASONAL DISTRIBUTION OF FINE MASS AND RECONSTRUCTED LIGHT EXTINCTION

Figure S.7 is a summary plot of reconstructed fine mass and the contribution of each species for the 20 monitoring regions, excluding Washington, D.C., in the IMPROVE Network. The summer months have the highest fine mass loadings at 19 of the 20 monitoring regions with two regions having nearly identical mass loadings in two seasons. In the Pacific Coastal Mountains region, fine mass concentrations are nearly the same in the summer and autumn seasons, while the West Texas fine mass loadings are nearly the same in spring and summer. In the Northern Rocky Mountains region, fine mass loadings are greatest during the autumn season primarily because of increased organic mass concentration. East of the Mississippi sulfates make up about 60-70% of the fine mass in all seasons, while in much of the inner-mountain west fine mass concentrations are somewhat evenly split between sulfates, carbon, and soil/dust mass concentrations.

Figure S.8 is a summary plot of reconstructed light extinction and the contribution of each species for the 20 monitoring regions, excluding Washington, D.C., in the IMPROVE Network. The addition of the effect of water on hygroscopic aerosols and the addition of coarse mass changes the seasonal trends somewhat. At 13 of the 20 monitoring regions, summer extinction is

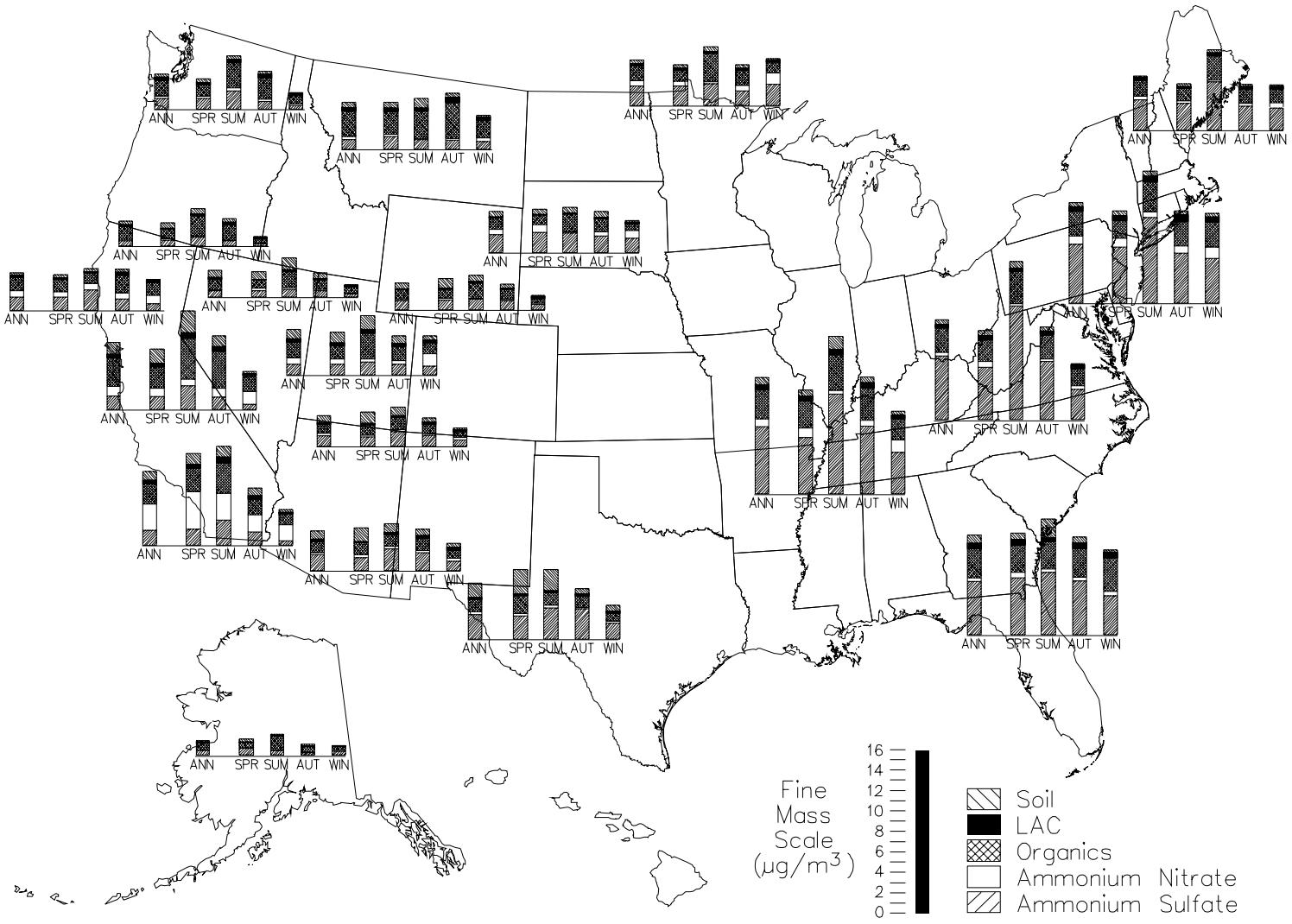

Figure S.7 *Summary plot of reconstructed fine mass and the fractional contribution of each species for the 20 monitoring regions in the IMPROVE Network, excluding Washington, D.C.*

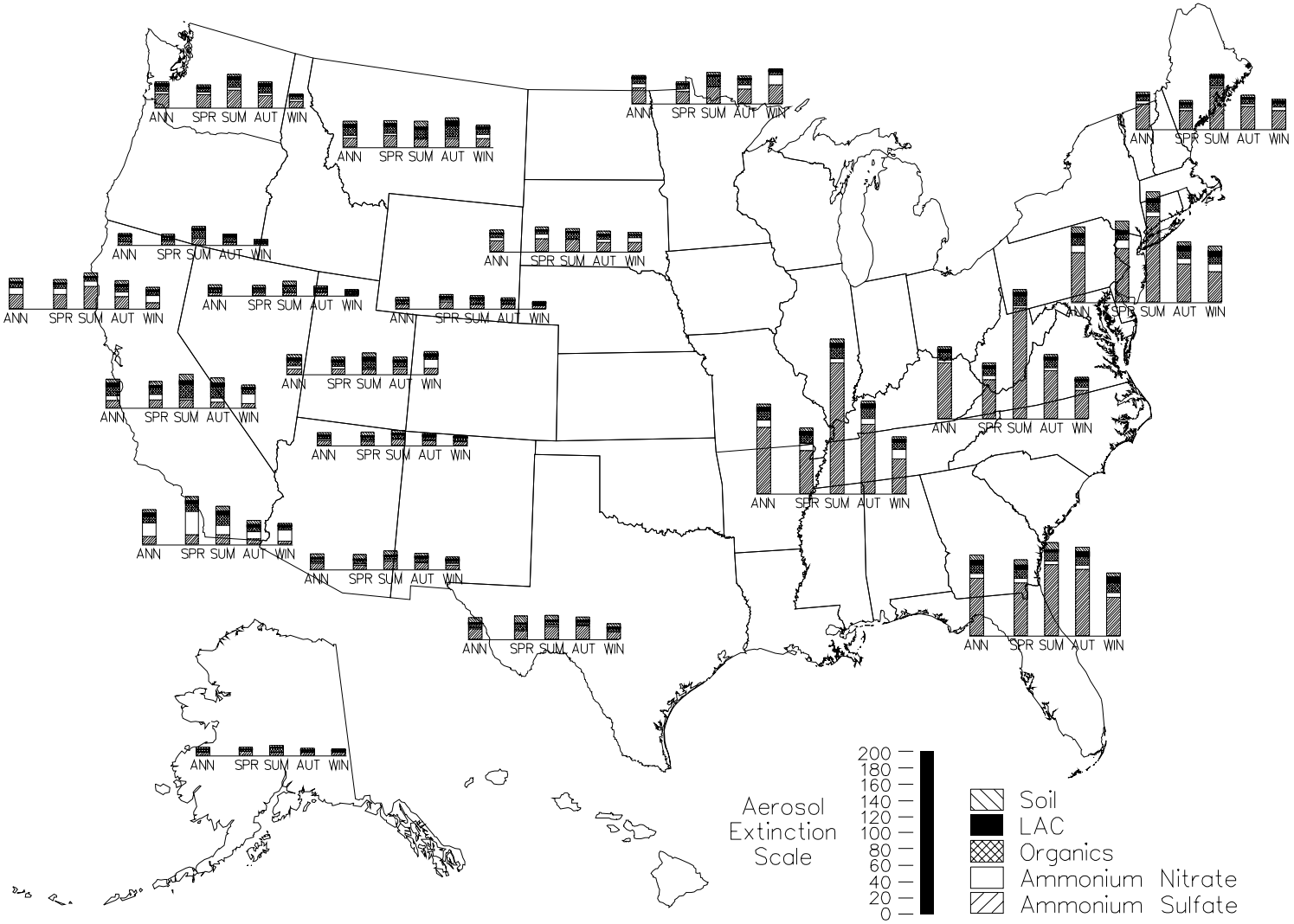

Figure S.8 *Summary plot of reconstructed light extinction and the fractional contribution of each species for the 20 monitoring regions in the IMPROVE Network, excluding Washington, D.C.*

the highest, with the largest difference between seasons being in the eastern United States, where sulfates in combination with high relative humidity make summer substantially hazier than any other season. Notice that sulfates, on a relative basis, contribute significantly more, because of high relative humidity, to extinction than to fine mass. West Texas, Sonoran Desert, Colorado Plateau, Great Basin, Sierra-Humboldt, Sierra-Nevada, Pacific Coastal Mountains, and Cascade Mountains regions also have, on the average, the highest extinction during the summer months, however, the differences between seasons tend to be not as pronounced. Three of the regions, Southern California, Central Rocky Mountains, and Northern Great Plains, have the highest extinction during the spring season. In the Southern California region, the springtime high is driven by increased nitrate extinction. In two regions, Cascade Mountains and Boundary Waters, winter has the highest extinction and again it is driven by nitrates, while in one region, Northern Rocky Mountains, spring is the season with greatest extinction.

S.5 CONTRIBUTION OF AEROSOL SPECIES TO PERIODS OF HIGH AND LOW (EXTREMES) FINE MASS CONCENTRATIONS

The chemical species contribution to extremes in fine mass is relevant to emissions control scenarios for the Class I areas represented by the IMPROVE monitoring sites where it is the goal to improve the haziest days, while maintaining visibility levels on the clearest days. Identification of the chemical species that impact the clearest and/or haziest days will provide a better understanding of potential sources of atmospheric particles responsible for visibility reduction during extreme fine mass events. For example, forest fires, whether they are prescribed burns or natural fires, occur sporadically and can cause particle carbon to have a large contribution to upper extremes of observed particle fine mass concentration at impacted sites. Also, secondary nitrate particles can have large contributions to upper extremes of fine particle mass during cold seasons, particularly in areas impacted by urban sources.

Spatial trends of fine particle data based on measurements from the IMPROVE Network indicate that, on average, sulfates constitute a major portion of particle fine mass in the eastern United States, particle carbon and soil/dust can have large contributions in the United States interior, desert mountain, and northwest regions, while nitrates are often major contributors to fine particle mass near many urban areas. This analysis contrasts the mean contribution of individual chemical species to the contribution of the same species to extremes in observed fine particle mass. It is illustrated that a chemical species contribution to the highest and lowest fine mass concentrations can be quite different from that species mean contribution. The analysis examined the contribution of sulfates, carbon, soil, and nitrate particles to extremes of observed fine particle mass.

On clean days, when fine mass concentrations are lowest, sulfate or carbon is the largest contributor to fine mass. However, on the highest fine mass days, or upper percentiles of observed fine mass, all species, including particle nitrates, can have large contributions, depending on the monitoring site and time of year.

For instance, sulfate is a major contributor to both the mean and upper extremes of fine mass in the eastern United States, with largest contributions to the upper extremes clustered in regions of high sulfur emissions. In the upper 2% of fine mass concentration, the sulfate contribution increases

between 20-30% over the mean sulfate contribution. For example, if the sulfates contribute 50% of the fine mass then, on the average, they contribute between 70-80% of the fine mass on the upper 2% time periods.

Carbon mass concentration exhibits a pattern generally increasing the mean contribution of fine mass concentrations from south-to-north. The carbon concentration increases during extreme high fine mass in the western United States that are likely related to forest fires. In the Central and Northern Rocky Mountains regions, the relative contribution of organics to fine mass increases from about 40-50% on the average to 50-70% on the extreme periods and at Yellowstone from 52% on the average to 75% on the highest fine mass time periods.

Particle nitrate contributions to fine mass are largest during the winter, and have substantially increased contributions to upper extremes of fine mass near urban areas and in the Midwest. For instance, along the California coast the average nitrate contribution to fine mass is 25-30%, while on the high fine mass days it is 60-65% and in the Midwest it is about 20-30% on the average and 40-45% on the highest fine mass periods. Interestingly, at Rocky Mountain National Park nitrates are only 7.3% of the fine mass on the average but 28.3% on the extreme days. The mean soil contribution to fine mass is largest in the western United States, with high soil contributions to upper extremes in the southwest and southeast coastal regions, where regional and long-range transport of wind-blown dust are responsible for extremes.

S.6 TEMPORAL TRENDS IN VISIBILITY AND AEROSOL CONCENTRATIONS

Referring to Figure S.9, the haziest days as represented by those days with the highest 20% fine mass concentrations, have nine sites with positive and significant dv slopes indicating that visibility is decreasing on the haziest days, eleven sites where visibility is improving at a statistically significant rate, and nine sites where visibility remains the same. At five of the nine sites that have decreasing visibility, sulfates are increasing at a significant rate (Great Smoky Mountains and Big Bend National Parks, and Chiricahua, Bandelier, and Great Sand Dunes National Monuments), four sites show increasing nitrates (Badlands, Mesa Verde, and Big Bend National Parks, and Chiricahua National Monument), and two sites (Jarbidge Wilderness Area and Bryce Canyon National Park) with increasing organics. The Great Smoky Mountains National Park's increase in haziness is primarily associated with a 259 $ng/m^3/yr$ increase in sulfates. This rate of increase in sulfates is 2½ times greater than at Big Bend National Park and a factor of 10 greater than at Bandelier and Great Sand Dunes National Monuments. Also, even though there are only two sites where increases in organics correspond to increases in haziness, there are seven sites, all in the inner-mountain west where organics are increasing in a statistically significant way. These are the same sites where the extreme fine mass concentrations are dominated by organics.

Of the eleven sites that show statistically significant trends toward improved visibility, six of these sites (Glacier, Mount Rainier, Redwood, and Canyonlands National Parks, Pinnacles National Monument, and San Gorgonio Wilderness Area) show decreases in sulfate mass concentration, eight sites (Mount Rainier, Redwood, Canyonlands, Petrified Forest and Acadia National Parks, Point Reyes National Seashore, Pinnacles National Monument, and San Gorgonio Wilderness Area) in nitrate concentrations, and seven sites (Mount Rainier, Redwood, Petrified Forest and

Acadia National Parks, Point Reyes National Seashore, Pinnacles National Monument, and San Gorgonio Wilderness Area) in organic mass concentration. At sites along the California coast and at San Gorgonio Wilderness Area, reductions in nitrate concentrations are the most significant contributors to improvement in visibility.

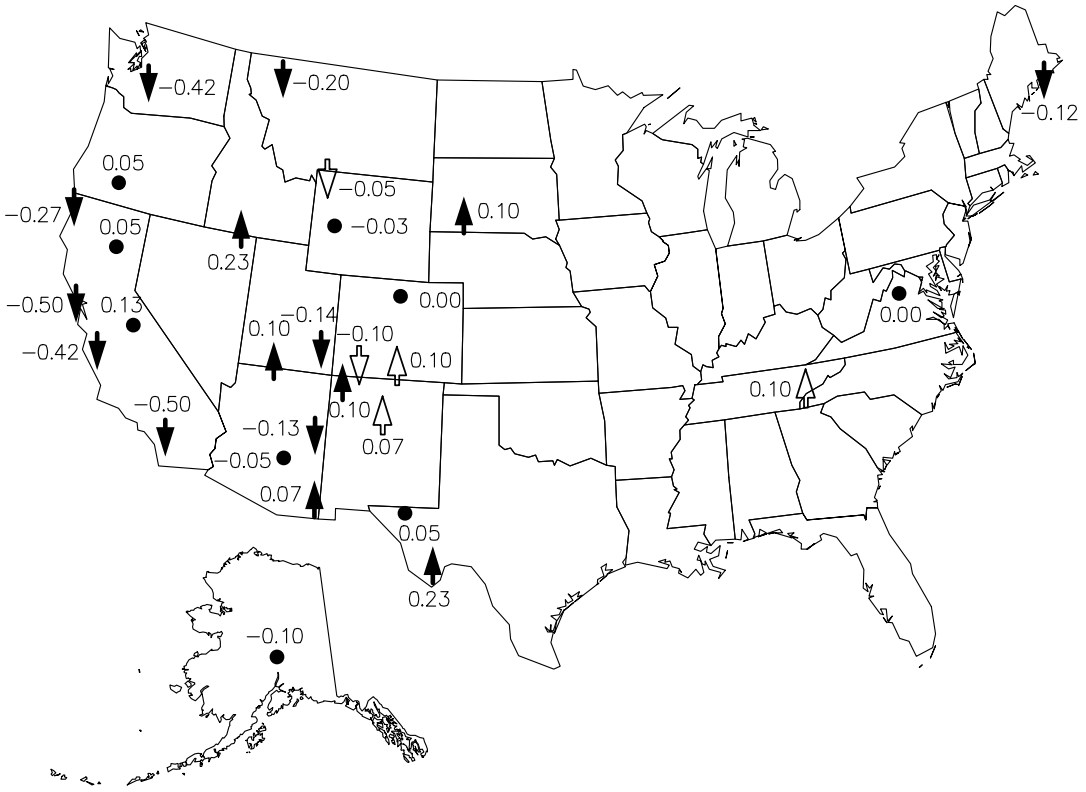

Figure S.9 *This map summarizes the trends in deciview (dv/yr) for group 90 (top 20% of fine mass) days. The icons mark the site locations, a solid dot indicates an insignificant slope, an empty arrow indicates a positive or negative slope that is significant in the range of $0.05<p\leq0.1$ level of probability, and a solid arrow indicates a positive or negative slope that is significant at better than 0.05 ($p\leq0.05$) level of probability.*

S.7 DIURNAL TRENDS IN SCATTERING AND EXTINCTION

The previous analysis, which focused on spatial and long-term trends, relied entirely on particle data that was collected twice weekly and each sample was 24 hrs in duration. On the other hand, at a few select sites transmissometers and nephelometers are operated along with the aerosol samplers. The optical instruments serve as a quality assurance check in that measured and reconstructed scattering/extinction should be equivalent and because these instruments run continuously, essentially collecting instantaneous data (10-min or 2-min time intervals), an examination of diurnal variations in visibility, as represented by the extinction and/or scattering coefficient, are possible.

Diurnal and seasonal patterns in measured b_{scat} and b_{ext} are similar for many sites. A common pattern is highest scattering or extinction during the summer, lowest during the winter with

scattering or extinction being somewhat higher at night. Usually, the differences between different hours of the day are not as large as the differences between seasons. In some cases, however, the average extinction varies by up to a factor of 5 from one time of day to another largely because of changes in relative humidity and the associated growth of hygroscopic aerosols. RH is typically driven mostly by an inverse relationship to average temperature. There are some sites that have unique diurnal or seasonal patterns in average b_{scat} or b_{ext}. In many cases, especially when the site is near a large urban area, there is evidence that these average values are dependent on mixing height. Higher mixing heights allow aerosols associated with local sources to reach the monitoring site.

S.8 RECOMMENDED FUTURE RESEARCH

Developing strategies to improve visibility requires an understanding of the relationship between the various aerosol species and atmospheric extinction. In this report and for applications where detailed physio-chemical aerosol characteristics are not known, a number of simplifying assumptions were made to make estimates of extinction from aerosol concentration measurements. Understanding the inherent uncertainties in linking aerosol species concentrations to extinction is essential if one is going to track progress in extinction change (change in visibility) as a function of changing emissions and resulting aerosol concentrations. Some key concerns are:

Organic Aerosol Measurement. The measurement of carbon mass remains responsible for much of the uncertainty in estimates of how various aerosol species affect visibility. Adjustments are made to carbon mass to correct for the adsorption of organic gases on the filter substrate as well as loss of volatile material from the substrate. This area needs to be considered in future studies. Also, the mass fractions of hydrogen and carbon in organics are based on an assumption of the hydrocarbon type. Future research should evaluate these fractions on the basis of the most common organic molecules in the samples.

Absorption Estimates and Measurement. The accurate estimation of absorption remains problematic. Absorption can be estimated by assigning a mass absorption efficiency to elemental carbon or it can be estimated from direct measurements of light attenuation as it passes through a filter medium on which the absorbing material has been collected. Some research has suggested that the various filter absorption measurement techniques yield values that are too high by factors on the order of 20-80%, while other techniques may underestimate absorption by the same amount. Even though all techniques are highly correlated, the absorption estimates can vary by more than factors of two. Furthermore, mass absorption efficiencies, which are required to estimate absorption from measurements of elemental carbon, have been reported in the literature that range from about 5–20 m^2/g with a value of 10 m^2/g being used by most researchers in the field. On a theoretical basis, it is hard to justify absorption efficiencies greater than about 5-8 m^2/g.

Apportionment of Carbon to General Source Categories. The attribution of smoke to fine particle mass and visibility impairment at points that are hundreds of kilometers distant are essential for meeting the requirements of the proposed $PM_{2.5}$ standard and proposed Regional Haze Rule.

Attribution of smoke to fine mass and/or extinction can only be achieved using yet to be developed monitoring methodologies.

Hygroscopicity of Aerosols. The relative humidity correction terms applied to sulfate and nitrate vary as a function of physio-chemical characteristics such as ammoniation and particle size, which to a large degree are dependent on the region of the country. For instance, sulfates tend to be more acidic in the eastern United States and tend toward larger particles than the western United States.

Coarse Particle Chemical and Optical Characteristics There has been very little work investigating coarse particle chemical and optical characteristics. It is usually assumed that coarse particles are primarily soil/dust, with scattering efficiencies of 0.4-0.6 m^2/g, and values that were derived from two studies that occurred in desert areas where dust can contribute as much as 50% of the particle extinction budget. Some recent studies suggest that significant fractions of coarse particles are organics and/or nitrates depending on the region of the country.

Other areas of concern that are secondary to these described issues are:

(1) How important are the mixing characteristics of aerosol species? Externally mixed particles are assumed, while it has been well documented that some species are internally mixed.

(2) What is the significance of scattering properties of sulfates as a function of ammoniation? This includes the water absorption properties of sulfates as a function of ammoniation.

(3) How important is the variability of ambient particle size to estimates of dry mass scattering efficiencies?

(4) Do carbon aerosols, other than elemental carbon, absorb light and if so what are the associated absorption efficiencies?

The answer to these questions may be regionally dependent. For instance, is the east different from the inner-mountain west or the northwest or the southwest?

In addition to the above refinements in the analyses conducted in this report, additional data analysis is recommended. For example, back trajectory analysis and spatial/temporal pattern analysis of episodes is recommended to determine the source region contributions to elevated concentrations.

S.9 REFERENCES

Sisler, J. F., *Spatial and Seasonal Patterns and Long Term Variability of the Composition of the Haze in the United States: An Analysis of Data from the IMPROVE Network*, Cooperative Institute for Research in the Atmosphere, Colorado State University, ISSN 0737-5352-32, 1996.

Sisler, J. F., Huffman, D., Latimer, D. A., Malm, W. C. and Pitchford, M. L., *Spatial and Temporal Patterns and the Chemical Composition of the Haze in the United States: An Analysis of Data from the IMPROVE Network 1988-1991*, Cooperative Institute for Research in the Atmosphere, Colorado State University, ISSN 0737-5352-26, 1993.

CHAPTER 1

IMPROVE NETWORK – CURRENT AND FUTURE CONFIGURATIONS

1.1 INTRODUCTION

The Regional Haze Rule [64 FR 35714, 1999] requires monitoring representative of each of the 156 visibility protected federal Class I areas (CIAs), as shown in Figure 1.1, beginning in January 2000 in order to track progress toward the national visibility goal. The deciview index calculated from ambient particle chemical speciation data was selected to track haze levels. This entails particle sampling and analysis of the major aerosol components using methods patterned after those utilized since 1987 by the IMPROVE Network [Joseph et al., 1987; Sisler, 1996] and consistent with the aerosol monitoring portion of the 1999 Visibility Monitoring Guidance document issued by EPA [64 FR 35 714, 1999].

The Interagency Monitoring of Protected Visual Environments (IMPROVE) program is a cooperative measurement effort designed:

(1) to establish current visibility and aerosol conditions in mandatory CIAs;

(2) to identify chemical species and emission sources responsible for existing man-made visibility impairment;

(3) to document long-term trends for assessing progress towards the national visibility goal; and

(4) with the enactment of the Regional Haze Rule, to provide regional haze monitoring representing all visibility-protected federal CIAs where practical.

The program is managed by the IMPROVE Steering Committee that consists of representatives from the U.S. Environmental Protection Agency (EPA), the four Federal Land Managers (FLMs—National Park Service, Forest Service, Fish and Wildlife Service, and Bureau of Land Management), the National Oceanic and Atmospheric Administration, four organizations representing state air quality organizations (State and Territorial Air Pollution Program Administrators/Association of Local Air Pollution Control Officials, Western States Air Resources Council, Northeast States for Coordinated Air Use Management, and Mid-Atlantic

Regional Air Management Association), and an Associate Member, the State of Arizona Department of Environmental Quality.

In 1999, the IMPROVE Network consisted of 30 monitoring sites in CIAs (see Figure 1.1), 20 of which began operation in 1987 with the others starting in the early 1990s. Each monitoring site includes $PM_{2.5}$ sampling on a twice per week schedule with subsequent analysis for the fine particle mass and major aerosol species as well as PM_{10} sampling and mass analysis [Sisler et al., 1993]. Many of the sites also include optical monitoring with a nephelometer or a transmissometer, and color photography to document scenic appearance. In addition, approximately 40 sites, most in remote areas, that use the same instrumentation, and monitoring and analysis protocols (called IMPROVE Protocol sites) were operated individually by federal or state organizations in recent years.

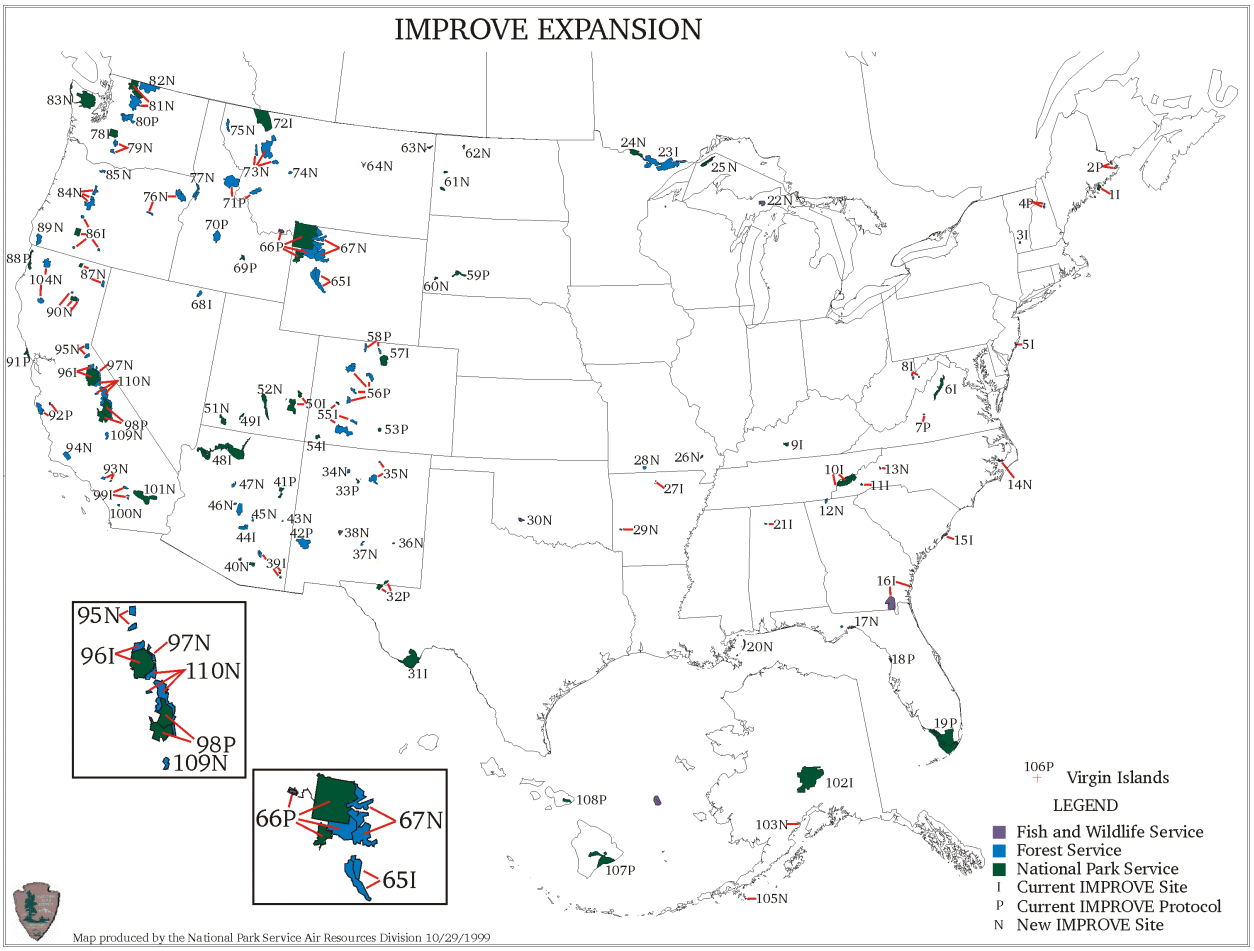

Figure 1.1 *Map showing all of the Federal Class I areas where visibility is deemed an important value and the locations of the original IMPROVE, IMPROVE Protocol and new IMPROVE sites.*

Beginning in 1998 EPA provided supplemental support to IMPROVE to expand the network in order to provide representative particle speciation monitoring that would be needed for the then anticipated Regional Haze Rule for all of the visibility-protected CIAs where it was

practical. In making the decision to support the expansion of the IMPROVE Network, EPA also considered the value of the $PM_{2.5}$ mass and speciation data in remote areas for use by states in their implementation of the $PM_{2.5}$ regulation [62 FR 38652, 1997]. Provisions were made in those regulations so that states could elect to use IMPROVE monitoring data to meet their requirements for regional background and transport monitoring sites.

EPA requested IMPROVE change some aspects of its monitoring protocol to increase the comparability of the monitoring to that required of states at their $PM_{2.5}$ compliance and speciation monitoring sites. The IMPROVE Steering Committee agreed to change the twice-weekly sampling schedule to the national every third day sampling, to add routinely operated collocated instruments at 10% of the sites in order to generate quality assurance data, and to provide all of the monitoring data to the Aerometric Information Retrieval System (AIRS) database. To accommodate these changes a new version of the IMPROVE sampler was developed that provides for more flexible sample schedule control and continuous monitoring of sample flow and temperature, while maintaining the same sample collection characteristics of the original version of the sampler.

This chapter briefly describes the current IMPROVE monitoring network with emphasis on the aerosol monitoring program that produced most of the data reported on in subsequent chapters, and it also describes the network expansion including site selection and changes in the monitoring equipment and protocols. None of the data summarized in this report were collected under changed protocols or at new sites. However, data generated by the expanded network will be available for public use several years prior to the preparation of the next IMPROVE report, so the description of the changes to the protocols and monitoring sites can serve to characterize these newly collected data.

1.2 CURRENT NETWORK

1.2.1 Particulate Samplers

The IMPROVE sampler was designed for the IMPROVE Network and has been operated extensively in the network and during field studies since the winter of 1987 [Malm et al., 1994 and Malm et al., 1989]. The IMPROVE sampler consists of four independent modules (see Figure 1.2). Each module incorporates a separate inlet, filter pack, and pump assembly, however, all modules are controlled by a singular timing mechanism. It is convenient to consider a particular module, its associated filter, and the parameters measured from the filter as a channel of measurement (i.e., module A). Modules A, B, and C are equipped with a 2.5 μm cyclone. The module A Teflon filter is analyzed for fine mass ($PM_{2.5}$) gravimetrically, nearly all elements with atomic mass number ≥11 (which is Na) and ≤82 (which is Pb) by proton induced x-ray emission (PIXE) and by x-ray florescence (XRF), elemental hydrogen by proton elastic scattering analysis (PESA), and for light absorption.

For module B, the sampled air is drawn through a carbonate denuder tube in the inlet to remove gaseous nitrates. The material collected from the filter is extracted ultrasonically in an aqueous solution that is subsequently analyzed by ion chromatography for the anions sulfate, nitrate, nitrite and chloride. At the Great Smoky Mountains and Shenandoah National Parks and

Dolly Sods Wilderness Area, the ammonium ion concentration is also measured using extracts from these filters in a separate colorimetric analysis.

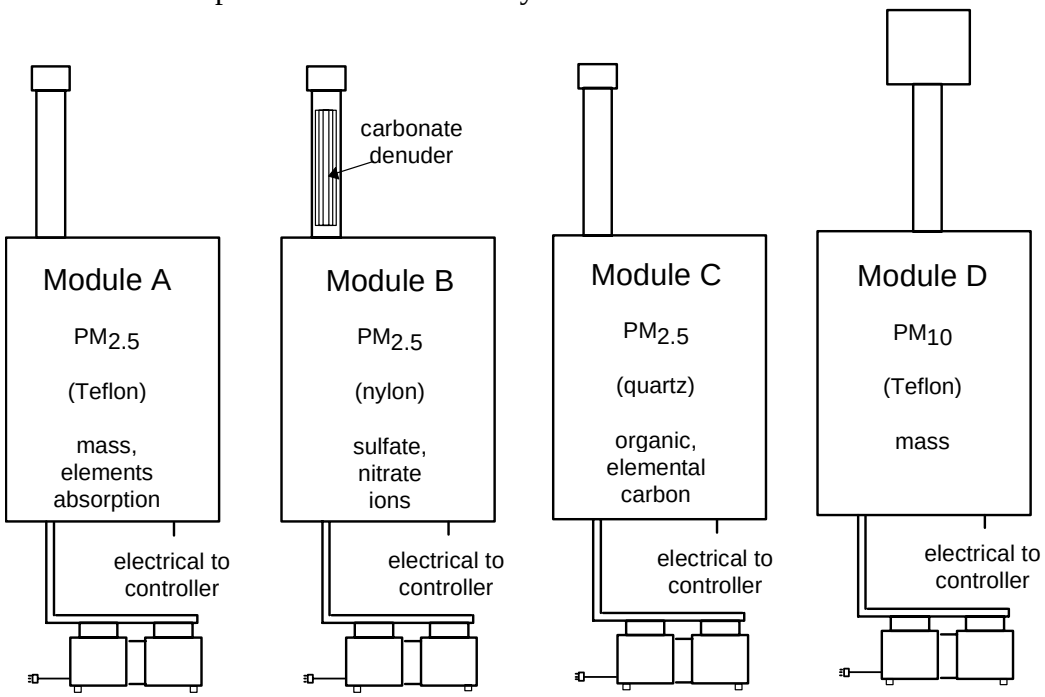

Figure 1.2 *Schematic view of the IMPROVE sampler showing the four modules with separate inlets and pumps. The substrates with analyses performed for each module are also shown.*

Module C utilizes tandem quartz fiber filters for the collection of fine particles; the front filter is analyzed for particulate carbon, while the second filter is used for an estimation of the organic carbon artifact associated with organic gases trapped on the filter substrate. Thermal optical reflectance (TOR) is the analytic technique used for determination of organic and elemental carbon [Chow et al., 1993].

Module D, fitted with a PM_{10} inlet, utilizes a Teflon filter, which is gravimetrically analyzed for mass (PM_{10}). Exposed cassettes from modules A, B, C, and D are stored in sealed plastic bags and shipped for storage and analysis.

1.2.2 Network Configuration

There are currently a number of monitoring sites in the United States that use IMPROVE instrumentation and follow IMPROVE protocol, however, not all sites are operated as part of the IMPROVE monitoring network. There are 49 sites that are used for the spatial distributions of aerosol mass and extinction analyses presented in Chapters 2 and 3. There are 51 sites in the contiguous United States that are used for the species contribution to extreme fine mass, which is discussed in Chapter 4. There are 29 sites with an 11-year record that extends from March 1988 to February 1999 and these data will be used in the 11-year trend analysis in Chapter 5. Table 1.1 summarizes this information as well as the monitoring site start date, whether it was part of

the IMPROVE monitoring network, indicated by an I, or operated by another agency but according to IMPROVE protocol, indicated by a P. In the table, the sites that were used for various analyses are indicated as S, E, or T, which stand for spatial distributions of mass and optical properties, species contribution to extreme concentrations, and trend analysis, respectively. The table also shows the aerosol modules operated at the site and whether that site was operated with an integrated nephelometer (N) or a transmissometer (Tr). Finally, at a number of these sites cameras were operated to document the visual impact of regional and layered hazes as a function of aerosol concentrations. Slides of a subset of the camera monitoring sites have been selected to represent the various haze conditions that occurred and have been transferred to CD-ROM. Storage of pictorial information in a digital format allows for maintenance of a permanent non-degrading visual image database. Those sites that have had the pictorial information transferred to CD-ROM and those sites under pictorial development are also summarized in Table 1.1.

Table 1.1 *Tabular summary of the sites used for spatial, trend, and extreme value analyses presented in this report. Also shown in the table is the protocol under which the site was operated, its start date, the type of equipment at the site and an indicator showing those sites that have selected color slides digitized and transferred to CD-ROM or in the slide development phase.*

Site	Protocol	Start Date	Analysis	Equipment	Slide Database
Alaska (AKA)					
Denali NP&P	I	3/88	SET	ABCD	
Appalachian Mountains (APP)					
Great Smoky Mountains NP	I	3/88	SET	ABCDN	X
Shenandoah NP	I	3/88	SET	ABCDTr	X
Dolly Sods WA	I	3/91	SE	ABCDN	X
James River Face WA	P	9/94	SE	ABCD	
Shining Rock WA	I	7/94	SE	ABCDN	
Boundary Waters (BWA)					
Boundary Waters Canoe Area	I	3/91	SE	ABCDN	◇
Cascade Mountains (CAS)					
Columbia River NSA	P	6/93	E	ABCDN	
Mount Rainier NP	I	3/88	SET	ABCDN	X
Snoqualmie Pass WA	P	7/93	SE	ABCDN	
Three Sisters WA	P	7/93	SE	ABCDN	
Central Rocky Mountains (CRK)					
Bridger WA	I	3/88	SET	ABCDTr	X
Great Sand Dunes NM	P	5/88	SET	ABCD	◇
Mount Zirkel WA	I	11/93	E	ABCDN	
Rocky Mountain NP	I	9/90	SET	ABCDTr	X
Weminuche WA	I	3/88	SET	ABCD	
Yellowstone NP	P	3/88	SET	ABCD	X
Colorado Plateau (CPL)					
Bandelier NM	P	3/88	SET	ABCDTr	X
Bryce Canyon NP	I	3/88	SET	ABCD	X
Canyonlands NP	I	3/88	SET	ABCDTr	X
Grand Canyon NP	I	3/88	SE	ABCDSoTr	X
Mesa Verde NP	I	3/88	SET	ABCD	X
Petrified Forest NP	P	3/88	SET	ABCDTr	

Table 1.1 *Continued.*

Site	Protocol	Start Date	Analysis	Equipment	Slide Spectrum
Great Basin (GBA)					
Jarbidge WA	I	3/88	SET	ABCDN	X
Great Basin NP	I	5/92	SE	ABCD	
Mid Atlantic (MAT)					
Edwin B. Forsythe (Brigantine) NWR	I	9/91	SE	ABCD	
Mid South (MDS)					
Upper Buffalo WA	I	6/91	SE	ABCDN	
Sipsey WA	I	3/92	SE	ABCD	
Mammoth Cave NP	I	3/91	SE	ABCDN	
Northeast (NEA)					
Acadia NP	I	3/88	SET	ABCDN	X
Lye Brook WA	I	3/91	SE	ABCD	X
Moosehorn NWR (Roosevelt Campobello US-CC)	P	12/94	SE	ABCD	
Northern Great Plains (NGP)					
Badlands NP	P	3/88	SET	ABCDTr	X
Northern Rocky Mountains (NRK)					
Glacier NP	I	3/88	SET	ABCDTr	X
Pacific Coast (PAC)					
Pinnacles NM	P	3/88	SET	ABCD	X
Point Reyes NS	P	3/88	SET	ABCD	X
Redwood NP	P	3/88	SET	ABCD	X
Sierra Nevada (SRA)					
Sequoia NP	P	7/93	SE	ABCD	
Yosemite NP	I	3/88	SET	ABCDTr	X
Sierra-Humboldt (SRH)					
Crater Lake NP	I	3/88	SET	ABCD	X
Lassen Volcanic NP	P	3/88	SET	ABCD	X
Sonoran Desert (SON)					
Chiricahua NM	I	3/88	SET	ABCDTr	X
Gila WA	I	3/94	E	ABCDN	
Tonto NM	I	3/88	SET	ABCD	
Southeast (SOE)					
Chassahowitzka NWR	P	4/93	SE	ABCD	
Okefenokee NWR	I	3/91	SE	ABCDN	
Cape Romain NWR	I	9/94	SE	ABCD	
Southern California (SCA)					
San Gorgonio WA	I	3/88	SET	ABCDTr	X
Wasatch (WAS)					
Lone Peak WA	P	11/93	SE	ABCDN	
Washington D.C. (WDC)					
Washington D.C.	P	3/88	E	ABCD	
West Texas (WTX)					
Big Bend NP	I	3/88	SET	ABCDTr	X
Guadalupe Mountains NM	P	3/88	SET	ABCDTr	X

NP&P = National Park and Preserve
NP = National Park
WA = Wilderness Area
NM = National Monument
NWR = National Wildlife Refuge
US-CC = U.S.-Canadian Commission
NS = National Seashore

NSA = National Scenic Area
I = Current IMPROVE site
P = Current IMPROVE protocol
◇ = Slide development phase
S = FM/Extinction Spatial Analysis
E = Extreme value analysis
T = Trend analysis

A = Module A aerosol sampler
B = Module B aerosol sampler
C = Module C aerosol sampler
D = Module D aerosol sampler
So = SO_2 afterfilter
N = Nephelometer
Tr = Transmissometer

The locations of all the sites listed in Table 1.1 are shown in Figure 1.3, along with the types of analysis (S, E, T) and presence of optical monitoring (O). The density of sites in the western United States is considerably greater than in the eastern United States. Therefore, data from the Clean Air Status and Trends Network (CASTNet), a program designed to track the sulfur dioxide emission reduction program, are used to "fill in" (described in Appendix A) sulfate and nitrate concentration data in the eastern United States to create a more accurate picture of the spatial variability of extinction.

1.3 FUTURE NETWORK CONFIGURATION

The IMPROVE Steering Committee devised a plan to expand the network to support the regional haze regulation monitoring needs with the following network design objectives: (1) minimize the number of monitoring sites needed to represent regional haze conditions for all of the CIAs where monitoring is possible, (2) continue at current monitoring sites that are representative of regional haze conditions in CIAs to preserve their value for trends analysis, and (3) ensure that every opportunity for input in the site selection process would be afforded to federal land management and state air quality organizations.

1.3.1 Site Selection Process

There are many examples of visibility-protected CIAs that are near to each other, so separate monitoring sites might not be needed. To determine which sites can be grouped together (objective 1) requires consideration of both technical and policy concerns for what constitutes representative monitoring for regional haze. Historical data collected at the current IMPROVE and IMPROVE Protocol sites show striking similarities in the average composition and concentration over distances exceeding 100 km [Sisler et al., 1993]. Site-to-site correlation analysis of aerosol data collected at sites in the same region typically produce highly significant relationships. Thus from a technical perspective, monitoring sites that are relatively near to each other in remote areas can be expected to collect similar data that might be considered redundant. The next section discusses representative monitoring from a policy perspective.

With respect to the second objective, the Steering Committee considers each of the original 30 IMPROVE sites to be representative of the regional haze conditions of the CIA for which it was selected. Reconsideration of the siting of any of these would only be done if requested by a state or land management organization. However, some of the IMPROVE Protocol sites were selected by the operating organization to represent air quality conditions for non-CIAs (typically Class II areas). IMPROVE Protocol sites would be candidates for selection as network expansion sites, but would only be chosen if they were the best of the sites being considered.

The last of these objectives reflects the Steering Committee's recognition of the responsibilities of state air quality and federal land management organizations identified in the Regional Haze Rule. While all of these organizations are represented on the Steering Committee, it was deemed prudent to explicitly solicit input from each individual state air quality agency, since no multi-state organization could be expected to speak for the diverse interests of each state. Moreover, states and the local federal land managers were looked to for

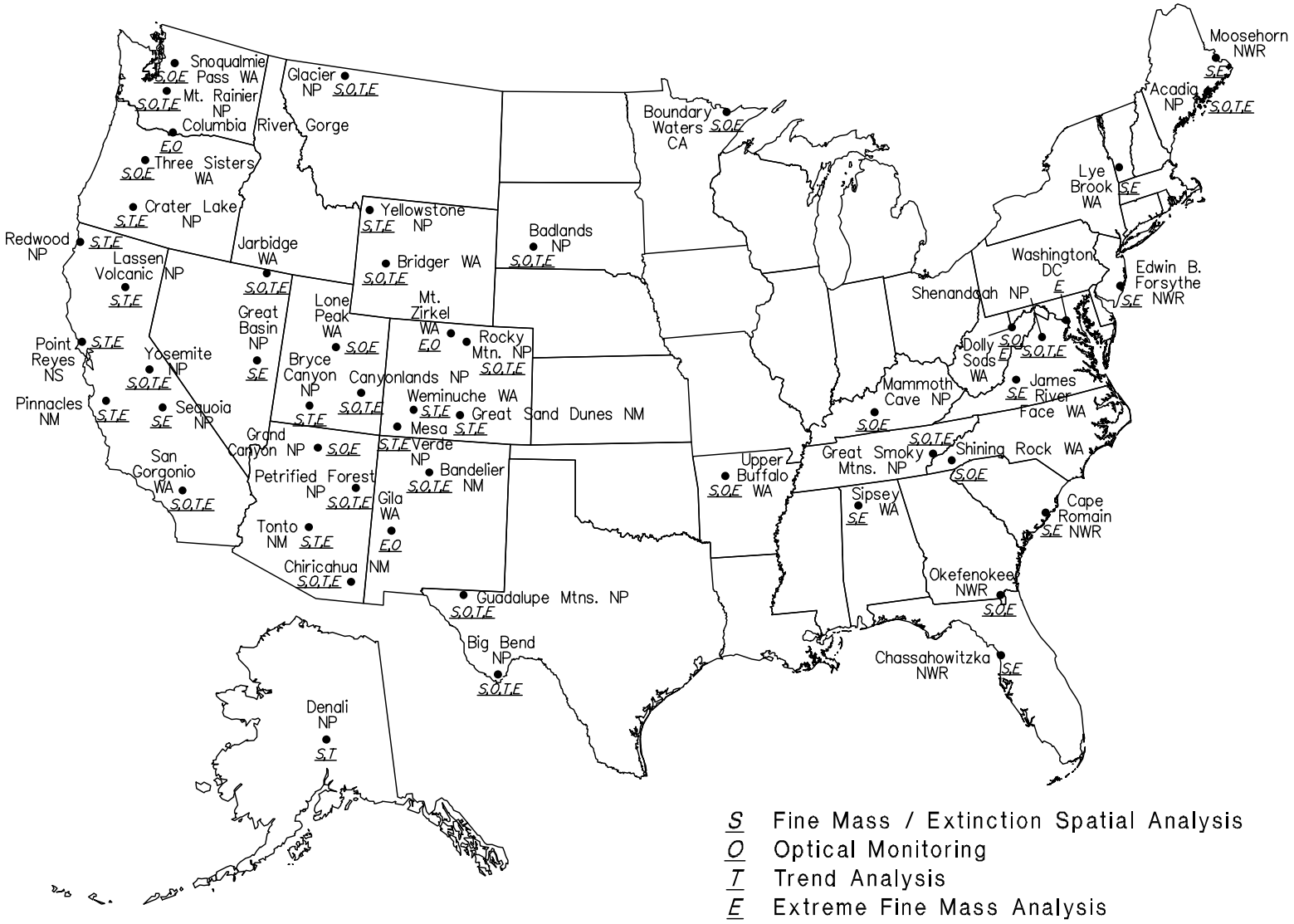

Figure 1.3 *A map of the IMPROVE sites used for the spatial, trend, and extreme value analyses.*

their knowledge and experience concerning air quality, meteorology and pollution emission conditions in their region. Communications and coordination with states was accomplished by a series of letters from the Steering Committee to the states distributed by STAPPA/ALAPCO and posted on the EPA AMTIC web page that described the network expansion plans, progress in site selection, and solicited input to the process. Over the 18-month planning process many states responded to this request for input with letters, email, or phone conversations, and in some cases with state- or site-specific meetings and field trips involving Steering Committee representatives.

1.3.1.1 Representative Monitoring for Regional Haze

Federal visibility protection is limited to specific well-defined locations, the 156 mandatory federal CIAs where visibility was deemed an important value (Figure 1.1). Visibility monitoring must be representative of these locations if the data are to be useful for tracking progress towards the visibility goal of eliminating man-made contributions to visibility impairment. Most of the CIAs are designated national wilderness areas for which the Wilderness Act restricts the siting of man-made items, including environmental monitoring equipment [Public Law 88-577, 1964; 16 USC section 1131, 1997]. Even for CIAs where monitoring is allowed (i.e., national parks), practical requirements such as power, security and access occasionally make it difficult to find a suitable monitoring site within the CIA boundary. Traditionally, the IMPROVE program has dealt with these restrictions by finding representative locations to site monitors that are as near to the CIAs as is practically possible so it could be reasonably claimed that the visibility monitored is the same as what would be experienced in the CIA.

The problems of finding representative monitoring locations are decreased considerably for sites where the primary objective is to monitor the regional haze aspect of visibility. EPA defines regional haze as "…visibility impairment that is produced by a multitude of sources and activities which emit fine particles and their precursors and which are located across a broad geographic area" [64 FR 35714, 1999]. EPA also recognizes a form of visibility impairment that is reasonably attributable to a nearby source or group of sources, which is addressed by the first phase of visibility protection regulations issued in 1980 [45 FR 80084, 1980]. The spatial scale of the impacts and the number and distribution of sources are important factors that distinguish regional haze from reasonably attributable impairment.

Since regional haze impacts are by definition those that are distributed over a broad geographic region, a representative monitoring site does not necessarily need to be located very near to the CIA being represented. It is more important that the monitoring site experience impacts from the same collection of regionally important emission sources that influence the CIA haze and be isolated as much as possible from sources of solely local impacts, even if the localized impacts affect the CIA. A distinction needs to be drawn between isolated individual sources (e.g., diesel generator at the visitor center or a nearby highway) that should be distant from regional haze monitoring sites and individually small but ubiquitous sources that are widely distributed throughout the region (e.g., suspended crustal material in a desert or organic material in a conifer forest) that need not be avoided. Being in or very near a CIA is not as important in selecting a representative regional haze monitoring site as having similar exposure to the regionally important sources of haze and isolation from emission sources with purely localized

impacts. The practical significance of the concept that representative monitoring for regional haze can be accomplished at a distance from the protected area is that it should be possible to find sites that represent more than one CIA where they are located within the same regional haze region.

A two-stage process was developed for selecting new monitoring sites. The first stage was to subdivide the 156 CIAs into three categories: those that required a separate monitoring site, those where two or more visibility-protected areas could be represented by a single monitoring site for regional haze, and those for which monitoring was impractical. The second stage involved selection of the actual locations for monitoring for the new sites. These two stages are described in the following separate sections.

1.3.1.2 Identification of CIA Clusters

Two location-related parameters, the horizontal distance and elevation range, were employed in the preliminary grouping of CIAs into clusters that might be represented by single monitoring sites. For this preliminary grouping it was arbitrarily decided that a monitoring site should be within 100 km and be at an elevation between the maximum and minimum elevation of the CIAs that it represents. The elevation criterion was soon determined to be unnecessarily restrictive for a number of locations and was relaxed by allowing the site to be within 10% or 100 feet of the elevation extremes of the CIA to be represented. As indicated above, the 30 IMPROVE sites operational in 1999 were expected to be part of the expanded IMPROVE Network to preserve and extend the long-term trend records.

The preliminary grouping criteria were implemented by drawing 100 km circles around the current IMPROVE sites and the centroids for each CIAs using Geographic Information System (GIS) software. From this a table was constructed that grouped into clusters all CIAs with overlapping circles or where the current IMPROVE site circle overlaps one or more CIAs. This generated 92 clusters; 57 of which contain a single CIA; 30 contained 2 or 3 CIAs, and the remaining 5 contained from 4 to 7 CIAs. The table also contained the maximum and minimum elevations of the CIAs, the current IMPROVE sites and the IMPROVE Protocol sites. Application of the elevation criterion subdivided 11 of the clusters for a total of 103 clusters in this preliminary assessment of the required size for regional haze monitoring of the 156 CIAs.

A letter from the IMPROVE Steering Committee explaining each of the criteria including the map and table showing the CIA clusters was sent to all of the state air quality offices and to the federal land managers asking for their comments (at www.epa.gov/ttn/amtic/visinfo.html). The letter specifically asked for comments on the desirability of grouping neighboring CIAs into clusters that would be represented by a single monitoring site, on the specific criteria used to determine the preliminary clusters, and on changes that should be made to improve the cluster groupings of CIAs that take into account their knowledge of factors that influence haze in the various regions (e.g., terrain, pollution source distributions and meteorology). The letter also asked for comments on the identification of one CIA, the Bering Sea Wilderness, as impractical for routine monitoring due to its location in the Bering Sea over 400 km from the nearest source of commercial power and potential field support staff.

Seventeen states responded to the letter with comments. Several states suggested reorganization and additions to the preliminary clusters, with a net effect of raising the number to 110. For a few CIAs the preliminary location and elevation criteria were violated in a minor way by the newly configured clusters, but in every case the new configuration was viewed as an improvement with respect to representative regional haze monitoring. In addition, the state of Alaska asked that the IMPROVE Steering Committee reconsider the siting of the existing site at Denali National Park and Preserve, which they thought was perhaps influenced by park staff and visitors. Figure 1.1 shows the locations of each of the resulting clusters and Table 1.2 lists each cluster and the names of the CIAs they contain. All of the state recommended changes were accepted by the Steering Committee as a blueprint for the site selection stage of the network expansion process.

Table 1.2 *Final list of Class I areas organized by clusters with numbers corresponding to the map in Figure 1.1. Each cluster will have one IMPROVE site to monitor regional haze.*

#	Represented Class I Areas	State	FLM
1	Acadia	ME	NPS
2	Moosehorn, Roosevelt Campobello	ME	FWS, US-CC
3	Lye Brook	VT	FS
4	Great Gulf, Presidential Range-Dry River	NH	FS
5	Edwin B. Forsythe (Brigantine)	NJ	FWS
6	Shenandoah	VA	NPS
7	James River Face	VA	FS
8	Dolly Sods, Otter Creek	WV	FS
9	Mammoth Cave	KY	NPS
10	Great Smoky Mountains, Joyce Kilmer-Slickrock	TN, NC	NPS, FS
11	Shining Rock	NC	FS
12	Cohutta	GA	FS
13	Linville Gorge	NC	FS
14	Swanquarter	NC	FWS
15	Cape Romain	SC	FWS
16	Okefenokee, Wolf Island	GA	FWS
17	St. Marks	FL	FWS
18	Chassahowitzka	FL	FWS
19	Everglades	FL	NPS
20	Breton	LA	FWS
21	Sipsey	AL	FS
22	Seney	MI	FWS
23	Boundary Waters	MN	FS
24	Voyageurs	MN	NPS
25	Isle Royale	MI	NPS
26	Mingo	MO	FWS
27	Upper Buffalo	AR	FS
28	Hercules-Glades	MO	FS
29	Caney Creek	AR	FS
30	Wichita Mountain	OK	FWS
31	Big Bend	TX	NPS

***Table 1.2** Continued.*

#	Represented Class I Areas	State	FLM
32	Guadalupe Mountains, Carlsbad Caverns	TX, NM	NPS
33	Bandelier	NM	NPS
34	San Pedro Parks	NM	FS
35	Wheeler Peak, Pecos	NM	FS
36	Salt Creek	NM	FWS
37	White Mountain	NM	FS
38	Bosque del Apache	NM	FWS
39	Chircahua NM, Chircahua W, Galiuro	AZ	NPS, FS
40	Saguaro	AZ	NPS, FS
41	Petrified Forest	AZ	NPS
42	Gila	NM	FS
43	Mount Baldy	AZ	FS
44	Superstition, Tonto	AZ	FS
45	Sierra Ancha	AZ	FS
46	Mazatzal, Pine Mountain	AZ	FS
47	Sycamore Canyon	AZ	FS
48	Grand Canyon	AZ	NPS
49	Bryce Canyon	UT	NPS
50	Canyonlands, Arches	UT	NPS
51	Zion	UT	NPS
52	Capitol Reef	UT	NPS
53	Great Sand Dunes	CO	NPS
54	Mesa Verde	CO	NPS
55	Weminuche, La Garita, Black Canyon of Gunnison	CO	FS
56	Maroon Bells, West Elk, Eagles Nest, Flat Tops	CO	FS
57	Rocky Mountain	CO	NPS
58	Mount Zirkel, Rawah	CO	FS
59	Badlands	SD	NPS
60	Wind Cave	SD	NPS
61	Theodore Roosevelt	ND	NPS
62	Lostwood	ND	FWS
63	Medicine Lake	MT	FWS
64	UL Bend	MT	FWS
65	Bridger, Fitzpatrick	WY	FS
66	Yellowstone, Grand Teton, Teton, Red Rock Lakes	WY	NPS, FWS
67	North Absoraka, Washakie	WY	FS
68	Jarbidge	NV	FS
69	Craters of the Moon	ID	NPS
70	Sawtooth	ID	FS
71	Anaconda-Pintler, Selway-Bitterroot	MT, ID	FS
72	Glacier	MT	NPS
73	Bob Marshall, Mission Mountains, Scapegoat	MT	FS
74	Gates of the Mountains	MT	FS
75	Cabinet Mountains	MT	FS
76	Eagle Cap, Strawberry Mountain	OR	FS
77	Hells Canyon	ID	FS

***Table 1.2** Continued.*

#	Represented Class I Areas	State	FLM
78	Mount Rainier	WA	NPS
79	Goat Rock, Mount Adams	WA	FS
80	Alpine Lakes, Snoqualmie Pass	WA	FS
81	North Cascades, Glacier Peak	WA	NPS, FS
82	Pasayten	WA	FS
83	Olympic	WA	NPS
84	Three Sisters, Mount Jefferson, Mount Washington	OR	FS
85	Mount Hood	OR	FS
86	Crater Lake, Diamond Peak, Mountain Lakes, Gearhart Mtn	OR	NPS, FS
87	Lava Beds, South Warner	CA	NPS, FS
88	Redwood	CA	NPS
89	Kalmiopsis	OR	FS
90	Lassen Volcanic, Caribou, Thousand Lakes	CA	NPS, FS
91	Point Reyes	CA	NPS
92	Pinnacles, Ventana	CA	NPS, FS
93	San Gabriel, Cucamonga	CA	FS
94	San Rafael	CA	FS
95	Desolation, Mokelumne	CA	FS
96	Yosemite, Emigrant	CA	NPS, FS
97	Hoover	CA	FS
98	Sequoia, Kings Canyon	CA	NPS, FS
99	San Gorgonio, San Jacinto	CA	FS
100	Agua Tibia	CA	FS
101	Joshua Tree	CA	NPS
102	Denali	AK	NPS
103	Tuxedni	AK	FWS
104	Marble Mountain, Yolla Bolly Middle Eel	CA	FS
105	Simeonof	AK	FWS
106	Virgin Islands	VI	NPS
107	Hawaii Volcanoes	HI	NPS
108	Haleakala	HI	NPS
109	Dome Land	CA	FS, BLM
110	Kaiser, Ansel Adams, John Muir	CA	FS

1.3.1.3 Selecting New Sites

To monitor the 110 CIA clusters, 80 new sites needed to be selected and the Denali IMPROVE site needed to be reconsidered. Twenty-five of the 80 clusters where new sites were required had IMPROVE Protocol sites as candidates that would be considered along with other alternative locations. The Air Quality Group of the University of California at Davis (UCD), the particle monitoring and analysis contractor for the IMPROVE Network, was tasked with coordinating the effort to select new monitoring sites. The Steering Committee also sought active participation by the local land managers and the state air quality offices for each new site. The response of these groups varied widely from site to site. In some cases, the land managers and/or state air quality organization were very active in identifying candidate sites, including

extensive field siting trips. For some of the new sites, the UCD staff worked with the local land manager over the phone and via email to develop candidate locations.

UCD prepared a document that described the procedures to be used for site selection that was circulated to all states and land management organizations in early 1999 (IMPROVE Particulate Monitoring Network Procedures for Site Selection at www.epa.gov/ttn/amtic/visinfo.html). This document identified three qualities required of a new site: (1) the site must represent all CIAs in the cluster, (2) it should be regionally representative, avoiding local pollution sources or areas with unusual meteorology, and (3) it must avoid nearby obstacles that could affect sample collection. The document contains specific siting criteria, much of it taken from EPA siting guidelines, that indicate minimum allowed distances from sources and obstacles, sampler inlet exposure rules, and the need for reliable 120 volt AC power, security and field staffing requirements.

Specific locations for nearly all sites were identified by the summer of 1999, and the last location was selected (for Breton Wilderness) by the end of October 1999. Various types of permits and/or leases were required to secure many of the sites. The processing time for these varied widely from site to site. As soon as possible site preparations were begun. These usually included construction of a shelter for the monitoring sites with AC power. In some cases, an existing shelter was used. The IMPROVE protocol for particle sampling required that the sampler operate at ambient temperatures. To accomplish this, samplers are housed in a ventilated shelter that provide shielding from direct sunlight. Shelter design varied to meet differing practical and aesthetic concerns for specific sites. Installation of the new version IMPROVE samplers (described below) at all 110 sites began in November and continued through the spring of 2000.

1.3.2 Protocol and Equipment Changes

At EPA's request, the IMPROVE Steering Committee agreed to a few protocol changes with respect to the particle monitoring in the network. These included changing the twice-weekly 24-hour duration sampling schedule to an every-third-day schedule that corresponds to the schedule of the national particulate network operated by state and local governments, addition of a 10% replicate sampling and analysis for $PM_{2.5}$ mass and composition to evaluate precision, and submission of all data to the AIRS database. In addition, the IMPROVE Steering Committee and the EPA Project Officer for the National $PM_{2.5}$ Speciation Monitoring Program have agreed to develop information to aid in determining the degree of comparability of data collected by the two programs.

The change to an every-third-day sampling schedule proved to be the most challenging of the agreed upon changes. The reason for this stems from one of the original IMPROVE design objectives, that field work would be made as simple, fast, and convenient as possible to enhance data recovery and in recognition of the fact that field operators were federal land management staff assigned this work as collateral duties. The original IMPROVE sampling schedule from midnight to midnight on Wednesday and Saturday combined with a sampler capable of two sampling periods of unattended operation controlled by a seven-day timer/controller meant that the operator could service the sampler any time on the same day every week (typically Tuesday).

This was both easy to remember and to fit into a busy schedule. Use of a seven-day timer to sample every third day would have required re-programming it each week, which was expected to produce unacceptable mistakes. A sampler with only a two-sampler period of unattended operation was also a problem since the service day would change each week and would include days the operator might normally be unavailable each week. To maintain the same day of the week service schedule, the sampler controller and number of unattended sampler periods needed to be changed.

A new version of the IMPROVE particle sampler was designed and produced at UCD. The objective was to build a sampler that would be comparable from a sample collection perspective but use state-of-the-art microprocessor technology to increase the control and provide feedback on operating status. The new version sampler was designed to be identical to the original IMPROVE sampler including the four modules to sample on various substrates (shown in Figure 1.2), the same materials and dimensions for each module from the sample inlet to the face of the filter and with the same flow controller and flow rates. Preliminary tests at UCD confirm the comparability of the original and new version samplers. Additional testing will be conducted at typical field sites during the first few years of sampling.

A microprocessor-based controller that can be programmed to sample any period of time on any schedule replaced the seven-day timer/controller. The microprocessor includes a memory card reader/writer that is being used to record flow-rate, sample temperature and other performance related information monitored continuously throughout the sample period. The original IMPROVE sampler flows were manually checked at the beginning and end of each sample period and the seasonal mean site temperature and pressure were used for flow calculations, so that for the infrequent cases where the final flow was outside of the allowed range or the temperature was seasonably abnormal, the sample volume could not be adequately determined. The microprocessor also permits programming changes to be distributed to the controller on data cards sent to the field locations by UCD.

The new version sampler has a four-filter manifold for each module in place of the original sampler two-filter manifolds. The manifold with the solenoids is directly above the filter cassettes and is raised or lowered as a unit to unload and load the filters. The four filter cassettes are held in a cartridge (shown in Figure 1.4) that is designed to only allow one orientation in the sampler. Fully prepared date- and site-labeled filter cartridges along with memory cards will be sent from the analysis laboratory to the field and returned in special mailing containers to prevent confusion concerning the order of sampling among the filters. If filter change service is performed on a sample day, the operator moves the cassette containing that day's filter to the open position in the newly loaded cartridge. The few minutes that it takes to perform this sample change is recorded by the microprocessor on the memory card so that the correct air volume is used to calculate concentrations.

The new version of the IMPROVE sampler makes it simple to add a fifth module at 10% of the monitoring sites to accommodate replicate sampling and analysis for mass and composition. This quality assurance module will be operated for each sample period and collect a replicate sample for any of the three $PM_{2.5}$ substrates (Teflon, nylon, or quartz) so that over time precision information can be developed for each type of data.

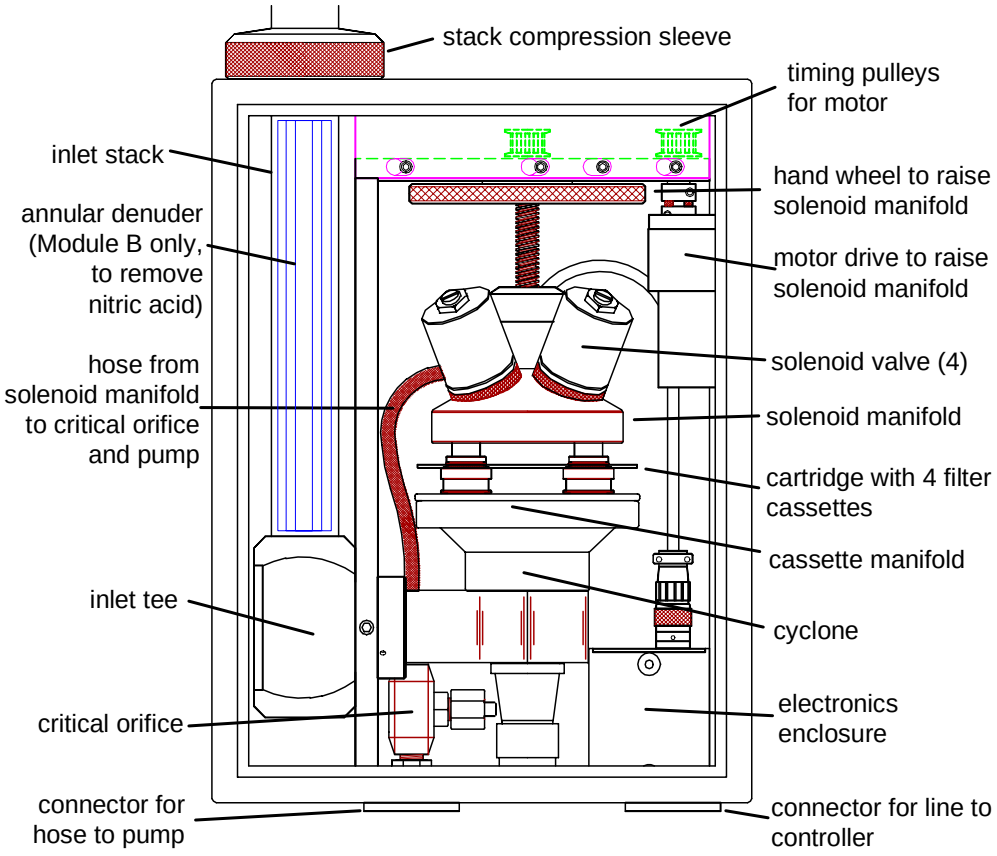

Figure 1.4 *Schematic of a new version of the IMPROVE sampler $PM_{2.5}$ module.*

The tentative approach agreed upon by EPA and IMPROVE to evaluate the comparability of the IMPROVE and the National $PM_{2.5}$ Speciation data sets involves having each network contribute samplers and analysis for up to three monitoring sites in the other's network for at least one year. In other words, IMPROVE samplers with IMPROVE mass and composition analysis would be operated by the speciation program at three of their typically urban sites, and speciation samplers with their analysis methods would by operated by IMPROVE at three of their remote sites. This permits long-term paired-data comparisons at six sites representing a range of concentrations and compositions likely to be experienced in either program.

1.4 CURRENT REPORT OBJECTIVES

This report is the third in a series of periodic reports that describe the data collected by the IMPROVE monitoring network. Following are the objectives of this report:

(1) to describe the spatial variation of aerosol species contributing to visibility impairment over the time frame from March 1996 through February 1999;

(2) to provide a first estimate of the apportionment of visibility impairment to these chemical species;

(3) to document long-term trends (11 years) of aerosol mass, its principal aerosol species, and visibility as expressed in terms of deciview;

(4) to examine how the contribution of various aerosol species changes at the extremes of fine mass distributions;

(5) to examine the inter-comparability of data collected in the IMPROVE Network and the Clean Air Status and Trends Network;

(6) to report on a number of special studies that were designed to examine the robustness of algorithms used to make extinction estimates from aerosol mass concentrations. The hygroscopicity of aerosol species is examined.

1.5 REFERENCES

16 USC section 1131, 1997.

45 FR 80084 and section 51.300-307, December 2, 1980.

62 FR 38652, July 18, 1997.

64 FR 35714, July 1, 1999.

Chow, J.C., Watson, J.G., Pritchett, L.C., Pierson, W.R., Frazier, C.A., and Purcell, R.G., The DRI thermal/optical reflectance carbon analysis system: description, evaluation, and applications in U.S. air quality studies, *Atmos. Environ.*, **27**(A), (8), 1185-1201, 1993.

Joseph, D. B., Metsa, J., Malm, W.C. and Pitchford, M. L. Plans for IMPROVE: a federal program to monitor visibility in class I areas, In: *Visibility Protection: Research and Policy Aspects*, P.S. Bhardwaja (Ed.), APCA, Pittsburgh, PA, 1987.

Malm, W.C., Sisler, J.F., Huffman, D., Eldred, R.A., and Cahill, T.A., Spatial and seasonal trends in particle concentration and optical extinction in the United States, *J. Geo. Res.*, **99**(D1), 1347-1370, 1994.

Malm, W.C., Gebhart, K.A., Latimer, D.A., Cahill, T.A., Eldred, R.A., Pielke, R., Stocker, R., and Watson, J. *National Park Service Report on the Winter Haze Intensive Tracer Experiment*, Final Report, 1989.

Public Law 88-577, 1964.

Sisler, J. F., *Spatial and Seasonal Patterns and Long Term Variability of the Composition of the Haze in the United States: An Analysis of Data from the IMPROVE Network*, Cooperative Institute for Research in the Atmosphere, Colorado State University, ISSN 0737-5352-32, 1996.

Sisler, J. F., Huffman, D., Latimer, D. A., Malm, W. C. and Pitchford, M. L., *Spatial and Temporal Patterns and the Chemical Composition of the Haze in the United States: An Analysis of Data from the IMPROVE Network 1988-1991*, Cooperative Institute for Research in the Atmosphere, Colorado State University, ISSN 0737-5352-26, 1993.

CHAPTER 2

AEROSOL MASS BUDGETS AND SPATIAL DISTRIBUTIONS

A detailed discussion and associated assumptions of how aerosol species mass is derived from IMPROVE aerosol measurements have been presented in Malm et al. [1994], Sisler et al. [1993], Sisler [1996] and only a summary will be presented here.

2.1 DETERMINATION OF AEROSOL SPECIES MASS

Most fine sulfates are the result of oxidation of sulfur dioxide (SO_2) gas to sulfate particles. In humid atmospheres, the oxidation typically occurs in clouds where sulfuric acid is formed within water droplets. If there is inadequate ammonia in the atmosphere to fully neutralize the sulfuric acid, as is sometimes the case, then the resulting aerosols are acidic. Under these circumstances solutions of continuously varying acidity are formed. The extremes of this continuum are ammonium sulfate (neutral) and sulfuric acid. The mass associated with the dry ammoniated sulfate ion can be estimated from independent measurements of sulfate (SO_4) and ammonium (NH_4) ions using:

$$[SULFATE] = (0.944)[NH_4^+] + (1.02)[SO_4^{2-}] \tag{2.1}$$

where [SULFATE] is the mass of the ammoniated sulfate ion. If only the sulfate ion is measured, as is the case in nearly every IMPROVE site, then one must assume a form of sulfate and multiply by an appropriate multiplication factor: 1.37*SO_4 or 4.125*S, if ammonium sulfate is assumed.

An average ambient particulate organic compound is assumed to have a constant fraction of carbon by weight. Organic carbon mass concentration from module C (OMC) is simply:

$$[OMC] = (1.4)[OC] \tag{2.2}$$

The factor of 1.4 was selected to adjust the organic carbon mass [OC] for other elements assumed to be associated with the organic carbon molecule [Watson et al., 1988].

Organic mass can also be estimated from the concentrations of H and S measured on the module A Teflon filter if certain assumptions are made [Malm et al., 1994]. It is assumed that during exposure to the vacuum of module A particle induced x-ray emission (PIXE) and proton elastic scattering (PESA) analyses all nitrates and water volatilize and do not contribute to the mass of H. It is further assumed that the remaining hydrogen can be apportioned between sulfates and organic

carbon. Assuming full neutralization of the sulfate ion, organic carbon by hydrogen (OCH) is calculated using:

$$OCH = 11(H - 0.25S) \tag{2.3}$$

The sulfur factor, H/S ratio, for ammonium sulfate is 8/32 or 0.25. The C/H ratio is 11 and operationally defined by forcing OCH to equal OC. Comparison of OCH to OC is used in data validation procedures and OCH is used to estimate organic mass when carbon is not explicitly measured.

Assuming that the collected nitrate ion is associated with fully neutralized nitrate aerosol, [NH_4NO_3], the ammonium nitrate mass, [NITRATE], is estimated from the nitrate ion mass concentration by using a multiplication factor of 1.29.

Soil mass concentration, [SOIL], is estimated by summing the elements predominantly associated with soil, plus oxygen for the common compounds (Al_2O_3, SiO_2, CaO, K_2O, FeO, Fe_2O_3, TiO_2), plus a correction for other compounds such as MgO, Na_2O, water, and carbonate [Malm et al., 1994].

The sum of the above four composites plus elemental carbon, referred to in this report as light-absorbing carbon (LAC), provides a reasonable estimate of the ambient fine mass concentration. The equation for this reconstruction of fine mass (RCFM) is then:

$$[RCFM] = [SULFATE] + [NITRATE] + [LAC] + [OMC] + [SOIL] . \tag{2.4}$$

Coarse mass (CM) is estimated gravimetrically by subtracting gravimetric fine mass ($PM_{2.5}$) concentration from total gravimetric mass (PM_{10}) concentration:

$$[CM] = [PM_{10}] - [PM_{2.5}] . \tag{2.5}$$

In the IMPROVE program, additional chemical analysis is not carried out on the coarse fraction. It is assumed that in rural or remote areas of the country the primary constituent of coarse mass is naturally occurring wind-blown dust along with some vegetative material [Noll et al., 1985; Noll, 1991].

The self-consistency and overall quality of the aerosol measurements are assured by redundancy and intercomparisons between independently measured species. A detailed description of validation and quality assurance procedures is available in Malm et al. [1994], Sisler et al. [1993], and Eldred et al. [1988]. In the most general sense, validation is a matter of comparing chemically related species that have been measured in different modules. Fortunately, the design of the IMPROVE sampler allows for redundancy between certain module A measurements and modules B and C measurements of the ions and carbons enabling quality control checks. For example, elemental sulfur mass times three should agree with the sulfate ion measured in module B. However, when comparing measured fine mass to RCFM, two complicating factors must be dealt with. First, under some conditions, a large portion of the nitrates (≥50%) can volatilize from the module A Teflon

filter; and second, the amount of residual water on the filter is a function of the relative humidity that the filter is weighed at because of water retention by soluble aerosol species.

2.2 ENSEMBLE AVERAGES

When reconstructed mass and/or extinction are presented as averages for some time period, the data must be aggregated into subsets of the larger database, then averages and related statistics are calculated for each of the subsets. There are a number of ways to aggregate the data and the strategy applied to any given aggregation is determined, at least in part, by the question being entertained. In this report, annual and seasonal aggregations of three years of data are presented. For instance, for summer averages data is aggregated over the months of June, July and August for the three years under consideration. This results in between 75 to 80 data points assuming up to nine samples per month. Other aggregations presented in this report require sorting the data into subgroups representing the days with the 20% lowest fine mass loadings, median 20%, and 20% highest fine mass loadings using measured fine mass as the sort variable. Sorting the three-year data set into three quintile yield data sets that contain fewer data points. Doing this on an annual basis yields even fewer data points, typically 18–20 observations.

Whatever criteria is used for sorting the data into subsets, at least two approaches reflecting different ways of handling missing values can be used for calculating summary statistics. The two approaches can yield significantly different results, particularly when the subsets of data are small. To understand this, consider the following extreme case; the sampling periods that correspond to the 20% highest fine mass concentrations for one season in one year of data yielding an ensemble of five data points (Table 2.1). In this example, there are two missing observations for nitrate, and one missing observation for the carbon data yielding only two observational periods without any missing values. The issue is, when reconstructing a variable such as reconstructed fine mass (RCFM): are only sampling periods with all variables present used in the reconstruction or are averages of each species calculated and then reconstructions carried out on the basis of these averages? By going with the former, (removing three observations) the RCFM is 10.75 $\mu g/m^3$ with a 14% contribution from OC. By using the second method, a RCFM value of 11.6 $\mu g/m^3$ is calculated with a 21% contribution from OC.

When removing the three observations with missing data either method yields identical results. By removing the observation with the high OC value, because nitrate is missing, skews the contribution of OC to the average RCFM for this ensemble as evidenced by the fact the measured fine mass is also highest for this observation. Other examples could be created and the question of the "best" way to do the ensemble averaging is currently under investigation and will be the subject of a forthcoming report and peer-reviewed journal articles.

In this report, the latter method is used to summarize average reconstructed mass and extinction as well as species concentrations/extinction. Specifically, by using measured fine mass as opposed to reconstructed fine mass as the sort variable larger, ensembles of data points are obtained. Then the average concentration for each species is calculated and the averages are then summed to estimate RCFM/extinction and the associated "budgets."

Table 2.1 *Five hypothetical observations that correspond to the 20% highest fine mass concentrations for one season as sorted by gravimetric fine mass (FM). Concentrations are given in $\mu g/m^3$.*

Observations	FM	Sulfate	Nitrate	Organics	Light-Absorbing Carbon (LAC)	Soil	RCFM
1	10	6	1	1	1	2	11
2	13	4	---	6	0.8	1	---
3	10	7	1.1	---	---	1	---
4	10	5	0.8	2	0.7	2	10.5
5	12	8	---	1	0.5	1	---
AVERAGE	11	6	0.96	2.5	0.75	1.4	10.75(11.61)

2.3 SPATIAL TRENDS IN AEROSOL CONCENTRATIONS

This section discusses the observed spatial variations in aerosol concentration and chemical composition throughout the United States on the basis of the IMPROVE measurements for the three-year period March 1996 through February 1999.

Aerosol concentrations and chemical composition vary because of a number of factors, including the spatial distribution of natural and anthropogenic emission sources and meteorological conditions. The highest aerosol concentrations tend to occur in significant urban or industrialized areas where emission densities are high. In addition, concentrations are highest when atmospheric dilution is minimal such as what occurs in stagnation periods or periods of limited mixing. Because sulfate and nitrate aerosols are formed from SO_2 and NO_x emissions and chemical reactions in the atmosphere, these aerosols are highest when photochemistry is strongest.

For example, concentrations of sulfates tend to be highest in areas of significant sulfur dioxide (SO_2) emissions such as the eastern United States where SO_2 is emitted from coal-fired stationary sources. Organic carbon concentrations tend to be highest in regions such as the Rocky Mountains and Pacific Northwest due in part to forest management practices and forest-product industries. Nitrates tend to be most prevalent in California where both NO_x emissions from motor vehicles and industry are high.

Spatial and temporal variations in aerosol composition and concentrations can be qualitatively examined through the use of annual and seasonal mass budgets. Mass budgets are the contribution of individual aerosol species to the reconstructed fine particle mass.

Average concentrations and chemical composition are calculated on the basis of measurements for each region. The heading of fine mass in the following discussion and tables is fine mass estimated from the summation of the individual aerosol species as described by Equation (2.4). The reconstructions are based on the summation of average concentrations for the time period reported as opposed to reconstructing the fine mass and then averaging. Data recovery is typically high

[Eldred et al., 1997] so a criteria for the number of data points required for a given average was not established. However, the validity of this assumption is currently being investigated and will be the topic for a future report and peer-reviewed publications.

Tables 2.2 and 2.3 show the reconstructed fine mass concentrations (RCFM) and coarse aerosol (CM) and the chemical composition (mass budgets) of the fine aerosol for each of the 21 regions in the United States, respectively. These concentrations and mass budgets are averaged over the entire three-year period to provide the annual average and over the three years for each of the four seasonal averages.

The characteristics of each of the regions (in alphabetic order) are discussed, followed by the spatial and temporal trends of the fine and coarse mass concentrations and the constituents of the fine-particle mass.

2.4 CHARACTERISTICS OF THE REGIONS

Alaska. The Alaska region has only one monitoring site, Denali National Park and Preserve, and it began operation in March 1988. The average concentrations of fine and coarse aerosols over the three-year period were 1.4 and 3.0 $\mu g/m^3$, respectively. The fine aerosol concentration was the lowest measured anywhere in the United States during this period. Both fine and coarse aerosol concentrations were largest in summer and smallest in winter. Organics were the largest contributor of fine particle mass (46.5%), followed by sulfate (31.4%), soil (11.7%), light-absorbing carbon (6.7%), and nitrate (3.6%). The concentrations of organics were largest in summer, perhaps due to the prescribed burning and forest fires that usually occurred during that season. The concentrations of light-absorbing carbon were largest in autumn.

Appalachian Mountains. This region has four sites reported here: Great Smoky Mountains and Shenandoah National Parks, both initiated in March 1988, Dolly Sods Wilderness Area in West Virginia, initiated in September 1991, and Shining Rock in North Carolina, which began monitoring in September 1994.

The average concentrations of fine and coarse aerosols for this region were 9.8 $\mu g/m^3$ and 4.5 $\mu g/m^3$, respectively. Both fine and coarse aerosol concentrations were maximum in summer and minimum in winter. Sulfate was by far the largest component of the fine particle mass. At 64%, sulfate was more than twice that of the next largest contributor, organics (23.8%). Other contributors included nitrate and light-absorbing carbon (both at 3.8%), and soil (4.6%). Except for nitrate and light-absorbing carbon, which had their maximum concentrations in winter and autumn, respectively, all other species had maximum concentrations in summer. The seasonal variation in sulfate concentrations is particularly strong with summer concentrations more than three times the winter concentrations.

Boundary Waters. This region in northern Minnesota is monitored at Boundary Waters Canoe Area in the Superior National Forest, which began monitoring in August 1991. Previously, this region was represented by two sites, Isle Royale National Park, which was discontinued in July 1991, and Voyageurs National Park, which has been downgraded to module A only.

Table 2.2 *Measured fine and coarse aerosol concentrations (in $\mu g/m^3$) for the 21 regions in the IMPROVE Network. Fine mass is reconstructed from the sum of individual species.*

Season	Reconstructed Fine Mass	Sulfate	Nitrate	Organics	Light-Absorbing Carbon	Soil	Coarse Mass
Alaska							
ANNUAL	1.4	0.45	0.05	0.67	0.10	0.17	3.0
Spring	1.6	0.70	0.06	0.46	0.09	0.28	3.2
Summer	2.1	0.44	0.03	1.37	0.10	0.15	3.2
Autumn	1.1	0.30	0.04	0.48	0.11	0.15	3.2
Winter	1.0	0.38	0.08	0.31	0.09	0.10	2.4
Appalachian							
ANNUAL	9.8	6.28	0.37	2.34	0.37	0.45	4.5
Spring	8.8	5.18	0.56	2.12	0.36	0.54	5.1
Summer	15.5	11.1	0.22	3.14	0.38	0.61	5.1
Autumn	9.2	5.66	0.35	2.33	0.41	0.42	4.0
Winter	5.6	2.98	0.34	1.71	0.33	0.20	3.5
Boundary Waters							
ANNUAL	4.5	1.89	0.57	1.47	0.19	0.34	3.6
Spring	4.0	1.90	0.50	1.05	0.14	0.40	3.3
Summer	5.8	2.17	0.12	2.83	0.23	0.41	4.1
Autumn	4.0	1.48	0.45	1.52	0.22	0.33	4.4
Winter	4.6	2.06	1.18	1.00	0.18	0.22	2.7
Cascade Mountains							
ANNUAL	3.4	1.01	0.21	1.66	0.27	0.28	3.2
Spring	3.0	1.04	0.20	1.16	0.20	0.36	2.6
Summer	5.3	1.83	0.29	2.42	0.36	0.38	4.5
Autumn	3.7	0.79	0.18	2.13	0.33	0.28	3.2
Winter	1.6	0.33	0.16	0.85	0.16	0.08	2.5
Central Rocky Mountains							
ANNUAL	2.6	0.81	0.16	0.96	0.13	0.54	3.4
Spring	3.0	0.87	0.22	0.86	0.12	0.90	3.7
Summer	3.4	1.01	0.14	1.44	0.15	0.62	4.0
Autumn	2.5	0.83	0.12	0.97	0.14	0.42	3.3
Winter	1.4	0.50	0.13	0.49	0.09	0.19	2.5
Colorado Plateau							
ANNUAL	3.0	1.03	0.20	0.94	0.17	0.64	4.3
Spring	3.3	0.89	0.24	0.98	0.16	1.06	5.3
Summer	3.8	1.44	0.19	1.23	0.18	0.79	4.8
Autumn	2.8	1.14	0.14	0.91	0.18	0.46	3.7
Winter	1.8	0.64	0.21	0.62	0.14	0.21	3.2
Great Basin							
ANNUAL	2.6	0.59	0.13	1.05	0.14	0.69	4.5
Spring	2.5	0.64	0.16	0.84	0.12	0.75	3.5
Summer	3.8	0.78	0.15	1.59	0.16	1.16	6.7
Autumn	2.4	0.63	0.12	0.94	0.13	0.58	4.0
Winter	1.2	0.26	0.10	0.61	0.12	0.12	2.7
Mid Atlantic							
ANNUAL	9.9	5.75	0.80	2.39	0.51	0.44	13.1
Spring	9.0	5.47	0.90	1.77	0.42	0.45	19.3
Summer	12.9	8.40	0.47	3.03	0.47	0.57	13.3
Autumn	9.0	4.92	0.69	2.38	0.59	0.44	8.2
Winter	8.8	4.36	1.08	2.47	0.58	0.30	10.6

***Table 2.2** Continued.*

Season	Reconstructed Fine Mass	Sulfate	Nitrate	Organics	Light-Absorbing Carbon	Soil	Coarse Mass
Mid South							
ANNUAL	11.4	6.60	0.76	2.86	0.48	0.72	5.2
Spring	10.2	5.55	0.91	2.68	0.44	0.63	5.7
Summer	15.4	9.80	0.34	3.52	0.46	1.33	6.6
Autumn	11.5	6.64	0.60	3.10	0.57	0.57	4.9
Winter	8.1	4.09	1.21	2.07	0.43	0.32	3.4
Northeast							
ANNUAL	5.3	2.96	0.32	1.56	0.25	0.25	3.7
Spring	4.5	2.55	0.33	1.14	0.21	0.30	4.0
Summer	7.8	4.70	0.21	2.37	0.28	0.28	3.6
Autumn	4.5	2.29	0.28	1.41	0.25	0.24	3.8
Winter	4.4	2.20	0.47	1.31	0.26	0.17	3.4
Northern Great Plains							
ANNUAL	4.0	1.71	0.52	1.13	0.14	0.45	5.5
Spring	4.3	1.96	0.73	0.91	0.13	0.53	5.7
Summer	4.4	1.91	0.14	1.71	0.15	0.52	6.1
Autumn	4.0	1.59	0.44	1.23	0.16	0.53	5.6
Winter	3.2	1.37	0.77	0.67	0.12	0.23	4.4
Northern Rocky Mountains							
ANNUAL	4.6	0.93	0.23	2.52	0.36	0.57	6.2
Spring	4.6	1.19	0.23	2.25	0.31	0.64	4.4
Summer	4.9	0.91	0.14	2.66	0.30	0.93	10.8
Autumn	5.5	0.84	0.20	3.48	0.51	0.52	6.1
Winter	3.3	0.78	0.35	1.70	0.31	0.18	3.3
Pacific Coastal Mountains							
ANNUAL	3.7	1.24	0.64	1.33	0.19	0.27	6.6
Spring	3.5	1.22	0.60	1.17	0.17	0.36	6.7
Summer	4.0	1.99	0.59	1.07	0.12	0.27	7.1
Autumn	4.0	1.11	0.55	1.77	0.26	0.32	7.4
Winter	3.0	0.64	0.82	1.24	0.20	0.11	5.4
Sierra-Humboldt							
ANNUAL	2.4	0.50	0.13	1.24	0.18	0.37	3.1
Spring	2.3	0.54	0.16	0.89	0.14	0.55	3.0
Summer	3.7	0.80	0.16	1.94	0.25	0.51	3.9
Autumn	2.6	0.46	0.12	1.52	0.21	0.31	2.6
Winter	0.9	0.17	0.07	0.47	0.11	0.08	2.6
Sierra Nevada							
ANNUAL	6.6	1.29	0.94	2.78	0.38	1.20	7.0
Spring	5.9	1.22	0.86	2.11	0.33	1.40	6.4
Summer	9.7	2.30	0.63	4.09	0.49	2.15	9.5
Autumn	7.2	1.18	0.93	3.56	0.47	1.09	8.6
Winter	3.7	0.50	1.27	1.48	0.23	0.22	3.6
Sonoran Desert							
ANNUAL	3.9	1.53	0.25	1.10	0.18	0.85	6.5
Spring	4.2	1.25	0.31	1.14	0.15	1.36	8.1
Summer	4.7	2.18	0.23	1.11	0.16	0.97	7.5
Autumn	4.1	1.77	0.19	1.25	0.22	0.62	5.9
Winter	2.6	0.90	0.27	0.88	0.18	0.41	4.1

Table 2.2 *Continued.*

Season	Reconstructed Fine Mass	Sulfate	Nitrate	Organics	Light-Absorbing Carbon	Soil	Coarse Mass
Southeast							
ANNUAL	9.8	5.22	0.40	2.86	0.51	0.81	9.5
Spring	9.9	5.61	0.49	2.73	0.50	0.60	10.4
Summer	11.3	6.12	0.32	2.71	0.35	1.86	10.8
Autumn	9.6	5.35	0.32	2.81	0.53	0.56	8.7
Winter	8.4	3.83	0.47	3.17	0.63	0.26	8.2
Southern California							
ANNUAL	7.2	1.47	2.49	2.04	0.37	0.83	6.5
Spring	9.0	1.53	3.72	2.25	0.40	1.06	6.8
Summer	9.6	2.45	2.60	3.03	0.50	1.06	8.8
Autumn	5.6	1.23	1.69	1.58	0.31	0.80	6.4
Winter	3.5	0.44	1.54	0.99	0.22	0.30	3.1
Wasatch							
ANNUAL	4.5	1.05	0.59	1.56	0.33	0.92	5.1
Spring	4.2	1.04	0.50	1.30	0.28	1.05	4.5
Summer	5.8	1.24	0.30	2.53	0.42	1.33	6.8
Autumn	3.9	1.06	0.36	1.35	0.33	0.76	4.7
Winter	3.9	0.86	1.26	1.01	0.28	0.47	4.4
Washington, D.C.							
ANNUAL	14.5	7.22	1.57	3.84	1.15	0.74	4.9
Spring	13.2	6.83	1.69	2.94	1.01	0.71	5.1
Summer	17.8	11.1	0.76	4.09	1.07	0.80	4.4
Autumn	13.9	6.12	1.64	3.99	1.29	0.85	5.9
Winter	13.1	4.68	2.25	4.36	1.26	0.59	4.4
West Texas							
ANNUAL	5.5	2.40	0.25	1.23	0.17	1.43	7.2
Spring	6.8	2.23	0.31	1.70	0.19	2.34	10.1
Summer	6.8	3.02	0.29	1.25	0.13	2.10	7.1
Autumn	5.0	2.91	0.15	1.12	0.18	0.60	5.3
Winter	3.3	1.53	0.23	0.79	0.16	0.61	5.9

Table 2.3 *Measured fine aerosol mass budgets (in %) for the 21 regions in the IMPROVE Network.*

Season	Sulfate	Nitrate	Organics	Light-Absorbing Carbon	Soil
Alaska					
ANNUAL	31.4	3.6	46.5	6.7	11.7
Spring	44.2	3.6	28.9	5.8	17.5
Summer	20.9	1.6	65.4	4.8	7.3
Autumn	27.9	3.3	44.7	9.9	14.2
Winter	39.6	8.7	32.3	9.2	10.2
Appalachian					
ANNUAL	64.0	3.8	23.8	3.8	4.6
Spring	59.1	6.3	24.2	4.1	6.2
Summer	71.9	1.4	20.2	2.5	4.0
Autumn	61.7	3.8	25.4	4.5	4.6
Winter	53.6	6.1	30.8	5.9	3.6

Table 2.3 *Continued.*

Season	Sulfate	Nitrate	Organics	Light-Absorbing Carbon	Soil
Boundary Waters					
ANNUAL	42.4	12.8	33.0	4.2	7.7
Spring	47.5	12.5	26.3	3.6	10.0
Summer	37.7	2.2	49.1	3.9	7.1
Autumn	37.0	11.2	38.1	5.4	8.2
Winter	44.4	25.4	21.5	3.8	4.8
Cascade Mountains					
ANNUAL	29.5	6.1	48.6	7.7	8.0
Spring	35.1	6.8	39.2	6.8	12.1
Summer	34.8	5.5	45.8	6.7	7.2
Autumn	21.3	4.8	57.4	8.9	7.6
Winter	21.1	10.1	53.8	10.2	4.8
Central Rocky Mountains					
ANNUAL	31.1	6.0	37.1	4.9	20.9
Spring	29.2	7.5	28.9	4.0	30.3
Summer	30.0	4.2	43.0	4.4	18.4
Autumn	33.5	5.0	39.0	5.7	16.9
Winter	35.7	9.3	35.2	6.4	13.4
Colorado Plateau					
ANNUAL	34.6	6.6	31.7	5.6	21.6
Spring	26.7	7.1	29.5	4.8	31.9
Summer	37.6	4.9	32.2	4.8	20.6
Autumn	40.3	5.0	32.2	6.2	16.4
Winter	35.1	11.7	34.1	7.8	11.3
Great Basin					
ANNUAL	22.6	5.1	40.4	5.3	26.6
Spring	25.6	6.4	33.6	4.7	29.8
Summer	20.3	3.9	41.5	4.1	30.1
Autumn	26.4	5.0	39.1	5.5	24.0
Winter	21.4	8.3	50.2	10.1	10.1
Mid Atlantic					
ANNUAL	58.1	8.1	24.2	5.2	4.4
Spring	60.6	10.0	19.6	4.7	5.0
Summer	65.0	3.6	23.4	3.6	4.4
Autumn	54.6	7.7	26.3	6.5	4.9
Winter	49.6	12.3	28.1	6.6	3.4
Mid South					
ANNUAL	57.8	6.6	25.0	4.2	6.3
Spring	54.4	8.9	26.3	4.4	6.2
Summer	63.5	2.2	22.8	3.0	8.6
Autumn	57.8	5.3	27.0	4.9	5.0
Winter	50.3	15.0	25.5	5.3	3.9
Northeast					
ANNUAL	55.4	6.0	29.2	4.7	4.7
Spring	56.3	7.3	25.1	4.6	6.7
Summer	60.0	2.7	30.2	3.6	3.6
Autumn	51.3	6.3	31.4	5.7	5.3
Winter	50.0	10.6	29.7	5.9	3.9

***Table 2.3** Continued.*

Season	Sulfate	Nitrate	Organics	Light-Absorbing Carbon	Soil
Northern Great Plains					
ANNUAL	43.2	13.2	28.6	3.6	11.4
Spring	46.0	17.3	21.3	3.0	12.4
Summer	43.1	3.2	38.5	3.5	11.7
Autumn	40.2	11.2	31.1	4.1	13.3
Winter	43.3	24.4	21.2	3.8	7.4
Northern Rocky Mountains					
ANNUAL	20.1	5.0	54.7	7.8	12.3
Spring	25.8	5.1	48.5	6.8	13.9
Summer	18.4	2.8	53.8	6.1	18.8
Autumn	15.1	3.5	62.8	9.3	9.3
Winter	23.4	10.7	51.2	9.4	5.3
Pacific Coastal Mountains					
ANNUAL	34.0	17.5	36.2	5.1	7.3
Spring	34.6	17.1	33.3	4.7	10.3
Summer	49.4	14.6	26.5	2.9	6.6
Autumn	27.8	13.6	44.2	6.4	7.9
Winter	21.4	27.2	41.0	6.6	3.8
Sierra-Humboldt					
ANNUAL	20.7	5.3	51.2	7.5	15.3
Spring	23.6	6.9	39.3	6.2	24.1
Summer	21.7	4.5	53.0	6.8	14.0
Autumn	17.3	4.6	58.1	8.1	11.8
Winter	18.7	7.5	52.5	12.6	8.7
Sierra Nevada					
ANNUAL	19.6	14.3	42.1	5.7	18.2
Spring	20.7	14.5	35.6	5.5	23.7
Summer	23.8	6.5	42.3	5.0	22.3
Autumn	16.3	12.8	49.3	6.5	15.1
Winter	13.6	34.4	39.8	6.3	6.0
Sonoran Desert					
ANNUAL	39.2	6.4	28.1	4.5	21.8
Spring	29.6	7.3	27.1	3.7	32.3
Summer	46.9	4.9	24.0	3.4	20.9
Autumn	43.7	4.7	30.9	5.3	15.4
Winter	34.1	10.1	33.4	7.0	15.4
Southeast					
ANNUAL	53.3	4.1	29.2	5.2	8.3
Spring	56.5	4.9	27.5	5.1	6.1
Summer	53.9	2.8	23.8	3.1	16.4
Autumn	55.9	3.3	29.3	5.5	5.9
Winter	45.8	5.6	38.0	7.6	3.1
Southern California					
ANNUAL	20.4	34.7	28.3	5.1	11.5
Spring	17.1	41.6	25.1	4.5	11.8
Summer	25.4	26.9	31.4	5.2	11.0
Autumn	21.9	30.2	28.1	5.5	14.2
Winter	12.6	44.2	28.3	6.3	8.6

Table 2.3 *Continued.*

Season	Sulfate	Nitrate	Organics	Light-Absorbing Carbon	Soil
Wasatch					
ANNUAL	23.6	13.3	35.1	7.3	20.6
Spring	24.9	12.1	31.3	6.7	25.1
Summer	21.3	5.2	43.5	7.2	22.9
Autumn	27.4	9.2	35.0	8.6	19.8
Winter	22.1	32.6	26.0	7.1	12.1
Washington, D.C.					
ANNUAL	49.7	10.8	26.4	7.9	5.1
Spring	51.8	12.9	22.3	7.6	5.4
Summer	62.3	4.2	23.0	6.0	4.5
Autumn	44.1	11.8	28.7	9.3	6.1
Winter	35.6	17.1	33.2	9.6	4.5
West Texas					
ANNUAL	43.9	4.6	22.4	3.0	26.1
Spring	32.9	4.6	25.1	2.8	34.5
Summer	44.4	4.3	18.4	1.9	30.9
Autumn	58.7	3.0	22.6	3.7	12.0
Winter	46.0	6.9	23.7	4.9	18.5

The average fine and coarse aerosol concentrations were 4.5 and 3.6 $\mu g/m^3$, respectively. The highest concentrations occurred during summer for fine aerosols and in the autumn for coarse aerosols, but there was not as strong a seasonal variation as in Alaska and the Appalachian Mountains. In this region, sulfate was the largest fraction of fine particle mass (42.4%), followed by organics (33%), and more distantly by nitrate (12.8%), soil (7.7%), and light-absorbing carbon (4.2%).

Cascade Mountains. This region in the states of Washington and Oregon has three monitoring sites reported here. Mount Rainier National Park southeast of Seattle was initiated in March 1988, Three Sisters Wilderness Area on the Willamette National Forest, and Snoqualmie Pass on the Snoqualmie National Forest were implemented in July 1993 and became fully operational September 1994.

Here the average fine and coarse aerosol concentrations were 3.4 and 3.2 $\mu g/m^3$, respectively. Fine and coarse aerosol concentrations reached their maxima in summer and minima in winter. Sulfate and nitrate concentrations had strong seasonal variations, with maxima in summer and minima in winter. This seasonal variation could be, in part, the result of seasonal variations in mixing and in photochemistry. In this region, organics were the single most significant contributor (48.6%) to fine particle mass. Sulfate (29.5%) contributed much less than organics. Nitrate contributed 6.1%, followed by soil (8%) then light-absorbing carbon (7.7%).

Central Rocky Mountains. The measurements in this region were made at five locations in the mountainous Class I areas of Colorado and Wyoming, including the Bridger and Weminuche Wilderness Areas, Rocky Mountain and Yellowstone National Parks, and Great Sand Dunes National Monument. Fine and coarse aerosol concentrations in this region averaged 2.6 and 3.4 $\mu g/m^3$, respectively. Like many of the other regions, concentrations, especially of sulfate,

organics, light-absorbing carbon, and coarse aerosol, were highest in summer and lowest in winter. The largest contributor to fine particle mass in this region was organics (37.1%), followed by sulfate (31.1%), soil (20.9%), nitrate (6.0%), and light-absorbing carbon (4.9%).

Colorado Plateau. This region in the "Four Corners'" states of the Southwest is the most intensively monitored in the IMPROVE Network. There are six sites, most of them within the so-called Golden Circle of National Parks: Bandelier, Bryce Canyon, Canyonlands, Grand Canyon, Mesa Verde, and Petrified Forest. A seventh site, Arches National Park, was discontinued in May 1992. In this region, fine and coarse aerosol concentrations averaged 3.0 and 4.3 $\mu g/m^3$, respectively. Fine and coarse aerosol concentrations were greatest in summer and spring, respectively, and least in winter. Concentrations of sulfate, organics, and light-absorbing carbon were also greatest in summer and smallest in winter. However, nitrate was highest in the spring and lowest in the autumn. Sulfate (34.6%) and organics (31.7%) contributed the most followed by soil (21.6%), nitrate (6.6%), and light-absorbing carbon (5.6%).

Great Basin. The Great Basin of Nevada has two sets of measurements at Jarbidge Wilderness Area in northeastern Nevada and Great Basin National Park, which began monitoring in March 1988 and May 1992, respectively. The fine and coarse aerosol concentrations averaged 2.6 and 4.5 $\mu g/m^3$, respectively. The fine mass concentration was the lowest of any of the regions in the contiguous 48 states. Perhaps this was due to the fact that this site was relatively remote from high emission density areas and was generally well ventilated. Both fine and coarse aerosol concentrations, as well as all of the fine aerosol components, experienced largest concentrations in the summer (except nitrate) and lowest concentrations in the winter (both winter and spring for light-absorbing carbon). The largest single contributors to fine particle mass at this region were organics (40.4%) and soil (26.6%). Sulfate was a smaller contributor (22.6%), followed by light-absorbing carbon (5.3%) and nitrate (5.1%).

Mid Atlantic. This region is represented by the Edwin B. Forsythe National Wildlife Refuge west of Atlantic City, New Jersey and began monitoring in September 1991. Fine and coarse aerosol concentrations averaged 9.9 and 13.1 $\mu g/m^3$, respectively. A moderate seasonality was evident with the highest fine and coarse aerosol concentrations occurring in the summer and spring, and the least in the winter and autumn, respectively. Sulfate, organics, and fine soil follow the same seasonal trend as for fine aerosol mass. Nitrates peaked in the winter at about two times its summer concentration, and light-absorbing carbon peaked in the winter as well but only showed a small seasonality. Sulfate comprises the bulk of the fine aerosol mass (58.1%) followed by organics (24.2%), nitrate (8.1%), light-absorbing carbon (5.2%), and soil (4.4%).

Mid South. Three sites are monitored for this region: Upper Buffalo Wilderness Area in north central Arkansas initiated in December 1991, Mammoth Cave National Park in Kentucky initiated in September 1991, and Sipsey Wilderness Area in northern Alabama initiated in March 1992. The average concentration of fine and coarse aerosols was 11.4 and 5.2 $\mu g/m^3$, respectively. Outside of Washington, D.C., which is an urban site, this region had the highest average concentration of fine aerosol. A modest seasonality was evident for fine and coarse aerosols with the minima occurring in the winter and the maxima in the summer. All fine aerosol constituents except nitrate and light-absorbing carbon follow the seasonality of fine aerosol. Nitrate had its maximum concentrations in the winter, while light-absorbing carbon was highest in the autumn. Sulfate (57.8%) composed the

bulk of fine aerosol followed by organics (25.0%), nitrate (6.6%), soil (6.3%), and light-absorbing carbon (4.2%).

Northeast. The northeastern United States is represented by measurements at three sites: Acadia National Park on the coast of Maine, which began monitoring in March 1988, Lye Brook Wilderness Area in southern Vermont, which began in September 1991, and Moosehorn National Wildlife Refuge on the border of Maine and New Brunswick, which began in December 1994. Fine and coarse aerosol concentrations averaged 5.3 and 3.7 $\mu g/m^3$, respectively. Although fine concentrations were largest in summer and least in winter, there was not a strong seasonal variation for coarse aerosol concentrations. Sulfate, organics, and light-absorbing carbon concentrations were also largest in summer. Nitrate concentrations reached their maximum in winter. The contributors to fine particle mass included sulfate (55.4%), organics (29.2%), nitrate (6.0%), light-absorbing carbon (4.7%), and soil (4.7%).

Northern Great Plains. Only one set of measurements was made in this region, at Badlands National Park in South Dakota. Fine and coarse aerosol concentrations averaged 4.0 and 5.5 $\mu g/m^3$, respectively. The maximum concentrations for fine mass and coarse mass occurred in the summer and were least in the winter. Sulfate (43.2%) contributed the most to fine mass and second were organics (28.6%), followed by nitrate (13.2%), soil (11.4%), and light-absorbing carbon (3.6%).

Northern Rocky Mountains. This region has measurements made at Glacier National Park in Montana, close to the Canada border. Fine aerosol and coarse aerosol concentrations averaged 4.6 and 6.2 $\mu g/m^3$, respectively. The strongest seasonality was shown by nitrate, with a significant winter peak, and coarse mass, which peaked in the summer. Sulfates peaked in the spring and organics and light-absorbing carbon peaked in the autumn. Organics were by far the largest contributor to fine particle mass (54.7%) followed by sulfate (20.1%), soil (12.3%), light-absorbing carbon (7.8%), and nitrate (5.0%).

Pacific Coastal Mountains. This region includes three Class I areas along and near the coast of northern California: Pinnacles National Monument, Point Reyes National Seashore, and Redwood National Park. In this region, the fine and coarse aerosol concentrations averaged 3.7 and 6.6 $\mu g/m^3$, respectively. There was no strong seasonal variation for fine and coarse concentrations, however, sulfate concentration was greatest in summer and least in winter, while nitrate showed the opposite trend, peaking in the winter and low in summer. Organics in this region were the largest single component of fine aerosol (36.2%), followed by sulfate (34%), nitrate (17.5%), soil (7.3%), and light-absorbing carbon (5.1%).

Sierra-Humboldt. The region further north in the Sierra Nevada and Humboldt Mountain Ranges was measured with sites at Crater Lake National Park in Oregon and Lassen Volcanic National Park in northern California. This region is relatively remote from high emission density areas. Its fine and coarse aerosol concentrations were relatively low, at 2.4 and 3.1 $\mu g/m^3$, respectively. Summer concentration of fine mass was generally about four times than during the winter. Organics contributed most of the fine particle mass (51.2%), followed by sulfate (20.7%), soil, (15.3%), light-absorbing carbon (7.5%), and nitrate (5.3%).

Sierra Nevada. The Sierra Nevada Mountains in California were monitored at two sites: Yosemite and Sequoia National Parks. Yosemite National Park has been monitored since March 1988. Sequoia National Park had modules A and D since March 1992 but was not fully instrumented until July 1993. Average fine and coarse aerosol concentrations were 6.6 and 7.0 $\mu g/m^3$, respectively. There was a strong seasonal variation of fine and coarse mass, with maximum concentrations in summer and minimum concentrations in winter. Sulfate concentrations, followed by organics, showed the largest seasonal variation between summer and winter, while nitrate concentration was greatest in the winter and least in summer. On a relative basis organics contributed more than twice what sulfate contributed (42.1% and 19.6%, respectively). Soil was the next largest contributor (18.2%), followed by nitrate (14.3%), and light-absorbing carbon (5.7%).

Sonoran Desert. This region in southeastern Arizona was monitored at two sites: Chiricahua and Tonto National Monuments that were initiated in March 1988. The three-year averages of fine and coarse mass concentrations in this region were 3.9 and 6.5 $\mu g/m^3$, respectively. These concentrations were highest in spring, summer, and fall and lowest in winter. The sulfate, organics, and soil components of fine particle mass had maxima in the summer, autumn, and spring, respectively, and minima in the winter. The contributions to fine particle mass were distributed between sulfate (39.2%) then organics (28.1%), followed by soil (21.8%), nitrate (6.4%), and light-absorbing carbon (4.5%).

Southeast. Previously, this region was designated as Florida, and is now represented by three sites at Chassahowitzka National Wildlife Refuge on the Gulf Coast north of Tampa, Florida, Okefenokee National Wildlife Refuge an inland site on the Georgia-Florida border, and Cape Romain National Wildlife Refuge on the South Carolina coast. Monitoring at these three sites began in April 1993, September 1991, and September 1994, respectively. The fine and coarse aerosol concentrations averaged 9.8 and 9.5 $\mu g/m^3$, respectively, with their concentrations highest in summer and lowest in winter. Sulfate and soil concentrations were greatest in the summer and least in the winter. Organics and light-absorbing carbon had their greatest concentrations in the winter, while nitrate concentrations were greater in the spring. Sulfate was found to be the largest contributor to fine particle mass (53.3%), followed by organics (29.2%), soil (8.3%), light-absorbing carbon (5.2%), and nitrate (4.1%).

Southern California. Measurements in this region were made in San Gorgonio National Monument, east of the Los Angeles metropolitan area. Fine and coarse aerosol concentrations were 7.2 and 6.5 $\mu g/m^3$, respectively. Like many sites in the IMPROVE Network, concentrations were highest in summer and lowest in winter. This site was the only site in the IMPROVE Network in which nitrate was a larger contributor to fine particle mass than either sulfate or organic carbon. The contributions were nitrate (34.7%), organics (28.3%), sulfate (20.4%), soil (11.5%), and light-absorbing carbon (5.1%).

Wasatch. This area is monitored at Lone Peak Wilderness Area above Provo, Utah to the north and east in the Wasatch Mountain Range. Monitoring began in December 1993 but suffered equipment failure in September 1994. It has since operated reliably. Fine and coarse aerosol concentrations averaged 4.5 and 5.1 $\mu g/m^3$, respectively, and were highest in the summer and least during winter. Concentrations of sulfate, organics, light-absorbing carbon, and soil were also highest in the summer and least in the winter. Nitrate, however, was exactly the opposite with

winter concentrations being more than four times as in summer. On average, organics comprised the bulk of fine mass (35.1%), followed by sulfate (23.6%), soil (20.6%), nitrate (13.3%), and light-absorbing carbon (7.3%).

Washington, D.C. This is a single monitoring site in the nation's capital, the only urban site of the network. Fine aerosol concentrations were higher here than anywhere in the IMPROVE Network. Fine and coarse mass concentrations averaged 14.5 and 4.9 $\mu g/m^3$, respectively. There was a moderate seasonal variation in fine aerosol concentrations; they ranged from 13.1 to 17.8 $\mu g/m^3$ in summer. However, the sulfate and nitrate components varied significantly by season. Sulfate concentrations were largest in summer and smallest in winter, while nitrate concentrations were largest in winter and smallest in summer. Fine particle mass consisted of sulfate (49.7%), organics (26.4%), nitrate (10.8%), light-absorbing carbon (7.9%), and soil (5.1%).

West Texas. Two measurement sites in west Texas were included: Big Bend and Guadalupe Mountains National Parks on or near the Mexico border in southwestern Texas, respectively, and have operated since March 1988. The fine and coarse aerosol concentrations averaged 5.5 and 7.2 $\mu g/m^3$, respectively. Minimum concentrations generally occurred during winter, while maximum concentrations occurred in summer for fine mass and spring for coarse mass. All components of fine mass showed seasonal variability except light-absorbing carbon, which remained relatively constant. Nitrate, and soil concentrations peaked during the spring, while sulfate and organics were lowest in the winter and nitrate was lowest in the autumn. Concentrations of organics were highest in the spring, while those of sulfates were highest in the summer. The contributions to fine particle mass was sulfate (43.9%), soil (26.1%), organics (22.4%), nitrate (4.6%), and light-absorbing carbon (3%).

In general, the following observations can be made. With few exceptions, aerosol concentrations were highest in summer and lowest in winter. In the eastern United States, sulfates contributed most to fine mass, while in southern California nitrates were the single largest contributor. In the desert Southwest, carbon, sulfates, and soil all contributed about equally to fine mass, while in the Northwest carbon and sulfate were the largest contributors.

2.5 SPATIAL TRENDS IN AEROSOL CONCENTRATIONS IN THE UNITED STATES

Because of the relatively large number of IMPROVE aerosol monitoring sites in the western United States, isopleth maps of the average aerosol concentrations measured over the three-year period from March 1996 through February 1999 could be drawn. Figures 2.1 through 2.8 show isopleth maps of the three-year average aerosol concentrations (PM_{10}, fine mass, coarse mass, sulfate, nitrate, organics, light-absorbing carbon, and soil). These figures provide us with information on how aerosol concentrations and mass budgets vary over the United States. Because Washington, D.C. is an urban site it is not included in the isopleth presentations.

2.5.1 PM_{10} Aerosol

Figure 2.1 shows isopleths of the PM_{10} gravimetric mass concentration measured during this three-year period. The highest concentrations occurred in the eastern United States. All the areas

east of the Mississippi River had concentrations in excess of 8 μg/m^3. The highest concentrations were in Edwin B. Forsythe National Wildlife Refuge in New Jersey at 23 μg/m^3, followed by the Southeast region, Sequoia National Park, and the Mid South, which experienced concentrations in excess of 15 μg/m^3. Outside of southern California and the Northern Rockies the least amount of PM_{10} concentrations occurred in the western United States, where there was a large swath extending from Oregon, northern California, Nevada, Utah, Wyoming, into northern Arizona, northern New Mexico and western Colorado, where the concentration of PM_{10} was less than 8.0 μg/m^3. The lowest concentration in the contiguous 48 states occurred at Lassen Volcanic National Park at only 5.1 μg/m^3 on average; the least was recorded at Denali National Park in Alaska at 4.5 μg/m^3. The strongest gradients were between regions of California and Nevada, where concentrations varied from 5.9 μg/m^3 at Great Basin National Park to an excess of 19 μg/m^3 at Sequoia National Park and Edwin B. Forsythe National Wildlife Refuge and Lye Brook Wilderness Area, where concentrations decreased from 23 to 8.2 μg/m^3.

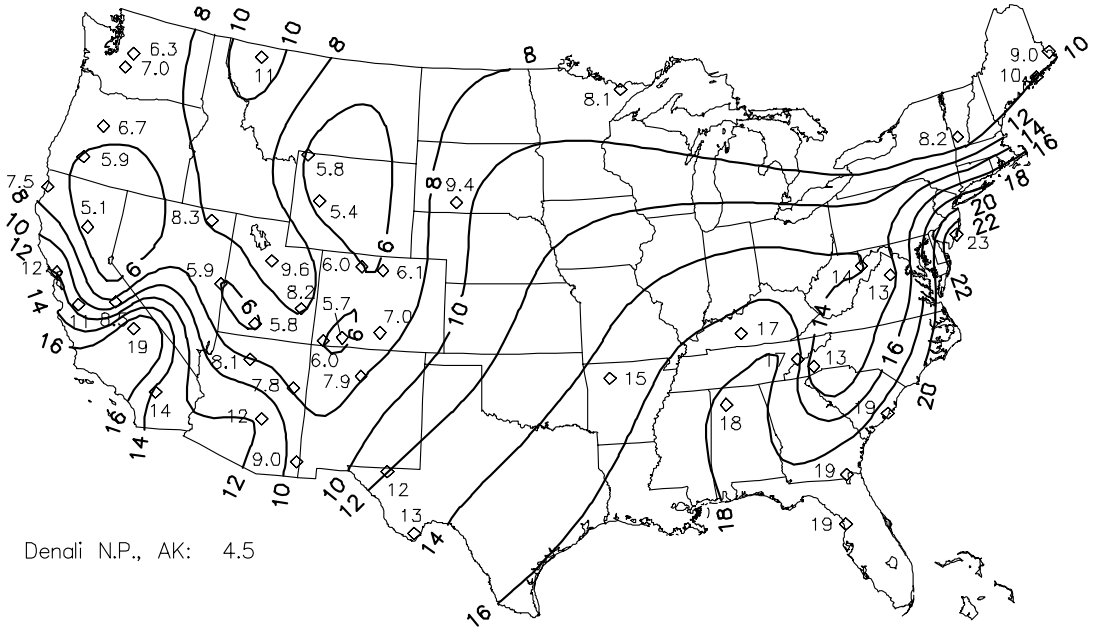

Figure 2.1 *Average PM_{10} mass concentrations (in μg/m^3) for each site in the IMPROVE Network, excluding Washington, D.C.*

2.5.2 Fine Aerosol

Figure 2.2 shows isopleths of the average reconstructed fine aerosol concentrations measured during the three-year period. Note the strong gradient in fine particle concentrations from southern California, a local maximum of 8.9 μg/m^3 to minima of 2.2 to 2.7 μg/m^3 observed in southern Oregon, Nevada, southern Utah, western Colorado, and Wyoming. This is a factor of four variations in average fine aerosol concentration. Also, note that fine aerosol concentrations increased again as one moves to the eastern United States with levels in excess of 9 μg/m^3 in Mammoth Cave National Park and Upper Buffalo and Sipsy Wilderness Areas. Thus, from the

minima in the western United States to the maxima in the eastern United States, there was about a factor of six difference in average concentration.

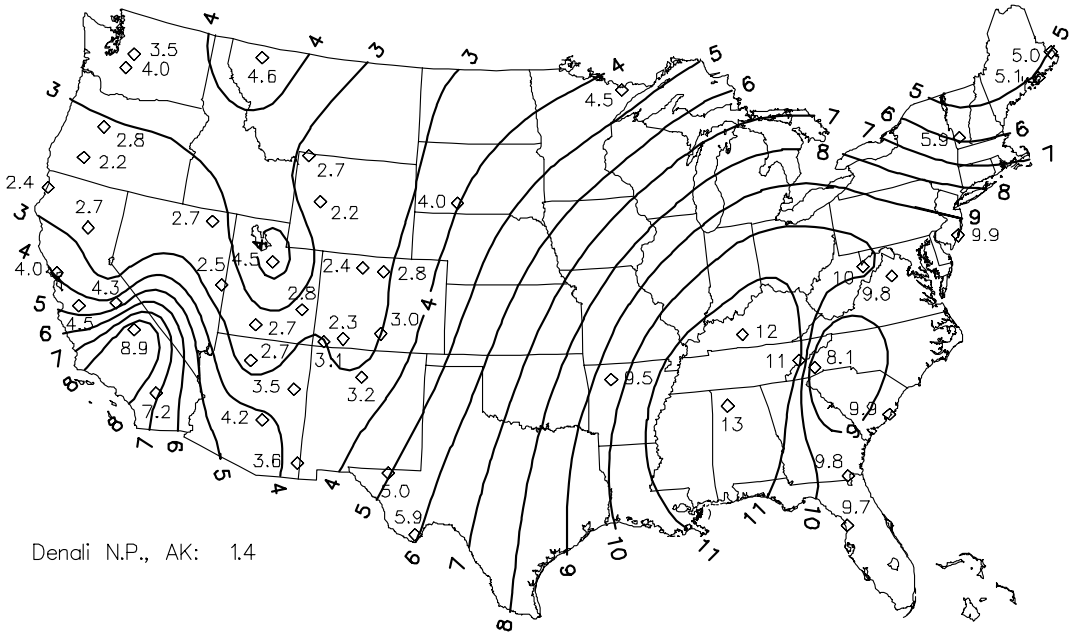

Figure 2.2 *Average fine mass aerosol concentrations (in μg/m^3) for each site in the IMPROVE Network, excluding Washington, D.C.*

2.5.3 Coarse Aerosol

Figure 2.3 shows isopleths of the three-year average coarse mass (CM) concentrations. There were a few local maxima from 7.5 to 13 μg/m^3 that were noticeable near southern Arizona, southern California, San Francisco, and the New Jersey coast. The lowest coarse aerosol concentrations occurred in the swath from the Pacific Northwest through Nevada to southern Utah. Concentrations in this region averaged around 3.5 μg/m^3. Throughout the United States coarse aerosol concentrations were generally in the factor-of-four range from 3 to 11 μg/m^3. The patterns in the eastern United States showed a steady north-south trend of increasing coarse aerosol concentrations with steepest gradients near the coast. Coarse aerosol concentrations in Alaska were not significantly lower than in the contiguous 48 states.

2.5.4 Fine Sulfate Aerosol

The average sulfate component of the fine aerosol measured over the three-year period is shown in Figure 2.4. Since sulfate is one of the two major components of fine particle mass, it was not surprising to observe gradients across the United States similar to what was observed for total fine particle mass. There was a strong gradient from high concentrations in southern California to low concentrations in southern Oregon and Nevada. There was also a strong gradient from the relatively low concentrations in the West to those in the East. There was about a factor of 18 between the lowest concentrations measured in Nevada and Oregon to the highest concentrations measured in

the Mid-South and Southern Appalachian Mountains. A relative maximum in sulfate concentration was observed in southern Arizona. The lower map in Figure 2.4 shows that sulfate constituted as little as 19% of fine particle mass in the Sierra-Nevada area to as much as 66% of total fine mass in Shining Rock Wilderness Area in North Carolina. On the Colorado Plateau sulfate was 31 to 37% of the fine particle mass.

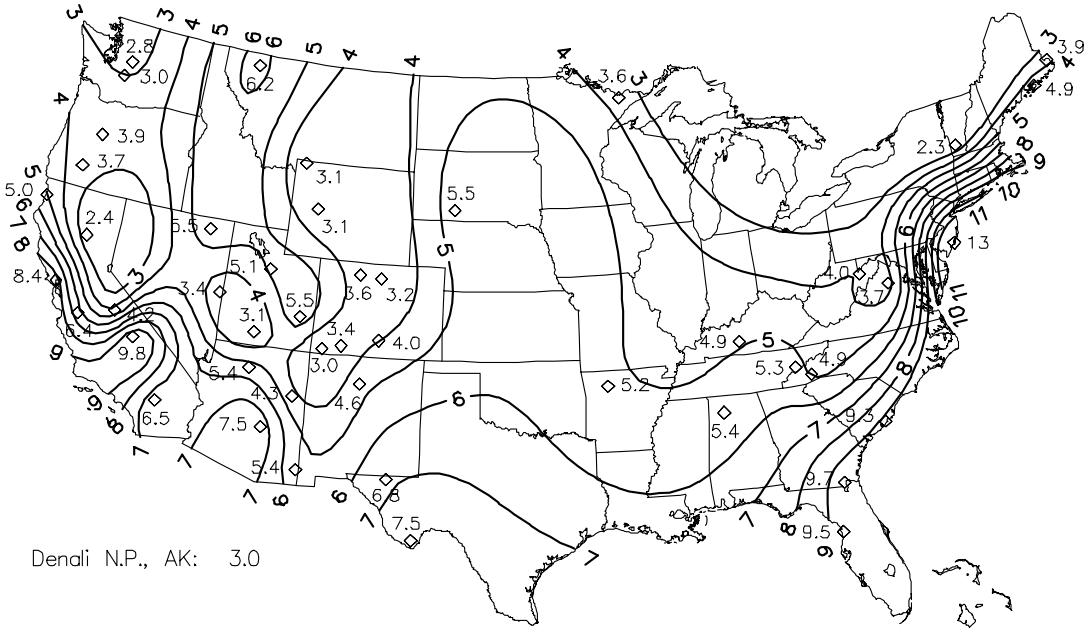

Figure 2.3 *Average coarse particle mass concentrations (in μg/m^3) for each site in the IMPROVE Network, excluding Washington, D.C.*

In the eastern United States, sulfate was the largest single component of fine particle mass. In the Boundary Waters, Sonoran Desert, and West Texas regions, sulfate is still the largest contributor to fine mass, however, it is followed closely by organic carbon. Sulfate was the second largest component of fine mass in all other regions studied except southern California and the Great Basin where sulfate is the third largest component.

2.5.5 Fine Nitrate Aerosol

Figure 2.5 shows isopleth maps of the nitrate concentration and nitrate mass fraction of fine aerosol, averaged over the three-year period. Note, the highest average concentration of 2.5 μg/m^3 was measured in San Gorgonio Wilderness, just east of the Los Angeles metropolitan area. There was a strong gradient from the high concentrations in the California coastal areas to the minima of 0.1 μg/m^3 measured in Oregon. There was a long swath of low nitrate concentrations extending from Oregon, Nevada, and Idaho into Utah, Wyoming, Colorado and into southern Arizona and southern New Mexico (<0.2 μg/m^3). Nitrate mass fractions were typically 4 to 12% except in California where they were 30% and higher. In the north central part of the United States, nitrates constituted over 12% of the fine aerosol mass. Nitrates were the largest single component of fine aerosol mass in southern California at San Gorgonio Wilderness Area.

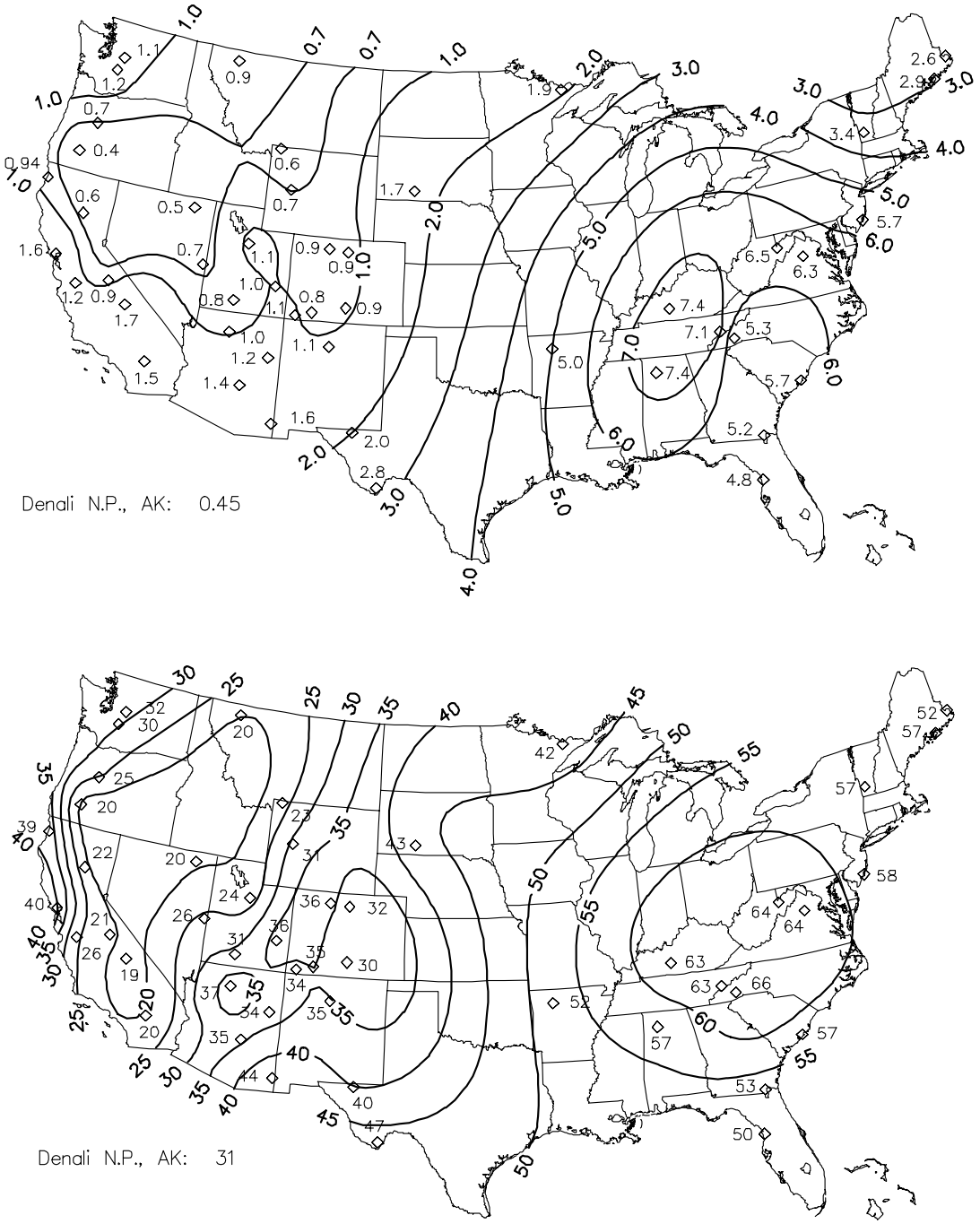

Figure 2.4 *Average fine sulfate aerosol concentrations (in μg/m^3) (top map) and sulfate fine mass (in %) (bottom map) for each site in the IMPROVE Network, excluding Washington, D.C.*

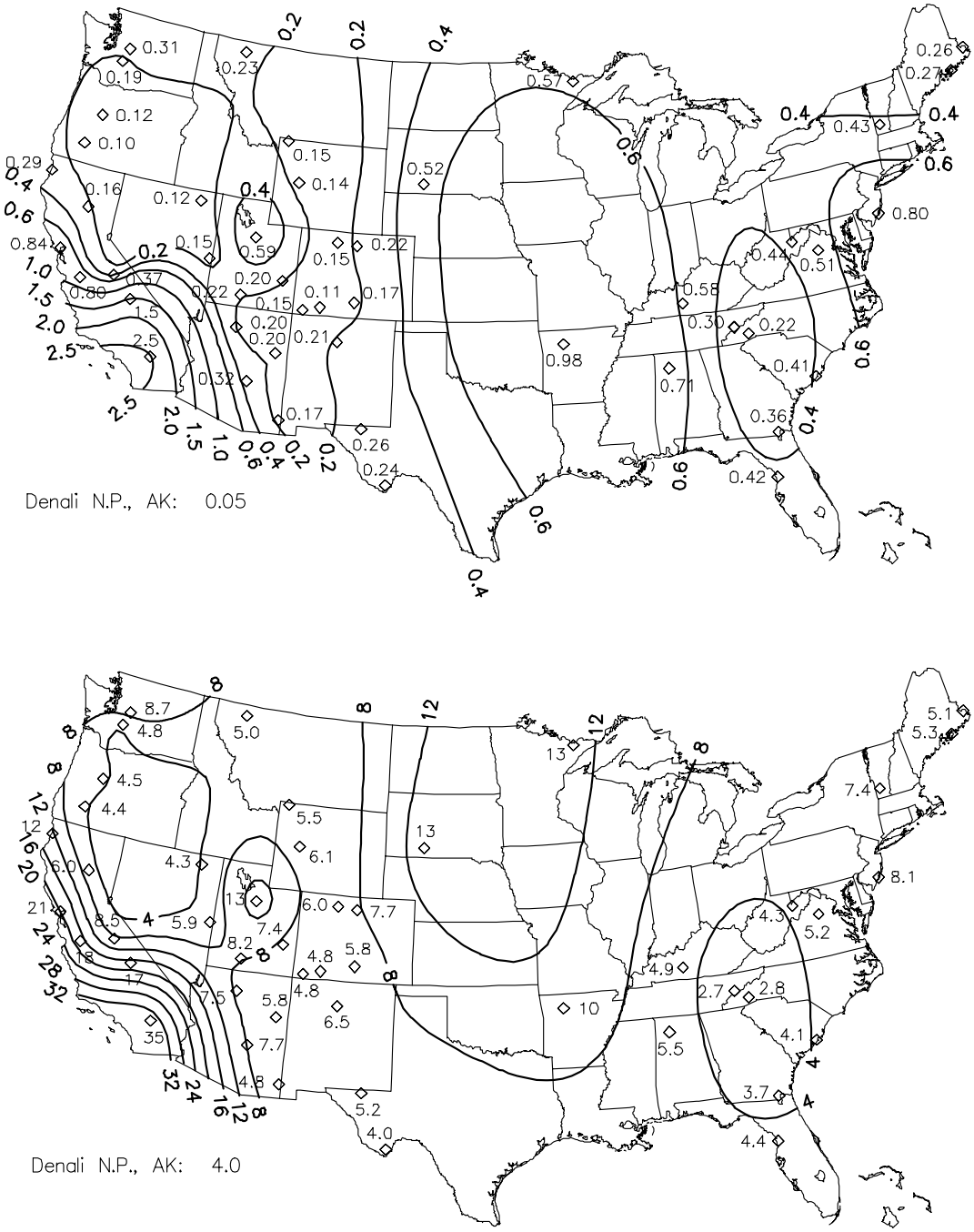

Figure 2.5 *Average fine nitrate aerosol concentrations (in μg/m^3) (top map) and nitrate fine mass (in %) (bottom map) for each site in the IMPROVE Network, excluding Washington, D.C.*

2.5.6 Fine Organic Aerosol

Figure 2.6 shows isopleth maps of the organic carbon mass concentration and organic mass fraction of the fine aerosol concentration, averaged over the three-year period. There was a significant spatial gradient from the lower Sierra-Nevada region, with average concentrations of 3.3 $\mu g/m^3$ to the inner-mountain region of Wyoming, Colorado, Oregon, Utah, and Arizona of 1.0 $\mu g/m^3$ or less. In the eastern United States, organics ranged generally between 1.5 to 3.4 $\mu g/m^3$. Except in the Sierra and Cascade Mountain regions, where organics were over half of the fine particle mass, organics generally constitute between 20 to 40% of the fine particle mass.

2.5.7 Fine Light-Absorbing Carbon Aerosol

Figure 2.7 shows isopleth maps of the light-absorbing carbon concentration and mass fraction of the fine aerosol, averaged over the three-year period. Note, light-absorbing carbon concentrations were lowest in the inner-mountain west and on the Colorado Plateau where light-absorbing carbon was generally less than 0.2 $\mu g/m^3$. Mass fractions were typically 4-5% of fine mass except in the Pacific Northwest where light-absorbing carbon contributed as much as 8.8% of the fine particle mass.

2.5.8 Fine Soil Aerosol

Figure 2.8 shows isopleth maps for fine soil. The contribution of soil to the fine aerosol in the United States was generally small, except for the elevated concentrations (>1 $\mu g/m^3$) in the southern tier of the United States. There was a quite noticeable north-south trend of increasing soil concentrations with the Northeast being the lowest. Soil contributed approximately 5 to 10% of the fine aerosol mass in the East. Except for Florida, all of the areas east of the Mississippi, the Pacific Northwest, and parts of California, soil contributed less than 10% to fine aerosol mass with much of the inner-mountain west in excess of 20%.

2.6 SUMMARY

The following were the major patterns observed in the three-year period of IMPROVE from March 1996 through February 1999:

(1) Spatial Patterns. Concentrations of fine particles (those most important in determining visibility) were highest in the eastern United States and in southern California and lowest in the relatively unpopulated areas of the West.

(2) Major Contributions to Fine Aerosol. The largest single component of the fine aerosol in the East was sulfate at 60-65% of the mass, while in the Pacific Northwest it was organics, and in southern California it was nitrates. In general, the largest mass fractions of the fine aerosol were sulfates, organics and in soil/dust. Of the 21 regions in the IMPROVE Network, carbon (organic plus light-absorbing carbon) was the largest single component in

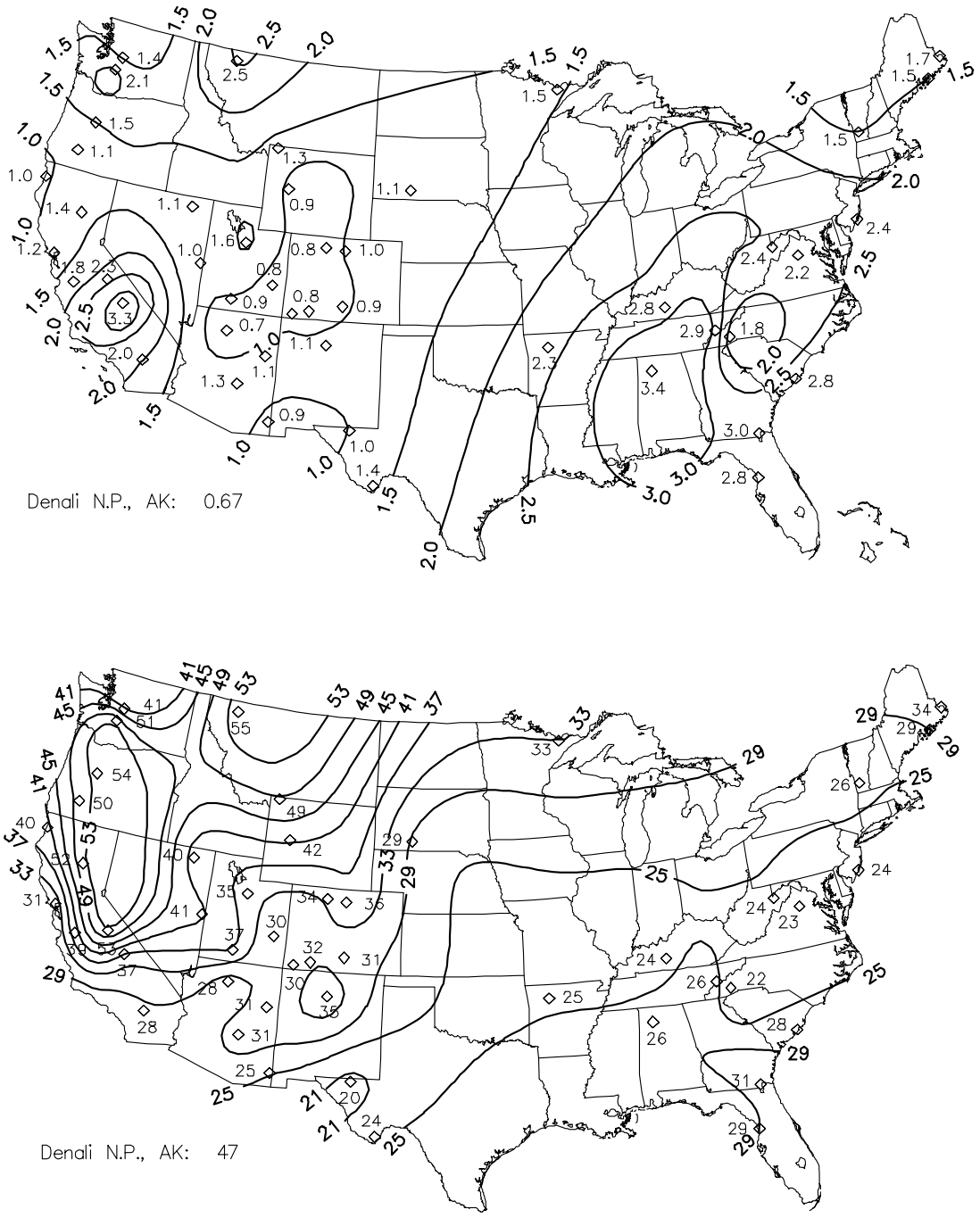

Figure 2.6 *Average fine organic aerosol concentrations (in μg/m^3) (top map) and organic fine mass (in %) (bottom map) for each site in the IMPROVE Network, excluding Washington, D.C.*

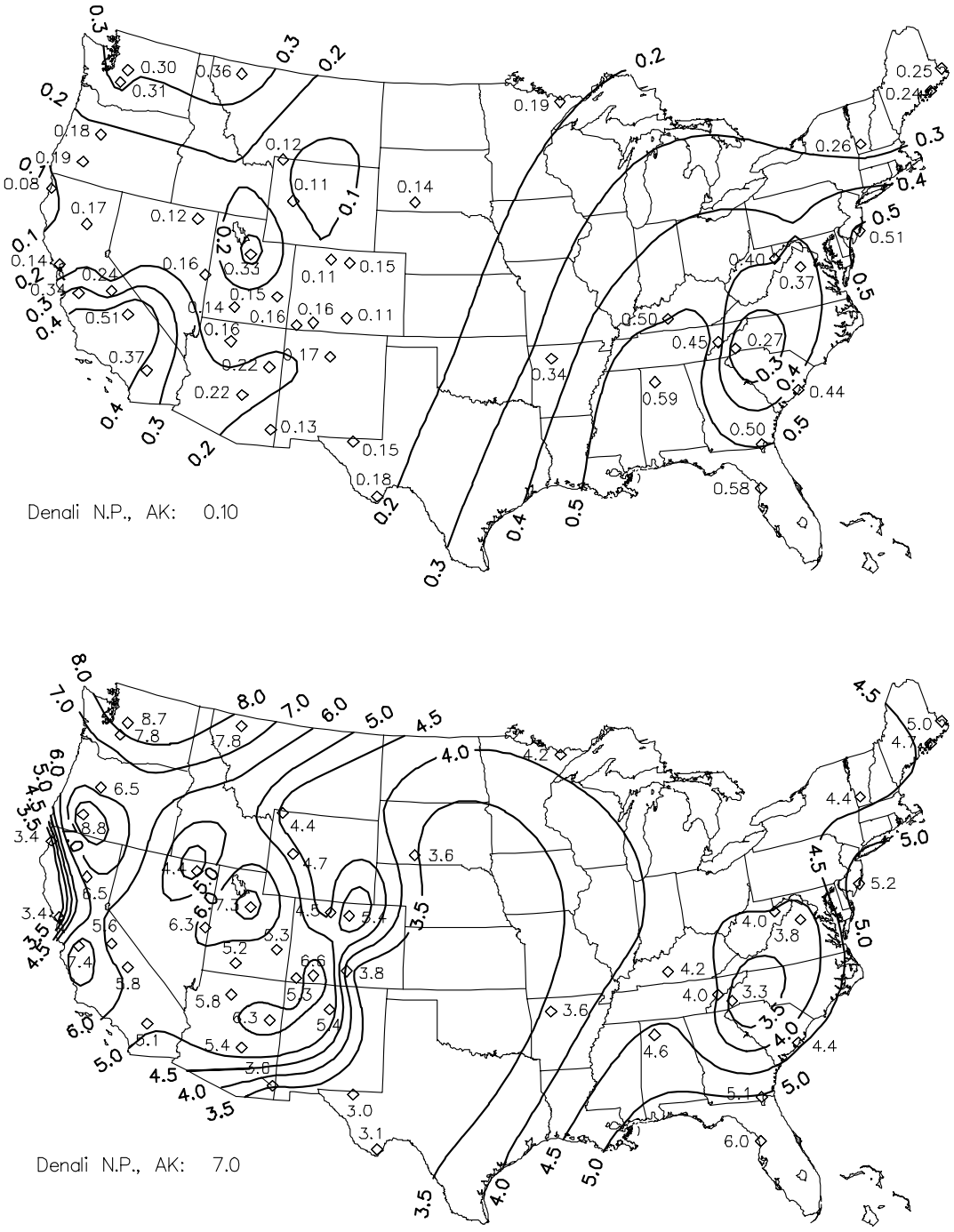

Figure 2.7 *Average light-absorbing carbon concentrations (in μg/m^3) (top map) and light-absorbing carbon fine mass (in %) (bottom map) for each site in the IMPROVE Network, excluding Washington, D.C.*

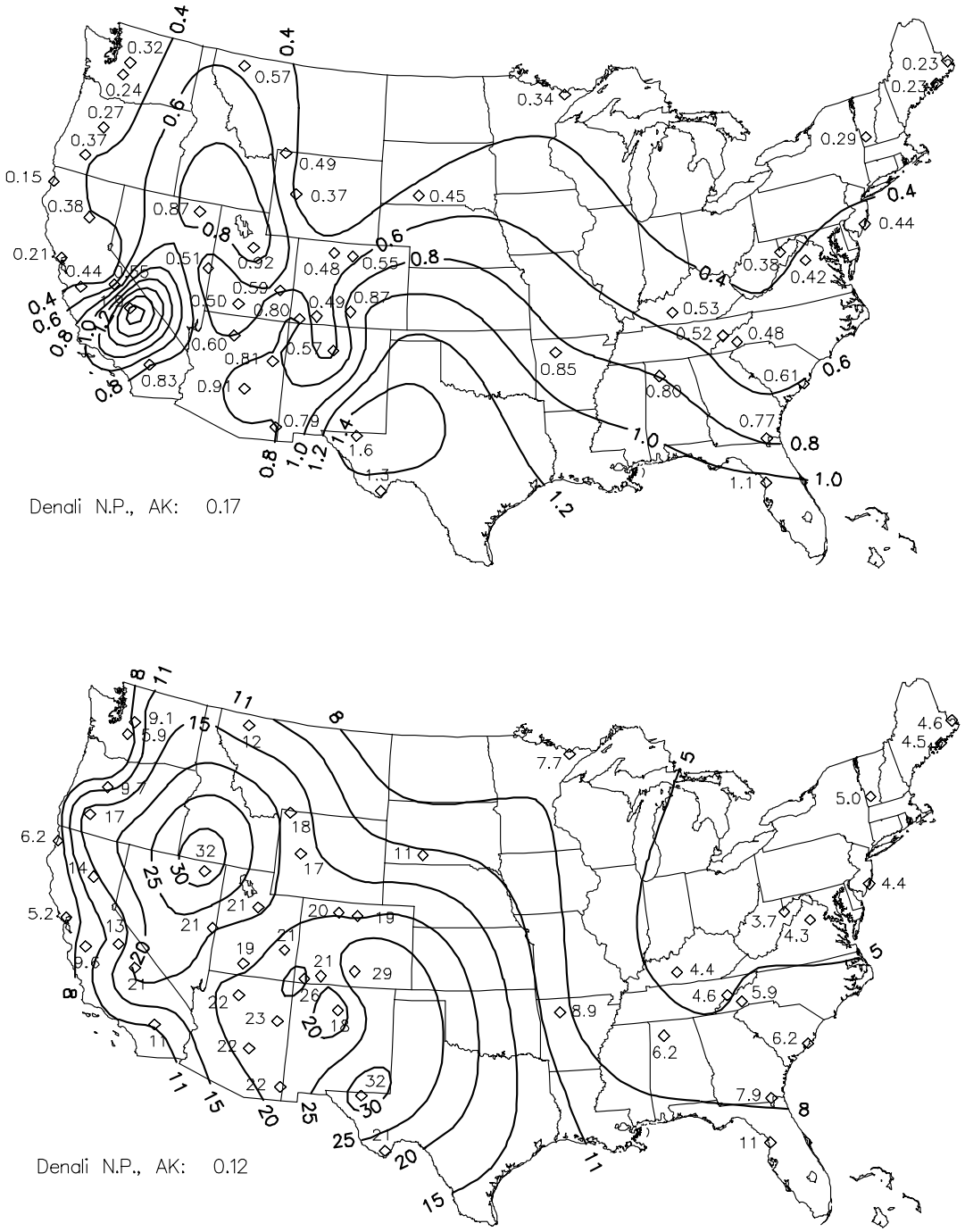

Figure 2.8 *Average fine soil aerosol concentrations (in μg/m^3) (top map) and soil fine mass (in %) (bottom map) for each site in the IMPROVE Network, excluding Washington, D.C.*

10 regions (Alaska, Cascade Mountains, Central Rocky Mountains, Colorado Plateau, Great Basin, Northern Rocky Mountains, Pacific Coastal Mountains, Sierra-Nevada, Sierra-Humboldt, and Wasatch). Sulfate was the largest single component of fine aerosol in 10 regions, primarily in the East (Appalachian Mountains, Boundary Waters, Mid Atlantic, Mid South, Northeast, Northern Great Plains Sonoran Desert, Southeast, Washington D.C. and West Texas), while nitrates were slightly greater than carbon in Southern California. Sulfate and carbon were approximately the same on the Colorado Plateau and Sonoran Desert.

(3) Smaller Contributors. After the contributions of organics and sulfate, soil was the next largest, followed by nitrate (except for nitrate in Southern California) and light-absorbing carbon.

(4) Seasonality. With a few exceptions, average fine mass concentrations, organics and sulfate components of fine mass were highest in summer. Soil concentrations were highest in spring or summer. On the other hand, nitrate concentrations were generally highest in winter or spring. Light-absorbing carbon exhibited relatively little seasonal variation.

(5) PM_{10}. The highest concentrations of PM_{10} occur in a region east of the Mississippi and south of the Great Lakes, followed by coastal and southern California. In the East, the high concentrations are driven by high fine mass, which contributes as much as 70% of PM_{10}.

2.7 REFERENCES

Eldred, R.A., Cahill, T.A., and Flocchini, R.G. Composition of $PM_{2.5}$ and PM_{10} aerosols in the IMPROVE Network, *J. Air and Waste Management Association*, **47**, 194-203, 1997.

Eldred, R.A., Cahill, T.A., Pitchford, M.L., and Malm, W.C., IMPROVE-A new remote area particulate monitoring system for visibility studies, *Proc. APCA (Air Pollution Control Assoc.) Ann. Mtg*., 81, 1-16, 1988.

Malm, W.C., Sisler, J.F., Huffman, D., Eldred, R.A., and Cahill, T.A., Spatial and seasonal trends in particle concentration and optical extinction in the United States, *J. Geo. Res*., **99**(D1), 1347-1370, 1994.

Noll, K.E., Pontius, A., Frey, R., and Gould, M., Comparison of atmospheric coarse particles at an urban and non-urban site, *Atmos. Environ*., **19**(11), 1931-1943, 1985.

Noll , K.E., Collection and characteristics of atmospheric coarse particles, Final Report, Dept. of Environmental Engineering, Illinois Institute of Technology, Chicago, 1991.

Sisler, J. F., *Spatial and Seasonal Patterns and Long Term Variability of the Composition of the Haze in the United States: An Analysis of Data from the IMPROVE Network*, Cooperative Institute for Research in the Atmosphere, Colorado State University, ISSN 0737-5352-32, 1996.

Sisler, J. F., Huffman, D., Latimer, D. A., Malm, W. C. and Pitchford, M. L., *Spatial and Temporal Patterns and the Chemical Composition of the Haze in the United States: An Analysis of Data from the IMPROVE Network 1988-1991*, Cooperative Institute for Research in the Atmosphere, Colorado State University, ISSN 0737-5352-26, 1993.

Watson, J.G., Chow, J.C., Pritchett, L.C., Pierson, W.R., Frazier, C.A., Purcell, R.G. and Olmez, I., *The 1987-88 Metro Denver brown cloud study*, Desert Research Institute, Doc 8810 1F2, Desert Research Institute, Reno, NV, 1988.

CHAPTER 3

SPATIAL DISTRIBUTIONS OF RECONSTRUCTED LIGHT EXTINCTION AND LIGHT-EXTINCTION BUDGETS

The model used to reconstruct the light extinction coefficient from aerosol measurements and to derive the reconstructed light extinction coefficient and other visibility metrics for the sites are presented and examined here. Using this model, the relative contribution of various aerosol components to total light extinction is combined into light-extinction budgets for the regions described in Chapter 1.

3.1 RECONSTRUCTING LIGHT EXTINCTION FROM AEROSOL MEASUREMENTS

The light-extinction coefficient, b_{ext} (expressed as inverse megameters, 1/Mm), is the sum

$$b_{ext} = b_{scat} + b_{abs} = b_{sg} + b_{sp} + b_{ag} + b_{ap} \tag{3.1}$$

where b_{scat} is the sum of scattering by gases and scattering by particles, and b_{abs} is the sum of absorption by gases and particles. Scattering by gases in the atmosphere, b_{sg}, is described by the Rayleigh scattering theory [vandeHulst, 1981] and will be referred to as Rayleigh scattering. The IMPROVE program assumes a standard value of 10 1/Mm. Scattering by particles, b_{sp}, is caused by both fine and coarse aerosol species and is the largest contributor to total light extinction in most locations [Malm et al., 1994a]. Absorption due to gases, b_{ag}, is primarily due to nitrogen dioxide (NO_2) and is assumed to be negligible because almost all monitoring sites are in rural locations [Trijonis and Pitchford, 1987]. Absorption by particles, b_{ap}, is caused primarily by carbon containing particles.

A particle in the atmosphere can be a mix (internal mixture) of various aerosol species, or in some cases its compositional structure may be restricted to one species (external mixture) such as $(NH_4)_2SO_4$. Furthermore, an internally mixed aerosol such as organic/sulfate/water particle can be externally mixed from wind-blown dust particles. Whether an aerosol is internally or externally mixed, it scatters and/or absorbs a specific fraction of radiant energy impinging on it. Following the suggestion of White [1986], an aerosol scattering/extinction per unit mass ratio will be referred to as specific scattering/extinction, as in specific gravity.

Most routine aerosol monitoring programs and many special study visibility characterization programs were designed to measure bulk aerosol species mass concentrations such as sulfates, nitrates, carbonaceous material, and selected elements [Heisler et al., 1980; Malm et al., 1994b; Tombach and Thurston, 1994; Watson et al., 1990; Macias et al., 1981]. They were not designed to determine the microphysical and chemical characteristics of these species.

The inherent limitations of estimating aerosol optical properties from bulk aerosol measurements have been addressed, at least in part, by a number of authors. For instance, Ouimette and Flagan [1982] have shown, from basic theoretical considerations, that if an aerosol is mixed externally or if in an internally mixed aerosol the index of refraction is not a function of composition or size, and the aerosol density is independent of volume, then:

$$b_{ext} = \sum_i \alpha_i m_i \tag{3.2}$$

where α_i is the specific scattering or absorption efficiency and m_i is the mass of the individual species.

Malm and Kreidenweis [1997] demonstrated from a theoretical perspective, that specific scattering of mixtures of organics and sulfates were insensitive to the choice of internal or external mixtures. Sloane [1983, 1984, 1986], Sloane and Wolff [1985], and more recently Lowenthal et al. [1995], Malm [1998], and Malm et al. [1997] have shown that differences in estimated specific scattering between external and internal model assumptions are usually less than about 10%. In the absence of detailed microphysical and chemical structure of ambient aerosols, the above studies demonstrate that a reasonable estimate of aerosol extinction can be achieved by assuming each species is externally mixed.

However, the issue of water uptake by hygroscopic species must be addressed. Implicit to the use of Equation (3.2) is an assumed linear relationship between aerosol mass and extinction. It is well known that sulfates and other hygroscopic species form solution droplets that increase in size as a function of relative humidity (RH). Therefore, if scattering is measured at various relative humidities the relationship between measured scattering and hygroscopic species mass can be quite nonlinear. A number of authors have attempted to linearize the model, in an empirical way, by multiplying the hygroscopic species by such a factor as 1/(1-RH) to account for the presence of water mass [White and Roberts, 1977; Malm et al., 1986]. However, Malm et al. [1989] and Gebhart and Malm [1989] proposed a different approach. They multiplied the hygroscopic species by a relative humidity scattering enhancement factor, f(RH), that is calculated on a sampling-period-by-sampling-period basis using Mie theory and an assumed size distribution and laboratory measured aerosol growth curves.

Measurements of hygroscopic species growth as a function of relative humidity show that species such as ammonium sulfate show zero growth until a relative humidity, referred to as the deliquescent relative humidity, is reached where they spontaneously form a solution droplet that is in equilibrium with water molecules in the ambient atmosphere. Conversely, when the relative humidity is decreased from some value greater than 80% the solution droplet retains water below the deliquescent point to a relative humidity where all water is spontaneously given up. This point is referred to as the crystallization relative humidity.

However, because the growth factor and light-scattering efficiency for ambient aerosols has previously been observed to be rather smooth, [Sloane 1983, 1984, 1986; Wexler and Seinfeld, 1991; Waggoner et al., 1981; Day et al., 2000; Malm et al. 2000] a “best estimate" for the sulfate and nitrate species growth, the laboratory growth curves, as measured by Tang [1996] were smoothed between the deliquescence and crystallization points. Malm [1998] and Malm et al., [1997] have demonstrated that in both the East (Great Smoky Mountains National Park) and West (Grand Canyon National Park) the best estimate growth model, in combination with measured size distributions, yields an f_T(RH) function that results in good agreement between measured and reconstructed scattering for particles less than 2.5 μm.

Therefore, the following equation is used to estimate reconstructed particle scattering:

$$\begin{aligned} b_{scat} = {} & (3) f_T(RH)[SULFATE] \\ & + (3) f_T(RH)[NITRATE] \\ & + (4) f_{org}(RH)[OMC] \\ & + (1)[SOIL] \\ & + (0.6)[CM] \end{aligned} \tag{3.3}$$

The brackets indicate the species concentration, 3 m^2/g is the dry specific scattering for sulfates and nitrates, 4 m^2/g for organic carbon, and 1 m^2/g and 0.6 m^2/g are the respective scattering efficiencies for soil and coarse mass. The efficiencies for fine soil and coarse mass are taken from a literature review by Trijonis and Pitchford [1987].

A dry scattering efficiency of 3 m^2/g is a nominal scattering efficiency based on a literature review by Trijonis et al. [1988, 1990] and a review by White [1990]. Trijonis' best estimate for sulfates and nitrates is 2.5 m^2/g with an error factor of 2, while for organics it is 3.75 m^2/g again with an error factor of 2. White took a somewhat different approach in that he reviewed 30 studies in which particle scattering and mass were measured. He then estimated a high and low scattering efficiency by using mass measurements to prorate the measured extinction. For sulfate, the low estimate was arrived at by assuming sulfate, nitrate, and organics scatter twice as efficiently as all other species, and for the high estimate he assumed that only sulfate was twice as efficient. His low and high sulfate mass scattering efficiencies for the rural west were 3.0 and 3.7 m^2/g, respectively. For organics his low estimate assumes organics and other non-sulfate species scatter half as efficiently as sulfates, and for the high estimate he assumes organics are three, and sulfates twice as efficient at scattering light as other species. His low and high estimates for organic mass scattering coefficients are 1.8 and 4.1 m^2/g. More recently, Malm et al. [1996] demonstrated that an assumption of dry specific scattering values given in Equation (3.3) yielded good agreement between measured and reconstructed extinction across the entire IMPROVE monitoring network.

Various functions for the hygroscopicity of organics have been proposed. Assumptions must not only be made about the solubility of organics but also on the fraction of organics that are soluble. It should be noted, models that treat water uptake for nonideal multicomponent solutions using theoretical and semi-theoretical thermodynamic relationships have been

developed and have been applied to both visibility and climate forcing problems [Saxena and Peterson, 1981; Pilinis et al., 1995; Saxena et al., 1986, 1993]. The correct treatment of the hygroscopicity of species in multicomponent mixtures—especially organic species—remains problematic, not only because of the lack of suitable mixture thermodynamic data but also because of the lack of information about other critical mixture properties. Given the variety of organic species, it is possible that a geographic variation in organic species exists, with large fractions of soluble species occurring in certain parts of the continent and much smaller fractions in other areas. However, field experiments and subsequent data analysis at Great Smoky Mountains and Grand Canyon National Parks [Malm et al., 1997; Malm and Kreidenweis, 1996 Malm et al., 2000] and, more generally, data collected in the IMPROVE Network [Malm et al., 1996] show that to within the uncertainty of the measurements and modeling assumptions, organics are not or are only weakly hygroscopic. Therefore, f_{org}(RH) for organics was set equal to one.

Equation (3.3) has been shown to give a good estimation of scattering for particles less than 2.5 μm, however, estimating extinction requires a knowledge of particle absorption. Mass absorption efficiencies of carbon vary by more than a factor of two as do direct measurements. Horvath [1993] has reviewed the measurement of absorption, while Fuller et al. [1999] has theoretically explored the variability of absorption efficiency as a function of carbon morphology. Although absorption can be estimated in a variety of ways, there is no one method that is generally accepted by the scientific community. For purposes of this report, carbon absorption is estimated using:

$$b_{abs} = 10[LAC] \tag{3.4}$$

where b_{abs} is particle absorption, LAC is the concentration of light-absorbing carbon as measured using the Thermal Optical Reflectance (TOR) analysis scheme [Chow et al., 1993], and 10 is the specific absorption for LAC, which has been used by a number of scientists [Horvath, 1993].

Because aerosol concentrations are derived from averages over long periods, the light scattering due to soluble species is derived using hourly RH values less than or equal to 98%, as given by the following equation:

$$b_{scat} = \alpha F_T \overline{C}\,, \tag{3.5}$$

where $\overline{C}$ is the average species concentration, α is the specific scattering, and

$$F_T = \overline{f_T(RH)}\,. \tag{3.6}$$

Using Equation (3.3), extinction budgets for a time interval may be calculated by replacing f_T(RH) with F_T and by using the average concentration of each species over the same time interval as the mass concentration.

Using the data from sites with collocated optical and RH data, a polynomial curve was fitted to the annual and seasonal data as defined by

$$F = b_0 + b_1(100/(100 - \overline{RH})) + b_2(100/(100 - \overline{RH}))^2 \tag{3.7}$$

where b_o = 0.33713, b_1 = 0.58601, and b_2 = 0.09164 with an R-square of 0.93 annually. Figure 3.1 shows the fitted curve plotted against annual average RH for IMPROVE sites with collocated RH data. Table 3.1 lists the regression results for annual and seasonal averaging periods. For those sites without collocated optical and RH data, the annual factors can be calculated using Equation (3.7) and estimates of annual average RH. (Five significant figures are used in the curve fit program used for this report and therefore are included here for reference.)

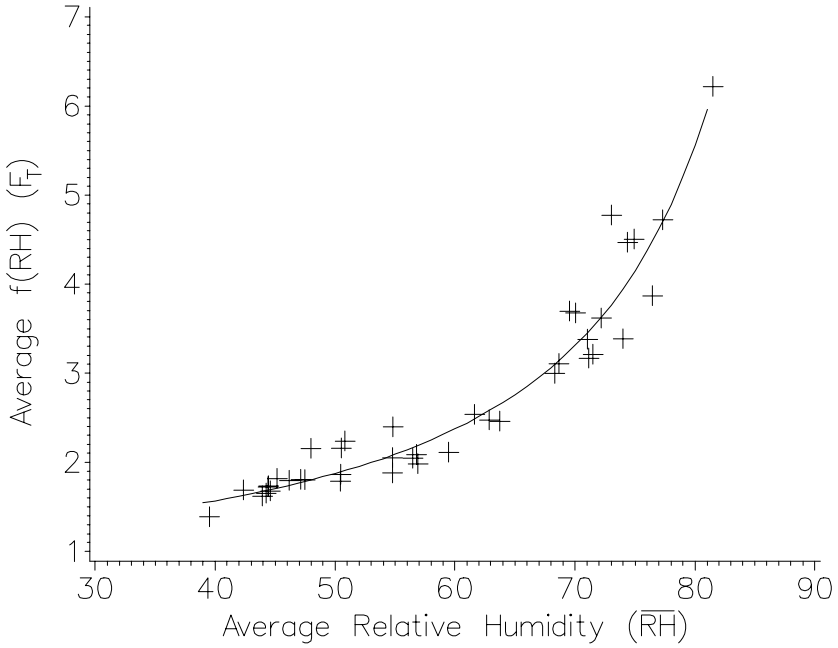

Figure 3.1 *Best-fit relation between a site's annual average RH and its annual average RH correction factor.*

Table 3.1 *Parameters of the best-fit equation relating the relative humidity light-extinction correction factors (F_T) to seasonal and annual average site relative humidity ($F = b_o + b_1(1/(1\text{-}RH)) + b_2(1/(1\text{-}RH))^2$.*

Season	b_0	b_1	b_2	R^2
Spring	-0.01097	0.78095	0.080147	0.93
Summer	-0.18614	0.99211	---	0.91
Autumn	-0.24812	1.01865	0.01074	0.93
Winter	0.34603	0.81984	---	0.77
ANNUAL	0.33713	0.58601	0.09164	0.93

Figure 3.2 is a flowchart, which details the process used to account for the effects of relative humidity at those sites with or without relative humidity sensors.

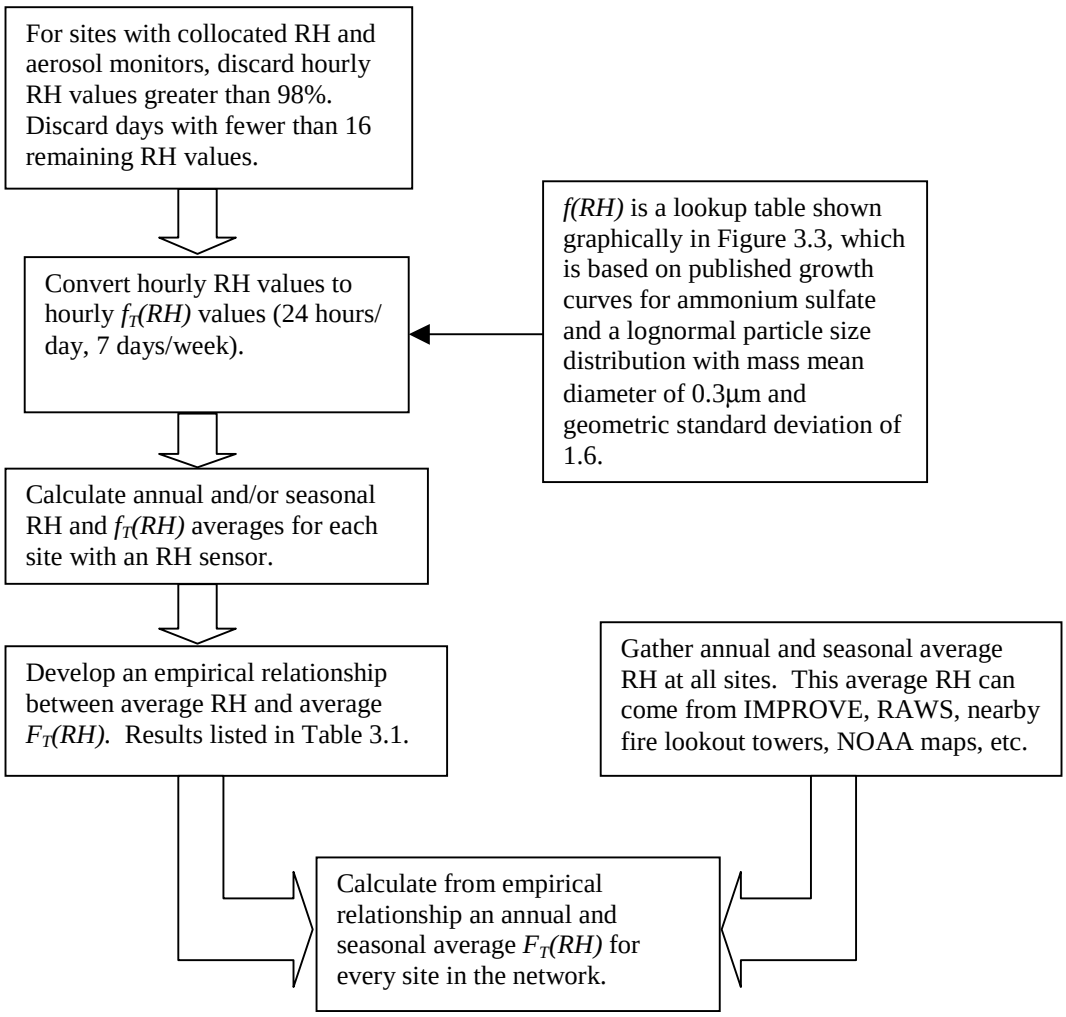

Figure 3.2 *The process by which IMPROVE data is used to develop site specific seasonal and annual RH correction factors.*

The extinction reconstruction process starting with the raw IMPROVE data through to the extinction calculation can be summarized:

(1) At those sites with collocated RH sensors and particle monitors, discard hourly RH values greater than 98% and discard days with less the 16 RH values.

(2) Convert the hourly RH to f(RH) values using the "smoothed" ammonium sulfate f_T(RH) versus RH lookup table shown graphically in Figure 3.3.

(3) Calculate annual and/or seasonal RH and f(RH) averages (F_T) (Equation (3.6)).

(4) Develop an empirical relationship between average RH and average F_T(RH) (Equation (3.7)).

(5) For the desired time period (annual or seasonal) find the average of the following species: sulfate, nitrate, organics, light-absorbing carbon, fine soil, and coarse mass.

(6) Using these averages calculate average reconstructed aerosol extinction according to the equation:

$$\begin{aligned} b_{ext} = {} & (3)F_T(RH)[\text{SULFATE}] \\ & + (3)F_T(RH)[\text{NITRATE}] \\ & + (4)[OMC] \\ & + (10)[LAC] \\ & + (1)[SOIL] \\ & + (0.6)[CM] \end{aligned} \tag{3.8}$$

where the parameters enclosed in the brackets are the average concentrations of each species.

The use of a 98% RH cutpoint is somewhat arbitrary, but it was chosen to allow for the likelihood that above 98%, precipitation would obscure visibility without regard to pollutant concentrations, and as an expedient measure because $f_T(RH)$ is infinite at 100% RH. The same $f_T(RH)$ was used in the first and second IMPROVE reports [Sisler et al., 1993; Sisler, 1996]. However, the assumptions used for estimating this curve will be investigated in light of more recent growth and particle size distribution data.

There are two ways reconstructed extinction is calculated in this report that are different from the 1996 IMPROVE report. First, the factor f(RH) that accounts for the relative humidity effects on hygroscopic aerosols has been upgraded with new relative humidity data from additional relative humidity monitoring sites and second, absorption is estimated from measurements of light-absorbing carbon rather than from transmission measurements of filter media. Therefore, some differences in aerosol extinction between this and the 1996 report are due to changes other than levels of aerosol mass concentration.

Visibility expressed as reconstructed deciview (dv) can now be calculated. The deciview is a visibility metric based on the light-extinction coefficient that expresses incremental changes in perceived visibility [Pitchford and Malm, 1994]. Because the deciview expresses a relationship between changes in light extinction and perceived visibility, it can be useful in describing visibility trends. A 1-dv change is about a 10% change in extinction coefficient, which is a small but perceptible scenic change under many circumstances. The deciview is defined by the following equation:

$$dv = 10\ln(b_{ext}/10) \tag{3.9}$$

The deciview scale is near zero for pristine atmosphere (dv = 0 for Rayleigh condition at about 1.8 km elevation) and increases as visibility is degraded.

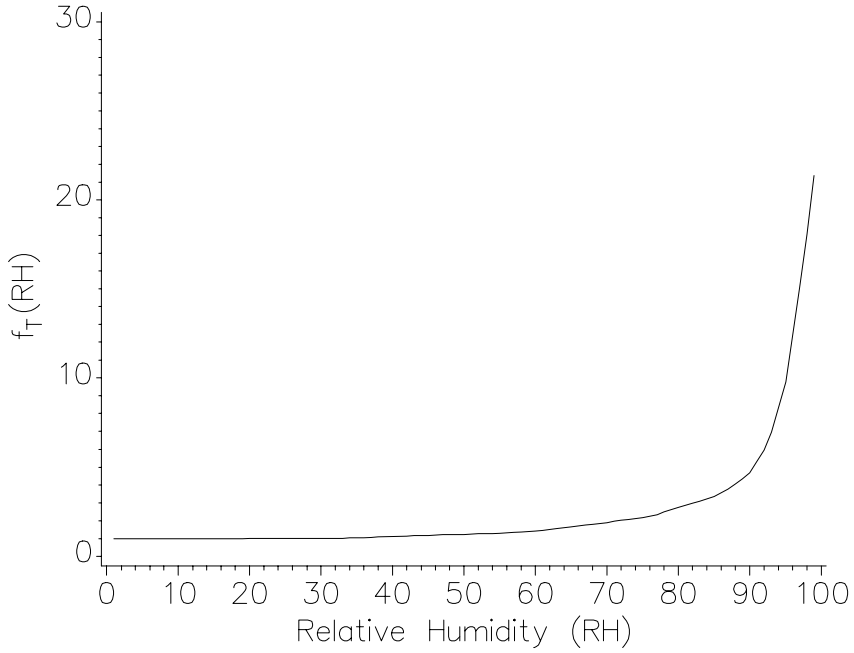

Figure 3.3 *RH factors (f_T (RH)) derived from Tang's ammonium sulfate growth curves smoothed between the crystallization and deliquescence points.*

3.2 RECONSTRUCTED LIGHT EXTINCTION AND LIGHT-EXTINCTION BUDGETS

Spatial patterns in the reconstructed light extinction are similar to those observed for aerosols since reconstructed light extinction is calculated from aerosol concentrations. However, because specific scattering of sulfates and nitrates are larger than other fine aerosols because of associated water, light-absorbing carbon has relatively high specific extinction, and coarse particle scattering contributes to total aerosol extinction, the extinction budgets are somewhat different from fine aerosol budgets.

3.2.1 Characteristics of the Regions

Tables 3.2, 3.3, and 3.4 summarize the seasonal and annual averages of the reconstructed light extinction coefficients for each of the 20 regions in the United States averaged over three years, March 1996 through February 1999.

Table 3.2 shows the breakdown of extinction among fine and coarse particle scattering and light absorption. In addition, this table shows the percentage of total light extinction (including Rayleigh scattering) that is caused by aerosol light extinction (both scattering and absorption). Also, the average relative humidity for each region is reported. Table 3.3 shows the aerosol light extinction as well as the contributions of sulfate, nitrate, organic carbon, light absorption, and coarse particles (including fine soil). Table 3.4 shows the aerosol light-extinction budgets: the fractions (percent) of

total aerosol (non-Rayleigh) light extinction contributed by sulfate, nitrate, organic carbon, light absorption, and coarse particles (including fine soil).

The characteristics of each region are briefly discussed.

Alaska. The Alaska region consists only of the measurements at Denali National Park and Preserve. The three-year annual average extinction is 20 1/Mm, of which aerosol extinction constituted 50%. The seasonal variation is small and varies from a low of 17.9 1/Mm in the winter to a high of 22.3 1/Mm in the summer. However, the extinction attributable to nitrate and organics show significant seasonal variation. Nitrate extinction ranges from a low of 0.3 1/Mm in the summer to a high of 0.8 1/Mm in the winter. Organic extinction, on the other hand, is highest in the summer at 5.5 1/Mm and lowest in the winter at 1.2 1/Mm. Sulfate is the largest contributor to aerosol extinction at an annual average of 38.9% and ranges from a seasonal high in the spring of 46.8% to a summer low of 28.2%. The next largest contributor is organics at a seasonal average of 27% ranges from a summer high of 44.4% to a winter low of 15.8%. The remaining contributors on an annual basis in order of importance are, soil and coarse particles (both at 19.9%), light-absorbing carbon (9.7%), and nitrate (4.5%).

Appalachian Mountains. This region consists of Dolly Sods Wilderness Area in West Virginia, Shenandoah, Great Smoky Mountains National Parks, and Shining Rock Wilderness Area in North Carolina. With an annual extinction of 98.5 1/Mm this region is typical of many eastern rural venues. The seasonal variation of extinction is about a factor of 3, ranging from 61 1/Mm in the winter to 169 1/Mm during summer. The seasonal variation is almost entirely due to sulfate extinction, which varies by a factor of 4 from 34.6 1/Mm in the winter to 136.3 1/Mm in the summer. Similarly, extinction due to organics, which averages 9.4 1/Mm annually, varies from a winter low of 6.8 1/Mm to 12.5 1/Mm during the summer. Nitrate extinction at 2.7 1/Mm is lowest in the summer and in the spring it peaks at 5.2 1/Mm and in the winter 4.0 1/Mm. The seasonal variation of sulfates, organics, and nitrates are driven by seasonal changes in meteorology and photochemistry. For sulfates and organics this leads to higher concentrations during the summer. This coupled with the fact that RH is highest in the summer leads to high specific scatttering for sulfate aerosols. Nitrates, on the other hand, are volatile. The lower temperatures during the winter and spring lead to higher concentrations of nitrates. Sulfate extinction comprises the largest fraction of aerosol extinction accounting for 77.1% annually and varies from a high during the summer of 85.7% down to 67.9% in the winter. The next highest contributor on an annual basis is organics (10.6%), followed by nitrate (4.6%), light-absorbing carbon (4.2%), and soil and coarse particles (3.5%).

Boundary Waters. The Boundary Waters Canoe Area represents this region in northern Minnesota, in the Superior National Forest. Annual average extinction here is about 44.6 1/Mm of which 78% is due to the ambient aerosol. The seasonal variation is significant, and ranges from a high in the winter of 52.9 1/Mm to as low as 36.3 1/Mm in the spring. Sulfate contributes the most to extinction (54.1%), the next largest contributor is organics (17%) followed by nitrate (16.3%), soil and coarse particles (7.2%) and light-absorbing carbon (5.4%).

Table 3.2 *Seasonal and annual averages of reconstructed total light-extinction coefficient (including Rayleigh) for the 21 regions in the IMPROVE Network. Also shown are the light scatterings resulting from fine and coarse aerosols, light absorption for carbonaceous aerosol, percentage of total extinction resulting from aerosol extinction and the average regional relative humidity.*

Season	Total Reconstructed Extinction (1/Mm)	Fine Reconstructed Scattering (1/Mm)	Coarse Scattering (1/Mm)	Absorption (1/Mm)	Percent Aerosol	Relative Humidity (%)
Alaska						
ANNUAL	20.0	7.0	2.0	1.0	50	65
Spring	20.0	6.9	2.2	0.9	50	56
Summer	22.3	9.2	2.1	1.0	55	64
Autumn	18.7	5.5	2.1	1.1	47	72
Winter	17.9	5.5	1.5	0.9	44	68
Appalachian						
ANNUAL	98.5	81.6	3.1	3.7	90	71
Spring	78.8	61.6	3.6	3.6	87	64
Summer	169.0	151.5	3.7	3.8	94	79
Autumn	88.9	71.9	2.8	4.1	89	69
Winter	61.0	45.4	2.3	3.3	84	71
Boundary Waters						
ANNUAL	44.6	30.3	2.5	1.9	78	71
Spring	36.3	22.4	2.4	1.4	72	61
Summer	48.0	32.8	2.9	2.3	79	69
Autumn	43.8	28.7	3.0	2.2	77	77
Winter	52.9	39.2	1.9	1.8	81	79
Cascade Mountains						
ANNUAL	41.5	26.6	2.2	2.7	76	77
Spring	37.6	23.7	1.9	2.0	73	76
Summer	50.9	34.3	3.1	3.6	80	71
Autumn	41.4	25.9	2.2	3.3	76	78
Winter	26.6	13.4	1.5	1.6	62	85
Central Rocky Mountains						
ANNUAL	23.8	10.0	2.6	1.3	58	56
Spring	27.7	13.4	3.1	1.2	64	64
Summer	26.2	11.7	3.0	1.5	62	46
Autumn	23.5	9.7	2.4	1.4	57	55
Winter	18.7	6.1	1.7	0.9	46	60
Colorado Plateau						
ANNUAL	25.6	10.7	3.2	1.7	61	48
Spring	26.2	10.3	4.2	1.6	62	45
Summer	28.3	12.8	3.7	1.8	65	41
Autumn	24.8	10.3	2.7	1.8	60	46
Winter	22.0	8.5	2.1	1.4	55	59
Great Basin						
ANNUAL	22.9	8.1	3.4	1.4	56	50
Spring	22.1	8.1	2.8	1.2	55	53
Summer	27.4	10.6	5.2	1.6	63	39
Autumn	22.0	7.7	3.0	1.3	55	47
Winter	17.5	4.6	1.8	1.2	43	59

***Table 3.2** Continued.*

Season	Total Reconstructed Extinction (1/Mm)	Fine Reconstructed Scattering (1/Mm)	Coarse Scattering (1/Mm)	Absorption (1/Mm)	Percent Aerosol	Relative Humidity (%)
Mid Atlantic						
ANNUAL	103.0	79.6	8.3	5.1	90	71
Spring	110.1	83.9	12.0	4.2	91	73
Summer	146.2	123.0	8.6	4.7	93	77
Autumn	84.6	63.4	5.3	5.9	88	69
Winter	79.5	57.0	6.7	5.8	87	67
Mid South						
ANNUAL	120.5	101.9	3.8	4.8	92	73
Spring	90.9	72.4	4.0	4.4	89	66
Summer	200.8	180.9	5.3	4.6	95	80
Autumn	124.3	105.1	3.5	5.7	92	74
Winter	79.6	63.0	2.3	4.3	87	71
Northeast						
ANNUAL	55.4	40.4	2.5	2.5	82	72
Spring	44.9	30.1	2.7	2.1	78	66
Summer	77.7	62.4	2.5	2.8	87	73
Autumn	51.7	36.6	2.5	2.5	81	76
Winter	47.1	32.3	2.2	2.6	79	73
Northern Great Plains						
ANNUAL	36.7	21.5	3.7	1.4	73	63
Spring	40.2	24.9	4.0	1.3	75	62
Summer	38.1	22.5	4.2	1.5	74	61
Autumn	34.8	19.3	3.9	1.6	71	60
Winter	33.6	19.5	2.9	1.2	70	69
Northern Rocky Mountains						
ANNUAL	41.8	23.9	4.3	3.6	76	76
Spring	42.2	25.7	3.3	3.1	76	76
Summer	41.7	21.3	7.4	3.0	76	69
Autumn	45.9	26.6	4.2	5.1	78	79
Winter	37.3	22.0	2.2	3.1	73	83
Pacific Coastal Mountains						
ANNUAL	47.3	31.2	4.2	1.9	79	72
Spring	45.9	29.9	4.4	1.7	78	72
Summer	53.9	38.2	4.5	1.2	81	71
Autumn	44.7	27.4	4.7	2.6	78	70
Winter	36.1	20.8	3.4	2.0	72	73
Sierra-Humboldt						
ANNUAL	23.8	9.8	2.2	1.8	58	61
Spring	22.8	9.1	2.3	1.4	56	63
Summer	32.7	17.3	2.9	2.5	69	69
Autumn	23.5	9.4	1.9	2.1	57	51
Winter	16.6	3.8	1.6	1.1	40	62
Sierra Nevada						
ANNUAL	45.1	26.0	5.4	3.8	78	51
Spring	42.6	24.1	5.2	3.3	77	59
Summer	51.1	28.4	7.8	4.9	80	42
Autumn	46.5	25.6	6.2	4.7	78	45
Winter	37.5	22.8	2.4	2.3	73	56

***Table 3.2** Continued.*

Season	Total Reconstructed Extinction (1/Mm)	Fine Reconstructed Scattering (1/Mm)	Coarse Scattering (1/Mm)	Absorption (1/Mm)	Percent Aerosol	Relative Humidity (%)
Sonoran Desert						
ANNUAL	29.4	12.9	4.7	1.8	66	42
Spring	28.6	10.9	6.2	1.5	65	35
Summer	32.9	15.8	5.5	1.6	70	41
Autumn	30.0	13.6	4.2	2.2	67	40
Winter	25.1	10.4	2.9	1.8	60	52
Southeast						
ANNUAL	109.2	87.7	6.5	5.1	91	75
Spring	103.5	81.6	6.8	5.0	90	70
Summer	124.8	103.0	8.3	3.5	92	77
Autumn	119.0	97.9	5.8	5.3	92	78
Winter	87.1	65.6	5.2	6.3	89	75
Southern California						
ANNUAL	52.8	34.4	4.7	3.7	81	48
Spring	68.9	49.7	5.1	4.0	85	54
Summer	57.2	35.8	6.3	5.0	83	44
Autumn	39.1	21.4	4.6	3.1	74	42
Winter	36.0	21.6	2.2	2.2	72	52
Wasatch						
ANNUAL	33.9	16.6	4.0	3.3	70	55
Spring	31.0	14.5	3.7	2.8	68	54
Summer	36.7	17.1	5.4	4.2	73	41
Autumn	31.1	14.2	3.6	3.3	68	54
Winter	38.0	22.1	3.1	2.8	74	70
Washington, D.C.						
ANNUAL	115.8	90.6	3.7	11.5	91	65
Spring	104.3	80.4	3.8	10.1	90	62
Summer	147.5	123.4	3.5	10.7	93	68
Autumn	116.3	89.0	4.4	12.9	91	68
Winter	97.0	71.3	3.2	12.6	90	62
West Texas						
ANNUAL	36.1	18.7	5.7	1.7	72	45
Spring	38.5	18.2	8.4	1.9	74	37
Summer	39.6	22.0	6.3	1.3	75	48
Autumn	37.1	21.4	3.8	1.8	73	49
Winter	28.8	13.0	4.1	1.6	65	47

Table 3.3 *Seasonal and annual averages of reconstructed aerosol light-extinction coefficient for the 21 regions in the IMPROVE Network. Also shown are light extinctions resulting from sulfate, nitrate, organic carbon, light-absorbing carbon, and soil and coarse particles.*

Season	Aerosol Reconstructed Extinction (1/Mm)	Sulfate (1/Mm)	Nitrate (1/Mm)	Organics (1/Mm)	Light-Absorbing Carbon (1/Mm)	Soil and Coarse (1/Mm)
Alaska						
ANNUAL	10.0	3.9	0.4	2.7	1.0	2.0
Spring	10.0	4.7	0.4	1.8	0.9	2.2
Summer	12.3	3.5	0.3	5.5	1.0	2.1
Autumn	8.7	3.2	0.4	1.9	1.1	2.1
Winter	7.9	3.5	0.8	1.2	0.9	1.5
Appalachian						
ANNUAL	88.5	68.2	4.0	9.4	3.7	3.1
Spring	68.8	47.9	5.2	8.5	3.6	3.6
Summer	159.0	136.3	2.7	12.5	3.8	3.7
Autumn	78.9	58.9	3.7	9.3	4.1	2.8
Winter	51.0	34.6	4.0	6.8	3.3	2.3
Boundary Waters						
ANNUAL	34.6	18.7	5.6	5.9	1.9	2.5
Spring	26.3	14.4	3.8	4.2	1.4	2.4
Summer	38.0	20.3	1.2	11.3	2.3	2.9
Autumn	33.8	17.3	5.3	6.1	2.2	3.0
Winter	42.9	22.4	12.8	4.0	1.8	1.9
Cascade Mountains						
ANNUAL	31.5	16.6	3.3	6.7	2.7	2.2
Spring	27.6	16.0	3.1	4.6	2.0	1.9
Summer	40.9	21.3	3.3	9.7	3.6	3.1
Autumn	31.4	14.3	3.1	8.5	3.3	2.2
Winter	16.6	6.8	3.2	3.4	1.6	1.5
Central Rocky Mountains						
ANNUAL	13.8	5.2	1.0	3.9	1.3	2.6
Spring	17.7	8.0	2.0	3.5	1.2	3.1
Summer	16.2	5.2	0.7	5.8	1.5	3.0
Autumn	13.5	5.1	0.8	3.9	1.4	2.4
Winter	8.7	3.3	0.8	2.0	0.9	1.7
Colorado Plateau						
ANNUAL	15.6	5.8	1.1	3.8	1.7	3.2
Spring	16.2	5.0	1.4	3.9	1.6	4.2
Summer	18.3	6.9	0.9	4.9	1.8	3.7
Autumn	14.8	5.9	0.7	3.6	1.8	2.7
Winter	12.0	4.6	1.5	2.5	1.4	2.1
Great Basin						
ANNUAL	12.9	3.2	0.7	4.2	1.4	3.4
Spring	12.1	3.7	0.9	3.4	1.2	2.8
Summer	17.4	3.6	0.7	6.4	1.6	5.2
Autumn	12.0	3.3	0.6	3.8	1.3	3.0
Winter	7.5	1.5	0.6	2.4	1.2	1.8

Table 3.3 *Continued.*

Season	Aerosol Reconstructed Extinction (1/Mm)	Sulfate (1/Mm)	Nitrate (1/Mm)	Organics (1/Mm)	Light-Absorbing Carbon (1/Mm)	Soil and Coarse (1/Mm)
Mid Atlantic						
ANNUAL	93.0	61.4	8.6	9.6	5.1	8.3
Spring	100.1	65.9	10.9	7.1	4.2	12.0
Summer	136.2	105.1	5.8	12.1	4.7	8.6
Autumn	74.6	47.2	6.6	9.5	5.9	5.3
Winter	69.5	37.8	9.3	9.9	5.8	6.7
Mid South						
ANNUAL	110.5	81.6	8.8	11.4	4.8	3.8
Spring	80.9	53.1	8.6	10.7	4.4	4.0
Summer	190.8	161.5	5.3	14.1	4.6	5.3
Autumn	114.3	85.3	7.5	12.4	5.7	3.5
Winter	69.6	42.3	12.4	8.3	4.3	2.3
Northeast						
ANNUAL	45.4	30.9	3.3	6.2	2.5	2.5
Spring	34.9	22.7	2.9	4.6	2.1	2.7
Summer	67.7	50.7	2.3	9.5	2.8	2.5
Autumn	41.7	27.6	3.4	5.6	2.5	2.5
Winter	37.1	22.4	4.7	5.2	2.6	2.2
Northern Great Plains						
ANNUAL	26.7	13.0	4.0	4.5	1.4	3.7
Spring	30.2	15.5	5.8	3.6	1.3	4.0
Summer	28.1	14.5	1.1	6.8	1.5	4.2
Autumn	24.8	11.2	3.1	4.9	1.6	3.9
Winter	23.6	10.8	6.1	2.7	1.2	2.9
Northern Rocky Mountains						
ANNUAL	31.8	11.1	2.8	10.1	3.6	4.3
Spring	32.2	14.0	2.8	9.0	3.1	3.3
Summer	31.7	9.3	1.4	10.6	3.0	7.4
Autumn	35.9	10.3	2.4	13.9	5.1	4.2
Winter	27.3	10.4	4.8	6.8	3.1	2.2
Pacific Coastal Mountains						
ANNUAL	37.3	17.9	8.0	5.3	1.9	4.2
Spring	35.9	17.5	7.7	4.7	1.7	4.4
Summer	43.9	26.9	7.0	4.3	1.2	4.5
Autumn	34.7	14.2	6.1	7.1	2.6	4.7
Winter	26.1	7.4	8.4	4.9	2.0	3.4
Sierra-Humboldt						
ANNUAL	13.8	3.9	1.0	5.0	1.8	2.2
Spring	12.8	4.3	1.2	3.6	1.4	2.3
Summer	22.7	7.9	1.7	7.8	2.5	2.9
Autumn	13.5	2.6	0.7	6.1	2.1	1.9
Winter	6.6	1.4	0.6	1.9	1.1	1.6
Sierra Nevada						
ANNUAL	35.1	8.6	6.3	11.1	3.8	5.4
Spring	32.6	9.2	6.5	8.4	3.3	5.2
Summer	41.1	9.4	2.6	16.4	4.9	7.8
Autumn	36.5	6.3	5.0	14.2	4.7	6.2
Winter	27.5	4.8	12.1	5.9	2.3	2.4

Table 3.3 *Continued.*

Season	Aerosol Reconstructed Extinction (1/Mm)	Sulfate (1/Mm)	Nitrate (1/Mm)	Organics (1/Mm)	Light-Absorbing Carbon (1/Mm)	Soil and Coarse (1/Mm)
Sonoran Desert						
ANNUAL	19.4	7.3	1.1	4.4	1.8	4.7
Spring	18.6	5.1	1.2	4.6	1.5	6.2
Summer	22.9	10.4	1.0	4.5	1.6	5.5
Autumn	20.0	7.8	0.8	5.0	2.2	4.2
Winter	15.1	5.4	1.5	3.5	1.8	2.9
Southeast						
ANNUAL	99.2	70.8	5.4	11.4	5.1	6.5
Spring	93.5	65.1	5.6	10.9	5.0	6.8
Summer	114.8	87.6	4.5	10.8	3.5	8.3
Autumn	109.0	81.9	4.8	11.2	5.3	5.8
Winter	77.1	47.2	5.7	12.7	6.3	5.2
Southern California						
ANNUAL	42.8	9.7	16.5	8.1	3.7	4.7
Spring	58.9	11.9	28.9	9.0	4.0	5.1
Summer	47.2	11.5	12.2	12.1	5.0	6.3
Autumn	29.1	6.4	8.8	6.3	3.1	4.6
Winter	26.0	3.9	13.7	4.0	2.2	2.2
Wasatch						
ANNUAL	23.9	6.6	3.7	6.3	3.3	4.0
Spring	21.0	6.2	3.0	5.2	2.8	3.7
Summer	26.7	5.6	1.4	10.1	4.2	5.4
Autumn	21.1	6.6	2.2	5.4	3.3	3.6
Winter	28.0	7.3	10.8	4.0	2.8	3.1
Washington, D.C.						
ANNUAL	105.8	61.7	13.5	15.3	11.5	3.7
Spring	94.3	55.0	13.7	11.8	10.1	3.8
Summer	137.5	100.2	6.8	16.4	10.7	3.5
Autumn	106.3	57.7	15.4	16.0	12.9	4.4
Winter	87.0	36.3	17.5	17.4	12.6	3.2
West Texas						
ANNUAL	26.1	12.5	1.3	4.9	1.7	5.7
Spring	28.5	10.0	1.4	6.8	1.9	8.4
Summer	29.6	15.5	1.5	5.0	1.3	6.3
Autumn	27.1	16.1	0.8	4.5	1.8	3.8
Winter	18.8	8.6	1.3	3.1	1.6	4.1

Table 3.4 *Seasonal and annual averages of percentage contributions to the reconstructed aerosol light-extinction coefficient (light-extinction budget) for the 21 regions in the IMPROVE Network for sulfate, nitrate, organic carbon, light-absorbing carbon, and soil and coarse particles.*

Season	Sulfate	Nitrate	Organics	Light-Absorbing Carbon	Soil and Coarse
Alaska					
ANNUAL	38.9	4.5	27.0	9.7	19.9
Spring	46.8	3.8	18.2	9.1	22.1
Summer	28.2	2.2	44.4	8.1	17.0
Autumn	37.4	4.4	21.9	12.1	24.2
Winter	43.8	9.6	15.8	11.3	19.5
Appalachian					
ANNUAL	77.1	4.6	10.6	4.2	3.5
Spring	69.6	7.5	12.3	5.3	5.2
Summer	85.7	1.7	7.9	2.4	2.3
Autumn	74.7	4.7	11.8	5.2	3.6
Winter	67.9	7.8	13.4	6.5	4.5
Boundary Waters					
ANNUAL	54.1	16.3	17.0	5.4	7.2
Spring	54.9	14.4	16.0	5.5	9.1
Summer	53.6	3.1	29.8	5.9	7.6
Autumn	51.2	15.6	18.0	6.4	8.8
Winter	52.3	29.9	9.3	4.1	4.3
Cascade Mountains					
ANNUAL	52.8	10.5	21.1	8.4	7.1
Spring	58.0	11.0	16.8	7.3	6.8
Summer	52.1	8.0	23.6	8.7	7.6
Autumn	45.4	9.9	27.1	10.5	7.1
Winter	41.1	19.2	20.6	9.8	9.3
Central Rocky Mountains					
ANNUAL	37.3	7.1	27.8	9.1	18.7
Spring	44.9	11.3	19.5	6.8	17.6
Summer	32.1	4.6	35.6	9.1	18.6
Autumn	37.6	5.6	28.7	10.4	17.6
Winter	37.8	9.5	22.9	10.5	19.3
Colorado Plateau					
ANNUAL	37.2	7.2	24.2	10.7	20.7
Spring	30.9	8.8	24.3	9.9	26.2
Summer	37.9	5.0	27.0	10.0	20.1
Autumn	40.2	5.0	24.6	11.9	18.3
Winter	37.8	12.4	20.5	11.8	17.5
Great Basin					
ANNUAL	24.8	5.6	32.6	10.7	26.3
Spring	31.0	7.7	28.0	9.7	23.6
Summer	20.7	3.9	36.6	9.1	29.7
Autumn	27.8	5.2	31.3	11.1	24.6
Winter	20.5	7.9	32.2	16.1	23.3

***Table 3.4** Continued.*

Season	Sulfate	Nitrate	Organics	Light-Absorbing Carbon	Soil and Coarse
Mid Atlantic					
ANNUAL	66.1	9.2	10.3	5.5	8.9
Spring	65.8	10.9	7.1	4.2	12.0
Summer	77.1	4.3	8.9	3.4	6.3
Autumn	63.3	8.9	12.7	7.9	7.2
Winter	54.3	13.4	14.2	8.4	9.6
Mid South					
ANNUAL	73.9	8.0	10.3	4.3	3.5
Spring	65.7	10.6	13.3	5.5	5.0
Summer	84.7	2.8	7.4	2.4	2.8
Autumn	74.6	6.5	10.8	5.0	3.1
Winter	60.7	17.8	11.9	6.2	3.4
Northeast					
ANNUAL	67.9	7.4	13.7	5.5	5.5
Spring	65.0	8.3	13.1	6.0	7.7
Summer	74.9	3.3	14.0	4.1	3.6
Autumn	66.1	8.2	13.5	6.1	6.1
Winter	60.4	12.6	14.1	7.0	6.0
Northern Great Plains					
ANNUAL	48.8	14.9	17.0	5.3	14.0
Spring	51.4	19.3	12.0	4.2	13.2
Summer	51.7	3.8	24.3	5.4	14.7
Autumn	45.2	12.7	19.8	6.6	15.7
Winter	45.7	25.7	11.3	5.1	12.1
Northern Rocky Mountains					
ANNUAL	34.8	8.7	31.7	11.3	13.4
Spring	43.6	8.6	27.9	9.8	10.2
Summer	29.2	4.5	33.5	9.5	23.3
Autumn	28.7	6.7	38.8	14.3	11.6
Winter	38.2	17.5	24.9	11.4	8.0
Pacific Coastal Mountains					
ANNUAL	47.9	21.5	14.2	5.0	11.4
Spring	48.7	21.5	13.1	4.6	12.1
Summer	61.3	16.0	9.8	2.7	10.3
Autumn	41.0	17.6	20.4	7.4	13.6
Winter	28.3	32.2	18.9	7.6	12.8
Sierra-Humbolt					
ANNUAL	27.8	7.1	35.9	13.2	15.9
Spring	33.4	9.5	27.9	10.9	18.3
Summer	34.8	7.3	34.2	11.0	12.6
Autumn	19.6	5.2	45.3	15.9	14.0
Winter	21.4	8.5	28.6	17.1	24.5
Sierra Nevada					
ANNUAL	24.4	17.8	31.6	10.7	15.4
Spring	28.3	19.8	25.8	10.1	16.0
Summer	23.0	6.3	39.8	11.8	19.0
Autumn	17.4	13.7	39.0	12.8	17.1
Winter	17.4	44.0	21.5	8.4	8.7

***Table 3.4** Continued.*

Season	Sulfate	Nitrate	Organics	Light-Absorbing Carbon	Soil and Coarse
Sonoran Desert					
ANNUAL	37.9	5.9	22.7	9.1	24.4
Spring	27.2	6.7	24.6	8.3	33.3
Summer	45.3	4.5	19.5	6.8	23.9
Autumn	39.2	4.0	25.1	10.8	20.9
Winter	35.5	10.0	23.3	12.1	19.0
Southeast					
ANNUAL	71.4	5.4	11.5	5.1	6.6
Spring	69.6	6.0	11.7	5.4	7.3
Summer	76.3	4.0	9.4	3.0	7.3
Autumn	75.1	4.4	10.3	4.9	5.3
Winter	61.2	7.4	16.5	8.2	6.7
Southern California					
ANNUAL	22.7	38.6	19.0	8.6	11.1
Spring	20.2	49.0	15.3	6.8	8.7
Summer	24.4	25.8	25.7	10.7	13.4
Autumn	21.8	30.1	21.7	10.7	15.8
Winter	15.1	52.9	15.2	8.5	8.4
Wasatch					
ANNUAL	27.8	15.7	26.2	13.7	16.7
Spring	29.7	14.4	24.8	13.2	17.8
Summer	20.8	5.1	38.0	15.7	20.3
Autumn	31.1	10.5	25.6	15.8	16.9
Winter	26.1	38.5	14.4	9.8	11.1
Washington, D.C.					
ANNUAL	58.4	12.7	14.5	10.9	3.5
Spring	58.4	14.5	12.5	10.7	4.0
Summer	72.9	5.0	11.9	7.8	2.5
Autumn	54.2	14.5	15.0	12.1	4.1
Winter	41.7	20.1	20.0	14.4	3.7
West Texas					
ANNUAL	47.8	5.0	18.8	6.4	22.0
Spring	35.1	5.0	23.9	6.7	29.4
Summer	52.3	5.1	16.9	4.3	21.4
Autumn	59.5	3.1	16.6	6.8	14.0
Winter	45.6	7.1	16.7	8.6	22.0

Cascade Mountains. Three sites, Mount Rainier National Park southeast of Seattle, Snoqualmie Pass to the northeast of Seattle, and Three Sisters Wilderness Area in Oregon now represent this region. The average annual extinction for this region is 41.5 1/Mm, of which 76% is due to aerosols. The seasonality is significant and ranges from a high in the summer of 50.9 1/Mm then drops to a low in the winter of 26.6 1/Mm. The seasonality is driven primarily by sulfate. Sulfate extinction ranges from a summer high of 21.3 1/Mm then drops to 6.8 1/Mm in the summer. Organics also show significant variance between seasons with an annual average value of 6.7 1/Mm and a minimum of 3.4 1/Mm in the winter to as high as 9.7 1/Mm in the summer. The largest contributor to aerosol extinction is sulfate (52.8%), followed by organics (21.1%), nitrate (10.5%), light-absorbing carbon (8.4%), and coarse extinction (7.1%).

Central Rocky Mountains. The measurements in this region were made at six locations in the mountainous Class I areas of Colorado and Wyoming, including the Bridger, Mount Zirkel, and Weminuche Wilderness Areas, Rocky Mountain and Yellowstone National Parks, and Great Sand Dunes National Monument. Monitoring began in the summer of 1994 at Mount Zirkel, and the other five sites have operated since March of 1988. The six sites show an annual average total extinction for the three-year period of 23.8 1/Mm, of which 58% is due to aerosol extinction. The seasonal variation is relatively small and has a maximum in the spring and summer of 27.7 and 26.2 1/Mm, respectively, and decreases to 18.7 1/Mm during the winter. Extinction due to organics, and absorption is highest in the summer and least in the winter. Organic extinction peaks at 5.8 1/Mm in the summer and drops in the winter to 2.0 1/Mm. Absorption ranges for 1.5 1/Mm in the summer and drops to 0.9 1/Mm in the winter. Sulfates (37.3%) contribute the most to extinction annually followed by organics (27.8%), soil and coarse (18.7%), light-absorbing carbon (9.1%), and nitrate is the smallest contributor (7.1%).

Colorado Plateau. This region in the Four Corners' states of the Southwest is the most intensively monitored in the IMPROVE Network. There are six sites, most of them within the so-called Golden Circle of National Parks: Bandelier, Bryce Canyon, Canyonlands, Grand Canyon, Mesa Verde, and Petrified Forest. The three-year annual average for total extinction is relatively low at 25.6 1/Mm, 61% of which is aerosol extinction. There is a very slight variance between seasons of total extinction ranging from 22 1/Mm in the winter to as high as 28.3 1/Mm during the summer. Sulfate extinction reaches its maximum at 6.9 1/Mm in summer and is lowest in winter at 4.6 1/Mm. Nitrate extinction is typically high during the winter at 1.5 1/Mm and lowest during the autumn at 0.7 1/Mm. The largest contribution to annual aerosol extinction is sulfate (37.2%) followed by organics (24.2%), soil and coarse particles (20.7%), light-absorbing carbon (10.7%), and nitrate (7.2%).

Great Basin. Two sites represent the Great Basin of Nevada, Jarbidge Wilderness Area in northeastern Nevada and Great Basin National Park. The annual average extinction during the three-year period for this region is quite low at 22.9 1/Mm, with 56% from aerosol extinction, the only region with less extinction is Alaska. A seasonal variation exists between 27.4 1/Mm during the summer and 17.5 1/Mm during the winter. On an annual basis the largest contributor to extinction is organics (32.6%) followed by soil and coarse particles (26.3%), and sulfate (24.8%). This region is unique in that sulfate is the third largest contributor to extinction. This holds for two out of the four seasons (summer and winter).

Mid Atlantic. This region, represented by the Edwin B. Forsythe National Wildlife Refuge, just west of Atlantic City, New Jersey, has an average annual reconstructed extinction of 103 1/Mm. There is a significant seasonality, with extinction moving from a high during the summer of 146.2 1/Mm, to 79.5 1/Mm in the winter. Sulfate extinction is 105.1 1/Mm in the summer and 37.8 1/Mm in the winter, and is responsible for most of the seasonality. Sulfates are responsible for about two thirds (66.1%) of the aerosol extinction, followed by organics (10.3%), nitrate (9.2%), soil and coarse particles (8.9%), and light-absorbing carbon (5.5%).

Mid South. Three sites represent this region: Sipsey Wilderness Area in northern Mississippi, Upper Buffalo Wilderness Area in northern Arkansas, and Mammoth Cave National Park in Kentucky. This region has the highest levels of reconstructed extinction. The average annual

reconstructed extinction is 120.5 1/Mm with a significant seasonal variation between the summer high of 200.8 1/Mm and the winter low of 79.6 1/Mm. Sulfate dominates the aerosol extinction and is responsible for much of the seasonality observed. Sulfate extinction is highest in the summer at 161.5 1/Mm and lowest in the winter at 42.3 1/Mm. Organics, and light-absorbing carbon all have seasonal trends that peak in the summer for organics and autumn for absorption but are lowest in the winter for organics and spring for absorption. On an annual average, sulfate contributes 73.9% of the aerosol extinction peaking in the summer (84.7%) and is least in the winter (60.7%). The next largest contributor annually is organics (10.3%), followed by nitrate (8%), light-absorbing carbon (4.3%), and soil and coarse particles (3.5%).

Northeast. The northeastern United States is represented by measurements at three sites: Acadia National Park and Moosehorn National Wildlife Refuge in Maine, and Lye Brook Wilderness Area in Vermont. The average annual extinction during the three-year period for the Northeast is 55.4 1/Mm of which aerosol extinction accounts for 82%. There is a significant seasonal variation from the spring minimum of 44.9 1/Mm and the highest during the summer at 77.7 1/Mm. Sulfates and organics are responsible for most of the seasonal variation with sulfates varying from 22.4 1/Mm to 50.7 1/Mm between winter and summer and organics varying between 4.6 1/Mm in the spring to 9.5 1/Mm in the summer. Nitrate extinction obtains its maximum during the winter at 4.7 1/Mm and its minimum at 2.3 1/Mm during the summer. The largest contributor to extinction is from sulfates at 67.9% annually. The next highest contributor is organics (13.7%), followed by nitrate (7.4%), and soil and coarse particles and light-absorbing carbon (both at 5.5%).

Northern Great Plains. Aerosol measurements were made at one site in this region, Badlands National Park in South Dakota, where reconstructed light extinction averaged 36.7 1/Mm. Unlike most other regions, extinction was highest in spring and lowest in winter. This seasonality is driven primarily by sulfate and nitrate extinction. Sulfate extinction reaches a maximum of 15.5 1/Mm in the spring and a minimum of 10.8 1/Mm in the winter. Nitrate extinction in the winter, 6.1 1/Mm, is almost six times its summer extinction of 1.1 1/Mm. The main contributor to annual extinction is sulfate, which accounts for 48.8% of the extinction. The next highest contributor is organics (17%), followed by nitrate (14.9%), soil and coarse particles (14%) and light-absorbing carbon (5.3%).

Northern Rocky Mountains. This region is represented by one site, Glacier National Park, which is close to the Canada border. The reconstructed light extinction coefficient is 41.8 1/Mm for an annual average of 76% due to aerosols. There is modest seasonality ranging between 45.9 1/Mm in the autumn down to 37.3 1/Mm during the winter. The seasonality is driven by sulfate and nitrate extinction. Sulfate and nitrate extinctions peak at 14 1/Mm and 4.8 1/Mm, during the spring and winter, respectively. The largest contributor to aerosol extinction is sulfate (34.8%) followed by organics (31.7%), soil and coarse particles (13.4%), light-absorbing carbon (11.3%), and nitrate (8.7%).

Pacific Coastal Mountains. This region includes three Class I areas near the coast of northern California: Pinnacles National Monument, Point Reyes National Seashore, and Redwood National Park. The average annual extinction during the three-year period for this area is 47.3 1/Mm with 79% due to aerosol extinction. The annual variance is moderate and ranges between 53.9 1/Mm during the summer and 36.1 1/Mm during the winter. Sulfate extinction reaches its maximum in the summer at 26.9 1/Mm when nitrate extinction is near its minimum at 7 1/Mm. When nitrate

extinction obtains its maximum of 8.4 1/Mm during the winter, sulfate extinction is at its minimum of 7.4 1/Mm. Organic extinction and absorption obtain their maxima in the autumn of 7.1 1/Mm and 2.6 1/Mm, respectively. On an annual basis, the largest contributor to aerosol extinction is sulfate (47.9%), followed by nitrate (21.5%), organics (14.2%), soil and coarse (11.4%), and light-absorbing carbon (5.0%). The contribution from sulfate shows considerable variation ranging from a high in the summer of 61.3% to 28.3% in the winter when its contribution is eclipsed by nitrate (32.2)%.

Sierra-Humboldt. The region in the Sierra Nevada and Humboldt Mountain Ranges was measured at Crater Lake National Park in Oregon and Lassen Volcanic National Park in northern California. For this region, total reconstructed light extinction averaged 23.8 1/Mm with maximum extinction in summer (32.7 1/Mm) and minimum extinction in winter (16.6 1/Mm). The seasonality is primarily due to variations in sulfate and organic extinctions and absorption. Organics contribute the most to extinction (35.9%), followed by sulfate (27.8%), soil and coarse particles (15.9%), light-absorbing carbon (13.2%), and nitrate (7.1%).

Sierra Nevada. Aerosols in the Sierra Nevada region are monitored at two sites: Yosemite and Sequoia National Parks. The average reconstructed light extinction is 45.1 1/Mm with a seasonal component that has a winter minimum of 37.5 1/Mm and a summer maximum of 51.1 1/Mm. The seasonality is driven primarily by organics and absorption with both species peaking during the summer at 16.4 1/Mm and 4.9 1/Mm, then dropping to their minimum at 5.9 1/Mm and 2.3 1/Mm during the winter. Sulfate, to a lesser extent, is responsible for the seasonality, its maximum occurs in the summer at 9.4 1/Mm and obtains its seasonal low in the winter at 4.8 1/Mm. Nitrate shows a very strong seasonal component with a winter high of 12.1 1/Mm to a summer low of 2.6 1/Mm. On an annual average, organics contribute the most to aerosol extinction (31.6%), followed by sulfate (24.4%), nitrate (17.8%), then soil and coarse particles (15.4%), and finally light-absorbing carbon (10.7%).

Sonoran Desert. This region in southeastern Arizona was measured at two sites: Chiracahua and Tonto National Monuments. The three-year average reconstructed extinction is 29.4 1/Mm and varies from a summer high of 32.9 1/Mm to a winter low of 25.1 1/Mm. The seasonality is due to changes in extinction from sulfate, organics, and absorption. Organics and absorption obtain their seasonal maxima of 5.0 1/Mm and 2.2 1/Mm during the autumn. Sulfate obtains its maximum extinction during the summer at 10.4 1/Mm and its minimum of 5.4 1/Mm in the winter. The largest contributor to extinction is sulfate (37.9%) followed by soil and coarse particles (24.4%), organics (22.7%), light-absorbing carbon (9.1%), and nitrate (5.9%).

Southeast. This region consists of three sites, Chassahowitzka National Wildlife Refuge north of Tampa, Florida, Okefenokee National Wildlife Refuge on the Georgia-Florida border, and Cape Romain National Wildlife Refuge on the South Carolina coast. The annual total extinction for this region is 109.2 1/Mm, 91% is due to aerosol extinction. A seasonal variance exists here, with summer having the most extinction of 124.8 1/Mm and winter the least at 87.1 1/Mm. The largest contributor to aerosol extinction is from sulfates (71.4%), followed by organics (11.7%), soil and coarse particles (6.6%), nitrate (5.4%), and light-absorbing carbon (5.1%).

Southern California. Measurements in this region were made in San Gorgonio Wilderness Area, east of the Los Angeles metropolitan area. Total reconstructed light extinction averaged over the three-year period was 52.8 1/Mm and varied from a seasonal high of 68.9 1/Mm in the spring to as little as 36.0 1/Mm in the winter. The seasonality is driven primarily by nitrates and to a lesser extent sulfate, organics, and absorption. This region is unique in that nitrates are by far the largest contributor to annual extinction (38.6%), followed by sulfate (22.7%), organics (19.0%), soil and coarse particles (11.1%), and light-absorbing carbon (8.6%).

Wasatch. This region is represented by the Lone Peak Wilderness Area northeast of Provo, Utah. It has an annual average extinction of 33.9 1/Mm. This area is somewhat unique in that it obtains the maximum light extinction during the winter of 38.0 1/Mm and the least during spring and autumn at 31.0 1/Mm and 31.1 1/Mm, respectively. This seasonality is driven by sulfate and nitrate extinction, which obtain their maximums during the winter of 7.3 1/Mm and 10.8 1/Mm, respectively, while organics and absorption peak in the summer at 10.1 1/Mm and 4.2 1/Mm, respectively. On average sulfate (27.8%) and organics (26.2%) contribute almost equally to aerosol extinction followed by soil and coarse particles (16.7%), nitrate (15.7%), and light-absorbing carbon (13.7%).

West Texas. Total light extinction reconstructed from the aerosol measurements at Big Bend and Guadalupe Mountains National Parks averaged 36.1 1/Mm over the three-year period. Seasonality is evident with the highest extinction in the summer (39.6 1/Mm) and the least during the winter (28.8 1/Mm). The seasonality is primarily due to sulfate, which is the largest contributor to aerosol extinction (47.8%), soil and coarse particles (22%), followed by organics (18.8%), light-absorbing carbon (6.4%), and nitrate (5%).

3.2.2 Spatial Trends in Reconstructed Light Extinction in the United States

Figure 3.4, based only on IMPROVE data, shows isopleths of the reconstructed aerosol light extinction coefficient (excluding Rayleigh) for the three-year period, March 1996 through February 1999. The highest light extinction (>100 1/Mm) occurs in the eastern United States; the highest extinction for a rural site occurs at Mammoth Cave at 130 1/Mm, then Sipsey Wilderness Area in northern Alabama at 128 1/Mm, followed by Cape Romain and Okefenokee National Wildlife Refuges at 106 1/Mm and 100 1/Mm, respectively. The lowest extinction (<20 1/Mm) generally occurs in the inner-mountain west in the Great Basin and Colorado Plateau regions. The lowest extinction for the contiguous 48 states is at Bridger Wilderness Area and Great Basin National Park at 12 1/Mm. The lowest extinction for the entire United States is at Denali National Park, with an annual extinction of 10 1/Mm. Crater Lake National Park and Jarbidge and Mount Zirkel Wilderness Areas have 13 1/Mm for annual extinction.

Because the majority of Class I areas with IMPROVE monitoring are located in the western United States, spatial coverage of the IMPROVE Network is sparse in the eastern United States. As a result, maps based on IMPROVE data alone, such as Figure 3.4, lack spatial resolution in the eastern United States, where visibility conditions are traditionally the worst. For comparison to Figure 3.4, Figure 3.5 shows the reconstructed aerosol light extinction coefficient using particle mass concentration data from IMPROVE monitoring sites (diamonds) and from monitoring sites in the Clean Air Status and Trends Network (CASTNet) [CASTNet, 1998] (plusses). Details of the

light extinction reconstruction algorithm applied to CASTNet data are given in Appendix A. At the time of this writing, CASTNet data were available only through 1998, therefore Figure 3.5 represents the three-year period, December 1995 through November 1998 instead of March 1996 through February 1999 that is used in the IMPROVE only isopleth maps. However, average aerosol mass concentrations, and hence reconstructed visibility conditions, for the respective time periods represented by Figures 3.4 and 3.5 should be comparable because the time periods for the two maps only differ by three out of 36 months. Figure 3.5 shows the highest light extinction coefficients, in excess of 120 1/Mm, occurring at monitoring locations in the eastern United States and in the general region defined by the Ohio River and Tennessee Valleys. This region of highest light extinction has better spatial resolution and larger geographic extent in the IMPROVE and CASTNet map than in the IMPROVE only map. The lowest extinction (<20 1/Mm) generally occurs in the rural western United States, as indicated by the reconstructed light extinction coefficient derived from both IMPROVE and CASTNet monitoring data in those regions. Similar combined monitoring network light extinction maps for the winter and summer seasons are shown in Appendix A.

Figure 3.6 shows the sulfate light extinction coefficient averaged over a three-year period of IMPROVE (March 1996 - February 1999). Note that the highest sulfate extinction occurs in the eastern United States, and the lowest sulfate extinction occurs in the Great Basin, Sierra-Nevada and Sierra-Humboldt regions. The major gradient in sulfate light extinction is from the eastern United States to the inner-mountain west. However, there is also a gradient from the Pacific Coastal Mountains and Cascade Mountains regions to the inner-mountain west. Sulfate extinction is more than 60% of the total aerosol light extinction east of the Mississippi, while in the Appalachian and Southeast regions sulfates contribute about three fourths of aerosol light extinction. In the season with the highest sulfate extinction (summer), its contribution to aerosol extinction is even greater at 80-90% in the eastern United States.

Figure 3.7 shows the nitrate light extinction. There is a gradient from east to west, with relatively high nitrate extinction east of the Mississippi River and south of the Great Lakes. However, the strongest gradient is from southern California to the California desert. Nitrate contributions to aerosol light extinction are generally less than 10%, except in California, where nitrate can contribute as much as 39% and the Northern Great Plains and Boundary Waters regions where nitrate extinction contributes to total aerosol extinction in excess of 15%.

Figure 3.8 shows isopleths of the light extinction due to organics throughout the United States, averaged over the three-year period. Note that extinction caused by organic carbon is largest in the eastern United States, Northern Rocky Mountains and Cascade Mountains regions, and lowest in the Colorado Plateau and Central Rocky Mountain regions. The fraction of aerosol light extinction contributed by organic carbon ranges from a high of 40% in the Sierra Nevada region to less than 15% in the Pacific Coastal Mountains region and eastern United States. Even though organics, on an absolute basis, are higher in the East than West, total aerosol extinction is significantly greater in the eastern United States.

Figure 3.9 shows isopleths of the extinction caused by absorption. Absorption is highest in the Southeast, Southern California, and Cascade Mountains regions and lowest in the inner-mountain west. However, the largest fraction of total extinction attributed to absorption is in the

Great Basin, Sierra-Nevada, Sierra-Humboldt, and Colorado Plateau regions, where 10% of extinction is absorption. Except for the coastal regions of northern California, most of the western United States has a contribution from absorption in excess of 6%.

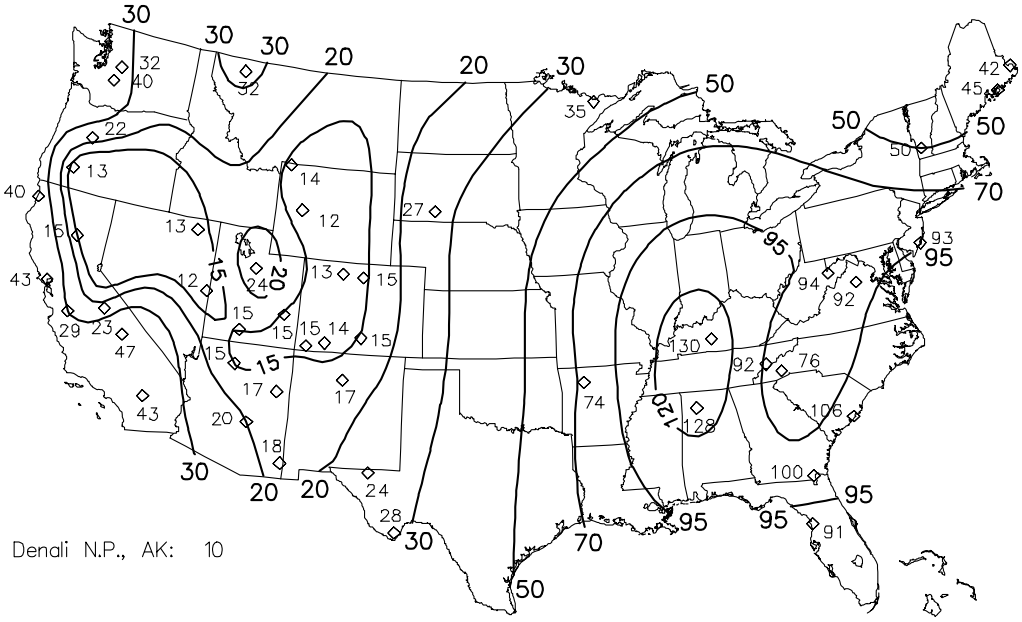

Figure 3.4 *Three-year averages of total reconstructed aerosol (Rayleigh is not included) light-extinction coefficient (1/Mm) for each site in the IMPROVE Network, excluding Washington, D.C.*

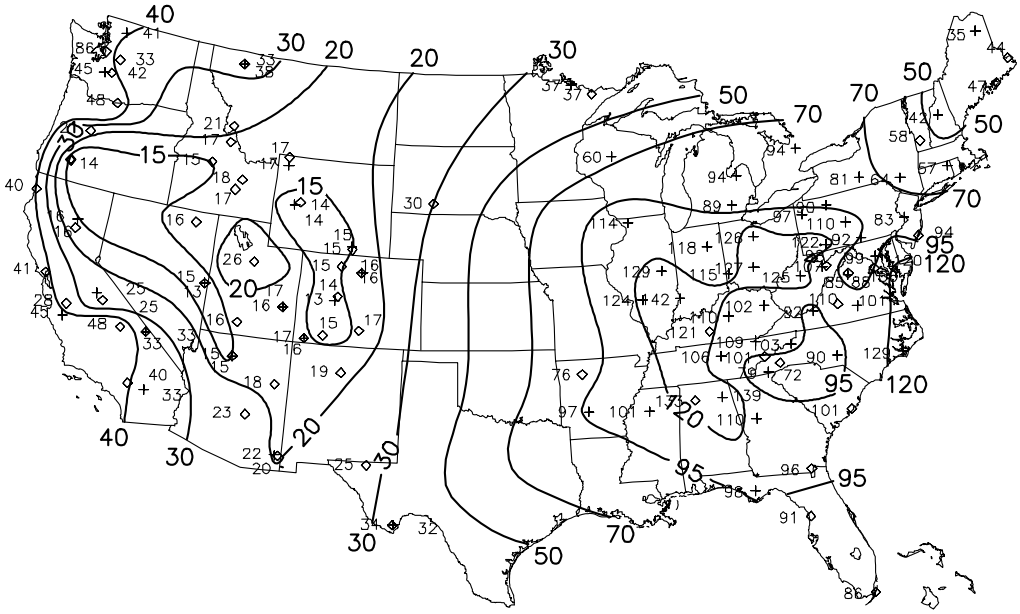

Figure 3.5 *Three-year averages of total reconstructed aerosol light-extinction coefficient (1/Mm) (Rayleigh is not included) for sites in the IMPROVE Network and CASTNet, excluding Washington, D.C.*

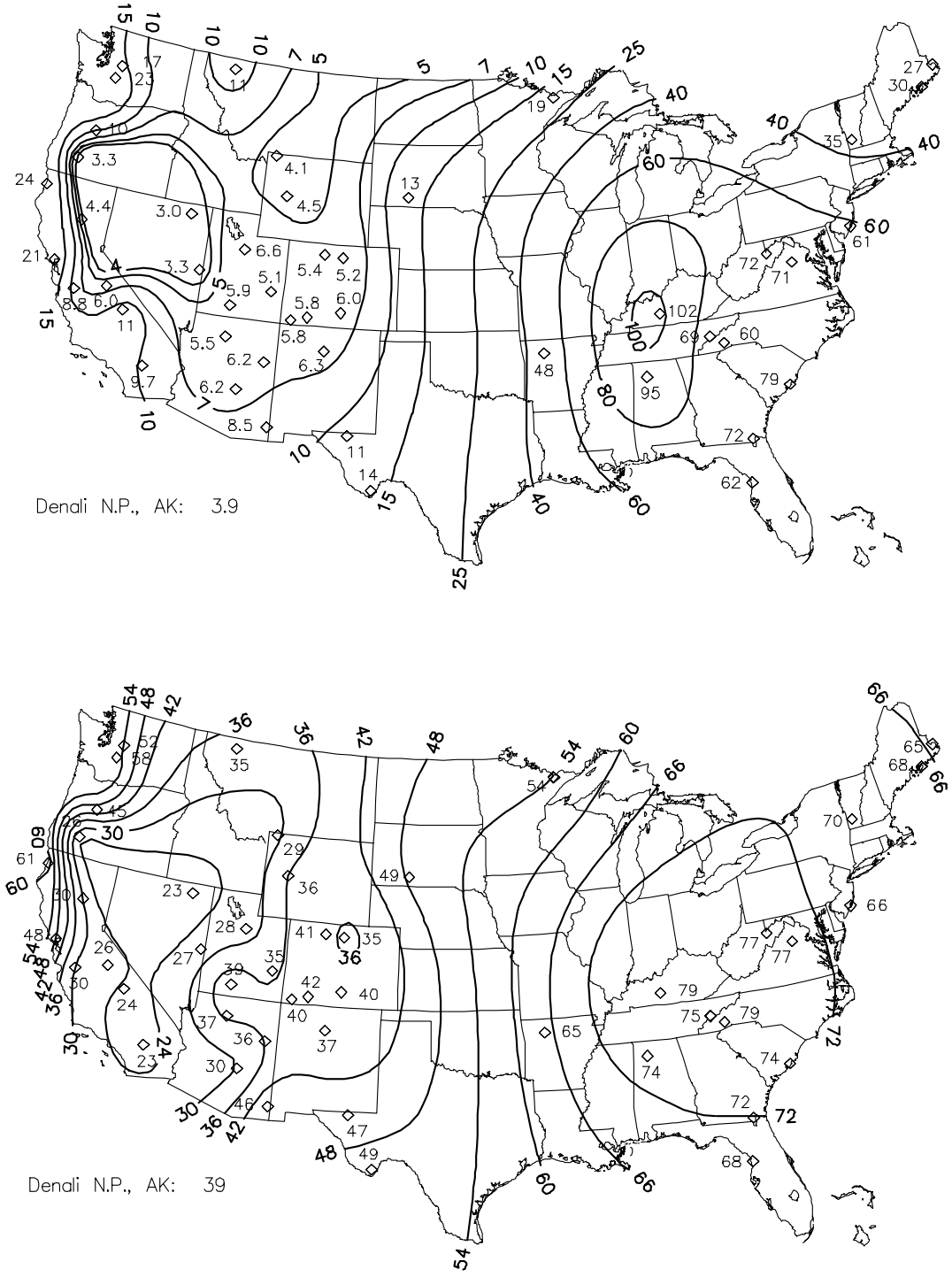

Figure 3.6 *Three-year averages of ammonium sulfate light-extinction coefficient in 1/Mm (top) and sulfate fraction in percent of aerosol light extinction (bottom), for each of the sites in the IMPROVE Network, excluding Washington, D.C.*

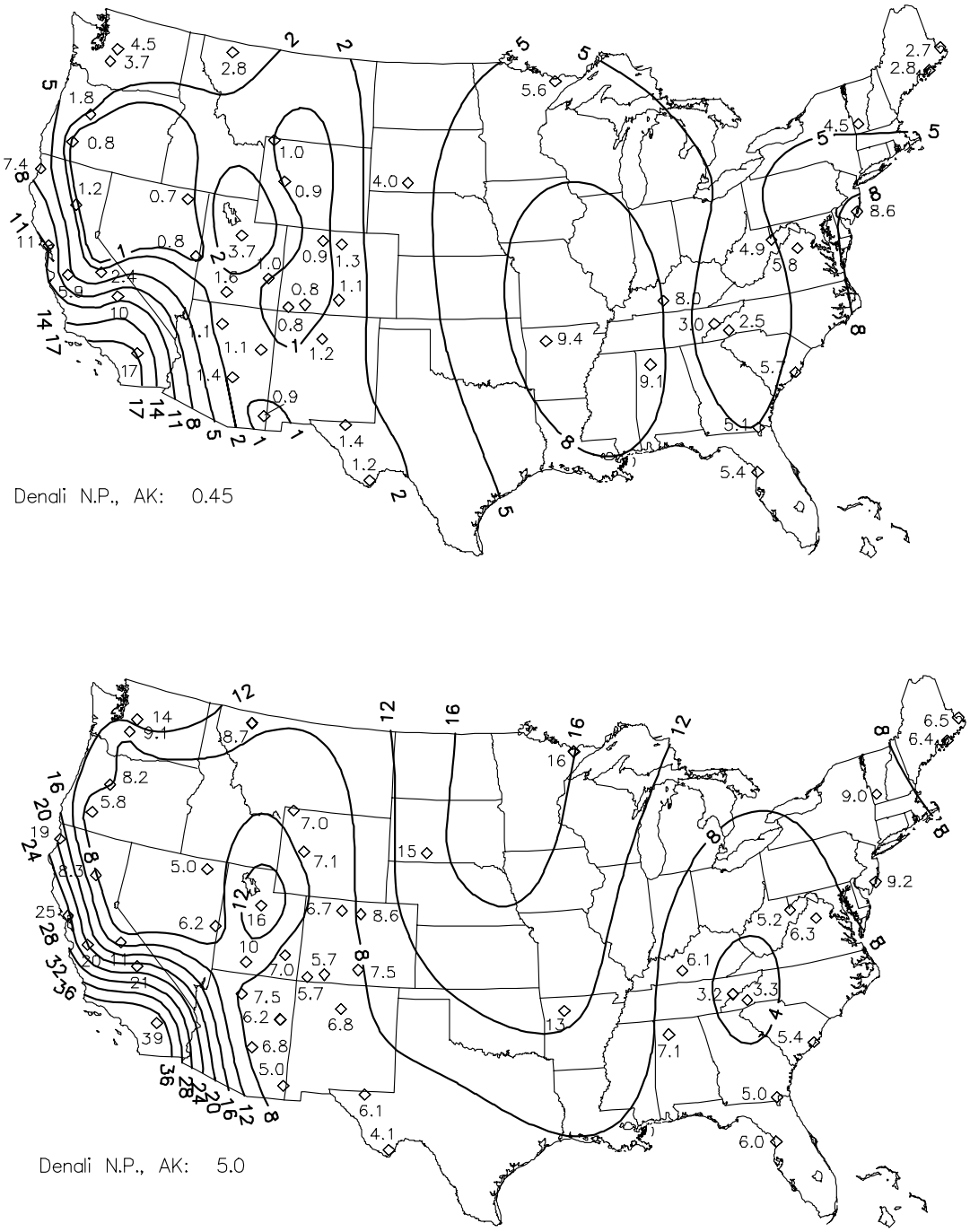

Figure 3.7 *Three-year averages of ammonium nitrate light extinction coefficient in 1/Mm (top) and nitrate fraction in percent of aerosol light extinction (bottom), for each of the sites in the IMPROVE Network, excluding Washington, D.C.*

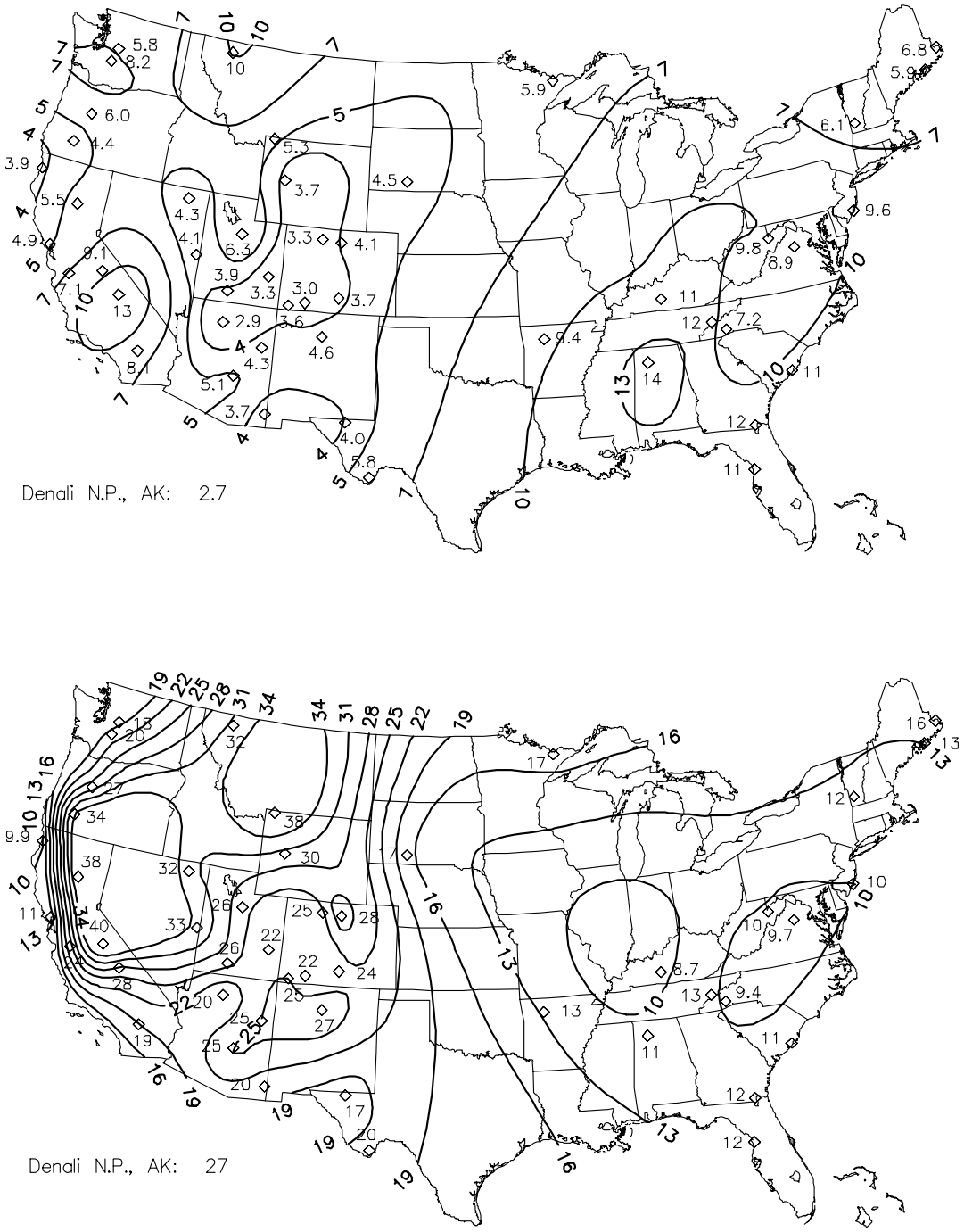

Figure 3.8 *Three-year averages of light extinction due to organic material in 1/Mm (top) and percent of aerosol extinction (bottom), for each of the sites in the IMPROVE Network, excluding Washington, D.C.*

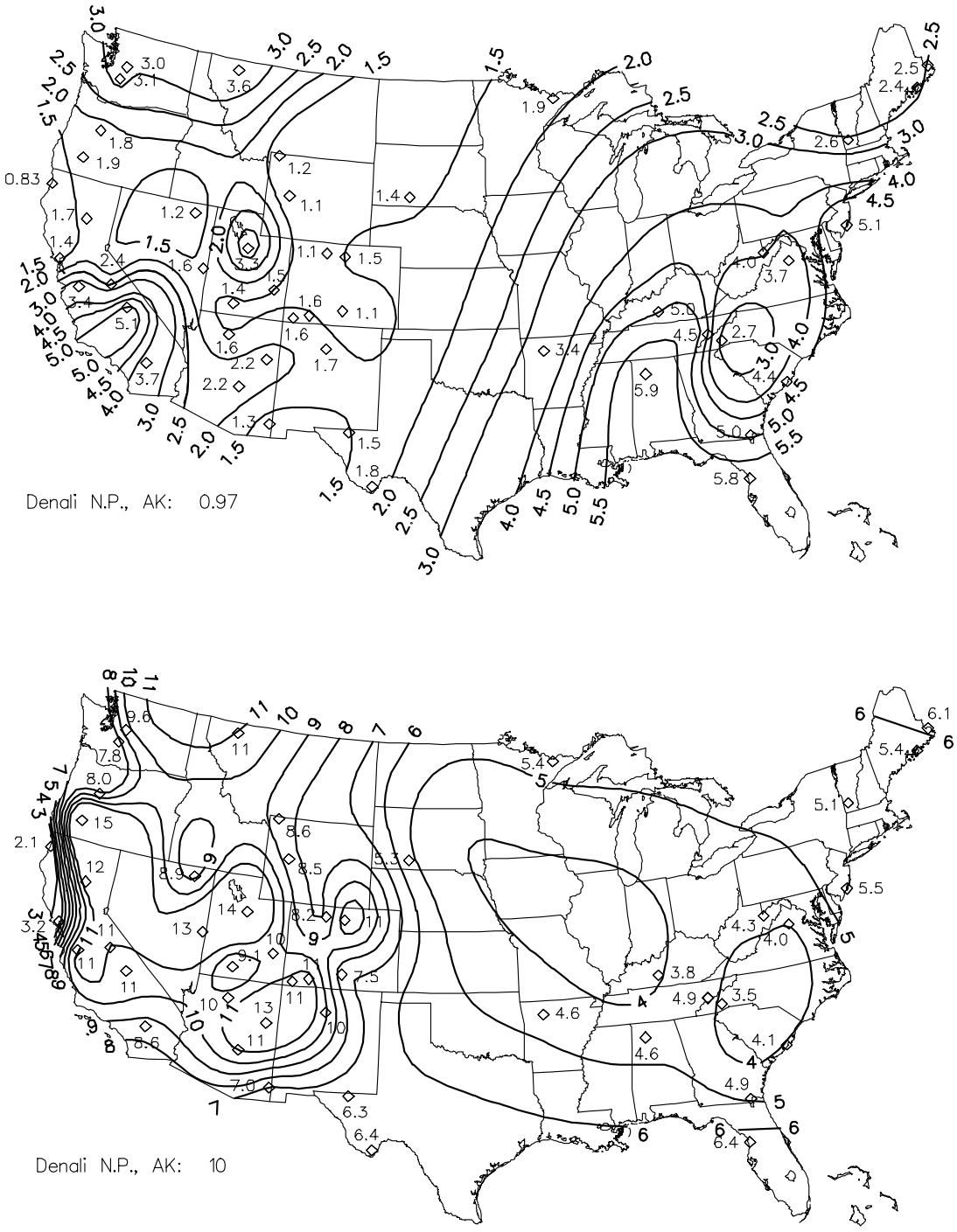

Figure 3.9 *Three-year averages of absorption in 1/Mm (top map) and absorption fraction in percent of aerosol light extinction (bottom map), for each of the sites in the IMPROVE Network, excluding Washington, D.C.*

Figure 3.10 shows isopleths of light extinction due to coarse material throughout the United States, averaged over the three-year period. Extinction caused by coarse material is highest in Southern California, Sonoran Desert, West Texas, Southeast, and eastern Coastal regions. The least contribution occurs in the Cascade Mountains, Colorado Plateau, and portions of the Central Rocky Mountain regions. The fraction of aerosol extinction contributed by coarse material shows an east-west dichotomy with the eastern United States having the lowest percentages in the Northeast and Appalachian regions at about 3% and the Great Basin area at 20-30%.

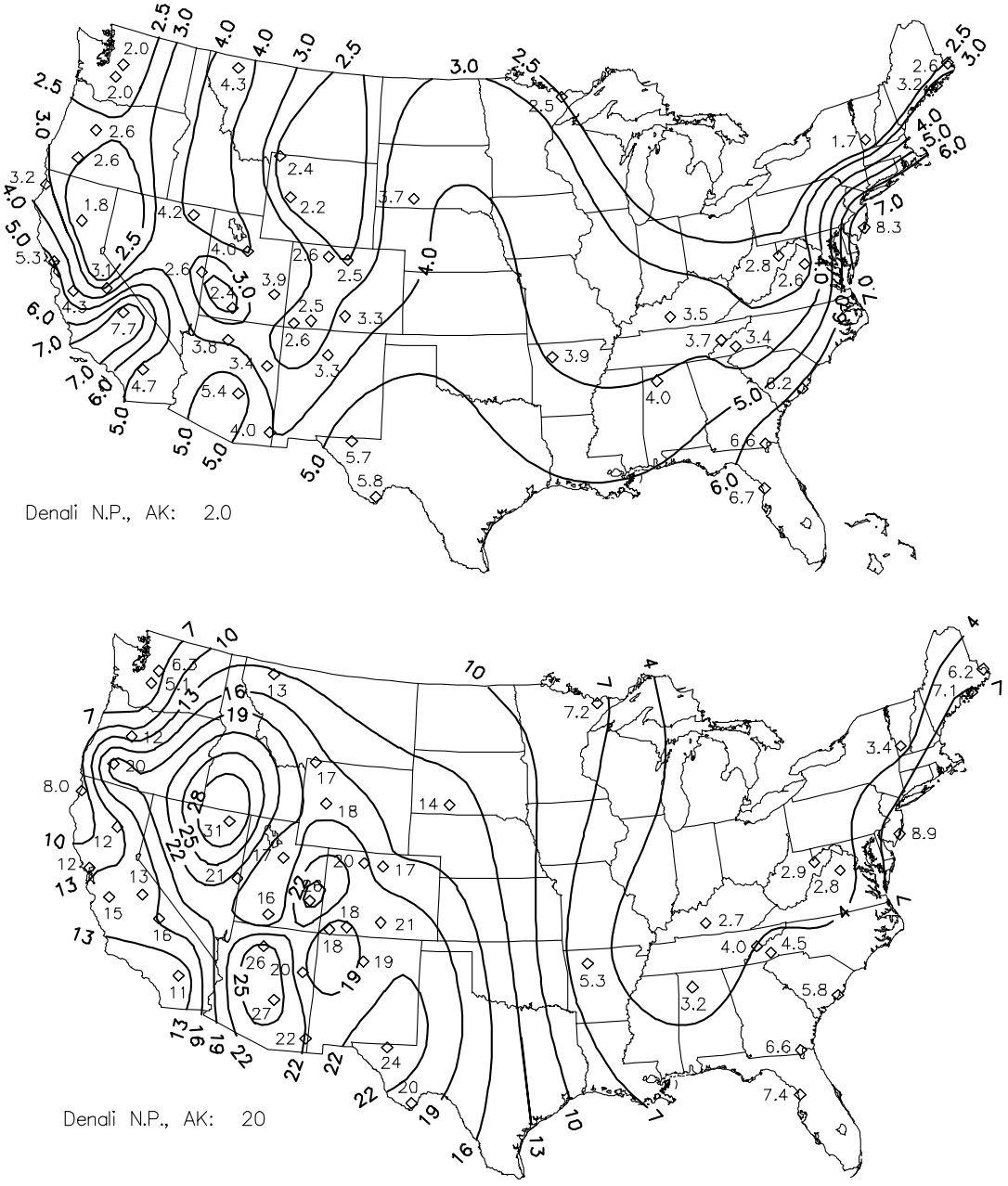

Figure 3.10 *Three-year averages of light extinction due to coarse material in 1/Mm (top map) and percent of aerosol extinction (bottom map), for each of the sites in the IMPROVE Network, excluding Washington, D.C.*

3.2.3 Spatial Trends in Visibility in the United States

Another way of displaying visibility estimates from aerosol data is by using the deciview (dv) scale. The deciview scale was designed to linearly relate to humanly perceived differences in visibility, which is not the case for light extinction. Particle free or Rayleigh conditions have a dv value of zero, and a change of 1 dv is a small but often noticeable change in perceived visibility.

Figure 3.11 shows isopleths of deciviews averaged over the three-year period using only IMPROVE data. There is a broad region that includes the Great Basin, most of the Colorado Plateau and portions of the Central Rocky Mountains that has visibility impairment of less than 10 dv. Moving in any direction from this region generally results in a gradient of increasing deciviews. West of the Sierra Nevada and the Southern California regions, dv values are in excess of 15. To the north a maximal value of 16 dv occurs at Mount Rainier National Park. The Cascade Mountain region and all of the eastern half of the United States have an excess of 13 dv of impaired visibility, and the region east of the Mississippi and south of the Great Lakes have impairment in excess of 23 dv, with the Mid-South region exceeding 25 dv. In fact, the highest annual dv value is reported at Mammoth Cave National Park and Sipsey Wilderness Area with an impairment of 26 dv.

Figure 3.12 is a deciview map calculated from IMPROVE and CASTNet data, analogous to Figure 3.5 showing the reconstructed light extinction coefficient. Spatial resolution of the deciview visibility index is enhanced in the eastern United States using the combined network data. Maximum values (≥26 dv) occur along the Ohio River and Tennessee Valleys.

Isopleths of deciviews for the winter, summer, spring, and autumn are shown in Figures 3.13 through Figure 3.16, respectively. The general spatial trend noted above for the annual average generally holds true for each season's average dv trend. Specifically, the least impairment or lowest dv values generally occur in all or part of the Great Basin, Colorado Plateau, and Central Rocky Mountains, with gradients of increasing dv values in any direction. A noticeable exception occurs during the winter and summer (Figures 3.13 and 3.14), at Lone Peak Wilderness Area in Utah, with 13 dv, likely due to haze originating in the urban Salt Lake City area.

The best visibility in the West occurs during the winter (Figure 3.13) with a minimum average of 4 dv at Jarbidge Wilderness Area. The region of 8 dv or less encompasses a broad expanse that covers the Sierra-Humboldt, Sierra-Nevada, Great Basin, Central Rocky Mountains, and the northwestern half of the Colorado Plateau. In the eastern half of the United States, the seasons of best visibility are winter and spring. In the Northeast and Southeast, the winter is best for visibility, while the Appalachian and Mid-West are variable among sites. However, all sites east of the Mississippi and south of the Great Lakes have impairment in excess of 20 dv for both the spring and winter.

Summertime visibilities (Figure 3.14), except for the Pacific Coastal Mountains, are generally the worst. Only small portions of the Great Basin and Central Rocky Mountains regions have impaired visibilities slightly below 10 dv. In the East, including the Upper Buffalo Wilderness Area, there is a broad region east of the Mississippi with more than 24 dv of impaired

visibility. Moreover, Mammoth Cave National Park and Sipsey Wilderness Area exceed 30 dv in impairment.

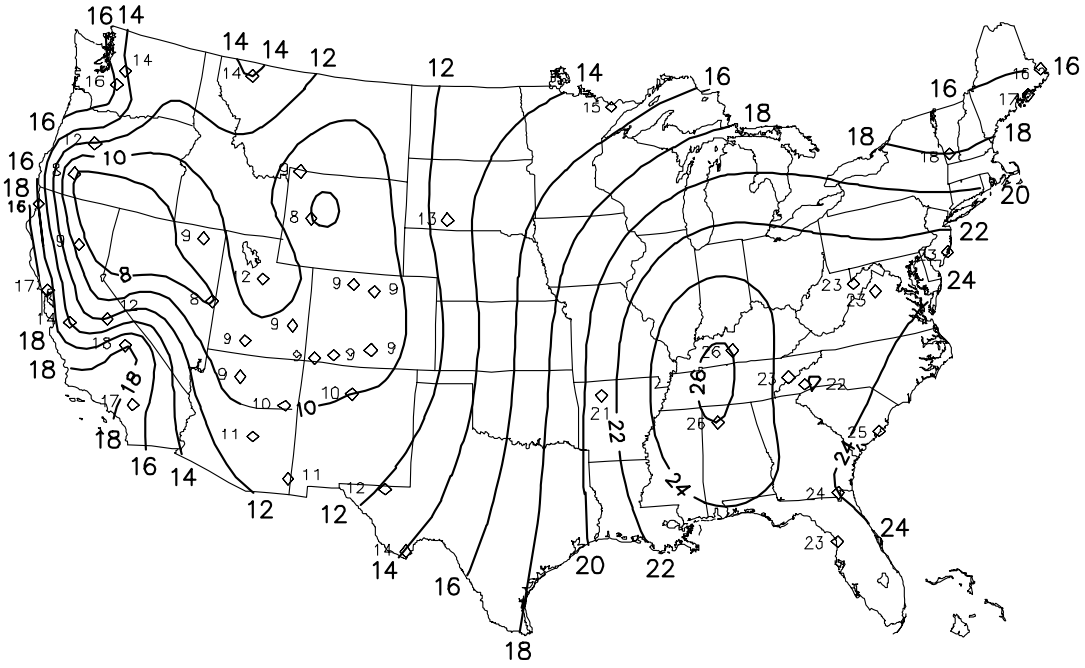

Figure 3.11 *Average visibility impairment in deciviews calculated from total (Rayleigh included) reconstructed light extinction for the three-year period, March 1996 through February 1999, of IMPROVE, excluding Washington, D.C.*

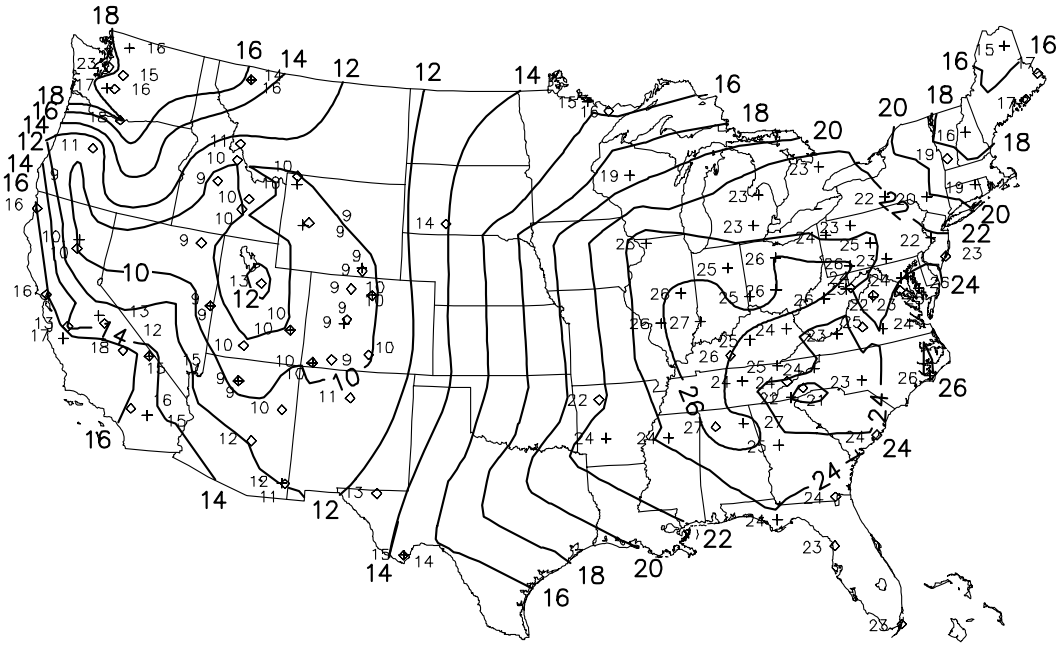

Figure 3.12 *Average visibility impairment in deciviews calculated from total (Rayleigh included) reconstructed light extinction for the three-year period, December 1995 through November 1998, of IMPROVE and CASTNet, excluding Washington, D.C.*

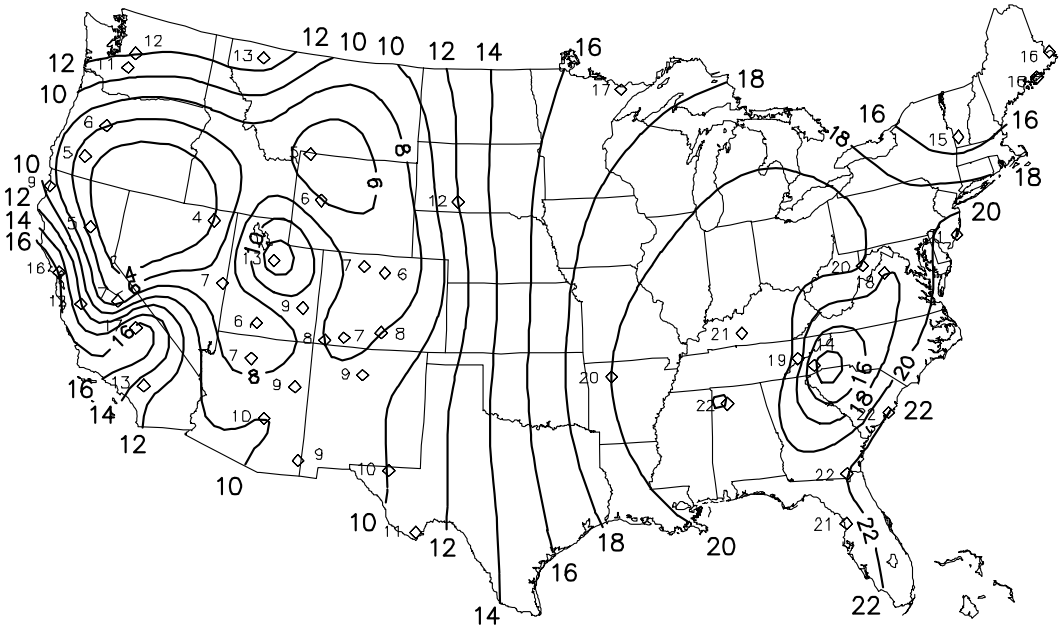

Figure 3.13 *Average winter visibility impairment in deciviews calculated from total (Rayleigh included) reconstructed light extinction for the three-year period, March 1996 through February 1999, excluding Washington, D.C.*

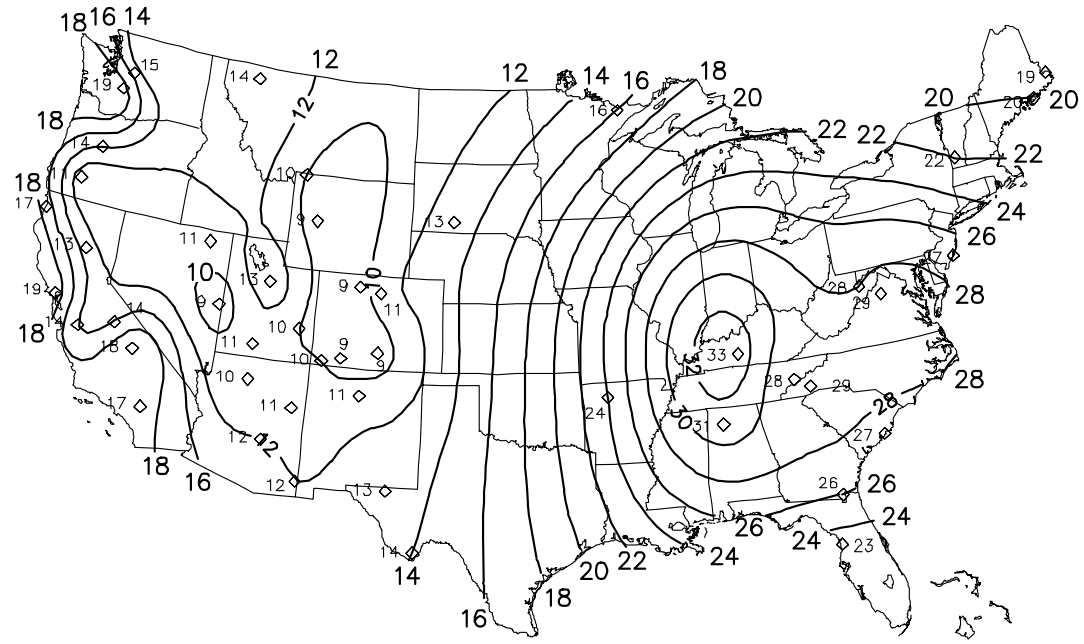

Figure 3.14 *Average summer visibility impairment in deciviews calculated from total (Rayleigh included) reconstructed light extinction for the three-year period, March 1996 through February 1999, excluding Washington, D.C.*

Visibility impairment in the spring (Figure 3.15) and autumn (Figure 3.16) are quite comparable. However, in the autumn the East is generally hazier than spring, while in the inner-mountain west, autumn is generally less impaired, particularly in the Central Rocky Mountains region. Southern California has better visibility in the autumn.

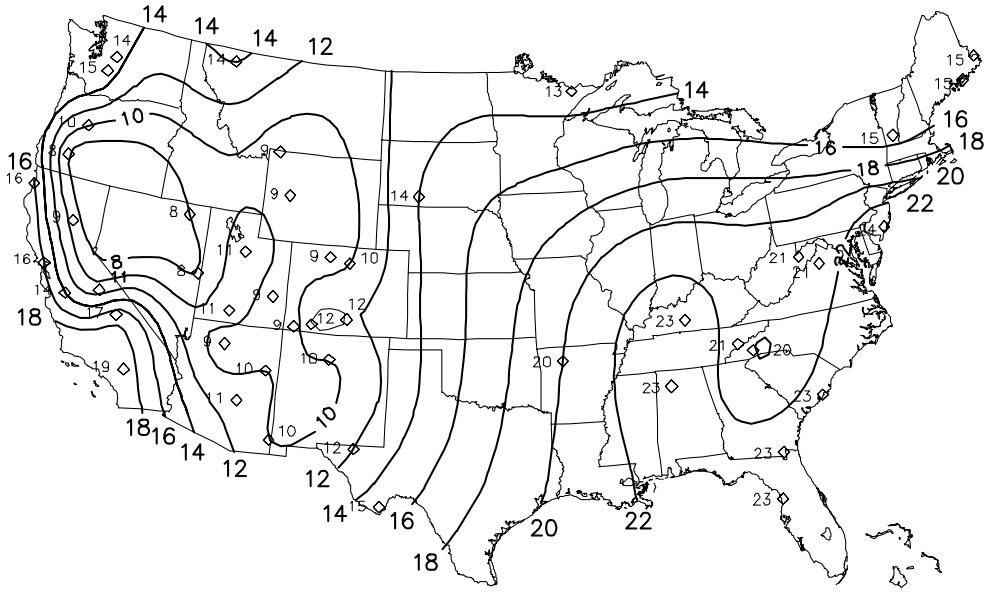

Figure 3.15 *Average spring visibility impairment in deciviews calculated from total (Rayleigh included) reconstructed light extinction for the three-year period, March 1996 through February 1999, excluding Washington, D.C.*

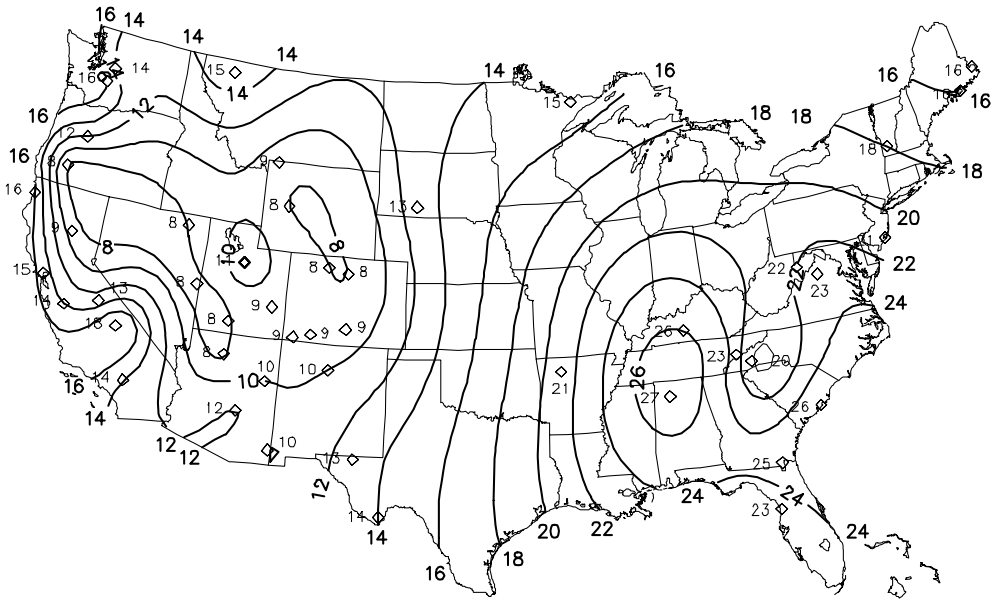

Figure 3.16 *Average autumn visibility impairment in deciviews calculated from total (Rayleigh included) reconstructed light extinction for the three-year period, March 1996 through February 1999, excluding Washington, D.C.*

3.3 SUMMARY

The following are the major patterns in light extinction reconstructed from aerosol measurements and relative humidity during the three-year period of IMPROVE (March 1996-February 1999):

(1) Spatial Patterns. Following the patterns observed in fine aerosol concentrations, reconstructed light extinction is highest in the eastern United States and in urban California and lowest in the nonurban west.

(2) Major Contributors to Light Extinction. Fine aerosols are the most effective in scattering light and are the major contributors to light extinction. In most cases, the sulfate component of fine aerosol is the largest single contributor to light extinction. This is because sulfate, being hygroscopic, generally has a higher light extinction efficiency than other species due to associated liquid water. This is especially true in the eastern United States, where relative humidity is high. In the Appalachian Mountains (Shenandoah and Great Smoky Mountains), sulfate accounts for nearly 80% of the total aerosol light extinction throughout the year, and more during the summer months. Sulfates contribute the least in the Great Basin region at about 25%, while along the Rocky Mountains the contribution is about 30-40%. In the Cascade Mountain region sulfates contribute significantly at 50-60%. Sulfates are the largest single contributor to light extinction in 17 of the 21 regions and are about comparable to organics in two of these regions, Northern Rocky Mountains and Wasatch.

(3) Nitrates are the single largest contributor to extinction in the Southern California region at 39% but also contribute significantly along the coastal areas of California at about 20-25%. Nitrates are 16% of extinction at Lone Peak Wilderness Area near Salt Lake City, while in the rest of the United States it is less than 10%.

(4) Organics are, in general, the second largest contributor to total aerosol extinction. It is the largest contributor in the Great Basin, Sierra-Humboldt, and Sierra Nevada regions at 33%, 36%, and 32%, respectively. It is the largest contributor at Yosemite National Park at 40% and on the order of about 10% in most of the eastern United States. In the Central Rocky Mountains and on the Colorado Plateau its contribution to extinction is about 20-25%.

(5) Light-absorbing carbon is on the order of about 10% in much of the western United States and on the order of 5% east of the Mississippi. In the three regions where organics are the largest contributors to extinction, the sum of organic and light absorbing carbon, or the contribution of carbon in general, to extinction is 40-50%.

(6) Fine and coarse soil/dust in the eastern United States is generally less than 5%, while in the Sonoran Desert, West Texas, Great Basin regions it contribution to extinction is on the order of 20-30%. In the Cascade Mountains region it is about 5%. In the rest of the United States soil/dust contributes between about 10 and 20% of extinction.

(7) Generally, reconstructed light extinction is highest in summer and lowest in winter; however, there are many exceptions to this general rule. Higher extinction occurs in summer generally

because of elevated sulfate and carbonaceous aerosol concentrations. Also, higher average RHs occur in the East during the summer, which increases extinction.

(8) The general spatial trend noted above for the annual average visibility levels generally holds true for each season's average visibility as well. Specifically, the least impairment occurs in all or part of the Great Basin, Colorado Plateau, and Central Rocky Mountains, with gradients of increasing dv values in any direction. The best visibility occurs during the winter and the worst in the summer. Visibility impairment in the spring and autumn are comparable.

3.4 REFERENCES

Chow, J.C., Watson, J.G., Pritchett, L.C., Pierson, W.R., Frazier, C.A., and Purcell, R.G., The DRI thermal/optical reflectance carbon analysis system: description, evaluation, and applications in U.S. air quality studies, *Atmos. Environ.*, **27**(A), (8), 1185-1201, 1993.

Clean Air Status and Trends Network (CASTNet) Deposition Summary Report (1987-1995), EPA/600/R-98-207, July, 1998.

Day, D.E., Malm, W.C., and Kreidenweis, S.M., Aerosol light scattering measurements as a function of relative humidity, *J. of Air & Waste Management Association*, 2000.

Fuller, K., Malm, W., and Kreidenweis, S., Effects of mixing on extinction by carbonaceous particles, *J. Geophys. Research*, **104**:15,941-15,954, 1999.

Gebhart, K.A. and Malm, W.C., An investigation of the size distributions of particulate sulfate concentrations measured during WHITEX, In Transactions of the AWMA/EPA Int'l Specialty Conference on Visibility and Fine Particles, edited by C.V. Mathai, Air and Waste Management Association, 157-169, 1989.

Heisler, S.L., Henry, R.C., Watson, J.G., and Hidy, G.M., "The 1978 Denver winter haze study volume II." ERT document #P-5417-1. Environmental Research and Technology, Inc., West Lake Village, CA, 1980.

Horvath, H., Atmospheric light absorption-A review, *Atmos. Environ.*, ***27***(A), 3, 293-317, 1993.

Lowenthal, D.H., Rogers, C.F., Saxena, P., Watson, J.G., and Chow, J.C., Sensitivity of estimated light extinction coefficients to model assumptions and measurement errors, *Atmos. Environ.*, ***29***, 751-766, 1995.

Macias, E.S., Zwicker, J.O. and White, W.H., Regional haze case studies in the southwestern U.S.—II. source contributions, *Atmos. Environ.*, **15**, 1987-1997, 1981

Malm W. C., Sisler J. F., Huffman D., Eldred R. A., and Cahill T. C., Spatial and seasonal trends in particle concentration and optical extinction in the U.S. *J. Geophys. Res*. **99**(D1):1347-1370, 1994a.

Malm, W.C., Cahill, T.A., Gebhart, K.A., and Waggoner, A., Optical characteristics of atmospheric sulfur at Grand Canyon, Arizona, in Visibility Protection, Research and Policy Aspects, edited by P.S. Bhardwaja, Air and Waste Management Association, Pittsburgh, PA, 418-433, 1986.

Malm, W.C., Iyer, H., Watson, J., and Latimer, D.A., Survey of a variety of receptor modeling techniques, In Transactions of the AWMA/EPA Int'l Specialty Conference on Visibility and Fine Particles, edited by C.V. Mathai, Air and Waste Management Association, 1989.

Malm, W.C., Gebhart, K.A., Molenar, J.V., Cahill, T.A., Eldred, R.A., and Huffman, D., Examining the relationship between atmospheric aerosols and light extinction at Mount Rainier and North Cascades National Parks, *Atmos. Environ.*, **28**, 347-360, 1994b.

Malm, W.C. and Kreidenweis, S.M., The effects of models of aerosol hygroscopicity on estimated scattering efficiencies, presented at the Air and Waste Management 89th Annual Meeting, Pittsburgh, PA, 1996.

Malm, W.C., Molenar, J.V., Eldred, R.A., and Sisler, J.F., Examining the relationship among atmospheric aerosols and light scattering and extinction in the Grand Canyon Area, *J. Geophys. Res.*,**101**(D14), 19251-19265, 1996.

Malm, W.C. and Kreidenweis, S.M., The effects of models of aerosol hygroscopicity on the apportionment of extinction, *Atmos. Environ.*, **31**, 1965-1976, 1997.

Malm, W.C., Day, D., and Kreidenweis, S.M., Comparison of measured and reconstructed scattering during an intensive field study at Great Smoky Mountains National Park, paper #97-WA70.02, presented at the Air and Waste Management 90th Annual Meeting, Pittsburgh, PA, 1997.

Malm, W.C., Examining the relationship between aerosol concentration and partial scattering efficiencies near the Grand Canyon, Presented at the 91st Annual Meeting of the Air and Waste Management Association, Pittsburgh, PA, 1998.

Malm, W.C., Day, D., and Kreidenweis, S.M., Light scattering characteristics of aerosols at ambient and as a function of relative humidity: part II---a comparison of measured scattering and aerosol concentrations using statistical models. *J. Air and Waste Management Association*, **50**, 174-182, 2000.

Ouimette, J.R. and Flagan, R.C., The extinction coefficient of multicoponent aerosols, *Atmos. Environ.*, **16**, 2405.

Pilinis C., Pandis S.N., and Seinfeld J.H., Sensitivity of direct climate forcing by atmospheric aerosols to aerosol size and composition, *J. Geophys. Res.*, **100**(D9), 18739-18754, 1995.

Pitchford, M.L. and Malm, W.C., Development and applications of a standard visual index, Presented at the Conference on Visibility and Fine Particles, Air and Waste Management Association, Vienna, Austria, September, *Atmos. Environ.*, **28**(5), 1049-1054, 1994.

Saxena P. and Peterson T.W., Thermodynamics of multicomponent electrolytic aerosols, *J. Colloid Interface Sci.*. **79**, 496-510, 1981.

Saxena P., Hudischewskyj A.B., Seigneur C., and Seinfeld J.H., A comparative study of equilibrium approaches to the chemical characterization of secondary aerosols, *Atmos. Environ.*, **20**,1471-1483, 1986.

Saxena P., Mueller P.K., Kim Y.P., Seinfeld J.H., and Koutrakis P., Coupling thermodynamic theory with measurements to characterize acidity of atmospheric particles, *Aerosol Sci. Technol*., **19**, 279-293, 1993.

Sloane C.S., Optical properties of aerosols-comparison of measurements with model calculations, *Atmos. Environ.*, **17**, 409-416, 1983.

Sloane C.S., Optical properties of aerosols of mixed composition, *Atmos. Environ.*, **18**, 871-878, 1984.

Sloane C.S., Effects of composition on aerosol light scattering efficiencies, *Atmos. Environ.*, **20**, 1025, 1986.

Sloane C.S. and Wolff, G.T., Change in aerosol optical properties with change in chemical composition, *Atmos. Environ.*, **19**, 669-680, 1985.

Stelson, A.W. and Seinfeld, J., Relative humidity and temperature dependence of the ammonium nitrate dissociation constant, *Atmos. Environ.*, **15**, 983, 1982.

Tang, I.N., Chemical and size effects of hygroscopic aerosols on light scattering coefficients, *J. Geophys. Res.*, **101**, (D14), 19245-19250, 1996.

Tombach, I. and Thurston, S.A., The quality of the SCENES measurements: the roles of data quality goals and evolving technology, in *Proc. Aerosols and Atmospheric Optics: Radiative Balance and Visual Air Quality*, *Air & Waste Management Assoc*., Pittsburgh, PA, 1994.

Trijonis, J.C. and Pitchford, M., *Preliminary extinction budget results from the RESOLVE program* edited by P.S. Bhardwaja, Air and Waste Management Association, Pittsburgh, PA, 1987.

Trijonis, J.C., McGown, M., Pitchford, M., Blumenthal, D., Roberts, P., White, W., Macias, E., Weiss, R., Waggoner, A., Watson, J., Chow, J., and Flocchini, R., RESOLVE Project Final Report: Visibility Conditions and Causes of Visibility Degradation in the Mojave Desert of California, NWC TP #6869, Naval Weapons Center, China Lake, CA, 1988.

Trijonis, J.C., Malm, W.C., Pitchford, M., White, W.H., Charlson, R., and Husar, R., Visibility: Existing and historical conditions-causes and effects, in *State Sci. State Technol. Rep. 24*, Natl. Acid Precip. Assessment Program, Washington, D.C., 1990.

vandeHulst, H.C., *Light scattering by small particles*, Dover Publications, New York, NY, 1981

Watson, J.G., Chow, J.C., Richards, L.W., Haase, D.L., McDade, C., Dietrich, L.D., Moon, D., Chinkin, L., and Sloane, C., The 1989-90 Phoenix urban haze study. Volume I: program plan. DRI document 8931.1F, prepared for Arizona Department of Environmental Quality, Phoenix, AZ, by Desert Research Institute, Reno, NV, 1990.

Wexler, A. and Seinfeld, J. Second-generation inorganic aerosol model, *Atmos. Environ.*, **25**A, 2731, 1991.

Waggoner, A.P., Weiss, R.E., Ahlquist, N.C., Covert, D.S., Will, S., and Charlson, R.J., Optical characteristics of atmospheric aerosols, *Atmos. Environ.*, **15**, 1891-1909, 1981.

White, W.H. On the theoretical and empirical basis for apportioning extinction by aerosols; a critical review, *Atmos. Environ.*, **20**, 1659-1672, 1986.

White, W.H. and Roberts, P.T., On the nature and origins of visibility-reducing aerosols in the Los Angeles Air Basin, *Atmos. Environ.*, **11**, 803-812, 1977.

White, W.H., Contributions to light scattering, In: Acidic Deposition: State of Science and Technology Report 24, J. Trijonis (lead author), National Acid Precipitation Assessment Program, Washington, DC, pp85-102, 1990.

CHAPTER 4

FINE PARTICLE MASS CONCENTRATION FREQUENCY DISTRIBUTIONS

The contributions of sulfates, carbon (organic plus light-absorbing carbon), soil, and nitrate particles to the fine mass concentration at various points of the fine mass concentration frequency distribution are summarized and displayed to illustrate which components are principal contributors during high and low concentration periods. Maps of chemical species' contribution to the mean and upper percentiles of particle fine mass show spatial trends in extreme contribution at IMPROVE (or IMPROVE protocol) sites across the contiguous United States. The chemical species contribution to extremes in fine mass is relevant to emissions control scenarios for the Class I areas represented by monitoring sites in which improvement is sought for the most impaired conditions as well as for more typical conditions.

4.1 DATA

Reconstructed fine mass (RCFM) concentrations were calculated following the procedures described in Section 2.1 using data from 51 monitoring sites. The site names and locations used for these assessments are indicated in Figure 1.3 and Table 1.2.

Unlike the analysis in Chapter 2, which displayed annual and seasonal means of reconstructed fine mass and its components, this chapter presents information at a number of points in the reconstructed fine mass frequency distributions for the selected monitoring sites. The chemical species contribution was calculated based upon the reconstructed fine mass rather than the gravimetric fine mass. This ensures that the sum of the components are always equal to 100% of the reconstructed fine mass. However, sample periods where all of the data needed to calculate fine mass components are not available and cannot be used because the reconstructed fine mass cannot be determined. This could result in a data analysis bias if missing data are not randomly distributed across the fine mass distribution. For example, the IMPROVE module B nylon filter clogs more readily under high fine mass loading than during average or low mass loading levels, so the nitrate data are more prone to be missing on days of high fine mass loading. To determine whether calculating species contributions to reconstructed rather than to gravimetric fine mass biased this analysis, the two approaches were compared. While the magnitude of species contribution changed somewhat between the two methods, general trends displayed in the frequency distributions and maps of species contributions to the mean and upper extremes of fine mass were similar.

4.2 RESULTS AND DISCUSSION

4.2.1 Fine Mass Frequency Distributions

Frequency distributions of fine mass at selected sites are shown in Figures 4.1a, 4.2a, 4.3a, and 4.4a, with mass concentration plotted as the abscissa on a logarithmic scale, and the number of samples per mass concentration bin, or *N per bin*, as the ordinate. Figures 4.1b, 4.2b, 4.3b, and 4.4b show the fractional contribution of individual chemical species to fine mass by mass concentration bin. The fine mass frequency distributions are separated into mass concentration bins covering three orders of magnitude, from 0.1 to 100 $\mu g/m^3$, with approximately equal bins widths on a logarithmic plot. The frequency distributions incorporate data from the entire period of record for selected sites. Color versions of the annual and seasonal frequency distributions for all sites listed in Table 1.2 are available on the internet (http://alta_vista.cira.colostate.edu /summary~data/fd.htm).

Figure 4.1a shows the fine mass frequency distribution at Shenandoah National Park. Data span the time period March 1988 through August 1999, as indicated by the Start and End dates on Figure 4.1a. *N Total* is the total number of sampling days included in the fine mass frequency distribution. Figure 4.1b shows the individual chemical species fraction of fine mass in each frequency distribution bin. Sulfates (solid line), have a steadily increasing contribution with increasing fine mass concentration at Shenandoah, and contribute in excess of 80% to fine mass on the days with highest fine mass concentration. On the cleanest days, when fine mass concentrations are less than approximately 3 $\mu g/m^3$, the particle carbon (dash-dot line) contribution is of approximately equal magnitude to sulfates. Soil (dashed line) and particle nitrate (dash-dot-dot line) are minor components of fine mass regardless of fine mass concentration, contributing approximately 10% or less over the entire range of fine mass concentration.

The fine mass frequency distribution at Big Bend National Park is shown in Figure 4.2a. The chemical species contribution to fine mass (Figure 4.2b) shows that sulfates and carbon are major contributors at low-to-mid-fine mass concentrations. However, the soil contribution increases with increasing fine mass concentration. On the days when fine mass concentrations at Big Bend are highest, soil dominates the fine mass fraction.

At Yellowstone National Park (Figure 4.3), particle carbon contributes about 50% at all but the highest fine mass concentrations. When the fine mass concentration at Yellowstone is greater than approximately 7 $\mu g/m^3$ the carbon contribution increases and can exceed 80%. At low fine mass concentrations (below approximately 2 $\mu g/m^3$), the relative contribution of the major chemical species to fine mass remains essentially constant.

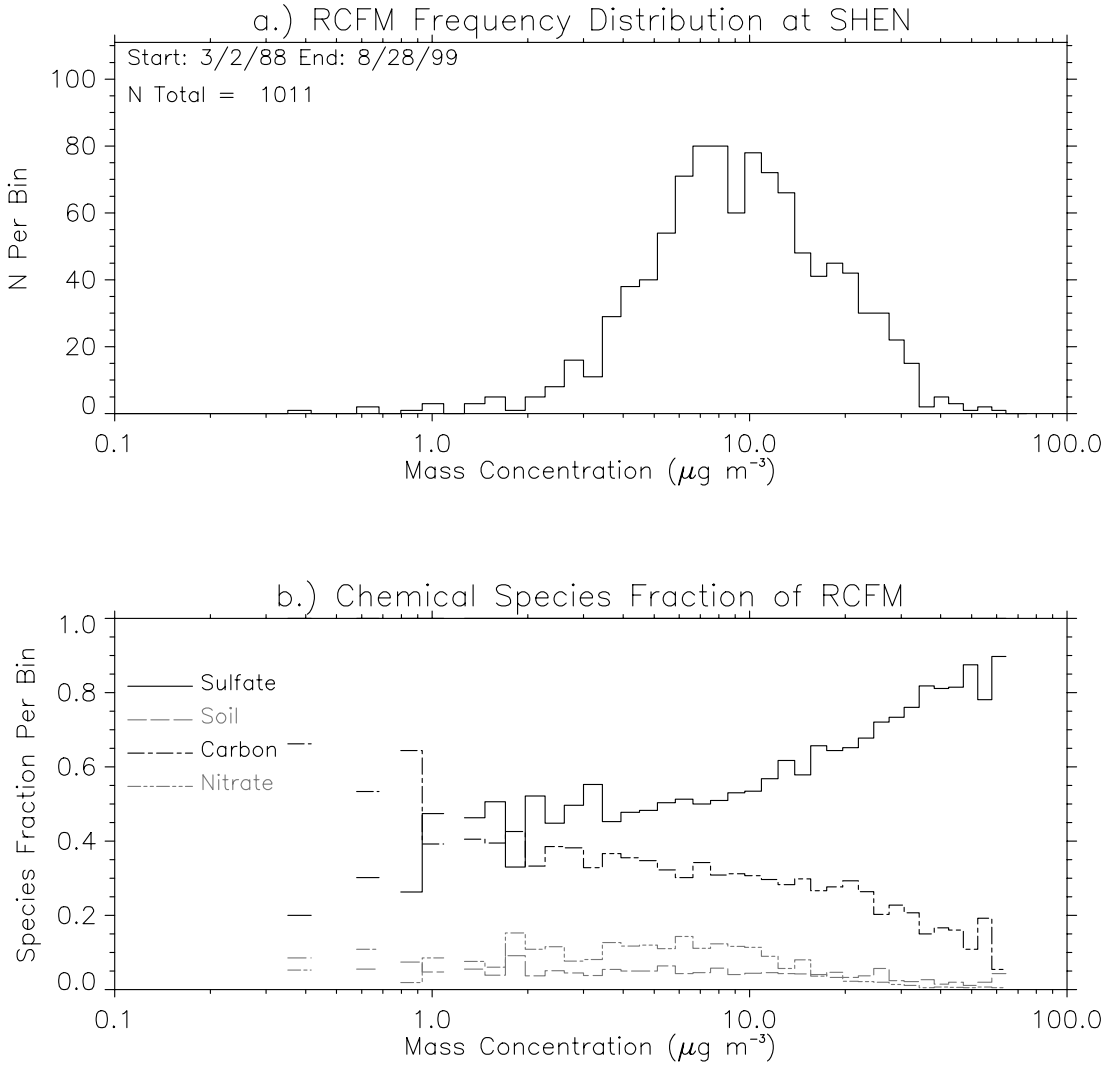

Figure 4.1 *(a) RCFM frequency distribution and (b) chemical species fractional contribution to RCFM by mass concentration bin at Shenandoah National Park.*

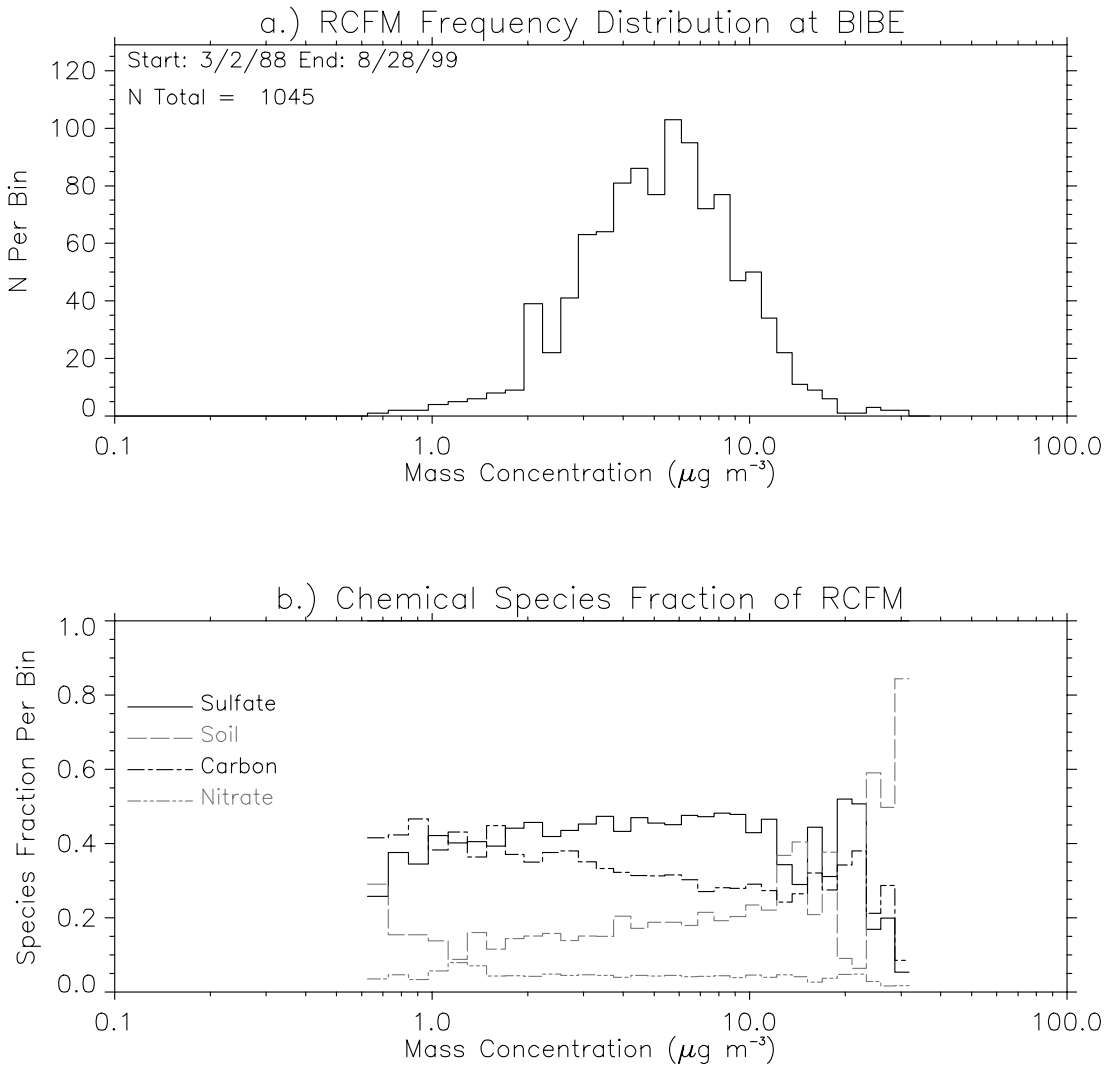

Figure 4.2 *(a) RCFM frequency distribution and (b) chemical species fractional contribution to RCFM by mass concentration bin at Big Bend National Park.*

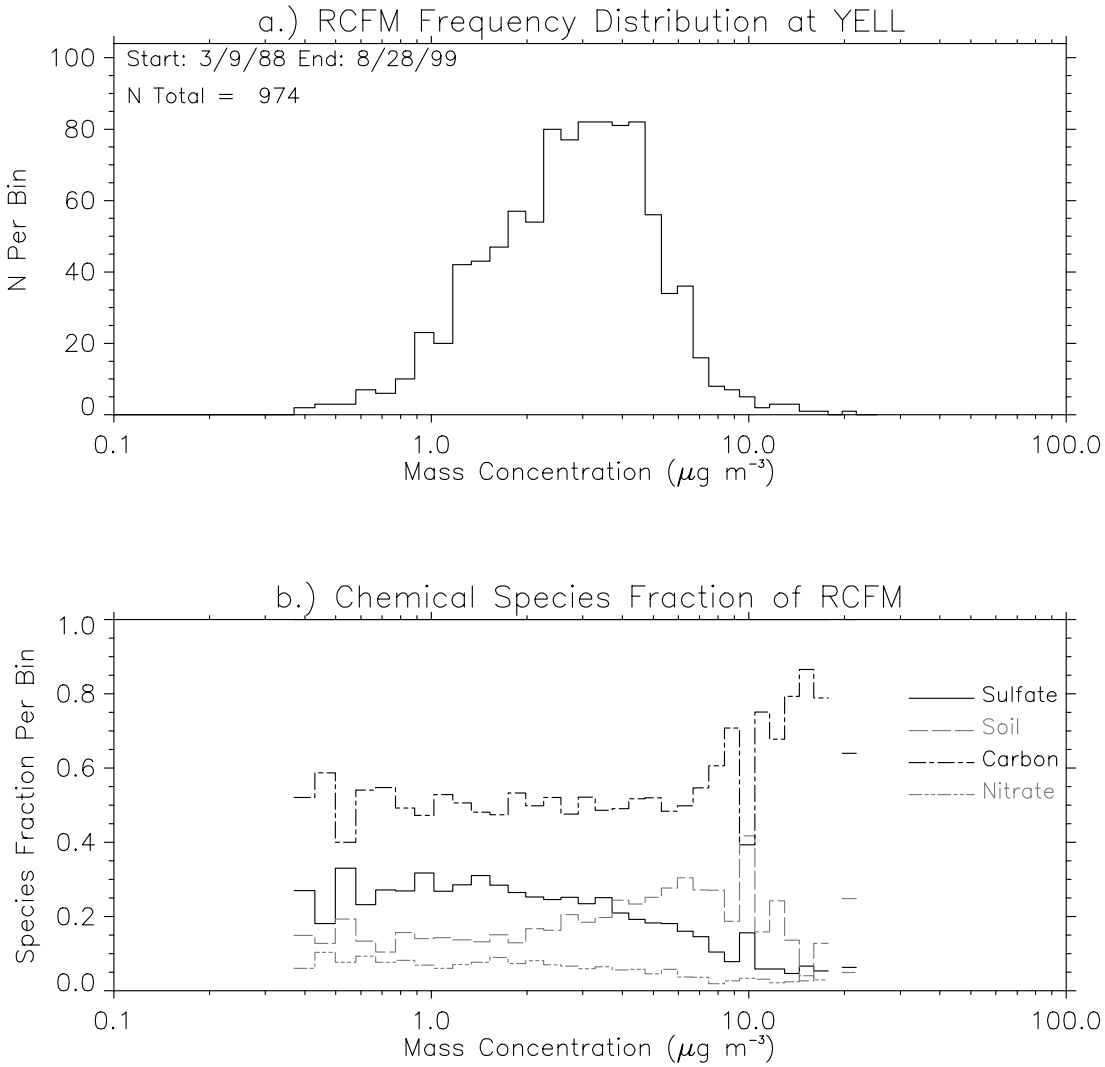

Figure 4.3 *(a) RCFM frequency distribution and (b) chemical species fractional contribution to RCFM by mass concentration bin at Yellowstone National Park.*

Figure 4.4a shows the wintertime fine mass frequency distribution at Yosemite National Park. During the winter at Yosemite, particle carbon has a majority contribution at most fine mass concentrations. However, when fine mass concentrations are high (in excess of 4 μg/m^3) the particle nitrate contribution to fine mass increases and can reach 50%.

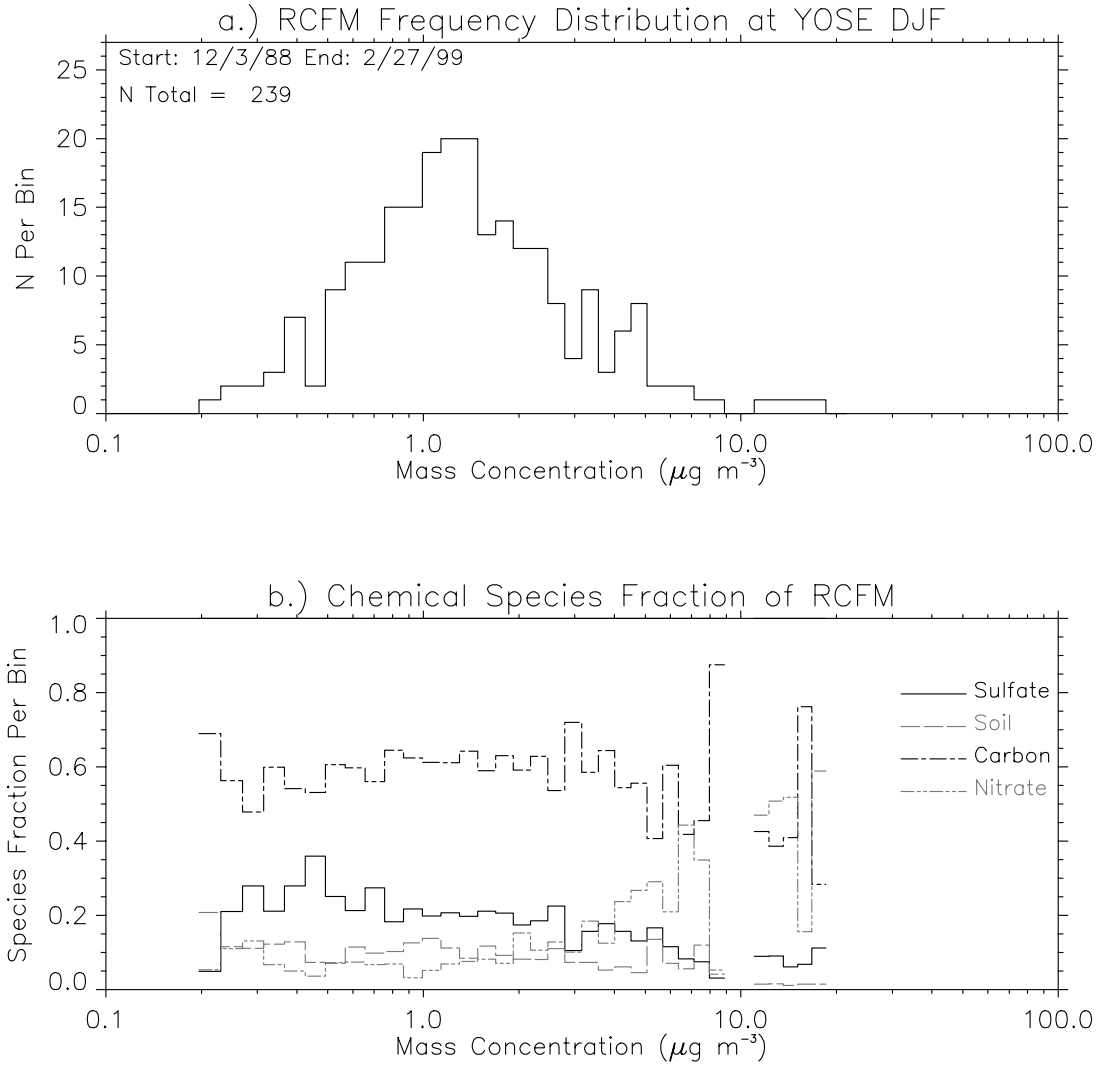

Figure 4.4 *(a) RCFM frequency distribution and (b) chemical species fractional contribution to RCFM by mass concentration bin at Yosemite National Park. Data shown are for winter only.*

Figure 4.5a shows the wintertime fine mass frequency distribution at Rocky Mountain National Park, with similar high particle nitrate contributions to the upper percentiles of fine mass as observed at Yosemite. At Rocky Mountain, particle nitrate contributes in excess of 25% fine mass when fine mass concentrations are greater than 4 μg/m^3. Particle carbon is the largest single contributor to wintertime mean fine mass at Rocky Mountain, although sulfates and nitrates have comparable contributions to particle carbon at both the upper and lower extremes of fine mass.

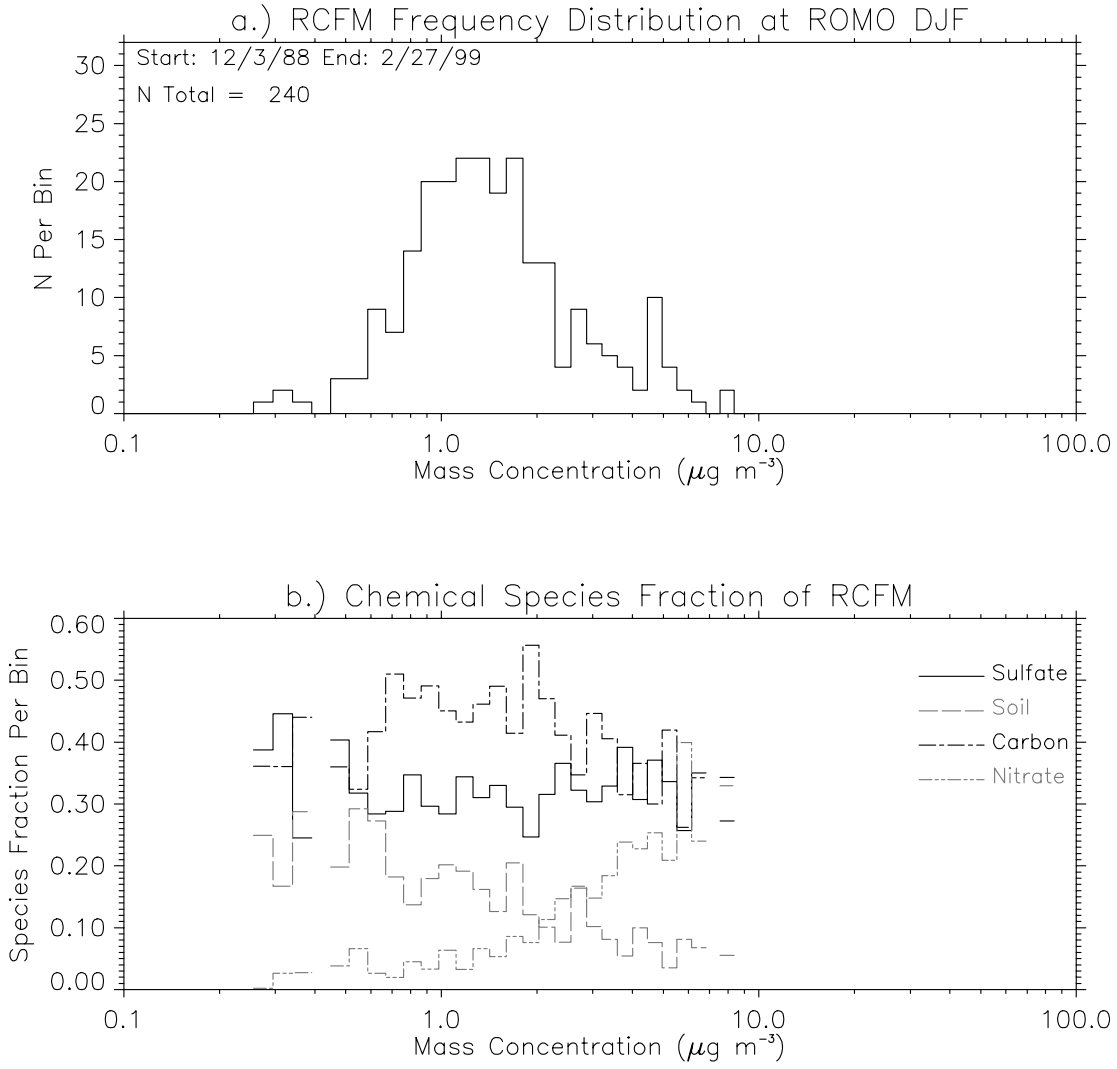

Figure 4.5 *(a) RCFM frequency distribution and (b) chemical species fractional contribution to RCFM by mass concentration bin at Rocky Mountain National Park.*

4.2.2 Maps of Chemical Species Contributions to Fine Mass (1994-1998)

Maps of mean chemical species percent contribution to reconstructed fine mass during December 1993 through November 1998 are shown in this section. A five-year period was chosen as a common period of record for all sites to display results on maps to show spatial patterns. Two maps are shown for each chemical species; the mean contribution during the specified time period, and the species contribution to an upper extreme, or percentile, of (reconstructed) fine mass. We represent the haziest days by the upper two percentiles of fine mass. The extreme contribution maps show the mean species contribution subtracted from the species contribution during the highest fine mass concentration days. In order to highlight regions where individual chemical species tend to dominate the highest fine mass concentration days, contours on the extreme contribution maps are shown for positive values only. We point out that all contours serve as guides to the eye and should be interpreted as approximations of spatial trends over large areas.

Discussion of chemical species contribution to low extremes of fine mass concentration is also included in this section. We represent the low fine mass concentration days, or clear days, by the lowest 20th percentile of fine mass. A larger percentile bracket is chosen for the low than high mass concentration days because the analytical measurements are less accurate at low mass concentrations, and incorporating more samples into the low extreme reduces uncertainty in the mean of those measurements. Clear day contributions can be inferred from the site specific frequency distribution plots.

An example of the chemical species contribution to the upper two percentiles of fine mass is the mean of the species pairwise contribution during the ten sampling days with highest fine mass concentration, based on 500 twice weekly IMPROVE samples available during a five-year period. A minimum of 70% of all possible sample periods must have complete chemical composition data for sites on the maps in this chapter except at Sipsey Wilderness where the criteria is relaxed to 64% to increase spatial coverage in the eastern United States.

The mean ammonium sulfate contribution to fine mass, expressed as a percent of fine mass, at IMPROVE monitoring sites across the United States, shown in Figure 4.6a, reaches a maximum of approximately 55% in the eastern United States. Note that values in Figure 4.6a are lower throughout much of the eastern United States sites than analogous values shown in Chapter 2, with discrepancies between the two chapters due to the different time periods, different averaging methods, and use of sulfur times three in place of the sulfate ion for calculations in this chapter.

Figure 4.6b shows sulfate contribution to the fine mass upper two percentiles, expressed as the mean contribution subtracted from the upper extreme contribution. By comparing Figures 4.6a and 4.6b we see that throughout much of the eastern United States the sulfate contribution to the upper extreme of fine mass exceeds the mean sulfate contribution. For example, the difference between the mean and upper two percentiles of sulfate contribution at Dolly Sods is 29%, or the contribution to the upper extreme is 84%, or the sum of the values for that site as

given by Figures 4.6a and 4.6b. Figure 4.6b indicates that the spatial extent of high sulfate contribution (sites greater than 20% in Figure 4.6b) to upper extremes of fine mass encompasses

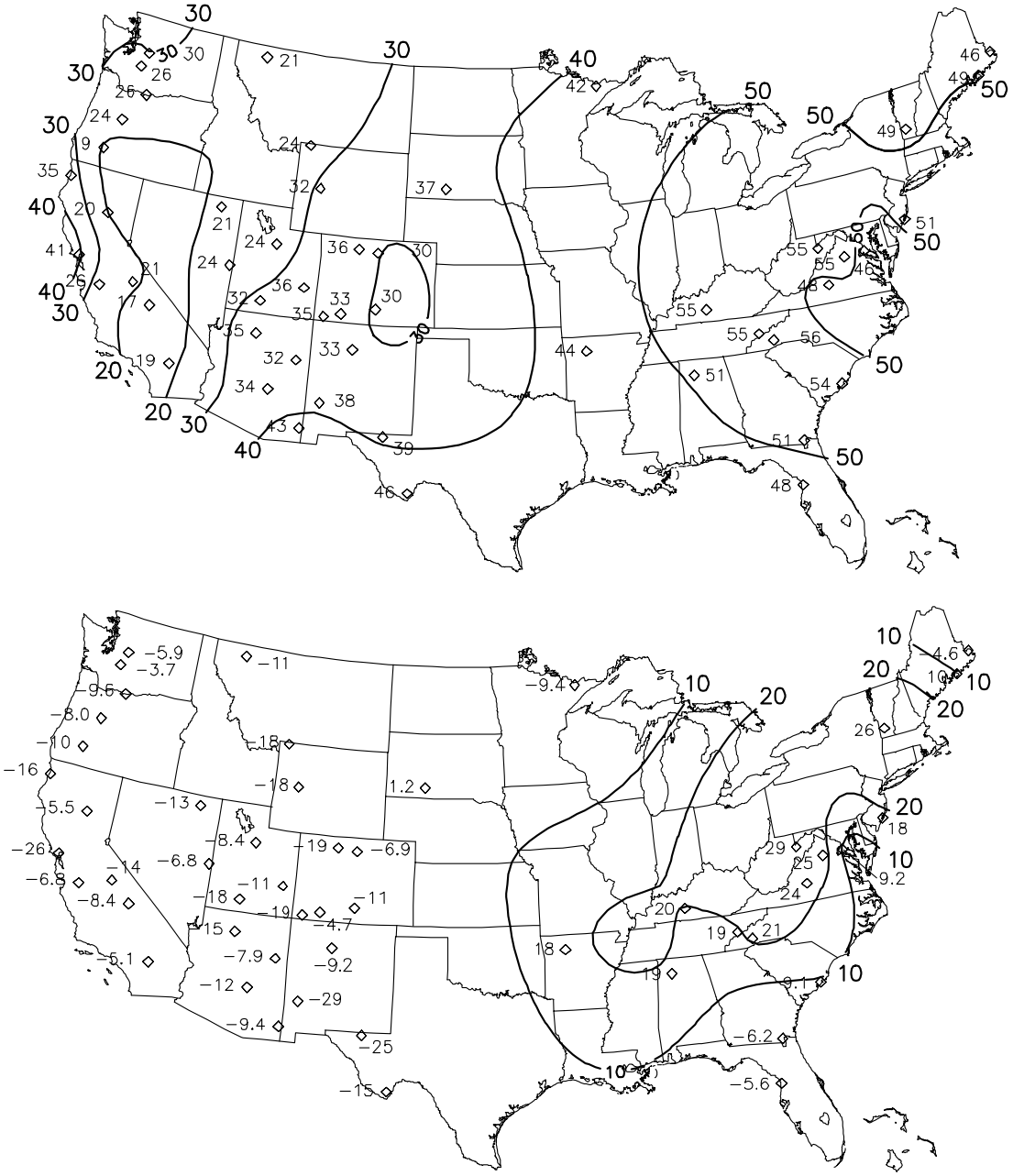

(a)

(b)

Figure 4.6 *(a) Map of mean sulfate contribution (%) to RCFM at IMPROVE monitoring sites across the United States. (b) Map of sulfate contribution to the upper two percentiles of RCFM (shown as the mean contribution subtracted from the upper extreme contribution).*

a region along the Ohio River Valley and northeast of Lye Brook. The true region of high sulfate contribution to the upper extreme of fine mass is likely more localized than the rather broad region in the eastern United States, where the mean sulfate contribution to fine mass exceeds approximately 50%. Negative values in Figure 4.6b indicate that the sulfate contribution to the upper extreme of fine mass is less than the mean for IMPROVE sites in the western United States and the most northerly and most southerly reaches of the eastern United States. In these regions, chemical species other than sulfate are major contributors to fine mass when particle fine mass concentrations are high.

The sulfate contribution to the lowest 20th percentile fine mass concentration days, or clean days, is about 5 to 10% less than the mean sulfate contribution (Figure 4.6a) in the eastern United States, and about 0 to 5% lower than the mean sulfate contribution in the western United States This translates to sulfate contributions on clean days of approximately 50% in the East and about 30% in the West.

The mean particle carbon contribution to fine mass, shown in Figure 4.7a, exhibits a general north-south gradient across the United States, with the highest values in the northwest United States. The difference between the carbon contribution to the mean and upper extreme of fine mass is shown in Figure 4.7b. At most western United States sites, the carbon contribution to the upper extremes is higher than the mean, while in the eastern United States only Moosehorn National Wildlife Refuge has a positive difference between the mean and upper extreme contributions. In the West, the carbon contribution to upper extremes of fine mass can be characterized by sporadic high values. For example, a 41% difference at Gila Wilderness Area in Figure 4.7b changes magnitude and location from year to year. These carbon 'hot spots' in the western United States may be related to wildland fires.

The particle carbon contribution to clean days is about 0 to 5% greater than the mean carbon contribution to fine mass at all IMPROVE sites shown in Figure 4.7a. Higher carbon contributions, approximately 15% in excess of the mean, are observed on clean days at monitoring sites in southern California.

The mean soil contribution to fine mass (Figure 4.8a) is about 5–10% along the eastern and western United States' coasts, and about 10–25% in the interior west. The soil contribution to the upper extremes of fine mass (Figure 4.8b) increases substantially from the mean in the southeast and throughout the southwest. Long-range dust transport from North African deserts may explain the large contribution of soil to the upper fine mass percentiles in the southeast states [Perry et al., 1997]. This source region is further evidenced by approximately 80% contribution of soil to the upper extremes of fine mass at Virgin Islands (not shown) during the summer and fall. High soil contributions to upper extremes of fine mass are also seen at sites in the southwest, particularly at Sequoia National Park (a difference of 35% from the mean) and Guadalupe Mountains National Park (a difference of 41% from the mean) in Figure 4.8b, which may be related to wind-blown dust originating in nearby arid regions.

Contributions of fine soil to clean days is generally within a few percent of the mean, therefore spatial patterns and magnitude of clean day fine soil contributions are roughly analogous to Figure 4.8a.

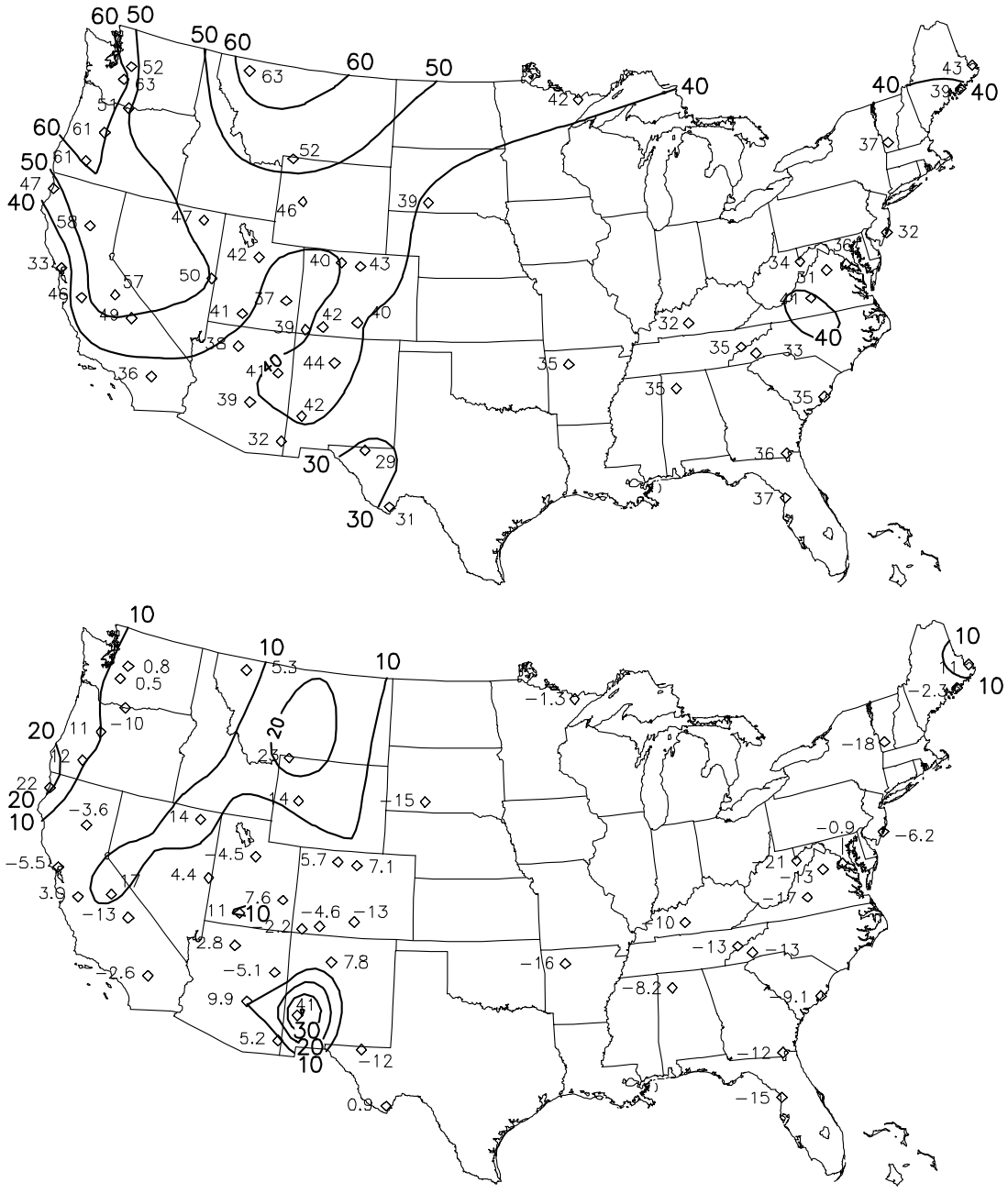

(a)

(b)

Figure 4.7 *(a) Map of mean particle carbon contribution to RCFM (%) at IMPROVE monitoring sites across the United States. (b) Map of particle carbon contribution to the upper two percentiles of RCFM (shown as the mean contribution subtracted from the upper extreme contribution).*

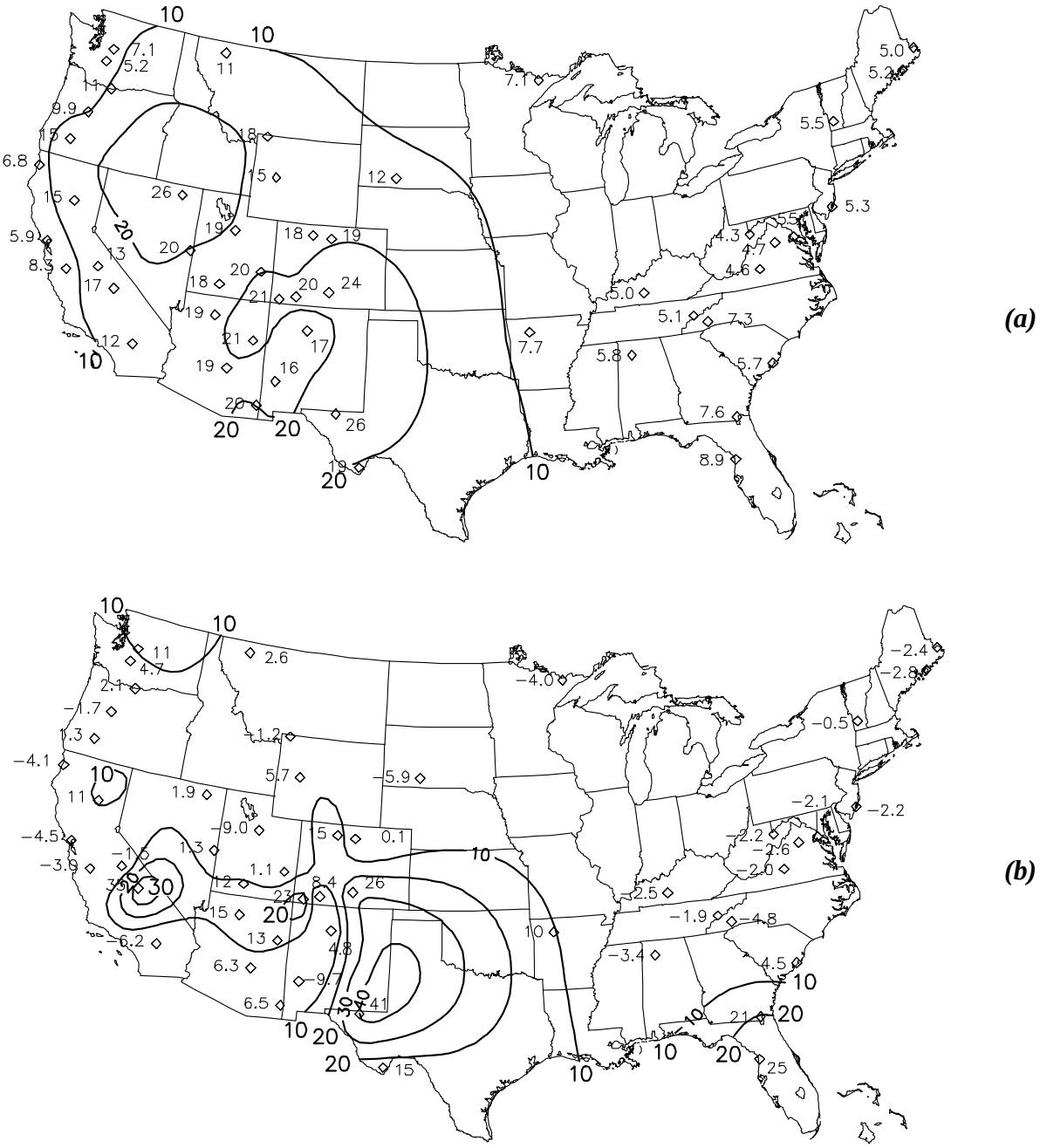

Figure 4.8 *(a) Map of mean soil contribution to RCFM (%) at IMPROVE monitoring sites across the United States. (b) Map of soil contribution to the upper two percentiles of RCFM (shown as the mean contribution subtracted from the upper extreme contribution).*

Because wintertime is generally the season when fine particle nitrate mass concentrations are at a maximum, and particle nitrate mass concentrations are often overwhelmed by other fine mass species during non-winter seasons, we show wintertime contributions to the mean (Figure 4.9a) and the upper extreme of fine mass (Figure 4.9b). The upper five percentiles are used to display the upper extreme for the wintertime maps so that statistics of the extreme values are derived from a sufficiently large number of data points.

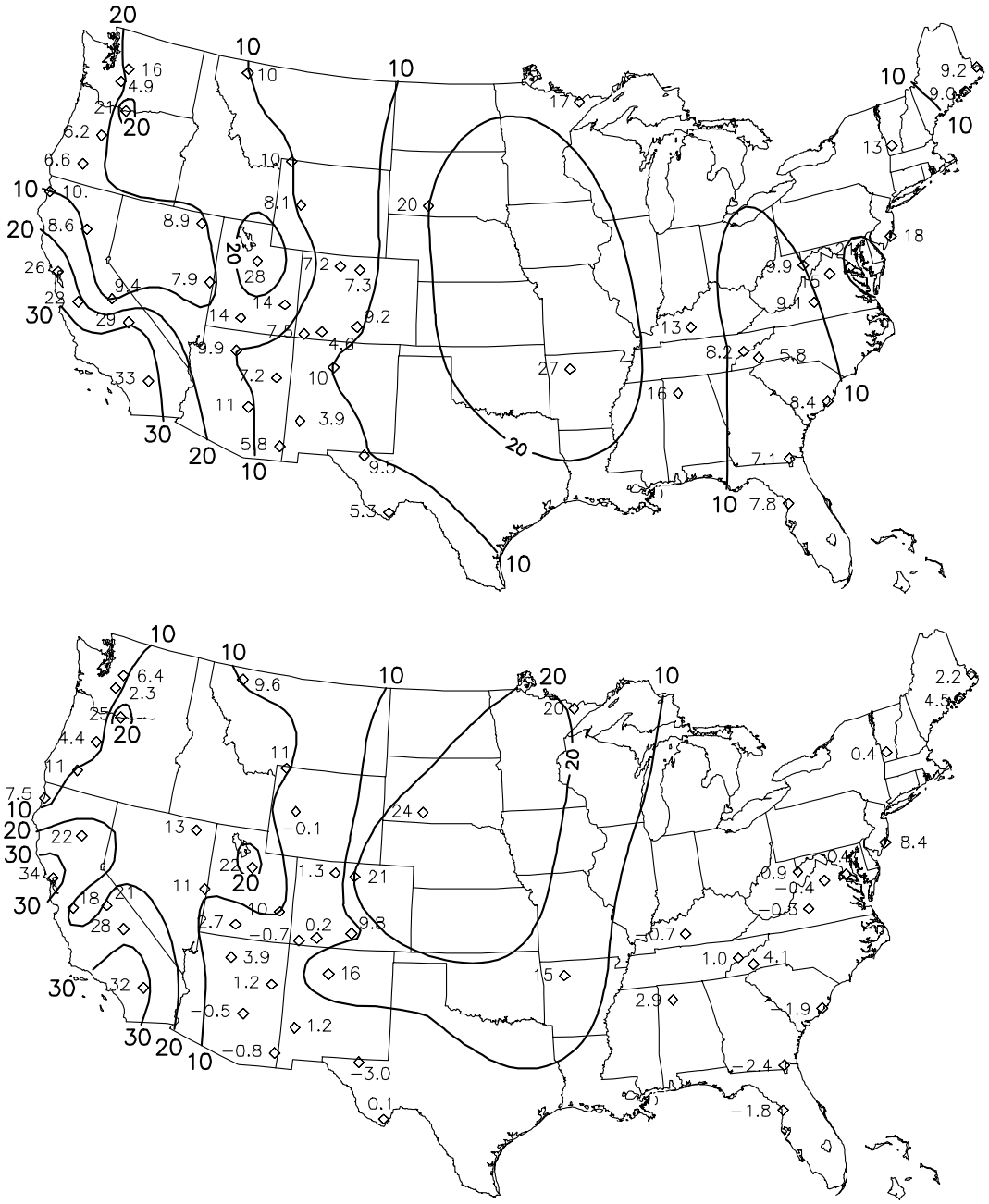

Figure 4.9 *(a) Map of mean particle nitrate contribution to RCFM (%) at IMPROVE monitoring sites across the United States. (b) Map of particle nitrate contribution to the upper five percentiles of RCFM (shown as the mean contribution subtracted from the upper extreme contribution). Data are shown for winter only.*

Figure 4.9b shows that many IMPROVE sites with high wintertime particle nitrate contributions to mean fine mass also have nitrate contributions to the upper extreme of fine mass well in excess of the mean. For example, Point Reyes National Seashore has a 26% contribution

to mean fine mass concentration, with an additional 34% contribution to the upper extreme of fine mass, or 60% particle nitrate contribution to the upper extreme of fine mass. Similar examples can be found at nearly all IMPROVE sites in California. Sites where the difference between the mean and upper extreme particle nitrate contribution to fine mass is 20% or more include most California sites, Columbia River, Lone Peak, Rocky Mountain, Boundary Waters, and Badlands. Among Midwest and eastern sites mean wintertime particle nitrate contributions to fine mass in excess of 27% and 21% occur at Upper Buffalo and Washington, D.C., respectively, although the contribution to upper extreme of fine mass at these sites is less than 20% in excess of the mean. In the eastern United States the nitrate contribution to the upper extremes of wintertime fine mass is typically very similar to the mean, with the exception of Edwin B. Forsythe (Brigantine), where particle nitrate contributes 26% of fine mass on high fine mass days, or a difference of 8% from the mean.

Particle nitrate contribution to fine mass on clear wintertime days is generally only a few percent less than the mean wintertime nitrate contribution shown in Figure 4.9a, including the central and eastern United States sites where mean particle nitrate contributions are greater than 10%. Exceptions are the particle nitrate impacted sites mentioned above, where clean day wintertime particle nitrate contribution to fine mass is approximately 5 to 20% below the mean. This is expected at the particle nitrate impacted sites because the mean nitrate contribution is strongly influenced by the large particle nitrate contribution on high fine mass concentration days.

For the wintertime maps shown in Figure 4.9, the minimum data requirement of 70% was relaxed to 60% at Mount Zirkel, Sipsey, and Shining Rock so that the nitrate maps included the same IMPROVE sites as the other chemical species maps.

4.3 SUMMARY

The particle sulfate, carbon, soil, and nitrate contributions to the fine mass frequency distribution are shown at selected IMPROVE monitoring sites to illustrate departures in the respective chemical species mean contributions to fine mass from the contribution of those species to the extremes of observed fine mass concentration. Maps of the mean and upper extremes of chemical species contribution are shown to illustrate spatial patterns in chemical species contributions to fine mass. Spatial patterns in chemical species contributions to extremes of observed fine mass concentration may be indicative of source regions for visibility reducing particles. In addition, the extreme value maps indicate the magnitude of chemical species contribution to what are likely the haziest days in a given region.

On the haziest days, or upper percentiles of observed fine mass, all major components of fine mass; sulfates, nitrates, carbon, and soil, can have large contributions to fine mass depending on region and time of year. Sulfate is a major contributor to both the mean and upper extremes of fine mass in the eastern United States, with largest contributions to the upper extremes clustered in regions of high sulfur emissions. Particle carbon exhibits a general increasing south-to-north gradient in mean contribution to fine mass, with sporadic high contributions to the upper extremes of fine mass in the western United States that may be related to wildland fires. The

mean soil contribution to fine mass is largest in the western United States, with high soil contributions to upper extremes in the southwest and southeast coastal regions likely related to regional and long-range transport of wind-blown dust. Particle nitrate contributions to fine mass are generally largest during the winter, and have substantially increased contributions to upper extremes of fine mass near urban areas.

On clear days, or the lowest 20th percentile of fine mass concentrations, sulfate and carbon are the largest contributors to fine mass. The sulfate contribution to fine mass on clear days is approximately 50% in the eastern United States, and approximately 20 to 30% in the western United States. Particle carbon contribution on clear days is approximately 40% in the East and from 40 to 60% in the West. Fine soil contributes a maximum of 20% to fine mass on clear days in the southwest United States, with contributions of only 5 to 10% during clear days in other regions of the United States. Particle nitrate contribution to fine mass on clear wintertime days is less than 10% at most IMPROVE sites, except for some monitoring locations near urban areas, and nearly all monitoring locations in the central United States, where particle nitrates contribute from 10 to 20% of fine mass on clean wintertime days.

4.4 REFERENCES

Perry K. D., Cahill T. A., Eldred R. A., Dutcher D. D., and Gill T. E., (1997) Long-range transport of North African dust to the eastern United States, *J. Geophys. Res.* 102(D10):11,225-11,238.

CHAPTER 5: See the Graphic Viewer for the latest trends

TRENDS ANALYSIS

Only recently has the IMPROVE aerosol network, initiated in March 1988, matured to a point where long-term trends of average ambient aerosol concentrations and reconstructed extinction can be assessed. There is now sufficient data to also examine trends in the aerosol concentrations and extinction for the clear and hazy days.

Characterization of trends, however, with only 11 years of data, can be a highly subjective exercise such that slopes and their significance can vary depending on the technique employed. Using ordinary least squares (OLS) regression approach is questionable with such small data sets as the results can be highly influenced by outliers plus standard deviations and standard errors can be large. In another approach, developed by Theil [1950], outlier data points do not as significantly influence the results. Slopes of trend lines are calculated for each site by first finding the slope between all possible pairs of data points, then sorting the results from smallest or most negative to the largest and finally, the median value in the case of an odd number of pairs is selected as the estimated slope, or in the case of even number of pairs the average of the two slopes that straddle the median is used as the estimate. The significance of the Theil slope is found by assuming that the "true" slope is zero, then calculating the probability that the estimated slope occurred by chance. This technique has also been adopted by the Environmental Protection Agency (EPA) for estimating trends in air quality data.

In this report, we examine trends of the distribution of $PM_{2.5}$ mass concentrations, reconstructed extinction and deciview, and their associated constituents at the IMPROVE sites with eleven years of data.

The trends are examined by sorting each year's data into three groups based on the cumulative frequency of occurrence of $PM_{2.5}$: lowest fine mass days, 0–20%; median fine mass days, 40-60%; and highest fine mass days, 80-100%. Each group is then labeled by its mid point (e.g., 10th, 50th, 90th percentiles). After sorting each group's average concentrations of $PM_{2.5}$ and selecting the associated principal aerosol species, scattering and/or absorption of each species, reconstructed light extinction, and deciview are calculated.

In addition to statistical concerns, there is always the underlying year-to-year variability due to meteorology. While the importance of meteorologically induced trends cannot be ignored, when trying to deduce the effect of emission changes, the role of meteorology is beyond the scope of this discussion.

The Theil slope estimates for a five-year rolling average of fine mass and deciview for the 90, 50, and 10 percentile groups are presented in Table 5.1. Each slope is paired with the probability for rejection. Plots of the data that went into the regressions can be found in Appendix B.

Table 5.1 *The Theil slope estimates for a five-year rolling average of fine mass and deciview for the 90, 50, and 10 percentile groups. Each slope is paired with the probability for rejection.*

Variable	Trend Coeff. Group 10	Significance Group 10	Trend Coeff. Group 50	Significance Group 50	Trend Coeff. Group 90	Significance Group 90
ACADIA NATIONAL PARK						
Particle mass (ng/m^3/yr)						
Fine Mass	-67.05	0.015	-133.08	0.000	-187.13	0.001
Sulfate	-39.21	0.005	-81.73	0.001	-95.43	0.191
Nitrate	-6.84	0.000	-10.01	0.015	-30.21	0.001
Organic	-11.12	0.119	-13.00	0.119	-69.13	0.015
Light-Absorbing Carbon	-11.20	0.000	-25.08	0.000	-35.58	0.000
Fine Soil	2.72	0.068	0.06	0.500	-1.32	0.500
Coarse Mass	-72.01	0.191	153.37	0.068	261.62	0.015
Particle extinction (1/Mm/yr)						
Total	-0.67	0.005	-1.21	0.000	-1.34	0.001
Sulfate	-0.41	0.005	-0.85	0.001	-1.00	0.191
Nitrate	-0.07	0.000	-0.10	0.015	-0.32	0.001
Organic	-0.04	0.119	-0.05	0.119	-0.28	0.015
Absorption	-0.11	0.000	-0.25	0.000	-0.36	0.000
Soil	0.00	0.068	0.00	0.500	0.00	0.500
Coarse	-0.04	0.191	0.09	0.068	0.16	0.015
Deciview **(dv/yr)**	-0.22	0.005	-0.23	0.000	-0.12	0.005
BADLANDS NATIONAL PARK						
Particle mass (ng/m^3/yr)						
Fine Mass	-46.29	0.001	-103.81	0.005	39.25	0.119
Sulfate	-7.60	0.281	-0.36	0.500	-8.24	0.386
Nitrate	2.93	0.191	-27.60	0.015	148.86	0.005
Organic	-18.98	0.001	-23.26	0.068	9.29	0.191
Light-Absorbing Carbon	0.17	0.500	-1.22	0.191	-5.79	0.191
Fine Soil	-20.13	0.005	-38.28	0.001	-97.54	0.001
Coarse Mass	11.61	0.500	-35.88	0.281	-280.13	0.001
Particle extinction (1/Mm/yr)						
Total	-0.12	0.035	-0.40	0.005	0.75	0.035
Sulfate	-0.06	0.281	0.00	0.500	-0.06	0.386
Nitrate	0.02	0.191	-0.21	0.015	1.13	0.005
Organic	-0.08	0.001	-0.09	0.068	0.04	0.191
Absorption	0.00	0.500	-0.01	0.191	-0.06	0.191
Soil	-0.02	0.005	-0.04	0.001	-0.10	0.001
Coarse	0.01	0.500	-0.02	0.281	-0.17	0.001
Deciview **(dv/yr)**	-0.05	0.068	-0.12	0.005	0.10	0.015

Table 5.1 *Continued.*

Variable	Trend Coeff. Group 10	Significance Group 10	Trend Coeff. Group 50	Significance Group 50	Trend Coeff. Group 90	Significance Group 90
BANDELIER NATIONAL MONUMENT						
Particle mass (ng/m^3/yr)						
Fine Mass	-64.47	0.005	-72.32	0.000	70.28	0.035
Sulfate	-35.89	0.005	-5.60	0.281	26.47	0.015
Nitrate	-1.35	0.119	-5.59	0.015	1.50	0.386
Organic	-23.71	0.015	-55.13	0.005	-14.73	0.068
Light-Absorbing Carbon	5.54	0.000	-4.27	0.015	-5.28	0.015
Fine Soil	-13.31	0.035	-10.30	0.191	41.48	0.005
Coarse Mass	-261.48	0.015	-310.53	0.119	139.00	0.035
Particle extinction (1/Mm/yr)						
Total	-0.35	0.005	-0.46	0.001	0.19	0.035
Sulfate	-0.20	0.005	-0.03	0.281	0.15	0.015
Nitrate	-0.01	0.119	-0.03	0.015	0.01	0.386
Organic	-0.10	0.015	-0.22	0.005	-0.06	0.068
Absorption	0.06	0.000	-0.04	0.015	-0.05	0.015
Soil	-0.01	0.035	-0.01	0.191	0.04	0.005
Coarse	-0.16	0.015	-0.19	0.119	0.08	0.035
Deciview **(dv/yr)**	-0.17	0.015	-0.18	0.001	0.07	0.068
BIG BEND NATIONAL PARK						
Particle mass (ng/m^3/yr)						
Fine Mass	26.97	0.191	51.01	0.035	285.08	0.001
Sulfate	-0.34	0.500	37.85	0.001	109.93	0.005
Nitrate	-0.67	0.386	3.01	0.119	11.02	0.068
Organic	7.87	0.191	-16.11	0.005	21.63	0.119
Light-Absorbing Carbon	-0.67	0.500	-0.45	0.500	1.27	0.500
Fine Soil	21.49	0.035	27.77	0.035	116.61	0.005
Coarse Mass	-41.71	0.119	116.98	0.068	568.37	0.005
Particle extinction (1/Mm/yr)						
Total	0.00	0.500	0.20	0.005	1.29	0.005
Sulfate	0.00	0.500	0.19	0.001	0.55	0.005
Nitrate	0.00	0.386	0.02	0.119	0.06	0.068
Organic	0.03	0.191	-0.06	0.005	0.09	0.119
Absorption	-0.01	0.500	0.00	0.500	0.01	0.500
Soil	0.02	0.035	0.03	0.035	0.12	0.005
Coarse	-0.03	0.119	0.07	0.068	0.34	0.005
Deciview **(dv/yr)**	0.00	0.500	0.07	0.005	0.23	0.005
BRYCE CANYON NATIONAL PARK						
Particle mass (ng/m^3/yr)						
Fine Mass	-23.83	0.005	-8.96	0.035	85.89	0.015
Sulfate	-15.18	0.005	-21.00	0.015	7.17	0.281
Nitrate	3.21	0.005	1.59	0.068	-9.23	0.068
Organic	-10.38	0.035	4.35	0.386	80.55	0.015
Light-Absorbing Carbon	3.79	0.005	3.50	0.068	12.24	0.015
Fine Soil	-7.93	0.035	2.26	0.191	-1.47	0.500
Coarse Mass	-124.55	0.035	-137.06	0.035	-203.40	0.001
Particle extinction (1/Mm/yr)						
Total	-0.18	0.035	-0.17	0.005	0.39	0.068
Sulfate	-0.11	0.005	-0.15	0.015	0.05	0.281
Nitrate	0.02	0.005	0.01	0.068	-0.07	0.068
Organic	-0.04	0.035	0.02	0.386	0.32	0.015
Absorption	0.04	0.005	0.04	0.068	0.12	0.015

Table 5.1 *Continued.*

Variable	Trend Coeff. Group 10	Significance Group 10	Trend Coeff. Group 50	Significance Group 50	Trend Coeff. Group 90	Significance Group 90
Soil	-0.01	0.035	0.00	0.191	0.00	0.500
Coarse	-0.08	0.035	-0.08	0.035	-0.12	0.001
Deciview **(dv/yr)**	-0.10	0.035	-0.08	0.015	0.10	0.035
BRIDGER WILDERNESS AREA						
Particle mass ($ng/m^3/yr$)						
Fine Mass	0.11	0.500	-34.08	0.035	-18.54	0.500
Sulfate	-9.31	0.068	-5.79	0.068	-20.63	0.015
Nitrate	0.11	0.500	-0.98	0.386	-0.14	0.500
Organic	4.12	0.119	-28.14	0.035	48.89	0.068
Light-Absorbing Carbon	3.36	0.001	4.66	0.015	9.22	0.068
Fine Soil	-2.65	0.015	-10.34	0.068	-43.10	0.015
Coarse Mass	-85.61	0.068	-69.01	0.035	-280.96	0.015
Particle extinction (1/Mm/yr)						
Total	-0.08	0.191	-0.14	0.035	-0.13	0.191
Sulfate	-0.06	0.068	-0.04	0.068	-0.13	0.015
Nitrate	0.00	0.500	-0.01	0.386	0.00	0.500
Organic	0.02	0.119	-0.11	0.035	0.20	0.068
Absorption	0.03	0.001	0.05	0.015	0.09	0.068
Soil	0.00	0.015	-0.01	0.068	-0.04	0.015
Coarse	-0.05	0.068	-0.04	0.035	-0.17	0.015
Deciview **(dv/yr)**	-0.05	0.191	-0.07	0.068	-0.03	0.386
CANYONLANDS NATIONAL PARK						
Particle mass ($ng/m^3/yr$)						
Fine Mass	-64.44	0.005	-83.14	0.005	-99.11	0.001
Sulfate	-43.08	0.005	-37.82	0.005	-27.35	0.001
Nitrate	-5.33	0.068	-4.75	0.119	-28.09	0.015
Organic	-10.52	0.015	-27.43	0.005	-16.74	0.281
Light-Absorbing Carbon	4.66	0.001	0.39	0.281	3.58	0.119
Fine Soil	-15.45	0.005	-15.83	0.000	-20.39	0.119
Coarse Mass	4.68	0.386	-73.71	0.386	-152.11	0.068
Particle extinction (1/Mm/yr)						
Total	-0.26	0.035	-0.34	0.015	-0.49	0.015
Sulfate	-0.22	0.005	-0.19	0.005	-0.14	0.001
Nitrate	-0.03	0.068	-0.02	0.119	-0.14	0.015
Organic	-0.04	0.015	-0.11	0.005	-0.07	0.281
Absorption	0.05	0.001	0.00	0.281	0.04	0.119
Soil	-0.02	0.005	-0.02	0.000	-0.02	0.119
Coarse	0.00	0.386	-0.04	0.386	-0.09	0.068
Deciview **(dv/yr)**	-0.13	0.035	-0.13	0.015	-0.14	0.015
CHIRICAHUA NATIONAL MONUMENT						
Particle mass ($ng/m^3/yr$)						
Fine Mass	30.24	0.068	25.91	0.119	96.33	0.005
Sulfate	-1.49	0.386	30.67	0.005	66.31	0.015
Nitrate	4.48	0.015	3.91	0.000	9.47	0.068
Organic	13.92	0.015	-23.18	0.035	-6.36	0.500
Light-Absorbing Carbon	4.16	0.001	-1.12	0.119	-2.61	0.281
Fine Soil	8.09	0.068	9.51	0.119	32.57	0.001
Coarse Mass	156.51	0.005	-22.06	0.119	-96.24	0.191
Particle extinction (1/Mm/yr)						
Total	0.23	0.000	0.08	0.119	0.27	0.015
Sulfate	-0.01	0.386	0.16	0.005	0.35	0.015

Table 5.1 *Continued.*

Variable	Trend Coeff. Group 10	Significance Group 10	Trend Coeff. Group 50	Significance Group 50	Trend Coeff. Group 90	Significance Group 90
Nitrate	0.02	0.015	0.02	0.000	0.05	0.068
Organic	0.06	0.015	-0.09	0.035	-0.03	0.500
Absorption	0.04	0.001	-0.01	0.119	-0.03	0.281
Soil	0.01	0.068	0.01	0.119	0.03	0.001
Coarse	0.09	0.005	-0.01	0.119	-0.06	0.191
Deciview **(dv/yr)**	0.10	0.001	0.03	0.119	0.07	0.035
CRATER LAKE NATIONAL PARK						
Particle mass ($ng/m^3/yr$)						
Fine Mass	-48.14	0.001	-48.84	0.035	112.28	0.015
Sulfate	-9.07	0.005	-9.38	0.119	-9.80	0.191
Nitrate	-0.72	0.281	-2.88	0.119	4.34	0.386
Organic	-27.45	0.001	-38.29	0.015	69.10	0.015
Light-Absorbing Carbon	-0.73	0.500	4.26	0.191	9.92	0.119
Fine Soil	-8.49	0.000	-7.92	0.015	30.49	0.005
Coarse Mass	-97.56	0.035	-98.77	0.015	-264.69	0.035
Particle extinction (1/Mm/yr)						
Total	-0.27	0.001	-0.24	0.068	0.20	0.191
Sulfate	-0.07	0.005	-0.07	0.119	-0.08	0.191
Nitrate	-0.01	0.281	-0.02	0.119	0.03	0.386
Organic	-0.11	0.001	-0.15	0.015	0.28	0.015
Absorption	-0.01	0.500	0.04	0.191	0.10	0.119
Soil	-0.01	0.000	-0.01	0.015	0.03	0.005
Coarse	-0.06	0.035	-0.06	0.015	-0.16	0.035
Deciview **(dv/yr)**	-0.18	0.005	-0.10	0.119	0.05	0.119
DENALI NATIONAL PARK AND PRESERVE						
Particle mass ($ng/m^3/yr$)						
Fine Mass	-18.55	0.015	-19.61	0.119	-48.62	0.191
Sulfate	-6.29	0.035	-19.14	0.068	-14.08	0.035
Nitrate	-0.11	0.500	-0.06	0.281	-1.89	0.119
Organic	-14.96	0.068	-3.98	0.281	1.29	0.500
Light-Absorbing Carbon	1.73	0.015	5.78	0.001	1.27	0.500
Fine Soil	-1.48	0.119	-11.07	0.015	-40.68	0.005
Coarse Mass	-108.05	0.191	-95.48	0.386	-290.46	0.015
Particle extinction (1/Mm/yr)						
Total	-0.12	0.191	-0.13	0.068	-0.34	0.119
Sulfate	-0.05	0.035	-0.16	0.068	-0.12	0.035
Nitrate	0.00	0.500	0.00	0.281	-0.02	0.119
Organic	-0.06	0.068	-0.02	0.281	0.01	0.500
Absorption	0.02	0.015	0.06	0.001	0.01	0.500
Soil	0.00	0.119	-0.01	0.015	-0.04	0.005
Coarse	-0.07	0.191	-0.06	0.386	-0.17	0.015
Deciview **(dv/yr)**	-0.08	0.191	-0.08	0.119	-0.10	0.191
GLACIER NATIONAL PARK						
Particle mass ($ng/m^3/yr$)						
Fine Mass	-73.28	0.005	-135.39	0.001	-134.39	0.035
Sulfate	-27.31	0.005	4.06	0.281	-36.23	0.005
Nitrate	-3.91	0.015	-3.01	0.015	-23.47	0.119
Organic	-23.93	0.035	-89.58	0.000	-50.96	0.281
Light-Absorbing Carbon	4.92	0.015	-2.24	0.281	-26.02	0.001
Fine Soil	-11.74	0.005	-28.37	0.000	-30.93	0.281
Coarse Mass	-222.54	0.015	-346.44	0.015	-190.79	0.281

Table 5.1 *Continued.*

Variable	Trend Coeff. Group 10	Significance Group 10	Trend Coeff. Group 50	Significance Group 50	Trend Coeff. Group 90	Significance Group 90
Particle extinction (1/Mm/yr)						
Total	-0.72	0.005	-0.70	0.005	-1.30	0.015
Sulfate	-0.33	0.005	0.05	0.281	-0.43	0.005
Nitrate	-0.05	0.015	-0.04	0.015	-0.28	0.119
Organic	-0.10	0.035	-0.36	0.000	-0.20	0.281
Absorption	0.05	0.015	-0.02	0.281	-0.26	0.001
Soil	-0.01	0.005	-0.03	0.000	-0.03	0.281
Coarse	-0.13	0.015	-0.21	0.015	-0.11	0.281
Deciview **(dv/yr)**	-0.28	0.005	-0.17	0.015	-0.20	0.015
GREAT SAND DUNES NATIONAL MONUMENT						
Particle mass (ng/m^3/yr)						
Fine Mass	-71.62	0.005	-84.16	0.005	-24.14	0.386
Sulfate	-15.95	0.015	0.80	0.386	18.05	0.015
Nitrate	-9.46	0.005	-3.13	0.191	0.72	0.500
Organic	-42.01	0.005	-42.24	0.001	10.48	0.386
Light-Absorbing Carbon	-0.55	0.119	-1.08	0.035	7.75	0.015
Fine Soil	-4.32	0.281	-37.62	0.015	-35.85	0.119
Coarse Mass	-294.48	0.001	-514.94	0.001	278.93	0.191
Particle extinction (1/Mm/yr)						
Total	-0.53	0.001	-0.56	0.001	0.30	0.035
Sulfate	-0.11	0.015	0.01	0.386	0.12	0.015
Nitrate	-0.06	0.005	-0.02	0.191	0.01	0.500
Organic	-0.17	0.005	-0.17	0.001	0.04	0.386
Absorption	-0.01	0.119	-0.01	0.035	0.08	0.015
Soil	0.00	0.281	-0.04	0.015	-0.04	0.119
Coarse	-0.18	0.001	-0.31	0.001	0.17	0.191
Deciview **(dv/yr)**	-0.30	0.001	-0.20	0.001	0.10	0.068
GREAT SMOKY MOUNTAINS NATIONAL PARK						
Particle mass (ng/m^3/yr)						
Fine Mass	0.60	0.500	-140.01	0.005	200.81	0.015
Sulfate	9.88	0.191	-98.08	0.035	259.17	0.005
Nitrate	-11.90	0.015	-34.91	0.001	-30.52	0.005
Organic	-15.89	0.386	-25.53	0.119	3.01	0.386
Light-Absorbing Carbon	2.63	0.386	-10.92	0.191	-15.09	0.068
Fine Soil	5.82	0.191	-5.39	0.191	27.64	0.281
Coarse Mass	4.13	0.500	44.85	0.281	-143.56	0.191
Particle extinction (1/Mm/yr)						
Total	0.02	0.500	-1.27	0.005	2.23	0.035
Sulfate	0.10	0.191	-0.96	0.035	2.53	0.005
Nitrate	-0.12	0.015	-0.34	0.001	-0.30	0.005
Organic	-0.07	0.386	-0.10	0.119	0.01	0.386
Absorption	0.03	0.386	-0.11	0.191	-0.15	0.068
Soil	0.01	0.191	-0.01	0.191	0.03	0.281
Coarse	0.00	0.500	0.03	0.281	-0.09	0.191
Deciview **(dv/yr)**	0.00	0.500	-0.15	0.005	0.10	0.068
GUADALUPE MOUNTAINS NATIONAL PARK						
Particle mass (ng/m^3/yr)						
Fine Mass	-2.60	0.386	35.69	0.119	281.09	0.015
Sulfate	10.65	0.281	51.06	0.005	1.82	0.386
Nitrate	1.90	0.191	1.31	0.068	8.11	0.068
Organic	-15.98	0.000	-18.30	0.001	-25.90	0.068

Table 5.1 *Continued.*

Variable	Trend Coeff. Group 10	Significance Group 10	Trend Coeff. Group 50	Significance Group 50	Trend Coeff. Group 90	Significance Group 90
Light-Absorbing Carbon	2.07	0.005	0.82	0.005	-7.36	0.015
Fine Soil	3.86	0.191	-4.24	0.500	276.83	0.000
Coarse	-42.21	0.068	-45.08	0.191	98.27	0.191
Particle extinction (1/Mm/yr)						
Total	-0.02	0.500	0.23	0.191	0.31	0.281
Sulfate	0.06	0.281	0.28	0.005	0.01	0.386
Nitrate	0.010	0.191	0.01	0.068	0.05	0.068
Organic	-0.06	0.000	-0.07	0.001	-0.10	0.068
Absorption	0.02	0.005	0.01	0.005	-0.07	0.015
Soil	0.00	0.191	0.00	0.500	0.28	0.000
Coarse	-0.03	0.068	-0.03	0.191	0.06	0.191
Deciview **(dv/yr)**	0.00	0.500	0.07	0.191	0.05	0.281
JARBIDGE WILDERNESS AREA						
Particle mass ($ng/m^3/yr$)						
Fine Mass	26.72	0.035	-12.37	0.386	173.22	0.035
Sulfate	-3.20	0.281	-11.13	0.015	-16.10	0.005
Nitrate	4.60	0.068	1.94	0.068	9.62	0.191
Organic	18.53	0.015	2.42	0.386	127.31	0.015
Light-Absorbing Carbon	3.41	0.001	4.83	0.005	16.93	0.005
Fine Soil	4.84	0.119	-7.64	0.500	25.08	0.191
Coarse Mass	-69.90	0.068	-50.04	0.068	142.48	0.068
Particle extinction (1/Mm/yr)						
Total	0.05	0.281	-0.02	0.386	0.81	0.035
Sulfate	-0.02	0.281	-0.06	0.015	-0.09	0.005
Nitrate	0.03	0.068	0.01	0.068	0.06	0.191
Organic	0.07	0.015	0.01	0.386	0.51	0.015
Absorption	0.03	0.001	0.05	0.005	0.17	0.005
Soil	0.01	0.119	-0.01	0.500	0.03	0.191
Coarse	-0.04	0.068	-0.03	0.068	0.09	0.068
Deciview **(dv/yr)**	0.03	0.281	0.00	0.500	0.23	0.035
LASSEN VOLCANIC NATIONAL PARK						
Particle mass ($ng/m^3/yr$)						
Fine Mass	-20.83	0.035	-10.56	0.386	138.58	0.015
Sulfate	-4.73	0.281	18.54	0.001	26.57	0.015
Nitrate	4.91	0.015	10.32	0.035	10.21	0.035
Organic	-19.72	0.035	-49.78	0.015	42.83	0.015
Light-Absorbing Carbon	0.78	0.119	-4.44	0.015	1.32	0.500
Fine Soil	-1.82	0.035	7.02	0.191	50.85	0.001
Coarse Mass	-239.74	0.001	-372.94	0.005	-616.48	0.000
Particle extinction (1/Mm/yr)						
Total	-0.22	0.001	-0.21	0.035	0.20	0.191
Sulfate	-0.04	0.281	0.14	0.001	0.20	0.015
Nitrate	0.04	0.015	0.08	0.035	0.08	0.035
Organic	-0.08	0.035	-0.20	0.015	0.17	0.015
Absorption	0.01	0.119	-0.04	0.015	0.01	0.500
Soil	0.00	0.035	0.01	0.191	0.05	0.001
Coarse	-0.14	0.001	-0.22	0.005	-0.37	0.000
Deciview **(dv/yr)**	-0.15	0.015	-0.10	0.035	0.05	0.281
MESA VERDE NATIONAL PARK						
Particle mass ($ng/m^3/yr$)						
Fine Mass	11.24	0.281	58.92	0.035	147.62	0.005

Table 5.1 *Continued.*

Variable	Trend Coeff. Group 10	Significance Group 10	Trend Coeff. Group 50	Significance Group 50	Trend Coeff. Group 90	Significance Group 90
Sulfate	-17.53	0.015	25.44	0.005	10.46	0.191
Nitrate	2.51	0.119	-1.64	0.119	13.39	0.001
Organic	10.21	0.068	-0.64	0.500	6.63	0.119
Light-Absorbing Carbon	11.02	0.000	6.57	0.015	5.81	0.119
Fine Soil	3.74	0.068	23.19	0.035	123.21	0.001
Coarse Mass	-262.62	0.001	-106.10	0.191	-29.78	0.386
Particle extinction (1/Mm/yr)						
Total	-0.13	0.119	0.17	0.005	0.30	0.035
Sulfate	-0.10	0.015	0.14	0.005	0.06	0.191
Nitrate	0.01	0.119	-0.01	0.119	0.07	0.001
Organic	0.04	0.068	0.00	0.500	0.03	0.119
Absorption	0.11	0.000	0.07	0.015	0.06	0.119
Soil	0.00	0.068	0.02	0.035	0.12	0.001
Coarse	-0.16	0.001	-0.06	0.191	-0.02	0.386
Deciview **(dv/yr)**	-0.08	0.119	0.05	0.005	0.10	0.015
MOUNT RAINIER NATIONAL PARK						
Particle mass ($ng/m^3/yr$)						
Fine Mass	-47.90	0.015	-139.61	0.005	-405.17	0.001
Sulfate	-24.41	0.001	-10.19	0.281	-120.82	0.035
Nitrate	-3.45	0.015	3.40	0.119	-25.01	0.005
Organic	-15.75	0.068	-100.30	0.001	-216.11	0.000
Light-Absorbing Carbon	-5.70	0.005	-23.66	0.000	-52.09	0.001
Fine Soil	-0.93	0.119	-8.92	0.005	5.57	0.119
Coarse Mass	-116.98	0.119	-66.25	0.119	-258.13	0.035
Particle extinction (1/Mm/yr)						
Total	-0.74	0.005	-0.81	0.068	-4.33	0.005
Sulfate	-0.47	0.001	-0.20	0.281	-2.32	0.035
Nitrate	-0.07	0.015	0.07	0.119	-0.48	0.005
Organic	-0.06	0.068	-0.40	0.001	-0.86	0.000
Absorption	-0.06	0.005	-0.24	0.000	-0.52	0.001
Soil	0.00	0.119	-0.01	0.005	0.01	0.119
Coarse	-0.07	0.119	-0.04	0.119	-0.16	0.035
Deciview **(dv/yr)**	-0.32	0.015	-0.15	0.119	-0.42	0.005
PETRIFIED FOREST NATIONAL PARK						
Particle mass ($ng/m^3/yr$)						
Fine Mass	-92.75	0.001	-93.89	0.005	-15.91	0.386
Sulfate	-35.45	0.005	-23.79	0.015	5.79	0.500
Nitrate	-0.67	0.386	-2.92	0.119	-1.54	0.191
Organic	-27.74	0.015	-29.74	0.015	-29.29	0.015
Light-Absorbing Carbon	-9.67	0.001	-25.03	0.000	-21.21	0.000
Fine Soil	-21.01	0.001	-6.21	0.386	19.27	0.281
Coarse Mass	-82.76	0.068	-216.12	0.015	-214.62	0.068
Particle extinction (1/Mm/yr)						
Total	-0.50	0.005	-0.67	0.005	-0.50	0.035
Sulfate	-0.19	0.005	-0.13	0.015	0.03	0.500
Nitrate	0.00	0.386	-0.02	0.119	-0.01	0.191
Organic	-0.11	0.015	-0.12	0.015	-0.12	0.015
Absorption	-0.10	0.001	-0.25	0.000	-0.21	0.000
Soil	-0.02	0.001	-0.01	0.386	0.02	0.281
Coarse	-0.05	0.068	-0.13	0.015	-0.13	0.068
Deciview **(dv/yr)**	-0.20	0.005	-0.25	0.005	-0.13	0.035

Table 5.1 *Continued.*

Variable	Trend Coeff. Group 10	Significance Group 10	Trend Coeff. Group 50	Significance Group 50	Trend Coeff. Group 90	Significance Group 90
PINNACLES NATIONAL MONUMENT						
Particle mass (ng/m^3/yr)						
Fine Mass	-85.05	0.015	-201.24	0.000	-378.19	0.000
Sulfate	-29.08	0.001	-49.38	0.001	-42.68	0.005
Nitrate	-38.92	0.000	-70.04	0.000	-215.57	0.000
Organic	-3.40	0.191	-78.71	0.000	-89.93	0.001
Light-Absorbing Carbon	-1.19	0.191	-13.60	0.005	-27.65	0.000
Fine Soil	-7.48	0.005	-3.46	0.386	11.77	0.035
Coarse Mass	-268.10	0.015	-409.69	0.000	-234.49	0.068
Particle extinction (1/Mm/yr)						
Total	-0.77	0.001	-1.61	0.000	-2.76	0.000
Sulfate	-0.22	0.001	-0.36	0.001	-0.32	0.005
Nitrate	-0.29	0.000	-0.52	0.000	-1.59	0.000
Organic	-0.01	0.191	-0.32	0.000	-0.36	0.001
Absorption	-0.01	0.191	-0.14	0.005	-0.28	0.000
Soil	-0.01	0.005	0.00	0.386	0.01	0.035
Coarse	-0.16	0.015	-0.25	0.000	-0.14	0.068
Deciview **(dv/yr)**	-0.30	0.001	-0.37	0.001	-0.42	0.000
POINT REYES NATIONAL SEASHORE						
Particle mass (ng/m^3/yr)						
Fine Mass	19.33	0.035	-117.00	0.035	-500.74	0.001
Sulfate	-0.08	0.500	-21.15	0.015	23.93	0.035
Nitrate	2.05	0.386	-24.50	0.068	-302.31	0.005
Organics	20.47	0.015	-83.76	0.035	-246.62	0.001
Light-Absorbing Carbon	1.94	0.035	-11.87	0.005	-52.65	0.001
Fine Soil	1.22	0.035	7.49	0.005	2.67	0.191
Coarse Mass	-798.63	0.000	-542.54	0.005	-653.07	0.005
Particle extinction (1/Mm/yr)						
Total	-0.38	0.035	-1.21	0.015	-5.09	0.005
Sulfate	0.00	0.500	-0.27	0.015	0.31	0.035
Nitrate	0.03	0.386	-0.32	0.068	-3.89	0.005
Organic	0.08	0.015	-0.34	0.035	-0.99	0.001
Absorption	0.02	0.035	-0.12	0.005	-0.53	0.001
Soil	0.00	0.035	0.01	0.005	0.00	0.191
Coarse	-0.48	0.000	-0.33	0.005	-0.39	0.005
Deciview **(dv/yr)**	-0.12	0.119	-0.25	0.015	-0.50	0.005
REDWOOD NATIONAL PARK						
Particle mass (ng/m^3/yr)						
Fine Mass	-40.78	0.001	-118.24	0.000	-233.53	0.000
Sulfate	-9.21	0.001	-10.25	0.015	-39.34	0.001
Nitrate	-4.20	0.001	-10.73	0.000	-20.40	0.015
Organic	-24.51	0.001	-94.26	0.000	-155.02	0.000
Light-Absorbing Carbon	-0.13	0.500	-12.32	0.000	-23.85	0.000
Fine Soil	2.66	0.015	3.67	0.068	0.50	0.500
Coarse Mass	-154.94	0.005	-11.14	0.500	-161.85	0.000
Particle extinction (1/Mm/yr)						
Total	-0.57	0.001	-1.02	0.000	-2.51	0.000
Sulfate	-0.24	0.001	-0.26	0.015	-1.01	0.001
Nitrate	-0.11	0.001	-0.28	0.000	-0.53	0.015
Organic	-0.10	0.001	-0.38	0.000	-0.62	0.000
Absorption	0.00	0.500	-0.12	0.000	-0.24	0.000

Table 5.1 *Continued.*

Variable	Trend Coeff. Group 10	Significance Group 10	Trend Coeff. Group 50	Significance Group 50	Trend Coeff. Group 90	Significance Group 90
Soil	0.00	0.015	0.00	0.068	0.00	0.500
Coarse	-0.09	0.005	-0.01	0.500	-0.10	0.000
Deciview **(dv/yr)**	-0.23	0.005	-0.20	0.001	-0.27	0.000
ROCKY MOUNTAIN NATIONAL PARK						
Particle mass ($ng/m^3/yr$)						
Fine Mass	-26.83	0.005	-66.59	0.001	20.03	0.191
Sulfate	-17.20	0.001	-22.72	0.015	-19.29	0.015
Nitrate	-8.38	0.005	-9.31	0.119	-12.18	0.281
Organic	-7.51	0.119	-43.85	0.015	10.08	0.386
Light-Absorbing Carbon	6.90	0.001	3.50	0.015	4.72	0.119
Fine Soil	-4.44	0.386	-1.49	0.386	38.86	0.068
Coarse Mass	94.15	0.281	-70.26	0.281	-76.56	0.119
Particle extinction (1/Mm/yr)						
Total	-0.05	0.119	-0.38	0.005	-0.08	0.068
Sulfate	-0.10	0.001	-0.13	0.015	-0.11	0.015
Nitrate	-0.05	0.005	-0.05	0.119	-0.07	0.281
Organic	-0.03	0.119	-0.18	0.015	0.04	0.386
Absorption	0.07	0.001	0.04	0.015	0.05	0.119
Soil	0.00	0.386	0.00	0.386	0.04	0.068
Coarse	0.06	0.281	-0.04	0.281	-0.05	0.119
Deciview **(dv/yr)**	-0.04	0.191	-0.15	0.015	0.00	0.191
SAN GORGONIO WILDERNESS AREA						
Particle mass ($ng/m^3/yr$)						
Fine Mass	36.67	0.281	-227.48	0.005	-852.61	0.000
Sulfate	3.39	0.191	4.91	0.500	-78.48	0.000
Nitrate	9.95	0.191	-90.74	0.005	-516.36	0.005
Organic	19.58	0.035	-55.48	0.035	-142.23	0.001
Light-Absorbing Carbon	-1.82	0.119	-11.65	0.015	-35.87	0.015
Fine Soil	12.85	0.119	-75.56	0.015	-60.51	0.001
Coarse Mass	-107.78	0.191	-687.65	0.015	-1113.99	0.000
Particle extinction (1/Mm/yr)						
Total	0.15	0.281	-1.46	0.015	-5.56	0.000
Sulfate	0.02	0.191	0.03	0.500	-0.52	0.000
Nitrate	0.07	0.191	-0.60	0.005	-3.42	0.005
Organic	0.08	0.035	-0.22	0.035	-0.57	0.001
Absorption	-0.02	0.119	-0.12	0.015	-0.36	0.015
Soil	0.01	0.119	-0.08	0.015	-0.06	0.001
Coarse	-0.07	0.191	-0.41	0.015	-0.67	0.000
Deciview **(dv/yr)**	0.03	0.386	-0.25	0.015	-0.50	0.001
SHENANDOAH NATIONAL PARK						
Particle mass ($ng/m^3/yr$)						
Fine Mass	-27.71	0.119	-268.58	0.001	-78.23	0.281
Sulfate	3.23	0.386	-155.40	0.005	-19.64	0.500
Nitrate	-10.16	0.386	-10.63	0.281	-6.08	0.191
Organic	-17.10	0.000	-76.79	0.005	26.94	0.500
Light-Absorbing Carbon	3.13	0.119	-20.23	0.005	-6.50	0.386
Fine Soil	-0.13	0.500	-1.35	0.191	-13.33	0.191
Coarse Mass	-51.55	0.281	-213.69	0.035	-353.70	0.000
Particle extinction (1/Mm/yr)						
Total	-0.03	0.386	-2.53	0.005	-0.41	0.191
Sulfate	0.04	0.386	-1.76	0.005	-0.22	0.500

Table 5.1 *Continued.*

Variable	Trend Coeff. Group 10	Significance Group 10	Trend Coeff. Group 50	Significance Group 50	Trend Coeff. Group 90	Significance Group 90
Nitrate	-0.12	0.386	-0.12	0.281	-0.07	0.191
Organic	-0.07	0.000	-0.31	0.005	0.11	0.500
Absorption	0.03	0.119	-0.20	0.005	-0.07	0.386
Soil	0.00	0.500	0.00	0.191	-0.01	0.191
Coarse	-0.03	0.281	-0.13	0.035	-0.21	0.000
Deciview **(dv/yr)**	0.00	0.281	-0.27	0.005	0.00	0.281
TONTO NATIONAL MONUMENT						
Particle mass ($ng/m^3/yr$)						
Fine Mass	-38.91	0.005	-41.63	0.015	-33.63	0.191
Sulfate	-36.22	0.001	-3.52	0.386	-19.57	0.119
Nitrate	5.74	0.191	3.07	0.191	-3.23	0.386
Organic	-15.13	0.005	-24.68	0.001	-21.05	0.281
Light-Absorbing Carbon	4.79	0.000	1.20	0.191	-8.39	0.068
Fine Soil	8.09	0.068	-17.50	0.191	16.72	0.068
Coarse Mass	-103.68	0.035	-268.76	0.005	106.70	0.191
Particle extinction (1/Mm/yr)						
Total	-0.25	0.001	-0.29	0.015	-0.21	0.191
Sulfate	-0.15	0.001	-0.02	0.386	-0.08	0.119
Nitrate	0.02	0.191	0.01	0.191	-0.01	0.386
Organic	-0.06	0.005	-0.10	0.001	-0.08	0.281
Absorption	0.05	0.000	0.01	0.191	-0.08	0.068
Soil	0.01	0.068	-0.02	0.191	0.02	0.068
Coarse	-0.06	0.035	-0.16	0.005	0.06	0.191
Deciview **(dv/yr)**	-0.10	0.005	-0.10	0.035	-0.05	0.281
WEMINUCHE WILDERNESS AREA						
Particle mass ($ng/m^3/yr$)						
Fine Mass	4.37	0.386	-30.09	0.005	-49.95	0.035
Sulfate	1.39	0.386	-22.69	0.015	8.64	0.191
Nitrate	1.61	0.005	0.95	0.068	7.36	0.005
Organic	-2.80	0.191	-19.95	0.015	-40.24	0.119
Light-Absorbing Carbon	1.90	0.191	-1.22	0.015	-3.66	0.119
Fine Soil	-1.00	0.500	3.43	0.119	-11.57	0.281
Coarse Mass	-132.37	0.068	-104.45	0.068	-234.32	0.015
Particle extinction (1/Mm/yr)						
Total	-0.06	0.386	-0.25	0.035	-0.29	0.119
Sulfate	0.01	0.386	-0.16	0.015	0.06	0.191
Nitrate	0.01	0.005	0.01	0.068	0.05	0.005
Organic	-0.01	0.191	-0.08	0.015	-0.16	0.119
Absorption	0.02	0.191	-0.01	0.015	-0.04	0.119
Soil	0.00	0.500	0.00	0.119	-0.01	0.281
Coarse	-0.08	0.068	-0.06	0.068	-0.14	0.015
Deciview **(dv/yr)**	-0.02	0.500	-0.10	0.015	-0.10	0.068
YELLOWSTONE NATIONAL PARK						
Particle mass ($ng/m^3/yr$)						
Fine Mass	-108.85	0.000	-97.55	0.005	2.64	0.386
Sulfate	-20.43	0.000	-11.13	0.005	-0.49	0.500
Nitrate	-9.18	0.001	-11.87	0.015	0.69	0.386
Organic	-60.94	0.000	-15.82	0.015	108.14	0.035
Light-Absorbing Carbon	-4.89	0.001	-4.89	0.005	-3.44	0.191
Fine Soil	-11.17	0.005	-49.24	0.001	-63.64	0.068
Coarse Mass	-249.71	0.000	-150.36	0.000	-999.63	0.000

***Table 5.1** Continued.*

Variable	Trend Coeff. Group 10	Significance Group 10	Trend Coeff. Group 50	Significance Group 50	Trend Coeff. Group 90	Significance Group 90
Particle extinction (1/Mm/yr)						
Total	-0.65	0.000	-0.39	0.005	-0.28	0.035
Sulfate	-0.13	0.000	-0.07	0.005	0.00	0.500
Nitrate	-0.06	0.001	-0.08	0.015	0.00	0.386
Organic	-0.24	0.000	-0.06	0.015	0.43	0.035
Absorption	-0.05	0.001	-0.05	0.005	-0.03	0.191
Soil	-0.01	0.005	-0.05	0.001	-0.06	0.068
Coarse	-0.15	0.000	-0.09	0.000	-0.60	0.000
Deciview **(dv/yr)**	-0.36	0.000	-0.15	0.015	-0.05	0.068
YOSEMITE NATIONAL PARK						
Particle mass ($ng/m^3/yr$)						
Fine Mass	-20.60	0.068	-24.45	0.068	270.37	0.035
Sulfate	-17.27	0.005	-15.74	0.191	-40.35	0.015
Nitrate	-5.40	0.015	-34.46	0.005	-39.00	0.005
Organic	4.86	0.386	18.59	0.005	302.48	0.035
Light-Absorbing Carbon	-1.48	0.068	-2.98	0.035	12.81	0.281
Fine Soil	-3.45	0.119	9.42	0.119	29.84	0.015
Coarse Mass	60.40	0.281	-239.78	0.015	-239.92	0.005
Particle extinction (1/Mm/yr)						
Total	-0.13	0.068	-0.34	0.035	0.72	0.068
Sulfate	-0.12	0.005	-0.10	0.191	-0.27	0.015
Nitrate	-0.04	0.015	-0.23	0.005	-0.26	0.005
Organic	0.02	0.386	0.07	0.005	1.21	0.035
Absorption	-0.02	0.068	-0.03	0.035	0.13	0.281
Soil	0.00	0.119	0.01	0.119	0.03	0.015
Coarse	0.04	0.281	-0.14	0.015	-0.14	0.005
Deciview **(dv/yr)**	-0.05	0.035	-0.12	0.015	0.13	0.119

5.1 SELECTED EXAMPLES OF TRENDS IN FINE MASS ($PM_{2.5}$) AND DECIVIEW

As an example, Figure 5.1 shows plots of the 10, 50, and 90 percentile groups at Pinnacles National Monument for both $PM_{2.5}$ and deciview. The sample year (SYEAR) on the horizontal axis begins in March of each year. The horizontal axis for the five-year rolling average indicates the center year of the five-year period (CYEAR) on the x-axis. Pinnacles has significant negative slopes for all subgroups for both deciview and $PM_{2.5}$. For instance, both the trends for group 90 in $PM_{2.5}$ and deciview (dv) are decreasing at a statistically significant rate of 378.2 ng/m^3 and 0.42 dv/yr. Figure 5.2 shows the same plots for Badlands National Park, a site with a significant group 90 positive slope for visibility impairment of 0.10 dv/yr but a decreasing trend in the group 50 and group 10 percentile. Plots for Big Bend National Park (Figure 5.3) demonstrates statistically significant positive trends in deciview for group 90 and group 50, while group 10 trends are insignificant.

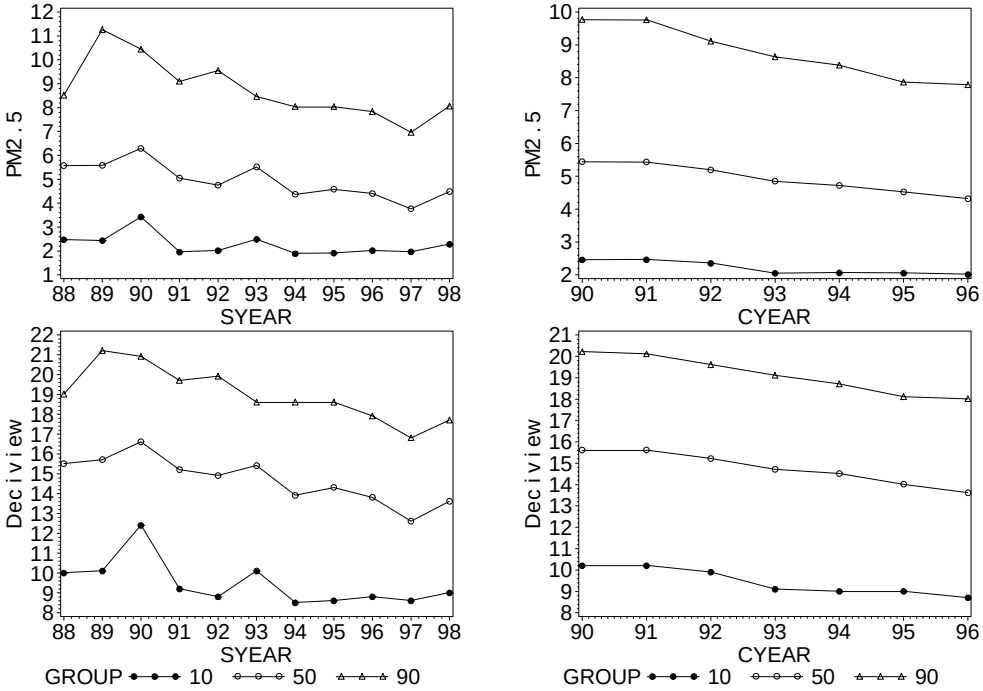

Figure 5.1 *Trends in annual and five-year rolling averages for $PM_{2.5}$ and deciview for Pinnacles National Monument.*

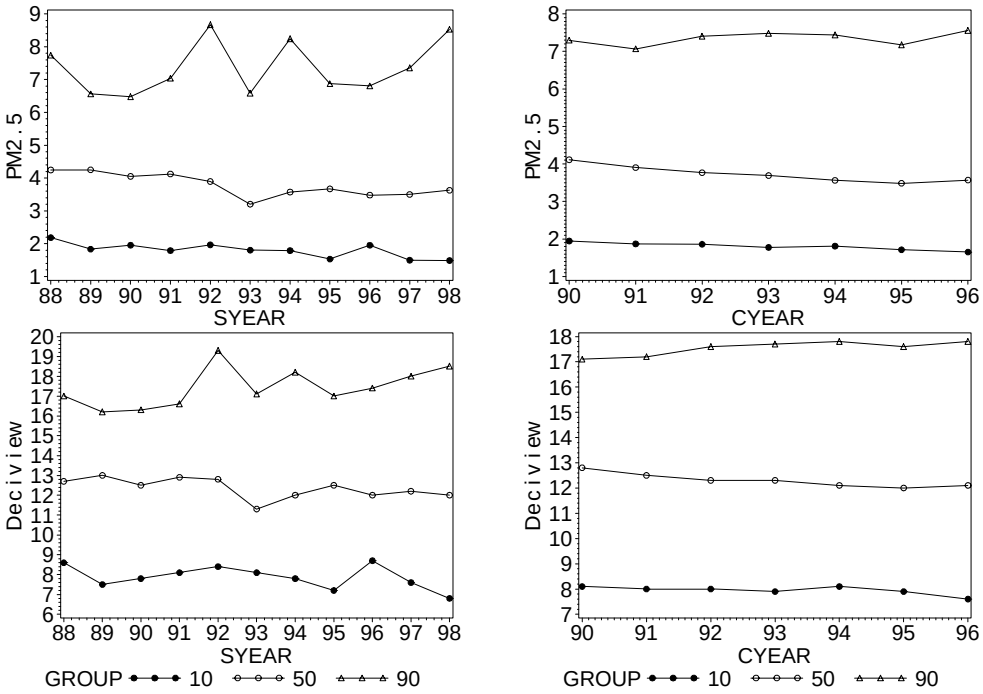

Figure 5.2 *Trends in annual and five-year rolling averages for $PM_{2.5}$ and deciview for Badlands National Park.*

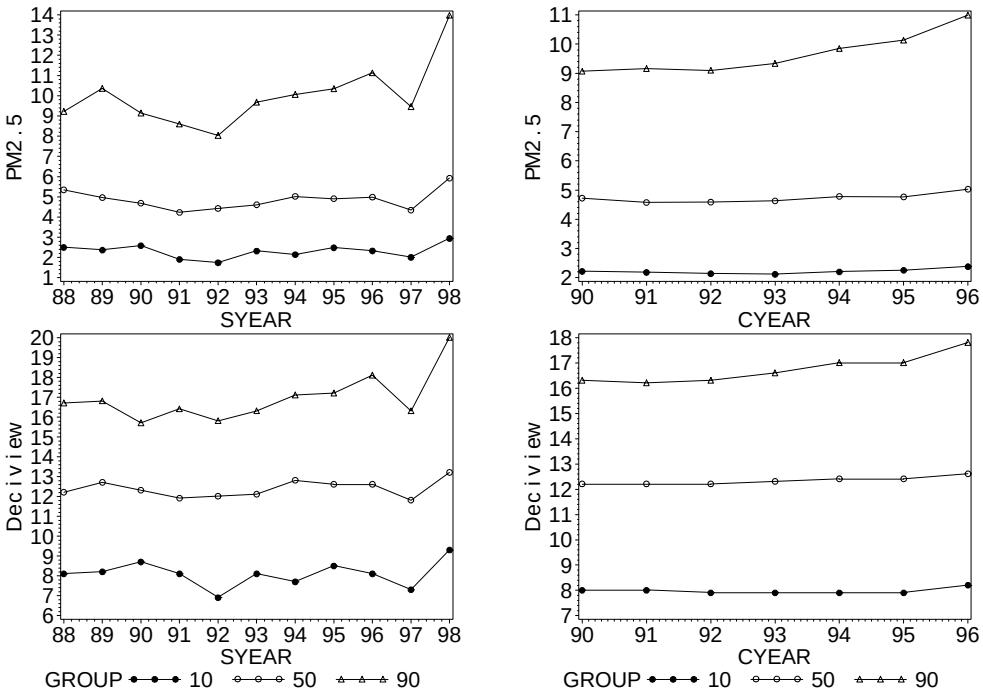

Figure 5.3 *Trends in annual and five-year rolling averages for $PM_{2.5}$ and deciview for Big Bend National Park.*

5.2 TRENDS IN $PM_{2.5}$ AND DECIVIEW ACROSS THE UNITED STATES

A map summarizing results of the trend analysis for the five-year rolling average deciviews and aerosol extinction are shown in Figures 5.4 and 5.5, respectively, for group 90. Similar presentations are made for sulfate, nitrate, organics, fine soil, and coarse mass in Figures 5.6, 5.7, 5.8, 5.9, and 5.10. (Additional maps of trends, using annual average data, in scattering and/or extinction for each species are presented in Appendix C.) The icons mark the site locations, a solid dot indicates an insignificant slope, the empty arrow indicates a positive or negative slope significant in the range of $0.05<p\leq0.1$ level of probability, and the solid arrow indicates a positive or negative slope that is significant at better than the 0.05 ($p\leq0.05$) level. A decreasing trend in deciview or extinction indicates improving visibility, while an increasing trend indicates worsening visibility.

Referring to Figure 5.4, group 90, the haziest days, has nine sites with positive and significant slopes indicating the visibility is getting worse on the haziest days, eleven sites where visibility is improving at a statistically significant rate, and nine sites where visibility remains the same. A summary of these sites follows:

Northern Great Plains: Badlands National Park, representing the Northern Great Plains region, has a statistically significant slope of 0.10 dv/yr. The trend toward increased haziness is driven by an increase in nitrate primarily in 1992 and forward as shown in Figure 5.11. (Temporal plots of group 90, 50 and 10 annual average species extinctions for all monitoring sites are presented in Appendix D.)

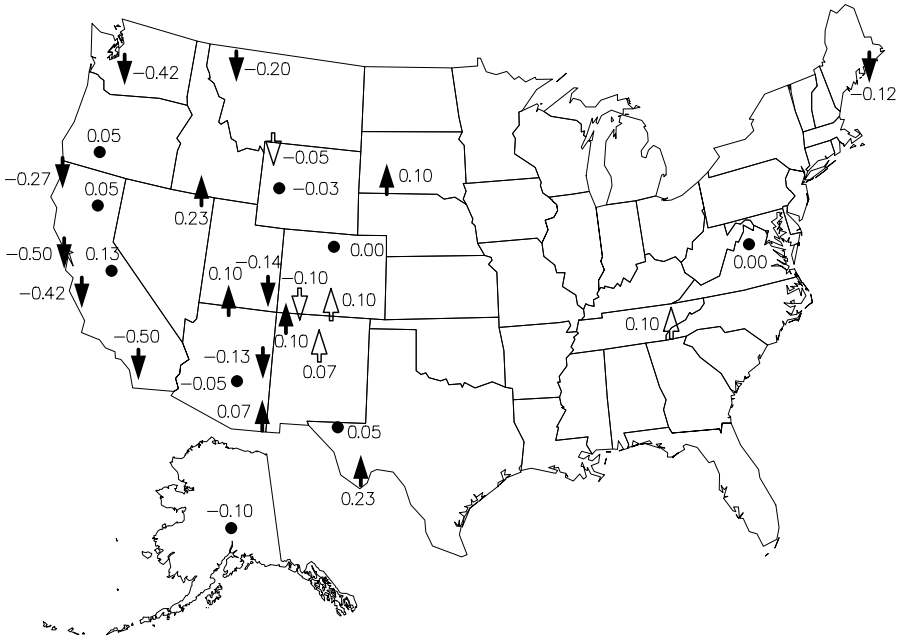

Figure 5.4 *Map summarizing the trends in deciview (dv/yr) for group 90 (top 20% of fine mass) days. The icons mark the site locations, a solid dot indicates an insignificant slope, the empty arrow indicates a positive or negative slope that is significant in the range of 0.05<p≤0.1 level of probability, and the solid arrow indicates a positive or negative slope that is significant at better than 0.05 (p≤0.05) level of probability.*

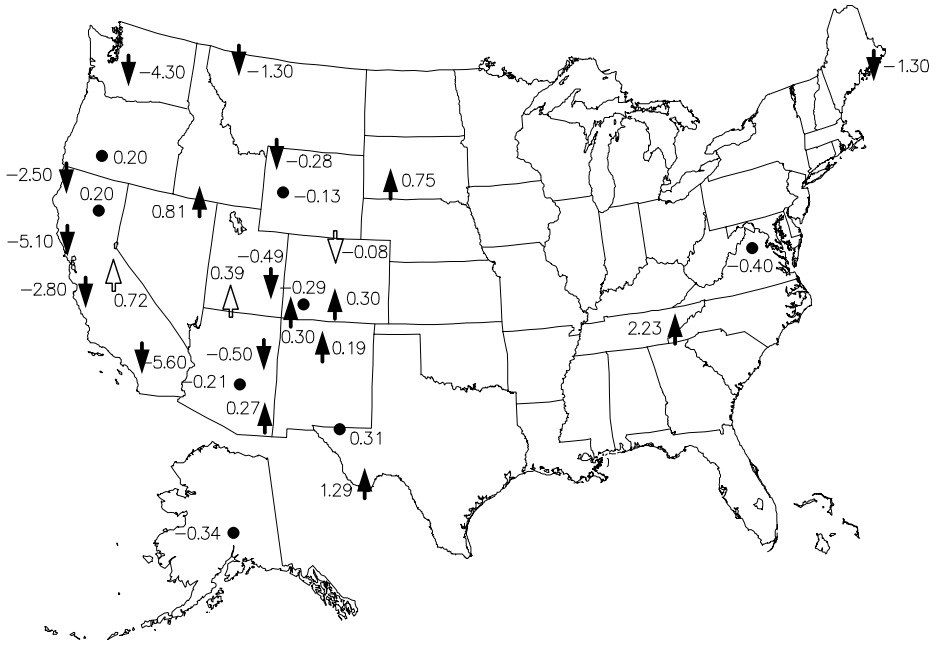

Figure 5.5 ***M****ap summarizing the trends in aerosol extinction (1/Mm/yr) for group 90 (top 20% of fine mass) days. The icons mark the site locations, a solid dot indicates an insignificant slope, the empty arrow indicates a positive or negative slope that is significant in the range of 0.05<p≤0.1 level of probability, and the solid arrow indicates a positive or negative slope that is significant at better than 0.05 (p≤0.05) level of probability.*

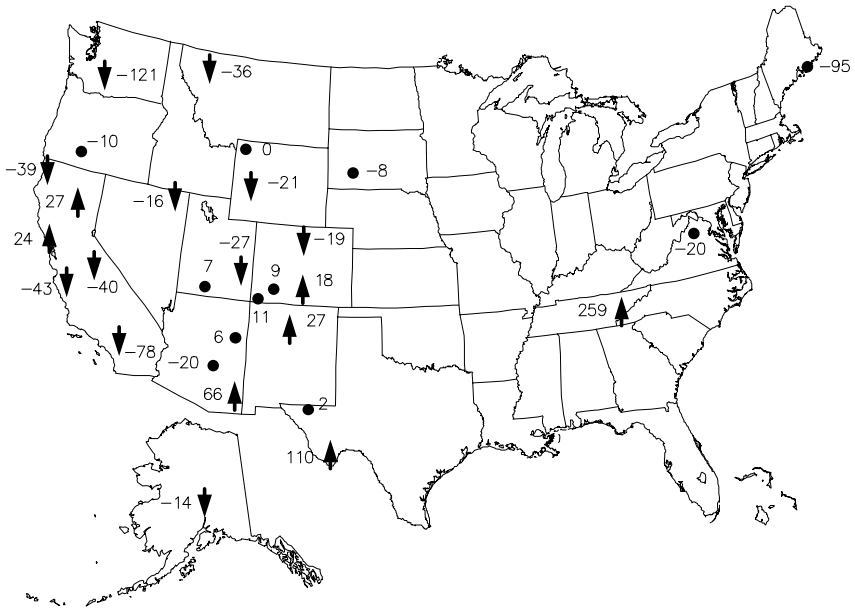

Figure 5.6 *Map summarizing the trends in sulfate mass concentration (ng/m^3/yr) for group 90 (top 20% of fine mass) days. The icons mark the site locations, a solid dot indicates an insignificant slope and the solid arrow indicates a positive or negative slope that is significant at better than 0.05 ($p \leq 0.05$) level of probability.*

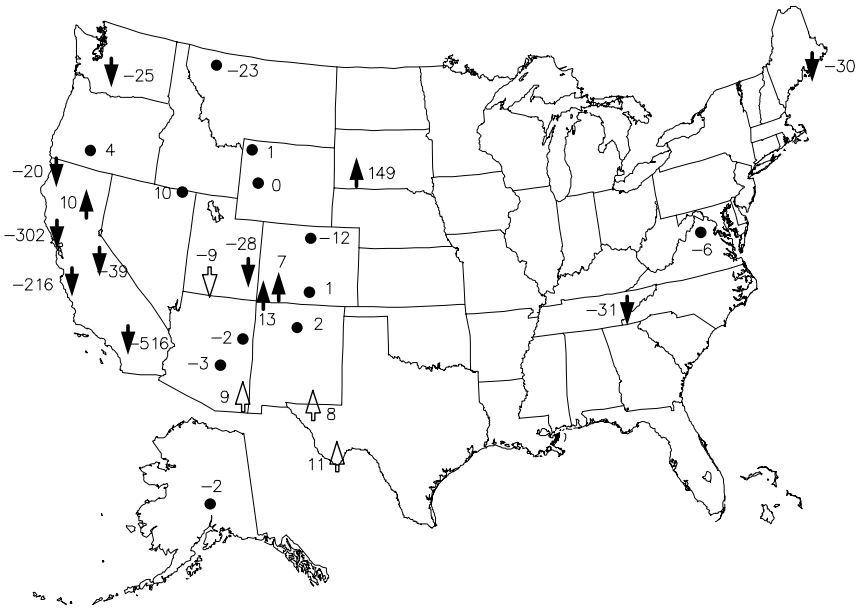

Figure 5.7 *Map summarizing the trends in nitrate mass concentration (ng/m^3/yr) for group 90 (top 20% of fine mass) days. The icons mark the site locations, a solid dot indicates an insignificant slope, the empty arrow indicates a positive or negative slope that is significant in the range of $0.05 < p \leq 0.1$ level of probability, and the solid arrow indicates a positive or negative slope that is significant at better than 0.05 ($p \leq 0.05$) level of probability.*

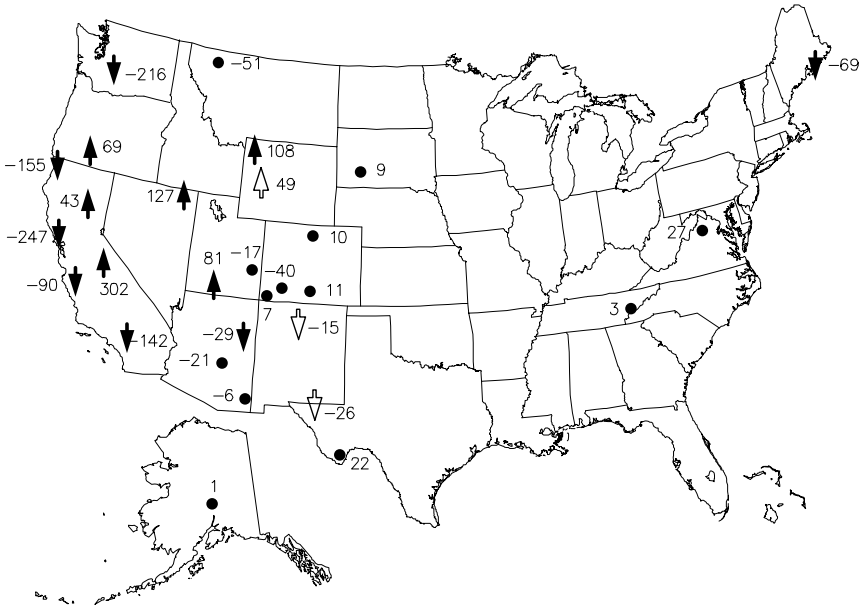

Figure 5.8 *Map summarizing the trends in organic mass concentration (ng/m^3/yr) for group 90 (top 20% of fine mass) days. The icons mark the site locations, a solid dot indicates an insignificant slope, the empty arrow indicates a positive or negative slope that is significant in the range of 0.05<p≤0.1 level of probability, and the solid arrow indicates a positive or negative slope that is significant at better than 0.05 (p≤0.05) level of probability.*

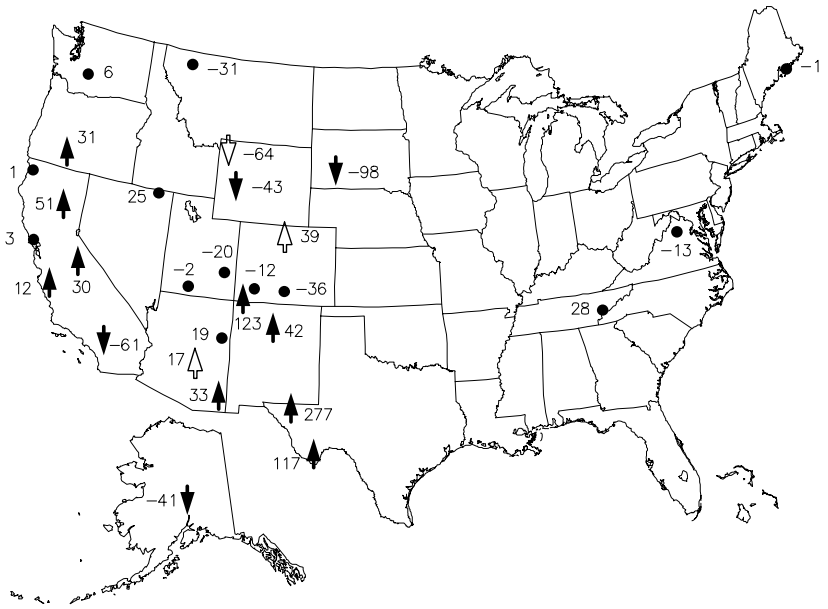

Figure 5.9 *Map summarizing the trends in fine soil mass concentration (ng/m^3/yr) for group 90 (top 20% of fine mass) days. The icons mark the site locations, a solid dot indicates an insignificant slope, the empty arrow indicates a positive or negative slope that is significant in the range of 0.05<p≤0.1 level of probability, and the solid arrow indicates a positive or negative slope that is significant at better than 0.05 (p≤0.05) level of probability.*

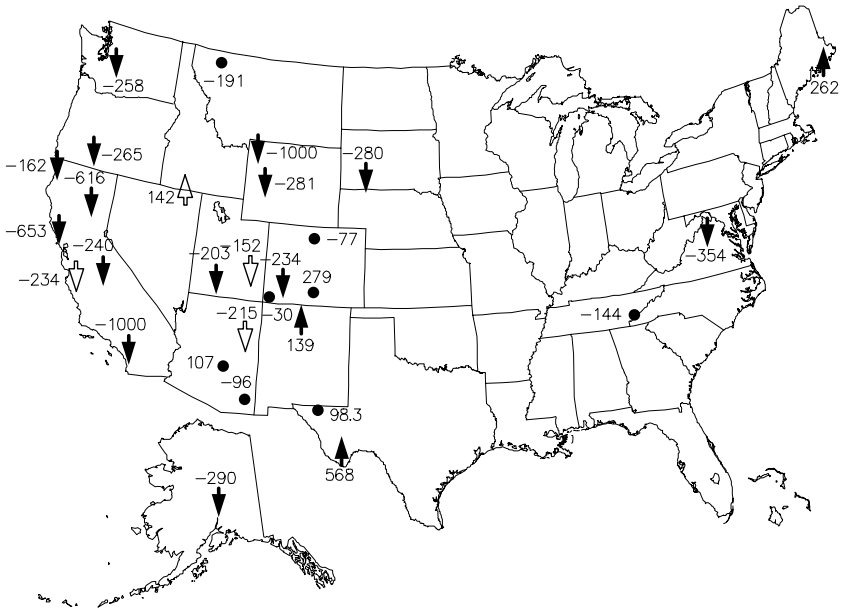

Figure 5.10 *Map summarizing the trends in coarse mass concentration (ng/m^3/yr) for group 90 (top 20% of fine mass) days. The icons mark the site locations, a solid dot indicates an insignificant slope, the empty arrow indicates a positive or negative slope that is significant in the range of $0.05<p\leq0.1$ level of probability, and the solid arrow indicates a positive or negative slope that is significant at better than 0.05 ($p\leq0.05$) level of probability.*

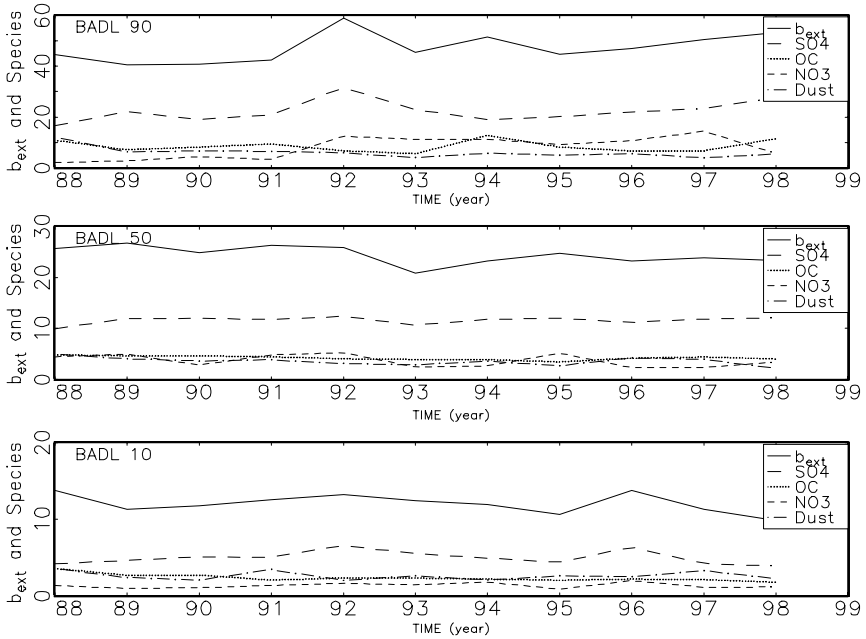

Figure 5.11 *Temporal plot of reconstructed extinction and extinction of constituent species for the group 90, 50, and 10 categories for Badlands National Park. The solid line corresponds to reconstructed extinction, the dashed line to sulfate scattering, the dotted line to organic scattering, the small dashed line to nitrate scattering, and the dot-dashed line to soil scattering. Units are in 1/Mm and time is in years.*

Great Basin: Jarbidge Wilderness Area in the Great Basin region has a significant slope of 0.23 dv/yr. The increasing haziness at Jarbidge is primarily driven by an increasing organic mass concentration as shown in Figures 5.8 and 5.12. These same figures show that sulfates are actually decreasing only to be offset by the organic mass fraction.

Central Rocky Mountains: Great Sand Dunes National Monument is the only monitoring site in the Central Rocky Mountain region to show a significant trend toward increasing haziness. Sulfates were shown to be increasing at a statistically significantly rate, while the slope of coarse mass was positive but not statistically significant (see Figures 5.6 and 5.10). These two species combine to form a significant trend in visibility that is driven primarily by one year (1994) when coarse mass was approximately twice that of other years (see Figure 5.13). Without the 1994 year visibility would be judged to not have changed at Great Sand Dunes. At Yellowstone National Park and Weminuche Wilderness Area, visibility is improving, while at Rocky Mountain National Park and Bridger Wilderness Area no change was recorded. Even though overall visibility is improving at Yellowstone, organics show a statistically significant increase in organics due primarily to two "fire" years in 1994 and 1996 (see Figure 5.14). The 1994 and 1996 fire years also show up as an increase in the organic mass concentration trends in the Sierra Nevada, Sierra-Humboldt, Great Basin, and parts of the Colorado Plateau and Central Rocky Mountain regions (see Figure 5.8).

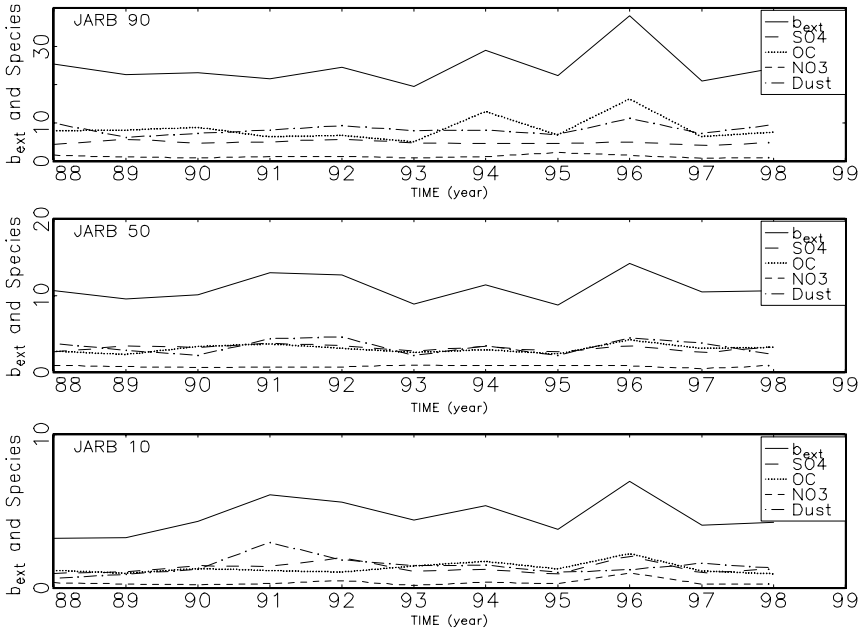

Figure 5.12 *Temporal plot of reconstructed extinction and extinction of constituent species for the group 90, 50, and 10 categories for Jarbidge Wilderness Area. The solid line corresponds to reconstructed extinction, the dashed line to sulfate scattering, the dotted line to organic scattering, the small dashed line to nitrate scattering, and the dot-dashed line to soil scattering. Units are in 1/Mm and time is in years.*

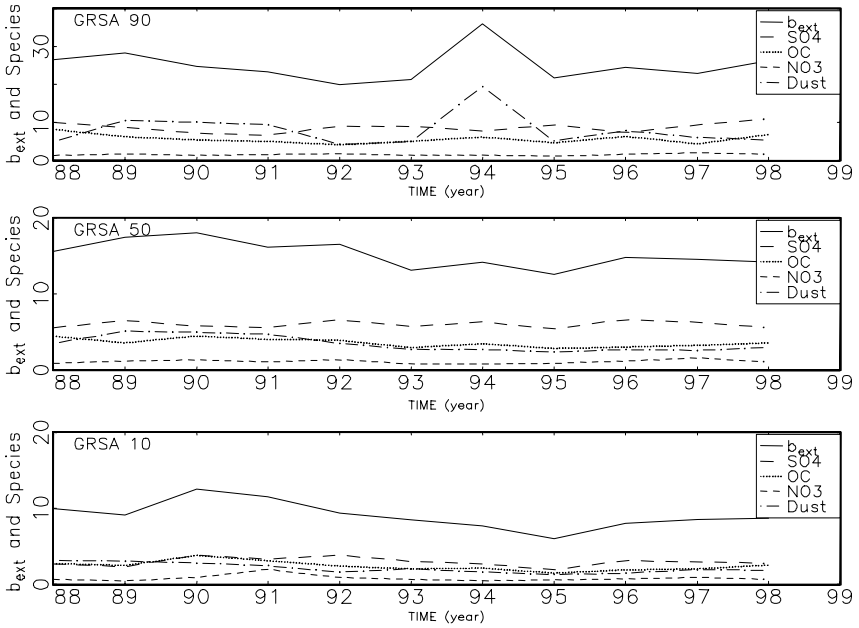

Figure 5.13 *Temporal plot of reconstructed extinction and extinction of constituent species for the group 90, 50, and 10 categories for Great Sand Dunes National Monument. The solid line corresponds to reconstructed extinction, the dashed line to sulfate scattering, the dotted line to organic scattering, the small dashed line to nitrate scattering, and the dot-dashed line to soil scattering. Units are in 1/Mm and time is in years.*

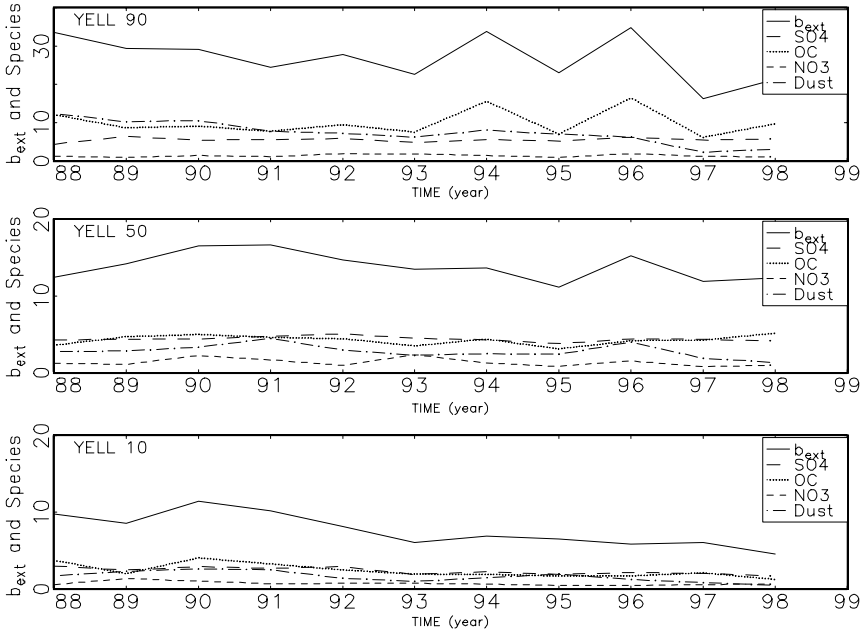

Figure 5.14 *Temporal plot of reconstructed extinction and extinction of constituent species for the group 90, 50, and 10 categories for Yellowstone National Park. The solid line corresponds to reconstructed extinction, the dashed line to sulfate scattering, the dotted line to organic scattering, the small dashed line to nitrate scattering, and the dot-dashed line to soil scattering. Units are in 1/Mm and time is in years.*

Colorado Plateau: Trends on the Colorado Plateau are mixed in that three sites show trends in increasing haziness, while two sites show visibility getting better. Bryce Canyon and Mesa Verde National Parks and Bandelier National Monument all show statistically significant increasing haziness in visibility and not all for the same reason. Sulfates are increasing at Bandelier, nitrates at Mesa Verde, and organics at Bryce Canyon (see Figures 5.15, 5.16, and 5.17). (Nitrates are actually decreasing at Bryce Canyon). Fine soil is increasing at Bandelier and Mesa Verde, while coarse mass is decreasing at Bryce Canyon and Bandelier. Two sites, Canyonlands and Petrified Forest National Parks show improvement in visibility. Sulfates, nitrates, and coarse mass concentrations have decreased at Canyonlands, while organics and coarse mass have gone down at Petrified Forest.

Sonoran Desert: Chiricahua National Monument shows an increase in haziness, while Tonto National Monument does not. Chiricahua shows significantly increasing trends in sulfates, nitrates, and fine soil (see Figure 5.18), while Tonto shows an increase in fine soil concentration.

West Texas: Big Bend National Park shows a significant increase in haziness primarily due to an increase in sulfates (see Figure 5.19). Nitrates, fine soil and coarse mass also show statistically significant increases. At Guadalupe Mountains National Monument, no trend is detected in visibility, however, nitrates and fine soil were shown to be increasing, while organics are decreasing.

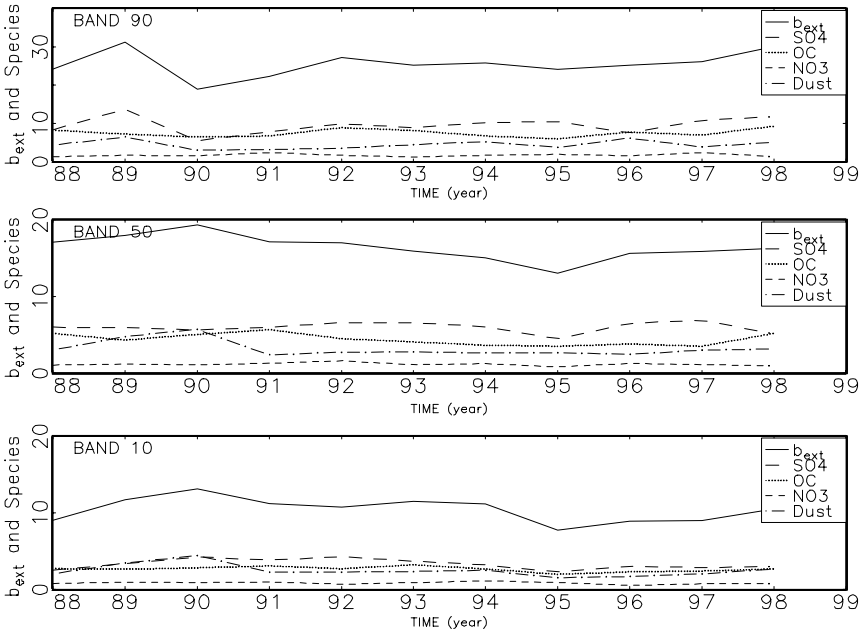

Figure 5.15 *Temporal plot of reconstructed extinction and extinction of constituent species for the group 90, 50, and 10 categories for Bandelier National Monument. The solid line corresponds to reconstructed extinction, the dashed line to sulfate scattering, the dotted line to organic scattering, the small dashed line to nitrate scattering, and the dot-dashed line to soil scattering. Units are in 1/Mm and time is in years.*

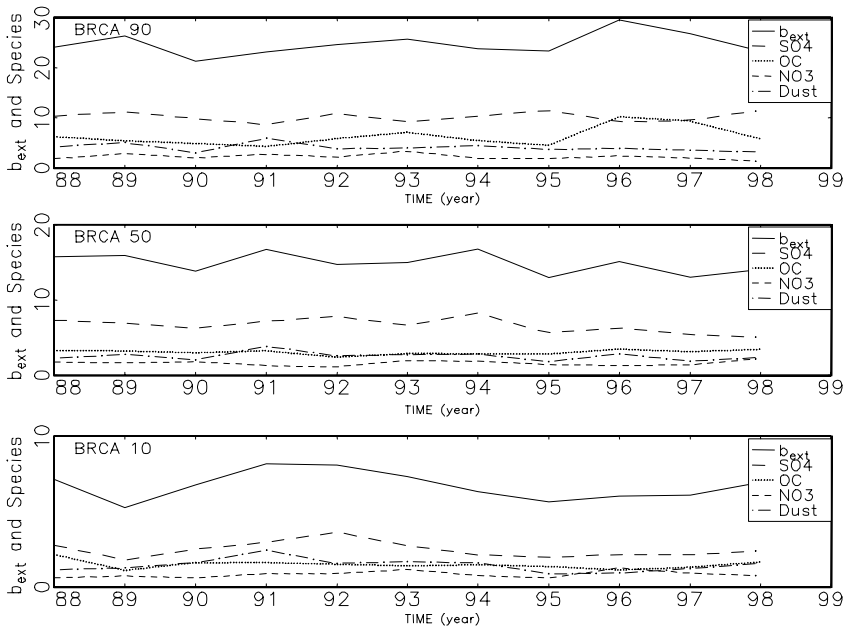

Figure 5.16 *Temporal plot of reconstructed extinction and extinction of constituent species for the group 90, 50, and 10 categories for Bryce Canyon National Park. The solid line corresponds to reconstructed extinction, the dashed line to sulfate scattering, the dotted line to organic scattering, the small dashed line to nitrate scattering, and the dot-dashed line to soil scattering. Units are in 1/Mm and time is in years.*

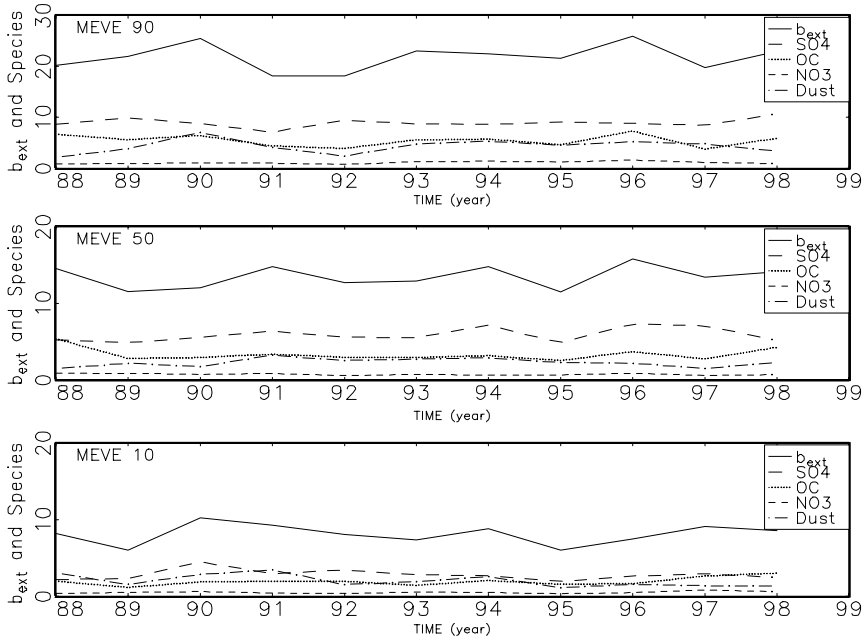

Figure 5.17 *Temporal plot of reconstructed extinction and extinction of constituent species for the group 90, 50, and 10 categories for Mesa Verde National Park. The solid line corresponds to reconstructed extinction, the dashed line to sulfate scattering, the dotted line to organic scattering, the small dashed line to nitrate scattering, and the dot-dashed line to soil scattering. Units are in 1/Mm and time is in years.*

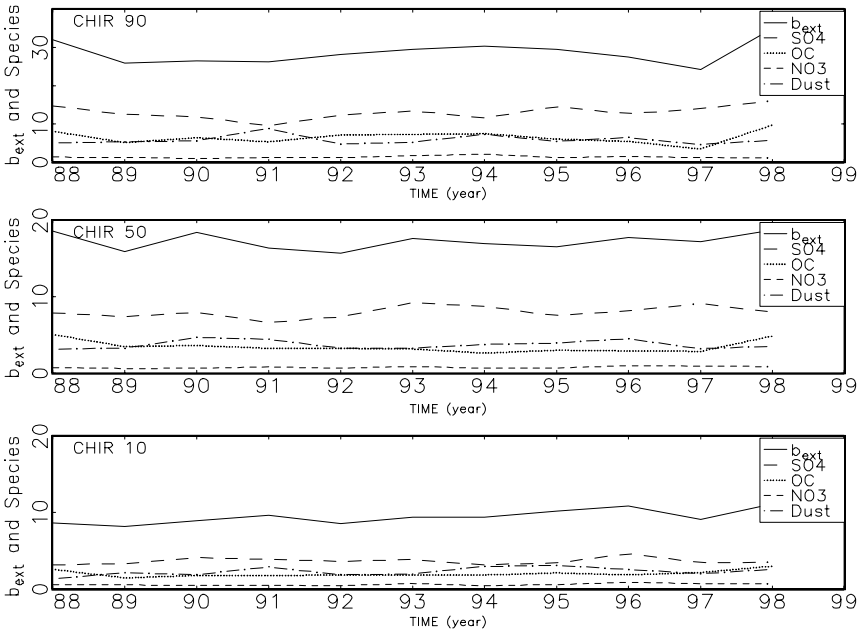

Figure 5.18 *Temporal plot of reconstructed extinction and extinction of constituent species for the group 90, 50, and 10 categories for Chiricahua National Monument. The solid line corresponds to reconstructed extinction, the dashed line to sulfate scattering, the dotted line to organic scattering, the small dashed line to nitrate scattering, and the dot-dashed line to soil scattering. Units are in 1/Mm and time is in years.*

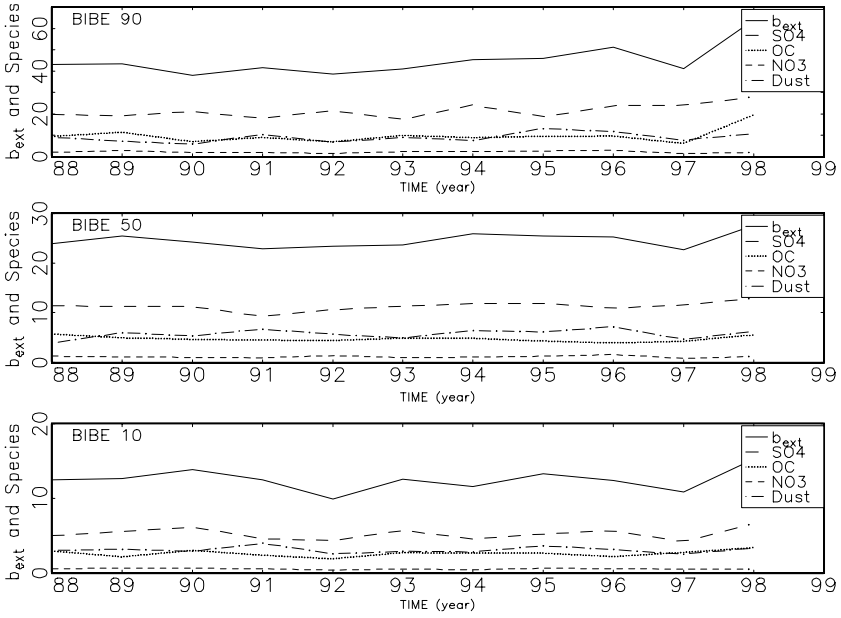

Figure 5.19 *Temporal plot of reconstructed extinction and extinction of constituent species for the group 90, 50, and 10 categories for Big Bend National Park. The solid line corresponds to reconstructed extinction, the dashed line to sulfate scattering, the dotted line to organic scattering, the small dashed line to nitrate scattering, and the dot-dashed line to soil scattering. Units are in 1/Mm and time is in years.*

Appalachian Mountains: Great Smoky Mountains National Park shows a significantly increasing haziness in visibility due to an increasing trend in sulfate concentration (see Figure 5.20). Nitrates have actually decreased, while all other species have remained the same. Shenandoah National Park on the other hand, did not show a change in visibility and sulfates have not changed in a statistically significant way.

At the remaining monitoring sites, visibility has not changed or improved. The good news is that at all western California monitoring sites, visibility has improved at a statistically significant rate primarily because of decreases in nitrate concentrations (see Figures 5.4 and 5.7). Also at most of these sites, organics and sulfates have decreased significantly. The sites along the Sierra range in California and southern Oregon have not shown a change in visibility. Glacier National Park has shown a decrease in haziness primarily because of a decrease in sulfate concentration. Acadia National Park has shown a trend in decreasing haziness because of reductions in nitrate and organic concentrations.

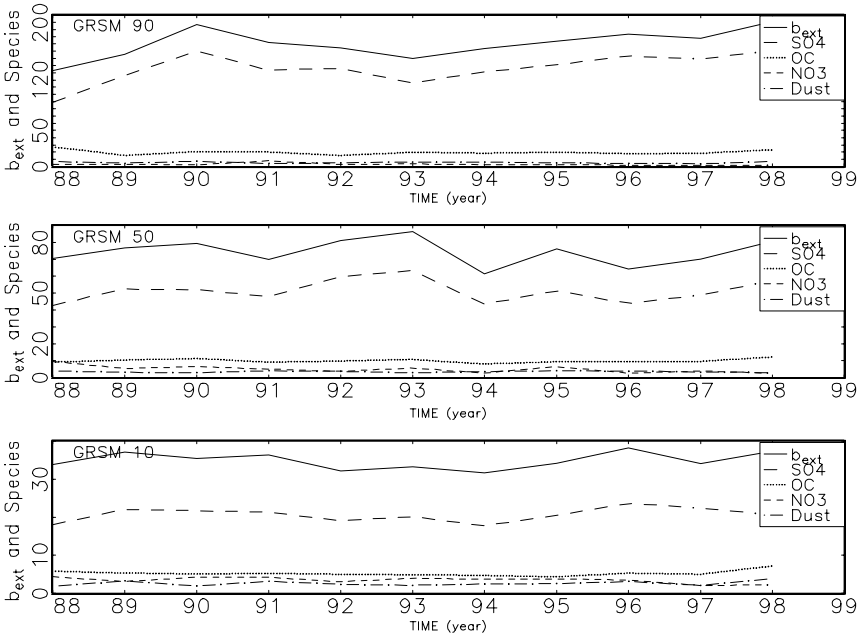

Figure 5.20 *Temporal plot of reconstructed extinction and extinction of constituent species for the group 90, 50, and 10 categories for Great Smoky Mountains National Park. The solid line corresponds to reconstructed extinction, the dashed line to sulfate scattering, the dotted line to organic scattering, the small dashed line to nitrate scattering, and the dot-dashed line to soil scattering. Units are in 1/Mm and time is in years.*

5.3 SEASONAL TRENDS IN FINE MASS AND EXTINCTION

Figure 5.21 is a map with bar plots showing annual and seasonal reconstructed fine mass and the contribution of each species for the 20 monitoring regions, excluding Washington, D.C., in the IMPROVE Network. (See Appendix E for the same plots but for each site by month instead of season.) The summer months have the highest fine mass loadings at 19 of the 20 monitoring regions with two regions having nearly identical mass loadings in two seasons. In the Pacific

Coastal Mountain region, fine mass concentrations are nearly the same in the summer and autumn seasons, while the West Texas fine mass loadings are nearly the same in spring and summer. The summer months are averages across June, July, and August, and at most sites east of the Mississippi it is August that has the highest mass loadings because sulfates are highest during that month. East of the Mississippi sulfates make up about 60-70% of the fine mass in all seasons.

At most sites in four of the western regions, Cascade Mountains, Central Rocky Mountains, Colorado Plateau, Great Basin, Seirra-Humboldt, Sonoran Desert, and Wasatch, sulfate concentrations are highest during the August-September timeframe, although fine mass concentrations are somewhat evenly split between sulfates, carbon, and soil/dust mass concentrations.

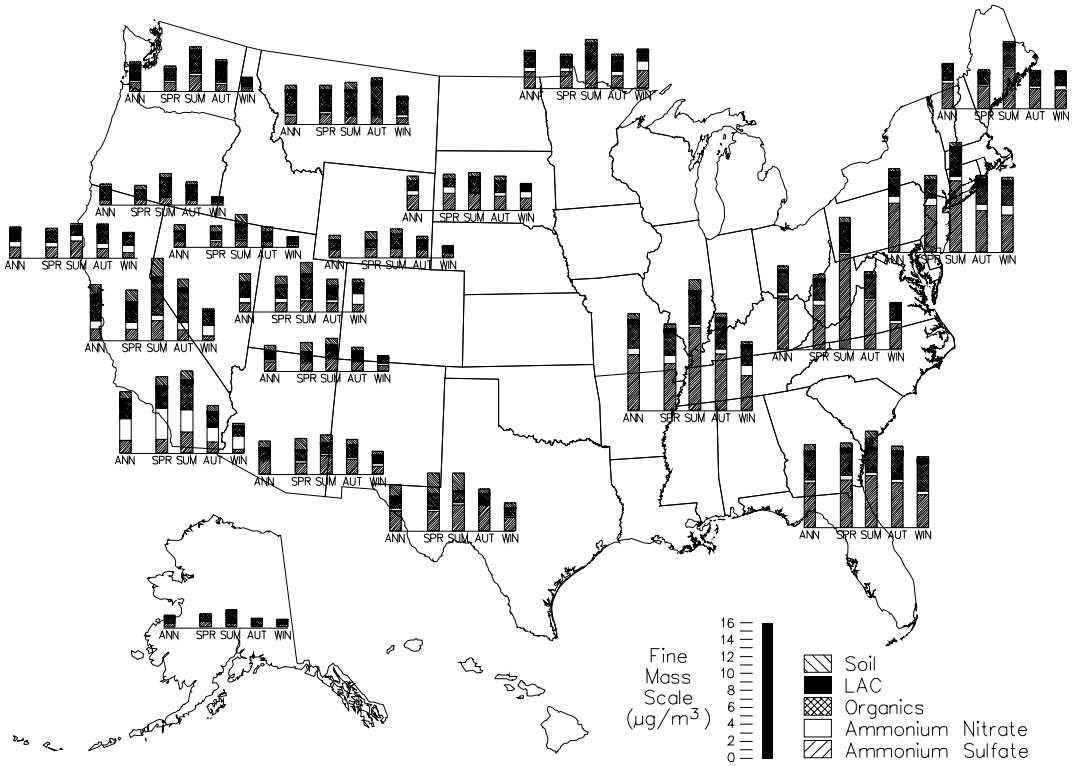

Figure 5.21 *Summary plot of reconstructed fine mass and the fractional contribution of each species for the 20 monitoring regions in the IMPROVE network (Washington, D.C. is not shown).*

At many sites in seven regions in the west, Cascade Mountains, Central Rocky Mountains, Colorado Plateau, Great Basin, Sierra-Nevada, Sierra-Humboldt, and Wasatch regions, August has the highest fine mass concentration because organic mass concentrations are elevated. These regions show increased trends in organic mass concentration

Even though the average summer fine mass concentrations are highest at most western United States sites, the month with the highest fine mass loading is May, and it also is primarily associated with elevated carbon mass concentrations. The sites are Weminuche, Bryce Canyon, Mesa Verde,

Petrified Forest, Chiricahua, Tonto, and Big Bend. Notice that these sites are a subset of those listed in the previous paragraph.

In the Northern Rocky Mountain region, fine mass loadings are greatest during the autumn season again primarily because of increased organic mass concentration

Figure 5.22 is a summary plot of reconstructed light extinction and the contribution of each species for the 20 monitoring regions, excluding Washington, D.C. The addition of the effect of water on hygroscopic aerosols and the addition of coarse mass changes the seasonal trends somewhat. At 13 of the 20 monitoring regions, summer extinction is the highest with the largest difference between seasons being in the eastern United States where sulfates, in combination with high relative humidity, make summer substantially hazier than any other season. Notice that sulfates, on a relative basis contribute significantly more, because of high relative humidity, to extinction than to fine mass. West Texas, Sonoran Desert, Colorado Plateau, Great Basin, Sierra-Humboldt, Sierra-Nevada, Pacific Coastal Mountains, and Cascade Mountain regions also have, on the average, the highest extinction during the summer months, however, the differences between seasons tend to not be as pronounced. Three of the regions, Southern California, Central Rocky Mountains, and Northern Great Plains, have the highest extinction during the spring season. In Southern California, the springtime high is driven by increased nitrate extinction. Two regions, Cascade Mountains and Boundary Waters, winter has the highest extinction and again it is driven by nitrates, while in the Northern Rocky Mountains region spring is the season with greatest extinction.

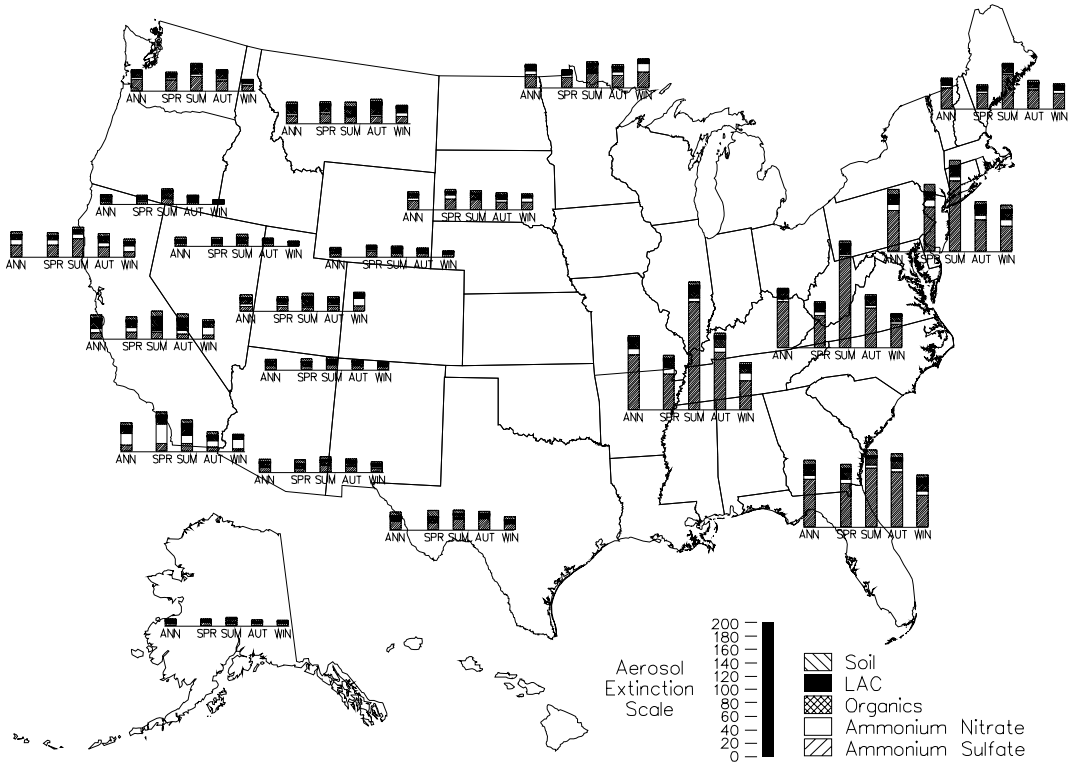

Figure 5.22 *Summary plot of reconstructed light extinction and the fractional contribution of each species for the 20 monitoring regions in the IMPROVE network (Washington, D.C. is not shown).*

5.4 DIURNAL TRENDS IN RELATIVE HUMIDITY AND SCATTERING AND EXTINCTION

One of the fundamental differences between the aerosol and optical measurements in the IMPROVE network is the sampling frequency. While the aerosol measurements are made twice weekly, the optical, temperature, and relative humidity (RH) measurements are made hourly. So, while the aerosol data are usually analyzed on a seasonal or annual basis, the optical data can be analyzed with respect to hour of day, or day of week. Diurnal patterns in optical and RH data are shown for all sites in Appendix F; data for a few sites are discussed in detail below.

5.4.1 Most Common Patterns

At many IMPROVE sites there are diurnal patterns in RH and b_{ext} or b_{scat} that are what would be expected simply based on average meteorology. On average, RH is higher at night, lower during midday, and higher during the winter than during the summer. This is due to the temperature dependence of RH. Warm air is able to hold more water than cool air, so for a constant amount of moisture in the atmosphere, RH (the ratio of actual moisture in the air to the total amount possible) rises and falls inversely with temperature.

Also, as expected based on RH alone, light extinction (b_{ext}) measured by the transmissometer or scattering (b_{scat}) measured by the nephelometer are often either in phase with RH or relatively independent of time of day. This is due to the RH dependence of scattering by hygroscopic aerosols such as sulfates and nitrates. Because the relationship between scattering and RH is nonlinear, small changes in RH can cause very large changes in light scattering when the RH is high (i.e., 70% or higher), but will cause relatively smaller changes when RH is low. The greater the fraction of light scattering due to hygroscopic aerosols, the more sensitive the light scattering will be to changes in RH. See Chapter 2 for details of reconstructed fine particle mass at each site and Chapter 3 for reconstructed light extinction. There are other factors that confound the relationship between RH and scattering, however, such as diurnal or seasonal differences in mean transport of pollutants to the site, atmospheric stability, precipitation, mixing heights, and/or rates of chemical processes.

Each site is unique, but patterns in RH and b_{ext} at Petrified Forest, Guadalupe Mountains, Great Basin, Badlands and Big Bend National Parks, and Jarbidge Wilderness Area are similar to those shown in Figure 5.23 for Pinnacles National Monument. Even though relative humidity is highest during the winter months, winter has the lowest extinction coefficient. The highest scattering or extinction is usually during the summer, lowest during the winter and scattering or extinction is somewhat, but not dramatically, higher at night than during the day. However, it is pointed out that at Pinnacles National Monument extinction during the nighttime hours is greater during the autumn season than the summer months.

Another group of sites, Canyonlands, Chiricahua, Bandelier, and Grand Canyon (both Hopi Point and below the rim) have similar patterns in measured RH, but have a different diurnal pattern in measured scattering or extinction. The graphs for data collected at Grand Canyon National Park (Hopi Point) are shown in Figure 5.24. At these sites, the highest scattering occurs during midday and lower hourly means are measured at night and with very little relative

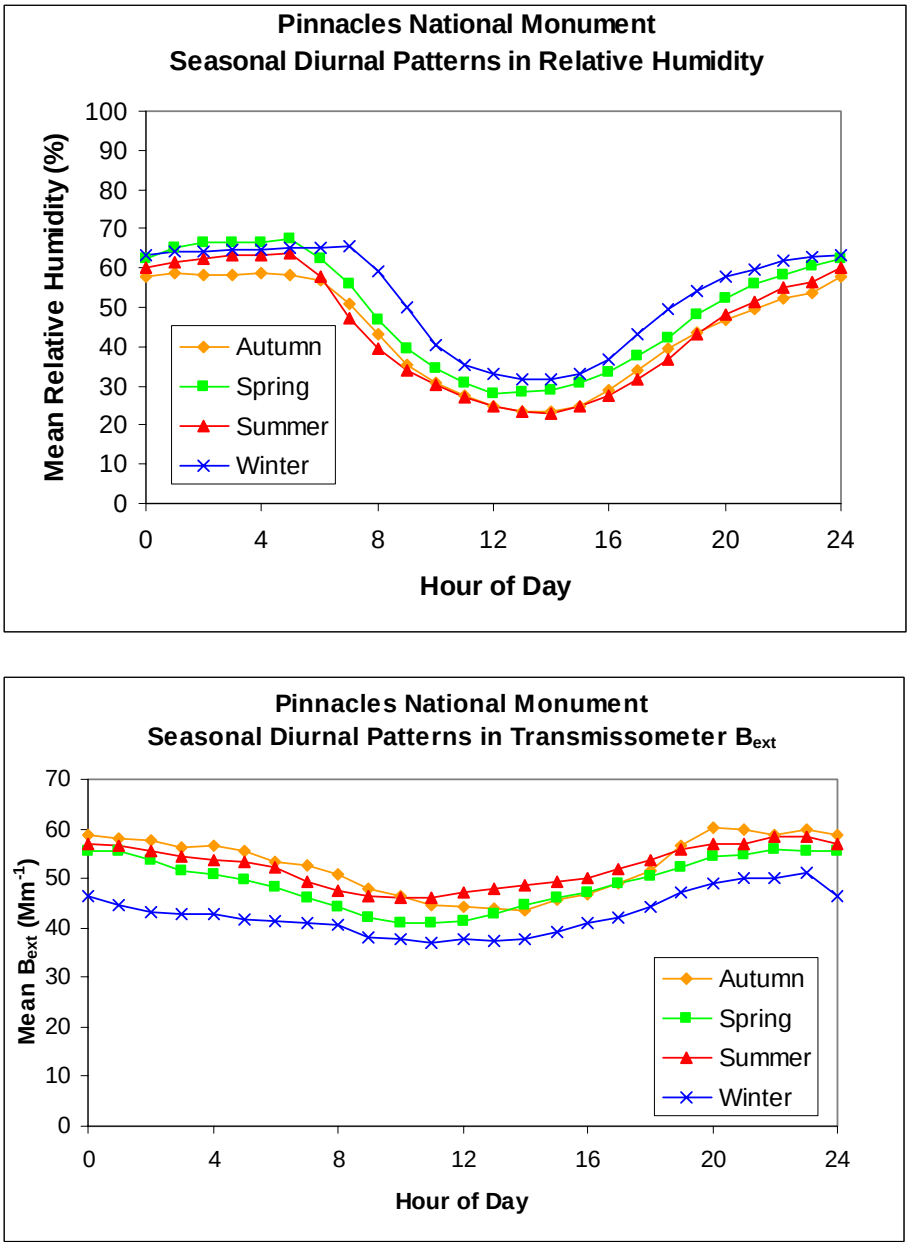

Figure 5.23 *Diurnal patterns by season for RH and b_{ext} measured at Pinnacles National Monument from 1988 to August 1993.*

humidity dependence. This is because the relative humidity tends to vary between 20 and 50% where there is very little particle growth and therefore little dependence on scattering as a function of relative humidity. At these sites, the transmissometer is located in such a manner as to measure air in or over canyons, where the diurnal particulate concentrations may be at least partially dependent on the height of the mixed layer. Higher mixing heights that occur during midday allow low-level aerosol concentrations to be mixed up to the elevation of the monitoring site. Note that at Grand Canyon during the winter, b_{ext} is much lower than during the warmer

seasons and there is virtually no diurnal variation in b_{ext} during the winter. This could well be because the top of the mixed layer only rarely reaches the transmissometer site path at Hopi Point during the winter. Also the in-canyon transmissometer at Grand Canyon has a similar diurnal pattern as the rim instrument but is about 30% higher indicating that the in-canyon haze is greater than on the rim.

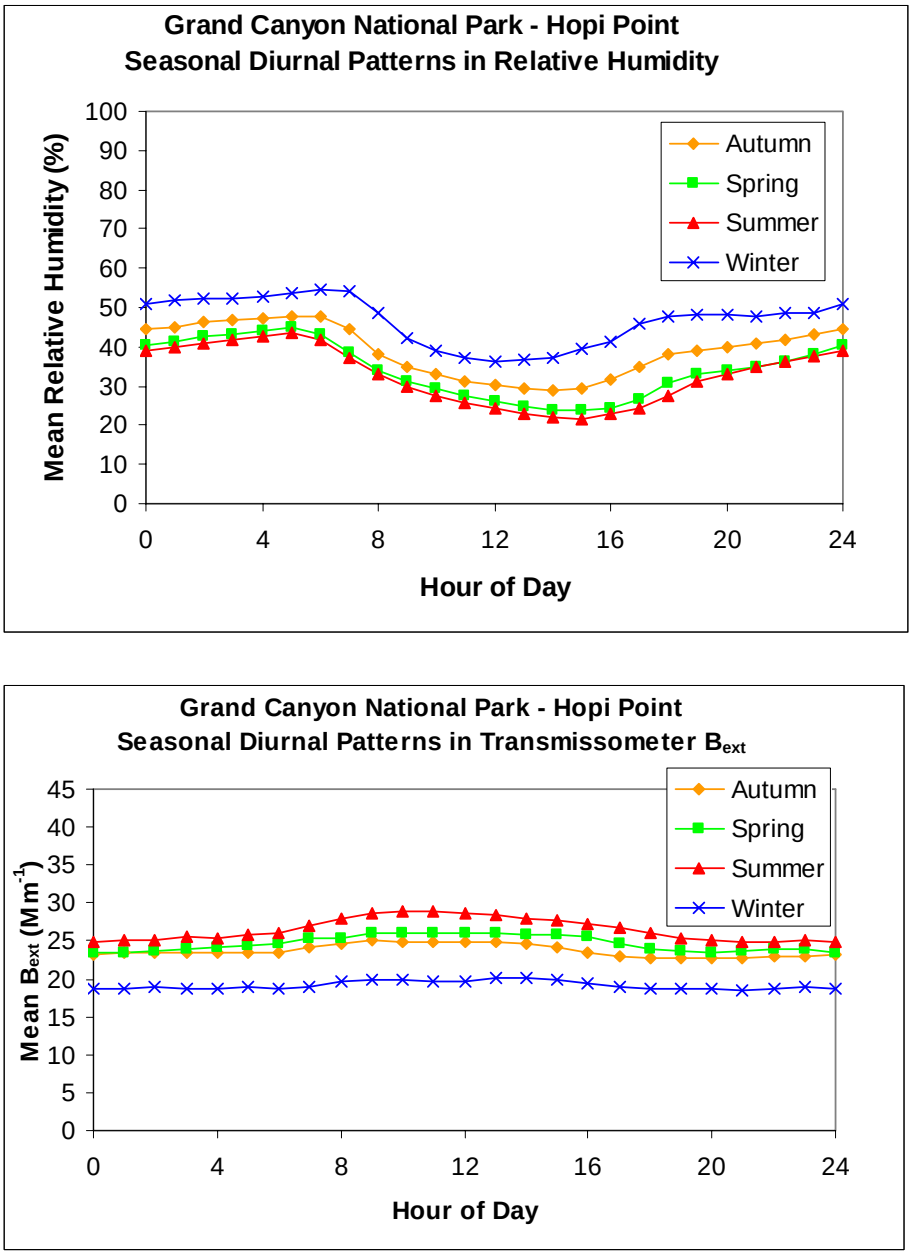

Figure 5.24 *Diurnal patterns by season for RH and b_{ext} measured at Grand Canyon National Park from 1986 to August 1997.*

Some sites have unique or distinct patterns that may be linked to nearby source regions (i.e., a city or group of cities) or local meteorology. Some of these are discussed in more detail in the following subsections.

5.4.1.1 Gila Cliff Dwelling National Monument/Gila Wilderness Area, New Mexico

Figure 5.25 shows the hourly average b_{scat} and RH values at Gila Wilderness Area. The diurnal differences in b_{scat} are very pronounced in the summer and almost nonexistent in the winter. In the summer, hourly average b_{scat} peaks at 5:00 a.m., with values almost twice those measured during the afternoon hours. Although RH also peaks near 5:00 a.m., the average RH is too low to account for the large change in b_{scat}. The peak in b_{scat} is an increase in particulate concentrations that occurs somewhat regularly during summer mornings. Spring and autumn exhibit similar but less pronounced patterns. Winter has the highest average RH and a strong diurnal pattern in RH, but almost no diurnal pattern in b_{scat}. Again these patterns are consistent with mixing of low elevational aerosol concentrations up to the elevation of the monitoring site.

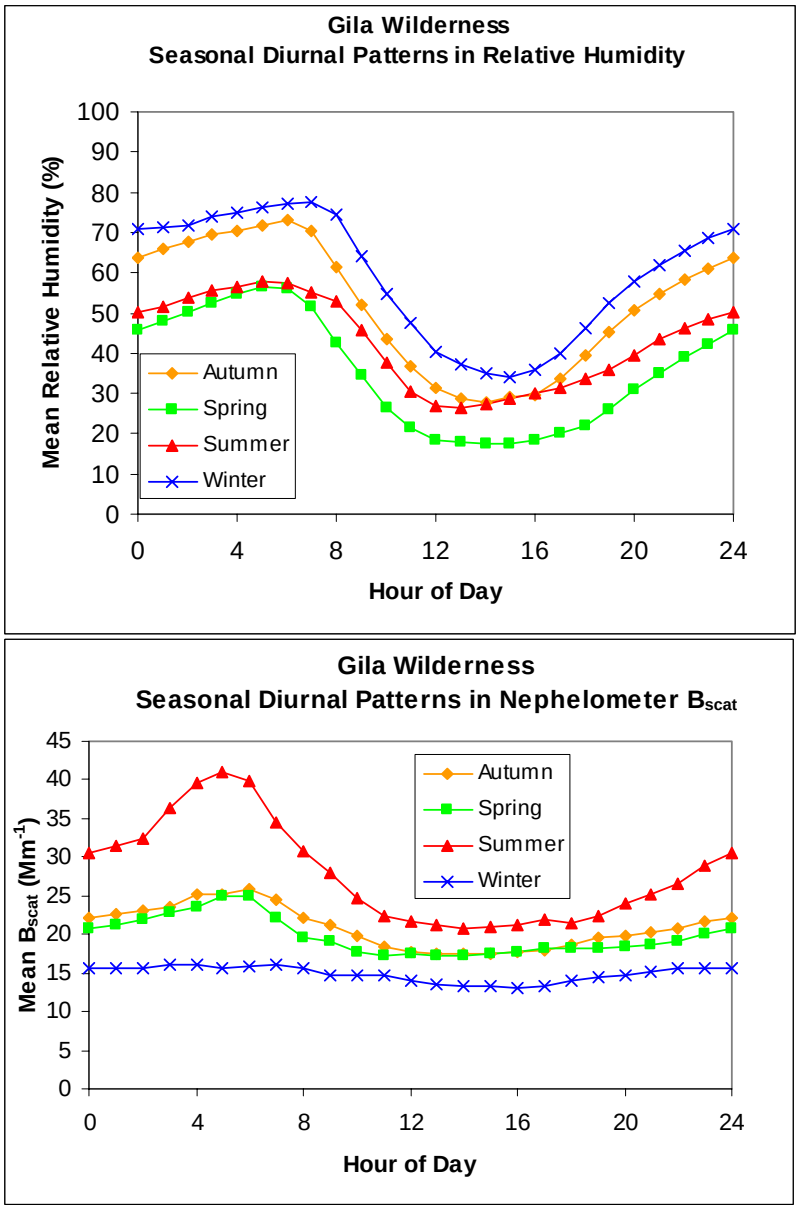

Figure 5.25 *Diurnal patterns by season for RH and b_{scat} measured at Gila Wilderness from 1994 to August 1997.*

The reconstructed extinction at Gila Wilderness is typical for sites in the Southwest. The haziest days occur in the summer with episodes dominated by organics and sulfates. The best visibility occurs in the winter.

5.4.1.2 Lone Peak Wilderness Area, Utah

Lone Peak Wilderness Area is located near the urban area of Provo and Salt Lake City, Utah. Winter weather in this area often alternates between periods of stagnation of several days or longer duration exacerbated by the nearby Wasatch Mountains to the east and Oquirrah Mountains to the west, interspersed with periodic winter storms bringing snow and/or rain that washes out any particulates in the atmosphere. Sites at high elevation, such as the nephelometer site in Lone Peak Wilderness, may often be above this stagnant surface layer.

Perhaps not surprisingly then, the worst episodes of impaired visibility at this site occur in the winter, with reconstructed extinction showing that these days are dominated by nitrates (see Chapter 3). And the periods with the best visibility also occur during the winter, probably either immediately following a cleansing winter storm or on days when the nephelometer site is above the surface layer of the atmosphere. During winter, the maximum hourly average b_{scat} occurs between 10:00 a.m. and 6:00 p.m., with the highest averages being more than twice the values during the remainder of the day. This suggests transport from the nearby urban areas during the afternoon when the mixing height is greatest. During spring, summer, and autumn, b_{scat} peaks between 10:00 a.m. and noon, tapers off throughout the day, then peaks again between 8:00 p.m. and 9:00 p.m. The second daily peak is most pronounced in the summer. These are shown in Figure 5.26.

5.4.1.3 San Gorgonio Wilderness Area, California

San Gorgonio Wilderness Area is located in a pass in the mountains east of the Los Angeles urban area. The diurnal pattern in regional meteorology, affected by the different responses of ocean, coast, and mountains to the daily heating cycle, is such that the urban air mass is often transported eastward through the mountain passes in the afternoon. The highest extinction days at San Gorgonio generally occur in the spring and summer with reconstructed extinction analysis showing episodes of high extinction that are dominated by nitrates (see Chapter 3). The best visibility at San Gorgonio occurs during the winter, with autumn falling between winter and spring/summer.

Although the diurnal pattern in RH at San Gorgonio is fairly typical of many sites, the diurnal pattern in b_{ext} is unique in the IMPROVE network. As shown in Figure 5.27, hourly average b_{ext} begins to rise at roughly 8:00 a.m., though the mean RH is relatively unchanged from previous hours. Average b_{ext} continues to rise throughout the day, peaking between 5:00 p.m. and 6:00 p.m. depending on the season, then drops rapidly, several hours before RH drops in the morning. This pattern suggests that the site at San Gorgonio is less affected by the Los Angeles urban area at night than during midday. This could be due to either diurnal changes in the height of the mixed layer, shifts in wind direction or a combination of these factors.

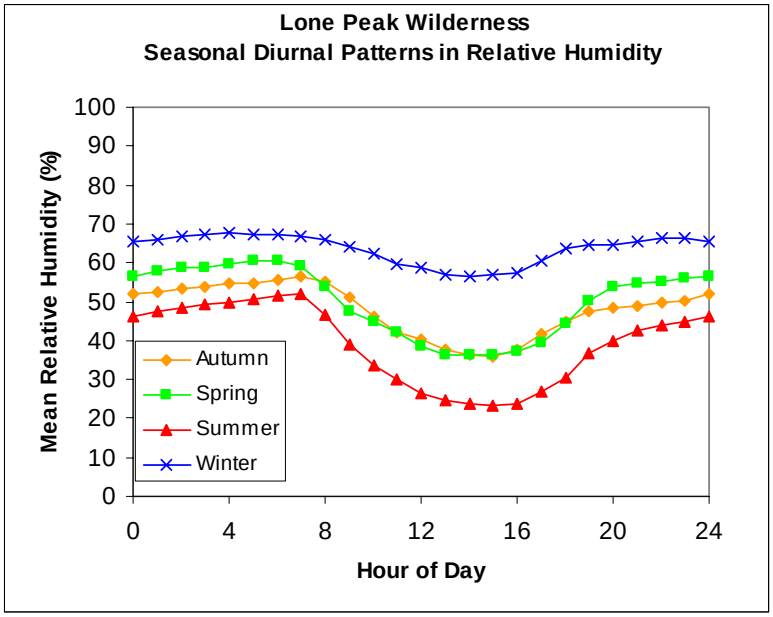

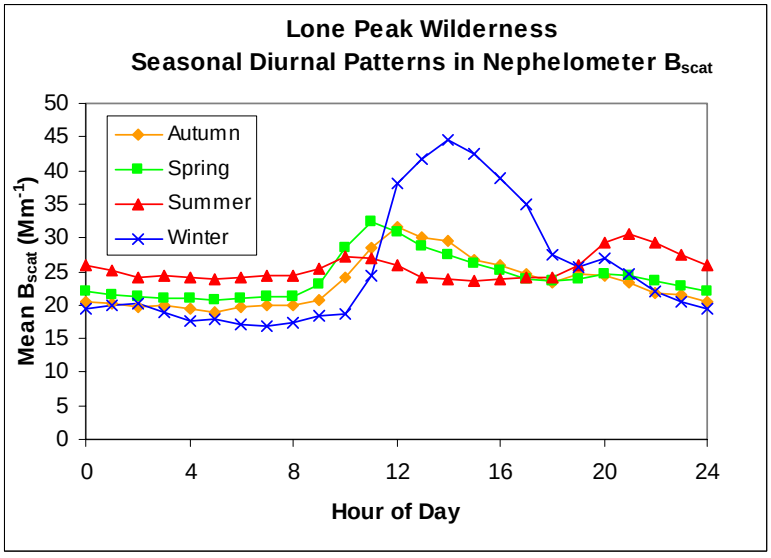

Figure 5.26 *Diurnal patterns by season for RH and b_{scat} measured at Lone Peak Wilderness from 1993 to August 1997.*

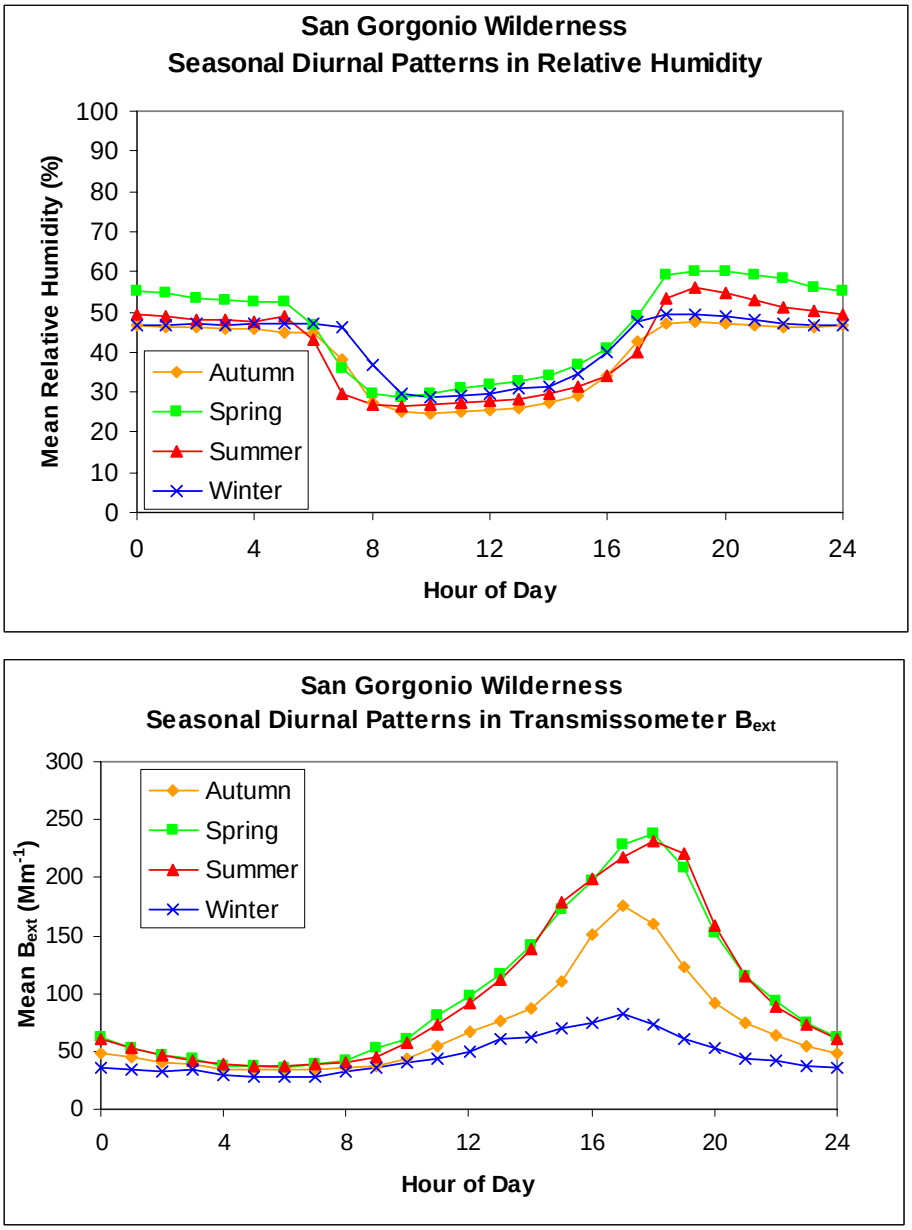

Figure 5.27 *Diurnal patterns by season for RH and b_{ext} measured at San Gorgonio Wilderness from 1989 to August 1997.*

5.4.1.4 Yosemite National Park, California

The transmissometer at Yosemite National Park is located on Turtle Back Dome west of the entrance to the main valley. The diurnal patterns in the b_{ext} and RH are shown in Figure 5.28. While the RH pattern is typical of many sites, the daily pattern in b_{ext} seems to be driven by a combination of RH and mixing height. Peaks in b_{ext} during all seasons tend to occur during mid-afternoon, though the time of the maximum hourly average varies by season, occurring slightly earlier in the day during warmer seasons. Mid-afternoon is the time of day when the mixing

height is likely to be high enough to allow haze from lower elevations to mix up as high as the site. As at San Gorgonio, some diurnal differences in pollutant concentrations may also be due to changes in wind direction driven partially by the complex terrain.

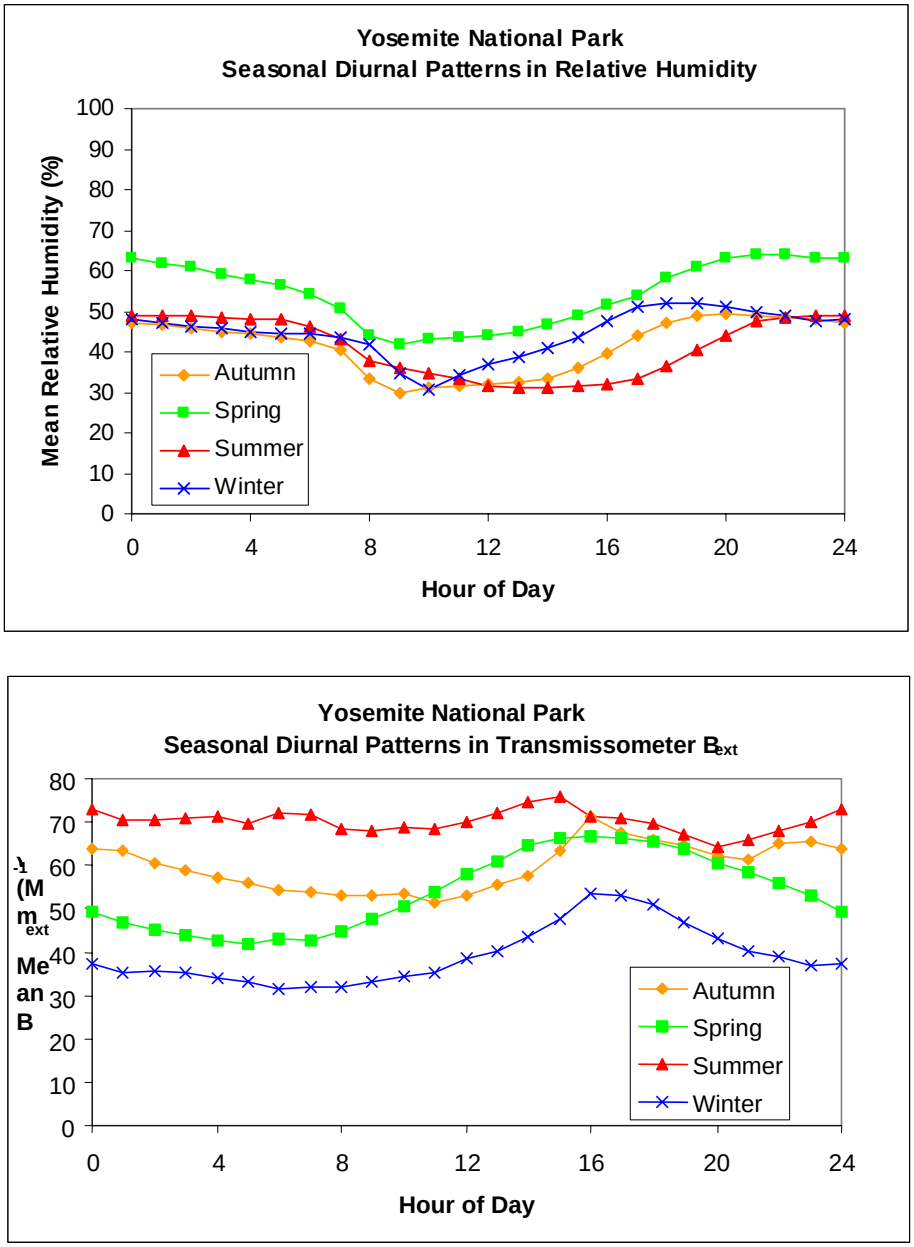

Figure 5.28 *Diurnal patterns by season for RH and b_{ext} measured at Yosemite National Park from 1988 to August 1997.*

5.4.1.5 Alpine Lake Wilderness Area at Snoqualmie Pass, Washington

The nephelometer is located on a ridge top at a ski area just east of Seattle. There are two interesting features in the diurnal b_{scat} pattern as shown in Figure 5.29. First is the rise in scattering occurring during mid-afternoon, beginning by noon and peaking by 9 p.m. during the

summer, and an hour or two earlier during the cooler seasons. This may be due to transport of haze from Seattle at the time of day when the mixing height is high enough to allow it. The hourly average RH is always relatively high, so slight changes in RH may also cause larger changes in scattering at this site as compared to drier areas. The second feature of interest in b_{scat} is the mid-morning peak occurring during winter only. This could be due to local traffic associated with the ski area.

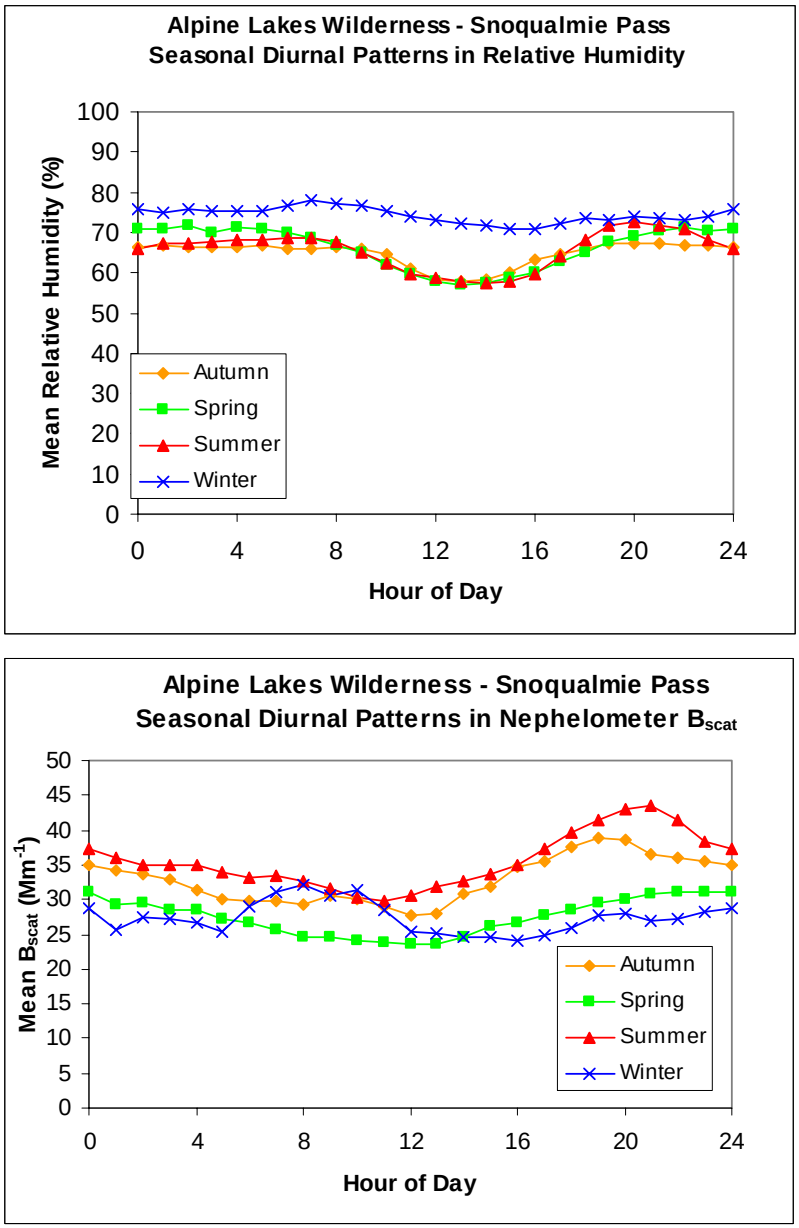

Figure 5.29 *Diurnal patterns by season for RH and b_{scat} measured at Snoqualmie Pass from 1993 to August 1997.*

5.4.1.6 Great Smoky Mountains National Park, Tennessee

Data for Great Smoky Mountains National Park are shown in Figure 5.30. Data at this site have features common to other sites in the eastern United States, such as Acadia National Park, Shining Rock Wilderness Area, Dolly Sods Wilderness Area, and Shenandoah National Park. The most dramatic property is that the hourly mean b_{scat} measured during the summer is more than twice as high as during the remaining seasons of the year. RH is high during all seasons, and the hourly means are nearly always above 70% during the summer. This is in the range of RH where small increases in RH cause large increases in scattering due to hygroscopic aerosols such as sulfates and nitrates. The largest fraction of the scattering at most eastern United States sites is due to sulfates. (See Chapters 2 and 3.) The diurnal pattern in mean scattering during the

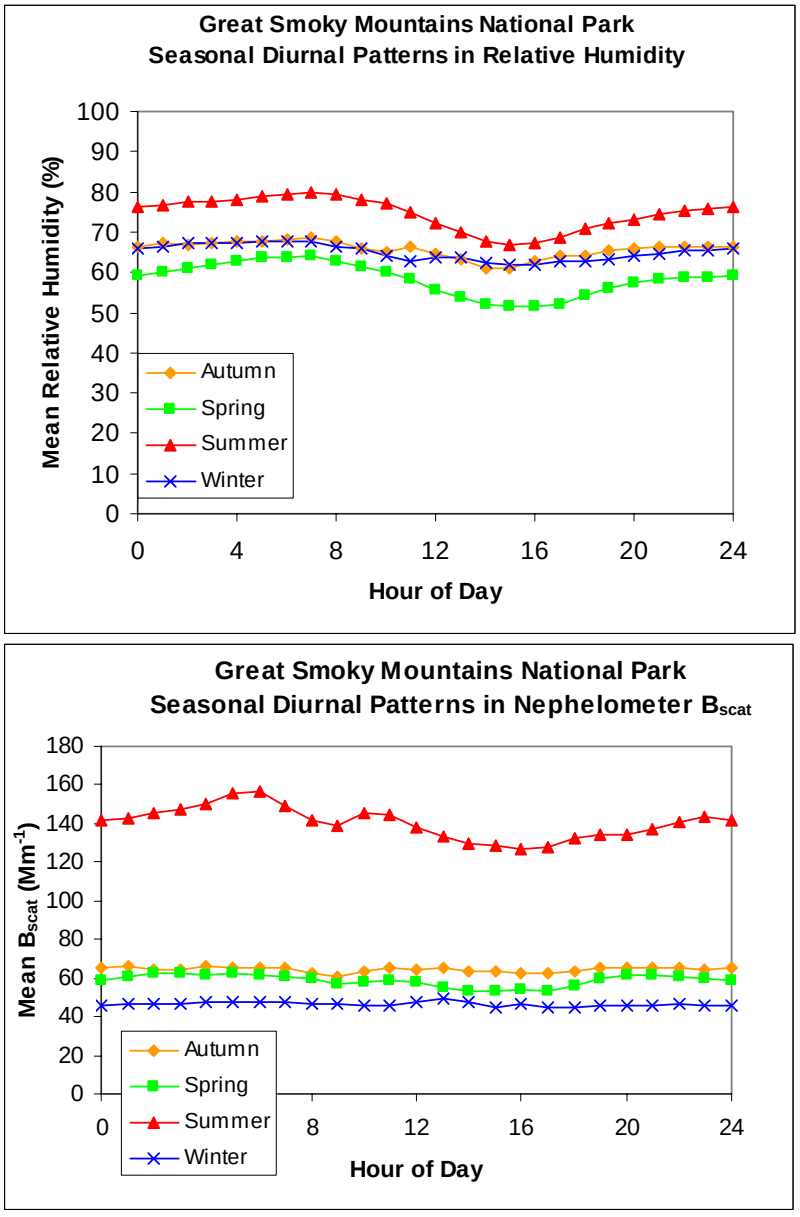

Figure 5.30 *Diurnal patterns by season for RH and b_{scat} measured at Great Smoky Mountains National Park from 1993 to August 1997.*

summer matches fairly closely the diurnal pattern in the RH, with a minimum in the late afternoon and higher values at night. Scattering during the remaining seasons is not dependent on time of day.

5.4.1.7 Boundary Waters Canoe Area, Minnesota

Graphs for this site are shown in Figure 5.31. This site is located in a very remote flat area of lakes and forest in northern Minnesota. Contrary to most sites in the IMPROVE Network, the highest scattering here occurs during the winter rather than during the summer. Lowest b_{scat} is during spring and fall with summer falling in between. RH is quite high on average, being

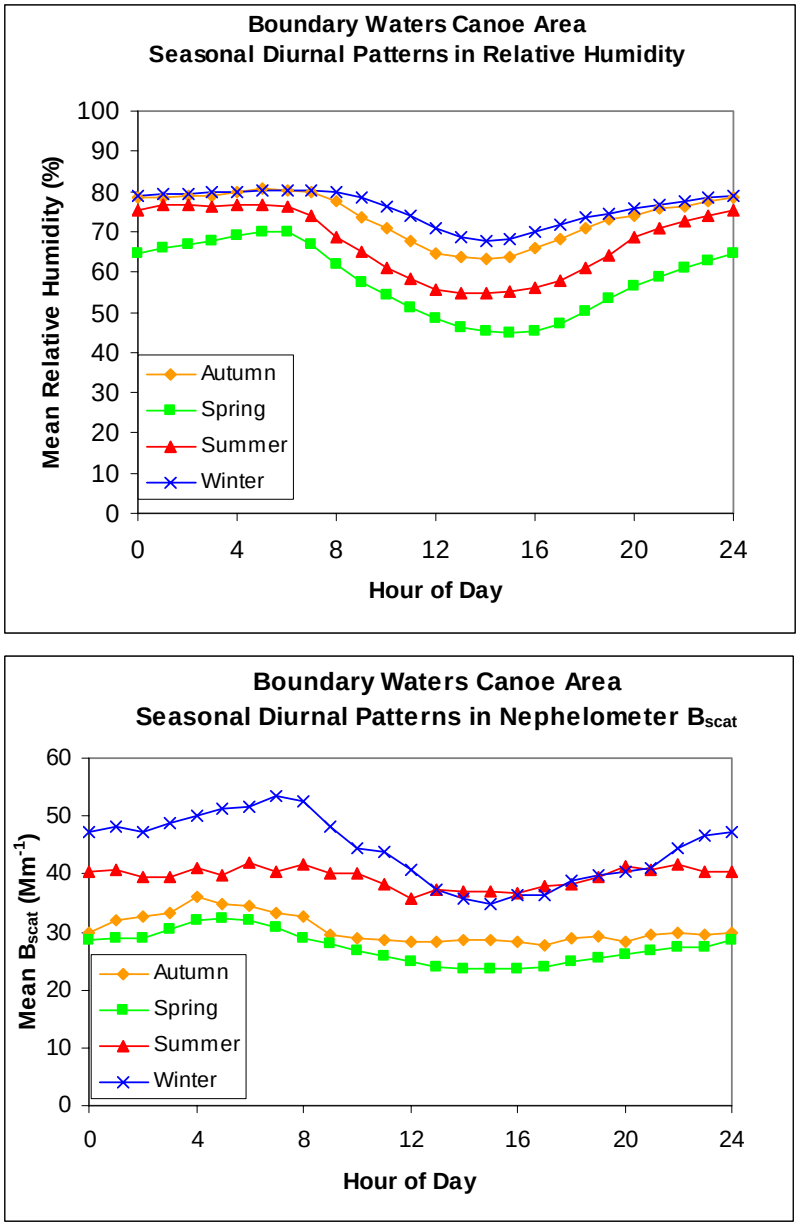

Figure 5.31 *Diurnal patterns by season for RH and b_{scat} measured at Boundary Waters Canoe Area from 1993 to August 1997.*

highest during the winter and lowest during the spring, although the nighttime averages for winter and fall are nearly identical, especially at night. It's possible that the high scattering measured from approximately 10 p.m. to 8 a.m. during the winter is associated with icy fog.

Diurnal and seasonal patterns in measured b_{scat} and b_{ext} are similar for many sites. A common pattern is highest scattering or extinction during the summer, lowest during the winter with scattering or extinction being somewhat higher at night. Usually, the differences between different hours of the day are not as large as the differences between seasons. In some cases, however, the average extinction varies by up to a factor of 5 from one time of day to another largely because of changes in relative humidity and the associated growth of hygroscopic aerosols. RH is typically driven mostly by an inverse relationship to average temperature. There are some sites that have unique diurnal or seasonal patterns in average b_{scat} or b_{ext}. In many cases, especially when the site is near a large urban area, there is evidence that these average values are dependent on mixing height. Higher mixing heights allow emissions from local sources to reach the monitoring site.

5.5 REFERENCES

Theil, H., A rank-invariant method of liner and polynomial regression analysis (I-III), *Proc. Kon. Ned. Akad. V. Wetensch. A.*, (53), 1950

CHAPTER 6

SPECIAL STUDIES

Developing strategies to improve visibility requires an understanding of the relationship between the various aerosol species and atmospheric extinction. In this report and for applications where detailed physio-chemical aerosol characteristics are not known, the following equation is used to estimate extinction under the assumptions of external mixing, constant dry specific scattering, and sulfate interpreted as ammonium sulfate:

$$b_{ext} = (3)([SULFATE] + [NITRATE])\, f(RH) + (4)[OMC]\, f_{org}(RH) + (1)[SOIL] + (0.6)[CM] + (10)LAC \quad (6.1)$$

where b_{ext} is the reconstructed extinction coefficient. The ratio between dry and wet scattering as a function of relative humidity (RH) is referred to as the relative humidity scattering enhancement factor, f(RH). f(RH) and f_{org}(RH) refer to the enhancement factors for sulfates and nitrates, and organics, respectively. [SULFATE] is the ammonium sulfate concentration, while [NITRATE], [OMC], [SOIL], [CM], and [LAC] are the concentrations of ammonium nitrate, organic carbon, soil, coarse mass, and light-absorbing carbon, respectively. Light-absorbing carbon [LAC] and elemental carbon [EC] are used interchangeably throughout the chapter. Coarse mass is assumed to be primarily crustal in nature. The coefficient numbers refer to the assumed dry specific scattering of the respective species in m^2/g. The choice of these specific scattering coefficients are discussed in Malm et al. [1994] and are basically best estimates based on an extensive literature review and reported in Trijonis and Pitchford [1987] and Trijonis et al. [1990].

Average f(RH) values for each sampling period are calculated using Tang's [1996] ammonium sulfate D/D_o curves smoothed between the crystallization and deliquescent points. The f(RH) values are calculated for each hour and then averaged up to the sampling period length assuming a lognormal sulfate species mass size distribution, with an assumed geometric mass mean diameter and geometric standard deviation. The f(RH) associated with nitrates was assumed to be the same as for sulfates, while f_{org}(RH) for organics is set equal to one.

Understanding the inherent uncertainties in linking aerosol species concentrations to extinction using Equation (6.1) is essential if one is going to track progress in extinction change (change in visibility) as a function of changing emissions and resulting aerosol concentrations. Some key concerns are:

- How important are the mixing characteristics of aerosol species? Equation (6.1) assumes externally mixed particles, while it has been well documented that some species are internally mixed.
- What is the significance of scattering properties of sulfates as a function of ammoniation? This includes the water absorption properties of sulfates as a function of ammoniation.
- How important is the variability of ambient particle size to estimates of dry mass scattering efficiencies?
- What are the hygroscopic characteristics of organics?
- Is the assumption that coarse mass is primarily crustal valid and if not does its mass scattering efficiency vary significantly?
- Do carbon aerosols, other than elemental carbon, absorb light and if so what are the associated absorption efficiencies?
- Are the assumptions inherent to estimating extinction from aerosol species regionally dependent? Is the east different from the inner-mountain west or the northwest or the southwest?

6.1 GREAT SMOKY MOUNTAINS STUDY

Over the past five years, a number of special studies have been designed to answer some of these questions. During the summer months, the national parks in the eastern United States and the eastern United States as a whole experience some of the worst visibility conditions in the nation. Typically, high relative humidity conditions combine with high aerosol loading to reduce visibility to as low as 5-10 km, which corresponds to extinction levels of 0.4-0.8 1/km (or 400-800 1/Mm) To study these conditions, the Southeastern Aerosol and Visibility Study (SEAVS) was conducted from July 15, 1995, through August 25, 1995, in Great Smoky Mountains National Park. The study was a collaborative effort between several universities, consulting firms, the Electric Power Research Institute (EPRI), and the National Park Service (NPS). The overall objectives of this research were to better understand the physical, chemical, and overall optical characteristics of the ambient aerosol under the humid conditions observed in the southeastern United States during the summer months, and the relationships between these characteristics and visibility issues.

This discussion will focus on theoretically exploring the scattering properties of ambient aerosols as a function of mixing assumptions, sulfate ammoniation, aerosol size characteristics, and hygroscopic properties. Initiatory experiments on the relationship between measured water uptake and aerosol composition have been carried out by Zhang et al. [1993] and McMurry et al. [1996]. They used tandem differential mobility analyzers (TDMA) in conjunction with mass size sampling systems to measure growth as a function of size, composition, and relative humidity (RH). Saxena et al. [1995] and Pitchford and McMurry [1994] used their data to theoretically explore how water might be apportioned between the inorganic and organic aerosol fractions and as a function of mixing characteristics. Saxena et al. [1995] concluded that aerosols behaved differently at Grand Canyon, Arizona, than at the more urban site of Claremont, California. At Grand Canyon, they concluded that organics add to water absorption by inorganics. In the RH range of 80-88%, they assert that about 25-40% of water uptake is attributable to organics. On the other hand, Pitchford and McMurry [1994], using the same data set, demonstrated that all the water could be accounted for by assuming that just sulfate and nitrates, were hygroscopic. At Claremont,

Saxena et al. [1995] show that in the RH range of 80-93% the net effect of organics is to diminish water absorption by inorganics by 25-35%.

A number of authors have discussed the limitations of trying to apportion scattering to specific species, commonly referred to as scattering budgets [McMurry et al., 1996; White, 1986; Malm and Kreidenweis, 1997]. However, the goal of the calculations presented in this report is not to apportion scattering to any particular species, but to examine the ability of various models to predict scattering by fine particles (less than 2.5 μm) as a function of relative humidity and to draw from these calculations a better understanding of the hygroscopic characteristics of various aerosol types.

Experiments were designed such that observables could be estimated or modeled in a number of different ways. Measured ambient scattering at ambient relative humidities will be compared to ambient reconstructed scattering, and the ability of aerosol scattering models to predict the ratio of wet-to-dry scattering as a function of humidity will be explored. Modeling ambient scattering and the wet-to-dry scattering ratio will serve to both explore the validity of aerosol growth and mixing models and associated assumptions, and provide an estimate of the hygroscopicity of aerosol species other than sulfates and nitrates.

6.1.1 Experimental Methods

6.1.1.1 Humidograph

The hygroscopic properties are examined using a humidograph with the ability to measure scattering as a function of humidity over ranges of about 15-95%. Day et al. [1997] describe the instrument design in some detail and therefore its operation will only be summarized here.

Air is drawn through a temperature controlled humidity conditioner and passed into a Radiance Research M903 integrating nephelometer. The humidity conditioner consists of Perma Pure Nafion dryers, while temperature is controlled by placing the dryers in a constant temperature water bath. Because temperature change in the sampling plumbing can cause unwanted and unknown RH changes, temperatures are monitored throughout the system.

6.1.1.2 Integrating Nephelometers

The details of ambient nephelometer measurements were covered in Malm et al. [1994] and Day et al. [1997] and as before will only be briefly reviewed here. Five Optec NGN-2 integrating nephelometers, in various configurations, were operated during SEAVS. One of the five Optec nephelometers utilized the open-air configuration and was operated using standard IMPROVE protocols [Air Resource Specialists, 1994]. The other four Optec nephelometers were operated at reduced flow rates (113 l/min) and were fitted with an inlet, to which a Bendix-240 cyclone, with a 2.5 μm cutpoint could be attached. Two of these nephelometers were operated with an inlet and a cyclone. The other two nephelometers were operated with the inlet but without the cyclone. The four nephelometers that were operated with the inlet and at a reduced flow rate were much more susceptible to heating the sample aerosol in the optical chamber than was the open-air nephelometer. These nephelometers were therefore configured

with a water jacket mounted on the back wall of the scattering chamber. This water jacket surrounded the light source where most of the heat in the system was generated. Water was circulated through the water jacket inside the nephelometer, then through a heat exchanger outside the nephelometer that was kept at ambient temperature by a large fan. Thermistors were placed inside the inlet, where sample air was assumed to be at ambient temperature, and at the sample exit, where sample air should be hottest if heating of the aerosol had occurred. Monitoring the difference in sample temperature between the inlet and the outlet of each nephelometer allowed determination of whether heating of the sample had occurred and if there was a subsequent change in sample RH. Generally, the degree to which the sample was heated was less than 0.5°C. The accuracy of the nephelometer measurements and degree of heating are discussed in some detail by Day et al. [1997].

6.1.1.3 Relative Humidity Sensors

Three Rotronics mp 100f combination relative humidity/temperature sensors were housed in PVC holders and aspirated by a fan. The reported accuracy of the relative humidity sensor is ±2% [Rotronic Instrument Corp., 1998]. The flow rate through the holder was approximately 120 l/min. The sensors were approximately 6 ft above ground level, 6 ft from each other, and mounted near the inlets of the nephelometers.

6.1.1.4 Particulate Samplers

IMPROVE particle samplers were used throughout the study. A detailed description of validation and quality assurance procedures is available in Malm et al. [1994], Sisler et al. [1993], and Eldred et al. [1988]. In the most general sense, validation is a matter of comparing chemically related species that have been measured in different channels. Details of standard methods for apportionment of measured mass to the various aerosol species are described in some detail in Malm et al. [1994], however, in this study sulfate ammoniation was explicitly addressed.

Most fine sulfates are the result of oxidation of SO_2 gas to sulfate particles. In humid atmospheres, the oxidation of SO_2 occurs primarily in the aqueous phase where sulfuric acid is formed within water droplets. If there is inadequate ammonia in the atmosphere to fully neutralize the sulfuric acid, as is sometimes the case, then the resulting aerosols are acidic. Under these circumstances solutions of continuously varying acidity are formed. The extremes of this continuum are ammonium sulfate (neutral) and sulfuric acid.

Therefore, the ammoniated sulfate mass is estimated from independent measurements of SO_4 and NH_4 ions using:

$$[SO_{4,mass}] = (0.944)[NH_4^+] + (1.02)[SO_4^{2-}] \qquad (6.2)$$

where $[SO_{4,mass}]$ is the mass of the ammoniated sulfate compound.

6.1.2 Estimating Particle Scattering

Measurements of scattering used in the following analysis were restricted to particles less than 2.5 μm. A particle in the atmosphere can be a mix (internal mixture) of various aerosol species or in some cases its compositional structure may be restricted to one species (external mixture) such as $(NH_4)_2SO_4$. Whether the particles are internally or externally mixed they scatter or absorb a specific fraction of radiant energy that can be theoretically calculated by invoking a number of assumptions concerning the chemical and physical properties of the assumed structure of the aerosol. Following the suggestion of White [1986] the scattering/extinction per unit mass will be referred to as specific scattering/extinction as in specific gravity.

Comparisons between measured and theoretically reconstructed scattering will be carried out using four models. First, an externally mixed aerosol model with constant dry specific scattering, one sulfate species and associated growth as a function of relative humidity for that sulfate species was assumed. Second, an external model with constant specific scattering was assumed but the mass associated with sulfate ammoniation was calculated using Equation (6.2) and the functional dependence of scattering on RH is based on measured pure-component sulfate hygroscopic growth curves interpolated to the measured degree of neutralization. Third, the same model is assumed but sulfate specific scattering is estimated from measured sulfur mass size distributions. Finally, an internally mixed aerosol model is used that is based on measured sulfate ammoniation and size distributions with an assumed mass size distribution for other aerosol species.

To make reference to the various models the following modifiers to variables will be used: *E* and *M* refer to externally and internally mixed models, respectively, e_c and e_s to specific scattering assuming a constant and size dependent value, S_c and S_a refer to a fixed sulfate species such as ammonium bisulfate, and ammoniated sulfate, respectively, while *B*, *C*, and *D* refer to the best estimate, crystallization, and deliquescent growth curves. For instance, $b_{scat}\_E\_e_s\_S_a\_B$ refers to modeled scattering assuming an external model (*E*), size dependent specific scattering coefficient (e_s), ammoniated sulfate (S_a), and best estimate hygroscopic growth curve (*B*). b_{scat} refers to modeled scattering, while $<b_{scat}>$ is measured scattering.

6.1.2.1 Aerosol Growth as a Function of Relative Humidity

Tang [1996] published data on growth curves, D/D_o, as a function of increasing and decreasing relative humidity for $(NH_4)_2SO_4$, NH_4HSO_4, and H_2SO_4. For increasing or decreasing RH, $(NH_4)_2SO_4$ and NH_4HSO_4 exhibit a hysteresis in the D/D_o vs RH relationship, with sharp discontinuities at the deliquescence (relative humidity at which the crystal abruptly absorbs water) and crystallization (relative humidity at which particle abruptly loses water and recrystalizes) humidities. However, because vertical atmospheric mixing during summer months in the eastern United States should almost always bring the aerosol into an RH environment that is in excess of 80% one can make the argument that the sulfate aerosol will always be on the crystallization (upper) branch of the aerosol growth curve. Furthermore, because mixtures of ammoniated sulfate compounds with other species have been shown to be hygroscopic below the deliquescent values [Sloane, 1984, 1986; Stelson and Seinfeld, 1982], and

because the growth factor and light-scattering efficiency for ambient aerosols has previously been observed to be rather smooth [Sloane, 1983, 1984, 1986; Wexler and Seinfeld, 1991; Waggoner et al., 1981] it is not known whether the upper or lower limb of the hysteresis curve applies for a particular aerosol sample. Therefore, as our "best estimate" for the sulfate species growth, the curves were smoothed between the deliquescence and crystallization points.

At the Great Smoky Mountains National Park monitoring site, the neutralization of the sulfate aerosols varied from sampling period to sampling period. As an estimate of sulfate compound hygroscopicity for aerosols whose molar ratios of ammonium to sulfate were somewhere between 0 and 2, a linear interpolation between growth curves was carried out based on NH_4 to SO_4 ratios.

When species with different hygroscopic characteristics, such as organics and sulfates, are internally mixed, a method for adjusting the aerosol hygroscopicity in response to changes in chemical composition is needed. Malm and Kreidenweis [1997] have demonstrated the application of the Zdanovskii-Stokes-Robinson (ZSR) model, which accounts for solute-solvent interactions but neglects solute-solute interactions. The use of the ZSR model for determination of the water content has been utilized by Saxena and Peterson [1981]. They examined the applicability of the ZSR assumptions to mixtures of inorganics, while Meng et al. [1995] applied it to mixtures of organics and inorganics. In the present case, the ZSR model assumptions were used to derive an equation for the hygroscopic growth of internally mixed particles when the growth characteristics of the externally mixed species are either known or can be approximated. Applying the ZSR model assumptions to the case of two solute species yields:

$$\left(\frac{D}{D_o}\right)^3 = \frac{\rho_{dry}}{\rho_{wet}}\left[z_1\frac{\rho_{wet1}}{\rho_{dry1}}\left(\frac{D_1}{D_{o,1}}\right)^3 + z_2\frac{\rho_{wet2}}{\rho_{dry2}}\left(\frac{D_2}{D_{o,2}}\right)^3\right] \tag{6.3}$$

D and D_o are the dry and wet particle diameter, ρ_{dry} and ρ_{wet} are the dry and wet densities and the subscript 1 and 2 refer to species one and two. The coefficients z_1 and z_2 are the mass fractions of each species. It should be noted that models that treat water uptake for nonideal, multicomponent solutions using theoretical and semi-theoretical thermodynamic relationships have been developed and have been applied to both visibility and climate forcing problems [Saxena and Peterson, 1981; Pilinis et al., 1995; Saxena et al., 1986, 1993]. The correct treatment of the hygroscopicity of species in multicomponent mixtures—especially organic species—remains problematic, not only because of the lack of suitable mixture thermodynamic data, but also because of the lack of information about other critical mixture properties.

6.1.2.2 Estimation of Size Dependent Specific Scattering

The analysis of DRUM measured sulfur size distributions is confined to the five stages that collect particles with a diameter below 2.5 μm. The size-resolution afforded by the five size cuts is quite limiting when estimating scattering efficiencies using Mie theory because particles collected on each stage cover quite a large variation in size. For instance, particles between 0.07 and 0.24 μm are collected on stage one. Therefore, the mass size distributions are usually "inverted" to yield a smoothed estimate of *dC/dlog(D)* [John et al., 1990]. DRUM measurements are inverted using the Twomey [1975] scheme, which is a nonlinear iterative algorithm that

accounts for the sampling efficiency as a function of particle size for each stage. The output of the inversion is 72 data pairs of *dC/dlog(D)* and *D*, where *C* is the concentration of sulfur and *D* is the aerodynamic diameter. Geometric mass mean diameter and geometric standard deviation are calculated for each of these sulfur size distributions using Stokes diameters.

Using Mie theory specific scattering was calculated from *dC/dlog(D)* distributions three different ways. First, the dry sulfate specific scattering (e_d) was calculated by estimating the dry scattering coefficient ($b_{scat,d}$), assuming water was not mixed with the particle (RH=0.0%), and dividing that scattering by dry ammoniated sulfate mass concentration. Because the "wet" size is measured by the DRUM sampler the dry size was calculated using the sampling period average (D/D_o) corresponding to the ambient RH. (D/D_o) was estimated as discussed above for each hour and then averaged up to twelve hours. Second, a wet ammoniated sulfate specific scattering (e_w) was arrived at by calculating the scattering of the sulfate species plus water ($b_{scat,w}$) and dividing it by the mass of sulfate species plus water. Finally, the water enhanced efficiency (e_{wd}) was calculated by dividing the scattering of the wet ammoniated sulfate species by dry ammoniated sulfate mass. The water associated with the ammoniated sulfate species mass was calculated assuming volume conservation between sulfate and water. The index of refraction of the "wet" aerosol was arrived at by volume weighting the index of refraction for sulfate species and water.

For the internally mixed model, the calculations were carried out in much the same way, however, the growth was estimated using Equation (6.3). As before the water associated with the internally mixed aerosol mass was calculated assuming volume conservation and the index of refraction of the "wet" aerosol was arrived at by volume weighting the index of refraction for sulfate species, nitrates, organics, and water. The indices of refraction used in the calculations were 1.41, 1.47, 1.53, 1.55, 1.55, 1.53, and 1.33 for sulfuric acid, ammonium bisulfate and sulfate, ammonium nitrate, organics, soil, and water, respectively.

6.1.2.3 The Externally Mixed – Constant Dry Specific Scattering Model

The following equation is used to estimate scattering under the assumptions of external mixing, constant dry specific scattering, and sulfate interpreted as ammonium bisulfate or sulfate mass adjusted for the level of ammoniation:

$$b_{scat} = (3)([SULFATE] + [NITRATE])\, f(RH) + (4)[OMC]\, f_{org}(RH) + (1)[SOIL] \qquad (6.4)$$

b_{scat} is the reconstructed scattering coefficient. The ratio between dry and wet scattering as a function of RH is referred to as the relative humidity scattering enhancement factor, f(RH). f(RH) and f_{org}(RH) refer to the enhancement factors for sulfates, nitrates, and organics, respectively. [SULFATE] is the SO_4 ion mass concentration adjusted either to a constant sulfate species type, such as ammonium bisulfate, or for its level of ammoniation. [NITRATE], [OMC], and [SOIL] are the concentrations of ammonium nitrate, organic carbon, and soil. The coefficient numbers refer to the assumed dry specific scattering of the respective species in m^2/g. The choice of these specific scatterings are discussed in Malm et al. [1994] and are basically best estimates based on an extensive literature review and reported in Trijonis and Pitchford [1987] and Trijonis et al. [1990].

Average *f*(RH) values for each sampling period were calculated using Tang's sulfate D/D_o curves. The *f*(RH) values were calculated for each hour and then averaged up to the sampling period length assuming a lognormal sulfate species mass size distribution with a geometric mass mean diameter of 0.3 μm and a geometric standard deviation, σ_g, of 1.5 was assumed. Estimates of *f*(RH) were derived for the deliquescent and crystallization curves as well as for curves that were smoothed between the crystallization and deliquescent points. The *f*(RH) associated with nitrates was assumed to be the same as for sulfates, while f_{org}(RH) for organics was set equal to one.

6.1.2.4 The Externally Mixed–Sulfate Ammoniated–Variable Specific Scattering Model

The following equation was used to estimate scattering:

$$b_{scat} = e_{wd}([SULFATE] + [NITRATE]) + (4)[OMC] f_{org}(RH) + (1)[SOIL] \quad (6.5)$$

e_{wd} is the ammoniated size and relative humidity dependent scattering efficiency of the wetted sulfate aerosol and the variables in the brackets are the dry mass concentrations of the various species. It is assumed that the nitrate and sulfate size distributions are the same and that nitrates scatter with the same efficiency as sulfate. The other variables are the same as those defined above.

6.1.2.5 The Internally Mixed Variable Mass and Size Scattering Model

The equation used to reconstruct scattering when the sulfate size distribution is known and a size distribution for organics and nitrates is assumed by:

$$b_{scat} = e_{wdm}([SULFATE] + [NITRATE] + [OMC]) + (1)[SOIL] \quad (6.6)$$

where e_{wdm} is the size and relative humidity dependent specific scattering for a sulfate, nitrate, and organic aerosol that is uniformly mixed. It is assumed that soil is externally mixed.

6.1.3 Results

6.1.3.1 Summary of Aerosol Measurements

$PM_{2.5}$ Measurements. Table 6.1 contains statistical summaries of the aerosol fine mass ($PM_{2.5}$) concentrations along with the fraction that each aerosol species contributes to reconstructed fine mass. All sampling periods were twelve hours in length starting at 7:00 a.m. Figure 6.1 shows temporal plots of measured fine mass and the five major aerosol species. The lowest concentrations of fine mass occurred on Julian day (JD) 216 when values of 3-4 $\mu g/m^3$ were recorded. Conversely, on JD 230 measured fine mass was 88 $\mu g/m^3$. Three relatively high soil episodes were recorded on JD=206-207, JD=215-216, and JD=225-232. On JD=207 soil was about 40-50% of the fine mass. The contributions of elemental carbon (EC) and nitrate to fine mass were small during the entire study period.

Table 6.1 *Statistical summary of aerosol species concentrations and the fraction of reconstructed fine mass attributed to certain species. FM, reconstructed FM, [SO_4] ion, [SULFATE], [NH_4NO_3], [OMC], [EC], [SOIL], [CM], and [NH_4] are gravimetric fine mass, reconstructed fine mass, sulfate ion mass, sulfate plus ammonium mass, neutralized nitrate mass, organic carbon mass, elemental carbon mass, soil mass, coarse mass, and ammonium ion mass, respectively.*

Variable	Mean ($\mu g/m^3$)	Std. Dev.	Minimum ($\mu g/m^3$)	Maximum ($\mu g/m^3$)	Fraction	N
FM	25.13	17.55	0.00	87.94	1.38	80
Reconstructed FM	18.09	12.34	3.66	59.41	---	80
[SO_4] ion	9.55	9.02	1.09	42.71	---	80
[SULFATE]	11.42	10.32	1.17	48.23	0.63	80
[NH_4NO_3]	0.20	0.11	0.07	0.70	0.01	80
[OMC]	4.56	1.79	1.40	8.60	0.25	80
[EC]	0.44	0.25	0.00	1.17	0.02	80
[SOIL]	1.47	1.56	0.02	8.33	0.08	80
[CM]	6.16	5.85	0.00	24.69	---	80
[NH_4]	1.79	1.30	0.06	4.98	---	80
NH_4/SO_4 molar ratio	1.10	0.30	0.30	1.85	---	80

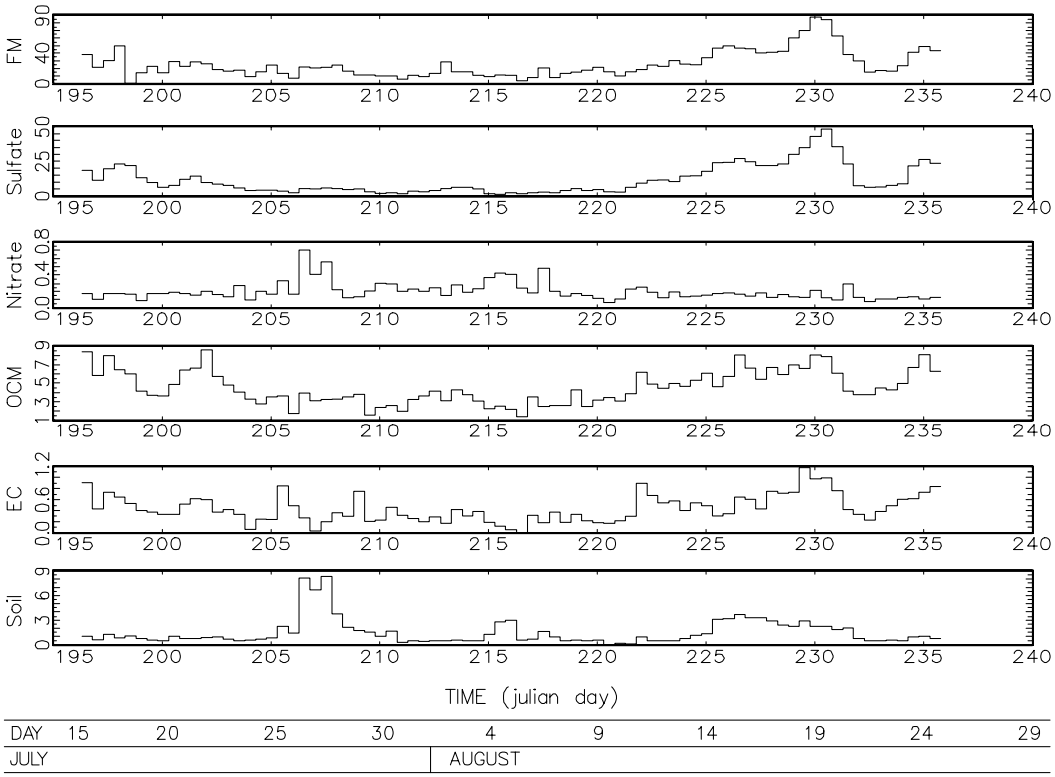

Figure 6.1 *Time lines of fine mass (FM), sulfate species mass (Sulfate), ammonium nitrate (Nitrate), organic mass (OCM), elemental carbon (EC), and soil (Soil). The time line is presented in Julian day, while concentrations are in $\mu g/m^3$.*

On the average, measured fine mass accounted for about 80% of the measured PM_{10} mass. Sulfates were the largest fraction of reconstructed fine mass at 63%. Organic carbon accounted for 25% of the fine mass, while soil contributed another 8%. Nitrates and EC were virtually tied for the lowest contribution to fine mass at 1% and 2%. It is worth noting that the mass fractions reported here are consistent with those found at other eastern monitoring sites [Sisler, 1996]. The average molar ratio of ammonium to sulfate ion was about 1, indicating that the sulfate ion was, on the average, about half neutralized.

Sulfur Mass Size Distributions. Figures 6.2 and 6.3 show two sulfur mass size distributions for two sampling periods. Figure 6.2 shows a mass size distribution for "larger sulfur particles", while Figure 6.3 is a more "typical distribution". Included on each graph are the Δ(sulfate mass)/Δ(log(*D*)) values derived directly from the DRUM sampler and from the results of the Twomey inversion calculation. The peak or maximum Δ(sulfur mass)/Δ(log(*D*)) curve for the more typical distribution occurred at about 0.45 μm, while for the "large" size distribution the maximum occurred at near 0.6 μm with most of the mass being above about 0.4 μm.

Table 6.2 is a statistical summary of the relative humidity, water mass associated with the sulfate species at ambient humidity, sulfate plus ammonium mass as measured with the IMPROVE and DRUM samplers, wet geometric mass mean diameter, and the geometric standard deviation. Various scattering parameters, which will be discussed in the next section, are also summarized.

The average ammoniated sulfate species concentrations are 14.95 and 14.02 $\mu g/m^3$ for the IMPROVE and DRUM samplers, respectively, which corresponds to a difference of 6.2%. The average geometric mass mean diameter at ambient RH is 0.36 μm with an average geometric standard deviation of 1.92.

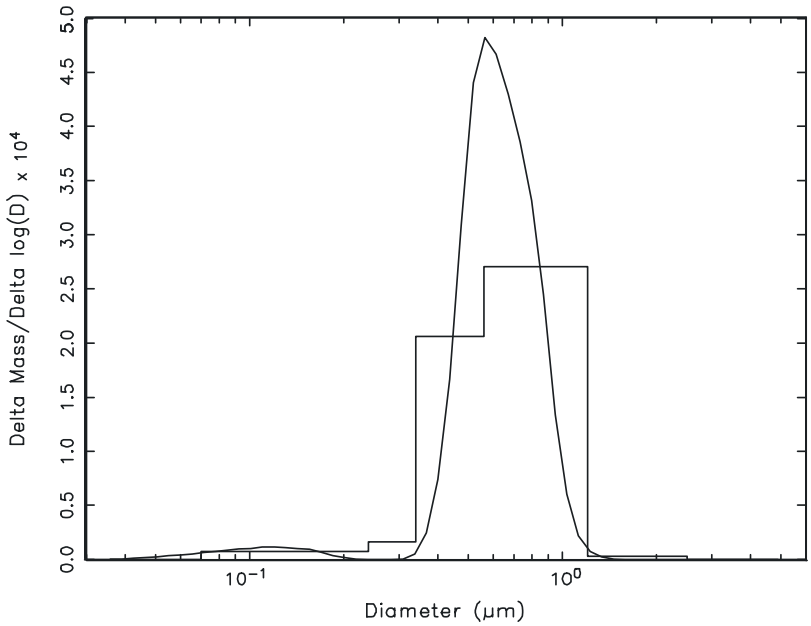

Figure 6.2 *An elemental sulfur mass size distribution at ambient RH for JD 229, which corresponds to a σ_g of 1.5 and a D_g equal to 0.60 μm. The smooth curve is the mass size distribution calculated using the Twomey [1975] inversion technique.*

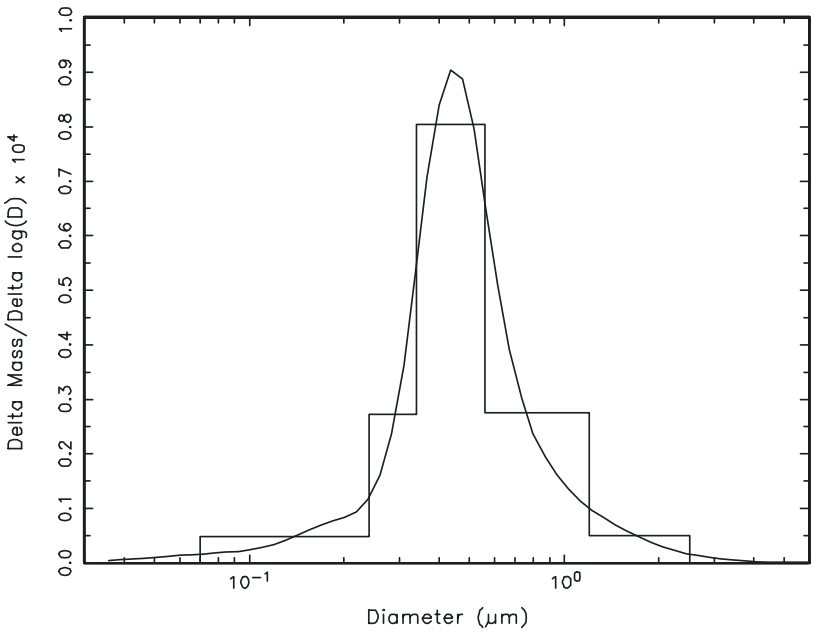

Figure 6.3 *A sulfur mass size distribution at ambient RH for JD 237, which corresponds to a σ_g of 1.8 and a D_g equal to 0.47 μm. The smooth curve is the mass size distribution calculated using the Twomey [1975] inversion technique.*

Table 6.2 *Statistical summary of DRUM data. WMASS is water mass associated with sulfate aerosol at ambient relative humidity, $SO_{4,mass}$ is sulfate plus ammonium mass, D_g and σ_g are the wet geometric mass mean diameter and standard deviation, respectively. e_d and e_w are the specific scattering of the dry and wet sulfate aerosol, while e_{wd} is wet scattering divided by the dry mass.*

Variable	Mean	Std. Dev.	Minimum	Maximum	N
RH (%)	74.99	8.94	51.66	92.24	45
WMASS ($\mu g/m^3$)	20.57	14.56	2.33	66.60	45
IMPROVE $SO_{4,mass}$ ($\mu g/m^3$)	14.95	11.37	2.09	48.23	45
DRUM $SO_{4,mass}$ ($\mu g/m^3$)	14.02	10.27	1.29	44.50	45
D_g (μm)	0.36	0.07	0.18	0.50	45
σ_g	1.92	0.27	1.47	2.37	45
e_d (m^2/g)	2.40	0.51	1.33	3.10	45
e_w (m^2/g)	3.58	0.61	1.76	4.60	45
e_{wd} (m^2/g)	9.64	3.25	3.04	19.12	45

Calculation of Sulfate Specific Scattering From Mass Size. The study's average dry specific scattering (e_d), wet specific scattering (e_w), and water enhanced specific scattering (e_{wd}) for sulfate are summarized in Table 6.2. e_d and e_w are 2.40 and 3.58 m^2/g, respectively. The mean dry specific scattering of 2.40 m^2/g is somewhat less than the 3.0 m^2/g used by a number of authors to estimate sulfate scattering [Trijonis et al., 1990]. The average enhanced specific scattering, e_{wd}, on the other hand, is 9.64 m^2/g at an average ambient relative humidity of 75%.

6.1.3.2 Comparison of Measured and Theoretical Predictions of Ambient Scattering

Results for the Externally Mixed Constant Specific Scattering Model. Because the average molar ratio of ammonium to sulfate ion was approximately one the ammonium bisulfate D/D_o curve was used to calculate the f(RH) function. [SULFATE] in Equation (6.4) was interpreted as ammonium bisulfate. Results of these calculations are summarized in Table 6.3 and shown in Figure 6.4, where measured and reconstructed scattering are scattered against each other. Also plotted in Figure 6.4 is the 1:1 line. The average sulfate scattering is 0.129 1/km, which in turn yields an average reconstructed scattering ($b_{scat}\_E\_e_c\_S_c\_f$(RH)), of 0.152 1/km, which is about 18% less than measured average scattering.

Table 6.3 *Statistical summary of measured scattering (<b_{scat}>), reconstructions of b_{scat} assuming different mixing rules and specific scattering and the scattering associated with each aerosol species. Except for f(RH), which is unitless, all units are in 1/km. The parenthetical values in the mean column are the fractional contribution of the respective species to the "best estimate" of reconstructed scattering. Variable descriptors are found at the bottom of the table.*

Variable	Mean	Std. Dev.	Minimum	Maximum	N
$< b_{scat}>$	0.185	0.133	0.045	0.611	45
$b_{scat}\_E\_e_c\_S_c\_f(RH)$	0.152	0.098	0.033	0.454	45
$b_{scat}\_E\_e_c\_S_a\_f(RH)$	0.164	0.118	0.037	0.537	45
$b_{scat}\_E\_e_s\_S_a\_B$	0.168	0.130	0.028	0.596	45
$b_{scat}\_E\_e_s\_S_a\_C$	0.168	0.129	0.028	0.596	45
$b_{scat}\_E\_e_s\_S_a\_D$	0.164	0.132	0.028	0.596	45
$b_{scat}\_M\_e_s\_S_a\_B$	0.182	0.134	0.033	0.626	45
RH (<95%)	74.99	8.94	51.66	92.24	45
f(RH)	3.29	1.07	1.44	6.57	45
$SO_4\_e_c\_S_c\_f(RH)$	0.129	0.093	0.020	0.420	45
$SO_4\_e_c\_S_a\_f(RH)$	0.140	0.113	0.024	0.502	45
$SO_4\_e_s\_S_a\_B$	0.143(0.85)	0.125	0.015	0.562	45
$SO_4\_e_s\_S_a\_C$	0.143	0.125	0.015	0.562	45
$SO_4\_e_s\_S_a\_D$	0.139	0.128	0.015	0.562	45
OC	0.021(0.13)	0.007	0.010	0.034	45
NO_3 *f(RH)*	0.002 (0.01)	0.001	0.001	0.004	45
Soil	0.002 (0.01)	0.002	0.000	0.008	45

E=external mixture
M=internal mixture
e_c=constant specific scattering
e_s=size dependent specific scattering
S_c=fixed sulfate species (NH_4HSO_4)
S_a=ammoniated sulfate species
B=best estimate sulfate growth curves
C=crystallization sulfate growth curves
D=deliquescent sulfate growth curves

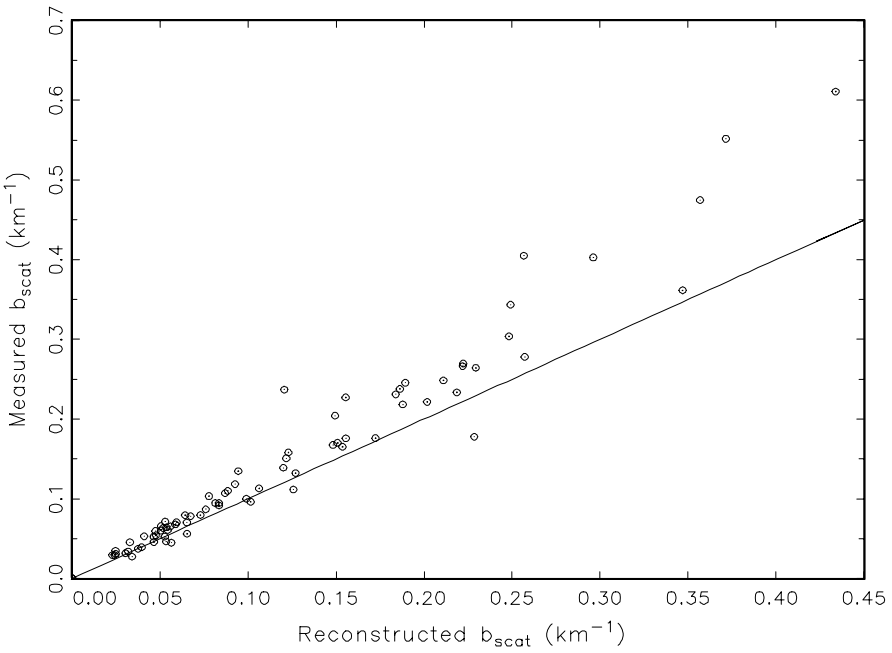

Figure 6.4. *An example of a measured f(RH) curve on sampling period corresponding to JD 205.29. The curve through the data points is a best fit using an equation with a functional form containing RH/(1-RH).*

An ordinary least square (OLS) regression yielded a very high R^2 of 0.95, however, the OLS regression line is about 1.31, implying measured scattering is about 30% greater than reconstructed. Similar discrepancies between reconstructed and measured scattering were noted previously [Gebhart and Malm, 1990] using data gathered at Shenandoah National Park. For the most part the use of Equation (6.4) and [SULFATE] as ammonium bisulfate or ammonium sulfate to reconstruct scattering works well for most western IMPROVE sites [Malm et al., 1996]. The inability to use Equation (6.4) and the associated assumptions to reconstruct scattering at nonurban eastern sites was part of the motivation for carrying out SEAVS.

The calculations were repeated using Equation (6.4) but with [SULFATE] explicitly adjusted for the ammonium ion concentration and the *f*(RH) function for the ammoniated sulfate aerosol species was calculated on a sampling-period-by-sampling-period basis using Tang's sulfate D/D_o curves that were smoothed between the crystallization and deliquescent points and interpolated between $(NH_4)_2SO_4$, NH_4HSO_4, and H_2SO_4, as described previously. $SO_4\_e_c\_S_a\_f$(RH) is 0.140 1/km, which in turns yields an average reconstructed scattering ($b_{scat}\_E\_e_c\_S_a\_f$(RH)), of 0.164 1/km, compared with 0.152 1/km for the case that did not use actual sulfate compound mass concentrations nor an estimation of the amount of water associated with each type of sulfate species. This is still about 11% lower than measured scattering. The R^2 of an OLS regression between reconstructed and measured scattering is again high at over 0.95 and the regression coefficient is 1.12, suggesting the measured scattering is about 12% greater than reconstructed.

Results for the Externally Mixed Model with Sulfate Specific Scattering Estimated From Mass Size Distributions. The same strategy described previously, for estimating D/D_o was used. However, to develop the range of possible ammoniated sulfate and associated water scattering allied with the crystallization, deliquescent, and best estimate branches of the growth curves, each was used in the reconstructed scattering calculation and the results are presented in Table

6.3 under $SO_4\_e_s\_S_a\_C$, $SO_4\_e_s\_S_a\_D$, and $SO_4\_e_s\_S_a\_B$, respectively. There are only small differences between the three estimations. The crystallization $SO_4\_e_s\_S_a\_C$ is almost the same as the best estimate $SO_4\_e_s\_S_a\_B$, while the deliquescent $SO_4\_e_s\_S_a\_D$ is about 3% less than the best estimate. Because other species also contribute to scattering, the net effect of the three different assumptions on total $PM_{2.5}$ scattering is even less. Reconstructed scattering varies between 0.168 1/km and 0.164 1/km. Furthermore, reconstructed scattering using this model (sulfate scattering efficiencies estimated from mass size distributions) is nearly the same as the constant dry specific scattering model but with sulfate ammoniation accounted for. Apparently, the biggest effect in achieving a close match between reconstructed and measured scattering is the adjustment for sulfate ammoniation and associated growth as a function of relative humidity.

Results of the calculation are further highlighted in Figure 6.5, where the range of scattering coefficients associated with using the crystallization, best estimate, and deliquescent branches of the growth curve is shown. Also shown in the scatter plot is the 1:1 line. A visual examination of the scatter plot shows that reconstructed and measured scattering compare quite favorably. An OLS regression between measured and reconstructed scattering using the "best estimate" growth curves yields an R^2 of 0.98, a slope of 1.00, and an offset of 0.014 1/km. The parenthetical values in Table 6.3 are the study-averaged fractional contribution of each species to fine specific scattering using the "best estimate" growth model. Sulfates, organics, nitrates, and soil contribute 85%, 13%, 1%, and 1%, respectively.

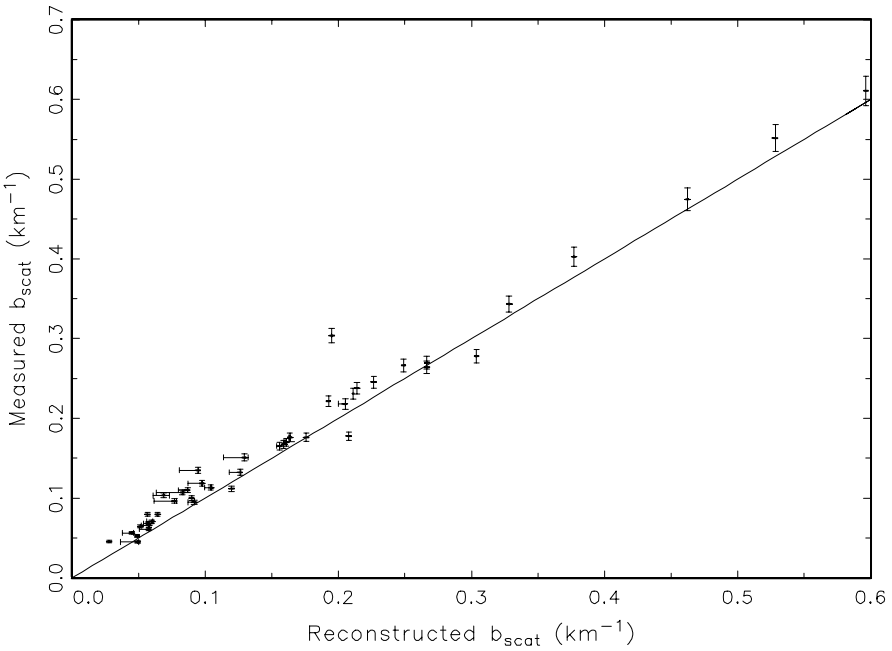

Figure 6.5 *A scatter plot of reconstructed and measured $PM_{2.5}$ scattering assuming external mixing but with measured sulfur size distributions. The range of reconstructed scattering was arrived at by assuming three different forms of Tang's D/D_o curves for $(NH_4)_2SO_4$, NH_4HSO_4, and H_2SO_4. The highest reconstruction is arrived at by using the crystallization branches, the middle value from a best estimate growth between the crystallization and deliquescence branches, while the lowest reconstruction was calculated using the deliquescent arm of the growth curves. Units are in 1/km.*

As an example of the temporal variability, Figure 6.6 shows the time lines of measured, ammoniated sulfate species, nitrate, organics, and soil scattering coefficients for the "best estimate" growth model. The units in Figure 6.6 are 1/km. Sulfate scattering varies from about 0.05 1/km to a high of over 0.6 1/km: over an order of magnitude change. Nitrate scattering varies around 0.002 1/km, while organics vary from about 0.004 to 0.04 1/km, also an order of magnitude change. However, the organic scattering coefficient is about an order of magnitude lower than that for sulfate. There is one soil episode occurring on JD 206-208, where the soil scattering is almost 0.01 1/km as compared to the more typical values of 0.002-0.003 1/km. It should be pointed out, however, that the episode soil scattering coefficient at 0.01 1/km is still about five times less than the lowest sulfate scattering coefficient.

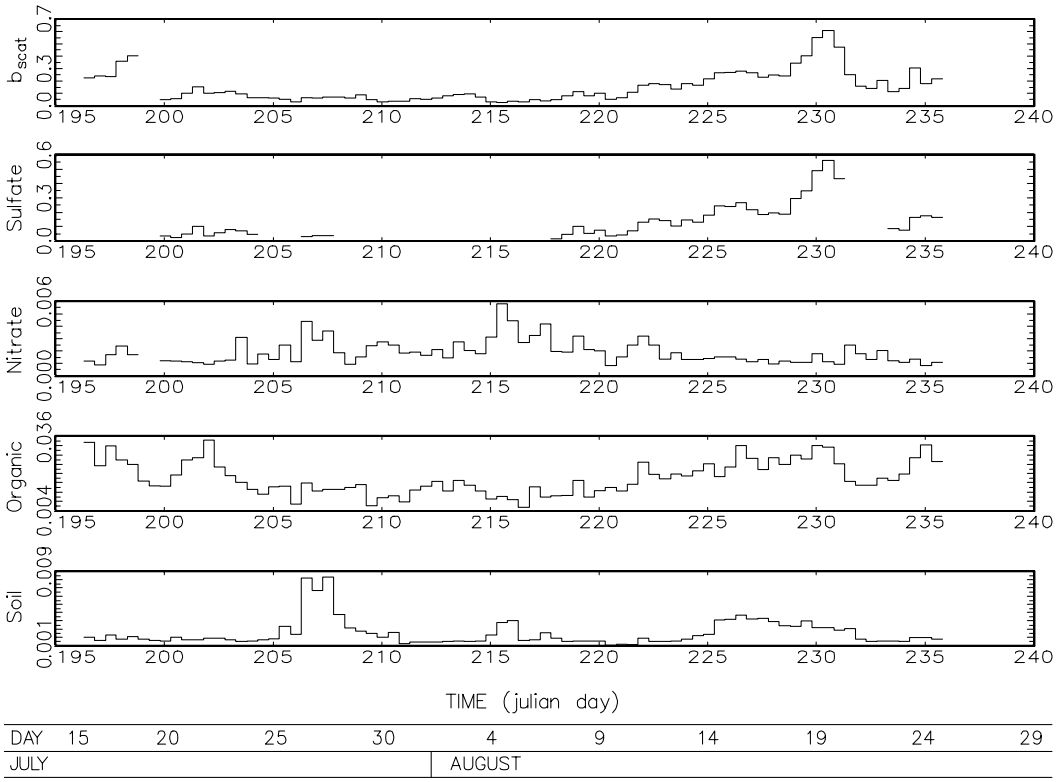

Figure 6.6 *Time lines showing measured <b_{scat}> (b_{scat}), sulfate species scattering (Sulfate), ammonium nitrate scattering (Nitrate), organic specific scattering (Organic), and soil scattering (Soil). The best estimate D/D_o growth curve and measured sulfur mass size distributions were used. Units on scattering are in 1/km, while time is presented as Julian day.*

Results for the Internally Mixed Model with Measured Sulfur Mass Size Distribution. For the internally mixed model, it was assumed that sulfates, nitrates, and organics were uniformly mixed, all with the same size distribution as sulfur. The growth of the mixed particle was calculated using Equation (6.4) for a three species mix and with D/D_o set equal to 1 for organics (that is, organics were considered nonhygroscopic), while nitrates were assumed to have the same hygroscopicity as sulfates. D/D_o for sulfate species was calculated using the "best estimate" growth curve as described above.

Results of the calculation are summarized in Table 6.3 as $b_{scat}\_M\_e_s\_S_a\_B$, while Figure 6.7 shows the internally and externally mixed model results plotted against measured scattering. The range of results for the internal and external model calculations is represented by the horizontal bars with the largest reconstructed scattering generally corresponding to the internal model and the lowest scattering with the external calculation. In most cases, the difference between the internal and external case is small, as expected. The average difference between the two calculations is only about 8%, with the internally mixed model yielding the higher reconstructed scattering estimates and in closer agreement with measurement.

An OLS regression between reconstructed scattering using the internally mixed model and measured scattering resulted in an R^2 of 0.97 with a slope of 0.97±0.025.

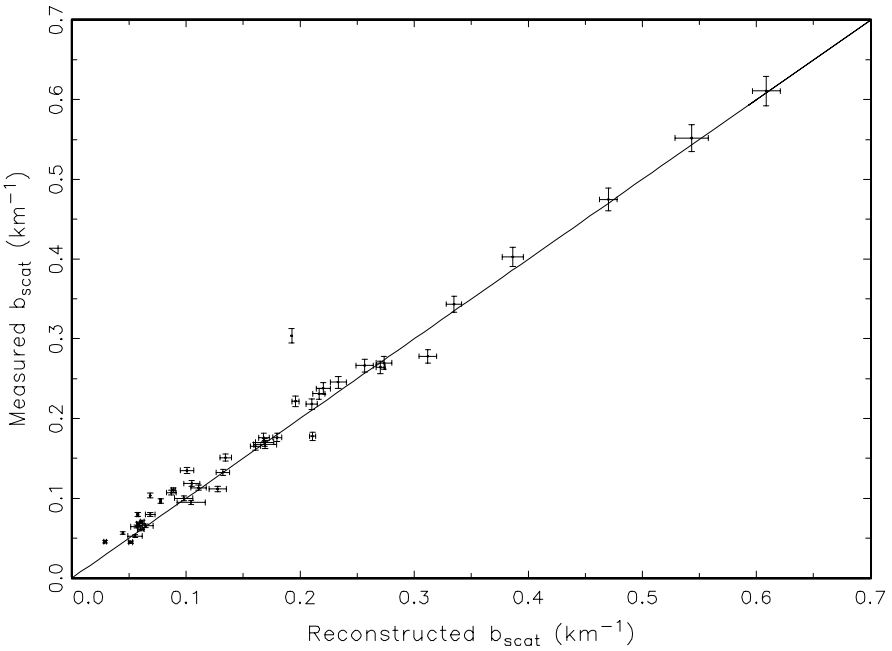

Figure 6.7 *Scatter plot of reconstructed and measured scattering along with the 1:1 line. The upper and lower bound of reconstructed scattering correspond to assuming an internally and externally mixed aerosol.*

6.1.3.3 Comparison of Measured and Theoretical Estimations of $b_{scat}(RH)/b_{scat,dry}$

Comparisons between measured and modeled calculations of $b_{scat}(RH)/b_{scat,dry}$ will be carried out using the latter three modeling approaches described previously. While most measurements were made from JD 196 to JD 235, the humidograph was only successfully operated from JD 203 to 225 and on JD 230, and the mass size measurements are available for most time periods between JD 199 and 207 and between JD 216 and 235. Therefore, out of 80 sampling periods where $b_{scat}(RH)/b_{scat,dry}$ model calculations could be done, there are only 24 overlapping time periods where all three model calculations can be compared. However, any single model comparison to $b_{scat}(RH)/b_{scat,dry}$ measurements can have more data points. For instance, the

comparison between measurements and the external model calculation, which does not rely on mass size distribution measurements, has 70 common sampling periods.

Figure 6.8 shows a comparison between measured and modeled $b_{scat}(RH)/b_{scat,dry}$ for JD 204.29. The three lines correspond to the model calculations, while the measured data points are represented by the uncertainty bars where uncertainty in the $b_{scat}(RH)/b_{scat,dry}$ ratio and relative humidity are shown. The solid line corresponds to the external-constant specific scattering model, $b_{scat}\_E\_e_c\_S_a\_f(RH)$, but with sulfate ammoniation and water uptake accounted for, the short dashed line is the external model with sulfate efficiency calculated from sulfur mass size distributions, $b_{scat}\_E\_e_s\_S_a\_B$, and the long dashed line corresponds to the internally mixed model, $b_{scat}\_M\_e_s\_S_a\_B$. In most cases, the external and mixed models agreed quite well with each other and with the measurements. However, there were a number of cases where all models agreed well with each other but the modeled $b_{scat}(RH)/b_{scat,dry}$ was well above measured values. One representative case is shown for JD 202.79 in Figure 6.9. In most cases, when modeled $b_{scat}(RH)/b_{scat,dry}$ was greater than the measured ratio, the organic fraction of fine mass was at its highest values. For instance, JD 202.79 corresponds to the sampling period with the highest organic concentration.

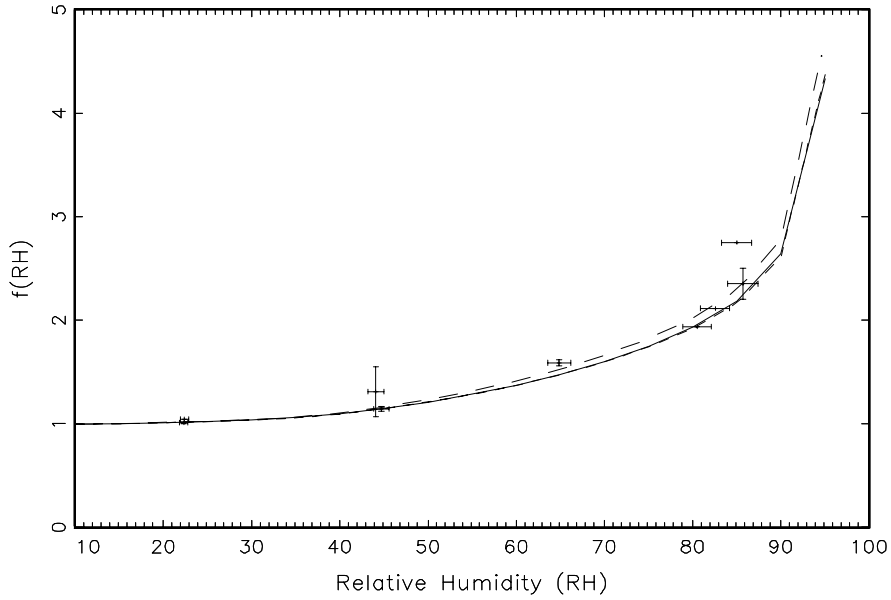

Figure 6.8 *f(RH), $b_{scat}(RH)/b_{scat,dry}$, is plotted as a function of relative humidity. The uncertainty bars represent the uncertainties in measured RH and f(RH), while the three lines correspond to the three model calculations. The solid line, small and large dashed lines correspond to external-constant specific scattering, external-variable specific scattering, and mixed model, respectively. Julian Day = 204.29.*

There are a few time periods where the mixed model $b_{scat}(RH)/b_{scat,dry}$ ratio was substantially lower than the ratios predicted by the external models. One example is shown in Figure 6.10 where the internally mixed and external model calculations bound the measured ratios. On JD 217 the internally mixed model ratios were lower than measured or external model predictions. The discrepancy between internally mixed and external model calculations occurred on the lowest sulfur concentration time periods. For those time periods, the mixed model predicts less of an increase in scattering as a function of relative humidity than do the external models.

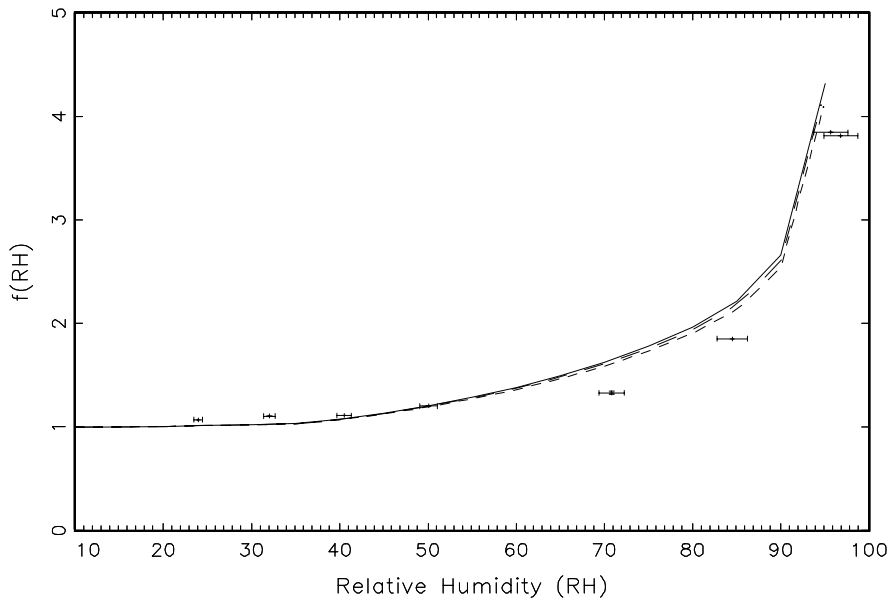

Figure 6.9 *f(RH), $b_{scat}(RH)/b_{scat,dry}$, is plotted as a function of relative humidity. The uncertainty bars represent the uncertainties in measured RH and f(RH), while the three lines correspond to the three model calculations. The solid line, small and large dashed lines correspond to external-constant specific scattering, external-variable specific scattering, and mixed model, respectively. Julian day = 202.79.*

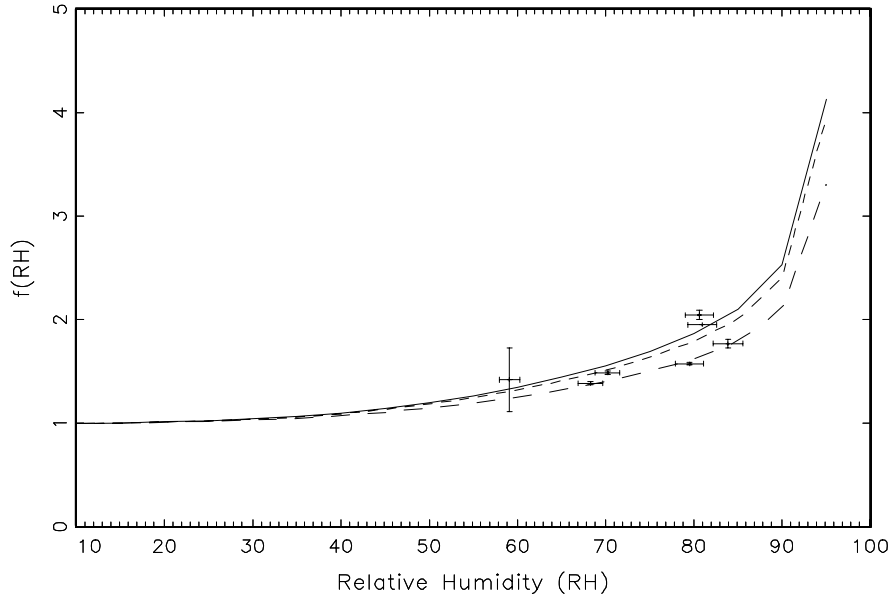

Figure 6.10 *f(RH), $b_{scat}(RH)/b_{scat,dry}$, is plotted as a function of relative humidity. The uncertainty bars represent the uncertainties in measured RH and f(RH), while the three lines correspond to the three model calculations. The solid line, small and large dashed lines correspond to external-constant specific scattering, external-variable specific scattering, and mixed model, respectively. Julian day = 206.79.*

Comparisons between measured and calculated $b_{scat}(RH)/b_{scat,dry}$ for the whole data set are shown in Figure 6.11 for the $b_{scat}\_E\_e_s\_S_a\_B$ model, while comparisons, using ordinary least square regressions, between measured and estimated ratios for all models are summarized in Table 6.4. Figure 6.11 shows that in general there is good agreement between measured and modeled $b_{scat}(RH)/b_{scat,dry}$ ratios. There are about eight data points where modeled ratios are significantly greater than measured values and at higher RH values model calculations appear to be slightly greater than measured ratios. The R^2 for regressions between measured and model calculations range from a high of 0.92 for the $b_{scat}\_E\_e_c\_S_a\_f(RH)$ to a low of 0.71 for the $b_{scat}\_M\_e_s\_S_a\_B$ model. All models yield $b_{scat}(RH)/b_{scat,dry}$ ratios that are about 20% greater than measured values. In all models, organics were assumed not to be hygroscopic. Assuming some hygroscopicity for organic aerosols would enhance the difference between measured and modeled $b_{scat}(RH)/b_{scat,dry}$ ratios.

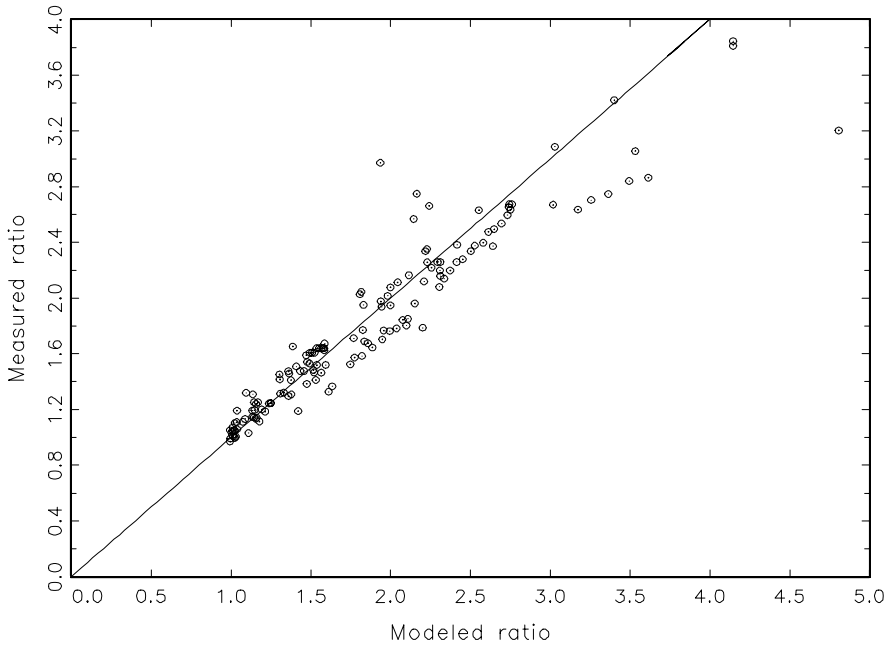

Figure 6.11 *Scatter plot of measured vs modeled $b_{scat}(RH)/b_{scat,dry}$ for the external mixture-variable sulfate size ($b_{scat}\_E\_e_s\_S_a\_B$) calculation. For reference the 1:1 line is also shown.*

Table 6.4 *Summary of ordinary least square regressions of measured and estimated $b_{scat}(RH)/b_{scat,dry}$ as the dependent and independent variables, respectively.*

Model	Intercept	Std error	Estimate	Std error	t-value	N	R^2
$b_{scat}\_E\_e_c\_S_a\_f(RH)$	0.31	0.023	0.79	0.012	0.000	368	0.92
$b_{scat}\_E\_e_s\_S_a\_B$	0.29	0.048	0.83	0.023	0.000	148	0.89
$b_{scat}\_M\_e_s\_S_a\_B$	0.43	0.079	0.82	0.042	0.000	148	0.71

Table 6.5 further summarizes the difference between the three model calculations. The numbers 1, 2 and 3 refer to averages of the differences over three relative humidity ranges

corresponding to 20-35%, 40-60%, and 75-95%. In all cases, the differences between the three models are accentuated at higher relative humidities with the external models yielding, in all cases, higher $b_{scat}(RH)/b_{scat,dry}$ ratios. The mean difference between external models is less than 1% for low RH values and only 3% at higher relative humidities. Differences between the internally mixed and external models is again small at low RH values and approach a mean difference on the order of 10% at the higher relative humidities. The maximum difference between the internally mixed and external models is about 30% for the 75-95% relative humidity range.

Table 6.5 *A summary of the percent differences between model estimations of $b_{scat}(RH)/b_{scat,dry}$ for three ranges of relative humidities. Number 1 refers to an average of $b_{scat}(RH)/b_{scat,dry}$ values between 20-35% RH, number 2 to average ratios between 40-60% RH, and number 3 to ratios between 75-95% RH.*

Variable	Number	Mean	Std. Dev.	Variance	Minimum	Maximum	N
$(b_{scat}\_M\_e_s\_S_a\_B)$ -	1	-0.60	0.60	0.36	-2.29	0.59	45
$(b_{scat}\_E\_e_s\_S_a\_B)$	2	-2.44	2.78	7.71	-9.55	3.26	45
	3	-6.91	8.24	67.83	-26.37	9.43	45
$(b_{scat}\_E\_e_c\_S_a\_f(RH))$ -	1	0.40	0.27	0.07	-0.05	1.20	45
$(b_{scat}\_E\_e_c\_S_a\_B)$	2	1.06	0.86	0.74	-0.30	4.70	45
	3	2.90	3.24	10.52	-0.97	16.78	45
$(b_{scat}\_M\_e_s\_S_a\_B)$ -	1	-1.00	0.71	0.50	-2.23	0.53	45
$(b_{scat}\_E\_e_c\_S_a\_f(RH))$	2	-3.51	2.79	7.76	-9.83	3.56	45
	3	-9.80	8.22	67.58	-29.17	10.39	45

6.1.4 Summary of the Great Smoky Mountains Study

The objective of calculations presented in this section were not to apportion scattering to any particular species but to examine the ability of various models to predict scattering of fine particles less than 2.5 μm both as a function of relative humidity and at ambient humidities. From these calculations it is possible to develop a better understanding of the sensitivity of scattering models to aerosol mixing assumptions, sulfate acidity, and the hygroscopic characteristics of various aerosol types.

A variety of aerosol scattering models was exercised. First, an externally mixed aerosol model where constant dry specific scattering was assumed, sulfate mass is assumed to be in the form of ammonium bisulfate and a functional dependence of scattering on relative humidity (RH), which was based on laboratory measured ammonium bisulfate growth, was used. Second, an external model with constant dry specific scattering was used but sulfate mass and changes in scattering efficiency due to growth as a function of relative humidity were accounted for as functions of sulfate ammoniation. Third, an externally mixed aerosol model was assumed, but with explicit incorporation of sulfate size and sulfate ammoniation with associated growth as a function of relative humidity accounted for. Finally, an internally mixed aerosol model that incorporated sulfate size, ammoniation, and associated sulfate hygroscopic growth was exercised. In all cases, only sulfates and nitrates were assumed to be hygroscopic.

When comparing model performance as it relates to predicting ambient scattering, the first and simplest model, which assumed only one type of sulfate species and constant dry specific scattering, performed the poorest. It predicted ambient scattering adequately at low scattering values but underpredicted scattering under high sulfate concentrations by about 30%. When the estimated mass of the sulfate species was corrected for its degree of ammoniation, model performance was improved substantially, and was further improved by estimating absorbed water as a function of sulfate ammoniation. Only slight improvement in model performance was achieved by explicitly accounting for variation in dry specific scattering coefficients due to changes in particle size distribution. The overall performance of the externally mixed model, with sulfate ammoniation, growth as a function of relative humidity and size, was excellent in that the averages between measured and predicted scattering were within 9% of each other, and an OLS regression between the two variables yielded an R^2 of 0.94. The effect of assuming the crystallization, deliquescent or best estimate branches of the sulfate growth curves was also explored. Each was used in the reconstructed scattering and it was shown that there were only small differences between the three estimations. The scattering associated with the crystallization curve was almost the same as the best estimate, while scattering calculated using the deliquescent curve was about 3% less than the best estimate.

For the internally mixed model, it was assumed that sulfates, nitrates, and organics were uniformly mixed, with nitrates, sulfates and organics all having the measured sulfur mass size distribution and soil mixed externally. The growth of the internally mixed particle was calculated using the ZSR assumptions with D/D_o as a function of RH set equal to 1 for organics, while nitrates were assumed to have the same hygroscopicity as sulfates. D/D_o for sulfate species was calculated using the "best estimate" growth curve. In general, the difference between the internal and external case is small. The average difference between the two calculations is only about 8%, with the internally mixed model yielding the higher reconstructed scattering estimates.

Comparison between measured and modeled $b_{scat}(\mathrm{RH})/b_{scat,dry}$ ratios were carried out using three of the four modeling approaches. Models used for the comparison were external with constant specific scattering but with sulfate ammoniation and associated growth accounted for, external with sulfate size, ammoniation, and growth incorporated, and the internally mixed model. In most cases, all three modeling approaches agreed well with each other, however, the ratios predicted by the internally mixed and external models under high relative humidity conditions differed from each other by as much as 30%, with the mixed model generally showing less increase in scattering with RH than the external models.

Measured ratios, in general, were well reproduced by all of the modeling approaches. The R^2s between measured and modeled ratios varied from 0.92 to 0.71 with the external models having the highest R^2. All models yielded ratios that were on the average, about 20% greater than those that were measured. The largest discrepancies occurred when organic mass concentrations were highest with modeled ratios being greater than those measured.

6.2 GRAND CANYON STUDIES

Two other studies were carried out at Grand Canyon, Arizona. National parks on the Colorado Plateau experience some of the best visibility in the continental United States. Annual average extinction, including Raleigh scatter, is about 31 1/Mm in the inner-mountain western United States as compared to rural eastern sites where the average extinction is near 130 1/Mm. In the eastern United States and at parks such as the Great Smoky Mountains, sulfates contribute most of the visibility degradation, whereas on the Colorado Plateau extinction is more evenly split between sulfates that make up about 23% of total extinction and carbon (scattering plus absorption), which may be as high as 33% depending on how absorption is estimated. About 10% of extinction is estimated to be associated with soil and coarse mass [Sisler, 1996; Malm et al., 1994]. While the fraction of extinction associated with sulfates is expected to decrease in the next two decades as a result of projected decreases in sulfur dioxide emissions, carbon emissions are expected to increase as prescribed fire activity by federal land managers is projected to increase by factors of 5-10 [Sandberg et al., 1979].

The accurate estimation of b_{abs} and coarse mass scattering remain problematic. Absorption can be estimated by assigning a mass absorption efficiency to elemental carbon or it can be estimated from direct measurements of light attenuation as it passes through a filter medium on which the absorbing material has been collected. Horvath [1993] reviewed the various filter absorption measurement techniques and concluded that, depending on scattering albedo and filter loading, measured absorption values are too high by factors on the order of 20-80%! Presumably, the overestimation of absorption is due to multiple scattering effects and/or light leakage from the edge of the filter medium. On the other hand, Eldred and Cahill [1994] clearly showed that absorption estimates decrease as filter aerial density increases. They collected multiple samples over the same time period but with different filter "masks" that results in varying aerial densities. Absorption, derived from the various filters with varying aerial density, showed a decrease as aerial density increased when absorption estimates should have been the same. These series of measurements suggest that absorption estimates based on filter transmittance underpredict by as much as a factor of two, depending on filter loading. They suggest that a fraction of absorbing particles were "shadowed" by nearest neighbors masking or blocking light from particles below the outermost particle layers.

Hitzenberger et al. [1999] compared a number of commonly employed absorption measurement techniques and showed that, even though all techniques were highly correlated, the absorption estimates varied by more than factors of two. Furthermore, mass absorption efficiencies have been reported in the literature that range from about 5–20 m^2/g [Horvath, 1993] with a value of 10 m^2/g being used by most researchers in the field. It is interesting to point out that Fuller et al. [1999], in a theoretical exploration of elemental carbon scattering and absorption as a function of elemental carbon physical characteristics and mixing assumptions, were unable to justify absorption efficiencies for elemental carbon as high as 10 m^2/g. They concluded that efficiencies in the range of 5-8 m^2/g were more likely.

In the IMPROVE monitoring network, elemental carbon (EC) is measured using the thermal optical reflectance (TOR) technique [Chow et al., 1993] and b_{abs} has been estimated using a laser integrated plate method (LIPM) and more recently with a hybrid integrating plate and sphere

(HIPS) instrument [Campbell et al., 1997]. Both measurements have been made on rather heavily loaded (more than a monolayer of deposit) Teflon filters. Absorption estimates using LIPM and HIPS are further corrected for aerial density effects, discussed above, that results in an upward scaling of about a factor of 1.7-2.0. Interestingly, comparison of b_{abs} derived from HIPS and corrected for variation in aerial density and 10*EC shows the b_{abs} measurement to be about a factor of two higher than absorption estimated from elemental carbon.

Malm et al. [1996], using IMPROVE data, compared reconstructed extinction with measured extinction and concluded that absorption estimated by LIPM and corrected for aerial density was needed to achieve closure between the two variables. Using 10*EC as the absorption estimate for reconstructing extinction fell short of measured extinction. On the other hand, one could use 10*EC as the absorption estimate and increase coarse mass scattering and achieve closure with about the same degree of accuracy as using b_{abs} as determined by LIPM. Together absorption and coarse mass scattering make up about 30-50% of aerosol extinction in the western United States [Malm et al., 1996; Sisler, 1996].

There has been very little work investigating coarse particle scattering. The value most often used for coarse scattering efficiency is 0.6 m^2/g, a value that was originally reported by Trijonis [1988] for a study carried out in the Mojave Desert, while White [1990] reported coarse mass scattering efficiencies of 0.34-0.45 m^2/g for data collected near Lake Mead and White and Macias [1990] reported a value of 0.4 m^2/g for data collected at Spirit Mountain, which is about 100 miles south of Las Vegas, Nevada. The inlet size cut (D_{aero}) for the coarse mode for the White [1990] and White and Macias [1990] studies was 15 μm, while the Trijonis [1988] study reported on data collected with an inlet corresponding to D_{aero}<10 μm. All these studies occurred in desert areas where dust can contribute as much as 50% of the particle extinction budget. Estimates of coarse mass scattering have not been made in other nonurban areas of the United States.

In part, it is the inability to conclusively apportion about 30-50% of the extinction budget between coarse mass scattering and particle absorption that has motivated the measurement program reported here. To investigate these issues a study was carried out from July 10, 1998 through August 8, 1998 on the south rim of Grand Canyon National Park.

Experiments were designed such that observables could be estimated or modeled in a number of different ways. Fine mass was gravimetrically determined for both D_{aero} < 10 and 2.5 μm, which can be compared to reconstructed mass based on measured species. Dry and ambient 2.5 μm scattering was measured, which in turn can be compared to reconstructed scattering based on aerosol species measurements. Open-air nephelometry was used to measure ambient scattering of fine and coarse particles that can be used to estimate coarse particle scattering, which in turn can be used with extinction measurements to develop independent estimates of absorption. Fine and coarse mass absorption was independently measured using two filter substrates and with an aethalometer. Scattering as a function of relative humidity was also measured with a humidograph allowing for estimates of $f(\mathrm{RH}) = b_{scat(wet)}/b_{scat(dry)}$, which in turn can be used to develop estimates of aerosol growth. Modeling ambient scattering and the wet-to-dry scattering ratio will serve to both explore the validity of aerosol growth and mixing models and associated assumptions, and provide an estimate of the hygroscopicity of aerosol species

other than sulfates and nitrates. The following discussion will focus on exploring the scattering properties of fine and coarse particulates under ambient conditions and particle absorption.

6.2.1 Experimental Methods

The details of the nephelometer and particle measurement program were discussed previously on the special study at Great Smoky Mountains.

6.2.1.1 Transmissometer

Transmissometers are calibrated to measure the irradiance, at 550 nm, of a light source after the light has traveled over a finite atmospheric path. The transmittance of the path is calculated by dividing the measured irradiance at the end of the path by the calibrated initial intensity of the light source. The average extinction of the path is calculated using Bouger's law from the transmittance and length of the path. The measurement is ambient in that air samples are not passed through an enclosed chamber.

Transmissometers employed in this study are the Optec, Inc., LPV-2 instruments, which have been in operation since 1986. Their use in remote locations such as national parks is discussed by Molenar *et a1*. [1989], while their use in urban settings is presented by Dietrich et al. [1989]. Careful operation of the transmissometer (daily cleaning of optics and pre and post calibrations) should result in extinction measurements with an accuracy of about 10% [Molenar *et a1*., 1989]. The transmissometer was located near the particle samplers but on the rim of the canyon. Therefore, the separation between the transmissometer and all other instruments was about 1.5 km.

6.2.1.2 Aethalometer

The aethalometer collects aerosol continuously on a quartz fiber filter, while measuring the optical transmittance through the filter [Hansen et al., 1982]. The rate of decrease of optical transmittance as a function of the rate of increase of filter loading has been found to be proportional to the atmospheric absorption. The aethalometer can be operated at a flow rate of 5-10 l/min and is purported to have an accuracy of about 10%. Its sample air was extracted from a sampling plenum that was also fitted with a 2.5 μm cyclone inlet.

6.2.2 Summary of Measurements

Table 6.6 summarizes the optical measurement in the form of mean, standard deviation, minimum, and maximum. The number of valid data points is also given. The extinction measurements, b_{ext}, were made with a transmissometer, while $b_{scat,open}$, $b_{scat,2.5\mu m}$, and $b_{scat,dry}$ refer to scattering measurements made with the open air nephelometer, the nephelometer fitted with a 2.5 μm inlet, and the nephelometer designed to operate with an inlet that dried the aerosol, respectively. The absorption measurement, $b_{abs,2.5\mu m}$, referred to in this table, was made with the aethalometer fitted with a 2.5 μm inlet. RH_{neph}, and RH_{trans} refer to the relative humidity measured at the nephelometer and transmissometer locations.

As a quality assurance check, the $b_{scat,dry}$ values derived from the Radiance Research nephelometer, which was run with an aerosol drying system, was compared to the Optec nephelometer derived scattering, which operated under ambient relative humidity conditions, when the relative humidity was less than 45%. For nearly neutralized sulfate aerosols, one would not expect significant growth below 45% relative humidity at Grand Canyon [Zhang et al., 1994]. Figure 6.12 shows the comparison for a 100 min averaging time along with the 1:1 line (R^2=0.92). The difference between the average scattering coefficients for the data presented in Figure 6.12 is less than 5% at 6.9 1/Mm and 6.5 1/Mm for the Radiance Research and Optec nephelometers, respectively.

Table 6.6 *Statistical summary of ten-minute optical and relative humidity measurements. The scattering and extinction values include Rayleigh scattering.*

Variable	Mean (1/Mm)	Std. Dev.	Minimum (1/Mm)	Maximum (1/Mm)	Valid
b_{ext}	23.06	11.23	7.70	192.8	6432
$b_{scat,open}$	20.59	6.62	8.40	63.00	5660
$b_{scat,2.5\mu m}$	18.03	7.96	7.80	86.80	6052
$b_{scat,dry}$	16.23	3.71	9.38	35.07	5875
$b_{abs,2.5\mu m}$	1.12	1.26	-3.33	46.27	6762
RH_{neph} (%)	42.39	25.32	5.73	100.00	6843
RH_{trans} (%)	34.56	22.35	4.46	97.80	6762

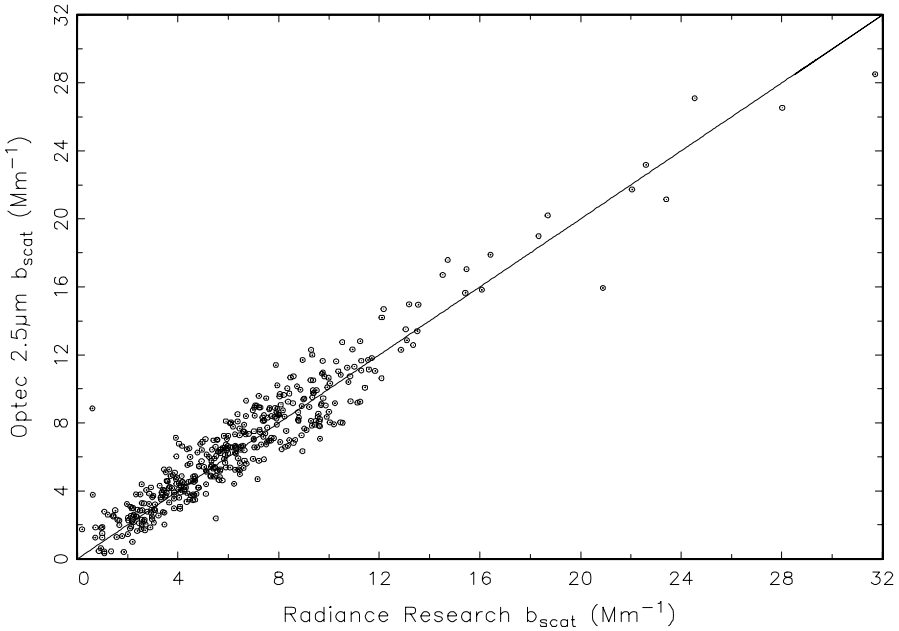

Figure 6.12. *Scatter plot of b_{scat} measured by the Radiance Research and Optec nephelometers for relative humidities less than 45%. The 1:1 line is shown for reference. Both instruments were fitted with a 2.5 µm cyclone inlet.*

A number of authors [Heintzenberg and Quenzel, 1973; Fitzgerald, 1977; Hasan and Lewis, 1983; Sloane et al., 1990] estimated that the MRI series of nephelometers see about half of the actual scattering from representative distributions of coarse particles because of large angle truncation errors (the MRI nephelometers integrated over angles between 8 and 168 degrees). White et al. [1994] used field measurements obtained in the Subregional Cooperative Electric Utility National Park Service, and Environmental Protection Agency Study (SCENES) [McDade and Tombach, 1987] to independently estimate the fraction of coarse particle scattering measured by these nephelometers. They regressed total scattering (b_{ext}-b_{abs}) against fine and coarse particle scattering as measured by the 1597 MRI integrating nephelometer fitted with and without a 2.5 μm cyclone inlet. The regression coefficient on coarse particle scattering was 2.3±13% consistent with the theoretically estimated factor of two.

Molenar [1997] carried out similar theoretical calculations of the expected underprediction of coarse particle scattering associated with the Optec nephelometer and showed that at 550 nm it will underestimate coarse particle scattering by 5-30%, depending on assumed particle size distributions.

Referencing Table 6.6, b_{ext} exceeds $b_{scat,2.5\mu m}$ by about 5 1/Mm or 37% of aerosol extinction, a significant fraction of the extinction budget. If the open air nephelometer indeed does measure most of the coarse particle scatter and most of the absorption is due to particles less than 2.5 μm, then $b_{ext} \cong b_{scat,open} + b_{abs,2.5\mu m}$. The sum of $b_{scat,open}$ and $b_{abs,2.5\mu m}$ is 21.7 1/Mm or about 1.35 1/Mm short of measured extinction. One could achieve closure if it is assumed that the aethalometer measurement of $b_{abs,2.5\mu m}$ is about 2.2 times underestimated or about 2.47 1/Mm instead of 1.12 1/Mm. On the other hand, the difference between the open air and fine particle (D_{aero}<2.5 μm) scattering is 2.56 1/Mm and is presumably associated with coarse particle scattering. Assuming for the moment that this value is one half of coarse particle scattering one can estimate coarse particle scattering to be 5.12 1/Mm. Then coarse plus fine particle scattering alone would be 23.15 1/Mm, which is very close to measured extinction without including absorption.

The degree to which absorption and/or coarse particle scattering are over or underestimated can be explored using regression analysis. Assuming that $b_{scat,open}$-$b_{scat,2.5\mu m}$ is proportional to coarse particle scattering and b_{ext}-$b_{scat,2.5\mu m}$ is coarse particle scattering plus absorption of both coarse and fine particles one can write the following equation:

$$(b_{ext} - b_{scat,2.5\mu m})_i = a_o + a_1(b_{scat,open} - b_{scat,2.5\mu m})_i + a_2(b_{abs,2.5\mu m})_i \qquad (6.7)$$

where i refers to the i^{th} sampling period and a_o, a_1, and a_2 are constants. This series of equations can be solved using ordinary least square (OLS) regression analysis.

Figure 6.13 shows the temporal plot of b_{ext} and $b_{scat,2.5\mu m}$ for 10.0 min time intervals starting at JD 161 and ending on JD 210 (June 10 – August 29). In most cases, the two variables co-vary with each other, however, during some time periods they are actually anti-correlated. For reference, the overall correlation is 0.62, while the correlation between two collocated samplers, $b_{scat,open}$ and $b_{scat,2.5\mu m}$ is 0.93. The insert in Figure 6.13 shows a time period from JD 181-183 where the variables are almost exactly out of phase with each other. The reader is reminded that

the transmissometer measurement is path averaged over 5 km and is about 1.5 km distant from the nephelometers.

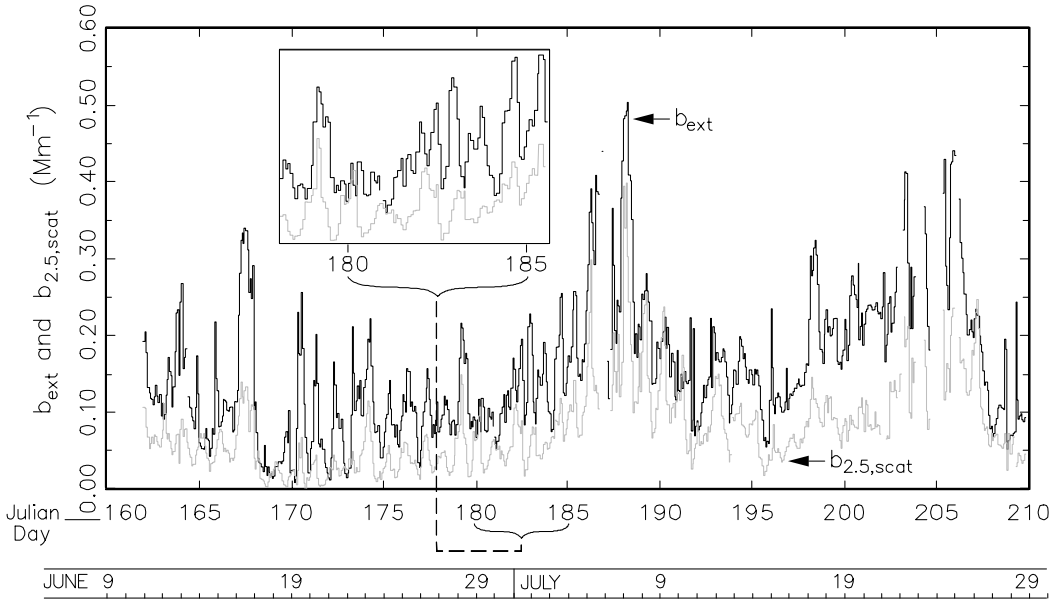

Figure 6.13 *Temporal plot of measured extinction and scattering by particles less than 2.5 μm. The time increment associated with each data point is 10 minutes.*

For purposes of the regression analysis, short temporal variability in the data was minimized by averaging to 16 hrs and requiring that the 16-hr data have at least 8 hrs of nonmissing values. Furthermore, because the relative humidity at the transmissometer site was lower than at the nephelometer location, only optical parameters were included in the averaged data set if the relative humidity was less than 60%. Figure 6.14 is a temporal plot of the averaged b_{ext}, $b_{scat,2.5\mu m}$, and $b_{abs,2.5\mu m}$ values.

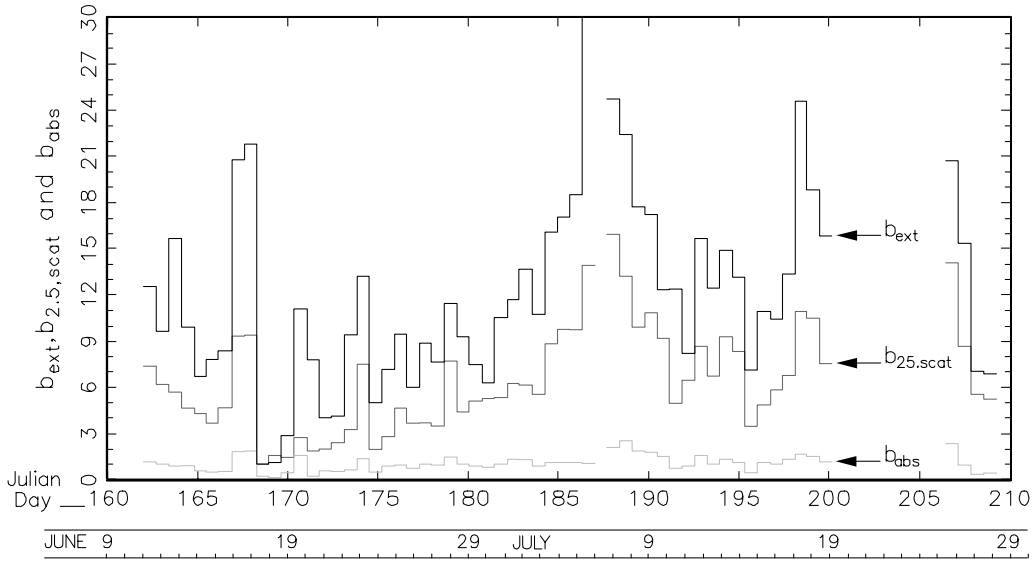

Figure 6.14 *Temporal plot of measured extinction, scattering and absorption by particles less than 2.5 μm for 16-hr time intervals*

Table 6.7 shows the results of the regression. The regression coefficients are highly significant with standard error for both coefficients being about 20%. Figure 6.15 is a scatter plot of reconstructed and measured extinction where reconstructed extinction is based on the regression coefficients presented in Table 6.7. For comparison the 1:1 line is also shown and R^2=0.87.

The coefficient associated with coarse particle scattering as determined by the nephelometers ($b_{scat,open}$-$b_{scat,2.5\mu m}$) suggests that coarse particle scattering is overestimated by about 18±19%. On the other hand, the coefficient associated with $b_{abs,2.5\mu m}$ implies that measured absorption is low by a factor of about 2.8±0.62! Changing the averaging time does alter the coefficients somewhat. For instance, for an averaging time of an hour the coefficient on coarse particle scattering remains unchanged and its significance level increases but the coefficient associated with absorption is reduced from 2.76 ±0.62 to 1.6 ± 0.35. However, the overall model R^2 is decreased to 0.36.

Table 6.7 *Summary of OLS regression with b_{ext}-$b_{scat,2.5\mu m}$ as the dependent variable and $b_{scat,open}$-$b_{scat,2.5\mu m}$, and $b_{abs,2.5\mu m}$ as independent variables. $b_{abs,2.5\mu m}$ refers to aethalometer measurements in this table.*

Valid cases: 49	Dependent variable: b_{ext}-$b_{scat,2.5\mu m}$			R^2=0.60	
Variable	Estimate	Std error	t-value	Prob t>|t|	Cor dep var
intercept	-0.0004	0.0007	-0.59	0.56	-------
$b_{scat,open}$-$b_{scat,2.5\mu m}$	0.82	0.19	4.27	0.00	0.67
$b_{ath,2.5\mu m}$	2.76	0.62	4.44	0.00	0.68

Because the nephelometers and transmissometer are not sampling the exact same air mass, the regression analysis should be viewed as semi-quantitative. However, the analysis strongly suggests that fine particle absorption as measured by the aethalometer is an underestimate of total absorption. The "calibration" factor for the aethalometer could be in error or there may be substantial coarse particle absorption.

6.2.3 Summary of Particulate Measurements

A statistical summary of fine and coarse particle (PM_{10}-$PM_{2.5}$) concentrations are presented in Table 6.8, while temporal plots are shown in Figures 6.16 and 6.17 for coarse and fine mass components, respectively. Organics (H) and organics (C) refer to organic mass estimates based on hydrogen and carbon, respectively. Because only module A was used to sample PM_{10} analysis is limited to PIXE, XRF, and PESA. Therefore, coarse carbon and nitrates cannot be explicitly determined and coarse organics must be estimated using Equation (6.8).

$$OCH = 11(H - 0.25S) \tag{6.8}$$

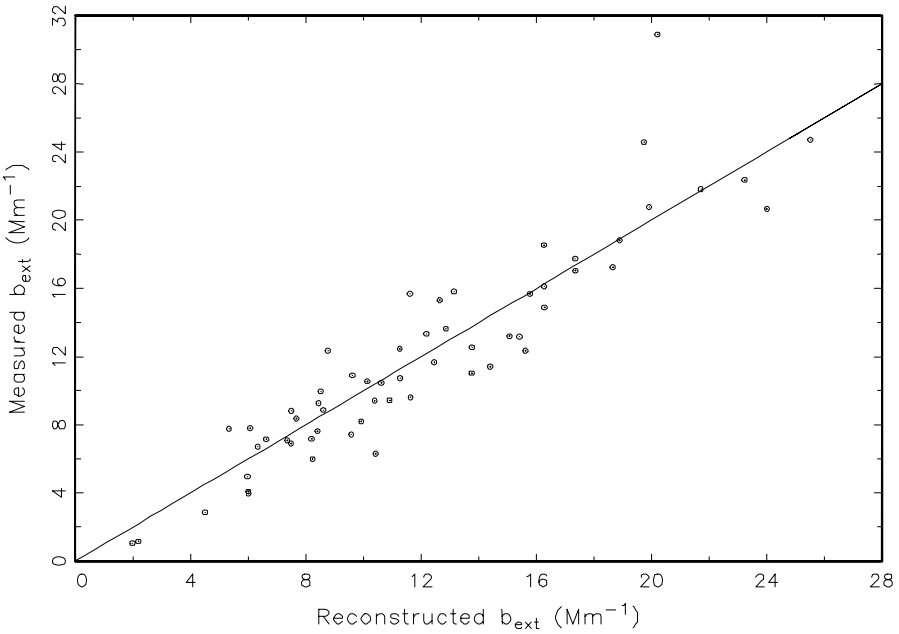

Figure 6.15 *Scatter plot, along with the 1:1 line, of measured and reconstructed extinction.*

Table 6.8 *Statistical summary of aerosol measurements.*

Variable	**Mean ($\mu g/m^3$)**	**Std. Dev. ($\mu g/m^3$)**	**Minimum ($\mu g/m^3$)**	**Maximum ($\mu g/m^3$)**	**Valid**
Coarse Mass	5.71	4.39	0.97	22.80	37
Coarse $(NH_4)_2SO_4$	0.14	0.13	0.00	0.44	37
Coarse organics (H)	2.70	1.54	0.64	7.30	37
Coarse Soil	4.14	4.30	0.27	24.31	37
	(3.06)	(3.18)	(0.20)	(17.99)	
Fine Mass	3.88	1.20	1.79	6.55	37
Reconstructed Fine Mass	3.68	1.05	1.67	6.02	37
$(NH_4)_2SO_4$	1.27	0.67	0.21	2.74	37
Organics (C)	1.52	0.42	0.64	2.18	37
Organics (H)	1.57	0.53	0.85	3.26	37
Elemental Carbon(EC)	0.10	0.08	-0.04	0.26	37
NH_4NO_3	0.20	0.12	0.03	0.55	37
Fine Soil	0.60	0.24	0.25	1.28	37

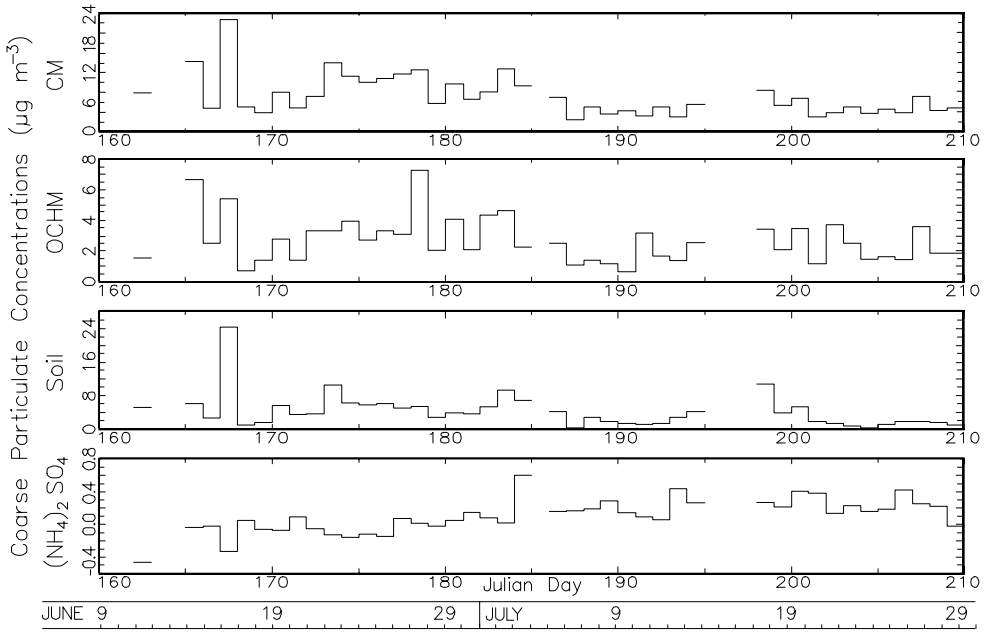

Figure 6.16 *Temporal plot of coarse particle (PM_{10}–$PM_{2.5}$ µm) concentrations. CM refers to gravimetric coarse mass and OCHM to organics by hydrogen.*

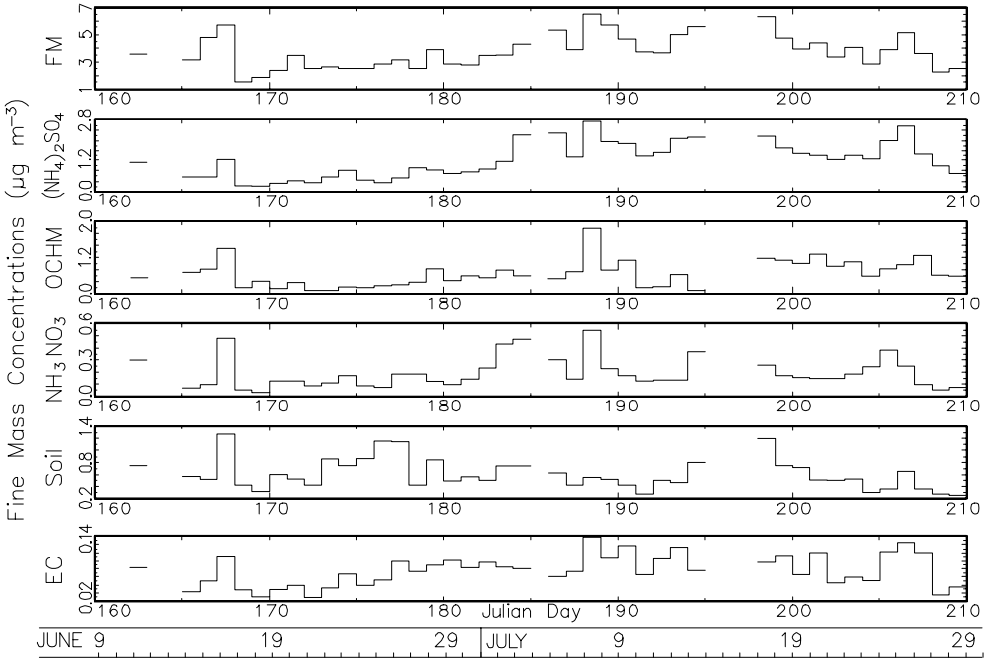

Figure 6.17 *Temporal plot of fine particle concentrations. FM refers to gravimetric fine mass, while OCHM is organics by hydrogen.*

Gravimetric coarse and fine mass on the average are about equal at 5.71 and 3.88 μg/m^3, respectively. Reconstructed and gravimetrically determined fine mass compare favorably at 3.88 and 3.68 μg/m^3, respectively, however, one can see that the sum of coarse mass constituents, without including elemental carbon and nitrates, are an overestimate of measured coarse mass. The sum of average coarse organics and soil alone are 6.84 μg/m^3, while measured average coarse mass is 5.71 μg/m^3. Apparently, the algorithms that have been developed for estimating fine mass constituents yield overestimates for their coarse counterparts.

To explore the degree to which coarse soil and organics are overdetermined, a regression analysis was carried out with CM as the dependent variable and coarse OCHM, ammonium sulfate, and soil as independent variables. The results are presented in Table 6.9. Sulfate concentrations are low and its coefficient is not statistically significant. The coefficient of determination (R^2) is high at 0.80 and the statistical significance of the coefficients associated with soil and OC are high. The regression results suggest that soil is overdetermined by 26%, while organic estimates are approximately correct. Table 6.8 also includes, parenthetically, coarse soil concentrations that have been corrected to the regression results (multiplied by 0.74).

Table 6.9 *Summary of results of an ordinary least square (OLS) regression with coarse mass as the dependent variable and soil and organics as the independent variables.*

Valid cases: 43	Dependent variable: CM			R^2=0.80	
Variable	Estimate	Std error	t-value	Prob t>|t|	Cor dep var
Soil	0.74	0.06	12.10	0.00	0.95
OC	1.00	0.12	8.42	0.00	0.91

Figure 6.18 shows a scatter plot of reconstructed and gravimetric fine mass along with a 1:1 line. The data points are scattered around the 1:1 line and the coefficient of determination for an OLS regression between the two variables is 0.78.

Referring to Table 6.8, organics are the largest fraction of fine mass, while soil is the largest fraction of coarse mass. Sulfates make up a small to negligible contribution to the coarse mode, while they are the second largest contributor to fine mass. Organics also contribute significantly to coarse mass. Referring to Figures 6.16 and 6.17, a number of interesting episodes present themselves. On JD 167 there was a coarse mass episode that reached 23 μg/m^3, while the corresponding fine mass concentration was about 6 μg/m^3. The coarse mode was made up primarily of soil but with a significant amount of organics present. In the fine mode, dust is also a large contributor at 1.28 μg/m^3 but organic concentrations are slightly higher at 1.47 μg/m^3 and sulfates are 1.22 μg/m. On JD 165, CM has the second highest value and coarse soil and organics are approximately equal with organics being slightly higher. Fine mass is not particularly high on that day. Coarse mass tends to be the highest during the early part of the sampling period (JD 160 to 188), while fine mass, other than the "dust" episode just discussed, was highest in the latter half of the study period (JD 188 to 210).

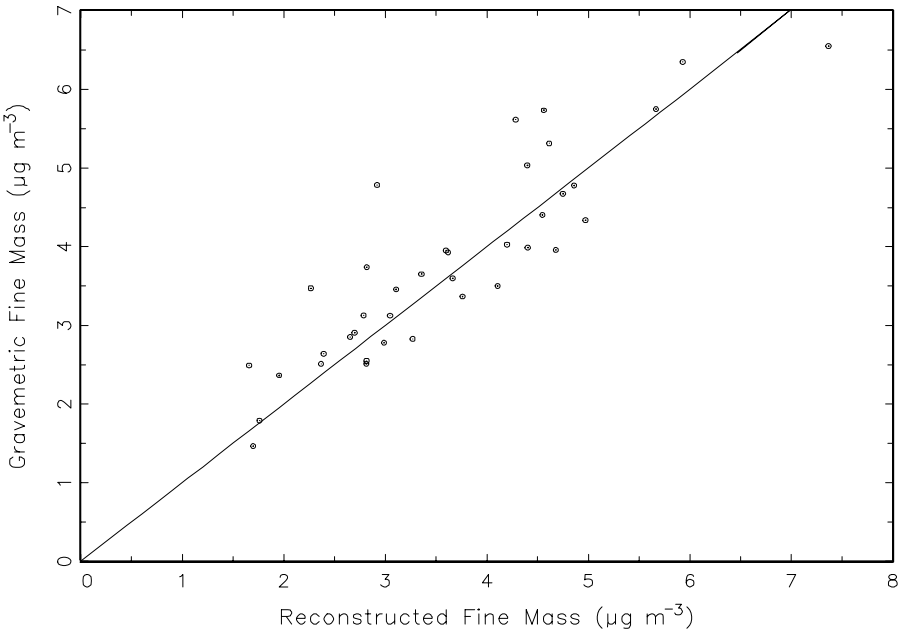

Figure 6.18 *Scatter plot, along with the 1:1 line, of measured and reconstructed fine mass.*

6.2.4 Estimates of Coarse Mass Scattering Efficiencies

Within the uncertainty of the regression analysis as defined by Equation (6.7), $b_{scat,open}$ - $b_{scat,2.5\mu m}$ gives an estimate of coarse particle scattering. Therefore, large particle scattering efficiency can be estimated by:

$$e_{CM} = (b_{scat,open} - b_{scat,2.5\mu m}) / CM. \tag{6.9}$$

From a physical perspective, $b_{scat,open}$ -$b_{scat,2.5\mu m}$ should be an underestimate of coarse particle scattering in that $b_{scat,open}$ undermeasures scattering due to all particles and therefore e_{CM} would be underestimated. Figure 6.19 is a scatter plot of coarse particle scattering efficiency (e_{CM}) and CM. Scattering efficiency is in units of m^2/g, while CM is in $\mu g/m^3$. The horizontal line corresponds to a scattering efficiency of 0.6 m^2/g, which is the "best estimate" suggested by Trijonis et al. [1990]. The lowest scattering efficiencies reported in the literature (0.34-0.45 m^2/g) were derived from measurements at Meadview during the SCENES study [White et al., 1994].

Referring to Figure 6.19, one can see that for CM mass concentrations above about 8.0 $\mu g/m^3$ estimated scattering efficiencies are consistent with the above referenced studies. However, for lower coarse mass concentrations efficiencies vary between about 0.5 and 1.2 m^2/g. Coarse mass efficiencies (e_{CM}) even as high as 0.6 m^2/g are hard to justify on a theoretical basis and to have mass scattering efficiencies as high as 1.0 m^2/g are even more difficult. For instance, assuming coarse soil has a mass median diameter (d_g) of 4.0 µm, geometric standard deviation (σ_g) of 2.0, index of refraction of 1.53, and density of 2.3 g/cm^3

yields a coarse mass scattering efficiency of about 0.35 m^2/g. Efficiencies as high as 0.6 m^2/g occur only when coarse soil particle mass mean diameters are near the 2.5 μm cyclone cut point.

Coarse mass scattering efficiencies as high as 1.0 m^2/g can occur if, as stated above, coarse soil mass size distributions are shifted to near the cyclone cut point, coarse particles are made up of other species that are less dense and therefore scatter more light on a per mass basis. The data does, to some degree reflect, these hypotheses. The highest coarse mass scattering efficiencies occur when the ratio of fine to coarse soil is greatest (0.4), and when this ratio is low (0.1-0.2), e_{CM} is lowest at about 0.4 m^2/g. Furthermore, the higher coarse mass efficiencies also occur when organics are the larger fraction of coarse mass and on the other hand when coarse organics make up only about 20% of the coarse mass the efficiencies drop to about 0.4 m^2/g.

A source of error in the above estimation of e_{CM}, is that the open-air nephelometer could be potentially biased from particles larger than 10.0 μm and therefore Equation (6.9) would necessarily be an overestimation of scattering by particles in the 2.5-10.0 μm range. Another potential source of error in the above estimation of e_{CM} is large particle (>2.5μm) "leakage" by the cyclone onto the PM2.5 substrates. CM estimates (PM_{10}-$PM_{2.5}$) would then be biased low and, therefore, CM scattering efficiencies biased high.

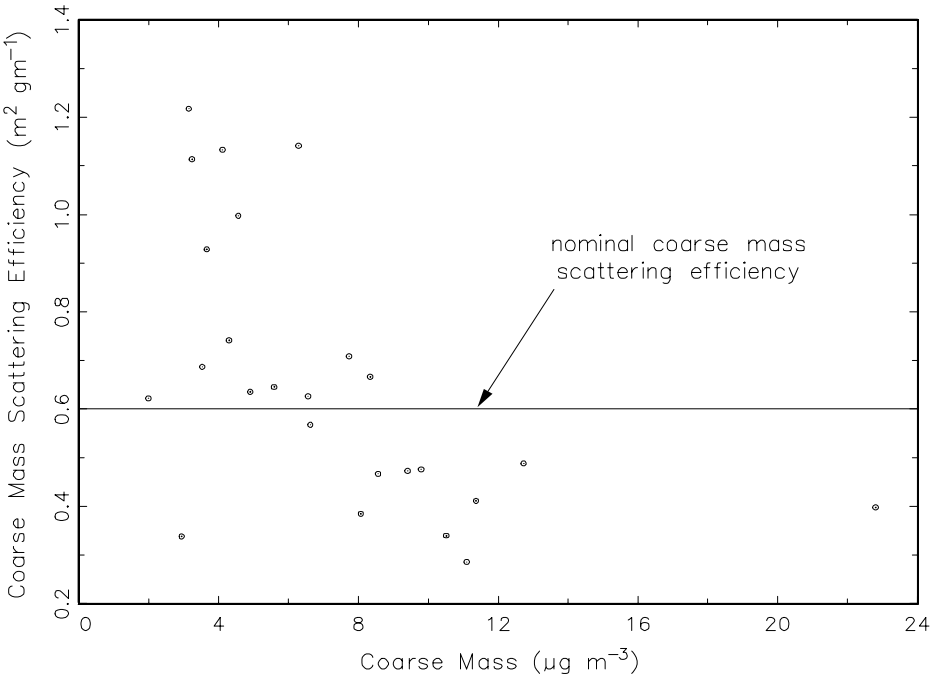

Figure 6.19 *Scatter plot of coarse mass scattering efficiency as a function of coarse mass concentration. The horizontal line corresponds to the mass coarse particle mass scattering efficiency that is typically used as a nominal value.*

6.2.5 Absorption Estimates

As sulfate concentrations decline, as a result of reduction in sulfur dioxide emissions, and organic and elemental carbon concentrations are projected to increase, as a result of increased urban populations and prescribed fire, the contribution of absorption to haze can be anticipated to increase. Yet there are no reliable means of estimating absorption. Most, if not all, absorption estimates rely on transmission measurements of aerosols collected on some filter media. Horvath [1993] reviewed many of these measurements. The absorption estimates are sensitive to the type of substrate used, optical configuration of the transmission measurement device, filter loading, and scattering albedo.

Arnott et al. [1999] developed a prototype photoacoustic spectrometer, which is undergoing initial field tests, while Moosmüller [1998] is developing an in-situ enclosed-folded path transmissometer that can be fitted with a size-selective inlet and thereby compared directly to nephelometers with size-selective inlets. Both instruments should go a long way toward resolving which of the many different filter type measurement schemes are most accurate.

In IMPROVE, absorption estimates have been derived from transmission measurements of the Module A Teflon filter using both LIPM and HIPS (see Section 6.2), while many other studies have employed a Nuclepore substrate. The aethalometer essentially makes a transmission measurement through a quartz type filter. In this field campaign, absorption estimates were derived by six different techniques: b_{lac} is 10 m^2/g * EC, $b_{ath,2.5\mu m}$ is the aethalometer measurement, LIPM is the laser integrated plate measurement on Teflon, HIPS is the hybrid integrated plate and sphere on Teflon, and NLIPM and NHIPS are the same measurements only on a Nuclepore substrate. CLIPM and CHIPS are coarse absorption derived from differencing PM_{10} and $PM_{2.5}$ LIPM and HIPS measurements on the associated Teflon filters.

Table 6.10 summarizes the absorption estimates. Not shown in Table 6.10 are the corrections for aerial density effects that have been routinely applied to LIPM and HIPS estimates. These corrections result in an upward scaling of about 1.7-2.0. It is interesting to note that the HIPS measurement, which is designed to compensate for filter reflectance effects, is lower than LIPM for Teflon filters but greater for Nuclepore substrates. The aethalometer and NLIPM, on the average, are within about 6% of each other and b_{lac} is about 30% greater than either of these two measurements. LIPM is about a factor of 2 greater than $b_{ath,2.5\mu m}$ or NLIPM, while HIPS is about a factor of 1.6 greater. Coarse absorption is on the order of about one half of fine absorption.

Figure 6.20 shows a multiple scatter plot of each of these variables scattered against each other. Each of the separate scatter plots will not be discussed as to how and why each variable is somewhat different than the next but are only included for completeness and for the interested reader. All variables are well correlated with each other but in some cases the differences between the variables are biased additively, while in other cases there is a multiplicative bias. For instance, LIPM has about a 1 1/Mm offset when compared to $b_{ath,2.5\mu m}$, while NHIPS when compared to $b_{ath,2.5\mu m}$ is lower by a multiplicative factor of about two. $b_{ath,2.5\mu m}$ and NLIPM compare the most favorably both on the average and across all values, while b_{lac} also compares

favorably with $b_{ath,2.5\mu m}$ and NLIPM. If the 1 1/Mm offset is subtracted from LIPM then it too compares well with $b_{ath,2.5\mu m}$, NLIPM, and b_{lac}. Finally, based on Figure 6.20, it is evident that coarse and fine absorption are correlated.

Table 6.10 *Statistical summary of absorption measurements.*

Variable	Mean (1/Mm)	Std. Dev. (1/Mm)	Minimum (1/Mm)	Maximum (1/Mm)	Valid
b_{lac}	1.38	0.68	0.07	2.56	21
$b_{ath,2.5\mu m}$	1.07	0.45	0.26	2.02	21
LIPM	2.19	0.63	0.92	3.69	21
HIPS	1.69	0.65	0.56	3.42	21
NLIPM	1.14	0.66	0.00	2.58	21
NHIPS	2.14	0.94	0.22	4.32	21
CLIPM	1.05	1.03	0.00	4.67	21
CHIPS	0.37	0.65	0.00	2.93	21

The solution of Equation (6.9) implies that absorption, as measured by the aethalometer, is an underestimate of absorption by an amount on the order of about 2. The regression coefficients, although quite significant, are sensitive to averaging time and in the broadest sense OLS type regressions are also sensitive to the inherent uncertainty of the measurements themselves [White, 1990]. It is further emphasized that the aethalometer measurements are for fine particle absorption, while b_{ext}-$b_{scat,2.5\mu m}$ is sensitive to fine and coarse particle absorption. LIPM measurements for coarse and fine particle absorption, after correcting for the 1/Mm fine particle offset (the correction isn't needed for coarse particle absorption because it is derived by differencing the PM_{10} and $PM_{2.5}$ absorption and the offset is thus subtracted out) are the same at about 1/Mm. Coarse particle HIPS is only 0.25 that of fine particle HIPS absorption.

Therefore, within the uncertainty of the analysis, regression results are consistent with absorption measurements. Total absorption, both fine and coarse, is on the order of about a factor of two greater than fine particle absorption by itself. Because the uncertainty of accurately measuring total absorption in the 1 to 3 1/Mm range by differencing optically derived variables (b_{ext}-$b_{scat,2.5\mu m}$ and $b_{scat,open}$-$b_{scat,2.5\mu m}$) the analysis should be viewed as semi-quantitative. It is clear, however, that total atmospheric absorption can be substantially underestimated if only fine particle absorption is considered.

Finally, a regression was carried out using:

$$b_{ath,2.5\mu m} = a_1(E1+E2) + a_2(O4+OP) + a_3(Soil) \tag{6.10}$$

where $b_{ath,2.5\mu m}$ is the absorption as determined using the aethalometer, E1, E2, O4, and OP are the carbon concentrations corresponding to the different temperatures over which carbon molecules are vaporized in the TOR technique [Chow et al., 1993], and Soil is fine particle soil. This type of analysis has been carried out by Huffman [1996] and Malm et al. [1996] but with $b_{abs,2.5\mu m}$ as determined by LIPM on Teflon and with the aerial density correction applied. In these previous analyses, absorption efficiencies associated with EC were on the order of 12 m^2/g

which, based on theoretical calculations, are unlikely unless rather severe assumptions are made concerning the density of elemental carbon [Fuller et al., 1999].

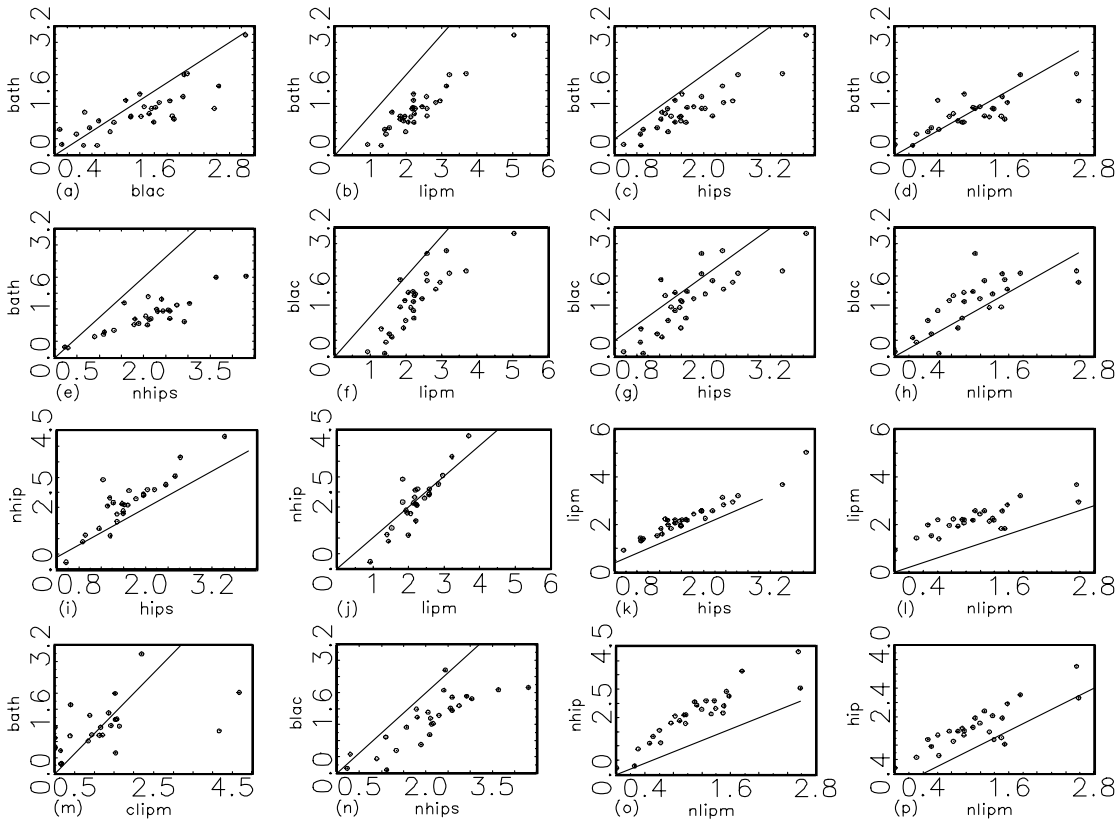

Figure 6.20 *Multiple scatter plots, along with 1:1 lines, of absorption measured in a number of different ways. lipm, hips, bath, and blac refer to laser integrated plate method, hybrid integrated plate and sphere instrument, aethalometer, and 10*EC where EC refers to elemental carbon, respectively. The lipm and hips measurements were made on Teflon, while nlipm and nhips are the lipm and hips techniques but on a Nuclepore substrates. clipm is absorption of coarse particles as measured using the lipm technique on a Teflon substrate.*

Using $b_{ath,2.5\mu m}$ data, Equation (6.10) yields 5.0, 0.8, and 0.5 m^2/g for E1+E2 (EC), O4+OP (high temperature) and pyrolized carbon, and soil, respectively. These absorption efficiencies are more in line with theoretical calculations. For more information on the effect of mixed carbon aerosols, in the form of enclosed chain aggregates, single carbon particles as a function of size and orientation, the reader is encouraged to read a detailed analysis of these considerations by Fuller et al. [1999].

Based on the above derived efficiencies 41%, 34%, and 25% of the absorption is identified with EC, high temperature and pyrolized carbon, and soil, respectively. Across the IMPROVE network, similar apportionments using LIPM yielded 41%, 45%, and 14%. Because the correlation between $b_{ath,2.5\mu m}$ and $b_{abs,2.5\mu m}$ using LIPM are high, the apportionments using either technique are nearly the same.

6.2.6 Reconciliation Between Measured and Scattering Reconstructed From Aerosol Measurements

The theoretical issues concerning reconstructing scattering and extinction from aerosol measurements are discussed in Section 6.1.2. In the most general sense, $b_{scat} \neq \Sigma e_i Mi$, where e_i are species specific mass extinction efficiencies and M_i are the associated species masses [Ouimette and Flagan, 1982]. However, a number of investigators have shown that both on a theoretical [Ouimette and Flagan, 1982] and empirical basis [Malm et al., 2000; Sloane, 1986; Malm, 1998] that the assumption of an externally mixed aerosol and $b_{scat}=\Sigma e_i M_i$ is only 5-10% different from internally mixed assumptions. Therefore, for the Grand Canyon study scattering estimates based on aerosol species measurements are made using:

$$b_{scat,2.5\mu m} = (2.2)([(NH_4)_2 SO_4] + [NH_3 NO_3])\, f(RH) + (4)[OMC] + (1)[SOIL] \qquad (6.11)$$

where $b_{scat,2.5\mu m}$ is scattering associated with particles less than 2.5 μm and enclosed in the brackets are aerosol species mass concentrations. The parenthetically enclosed numerals in front of OMC and SOIL are the optimal dry mass scattering efficiencies as reviewed by White [1990] and Malm et al. [1994]. Furthermore, a nominal mass scattering efficiency value of 3.0 m^2/g was recommended for ammonium sulfate, however, more recent mass size distribution measurements of sulfate suggest a value of about 2.2 m^2/g for the Grand Canyon region [Malm and Pitchford, 1997]. The ratio between dry and wet scattering as a function of RH is the relative humidity scattering enhancement factor, *f*(RH).

For the purposes of the calculations presented here, *f*(RH) was calculated on the basis of Tang's [1996] curves for ammonium sulfate but smoothed between the deliquescent and crystallization branches. Based on size distributions of sulfate at Grand Canyon National Park [Malm and Pitchford, 1997], the assumed geometric mass mean diameter (d_g) was 0.2 μm, while the geometric standard deviation (σ_g) was 2.3. Summary statistics for the *f*(RH) factor, measured and reconstructed PM2.5 scattering as well as scattering associated with each species assuming nominal dry scattering efficiencies and an external mixture are shown in Table 6.11.

Table 6.11 *Statistical summary of measured $b_{scat,2.5\mu m}$, reconstructed scattering, as well as the scattering associated with each aerosol species assuming an external mixture. OCHM refers to organics derived from hydrogen.*

Variable	Mean (1/Mm)	Std. Dev. (1/Mm)	Minimum (1/Mm)	Maximum (1/Mm)	Valid
$b_{scat,2.5\mu m}$	7.03	3.54	1.94	15.50	36
Reconstructed	10.39	4.01	4.91	19.71	36
$(NH_4)_2SO_4$	3.45	2.64	0.76	11.52	36
NH_4NO_3	0.49	0.32	0.10	1.35	36
OCHM	5.82 (2.62)	1.82 (0.82)	3.38 (1.52)	10.08 (4.52)	36
$Soil_{scat}$	0.63	0.26	0.25	1.28	36
f(RH)	1.40	0.58	1.00	4.13	36

The use of nominal scattering efficiencies have, for the most part, worked well for developing estimates of scattering from measured aerosol species concentrations [Malm et al., 1994, 2000; Trijonis et al., 1990]. However, Figure 6.21, a scatter plot of reconstructed and measured scattering, along with the 1:1 line, for the Grand Canyon data set shows poor agreement between these two variables. The estimated or reconstructed scattering is, on the average, overestimated by 3.36 1/Mm or about 50% of measured fine particle scattering.

The choice of nominal scattering efficiencies presented in Equation (6.11) can be explored using multiple linear regression analysis first proposed by White and Roberts [1977] and used by many other authors [Trijonis et al., 1990]. The use of the f(RH) term linearizes the otherwise nonlinear response of hygroscopic aerosol scattering to ambient relative humidity. The results of the regression are presented in Table 6.12. The dependent variable is $b_{scat,2.5\mu m}$, while $[(NH_4)_2SO_4] + [NH_4NO_3]$, organics, and soil are the independent variables. If the choice of nominal scattering coefficients are consistent with measured scattering and the variables are not excessively collinear with each other, then the regression coefficients would equal one.

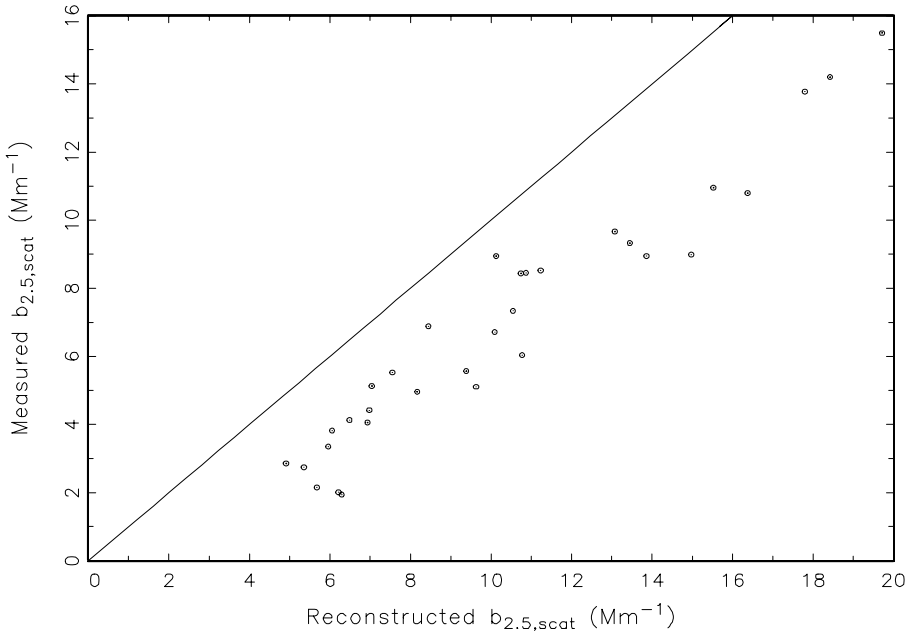

Figure 6.21 *Scatter plot of measured and reconstructed fine particle scattering along with the 1:1 line when nominal values of mass scattering efficiencies were used.*

The coefficient of determination (R^2) is high at 0.91 and the standard errors are small for sulfates (±6%) and organics (±16%), while the regression coefficient associated with soil is not significant. The regression results imply that the assumed dry mass scattering efficiency estimates for sulfates was about right at 2.2 m^2/g, while organics are high by about 65%. Figure 6.22 is the same data as shown in Figure 6.21 but with the organic mass scattering efficiency reduced to 1.8 m^2/g instead of the nominal value of 4.0. The data points are scattered about the 1:1 line and the overall R^2 is near 0.91. Table 6.11 also shows the scattering estimates for organics with the reduced scattering efficiencies parenthetically.

Table 6.12 *Summary table of an ordinary least square regression with $b_{scat,2.5\mu m}$ as the dependent variable and estimates of scattering by sulfate + nitrate, organic by hydrogen, and soil as the independent variables.*

Valid cases: 36	Dependent variable: $b_{scat,2.5\mu m}$			R^2=0.91	
Variable	Estimate	Std error	t-value	Prob t>|t|	Cor dep var
$(NH_4)_2SO_4$+NH_4NO_3	1.01	0.06	17.78	0.000	0.97
OCHM	0.45	0.07	6.17	0.000	0.94
Soil	0.79	0.48	1.64	0.11	0.83

Figure 6.22 *Scatter plot of measured and reconstructed fine particle scattering along with the*

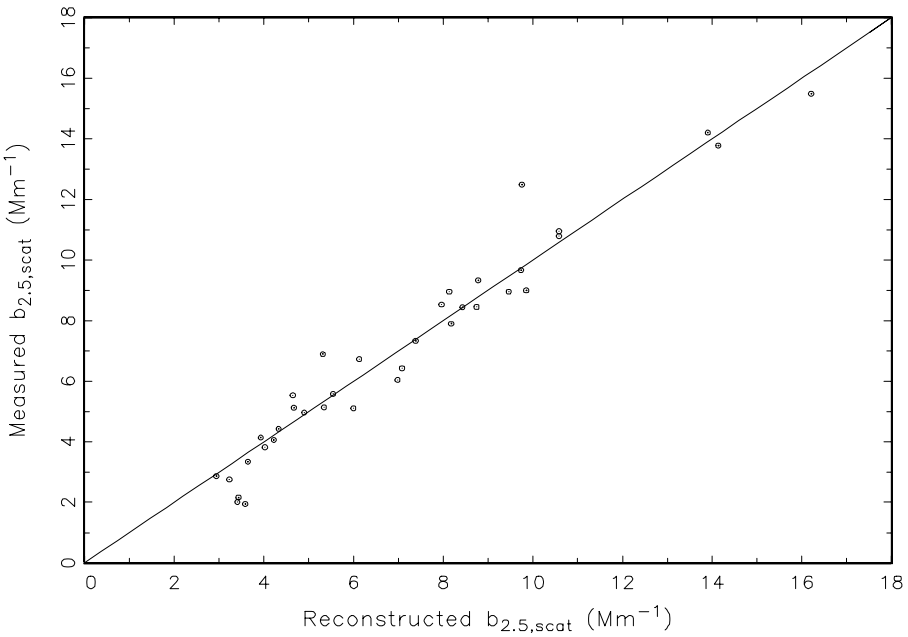

1:1 line when the nominal value of the organic dry mass scattering efficiency was lowered from 4.0 m^2/g to 1.2 m^2/g.

The lower fine organics mass scattering efficiency is consistent with comparatively high coarse mass efficiencies. Only 37% of measured organics are in the fine mode suggesting, assuming something like a lognormal mass size distribution, that the average organic mass mean diameter may be shifted toward the 2.5 μm cutpoint of the cyclone used to separate particles into the "fine" and "coarse" mode.

6.3 HYGROSCOPIC CHARACTERISTICS OF AEROSOLS AT GRAND CANYON AND GREAT SMOKY MOUNTAINS NATIONAL PARKS

The ability of atmospheric particulates to absorb water can be a significant factor in determining its scattering cross section and hence its effect on visibility and/or radiative forcing. For instance, at 90% relative humidity the scattering cross section of typical ammonium sulfate aerosols can be increased by a factor of five or more over that of a dry particle. The hygroscopicity of pure as well as inorganic salts has been studied in the laboratory [Tang, 1996]. It has been well established that inorganic pure salts exhibit deliquescent properties when exposed to moist atmospheres. Moreover, droplet growth can be estimated for both pure and mixed inorganic aerosols purely on the basis of chemical equilibrium equations along with mass concentrations and ion balances [Saxena and Hildemann, 1996; Kim et al., 1994].

On the other hand, organics and their affinity for water, especially those found in the ambient atmosphere, are less well characterized. Organic particulate matter contains hundreds of compounds that cover a wide range of carbon numbers and functional groups Saxena and Hildemann [1996]. They further point out that only a small fraction of potentially nonpolar organics are typically extracted from ambient samples because organic solvents used are typically nonpolar. However, Cadle and Groblicki [1982] and Turpin et al. [1997] have carried out water extractions that would consist of polar organics. Dicarboxylic acids, ketoacids and dicarbonyls have been identified in these extractions although there may be unidentified compounds as well. Typically, less than 10% of the organic matter is identified.

Rather than attempting to identify specific compounds that may be hygroscopic some workers have explicitly measured water uptake of organic material emitted by various source types. For instance, McDow et al. [1994] measured water uptake by diesel soot, automobile exhaust and wood smoke particles. They found that all three emission types absorbed water with wood smoke sample weight increasing by about 10% as sample relative humidity increased from 40-90%. Over the same range of relative humidities, diesel soot sample weight increased by only 2-3%. Chughtai et al. [1999] examined the hydration characteristics of BP2000 (commercially available carbon black), n-hexane, diesel, JP8 (aviation fuel), pine needle, Utah coal, and acetylene. They examined water adsorption isotherms between 20 and 85% relative humidity. They concluded that black carbons produced from a variety of fuel types generally increased with age and surface oxidation and that at high relative humidities (83%) large surface areas determine the adsorption capacity, while at lower humidities the surface functional groups play the most significant role. However, even at 83% relative humidity the water uptake was less than 10% of total mass for all carbon species other than BP2000. Because of its large surface area BP2000 absorbed about 40% of its mass in water. Consequently, they concluded that commercial carbon blacks are not acceptable models for fuel produced carbons.

Other workers have experimentally measured growth of ambient particles as a function of relative humidity [Zhang et al., 1993, 1994; McMurry et al., 1996] using tandem differential mass analyzers (TDMA). One study was carried out at Meadview, Arizona (west end of Grand Canyon) over a 31-day period during the summer of 1991, a second at Hopi Point Arizona (midpoint of Grand Canyon), a 13-day period during winter 1990, while a third was implemented at Claremont, California over an 11-day period during the summer of 1987. A TDMA consists

of two DMAs operated in series. The first DMA is used to select a size, while the second is used to measure the growth of these particles as relative humidity is varied. Usually, a MOUDI size sampler [Marple et al., 1991] is run concurrent with the TDMA to derive estimates of particle composition.

At Grand Canyon, the particles are grouped into three categories: more hygroscopic containing sulfates nitrates and some carbon, less hygroscopic containing carbon mass not accounted for by the number fraction of the more hygroscopic particles, and hydrophopic. Saxena and Hildemann [1996], based on their modeling assumptions, concluded that at Grand Canyon organics add to water absorption by inorganics, while at Claremont the net effect of organics is to diminish water absorption by inorganics. On the other hand, Pitchford and McMurry [1994] were able to show that if one assumed sulfates uptake water at the same rate as measured in the laboratory, they alone could account for all water absorption at Grand Canyon.

Other studies, originally initiated by Covert et al. [1979] examined the scattering characteristics of ambient aerosols as a function of relative humidity. One nephelometer was operated at 30% relative humidity, while a second at variable relative humidity. They made limited measurements $f(RH)=b_{wet}/b_{dry}$ at Tyson, Missouri and Point Reyes, California. The instrumentation was modified and additional measurements of b_{wet}/b_{dry} were made in rural West Virginia and University of Houston, Texas [Waggoner et al., 1983]. Humidity was controlled by first diluting sample air with dry air and then humidifying with a variable amount of water vapor. They also operated a heater and cooler in series with the humidifier (thermidograph), which allowed them to infer compositional structure of the aerosol.

They were able to dry the aerosol to about 30% RH and their first *f(RH)* data points start at about 35%. The singular most interesting feature of their *f(RH)* curves for Shenandoah is that they appear to be continuous over the range of RH values that they measured; that is they did not show evidence of supersaturation. On the other hand, at Houston, Texas, they concluded that the particles were supersaturated about 1/3 of the time. The range of *f(RH)* values at 90% RH varied from a low of about 1.5 to a high of about 2.2- 2.6. Moreover, at Shenandoah, the thermogram measurement allowed them to extract only sulfate scattering at 65-70% RH and it was their conclusion that at 70% RH all the water, within the uncertainty of their measurements, is associated with the ammonium plus sulfate fraction of fine particle mass.

The understanding of the hygroscopic properties of ambient aerosols was in part the motivation for two measurement programs included in this report. The inability to conclusively apportion about 30-50% of the extinction budget between coarse mass scattering and particle absorption at many of our national parks is also seen as important motivating factors.

To address these issues, two studies were carried out, one in the eastern United States at Great Smoky Mountains National Park and the other at Grand Canyon National Park. The design of the Great Smoky study was discussed in Section 6.1, while the Grand Canyon study is presented in Section 6.2. This section will focus on the qualitative and quantitative aspects of measured *f(RH)* curves as a function of aerosol species concentrations. A statistical technique to estimate the aerosol growth of individual species will be presented and results from the two studies compared.

6.3.1 General Features of the $f(RH) = b_{scat}(RH)/b_{scat,Dry}$ Curves

The ratio between dry and wet scattering as a function of RH is referred to as the relative humidity scattering enhancement factor, *f(RH)*. Figure 6.23 shows all the *f(RH)* data points for the Great Smoky data set, while Table 6.13 gives a statistical summary of that data. Over the course of the study, ammonium to sulfate molar ratios varied from a low of 0.30 to a high of 1.85 with an average of 1.1±0.30. A single outstanding feature of the data, although not explicitly observable from the data presentation in Figure 6.23, is the lack of evidence for deliquescence. In spite of the fact that the aerosol was typically dried to about 5-10% the scattering enhancement factor, *f(RH)*, for the most part showed a continuous increase from less than 20%.

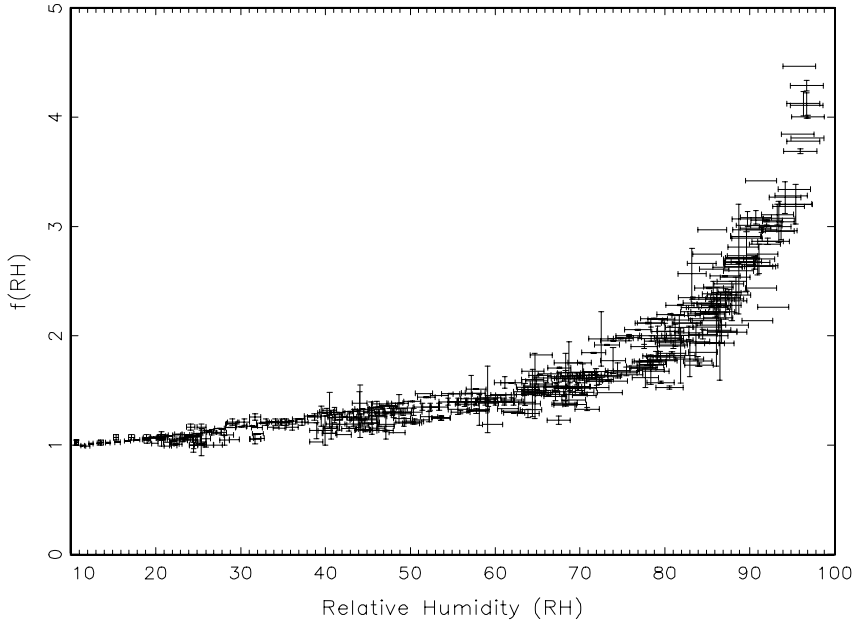

Figure 6.23 *Scatter plot of all measured f(RH) data points collected during the Great Smoky study.*

Figure 6.24, a curve similar to Figure 6.23, shows the *f(RH)* data collected at Grand Canyon. Because of the increased number of data points the average of all *f(RH)* values for a given run and within a given RH range is plotted instead of individual data points. A statistical summary of the data is presented in Table 6.14. As with the Great Smoky data set the *f(RH)* curves did not show evidence of deliquescence in that the curves showed a continuous increase with increasing relative humidity. However, while the Great Smoky data set showed increases in *f(RH)* starting at relative humidity values around 20%, the Grand Canyon data set did not show substantial increases until 40-50%.

Referring to Tables 6.13 and 6.14 the mean *f(RH)* in the 20-25% relative humidity range at Great Smoky was 1.06, while at Grand Canyon it was 1.0; in the 35-40% relative humidity range the *f(RH)* was 1.21, at Great Smoky, while at Grand Canyon it was only 1.05. In the higher relative humidity ranges, the Great Smoky *f(RH)* values always exceeded those of Grand Canyon but by smaller fractional amounts.

Table 6.13 *Statistical summary of mean f(RH) values in selected relative humidity ranges for the Great Smoky data set.*

Relative Humidity	Mean	Std. Dev.	Predicted	Minimum	Maximum	N
20<RH≤25	1.06	0.036	1.01	0.99	1.16	36
25<RH≤30	1.11	0.07	1.04	1.00	1.21	18
30<RH≤35	1.16	0.06	1.06	1.05	1.25	17
35<RH≤40	1.21	0.07	1.09	1.03	1.29	12
40<RH≤45	1.22	0.08	1.14	1.10	1.38	27
45<RH≤50	1.27	0.08	1.20	1.11	1.38	29
50<RH≤55	1.33	0.10	1.27	1.20	1.47	17
55<RH≤60	1.38	0.08	1.35	1.19	1.51	17
60<RH≤65	1.45	0.10	1.45	1.29	1.68	26
65<RH≤70	1.55	0.12	1.58	1.23	1.82	33
70<RH≤75	1.65	0.17	1.73	1.33	1.98	23
75<RH≤80	1.83	0.17	1.91	1.57	2.16	31
80<RH≤85	2.10	0.23	2.12	1.53	2.75	43
85<RH≤90	2.46	0.29	2.43	1.93	3.07	48
RH>90	3.17	0.29	3.01	2.14	4.47	40

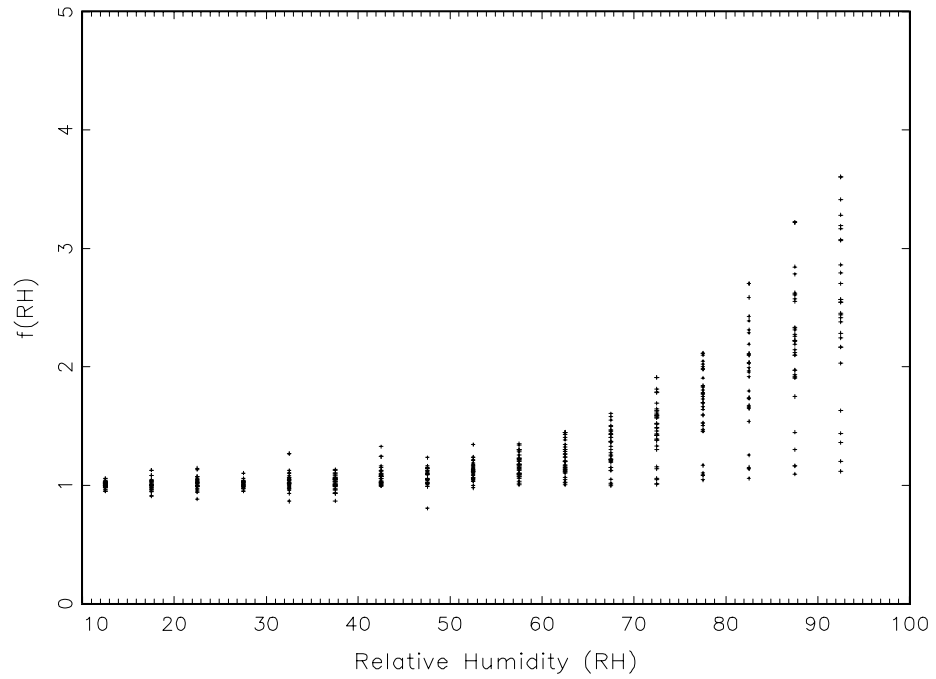

Figure 6.24 *Scatter plot of measured f(RH) data points that have been averaged into 5% relative humidity "bins" for the Grand Canyon data set. The total number of data points for this data set was approximately 7500.*

Table 6.14 *Statistical summary of mean f(RH) values in selected relative humidity ranges for the Grand Canyon data set. Also shown are the corresponding theoretical estimates of f(RH).*

Relative Humidity	Mean	Std. Dev.	Predicted	Minimum	Maximum	N
15≤RH<20	0.99	0.08	1.00	0.68	1.47	350
20≤RH<25	1	0.09	1.00	0.68	1.54	195
25≤RH<30	1.01	0.1	1.00	0.71	1.43	343
30≤RH<35	1.03	0.11	1.00	0.6	1.39	327
35≤RH<40	1.05	0.12	1.01	0.65	1.5	319
40≤RH<45	1.08	0.13	1.06	0.69	2.18	361
45≤RH<50	1.10	0.13	1.11	0.63	1.66	395
50≤RH<55	1.15	0.13	1.17	0.74	1.56	493
55≤RH<60	1.21	0.15	1.24	0.87	1.89	559
60≤RH<65	1.27	0.18	1.33	0.65	1.82	557
65≤RH<70	1.36	0.19	1.43	0.83	1.84	829
70≤RH<75	1.46	0.24	1.55	0.94	2.43	622
75≤RH<80	1.63	0.32	1.70	0.71	3.58	620
80≤RH<85	1.92	0.38	1.87	0.94	4	725
85≤RH<90	2.24	0.48	2.14	1.07	4.84	835

Figure 6.25 shows a "typical" run carried out on Julian day 212. The solid line corresponds to a theoretical prediction of *f(RH)*, which will be discussed in the next section. On this day, 48% and 8% of the fine mass was in the form of sulfates and nitrates, respectively, and significant growth did not occur until about 60% relative humidity. Figure 6.26, another growth curve where sulfates and nitrates made up 39% and 7% of the fine mass, shows an increase in *f(RH)* starting at 45-50% relative humidity rather than at 60%.

Figures 6.25 and 6.26 correspond to hygroscopic inorganic (sulfates and nitrates) fractions of 56% and 46%, respectively, and should be contrasted with Figure 6.27, which shows the *f(RH)* curve on a day when the 24-hr average inorganic hygroscopic fraction was only 22%. Again the solid lines represent theoretical *f(RH)* curves based on measured aerosol concentrations. Julian day 217 was associated with smoke from a forest fire on the north rim of the Grand Canyon. The measured ambient extinction and scattering showed short-term variability throughout the day and therefore the 24-hr aerosol measurement is unlikely to be representative of the time the *f(RH)* curve was measured. In fact, the *f(RH)* curve shown in Figure 6.27 does not show a continuous increase in *f(RH)* over the whole relative humidity range. *f(RH)* increases from 40-57% relative humidity and then is suppressed somewhat with less increase in the 65-80% range.

Figure 6.28 shows a similar plot for the Great Smoky data set. On Julian days 207, 211 and 224 the hygroscopic inorganic fractions were 32.6, 42.7, and 63.5%, respectively. The higher the fraction content of inorganic hygroscopic material the greater the increase in *f(RH)* as a function of relative humidity.

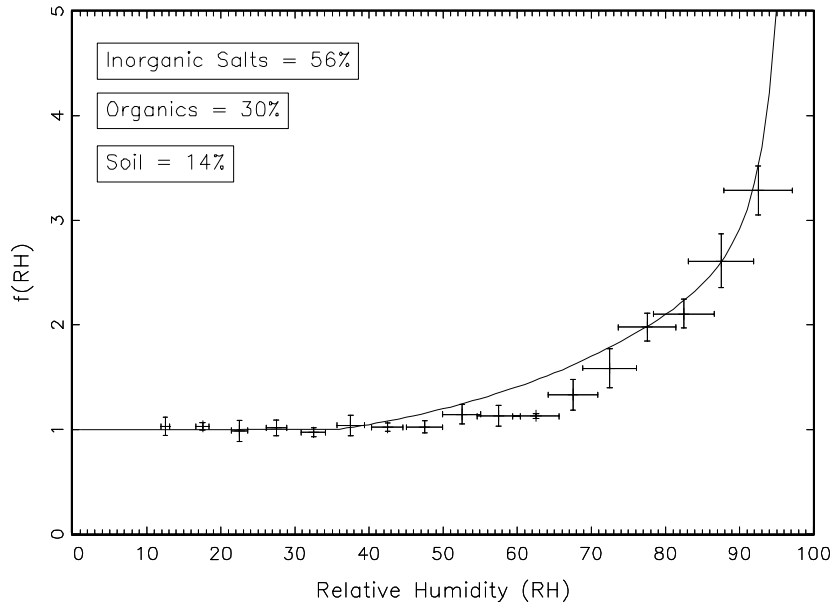

Figure 6.25 *Plot of measured f(RH) on Julian day 212 are presented as data points with uncertainty bars. The uncertainty bars represent a ±5% uncertainty for measured relative humidity, while the uncertainty bars for f(RH) represent one standard deviation of all measurements made within one 5% relative humidity range. The solid line is the result of a theoretical estimate of f(RH). On Julian day 212 the inorganic fraction of fine mass was 56%, organics 30% and soil 14%.*

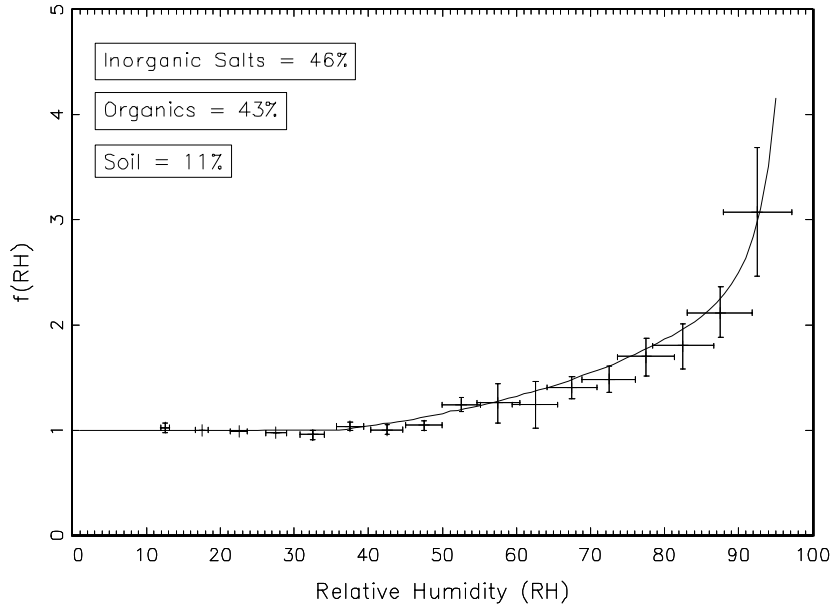

Figure 6.26 *Plot of measured f(RH) on Julian day 204 are presented as data points with uncertainty bars. The uncertainty bars represent a ±5% uncertainty for measured relative humidity, while the uncertainty bars for f(RH) represent one standard deviation of all measurements made within one 5% relative humidity range. The solid line is the result of a theoretical estimate of f(RH). On Julian day 204 the inorganic fraction of fine mass was 46%, organics 43% and soil 9%.*

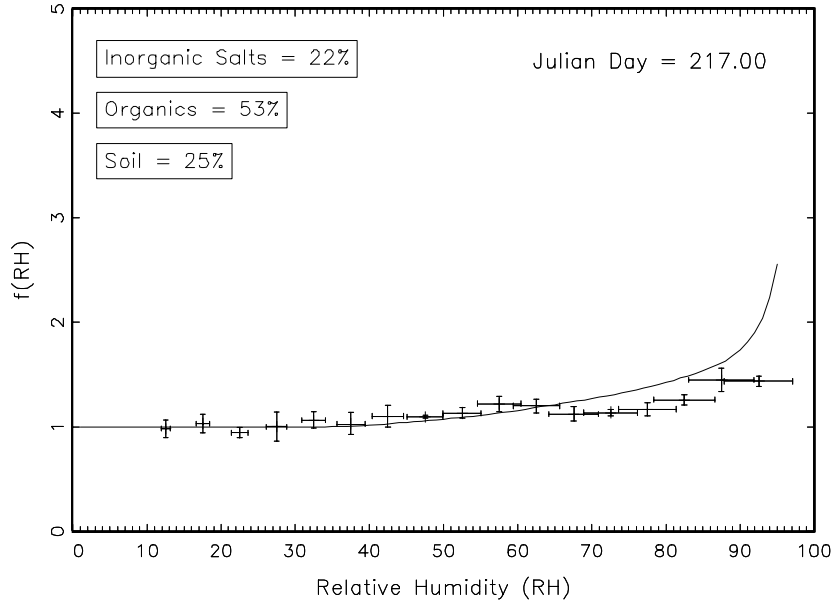

Figure 6.27 *Plot of measured f(RH) on Julian day 217 are presented as data points with uncertainty bars. The uncertainty bars represent a ±5% uncertainty for measured relative humidity, while the uncertainty bars for f(RH) represent one standard deviation of all measurements made within one 5% relative humidity range. The solid line is the result of a theoretical estimate of f(RH). On Julian day 217 the inorganic fraction of fine mass was 22%, organics 53% and soil 25%.*

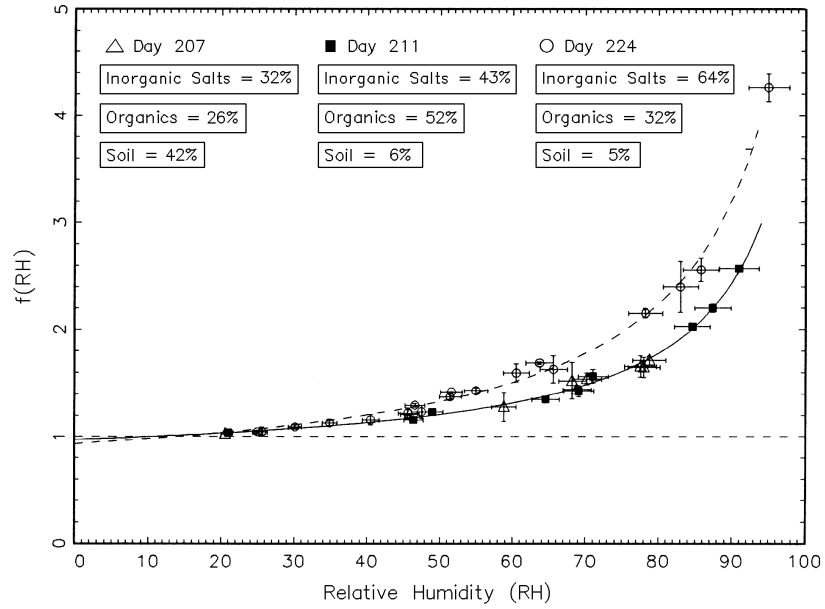

Figure 6.28 *Plot of measured f(RH) on Julian days 207, 211, and 224 for the Great Smoky data set. The uncertainty bars represent a ±5% uncertainty for measured relative humidity, while uncertainty bars on the f(RH) function reflect the instrumental uncertainty associated with the humidograph. The solid line is the result of a theoretical estimate of f(RH). The enclosed captions reflect the relative amounts of inorganic, organic, and crustal material.*

6.3.3 Comparison of Measured *f(RH)* With Theoretical Predictions

Malm et al. [2000] report on a comparison between measured and modeled $b_{scat}(RH)/b_{scat,dry}$ ratios for the Great Smoky data set. Models, described previously, used for the comparison were external with constant mass scattering but with sulfate ammoniation and associated growth accounted for, external with sulfate size, ammoniation, and growth incorporated, and the mixed model. In most cases, all three modeling approaches agreed well with each other, however, the ratios predicted by the internally mixed and external models at times differed from each other under high relative humidity conditions by as much as 30%, with the internally mixed model showing less increase in scattering than the external models.

Measured ratios, in general, were well reproduced by all of the modeling approaches. The R^2 between measured and modeled ratios varied from 0.92 to 0.71, with the external models having the highest R^2. All models, under higher relative humidity conditions, yielded ratios that were on the average greater than those that were measured. The largest discrepancies occurred when organic mass concentrations were highest with modeled ratios being greater than those measured.

For the Grand Canyon study, size distribution data were not available and because little difference is observed between the internally mixed and external models only the external model will be considered here. The following equation is used to estimate scattering under the assumptions of external mixing, constant dry mass scattering efficiencies, and sulfate interpreted as ammonium sulfate:

$$b_{scat} = (2.2)\, f(RH)[SULFATE + NITRATE] + (1.8)\, f_{org}(RH)[OMC] + (1)[SOIL] \qquad (6.12)$$

b_{scat} is the scattering coefficient; [SULFATE] is the SO_4 ion mass concentration adjusted to ammonium sulfate; [NITRATE], [OMC], and [SOIL] are the concentrations of ammonium nitrate, organic carbon, and soil, respectively. The coefficient numbers refer to the assumed dry mass scattering efficiencies of the respective species in units of m^2/g. *f(RH)* and $f_{org}(RH)$ refer to the scattering enhancement factors for sulfates, nitrates, and organics, respectively. The choice of mass scattering efficiencies is discussed in Malm and Day [2000] and is based on recent measurements of sulfur size distributions and on multiple regression analysis of measured $PM_{2.5}$ scattering and aerosol mass concentrations.

The function, *f(RH)*, was calculated on a sampling-period-by-sampling-period basis using Tang's sulfate D/D_o curves. Estimates of *f(RH)* are based on growth curves that were smoothed between the crystallization and deliquescent points. A lognormal sulfate species mass size distribution with a geometric mass mean diameter of 0.2 μm and a geometric standard deviation, σ_g of 2.3 was assumed. The *f(RH)* associated with nitrates was assumed to be the same as for sulfates, while $f_{org}(RH)$ for organics was set equal to one.

As pointed out previously the *f(RH)* curves were continuous showing little evidence for deliquescence. One question we wished to address was the validity of using growth curves that have been smoothed between the deliquescent and crystallization branches. Figures 6.25, 6.26 and 6.27 show the theoretical calculation of the growth curves as solid lines, while the data

points with associated error bars are measured. Figure 6.26 shows a case where measured and predicted estimates compare quite favorably, and the growth curves smoothing assumption appears to reproduce measured data. However, Figure 6.25 shows a case where growth assumptions result in an overprediction of scattering in the 50-75% relative humidity range. There were a number of sampling periods where the estimated *f(RH)* curves were overestimated in this same relative humidity region.

The differences between measured and estimated *f(RH)* values for different relative humidity regions is summarized in Table 6.14. The average of all measured *f(RH)* values within a certain relative humidity range compare favorably to theoretically predicted values, however, the agreement is slightly better at low and high relative humidities than at mid-range humidities. Moreover, under high relative humidity conditions the average measured values are about 2-5% greater than predicted, while around 60% relative humidity the predicted values on the average are about 5% greater. At low relative humidities, measured *f(RH)* shows growth starting as low as 25% RH and increasing slowly to 1.05 at the 35-40% RH range, while the theoretical calculations show zero growth or no change from one in this same range.

An ordinary least square (OLS) regression between measured and predicted *f(RH)* values yields an R^2= 0.82 with slope of 1.02 ±0.006 when the intercept term is forced through zero. The implication is that, on the average, predicted *f(RH)* values are about 2% greater than measured.

Table 6.13 summarizes that same information for the Great Smoky data set for the assumptions of an externally mixed aerosol with corrections for ammoniation and particle size. In the case of the Great Smoky data set, there is some bias in that *f(RH)*, and thereby growth, is underpredicted at lower RH values but overpredicted above about 70% RH. The overall R^2, however, associated with an OLS regression between the two variables is 0.92.

6.3.3.1 Statistical Estimates of $b_{scat}(RH)/b_{scat,dry}$

The amount of scattering at a specific relative humidity can be estimated using:

$$b_{scat,water}(RH) = a_0 + a_1 Sulfate + a_2 Organic + \ldots + a_n Other\ Species \qquad (6.13)$$

where $b_{scat,water}(RH)$ is scattering due to water at some RH, $a_1 = e_s[f(RH)_s+1]$, $a_2=e_{oc}[f(RH)_{oc}+1]$ and so forth. a_o is interpreted as scattering associated with residual water. e_s and e_{oc} are the average dry mass scattering coefficients associated with sulfates and organics, respectively. $b_{scat,water}(RH)=b_{scat}(RH)-b_{scat,dry}$ is calculated on a sampling-period-by-sampling-period basis by estimating $b_{scat}(RH)$ using measured $b_{scat}(RH)/b_{scat,dry}$ ratios and then differencing scattering at some RH and dry scattering. Equation (6.13) can then be solved at specific humidities using OLS regressions with or without an intercept.

For the Great Smoky data set, the coefficients for sulfate are highly significant for all relative humidities for both the intercept and nonintercept models, while the coefficient associated with organics is significant at better than the 5% level for humidities greater than 50% for the zero

intercept model and greater than 25% for the nonzero model. R^2s varied from a low of 0.89 to a high of 0.98.

Figure 6.29 is a plot of the *f(RH)* curves derived from the OLS analysis with an intercept term for sulfates and organics assuming e_s=2.4±0.5 m^2/g and e_{oc}=4.0 m^2/g. The error bars represent the standard error of the regression coefficients, while the rectangle enclosing each error bar is associated with the standard deviation of the theoretically calculated dry scattering coefficients (2.4±0.5 m^2/g) that are based on measured sulfate size distributions. The solid lines are the theoretically calculated *f(RH)* curves for ammonium bisulfate and sulfuric acid assuming D_g=0.36 μm and σ_g = 1.92 [Malm et al., 2000]. The average molar ratio of ammonium to sulfate for the study was near one, however, on the higher sulfate days the molar ratio tended to values less than one, while on lower sulfate concentration days the sulfate aerosols were more neutralized. It is the higher mass concentrations that tend to influence the regression coefficients most and therefore the statistically derived *f(RH)* curve is somewhat greater than the ammonium bisulfate curve but significantly less than the sulfuric acid *f(RH)* curve.

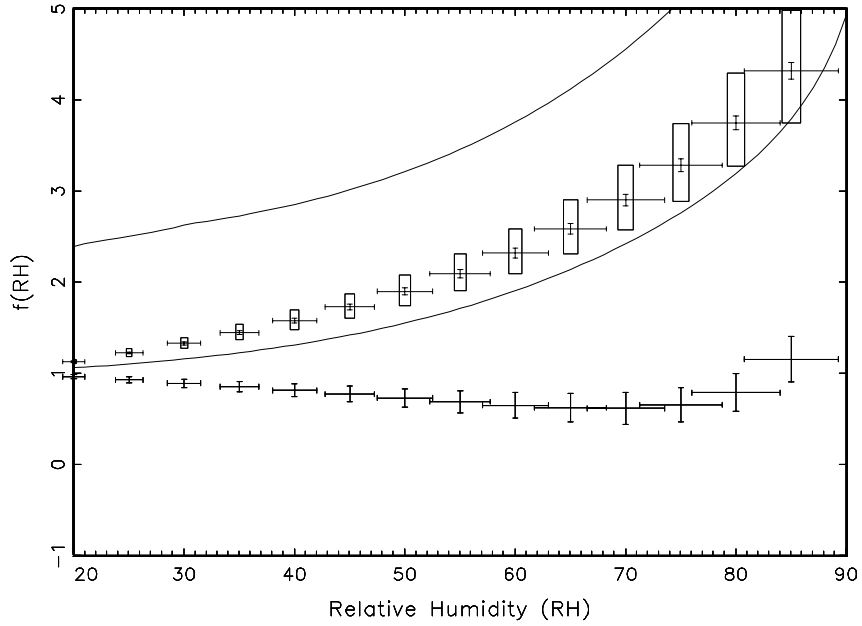

Figure 6.29 *f(RH) is plotted as the solid and broken line for ammonium bisulfate and sulfuric acid, respectively, while the single data points with error bars show the OLS regression with an intercept derived f(RH) for sulfates and organics. The error bars correspond to the standard errors of the regression coefficients, while the upper and lower edges of the rectangle represent the f(RH) that corresponds to ±1 standard deviation of dry mass scattering efficiency that was calculated from measured size distributions.*

An interesting feature of the regressions is the highly significant negative regression coefficients associated with organics. The implication of a negative regression coefficient is reflected in the organic *f(RH)* curves shown in Figure 6.29. An *f(RH)* curve less than one implies that organics would be less efficient at scattering light than predicted by an equation of the type given in Equation (6.14):

$$[OMC] = (1.4)[OC] \quad (6.14)$$

or that the effect of organics is to reduce the ability of sulfates in a sulfate organic mixture to absorb water and thereby reduce the specific scattering efficiency of the mixture. Although the organic *f(RH)* curve is slightly less than one at all relative humidities, *f(RH)*±standard error, for the most part, overlaps one. Therefore any interpretation concerning organic suppression of water absorption should be considered speculative.

The intercept term is identified as residual or unaccounted for water scattering and varies from about 0.6 1/Mm at 20% RH to 2.82 1/Mm at 65% RH. Because dry scattering was measured at about 15% RH and because nitrates were not included in the regression analysis some residual water scattering can be expected. Theoretical estimates of average nitrate scattering vary from about 0.04 1/Mm at 20% RH to 2.0 1/Mm at 85% RH, while the average sulfate scattering at 15% RH is estimated to be 1.8 1/Mm. Therefore, an intercept term on the order of 2-3 1/Mm is consistent with expected residual water scattering.

Figure 6.30 is for the Grand Canyon data set and is similar to Figure 6.29. The sulfate regression coefficient is significant at less than 1% at all humidities greater than 40%, while the regression coefficient associated with all other species are not statistically significant. Moreover, the intercept term is not statistically different from zero. The R^2s varied between 0.6-0.75. As before the error bars represent the standard error of the regression coefficients, while the rectangle enclosing each error bar represents the standard deviation of theoretically calculated dry scattering coefficients that were based on measured sulfate size distributions [Malm and Pitchford, 1997]. Even though the organic regression coefficients were not statistically significant, the implied organic *f(RH)* curve is included for reference. The solid line corresponds to the theoretically derived *f(RH)* curve for ammonium sulfate assuming a D_g=0.3, a σ_g=2.3 and a D/D_o curve that was interpolated between the deliquescent and crystallization branches of the ammonium sulfate hysteresis curve. On the average, the statistically derived *f(RH)* curves agree well with the ammonium sulfate *f(RH)* curve.

6.3.4 Summary of Hygroscopic Characteristics of Aerosols

The understanding of the hygroscopic properties of ambient aerosols as they relate to visibility impairment was in part the motivation for two measurement programs reported on in this report. Two studies, one at Great Smoky Mountains National Park, the other at Grand Canyon National Park, were designed to enhance our understanding of the hygroscopicity of various aerosol types. The Great Smoky study was carried out from July 15, 1995 through August 25, 1995, while the Grand Canyon study was conducted from July 10, 1998 through August 8, 1998 on the south rim of the Grand Canyon. Scattering as a function of relative humidity was measured with a humidograph allowing for estimates of $f(RH) = b_{scat(wet)}/b_{scat(dry)}$, which is used to develop a better understanding of aerosol growth. Modeling scattering as a function of relative humidity serves to both explore the validity of aerosol growth and mixing models and associated assumptions, and provide an estimate of the hygroscopicity of aerosol species other than sulfates and nitrates.

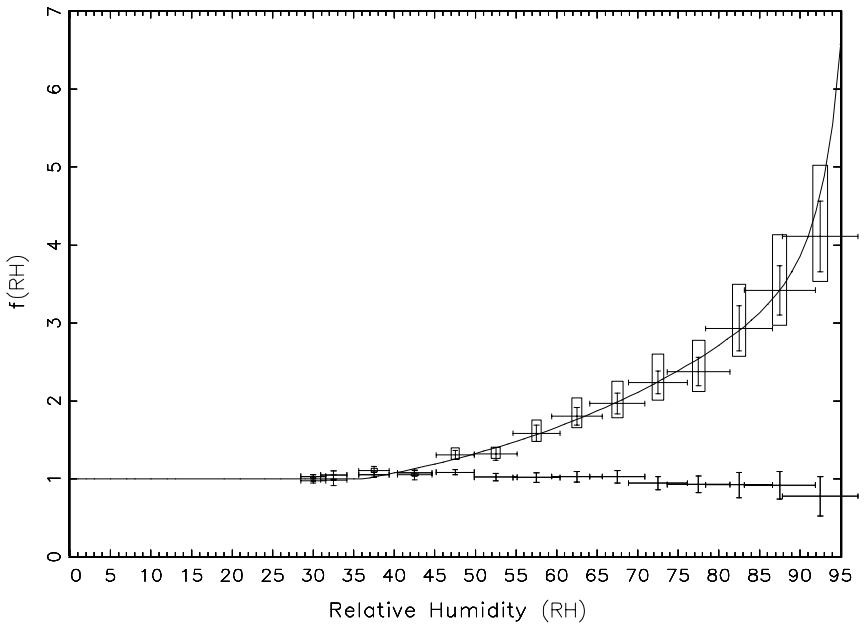

Figure 6.30 *f(RH) is plotted as the solid line for ammonium sulfate, while the single data points with error bars show the OLS regression with an intercept derived f(RH) for sulfates and organics. The error bars correspond to the standard errors of the regression coefficients, while the upper and lower edges of the rectangle represent the f(RH) that corresponds to ±1 standard deviation of dry mass scattering efficiency that was calculated from measured size distributions.*

The *f(RH)* function was smoothly increasing as a function of increasing relative humidity for both data sets. However, for the most part, the *f(RH)* at Great Smoky began to increase at relative humidities of around 20%, while at Grand Canyon increases did not take place until approximately 40-45% and in some cases not until 60%. At Grand Canyon, the *f(RH)* was more varied than at Great Smoky. For instance, in the range of 80-85% relative humidity the *f(RH)* values varied between 1.53 and 2.75 at Great Smoky, while at Grand Canyon the range was from near 1 to 4.0. Part of the explanation of these differences is that in the eastern United States sulfates make up a large fraction of fine mass, while in the West sulfates plus nitrates can actually be a small fraction of fine mass, with organics and soil dust being the major contributors. In general, as organics and soil dust increase the increase of *f(RH)* with humidity decreases.

A variety of scattering models were used to estimate measured *f(RH)* curves. At Great Smoky, an externally mixed aerosol model was assumed with and without sulfate ammoniation, and with and without accounting for sampling-period-to-sampling-period shifts in size distribution. These same variations were explored assuming a mixed aerosol model. The sensitivity to using the deliquescent and crystallization branches as well as a curve smoothed between the deliquescent and crystallization points of D/D_o curves as a function of relative humidity for inorganic salts was also explored. The single most important variables to predicting scattering as a function of relative humidity was accounting for aerosol growth as a function of

sulfate ammoniation and using the smoothed D/D_o growth curves. Changes in *f(RH)* as a function of assumptions concerning mixing were less than 10% on the average.

At Grand Canyon, only the external model was used; sulfate was assumed to be in the form of ammonium sulfate and a smoothed *f(RH)* curve was used based on size distribution measurements made in previous studies. An OLS regression between measured and predicted *f(RH)* values yields a R^2= 0.82 with a slope of 1.02 ±0.006 when the intercept term is forced through zero. The implication being that on the average predicted *f(RH)* values are about 2% greater than measured.

Finally, a model was developed to estimate the *f(RH)* function associated with individual aerosol species. The scattering associated with aerosol water can be shown to relate to aerosol species in a linear way for a given relative humidity. The regression coefficients are functions of dry mass scattering efficiency and $f(RH)= b_{scat}(RH)/b_{scat,dry}$ at a specified relative humidity. The resulting *f(RH)* curve, that is associated with a given data set is interpreted as a weighted average *f(RH)* over the time period corresponding to that data set. At Great Smoky, the measured *f(RH)* was on the average slightly greater than a theoretical curve for ammonium bisulfate implying slightly more growth than would have been predicted from the measured ammoniation (average molar ratio of ammonium to sulfate was one) and size parameters, while at Grand Canyon the measured *f(RH)* curve was nearly identical to the theoretical curve for ammonium sulfate assuming a smoothed D/D_o curve

For both data sets, organics were, within the statistical uncertainty of the regression analysis, judged to be weakly to nonhygroscopic. In fact, for the Great Smoky data set, organics may have repressed the ability of sulfates to absorb water.

6.4 REFERENCES

Air Resource Specialists, Standard operating procedures and technical instructions for nephelometer systems, ARS, 1901 Sharp Point Drive, Ste. E., Ft. Collins, CO 80525, 1994.

Arnott, W.P., Moosmüller, H., Rogers, C.F., Jin, T., and Bruch, R., Photoacoustic spectrometer for measuring light absorption by aerosol: instrument description, *Atmos. Environ.*, **33**, 2845-2852, 1999.

Cadle, S.H. and Groblicki, P.J., An evaluation of methods for the determination of organic and elemental carbon in particulate samples, in G.T. Wolff and R.L. Klimisch (eds.), *Particulate Carbon-Atmospheric Life Cycle*. Plenum Press, New York, pp. 89-109, 1982.

Campbell, D., Perley, B.P., and Eldred, R.A., Measurement of the aerosol absorption coefficient for the IMPROVE Network, *Proceedings Specialty Conference Visual Air Quality: Aerosols and Global Radiation Balance, American Geophysical Union and Air and Waste Management Association*, Pittsburgh, PA, 281-291, 1997.

Chow, J.C., Watson, J.G., Pritchett, L.C., Pierson, W.R., Frazier, C.A., and Purcell, R.G., The DRI thermal/optical reflectance carbon analysis system: Description, evaluation, and applications in U.S. air quality studies, *Atmos. Environ.,* **27A**(8), 1185-1201, 1993.

Chughtai, A.R., Williams, G.R., Atteya, M.M.O., Miller, N.J., and Smith, D.M., Carbonaceous particle hydration, *Atmos. Environ*., **33**, 2679-2687, 1999.

Covert, D.S., Waggoner, A.P., Weiss, R.E., Ahlquist, N.C., and Charlson, R.J., Atmospheric Aerosols, Humidity and Visibility, In *Character and Origins of Smog Aerosols*, John Wiley & Sons, 559-581, 1979.

Day, D.E., Malm, W.C., and Kreidenweis, S.M., Seasonal variations in aerosol composition acidity at Shenandoah and Great Smoky Mountains National Parks, *J. Air & Waste Management Assoc.,* **47**(3), 411-418, 1997.

Dietrich, L., Molenar, J.V., and Faust, J.F., Transmissometer extinction measurements in an urban environment, In *Transactions Visibility and Fine Particles*, (edited by C.V. Mathai), AWMA, Pittsburgh, PA, 374-383, 1989.

Eldred, R.A. and Cahill, T.A., Trends in elemental concentrations of fine particles at remote sites in the United States, *Atmos. Environ.,* **28**(5), 1009-1019, 1994.

Eldred, R.A., Cahill, T.A., Pitchford, M., and Malm, W.C., IMPROVE-A new remote area particulate monitoring system for visibility studies, *Proceedings 81st Annual Meeting of the Air Pollution Control Association*, Pittsburgh, PA, 1988.

Fitzgerald, J.W., Angular truncation error of the integrating nephelometer in the fog droplet size range, *J. Appl. Met*., **16**, 198-204, 1977.

Fuller, K.A., Malm, W.C., and Kreidenweis, S.M., Effects of mixing on extinction by carbonaceous particles, *J. Geophys. Res*., **104**(D13), 15941-15954, 1999.

Gebhart, K. A. and Malm, W. C., An investigation of the size distributions of particulate sulfate concentrations measured during WHITEX, In *Transactions Visibility and Fine Particles*, (edited by C.V. Mathai), AWMA, Pittsburgh, PA, 157-169, 1990.

Hansen, A.D.A., Rosen, H., and Novakov, T., Real-time measurements of the absorption coefficient of aerosol particles, *Appl. Optics*, **21**, 3060, 1982.

Hasan, H. and Lewis, C.W., Integrating nephelometer response corrections for biomodal size distributions, *Aerosol Sci. Technol*. **2**, 443-453, 1983.

Heintzenberg, J. and Quenzel, H., On the effect of the loss of large particles on the determination of scattering coefficients with integrating nephelometers, *Atmos. Environ.,* **7**, 503-507, 1973.

Hitzenberger, R., Jennings, S.G., Larson, S.M., Dillner, A., Cachier, H., Galambos, Z., Rouc, A., and Spain, T.G., Intercomparison of measurement methods for black carbon aerosols, *Atmos. Environ.,* **33**, 2823-2833, 1999.

Horvath, H., Atmospheric light absorption-A review, *Atmos. Environ.,* **27**(A), 293-317, 1993.

Huffman, H.D., Comparison of the light absorption coefficent and carbon measures for remote aerosols: an independent analysis fo data from the IMPROVE network-I, *Atmos. Environ.,* **30**, 73-83, 1996.

John W., Wall, S.M., Ondo, J.L., and Winklmayr W., Modes in the size distributions of atmospheric inorganic aerosol, *Atmos. Environ.,* **24**, 2349-2359, 1990.

Kim, Y.P., Pun, B. K. –L., Chan, C.K, Flagan, R.C., and Seinfeld, J.H., Determination of water activity in ammonium sulfate and sulfuric acid mixtures using levitated single particles, *Aerosol Sci. Tech*., **20**, 275-284, 1994.

Malm, W.C., Examining the relationship between aerosol concentration and partial scattering efficiencies near the Grand Canyon, presented at the *91st Annual Meeting and Exhibition of the Air and Waste Management Association*, Pittsburgh, PA, 1998.

Malm, W.C. and Day, D.E., Optical properties of aerosols at Grand Canyon National Park, accepted for publication in *Atmos. Environ*., 2000.

Malm, W.C. and Kreidenweis, The effects of aerosol hygroscopicity on the apportionment of extinction, *Atmos. Environ.,* **31**, 1965-1976, 1997.

Malm, W.C. and Pitchford, M.L., Comparison of calculated sulfate scattering efficiencies as estimated from size-resolved particle measurements at three national locations, *Atmos. Environ.,* **31**, 1315-1325, 1997.

Malm, W.C., Day, D.E., and Kreidenweis, S.M., Light scattering characteristics of aerosols as a function of relative humidity: Part I-a comparison of measured scattering and aerosol concentrations using the theoretical models, *J. Air and Waste Management Assoc.*, **50**, 2000.

Malm, W.C., Molenar, J.V., Eldred, R.A., and Sisler, J.F., Examining the relationship among atmospheric aerosols and light scattering and extinction in the Grand Canyon area, *J. Geophys. Res.,* **101**, 19251-19265, 1996.

Malm, W.C., Sisler, J.F., Huffman, D., Eldred, R.A., and Cahill, T.A., Spatial and seasonal trends in particle concentration and optical extinction in the United States, *J. Geophys. Res.* **99**, 1347-1370, 1994.

Marple, V.A., Rubow, K.L., and Behm, S.M., A microorifice uniform deposit impactor (MOUDI): description, calibration, and use, *Aerosol Sci. Technol*., **14**, 434, 1991.

McDade, C.E. and Tombach, I.H., Goals and initial findings from SCENES, In *Transactions Visibility Protection, Research and Policy Aspects,* (edited by Bhardwaja, P.S.) APCA, Pittsburgh, PA, 1987.

McDow, S.R., Vartianen, M., Sun, Q., Hong, Y., Yao, Y., and Kamens, R.M., Combustion aerosol water content and its effect on polycyclic aromatic hydrocarbon reactivity, Atmos. Environ., **29**, 791-797, 1994.

McMurry, P.H., Zhang, X., and Lee, C.-T., Issues in aerosol measurement for optics assessment, *J. Geophys. Res*., **101**, 19189-19197, 1996.

Meng, Z., Seinfeld, J.H., and Saxena, P., Gas/aerosol distribution of formic and acetic acids, *Aerosol Sci. Technol.*, **23**, 561-578, 1995.

Molenar, J.V., Analysis of the real world performance of the Optec NGN-2 ambient nephelometer, *Proceedings of Visual Air Quality, Aerosols, and Global Radiation Balance,* AWMA, Pittsburgh, PA., 243-265, 1997.

Molenar, J.V., Dietrich, D.L., and Tree, R.M., Application of a long range transmissometer to measure the ambient atmospheric extinction coefficient in remote pristine environments, In *Transactions Visibility and Fine Particles*, (edited by C.V. Mathai), AWMA, Pittsburgh, PA., 1989.

Moosmüller, H., Personal communication, 1998.

Ouimette, J.R. and Flagan, R.C., The extinction coefficient of multicomponent aerosols, *Atmos. Environ.*, **16**, 2405-2419, 1982.

Pilinis, C., Pandis, S. M., and Seinfeld, J. H., Sensitivity of direct climate forcing by atmospheric aerosols to aerosol size and composition, *J. Geophys. Res.*, **100**, 18739-18754, 1995.

Pitchford, M. L. and McMurry, P. H., Relationship between measured water vapor growth and chemistry of atmospheric aerosol for Grand Canyon, Arizona, in winter 1990, *Atmos. Environ*., 28, 827-839, 1994.

Rotronic Instrument Corp. Humidity-temperature meteorological pro, MP-100F, Fact Sheet, Rotronic Instrument Corp, 160 E. Main Street, Huntingdon, NY 11743, 1998.

Sandberg, D.V., Pierovich, J.M., Fox, D.G., and Ross, E.W., Effects of Fire on Air, General Technical Report WO-9, U.S. Department of Agriculture, U.S. Forest Service, Washington, D.C., 1979.

Saxena, P. and Hildemann, L.M., Water-soluble organics in atmospheric particles: a critical review of the literature and application of thermodynamics to identify candidate compounds, *J. Atmos. Chemistry*, **24**, 57-109, 1996.

Saxena, P. and Peterson, T.W., Thermodynamics of multicomponent electrolytic aerosols, *J. Colloid Interface Sci.*, **79**, 496-510, 1981.

Saxena, P., Hudischewskyj, A.B., Seigneur, C., and Seinfeld, J.H., A comparative study of equilibrium approaches tot he chemical characterization of secondary aerosols, *Atmos. Environ.,* **20**, 1471-1483, 1986.

Saxena, P., Mueller, P.K., Kim, Y.P., Seinfeld, J.H., and Koutrakis, P., Coupling thermodynamic theory with measurements to characterize acidity of atmospheric particles, *Aerosol Sci. Technol.*, **19**, 279-293, 1993.

Saxena P., Hildemann L. M., McMurry P. H., and Seinfeld, J. H., Organics alter hygroscopic behavior of atmospheric particles, *J. Geophys. Res.* **100**, 18755-18770, 1995.

Sisler, J. F., *Spatial and Seasonal Patterns and Long Term Variability of the Composition of the Haze in the United States: An Analysis of Data from the IMPROVE Network,* Cooperative Institute for Research in the Atmosphere, Colorado State University, ISSN 0737-5352-32, 1996.

Sisler, J. F., Huffman, D., Latimer, D. A., Malm, W. C. and Pitchford, M. L., *Spatial and Temporal Patterns and the Chemical Composition of the Haze in the United States: An Analysis of Data from the IMPROVE Network 1988-1991,* Cooperative Institute for Research in the Atmosphere, Colorado State University, ISSN 0737-5352-26, 1993.

Sloane, C.S., Optical properties of aerosols—comparison of measurement with model calculations, *Atmos. Environ.*, **17**, 409-416, 1983.

Sloane, C.S., Optical properties of aerosols of mixed composition, *Atmos. Environ.*, **18**, 871-878, 1984.

Sloane, C.S., Effect of composition on aerosol light scattering efficiencies, A*tmos. Environ.*, **20**(5), 1025-1037, 1986.

Sloane, C.S., Rood, M.J., and Rogers, F.C., Reconciliation of aerosol particle size measurements, In *Transactions Visibility and Fine Particles,* (edited by Mathai C.V.), AWMA, Pittsburgh, PA., 1990.

Stelson A.W. and Seinfeld J.H., Relative humidity and temperature dependence of the ammonium nitrate dissociation constant, *Atmos. Environ.*, **15**, 983, 1982.

Tang, I. N., Chemical and size effects of hygroscopic aerosols on light scattering coefficients, *J. of Geo. Research*, **101**, 19245-19250, 1996.

Trijonis, J.C., RESOLVE project final report, Visibility conditions and causes of visibility degradation in the Mojave Desert of California, NWC Tech. Pap. 6869, Naval Weapons Center, China Lake, CA., 1988.

Trijonis, J.C. and Pitchford, M., *Preliminary extinction budget results from the RESOLVE program*, edited by P.S. Bhardwaja, Visibility Protection Research and Policy Aspects, Air Pollution Control Association, Pittsburgh, PA., 1987.

Trijonis, J.C., Malm, W.C., Pitchford, M., White, W.H., Charlson, R., and Husar, R., Visibility: Existing and historical conditions - Causes and effects. In *State Sci. State Technol. Rep. 24, Natl. Acid Precip. Assessment Program*, Washington, D.C., 1990

Turpin, B.J., Saxena, P., Allen, G., Koutrakis, P., McMurry, P., and Hildemann, L., Characterization of the southwestern desert aerosol, Meadview, Arizona, *J. Air and Waste Management Assoc.*, **47**, 344-356, 1997.

Twomey, S., Comparison of constrained linear inversion and an iterative non-linear algorithm applied to the indirect estimation of particle size distributions, *J. Comput. Phys*. **18**, 188-200, 1975.

Waggoner, A.P., Weiss, R.E., Ahlquist, N.C., Covert, D.S., Will, S., and Charlson, R.J., Optical characteristics of atmospheric aerosols, *Atmos. Environ.,* **15**, 1891-1909, 1981.

Waggoner, A. P., Weiss, R. E., and Larson, T. V., In-situ rapid response measurement of $H_2SO_4/(NH_4)_2SO_4$ aerosols in urban Houston: a comparison with rural Virginia, *Atmos. Environ.,* **17**, 1723-1731, 1983.

Wexler A. and Seinfeld J., Second-generation inorganic aerosol model, *Atmos. Environ.,* **25A**(12), 2731, 1991.

White, W. H., On the theoretical and empirical basis for apportioning extinction by aerosols: a critical review, *Atmos. Environ.,* **20**, 1659-1672, 1986.

White, W.H., Contributions to light scattering, In *Acidic Deposition: State of Science and Technology, Tech. Rep. 24*, pp. 85-102, Natl. Acid Precip. Assess. Program, Washington, D.C., 1990

White, W.H. and Macias, E.A., Light scattering by haze and dust at Spirit Mountain, Nevada, In *Transactions Visibility and Fine Particles*, (edited by C. V. Mathai), AWMA, Pittsburgh, PA., 1990.

White, W.H. and Roberts, P.T., On the nature and origins of visibility-reducing aerosols in the Los Angeles Air Basin, *Atmos. Environ.*, **11**, 803-812, 1977.

White, W.H., Macias, E.S., Nininger, R.C., and Schorran, D., Size-resolved measurements of light scattering by ambient particles in the southwestern U.S.A., *Atmos. Environ.*, **28**, 909-921, 1994.

Zhang, X.Q., McMurry, P.H., Hering, S.V., and Casuccio, G.S., Mixing characteristics and water content of submicron aerosols measured in Los Angeles and at the Grand Canyon, *Atmos. Environ*., **27**A, 1593-1607, 1993.

Zhang, X.Q., Turpin, B.J., McMurry, P.H.,Hering, and S.V.,Stolenberg, M.R., Mie theory evaluation of species contributions to 1990 wintertime visibility reduction in the Grand Canyon, *J. Air Waste Management Assoc.*, **44**, 153-162, 1994.

APPENDIX A

VISIBILITY MAPS DERIVED FROM MEASURED AND SPATIALLY INTERPOLATED IMPROVE AND CDN DATA

Because the majority of Class I areas with IMPROVE monitoring are located in the western United States, spatial coverage of the IMPROVE network is sparse in the eastern United States. As a result, maps of a visibility index, such as the light extinction coefficient (b_{ext}) or deciview (dv) based on IMPROVE data [Malm *et al*., 1994; Sisler, 1996; Sisler *et al*., 1993; Chapter 3.2.2] lack spatial resolution in the eastern United States, where visibility conditions are traditionally the worst.

High-resolution maps of b_{ext} derived from airport visual range observations are available [Falke and Husar, 1998]. While these maps have detailed spatial resolution, they have limitations due to the human observation method from which they are derived. For example, the observationally based b_{ext} estimates are truncated at a minimum threshold and the observer system on which these maps are based is no longer widely used in the United States, rendering observationally based b_{ext} maps obsolete for future trend analysis. In contrast, b_{ext} reconstructed from aerosol mass concentration data can be used to estimate visibility conditions on the cleanest and haziest conditions, and these data can be combined with future monitoring for long-term trend analyses. Perhaps the greatest advantage of b_{ext} maps reconstructed from aerosol mass concentration data, over those estimated from visual range, is reconstructed aerosol b_{ext} allows for apportionment of visibility impairment to specific aerosol species.

In this section, IMPROVE and the CASTNet Deposition Network (CDN) data are combined to show spatial patterns in mean sulfate and nitrate mass concentration, as well as reconstructed b_{ext}, across the contiguous United States. The particle sulfate and nitrate maps represent mass concentrations reported by two networks, while the visibility maps are derived using the IMPROVE algorithm to reconstruct b_{ext} [Chapter 3.1]. Because routine CDN sampling protocol does not include measurements of all chemical species necessary to reconstruct b_{ext}, concentrations at CDN monitoring locations for species other than sulfates and nitrates are estimated by spatial interpolation of IMPROVE data.

In using the deposition network data as a surrogate for IMPROVE data in the b_{ext} algorithm, we adopt the assumption that sulfates and nitrates are responsible for the majority of light extinction at most CDN monitoring locations, particularly in the eastern United States where spatial coverage of IMPROVE sites is sparse. If chemical species other than sulfates and nitrates constitute a large portion of the extinction budget at a CDN site, then the point estimated b_{ext} will

rely heavily on interpolated IMPROVE fields and will contain uncertainties associated with the interpolation. However, in support of our underlying assumption, sulfates (as ammonium sulfate) contribute 70% or more to the annual average particle b_{ext} in the eastern United States based on IMPROVE data, while the contribution of other chemical species to the extinction budget is approximately 10% or less [Chapter 3.2.1]. Particle nitrates can also play a significant role in visibility reduction. For example, nitrates contribute approximately 30% to annual particle b_{ext} near some IMPROVE sites in southern California [Chapter 3.2.2]. CDN data shown in this section indicate high wintertime particle nitrate mass concentrations throughout large urban and agricultural regions of the Midwest, which may indicate nitrates are major contributors to the particle light extinction budget in that region during the cold season.

Before using CDN particle sulfate and nitrate mass concentrations as surrogates for IMPROVE protocol measurements, we compared the respective data sets. Results from this comparison show mean sulfate mass concentrations are comparable, however, bias between particle nitrate mass concentrations are observed at many nearby sites from the respective networks [Ames and Malm, 2000; Appendix G]. Field comparisons have shown good agreement between sulfate, although particle nitrate mass concentrations measured by CDN samplers, which use Teflon substrates to collect particles, may be underestimated by about 10% [Clean Air Status and Trends Network, 1998] compared to measurements from collocated samplers that collect particle nitrate on denuded nylon substrates. Other comparison studies have reported particle nitrate undersampling, attributed to particle nitrate volatilization from Teflon filters, of 60% during the summer, and 30% on an annual basis [Chow et al., 1994; Hering and Cass, 1999]. If particle nitrate volatilization occurs in the CDN samplers, then particle nitrate mass concentrations reported by that network may be a lower-bound estimate of the true ambient mass concentration. On the other hand, particle nitrate mass concentrations reported by the CDN may overestimate fine particle nitrate as measured by IMPROVE protocol samplers if measurable particle nitrate mass resides in the coarse mode.

A.1 METHOD

Reconstructed b_{ext} is calculated using data from the three-year period December 1995 through November 1998, and for the summer (June, July, August) and winter (December, January, February) seasons during that time period. The b_{ext} reconstruction follows the method in Chapter 3.1. All b_{ext} values in this section refer to mean aerosol b_{ext}. IMPROVE sulfate mass concentration is estimated from module A elemental S. Descriptions of the IMPROVE sampling modules, the chemical species that they collect, and related analytical methods are given in Chapter 2.1. CDN sulfate and nitrate ion mass concentrations are obtained from Teflon substrates. Hourly relative humidity (RH) measurements at IMPROVE and CDN sites are averaged following the method outlined in Chapter 3.1, and the relative humidity correction factor (F_T(RH)) is determined using Equation 3.7 and appropriate coefficients for seasonal or season weighted annual mean RH at all IMPROVE and CDN sites.

A minimum 70% of the possible measurements is required to calculate the mean particle mass concentration at any site for the three-year and summer periods, and a minimum of 60% is required for the winter period. Tallying sites in the combined IMPROVE/CDN data set shows 123 sites meet the valid data requirement for sulfate during the three-year period (60 IMPROVE,

63 CDN). Figure A.1 is a map showing the corresponding site abbreviations, and Table A.1 lists the site abbreviations, the state where the monitoring sites reside, and site names. Fifty IMPROVE and 63 CDN sites meet minimum data requirement for particle nitrate during the three-year period. The number of sites meeting the minimum data requirement for winter and summer periods is similar to those for the three-year period. A minimum of 50% valid data is required to calculate seasonal RH.

The criteria to calculate b_{ext} at any monitoring site is that sufficient sulfate measurements are available to calculate a mean for the desired time period. To calculate b_{ext} at sites where chemical concentration data other than sulfate are missing, available species mass concentration data are interpolated to a 0.5 degree latitude/longitude grid across the contiguous United States, and data are taken from the nearest grid value. Generally, data missing are at CDN sites for species other than sulfate and nitrate, for which species mass concentrations are taken from interpolated IMPROVE data. However, some interpolated data are used at IMPROVE sites without either of sampling modules B, C, or D. For example, interpolated particle nitrate mass concentrations derived from the combined data set are used at IMPROVE sites operating without module B which collects particle nitrate.

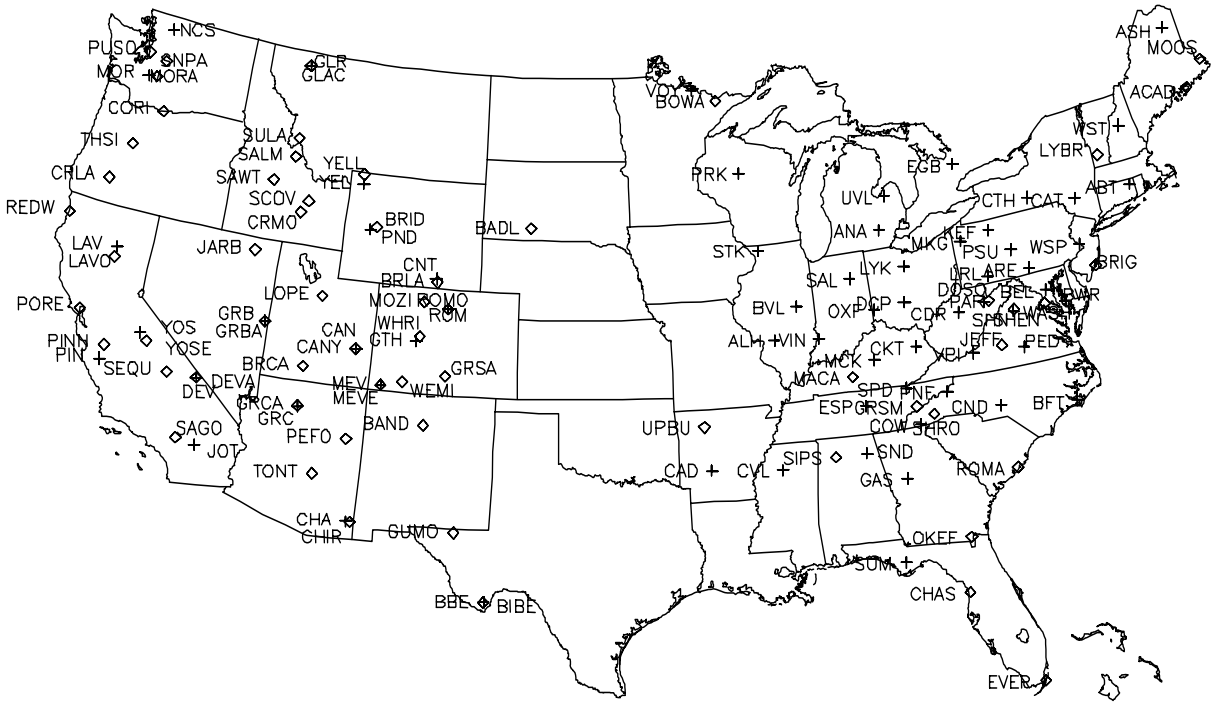

Figure A.1 *Map of monitoring sites, showing site abbreviations, from the IMPROVE network (diamonds) and the CDN (plusses) used in this analysis.*

IMPROVE organic carbon (OC), elemental carbon (EC), fine soil, and coarse mass (CM) are interpolated using a minimum curvature spline surface, which is appropriate for interpolation of the relatively low spatial density data set. (Isopleths of IMPROVE data interpolated using the spline method are shown in Chapter 2.5, and are similar to the interpolated fields used for this

analysis, although they correspond to a three-year period advanced one season from maps shown in this section). Concentrations for combined IMPROVE and CDN fields are interpolated using a nearest neighbor triangulation interpolation. The triangulation method provides more accurate interpolations than the spline method, in our opinion, for high density data sets. Maps shown in this section show contours of the triangulated fields. All interpolated fields, particularly at locations where estimates were made using interpolated data, were checked for reasonable behavior. For example, the IMPROVE site BRIG on the New Jersey coast, has high CM concentrations relative to other IMPROVE sites in the northeastern United States, likely due to sea salt. It is unlikely that this maritime CM extends inland any great distance, therefore BRIG was removed from the CM interpolation so as not to overestimate CM concentrations at neighboring, although more inland, CDN sites.

Mean CDN particle mass concentrations are converted to ambient pressure based on site elevation, although are not converted ambient temperature. IMPROVE data represent ambient sampling conditions. Sulfate and nitrate mass concentrations from both networks are converted to mass concentrations of fully neutralized ammonium salts. Due to an anticipated bias of CDN measurements to coarse particle nitrate, the three-year mean particle nitrate mass concentrations at 11 western CDN sites (PND, YEL, ROM, GRC, MEV, CAN, GRB, CHA, BBE, CNT, GTH) are adjusted to fine particle nitrate using a temperature and fine soil correlation model (Appendix G). Similar adjustments are not made to CDN nitrate data in other regions of the country, or for winter or summer data, because appropriate algorithms have not yet been developed.

Table A.1 *IMPROVE and CDN monitoring sites used in this analysis.*

IMPROVE			CDN		
Abbreviation	**State**	**Name**	**Abbreviation**	**State**	**Name**
ACAD	ME	Acadia NP	ABT	CT	Abington
BADL	SD	Badlands NP	ALH	IL	Alhambra
BAND	NM	Bandelier NM	ANA	MI	Ann Arbor
BIBE	TX	Big Bend NP	ARE	PA	Arendtsville
BOWA	MN	Boundary Waters CA	ASH	ME	Ashland
BRCA	UT	Bryce Canyon NP	BBE	TX	Big Bend NP
BRID	WY	Bridger WA	BEL	MD	Beltsville
BRIG	NJ	Brigantine NWR	BFT	NC	Beaufort
BRLA	WY	Brooklyn Lake	BVL	IL	Bondville
CANY	UT	Canyonlands NP	BWR	MD	Blackwater NWR
CHAS	FL	Chassahowitza NWR	CAD	AR	Caddo Valley
CHIR	AZ	Chiricahua NM	CAN	UT	Canyonlands NP
CORI	OR	Columbia River NSA	CAT	NY	Claryville
CRLA	OR	Crater Lake NP	CDR	WV	Cedar Creek
CRMO	ID	Craters of Moon NM	CHA	AZ	Chiricahua NM
DEVA	CA	Death Valley NP	CKT	KY	Crockett
DOSO	WV	Dolly Sods WA	CND	NC	Candor
EVER	FL	Everglades NP	CNT	WY	Centennial
GLAC	MT	Glacier NP	COW	NC	Coweeta
GRBA	NV	Great Basin NP	CTH	NY	Connecticut Hill
GRCA	AZ	Grand Canyon NP	CVL	MS	Coffeeville
GRSA	CO	Great Sand Dunes NM	DCP	OH	Deer Creek

Table A.1 *(Continued.)*

IMPROVE			CDN		
Abbreviation	**State**	**Name**	**Abbreviation**	**State**	**Name**
GRSM	TN	Great Smoky Mountains NP	DEV	CA	Death Valley NP
GUMO	TX	Guadalupe Mountains NP	EGB	ON	Egbert
JARB	NV	Jarbidge WA	ESP	TN	Edgar Evins
JEFF	VA	Jefferson NF	GAS	GA	Georgia Station
LAVO	CA	Lassen Volcanic NP	GLR	MT	Glacier NP
LOPE	UT	Lone Peak WA	GRB	NV	Great Basin NP
LYBR	VT	Lye Brook WA	GRC	AZ	Grand Canyon NP
MACA	KY	Mammoth Cave NP	GTH	CO	Gothic
MEVE	CO	Mesa Verde NP	JOT	CA	Joshua Tree NM
MOOS	ME	Moosehorn NWR	KEF	PA	Kane Exp. Forest
MORA	WA	Mount Rainier NP	LAV	CA	Lassen Volcanic NP
MOZI	CO	Mount Zirkel WA	LRL	PA	Laurel Hill
OKEF	GA	Okefenokee NWR	LYK	OH	Lykens
PEFO	AZ	Petrified Forest NP	MCK	KY	Mackville
PINN	CA	Pinnacles NM	MEV	CO	Mesa Verde NP
PORE	CA	Point Reyes NS	MKG	PA	M.K. Goddard
PUSO	WA	Puget Sound	MOR	WA	Mount Rainier NP
REDW	CA	Redwood NP	NCS	WA	North Cascades NP
ROMA	SC	Cape Romain NWR	OXF	OH	Oxford
ROMO	CO	Rocky Mountain NP	PAR	WV	Parsons
SAGO	CA	San Gorgonio WA	PED	VA	Prince Edward
SALM	ID	Salmon	PIN	CA	Pinnacles NM
SAWT	CO	Sawtooh NF	PND	WY	Pinedale
SCOV	ID	Scoville DOE Lab	PNF	NC	Cranberry
SEQU	CA	Sequoia NP	PRK	WI	Perkinstown
SHEN	VA	Shenandoah NP	PSU	PA	Penn State
SHRO	NC	Shining Rock WA	ROM	CO	Rocky Mountain NP
SIPS	AL	Sipsey WA	SAL	IN	Salamonie Reservoir
SNPA	WA	Snoqualmie Pass NF	SHN	VA	Shenandoah NP - Big Meadows
SULA	MT	Sula Peak	SND	AL	Sand Mountain
THSI	OR	Three Sisters WA	SPD	TN	Speedwell
TONT	AZ	Tonto NM	STK	IL	Stockton
UPBU	AR	Upper Buffalo WA	SUM	FL	Sumatra
WASH	DC	Washington, D.C.	UVL	MI	Unionville
WEMI	CO	Weminuche WA	VIN	IN	Vincennes
WHRI	CO	White River NF	VOY	MN	Voyageurs NP
YELL	WY	Yellowstone NP	VPI	VA	Horton Station
YOSE	CA	Yosemite NP	WSP	NJ	Washington Crossing
			WST	NH	Woodstock
			YEL	WY	Yellowstone NP
			YOS	CA	Yosemite NP - Turtleback Dome

NP = National Park
NM = National Monument
CA = Canoe Area
WA = Wilderness Area
NWR = National Wildlife Refuge
NSA = National Scenic Area
NS = National Seashore
NF = National Forest

A.2 RESULTS AND DISCUSSION

Combined IMPROVE and CDN nitrate, sulfate and b_{ext} maps for the three-year period, December 1995 through November 1998 are shown in Figures A.2 through A.4.

Figure A.2 is a map of mean particle nitrate mass concentrations, indicating maximum nitrate concentrations in excess of 3 $\mu g/m^3$ across the northern Midwest, with high particle nitrate concentrations also observed near some urban areas. Figure A.3 shows mean sulfate mass concentrations, indicating the highest mean sulfate mass concentrations, in excess of 7 $\mu g/m^3$ for the three-year period, occur at monitoring locations along the Ohio River and Tennessee Valleys. Note in Figure A.3 that the southeast boarder of the 7 $\mu g/m^3$ sulfate mass concentration contour reflects terrain features of the Appalachian Mountain chain.

Figure A.4 (also Figure 3.5 in Chapter 3.2.2) is a map of the reconstructed b_{ext} based on combined IMPROVE and CDN data. Mean reconstructed aerosol b_{ext} exceeds 120/Mm in a region of the eastern United States roughly corresponding to the region of maximum sulfate mass concentration shown in Figure A.2. Note that the region encompassed by the 120/Mm contour in the combined map is larger and has more spatial resolution than the same 120/Mm region based on IMPROVE data alone. Differences between some IMPROVE b_{ext} point values in Figure 3.4 compared to those in Figure 3.5 can be attributed to the different time periods for the respective maps, and the fact that F_T(RH) is calculated using Equation 3.17 at all sites in Figure 3.5, while in Figure 3.4 site specific values are used at some IMPROVE sites.

Comparison of mean IMPROVE and the CDN particle mass concentrations and b_{ext} values was performed at nearby monitoring sites. Table A.2 shows the root mean square (RMS) relative difference (expressed as a percent of the CDN mean) in means of sulfate and nitrate particle mass concentration, RH, and reconstructed b_{ext} for sites from the two networks within 50 km. These are a subset of the comparison sites in Appendix G, where sites separated by more than 50 km have been excluded, and the LYBR-LYE pair is excluded because data from LYE did not meet the minimum requirement for this analysis. The RMS difference for nitrate is higher than for sulfate, reflecting bias in the respective particle nitrate measurement from the two networks at the primarily western United States comparison sites. It is not surprising that the RMS difference for reconstructed b_{ext} is less than that of other quantities shown in Table A.2. Due to the proximity of comparison sites incorporated in RMS difference example, the same IMPROVE data are used in the reconstructed b_{ext} algorithm for quantities other than sulfate, nitrate, and RH.

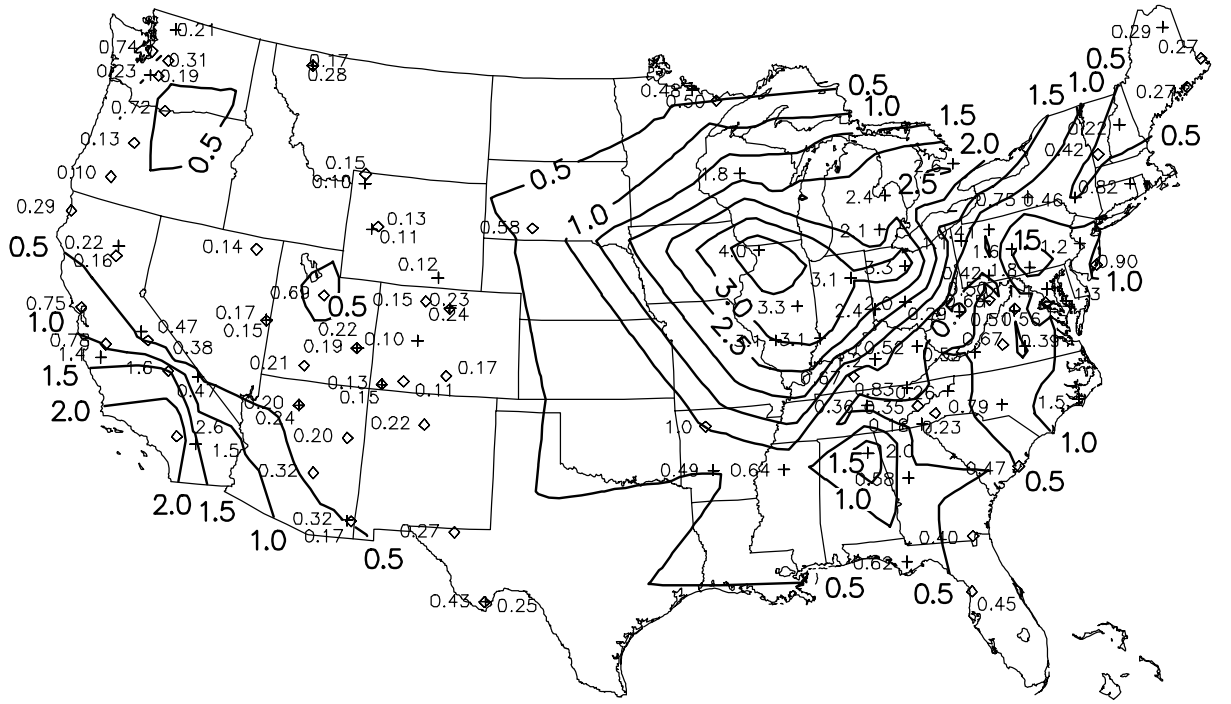

Figure A.2 *December 1995 through November 1998 mean particle nitrate (as ammonium nitrate) mass concentrations.*

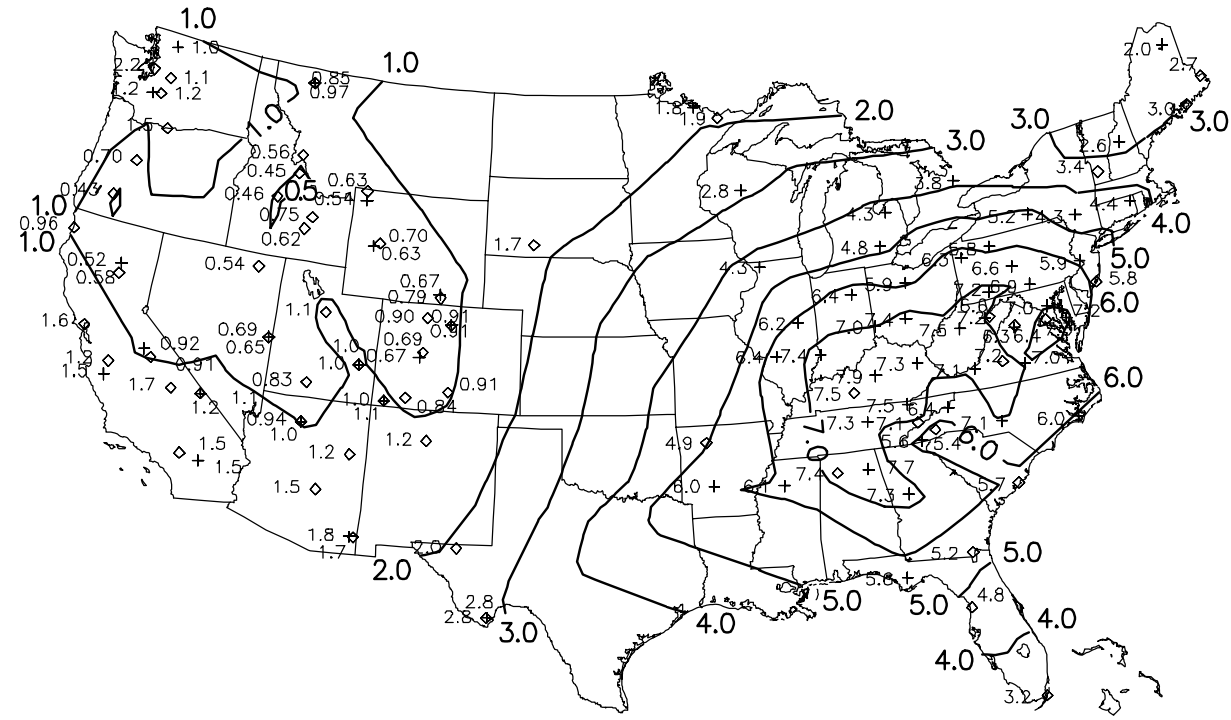

Figure A.3 *December 1995 through November 1998 mean particle sulfate (as ammonium sulfate) mass concentrations.*

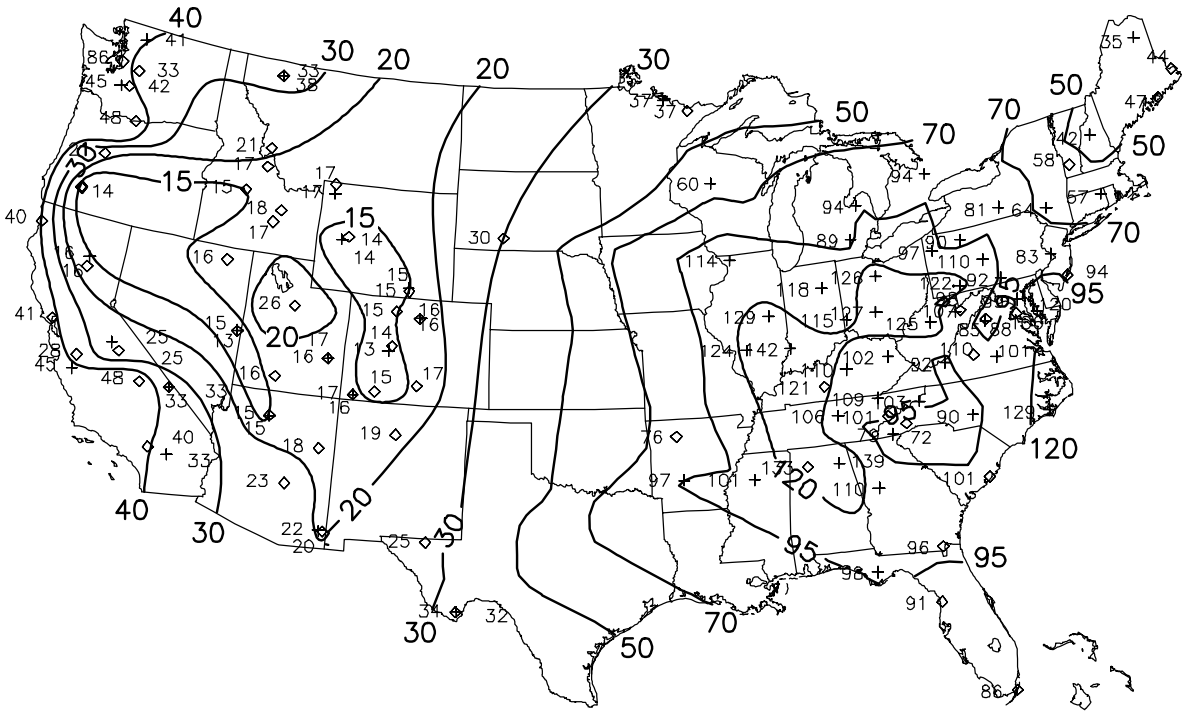

Figure A.4 *December 1995 through November 1998 mean reconstructed aerosol b_{ext}.*

Table A.2 *RMS percent difference for annual mean sulfate, nitrate, RH and reconstructed b_{ext} at nearby IMPROVE and CDN sites.*

Quantity	N	RMS Difference (%)
Sulfate	18	9
Nitrate	15	30
RH	15	9
Reconstructed b_{ext}	18	6

Seasonal maps of particle sulfate and nitrate mass concentration are shown in Figures A.5 through A.8. Figure A.5 indicates high wintertime particle nitrate concentrations throughout a large region of the northern Midwest, with maximum wintertime nitrate mass concentrations in excess of 4 $\mu g/m^3$ at CDN sites in Illinois, Indiana, and Ohio. This broad region of high particle nitrate mass concentrations is not captured by the IMPROVE Network. It is interesting to note the CDN site in Stockton, Illinois, which is not shown in Figure A.5 because the available data represent approximately 50% of the possible samples for the three-year winter period, has a wintertime mean particle nitrate mass concentration of 8 $\mu g/m^3$. Furthermore, Stockton, Illinois, nitrate data are shown in the map for three-year period (Figure A.2) because the data requirement specified for the entire three-year period are met at this site. Figure A.6 is a map of the wintertime mean sulfate mass concentration showing maximum values in excess of 4 $\mu g/m^3$ throughout much of the eastern United States. Higher wintertime sulfate concentrations are

confined generally east of the Appalachian mountains with a local minimum in the southeast United States at high elevation sites situated above the mixed layer for much of the winter.

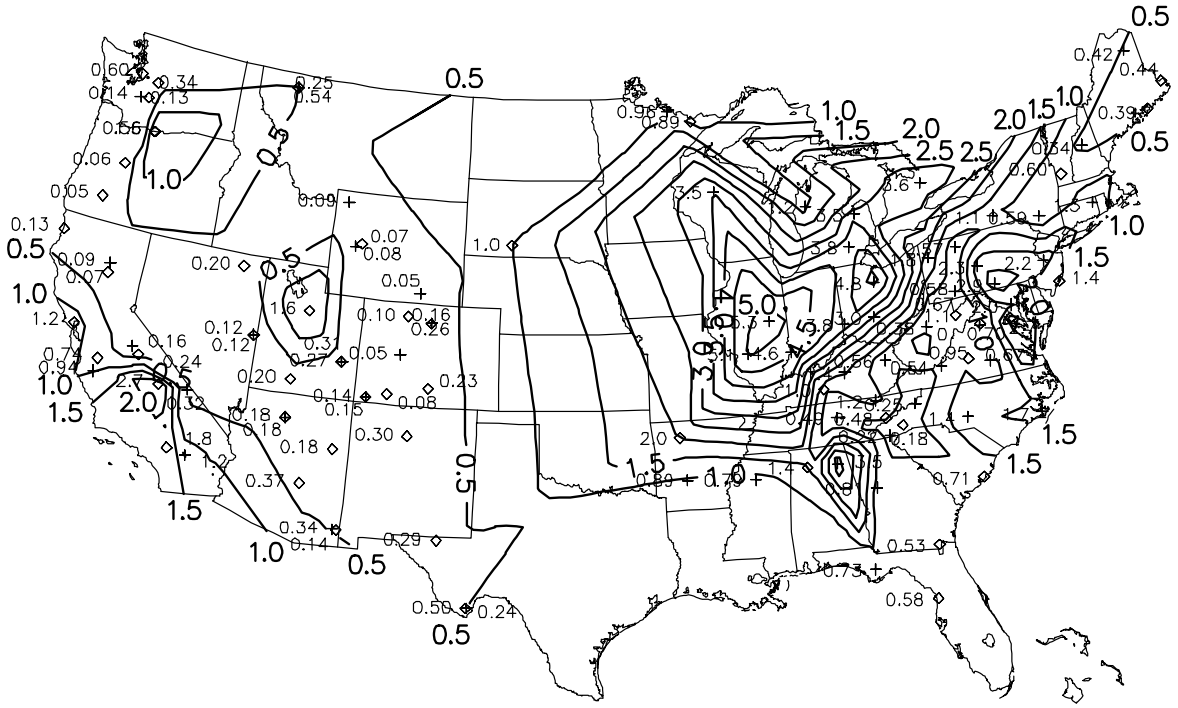

Figure A.5 *December 1995 through November 1998 mean winter particle nitrate mass concentrations.*

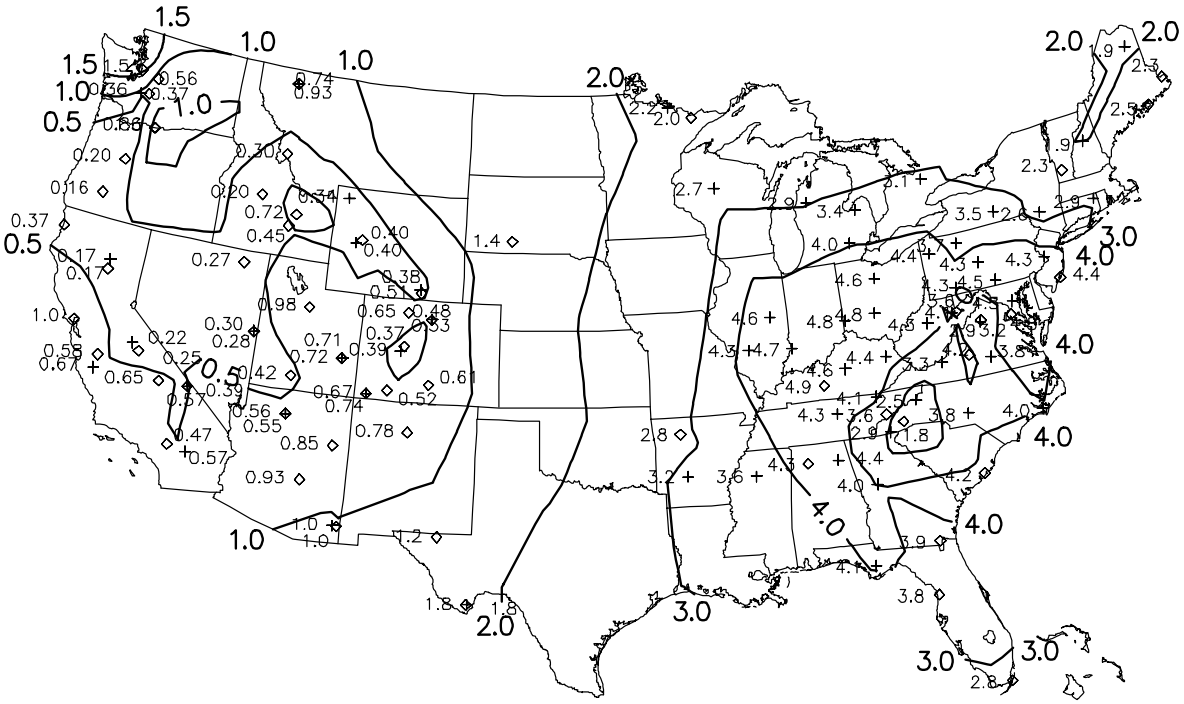

Figure A.6 *December 1995 through November 1998 mean winter sulfate mass concentrations.*

Figure A.7 is a map of summertime particle nitrate mass concentrations for the three-year period, showing values in excess of 1 $\mu g/m^3$ at some Midwest and California monitoring locations. It is interesting to note that the spatial pattern of particle nitrate seen during the winter, when particle nitrate mass concentrations are generally at a maximum, is essentially preserved in the summer nitrate map, although with lower magnitude. Figure A.8 is a map of mean summertime sulfate mass concentrations, showing maximum values in excess of 12 $\mu g/m^3$ centered over Kentucky and West Virginia, with steep decreasing concentration gradients in all directions away from the maximum. This contrasts with the winter sulfate map, where the region of maximum sulfate mass concentration in the eastern United States is comparatively broad, and mass concentration gradients exhibit a more gradual decline away from the highest wintertime values.

Figure A.9 is a map of reconstructed b_{ext} for the winter three-year period, showing many CDN sites in the northern Midwest with wintertime b_{ext} in excess of 100/Mm, generally corresponding to the region of high wintertime particle nitrate mass concentration. Wintertime b_{ext} is at a minimum (less than 10/Mm) in the western United States, Great Basin and Rocky Mountain regions, with local minimum b_{ext} in the eastern United States (less than 50/Mm) at a few high elevation sites along the Appalachian Mountain chain. Figure A.10 is a map of summertime b_{ext}, indicating a region of maximum b_{ext} (in excess of 170/Mm) along the Ohio River and Tennessee Valleys. The region of highest b_{ext} corresponds to monitoring sites where both sulfate and RH are high. For example, an increase in RH from 78% to 83% translates to a 31% increase in F_T(RH) as calculated by Equation 3.17. When the bulk of the light extinction budget is made up of hygroscopic chemical species, small changes in RH can have a strong influence on reconstructed b_{ext}, particularly at high RH values.

Table A.3 shows the RMS percent difference in winter sulfate, nitrate, and reconstructed b_{ext} and CDN and IMPROVE sites within approximately 50 km, while Table A.4 shows these values for the summertime comparison. Note that the sites used for the comparison are located primarily in the western United States and the large magnitude particle nitrate RMS difference likely reflects a sampling bias between IMPROVE and CDN specific to this region.

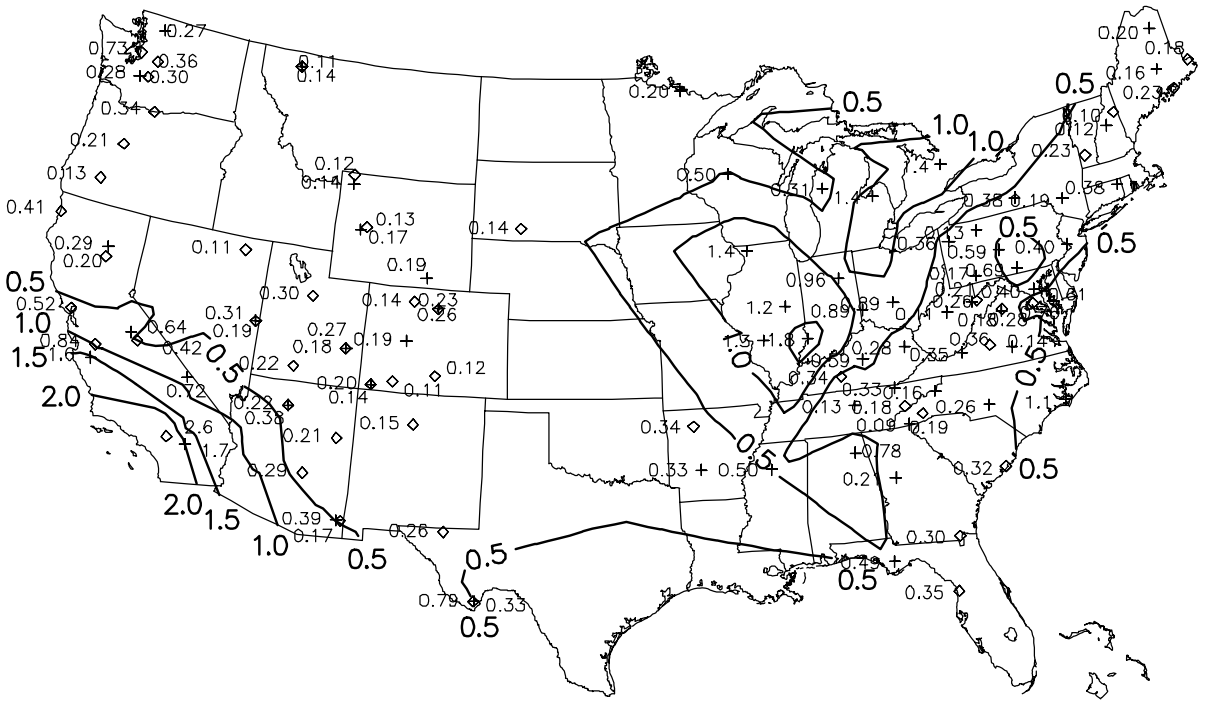

Figure A.7 *December 1995 through November 1998 mean summer particle nitrate mass concentrations.*

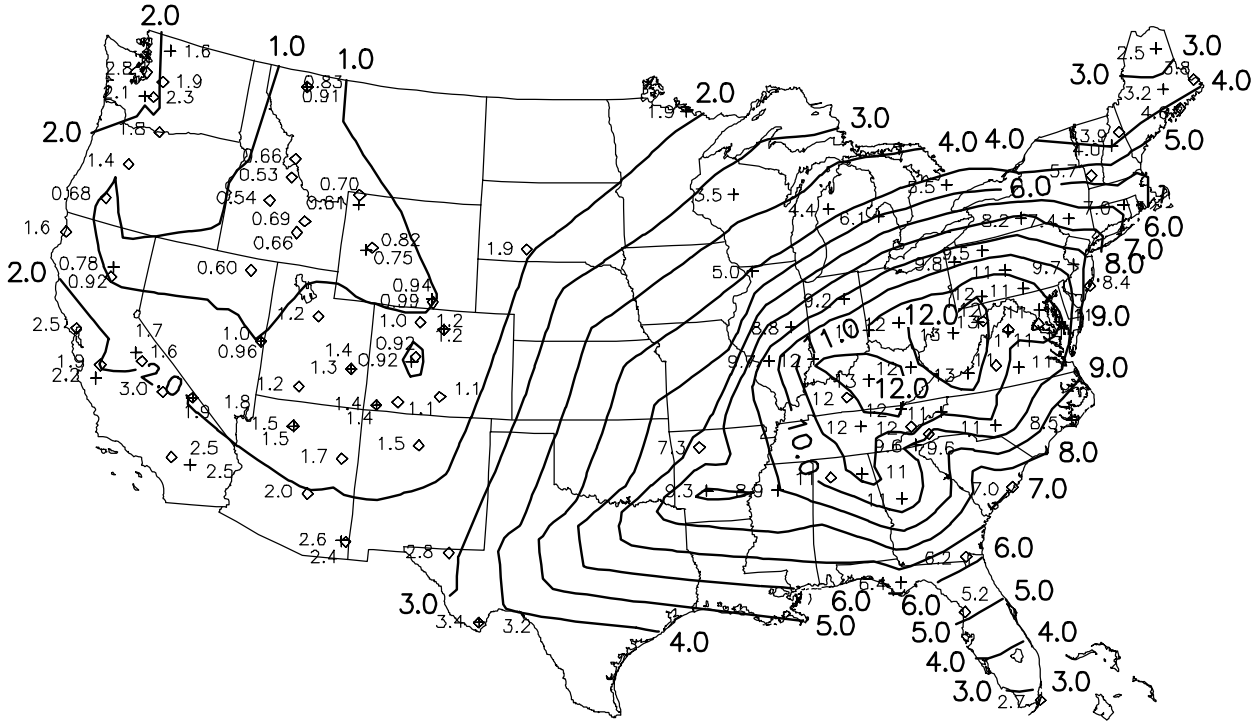

Figure A.8 *December 1995 through November 1998 mean summer sulfate mass concentrations.*

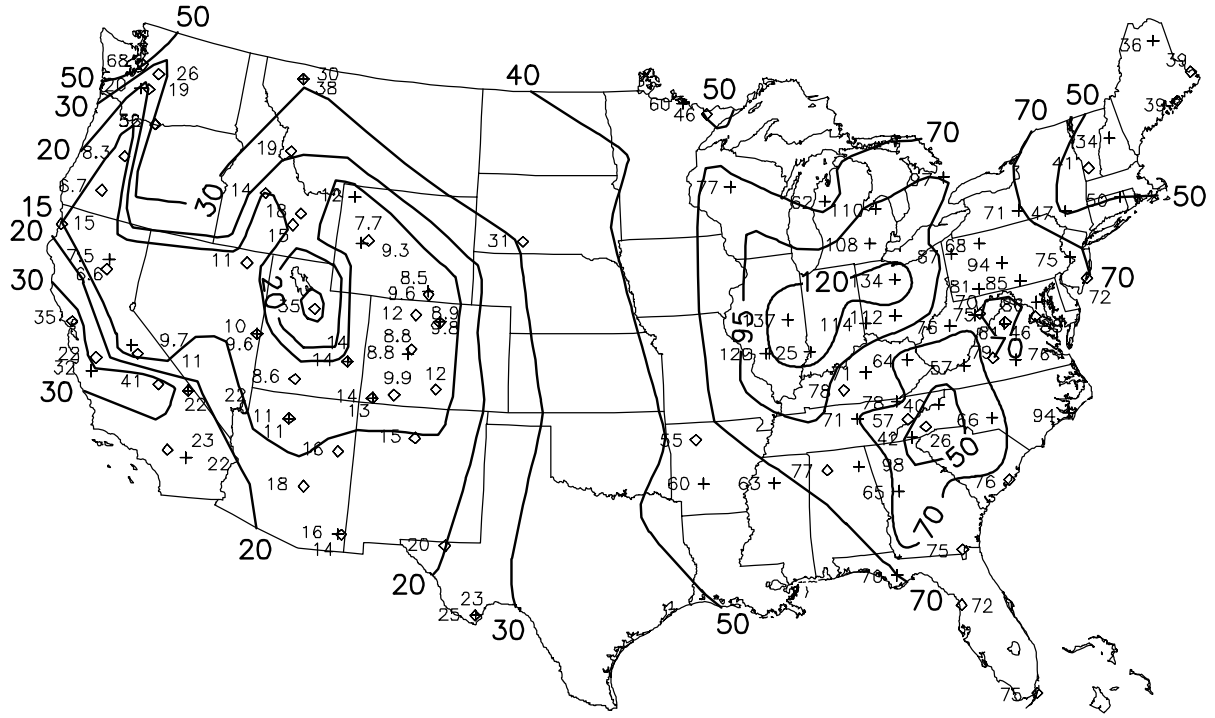

Figure A.9 *December 1995 through November 1998 mean winter reconstructed aerosol* b_{ext}.

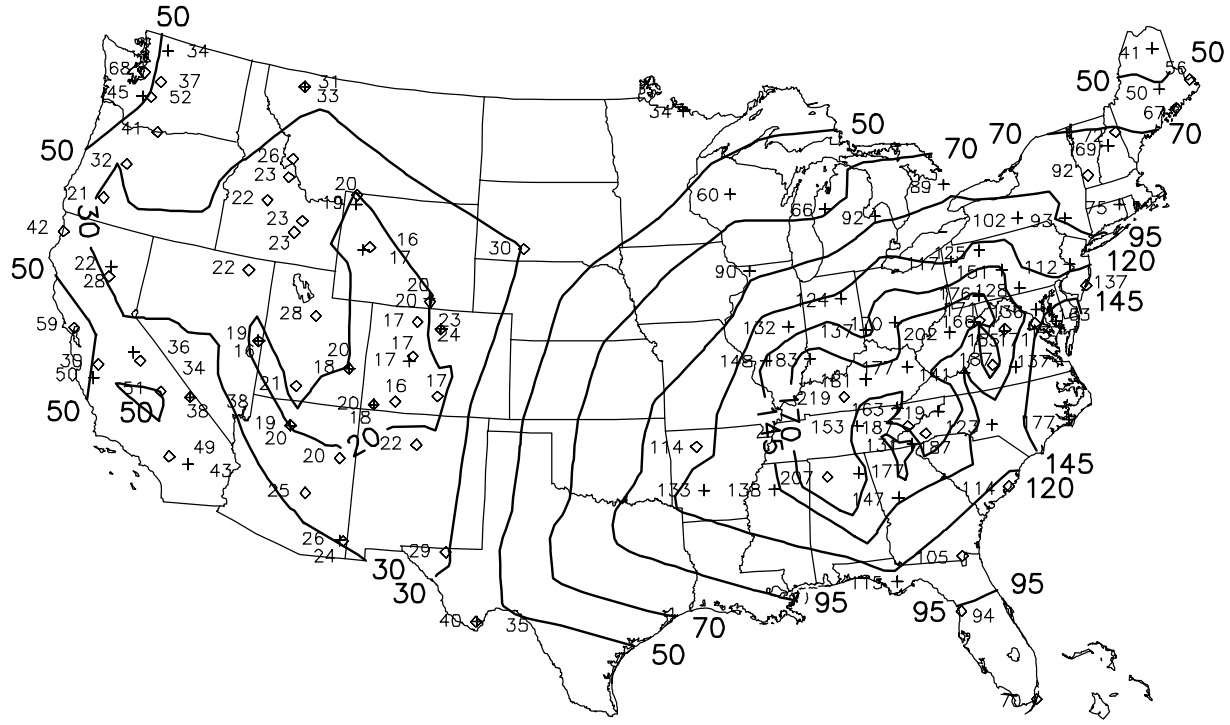

Figure A.10 *December 1995 through November 1998 mean summer reconstructed aerosol* b_{ext}.

Table A.3 *RMS difference for wintertime mean sulfate, nitrate, RH and reconstructed b_{ext} at nearby IMPROVE and CDN sites.*

Quantity	N	RMS difference (%)
Sulfate	17	14
Nitrate	14	43
RH	15	7
Reconstructed b_{ext}	17	12

Table A.4 *RMS difference for summertime mean sulfate, nitrate, RH and reconstructed b_{ext} at nearby IMPROVE and CDN sites.*

Quantity	N	RMS difference (%)
Sulfate	18	8
Nitrate	15	36
RH	18	10
Reconstructed b_{ext}	16	14

A.3 SUMMARY

Sulfate and nitrate particle mass concentrations from the CDN were combined with IMPROVE data to enhance spatial resolution of reconstructed aerosol b_{ext} maps. The spatial resolution of the combined b_{ext} maps in the eastern United States is greatly enhanced over maps based on IMPROVE data alone, particularly in the eastern United States where visibility conditions are traditionally the worst in the nation.

This analysis, which incorporates data from the three-year December 1995 through November 1998 period, illustrates that the haziest conditions in the United States occur in the Midwest and eastern United States, particularly along the Ohio River and Tennessee Valleys, in a region where mean b_{ext} exceeds 120/Mm. This region corresponds in general to the region of maximum sulfate mass concentration for the three-year period. Maximum summertime sulfate mass concentrations, in excess of 12 $\mu g/m^3$, center over Kentucky and West Virginia. These high summer sulfate mass concentrations, combined with mean RH values in excess of 80% at some sites, strongly influence spatial patterns of the summer b_{ext} maps, which exceeds 170/Mm across much of the eastern United States west of the Appalachian Mountains. Nitrates have a wintertime maximum particle mass concentration in excess of 4 $\mu g/m^3$ centered over Illinois, Indiana and Ohio, which corresponds to the regions of maximum wintertime b_{ext} in excess of 120/Mm.

In this analysis we assume sulfate and nitrate have the majority contribution to the particle light extinction budget at sites where b_{ext} is estimated using interpolated chemical mass concentration fields. This assumption likely holds at most eastern United States monitoring locations, where sulfates are major contributors to particle mass. The interpolations could be improved by incorporating factors such as terrain forcing, seasonal varying mixing heights, and measurements from sources other than IMPROVE to serve as basis for the interpolations, where

available. The disparity between IMPROVE and CDN particle nitrate mass concentration measurements remains troubling and should be further addressed, particularly in regions where particle nitrate mass concentrations are high and likely have a large contribution to b_{ext}. This type of analysis is also strongly influenced by RH, and could benefit from more refined and regionally specific estimates of the RH correction factor applied to hygroscopic aerosol species in the b_{ext} algorithm. Further applications of these combined b_{ext} data could be to refine regional chemical species b_{ext} budgets, or as a source of comparison data for b_{ext} maps estimated from human observations, or for comparison to remotely sensed estimates of aerosol optical depth in lower levels of the atmosphere.

A.4 REFERENCES

Ames R. B. and Malm W. C., Comparison of sulfate an nitrate particle mass concentrations from IMPROVE and CDN, submitted to *Atmospheric Environment*, 2000.

Chow, J. C.; Fujita, E. M.; Watson, J. G. ; Lu, Z., Lawson, D. R., Ashbaugh, L. L., Evaluation of filter-based aerosol measurements during the 1987 Southern California Air Quality Study, Environmental Monitoring and Assessment, *Environ. Monit. Assess.*, **30**(1):49-80, 1994.

Clean Air Status and Trends Network (CASTNet) Deposition Summary Report (1987-1995), EPA/600/R-98-207, July, 1998.

Falke S. F. and Husar R. B., Maps of $PM_{2.5}$ over the U.S. derived from regional $PM_{2.5}$ and surrogate visibility and PM_{10} monitoring data, Presented at the AWMA 90th annual meeting, 1998.

Hering S. and Cass G., The magnitude of bias in the measurement of $PM_{2.5}$ arising form volatilization of particulate nitrate from Teflon filters, *J. Air and Waste Management Association*, **49**(6):725-733, 1999.

Malm W. C., Sisler J. F., Huffman D., Eldred R. A., and Cahill T. C., Spatial and seasonal trends in particle concentration and optical extinction in the U.S. *J. Geophys. Res.* **99**(D1):1347-1370, 1994.

Sisler, J. F., *Spatial and Seasonal Patterns and Long Term Variability of the Composition of the Haze in the United States: An Analysis of Data from the IMPROVE Network,* Cooperative Institute for Research in the Atmosphere, Colorado State University, ISSN 0737-5352-32, 1996.

Sisler, J. F., Huffman, D., Latimer, D. A., Malm, W. C. and Pitchford, M. L., *Spatial and Temporal Patterns and the Chemical Composition of the Haze in the United States: An Analysis of Data from the IMPROVE Network 1988-1991*, Cooperative Institute for Research in the Atmosphere, Colorado State University, ISSN 0737-5352-26, 1993.

APPENDIX B

The plots included in this appendix show the trends in annual and five-year rolling averages for $PM_{2.5}$ and deciview for sites in the IMPROVE monitoring network. The sites are in alphabetical order.

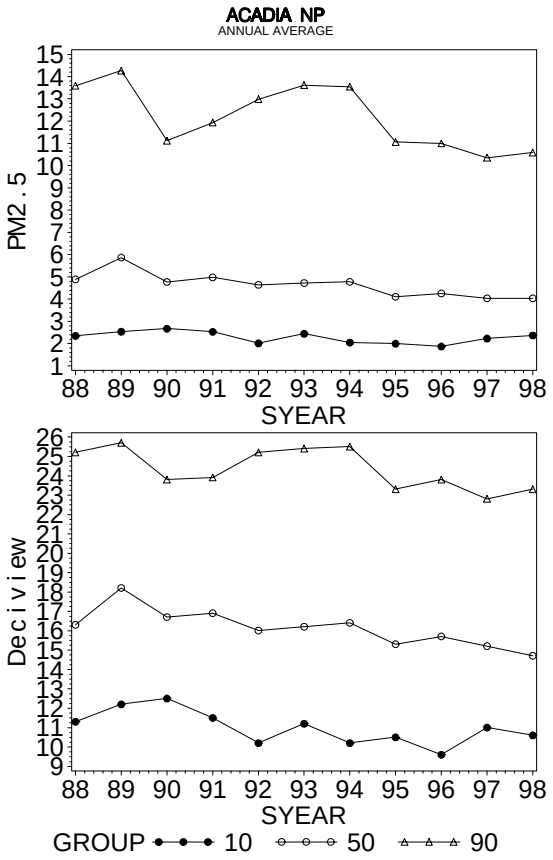
ACADIA NP
ANNUAL AVERAGE
PM2.5
SYEAR
Decivview
SYEAR
GROUP 10 50 90

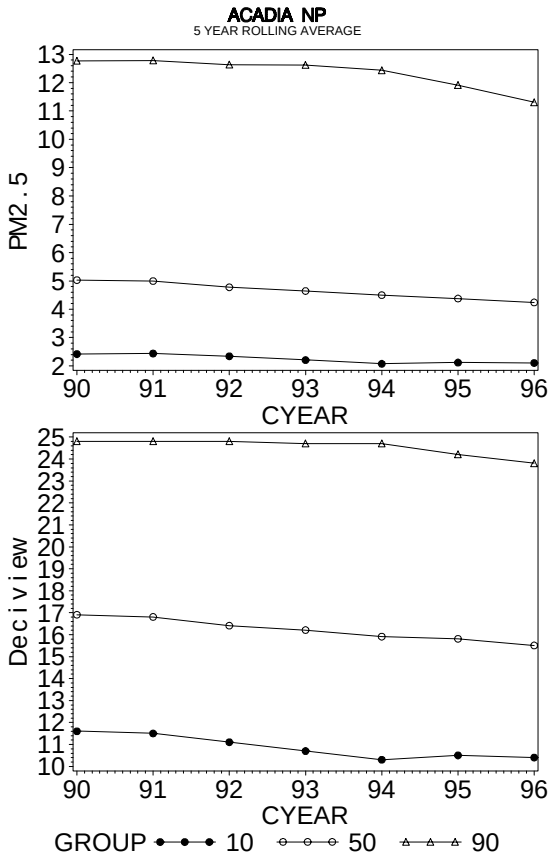
ACADIA NP
5 YEAR ROLLING AVERAGE
PM2.5
CYEAR
Decivview
CYEAR
GROUP 10 50 90

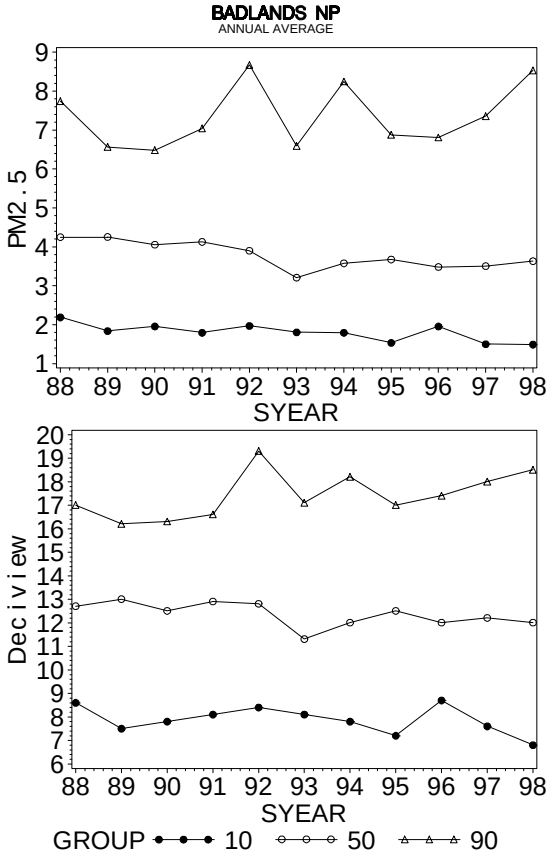
BADLANDS NP
ANNUAL AVERAGE
PM2.5
SYEAR
Decivview
SYEAR
GROUP 10 50 90

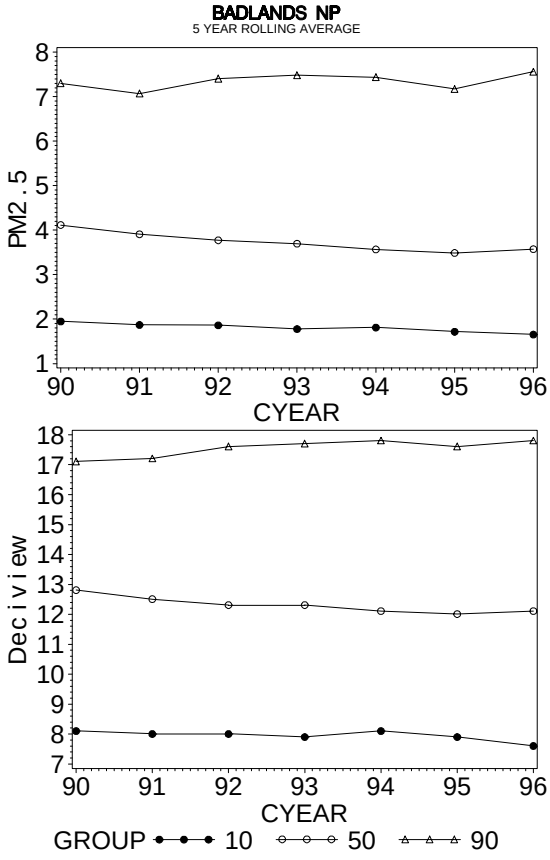
BADLANDS NP
5 YEAR ROLLING AVERAGE
PM2.5
CYEAR
Decivview
CYEAR
GROUP 10 50 90

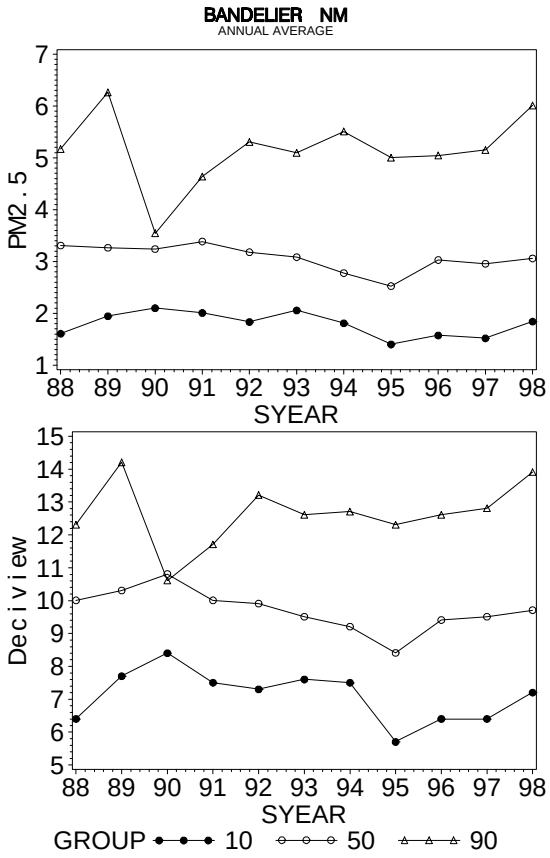
BANDELIER NM
ANNUAL AVERAGE
PM2.5
SYEAR
Deciview
SYEAR
GROUP 10 50 90

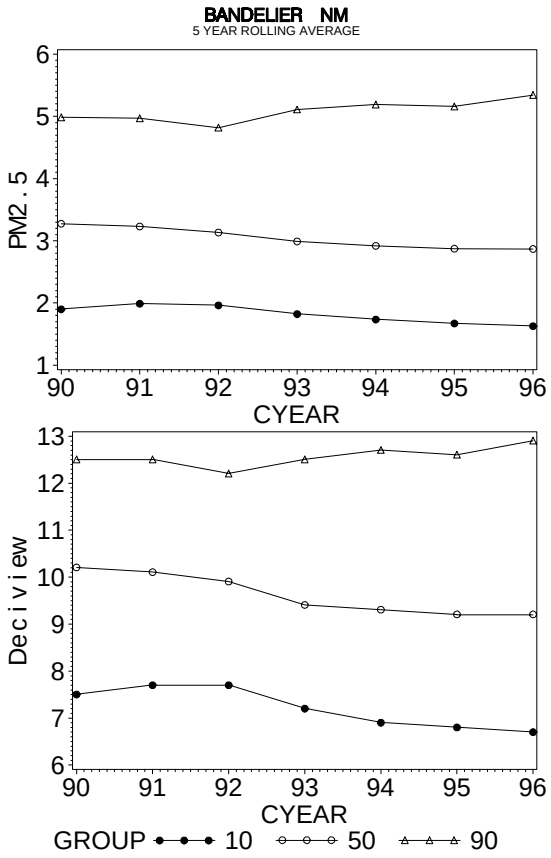
BANDELIER NM
5 YEAR ROLLING AVERAGE
PM2.5
CYEAR
Deciview
CYEAR
GROUP 10 50 90

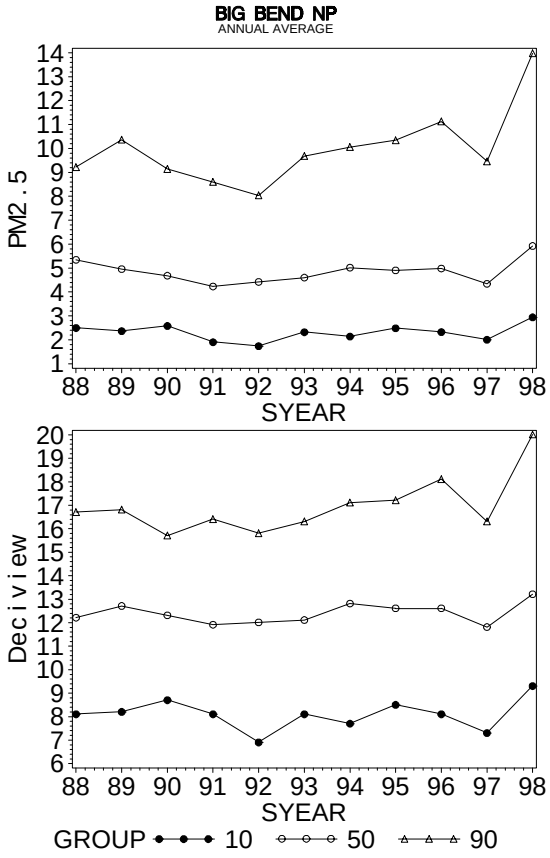
BIG BEND NP
ANNUAL AVERAGE
PM2.5
SYEAR
Deciview
SYEAR
GROUP 10 50 90

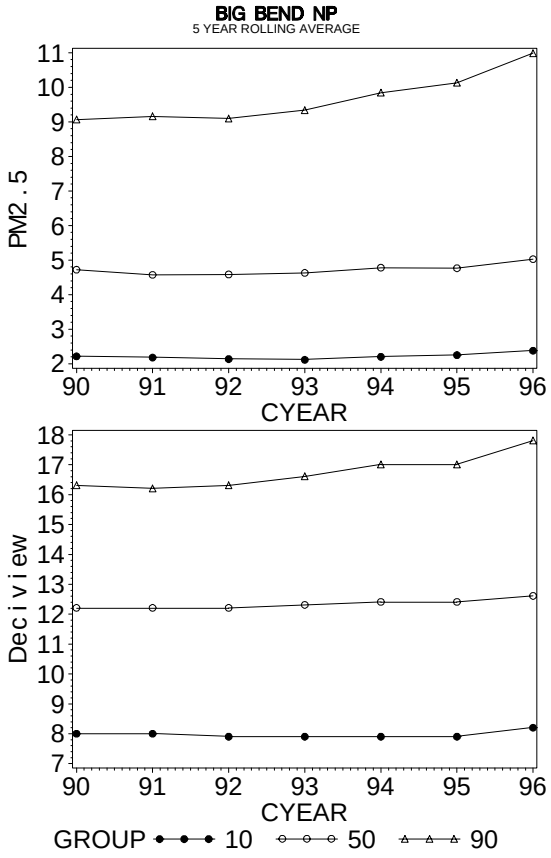
BIG BEND NP
5 YEAR ROLLING AVERAGE
PM2.5
CYEAR
Deciview
CYEAR
GROUP 10 50 90

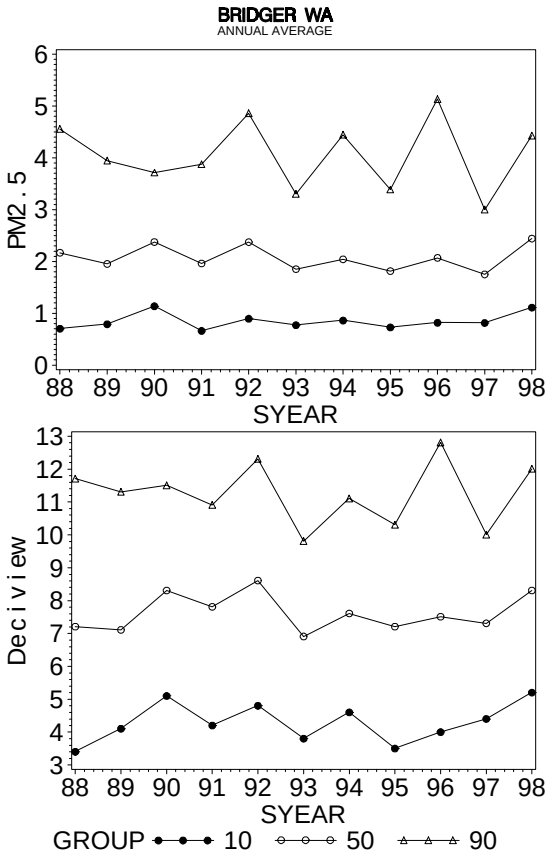
BRIDGER WA
ANNUAL AVERAGE
PM2.5
SYEAR
Deciview
SYEAR
GROUP 10 50 90

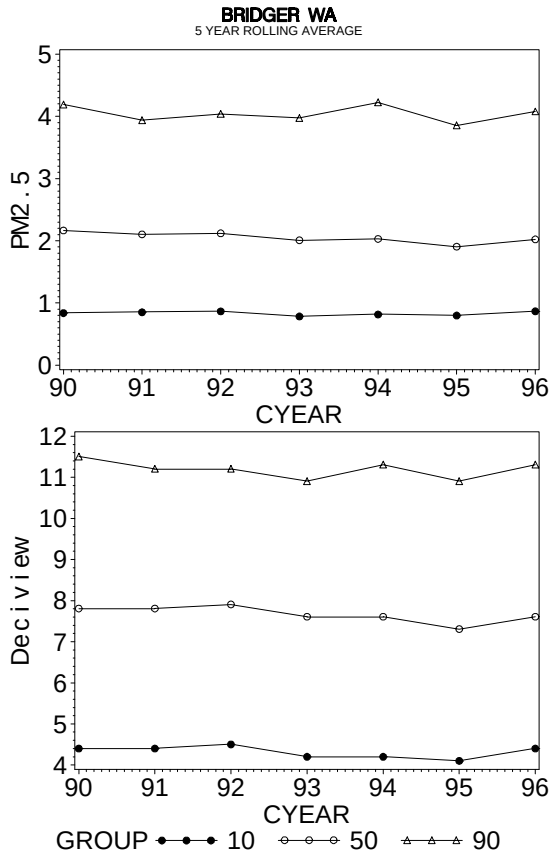
BRIDGER WA
5 YEAR ROLLING AVERAGE
PM2.5
CYEAR
Deciview
CYEAR
GROUP 10 50 90

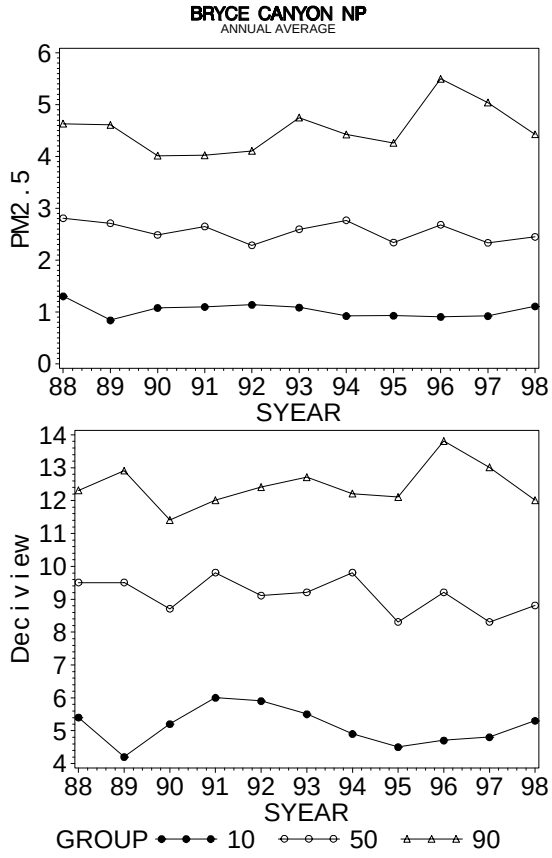
BRYCE CANYON NP
ANNUAL AVERAGE
PM2.5
SYEAR
Deciview
SYEAR
GROUP 10 50 90

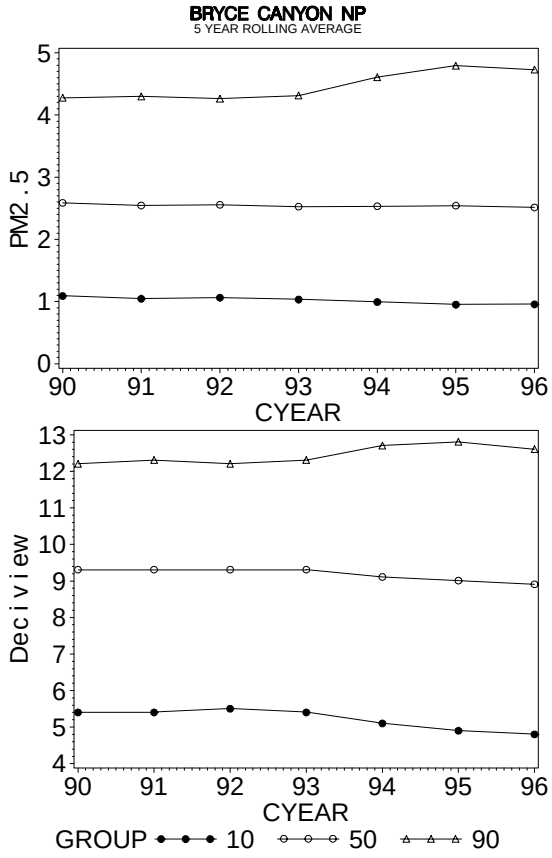
BRYCE CANYON NP
5 YEAR ROLLING AVERAGE
PM2.5
CYEAR
Deciview
CYEAR
GROUP 10 50 90

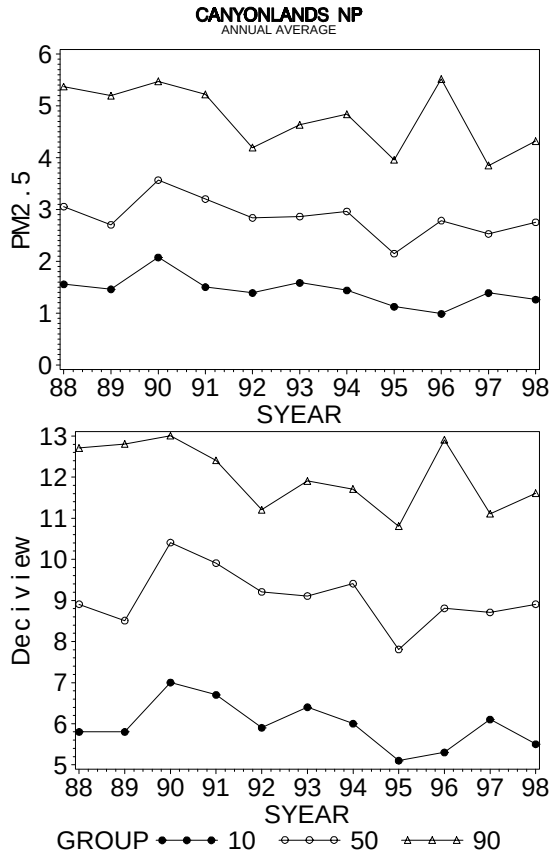
CANYONLANDS NP
ANNUAL AVERAGE
PM2.5
SYEAR
Deciview
SYEAR
GROUP 10 50 90

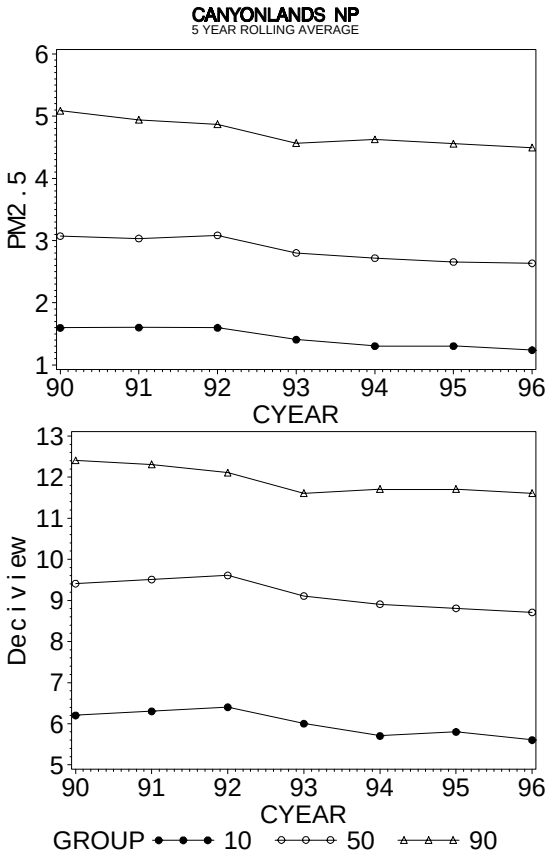
CANYONLANDS NP
5 YEAR ROLLING AVERAGE
PM2.5
CYEAR
Deciview
CYEAR
GROUP 10 50 90

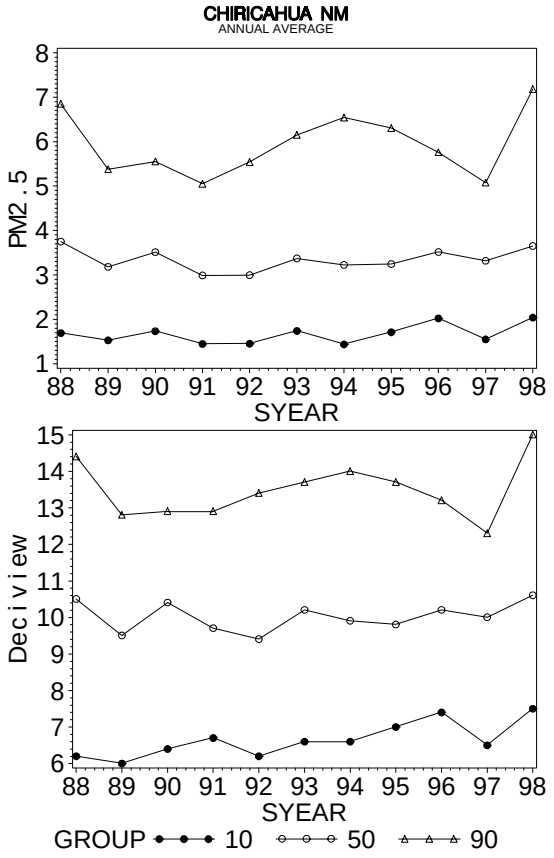
CHIRICAHUA NM
ANNUAL AVERAGE
PM2.5
SYEAR
Deciview
SYEAR
GROUP 10 50 90

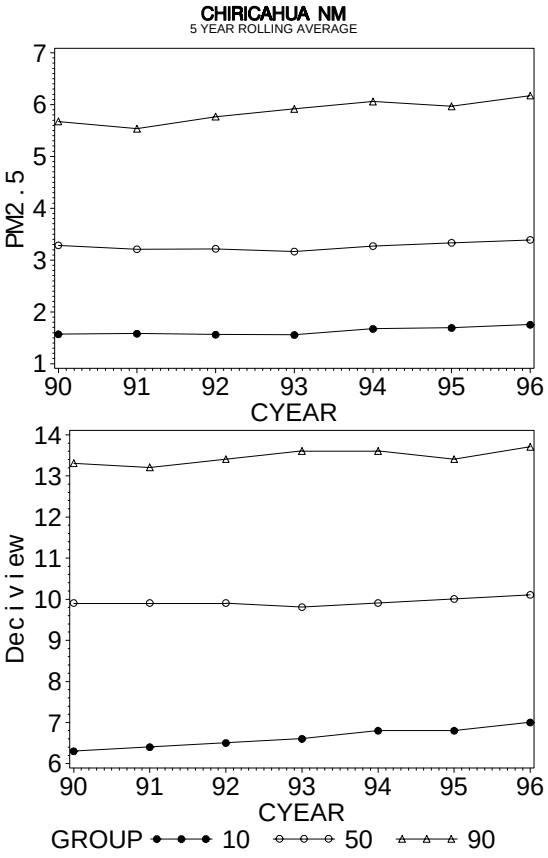
CHIRICAHUA NM
5 YEAR ROLLING AVERAGE
PM2.5
CYEAR
Deciview
CYEAR
GROUP 10 50 90

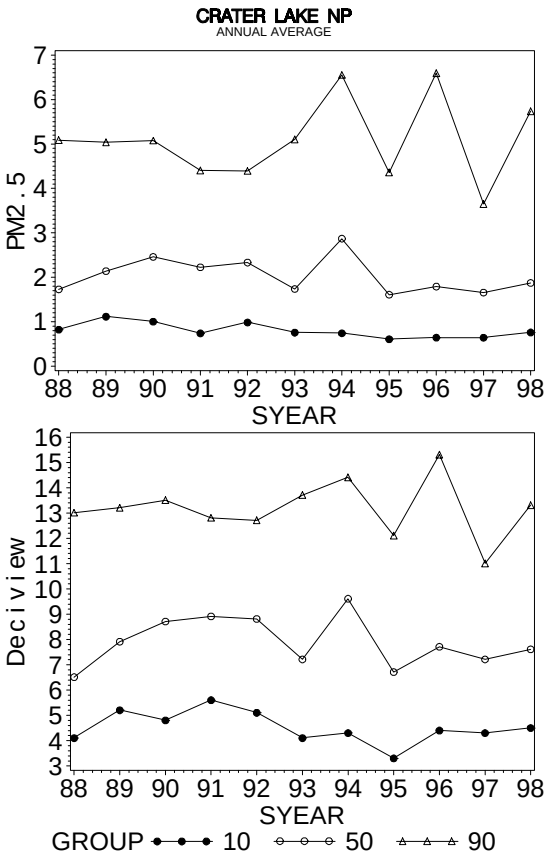
CRATER LAKE NP
ANNUAL AVERAGE
PM2.5
SYEAR
Decivview
SYEAR
GROUP 10 50 90

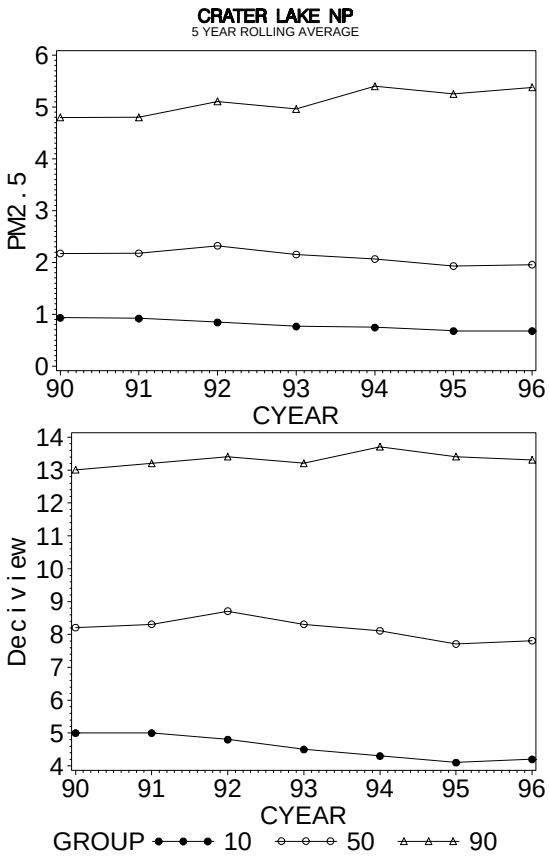
CRATER LAKE NP
5 YEAR ROLLING AVERAGE
PM2.5
CYEAR
Decivview
CYEAR
GROUP 10 50 90

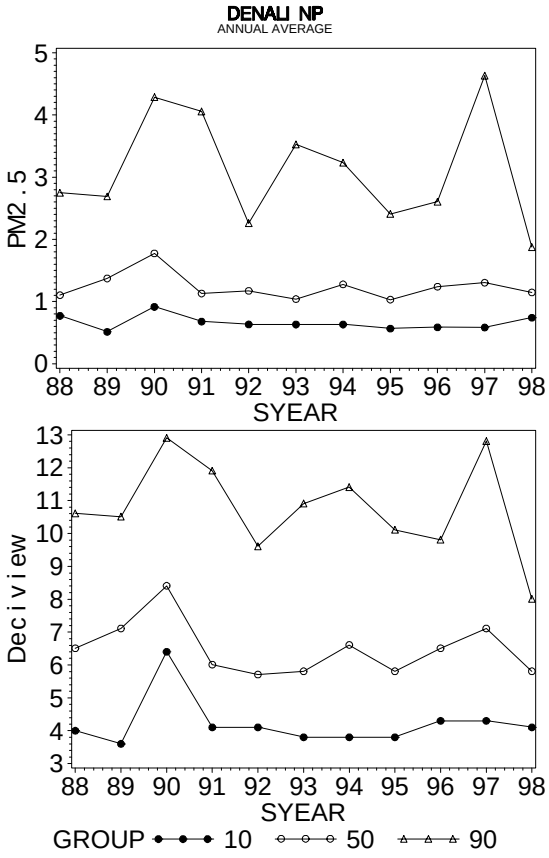
DENALI NP
ANNUAL AVERAGE
PM2.5
SYEAR
Decivview
SYEAR
GROUP 10 50 90

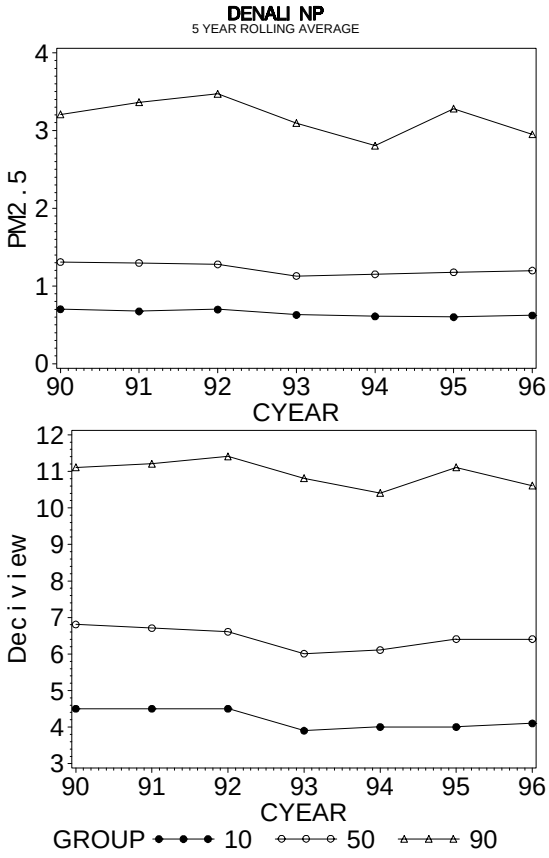
DENALI NP
5 YEAR ROLLING AVERAGE
PM2.5
CYEAR
Decivview
CYEAR
GROUP 10 50 90

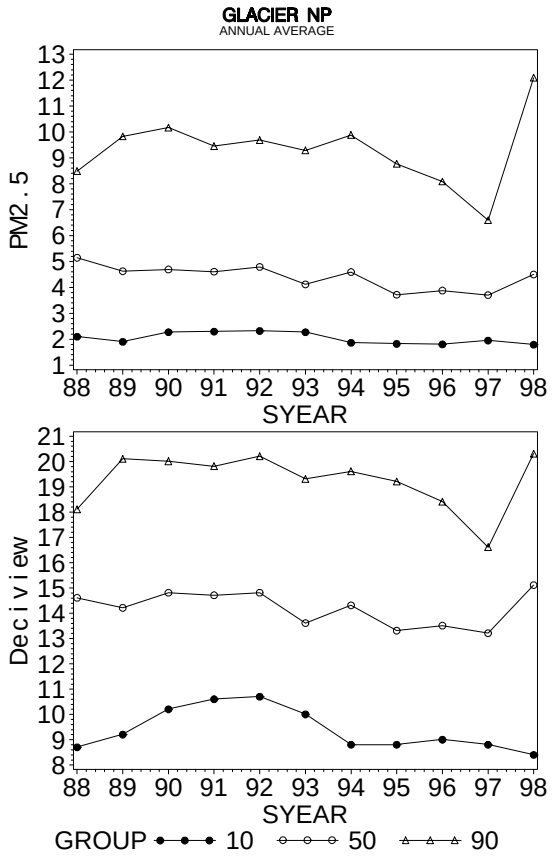
GLACIER NP
ANNUAL AVERAGE
PM2.5
SYEAR
Deciview
SYEAR
GROUP 10 50 90

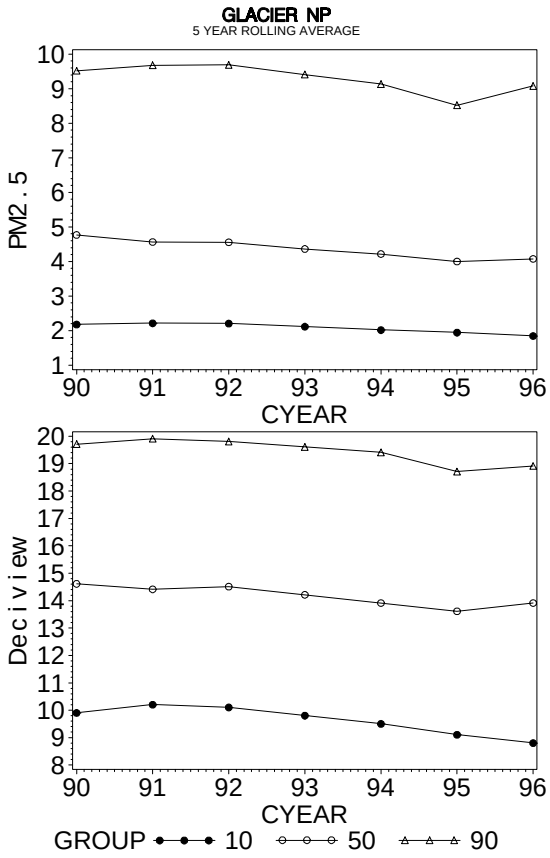
GLACIER NP
5 YEAR ROLLING AVERAGE
PM2.5
CYEAR
Deciview
CYEAR
GROUP 10 50 90

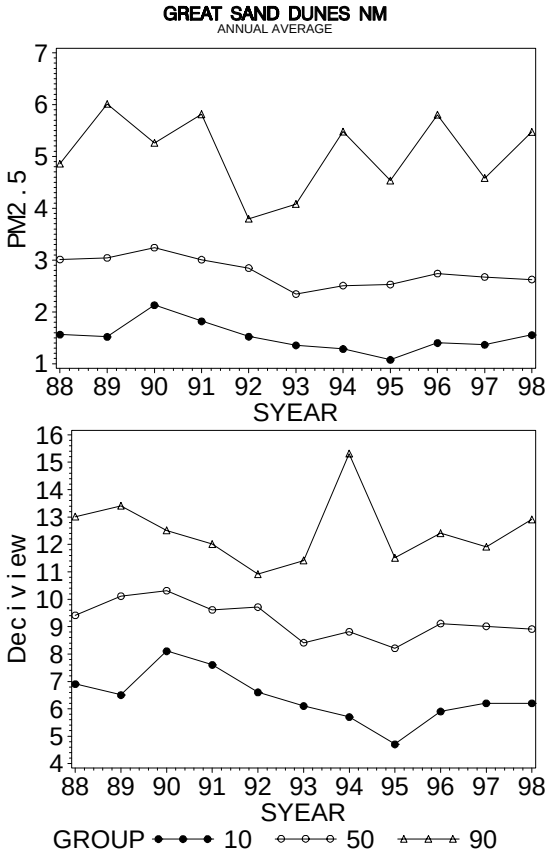
GREAT SAND DUNES NM
ANNUAL AVERAGE
PM2.5
SYEAR
Deciview
SYEAR
GROUP 10 50 90

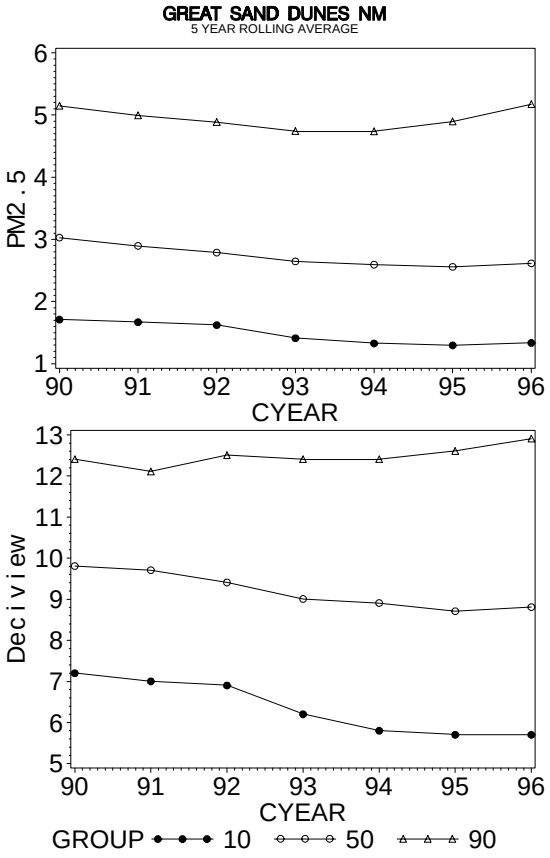
GREAT SAND DUNES NM
5 YEAR ROLLING AVERAGE
PM2.5
CYEAR
Deciview
CYEAR
GROUP 10 50 90

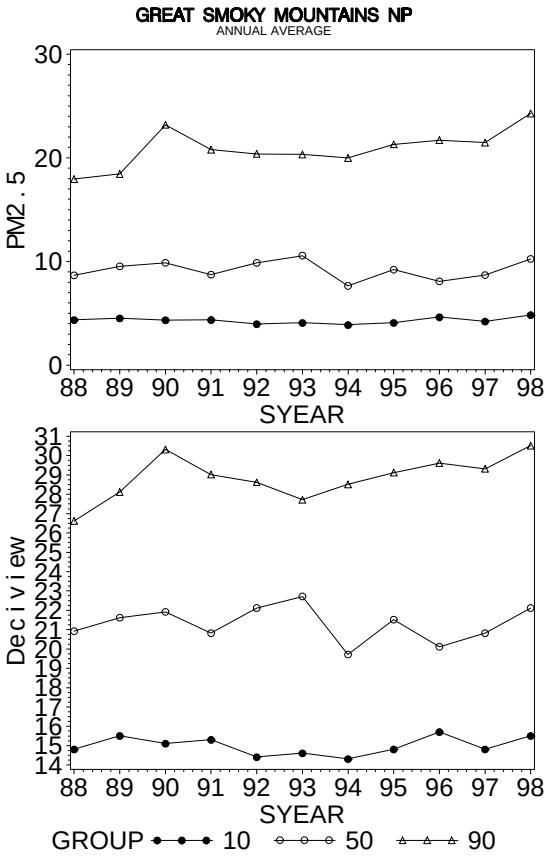
GREAT SMOKY MOUNTAINS NP
ANNUAL AVERAGE
PM2.5
SYEAR
Deciview
SYEAR
GROUP 10 50 90

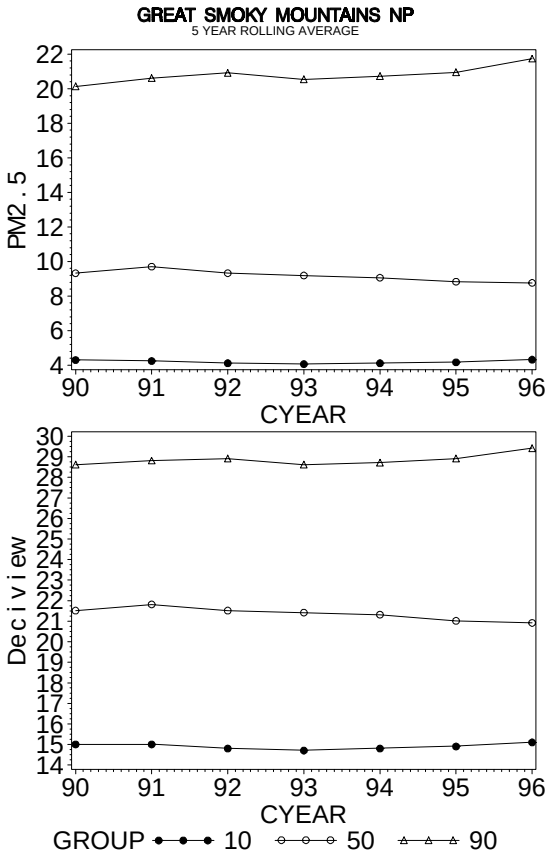
GREAT SMOKY MOUNTAINS NP
5 YEAR ROLLING AVERAGE
PM2.5
CYEAR
Deciview
CYEAR
GROUP 10 50 90

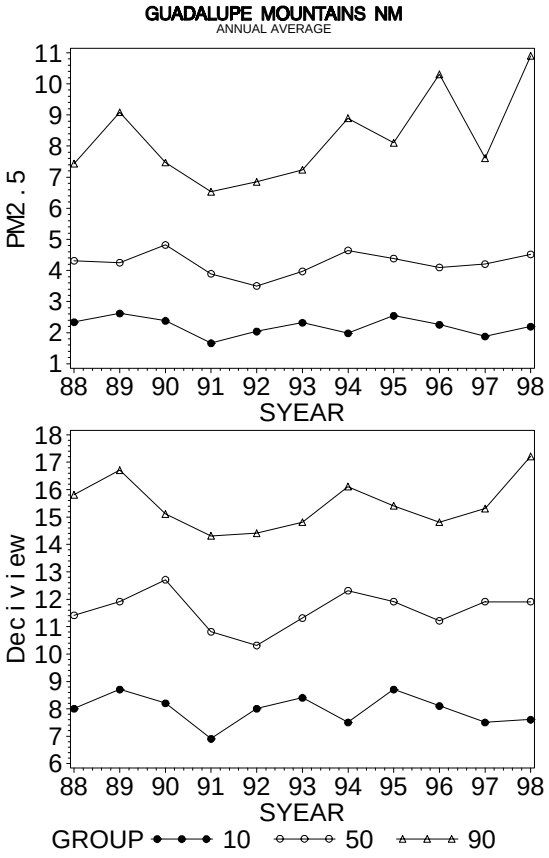
GUADALUPE MOUNTAINS NM
ANNUAL AVERAGE
PM2.5
SYEAR
Deciview
SYEAR
GROUP 10 50 90

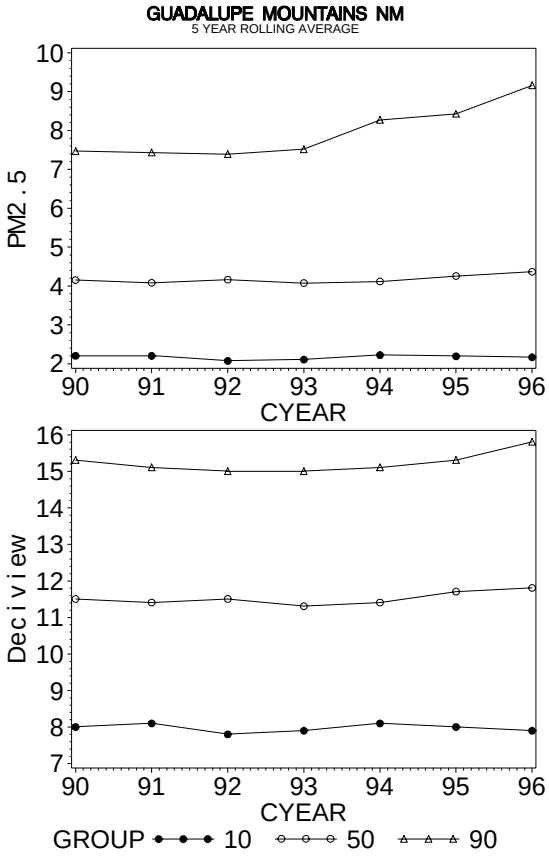
GUADALUPE MOUNTAINS NM
5 YEAR ROLLING AVERAGE
PM2.5
CYEAR
Deciview
CYEAR
GROUP 10 50 90

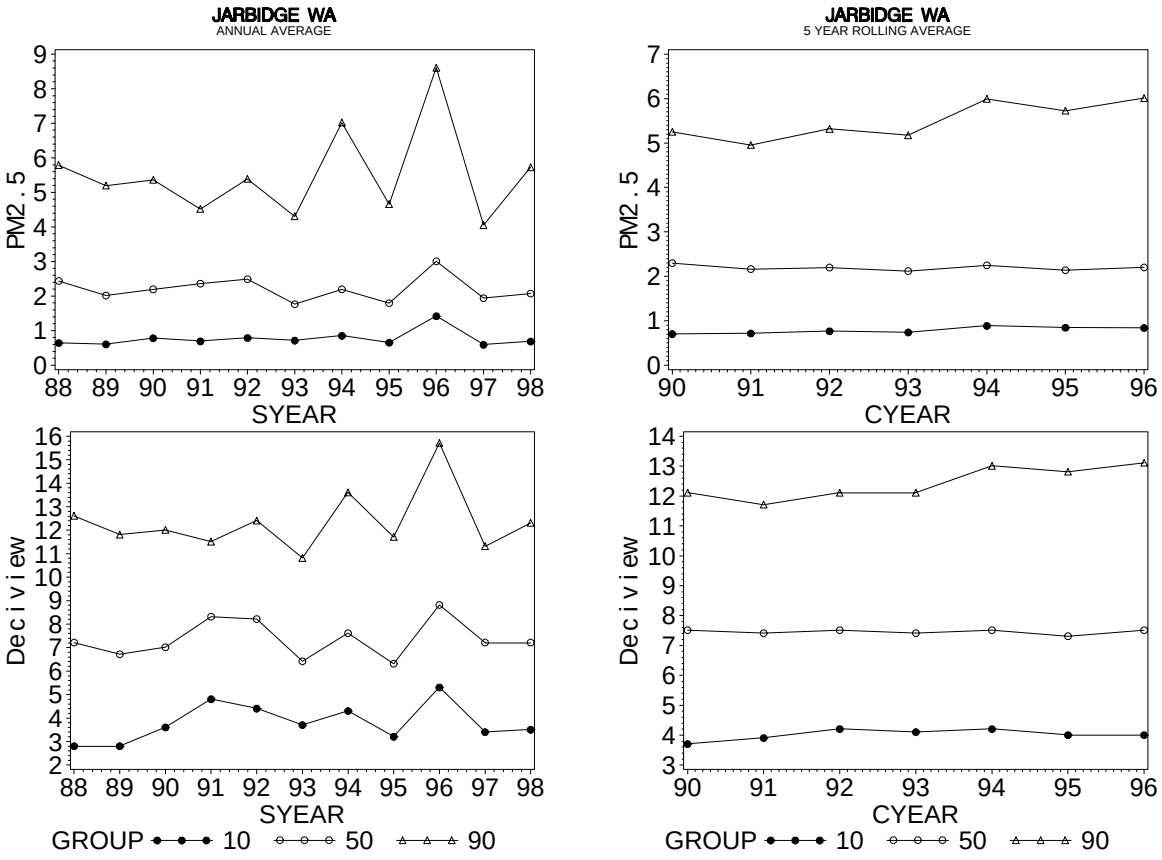
JARBIDGE WA
ANNUAL AVERAGE
PM2.5
SYEAR
Deciview
SYEAR
GROUP 10 50 90

JARBIDGE WA
5 YEAR ROLLING AVERAGE
PM2.5
CYEAR
Deciview
CYEAR
GROUP 10 50 90

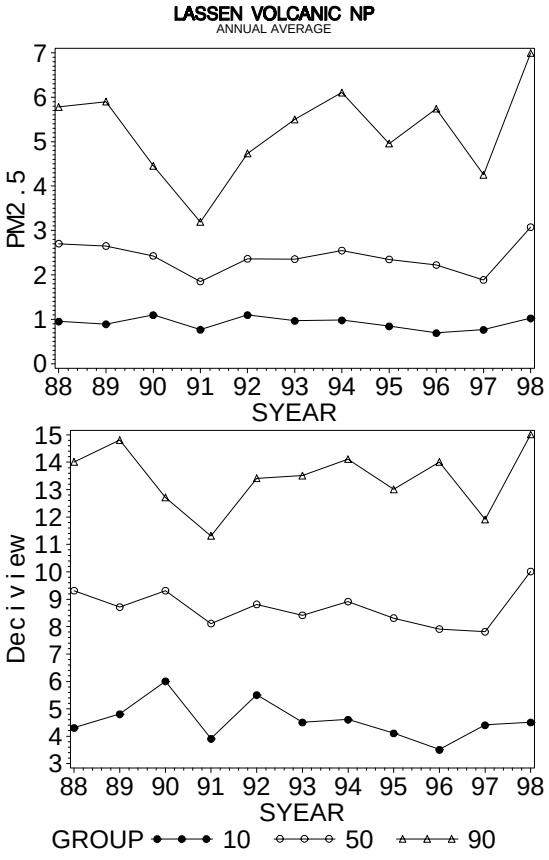
LASSEN VOLCANIC NP
ANNUAL AVERAGE
PM2.5
SYEAR
Deciview
SYEAR
GROUP 10 50 90

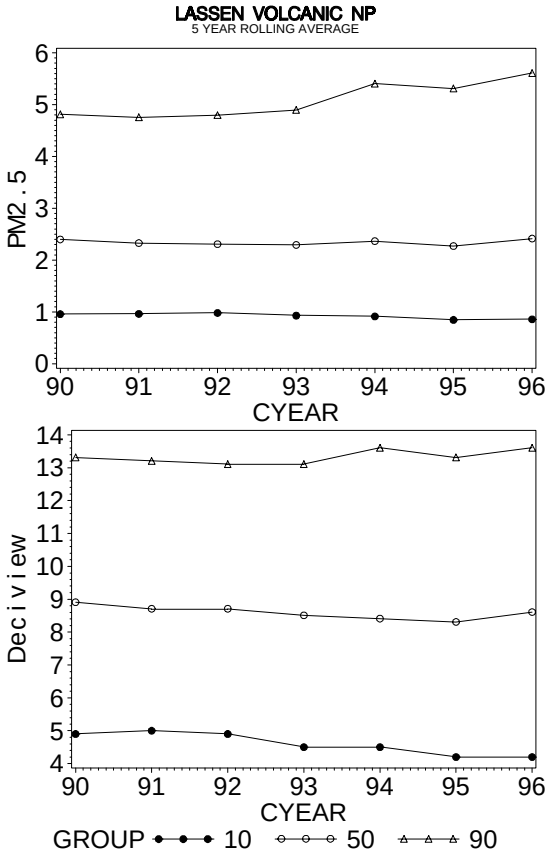
LASSEN VOLCANIC NP
5 YEAR ROLLING AVERAGE
PM2.5
CYEAR
Deciview
CYEAR
GROUP 10 50 90

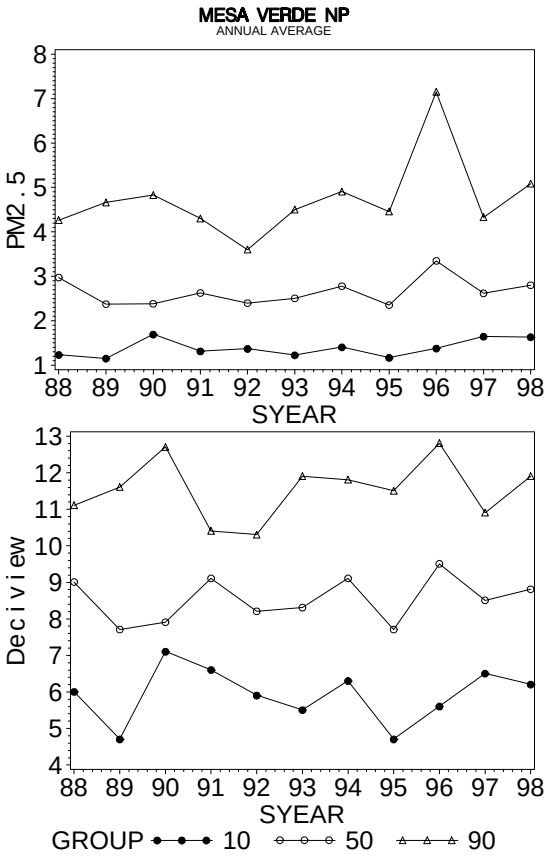
MESA VERDE NP
ANNUAL AVERAGE
PM2.5
SYEAR
Deciview
SYEAR
GROUP 10 50 90

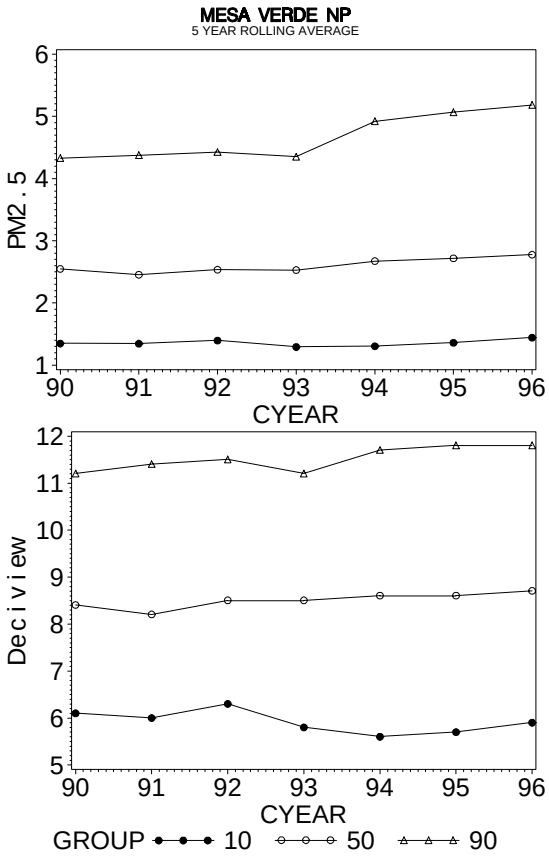
MESA VERDE NP
5 YEAR ROLLING AVERAGE
PM2.5
CYEAR
Deciview
CYEAR
GROUP 10 50 90

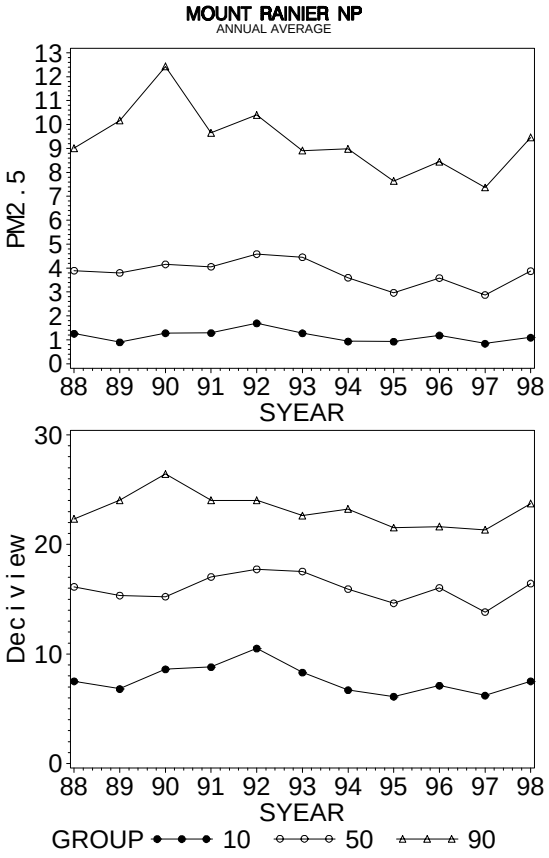
MOUNT RAINIER NP
ANNUAL AVERAGE
PM2.5
SYEAR
Deciview
SYEAR
GROUP 10 50 90

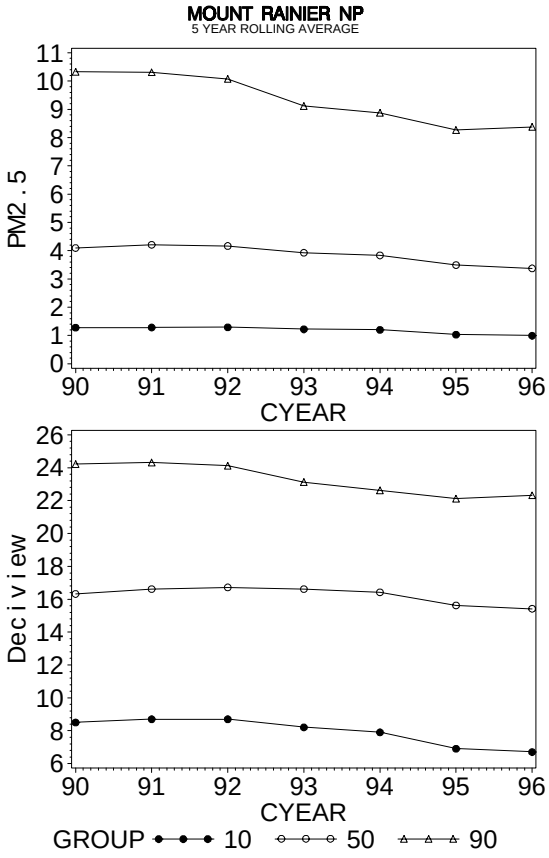
MOUNT RAINIER NP
5 YEAR ROLLING AVERAGE
PM2.5
CYEAR
Deciview
CYEAR
GROUP 10 50 90

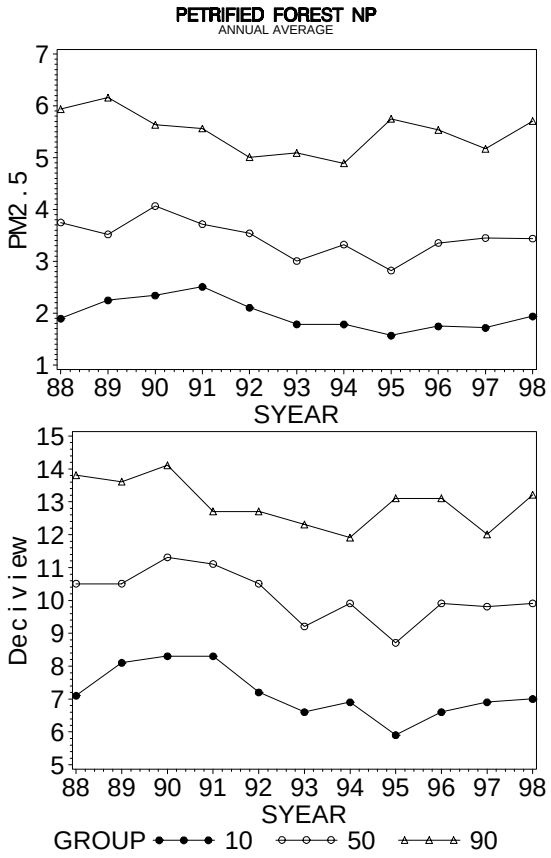
PETRIFIED FOREST NP
ANNUAL AVERAGE
PM2.5
SYEAR
Deciview
SYEAR
GROUP 10 50 90

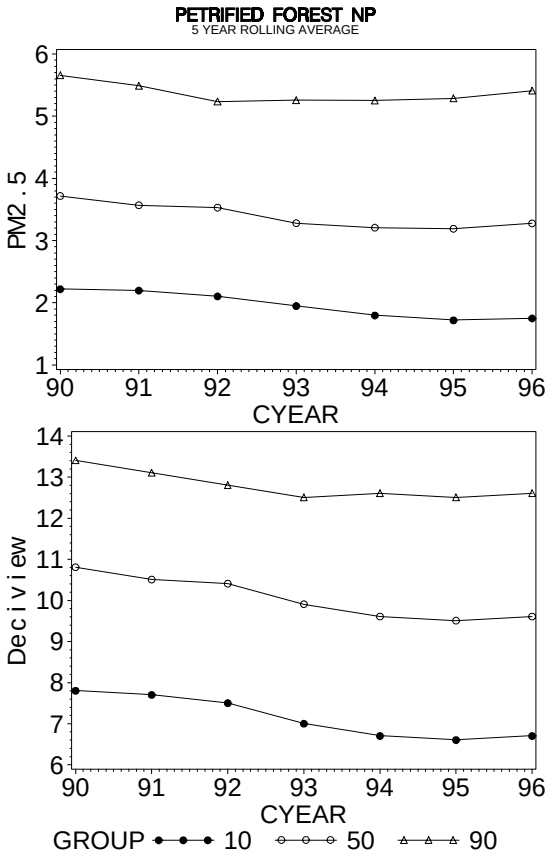
PETRIFIED FOREST NP
5 YEAR ROLLING AVERAGE
PM2.5
CYEAR
Deciview
CYEAR
GROUP 10 50 90

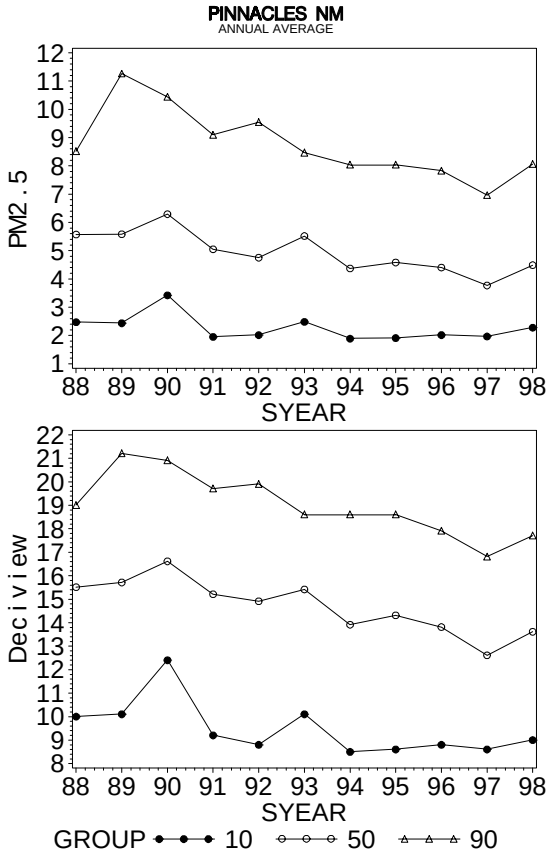
PINNACLES NM
ANNUAL AVERAGE
PM2.5
SYEAR
Deciview
SYEAR
GROUP 10 50 90

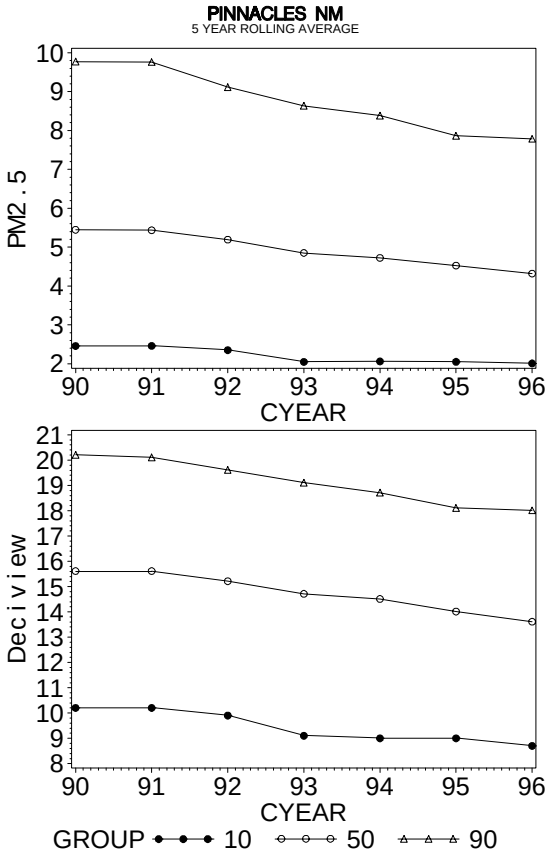
PINNACLES NM
5 YEAR ROLLING AVERAGE
PM2.5
CYEAR
Deciview
CYEAR
GROUP 10 50 90

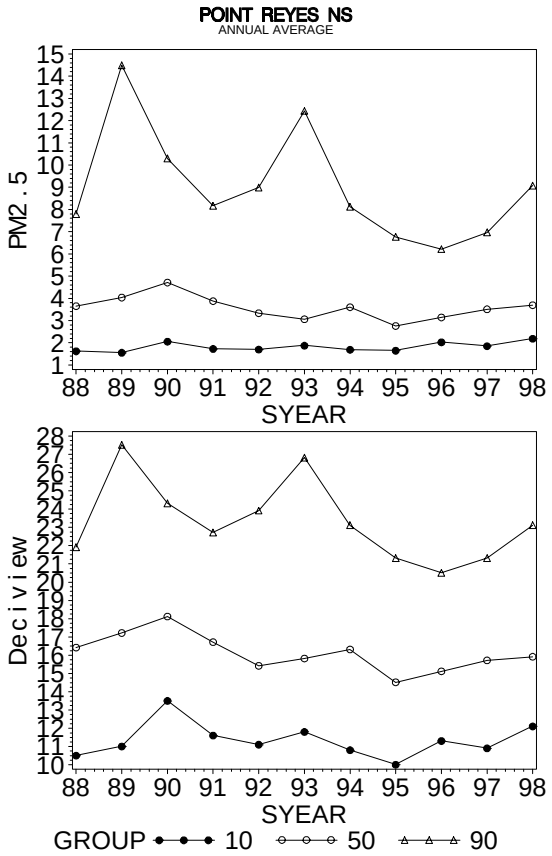
POINT REYES NS
ANNUAL AVERAGE
PM2.5
SYEAR
Deciview
SYEAR
GROUP 10 50 90

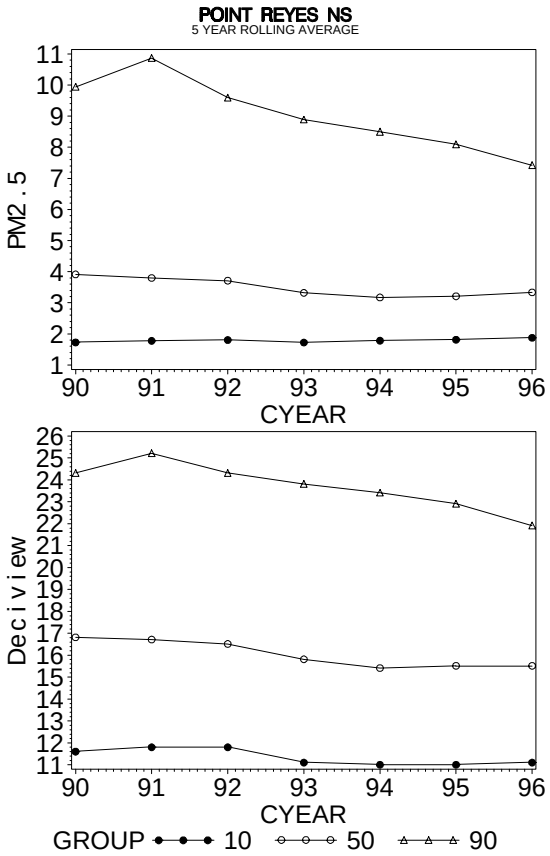
POINT REYES NS
5 YEAR ROLLING AVERAGE
PM2.5
CYEAR
Deciview
CYEAR
GROUP 10 50 90

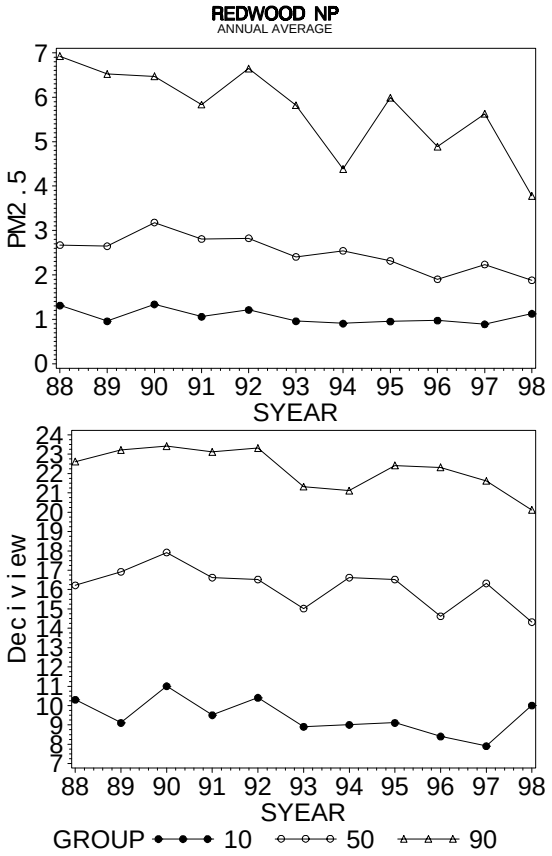
REDWOOD NP
ANNUAL AVERAGE
PM2.5
SYEAR
Deciview
SYEAR
GROUP 10 50 90

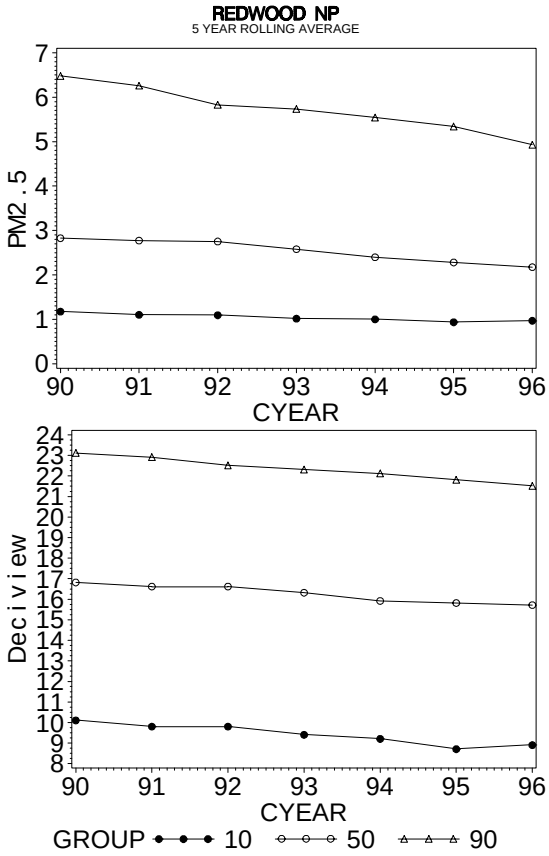
REDWOOD NP
5 YEAR ROLLING AVERAGE
PM2.5
CYEAR
Deciview
CYEAR
GROUP 10 50 90

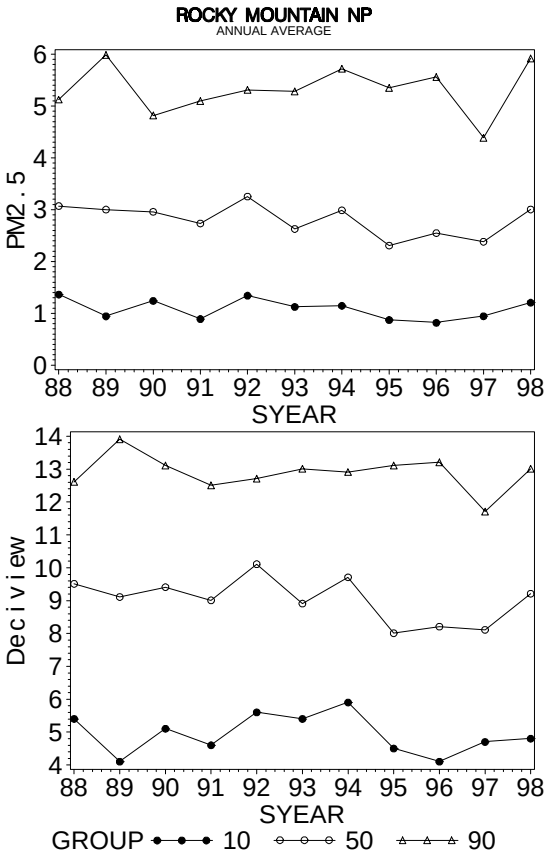
ROCKY MOUNTAIN NP
ANNUAL AVERAGE
PM2.5
SYEAR
Deciview
SYEAR
GROUP 10 50 90

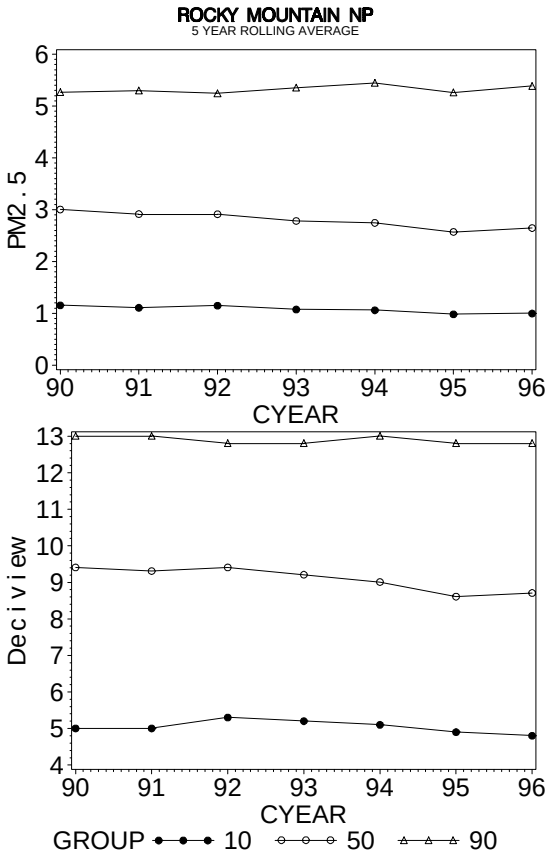
ROCKY MOUNTAIN NP
5 YEAR ROLLING AVERAGE
PM2.5
CYEAR
Deciview
CYEAR
GROUP 10 50 90

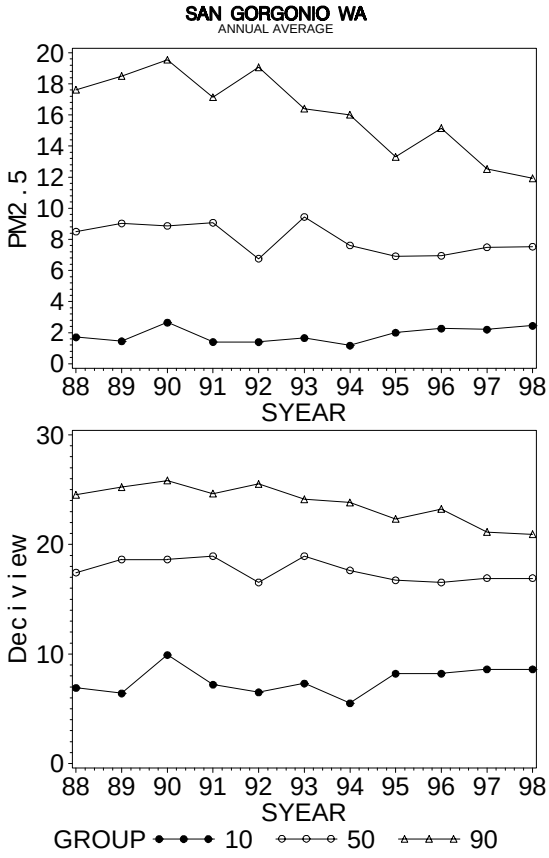
SAN GORGONIO WA
ANNUAL AVERAGE
PM2.5
SYEAR
Deciview
SYEAR
GROUP 10 50 90

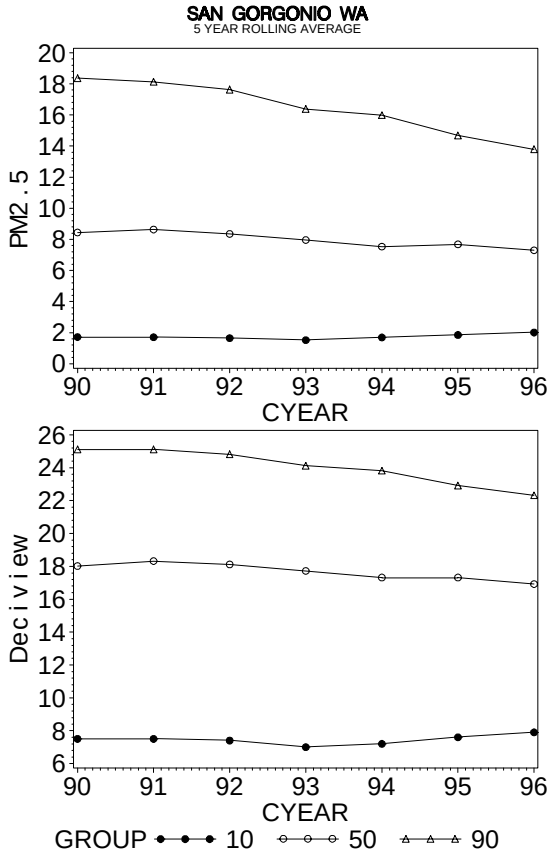
SAN GORGONIO WA
5 YEAR ROLLING AVERAGE
PM2.5
CYEAR
Deciview
CYEAR
GROUP 10 50 90

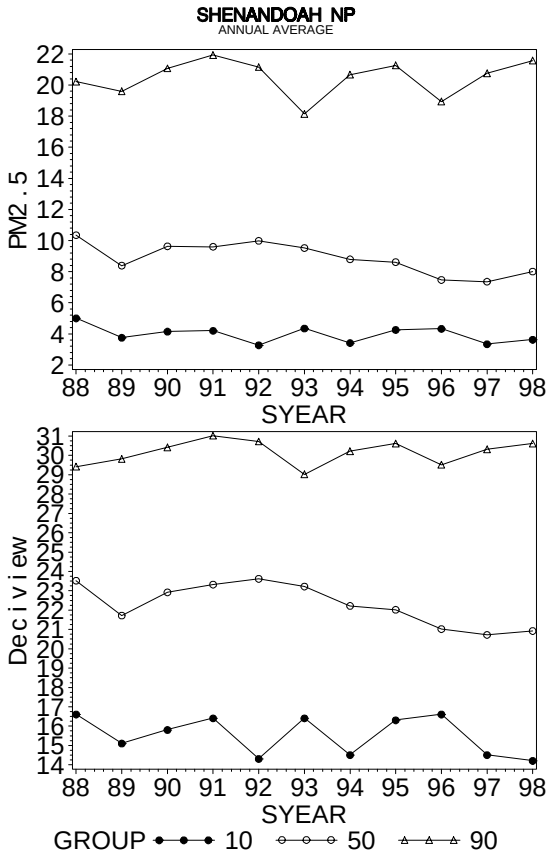
SHENANDOAH NP
ANNUAL AVERAGE
PM2.5
SYEAR
Deciview
SYEAR
GROUP 10 50 90

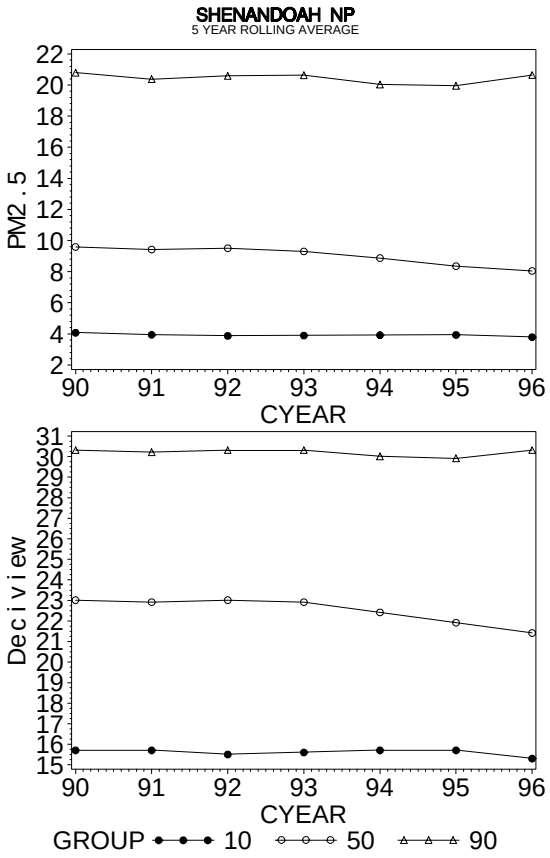
SHENANDOAH NP
5 YEAR ROLLING AVERAGE
PM2.5
CYEAR
Deciview
CYEAR
GROUP 10 50 90

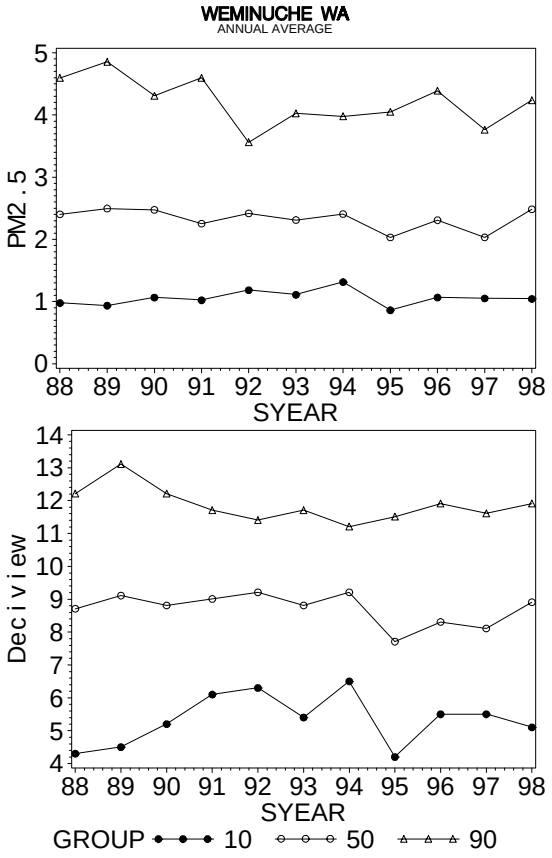
WEMINUCHE WA
ANNUAL AVERAGE
PM2.5
SYEAR
Deciview
SYEAR
GROUP 10 50 90

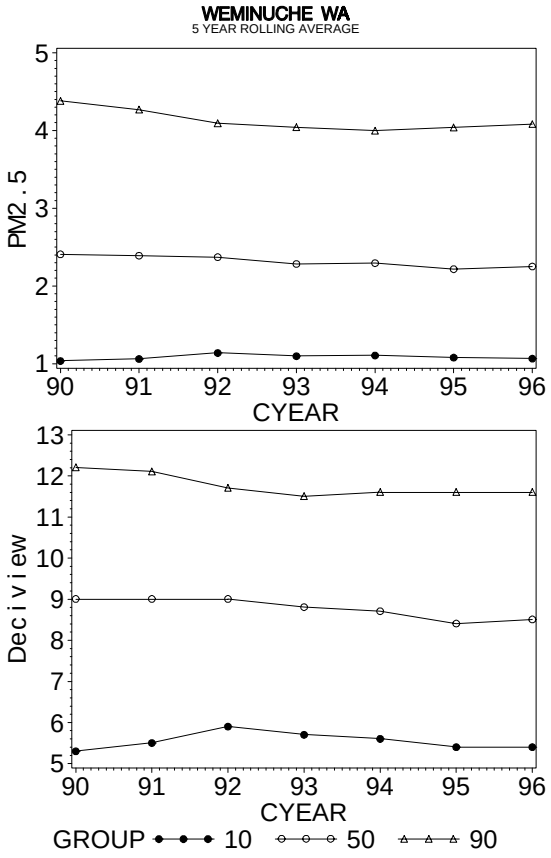
WEMINUCHE WA
5 YEAR ROLLING AVERAGE
PM2.5
CYEAR
Deciview
CYEAR
GROUP 10 50 90

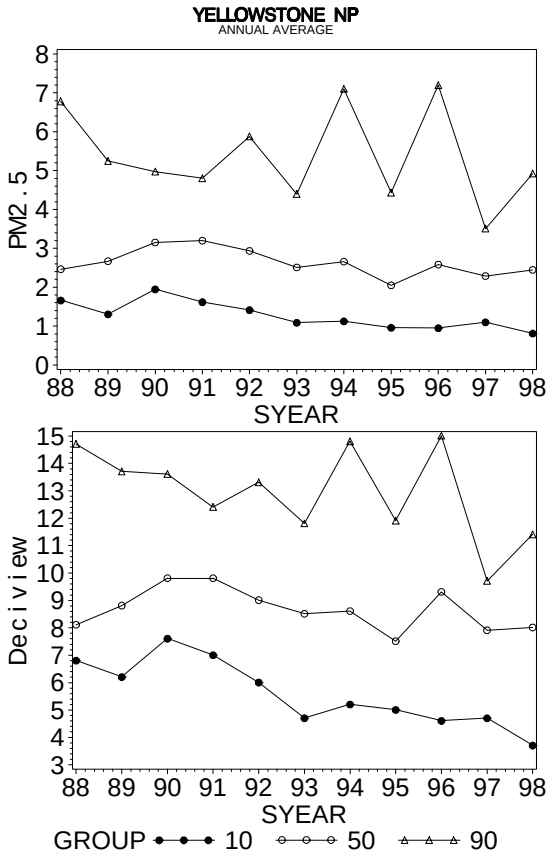
YELLOWSTONE NP
ANNUAL AVERAGE
PM2.5
SYEAR
Deciview
SYEAR
GROUP 10 50 90

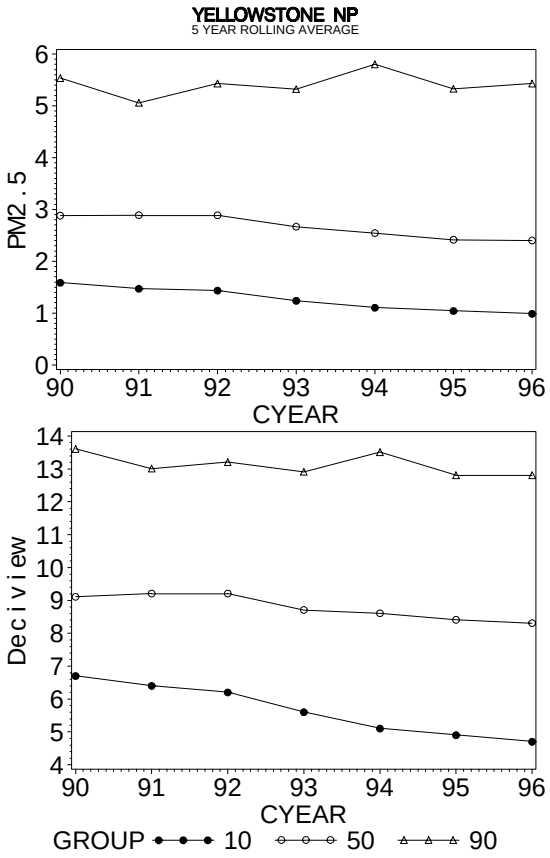
YELLOWSTONE NP
5 YEAR ROLLING AVERAGE
PM2.5
CYEAR
Deciview
CYEAR
GROUP 10 50 90

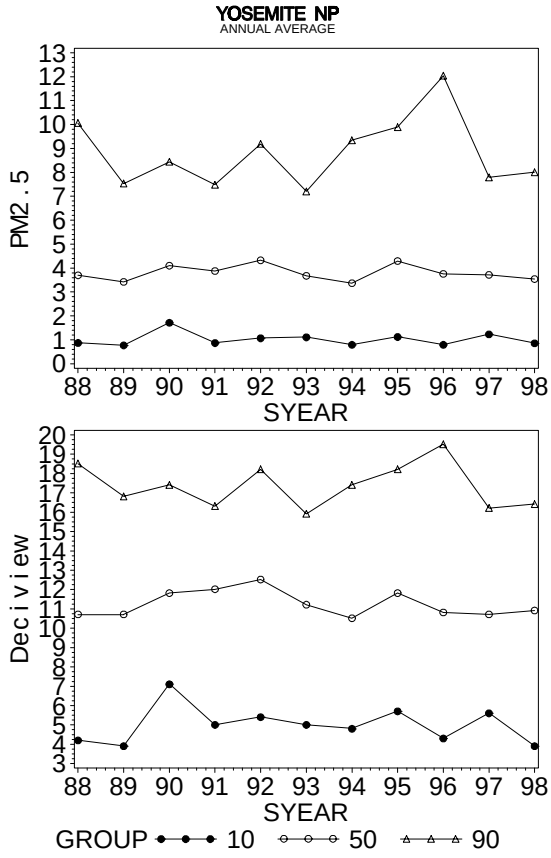
YOSEMITE NP
ANNUAL AVERAGE
PM2.5
SYEAR
Deciview
SYEAR
GROUP 10 50 90

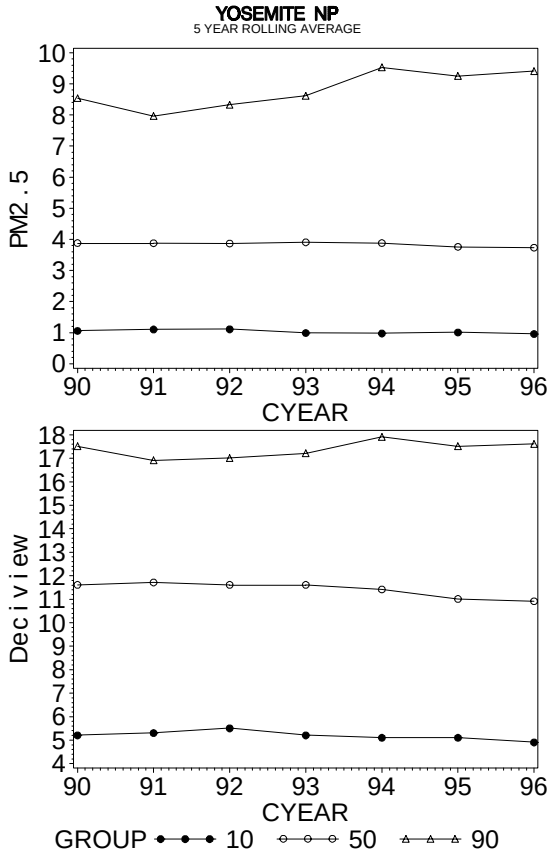
YOSEMITE NP
5 YEAR ROLLING AVERAGE
PM2.5
CYEAR
Deciview
CYEAR
GROUP 10 50 90

APPENDIX C

The maps contained in this appendix summarize the trends for group 90 (top 20% of fine mass) days. The icons mark the site locations, a solid dot indicates an insignificant slope, the empty arrow indicates a positive or negative slope that is significant in the range of $0.05<p\leq0.1$ level of probability, and the solid arrow indicates a positive or negative slope that is significant at better than 0.05 ($p\leq0.05$) level of probability.

ABSORPTION – Worst 20%

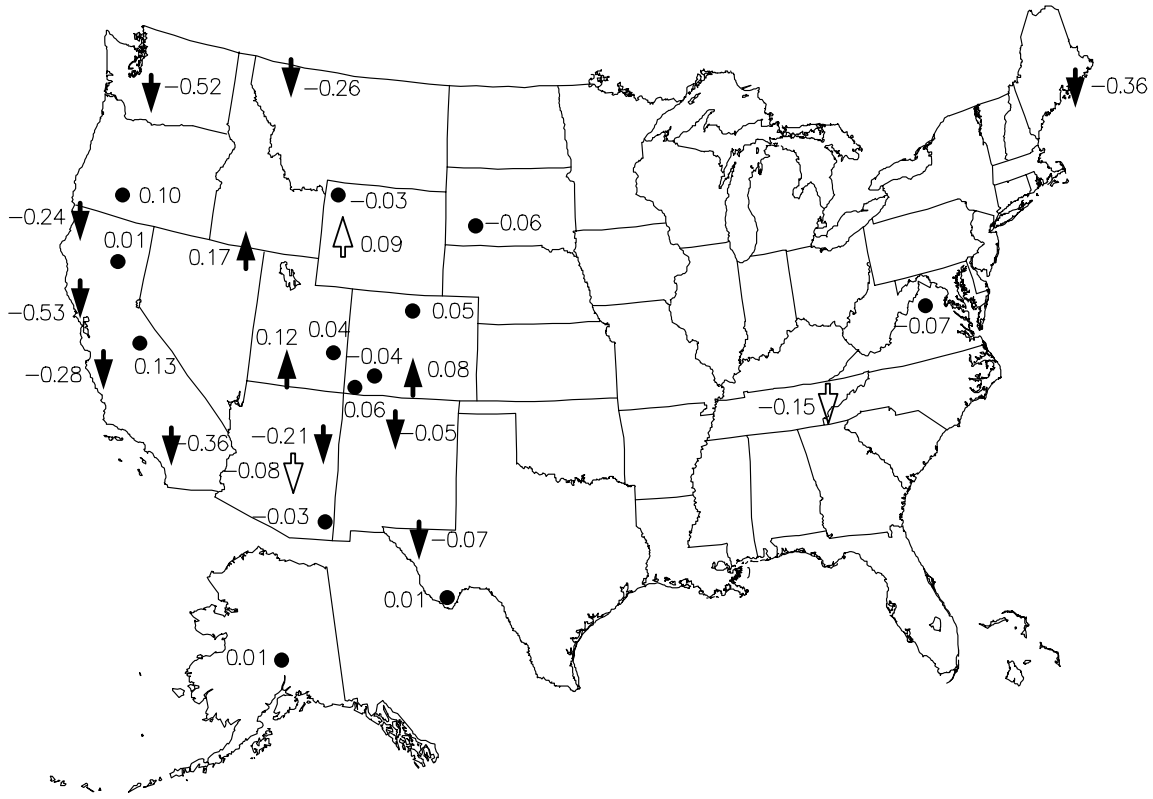

AEROSOL Bext – Worst 20%

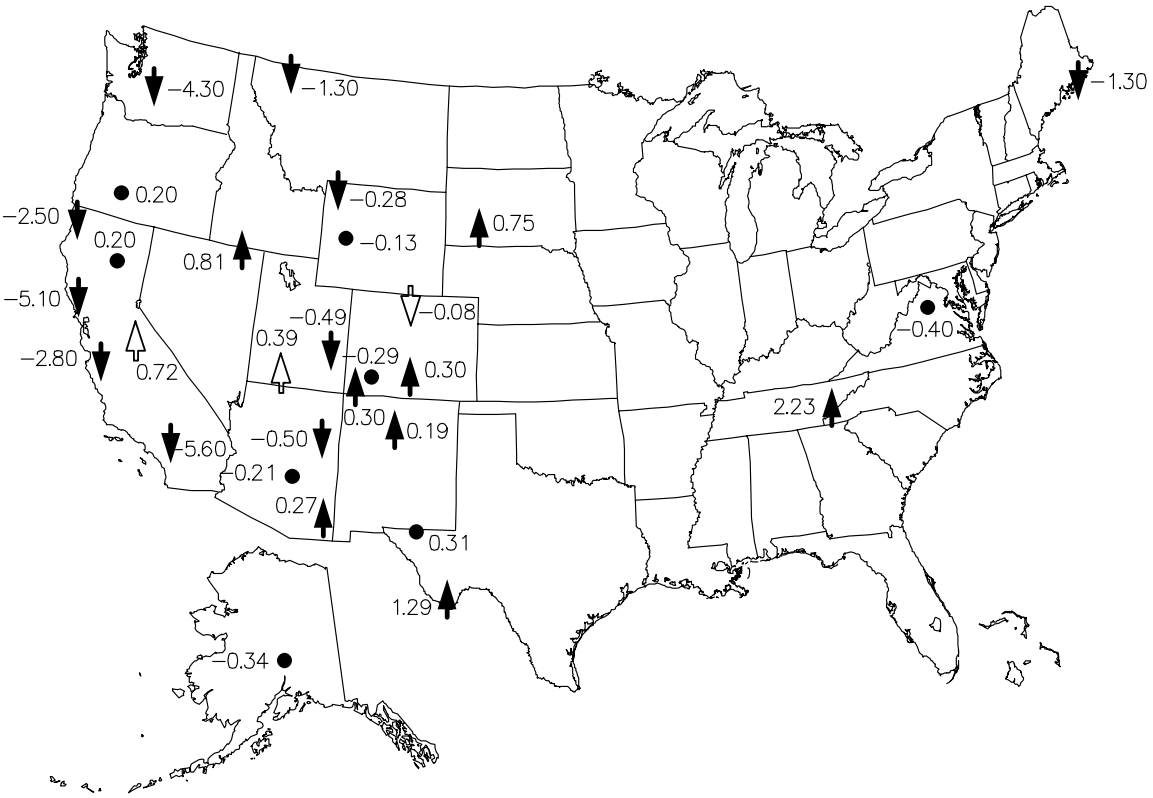

Coarse Mass – Worst 20%

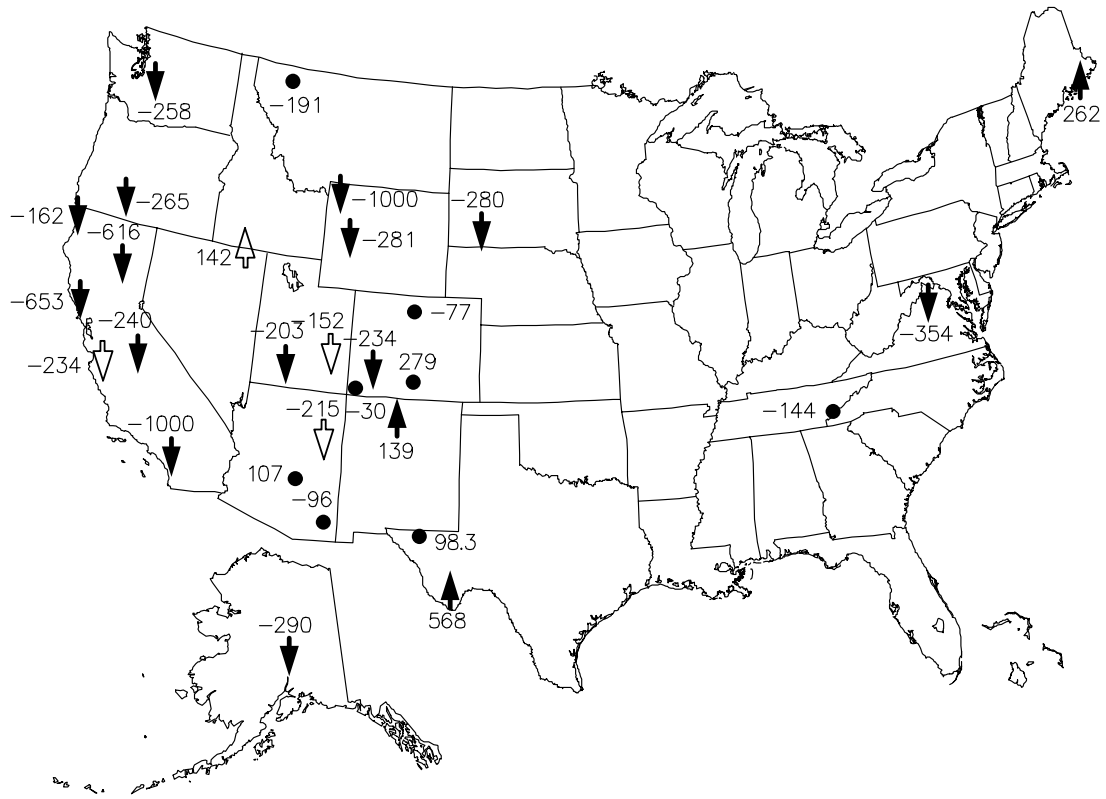

Deciview – Worst 20%

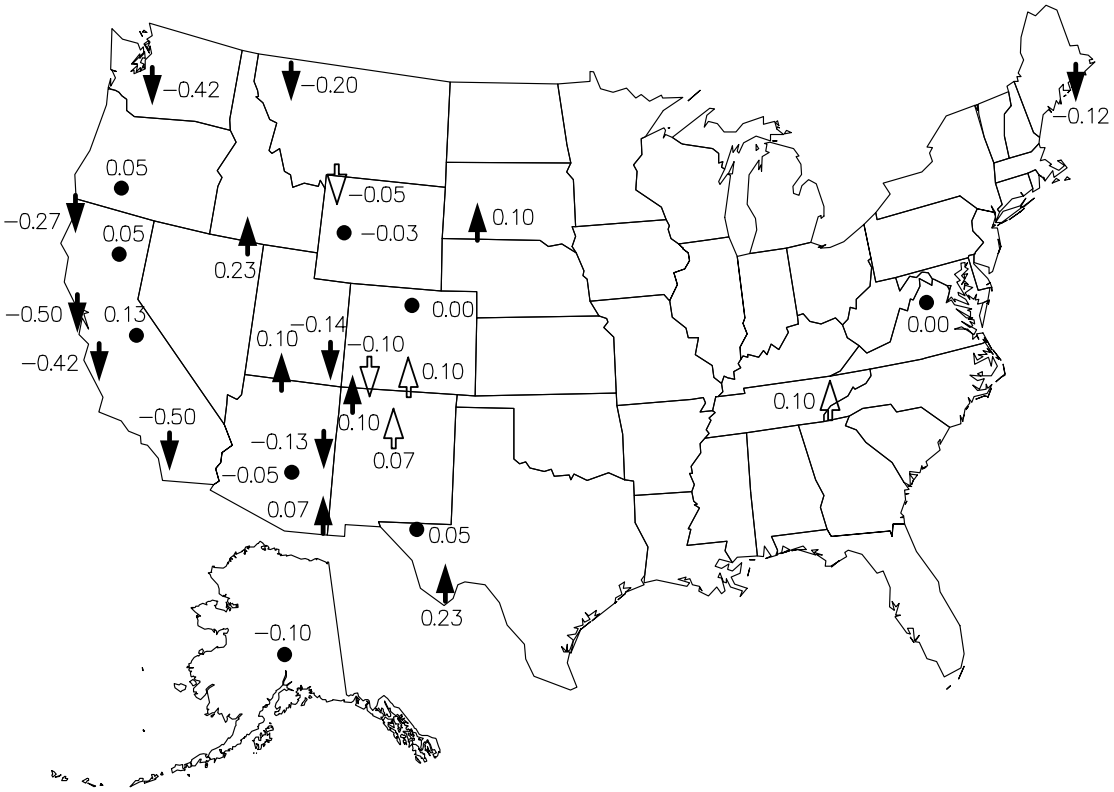

FINE + COARSE Bscat – Worst 20%

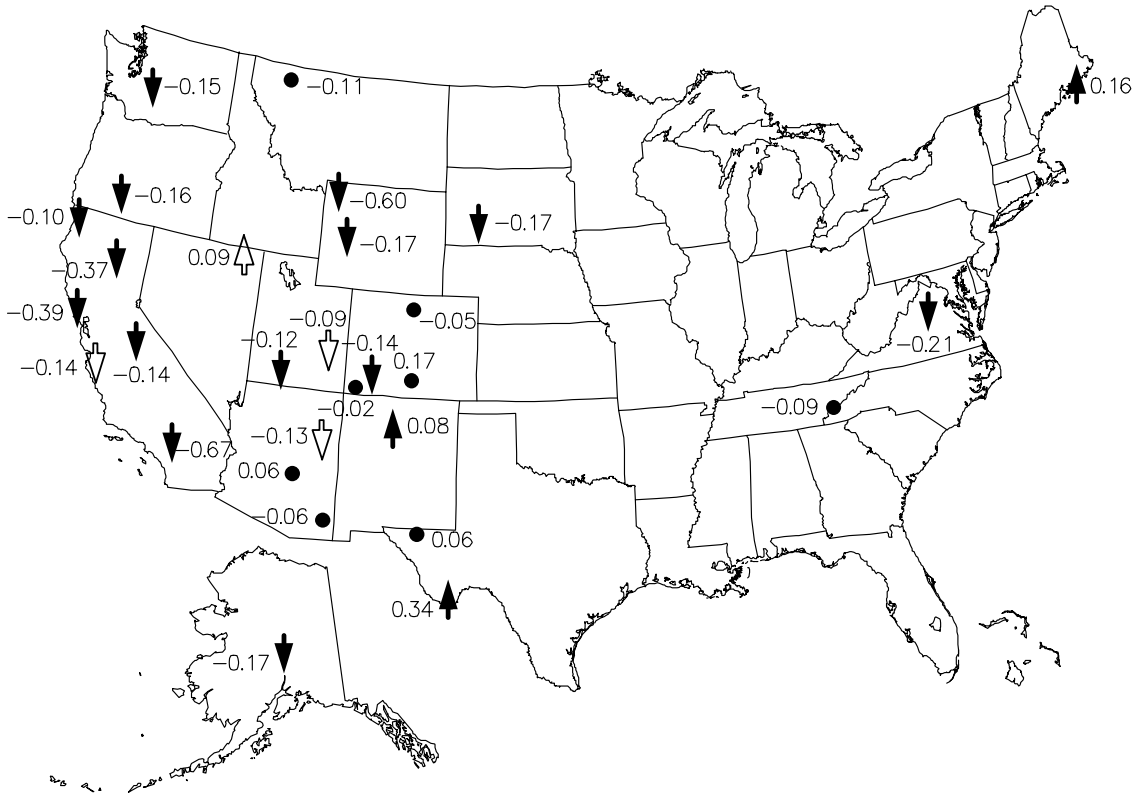

FINE MASS – Worst 20%

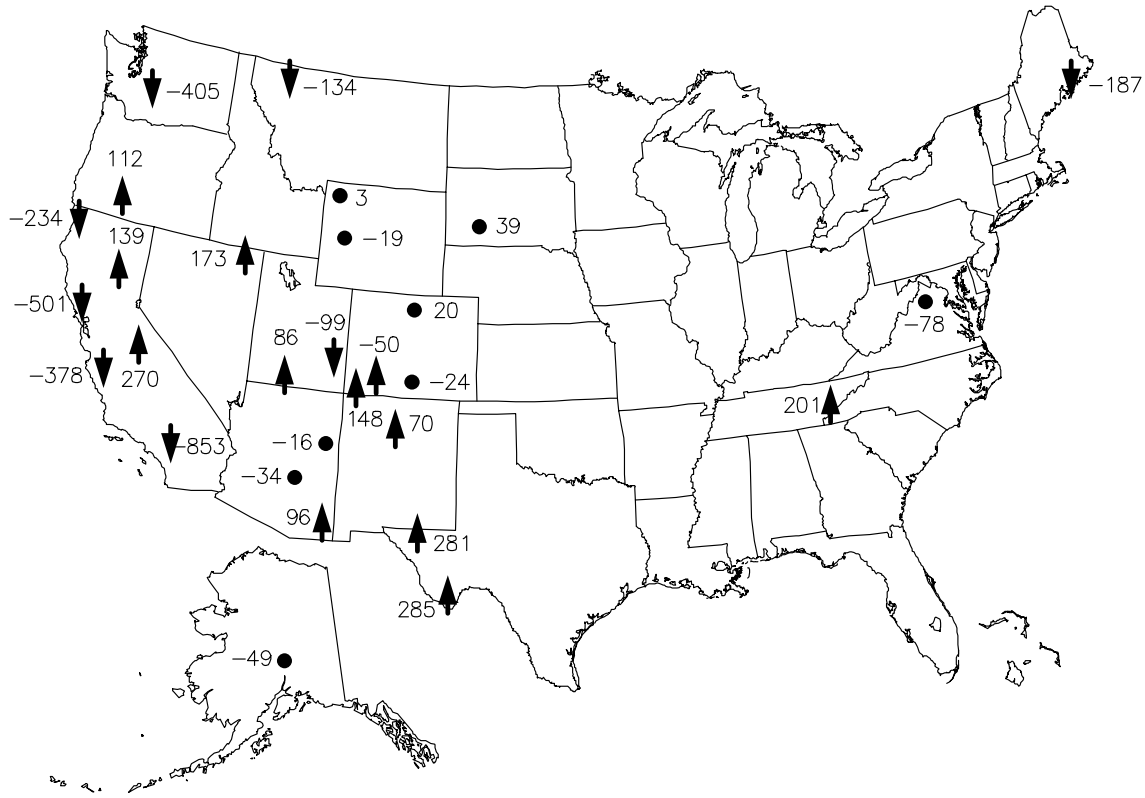

FINE SOIL – Worst 20%

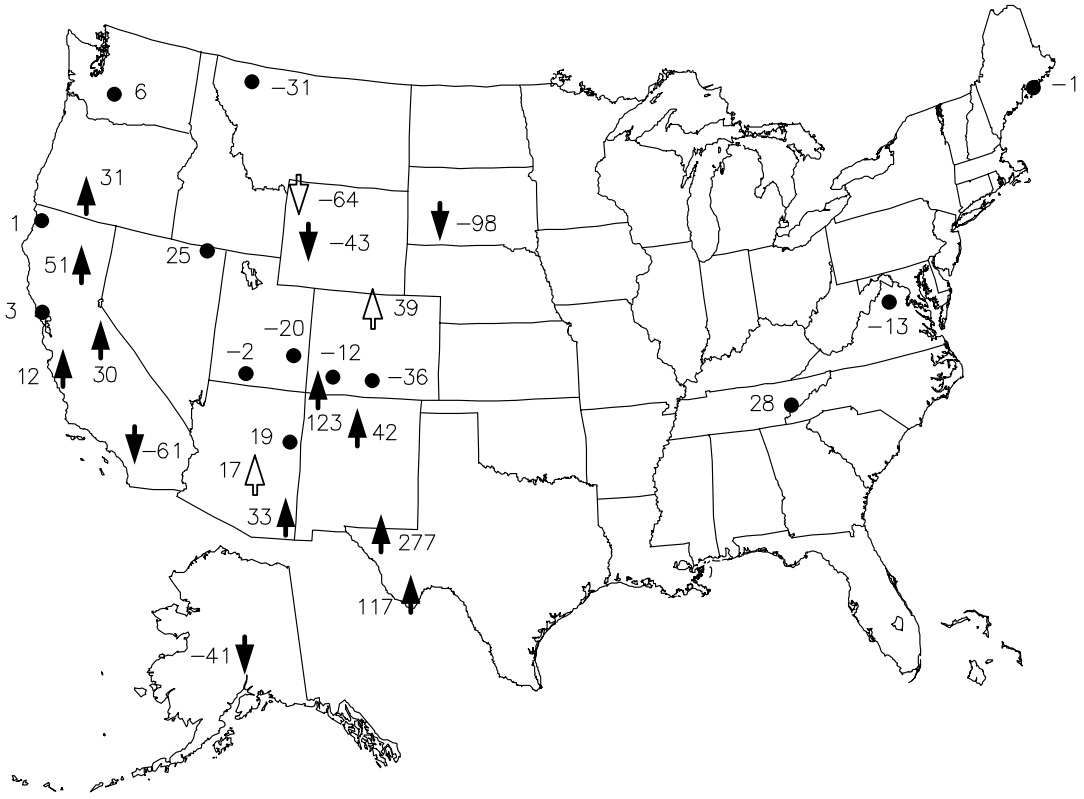

NITRATE – Worst 20%

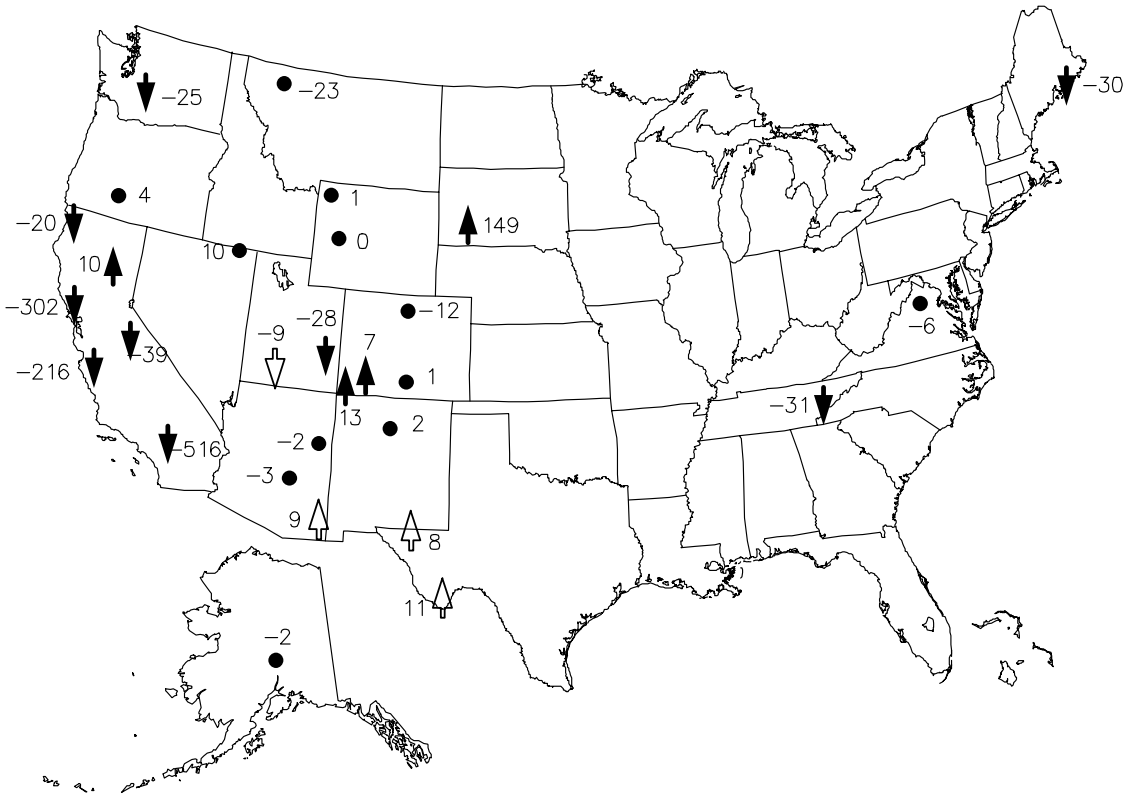

NITRATE Bscat – Worst 20%

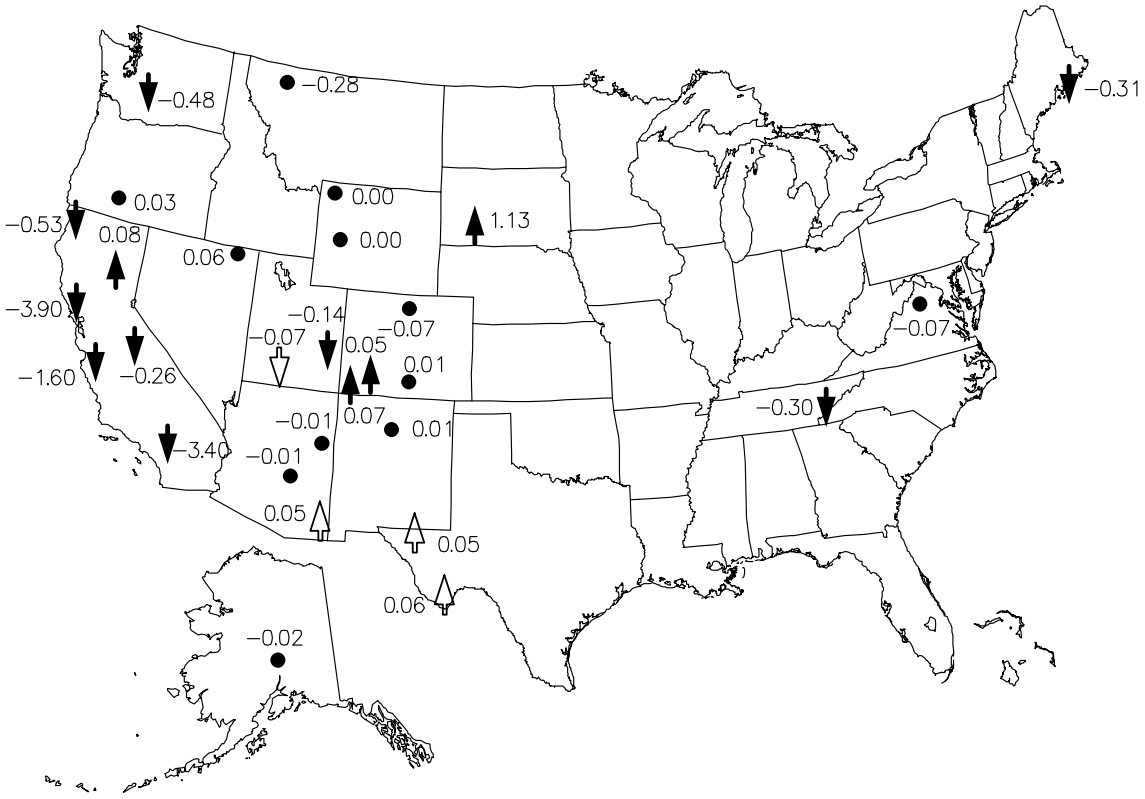

ORGANICS – Worst 20%

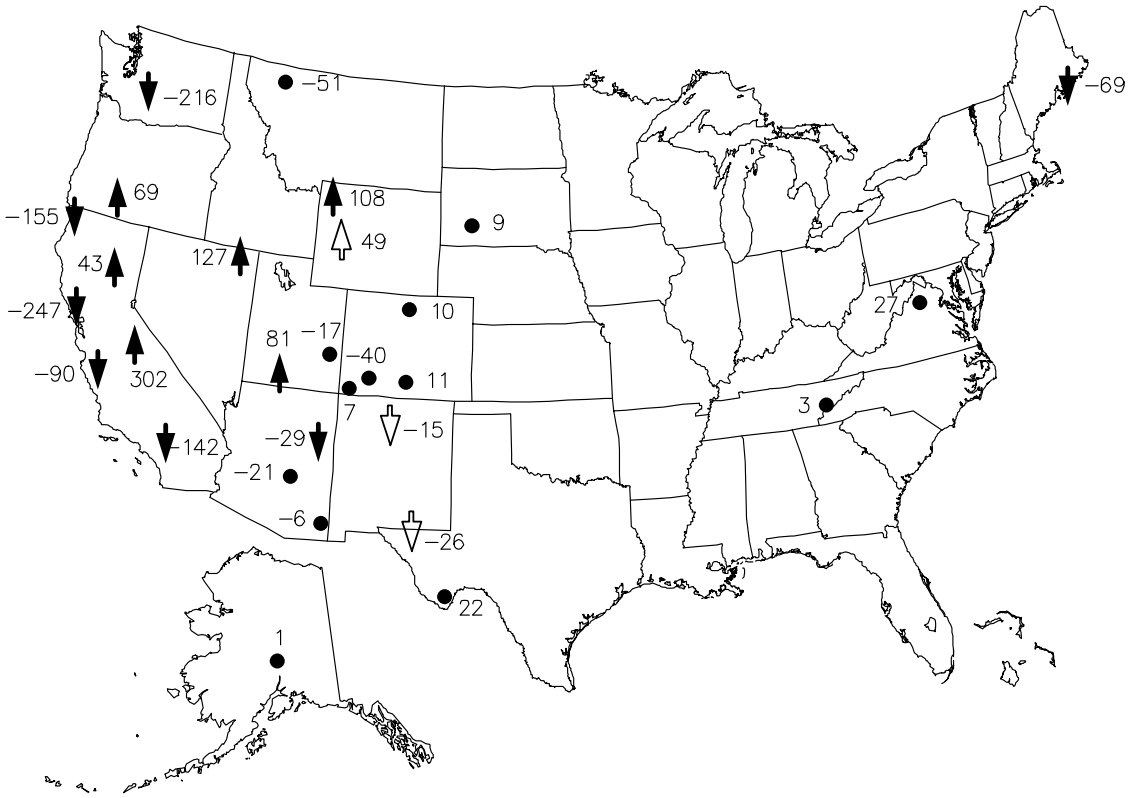

ORGANIC Bscat – Worst 20%

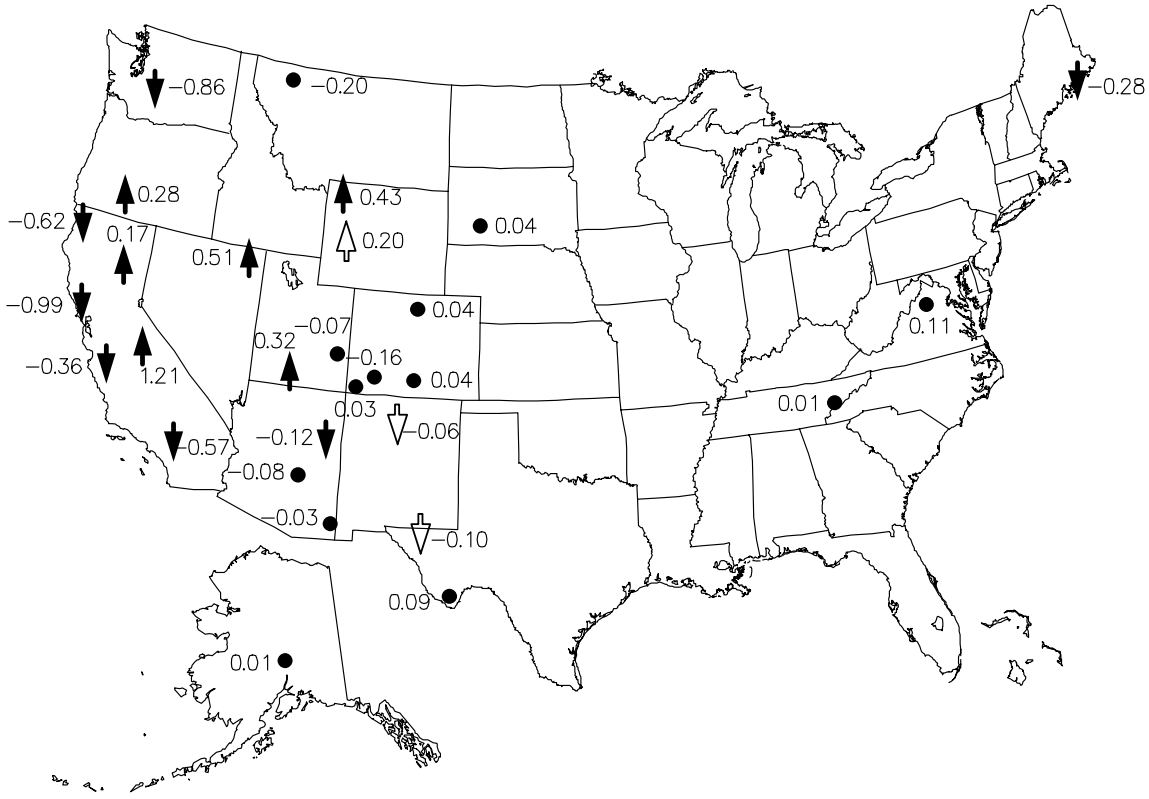

SULFATE – Worst 20%

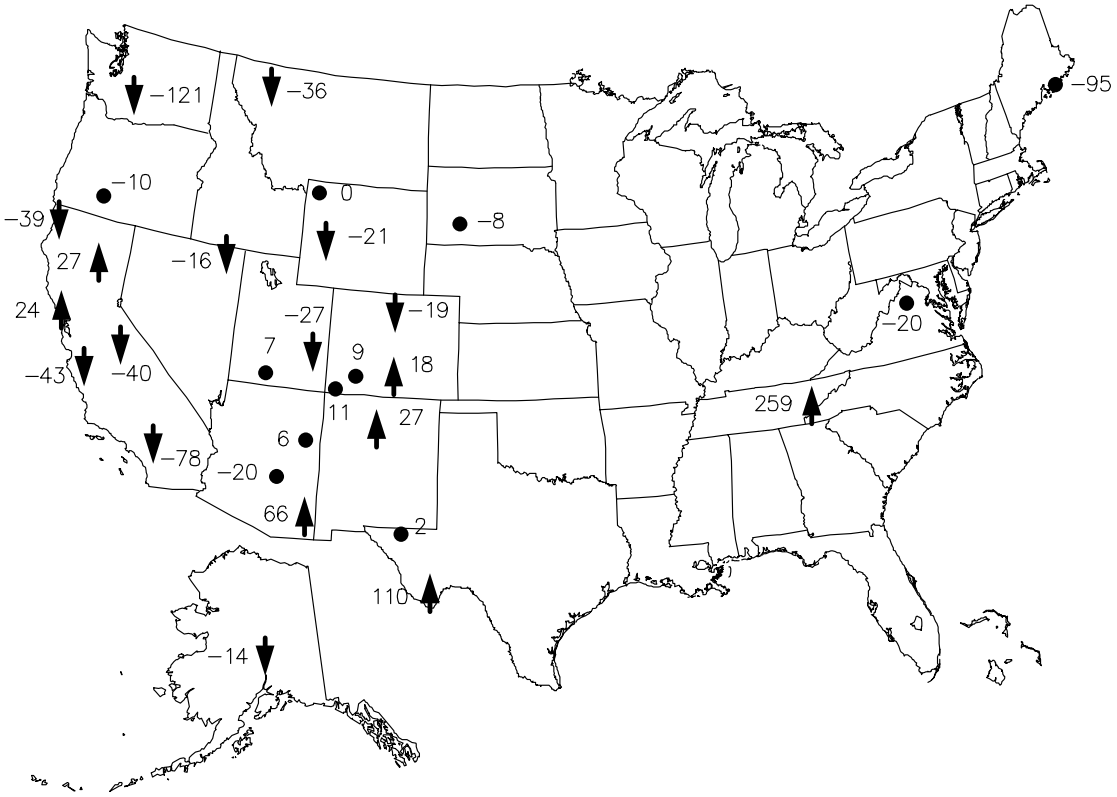

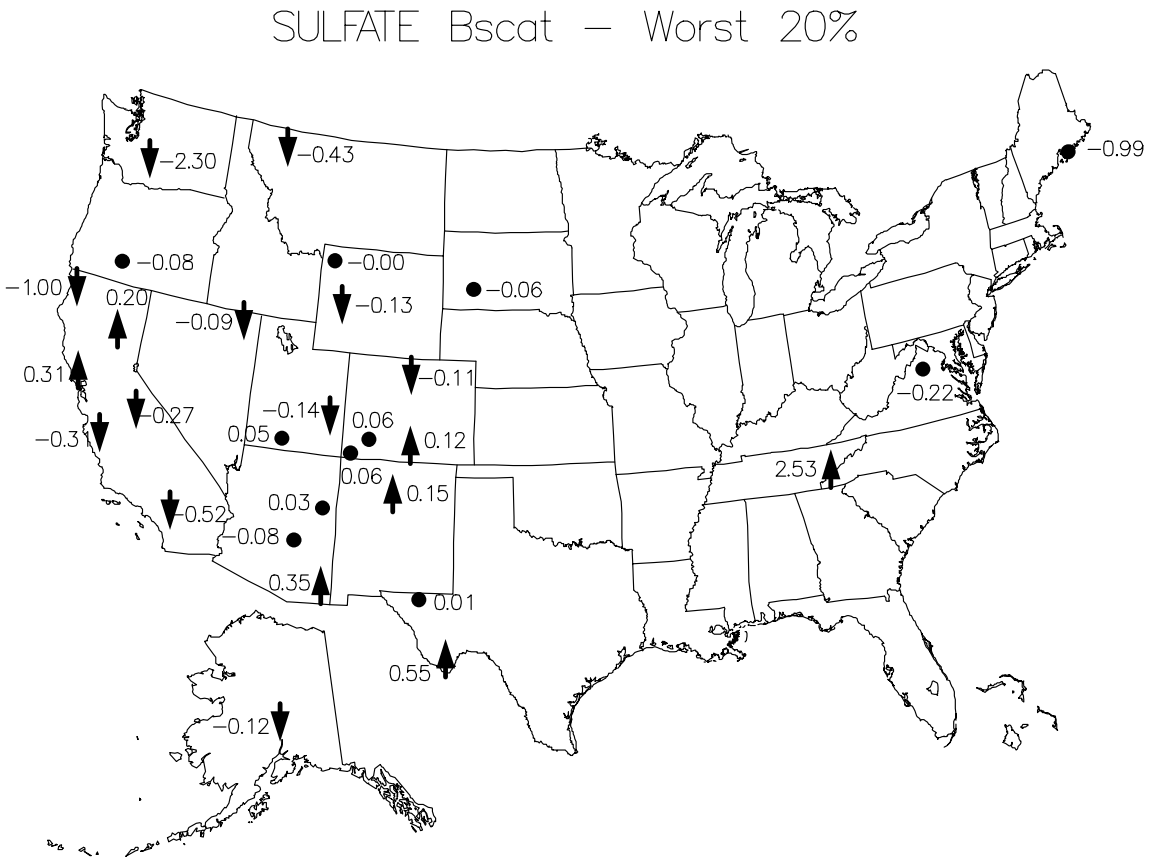
SULFATE Bscat – Worst 20%
−2.30
−0.43
−0.99
−0.08
−0.00
−0.06
−1.00
0.20
−0.13
−0.09
0.31
−0.11
−0.22
−0.27
−0.14
0.06
−0.31
0.05
0.12
2.53
0.06
0.15
0.03
−0.52
−0.08
0.35
0.01
0.55
−0.12

APPENDIX D

This appendix contains temporal plots of reconstructed extinction and extinction of constituent species for the group 90, 50, and 10 categories. The solid line corresponds to fine mass, the dotted line to sulfate, the solid-dotted line to organics, the small-dashed line to nitrates, and long-dashed line to soil. Units are in 1/Mm and time is in years.

APPENDIX E

MONTHLY RECONSTRUCTED FINE MASS AND BUDGETS FROM THE IMPROVE NETWORK – MARCH 1996 THROUGH FEBRUARY 1999

ACADIA NP

FINE MASS

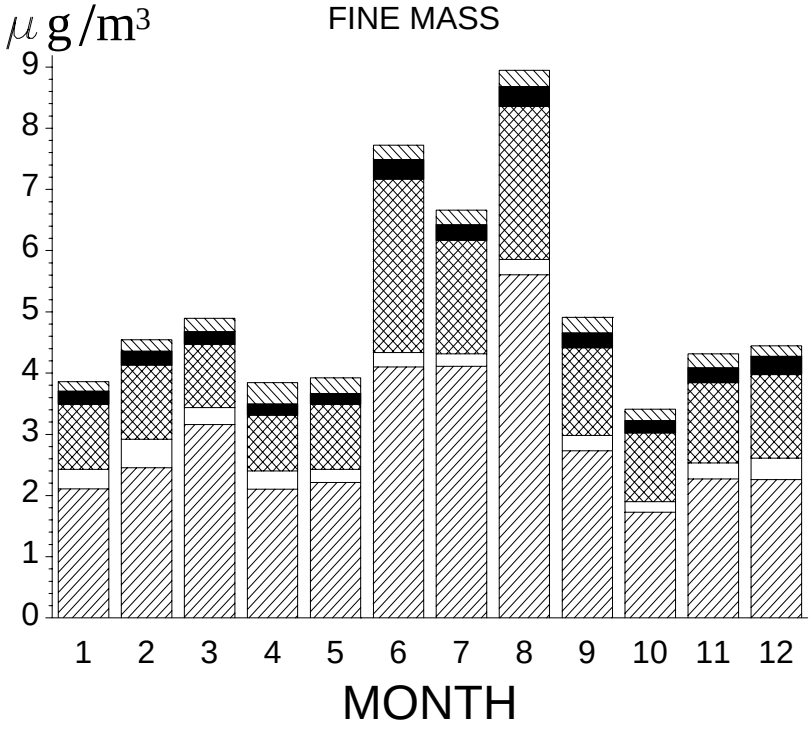

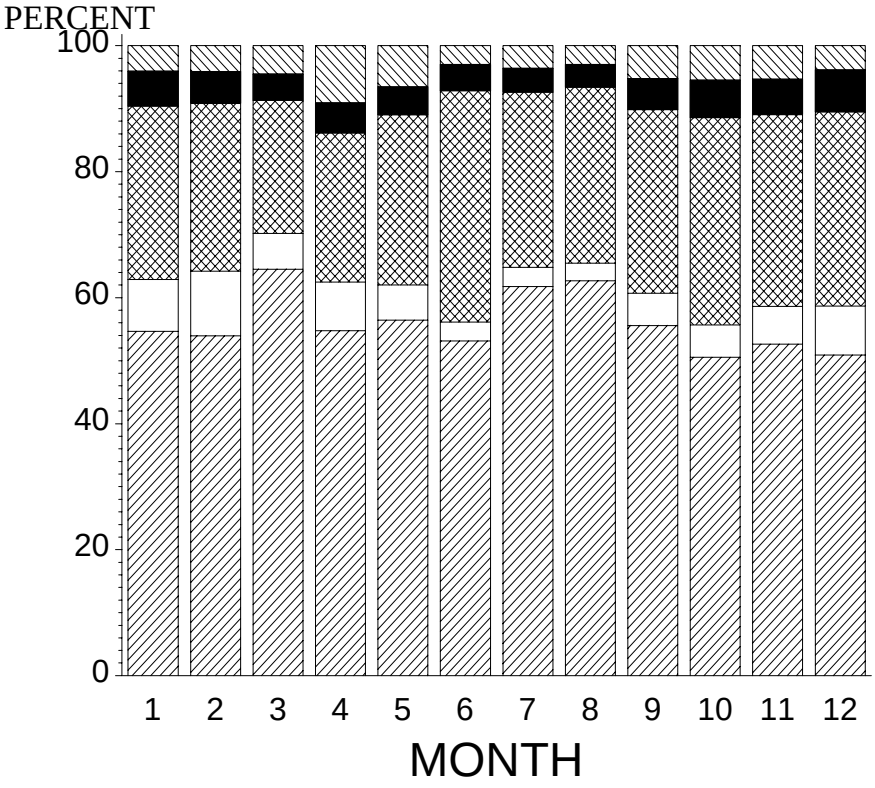

SULFATE NITRATE ORGANIC LAC SOIL

BADLANDS NP

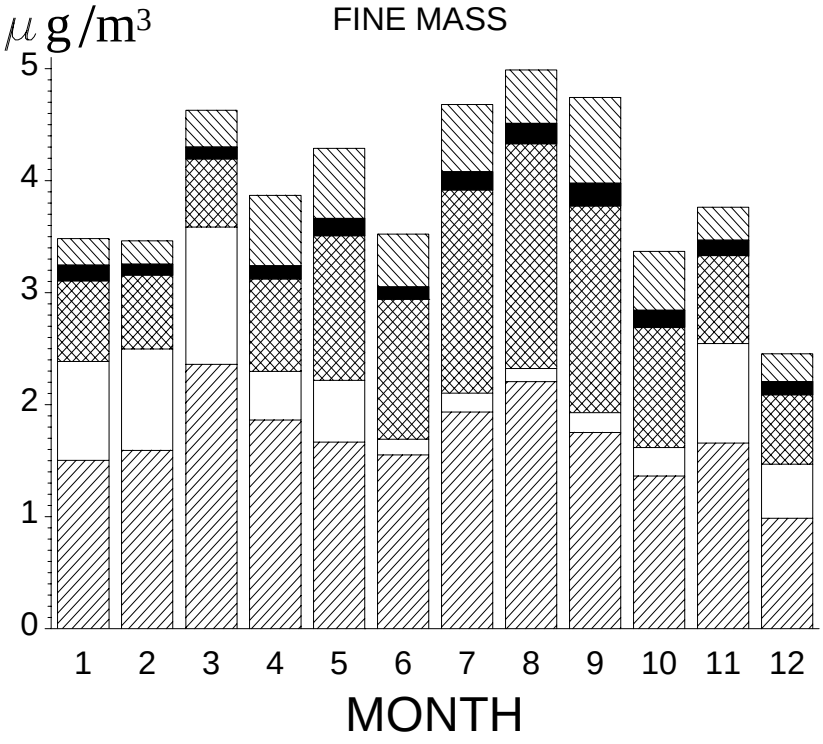

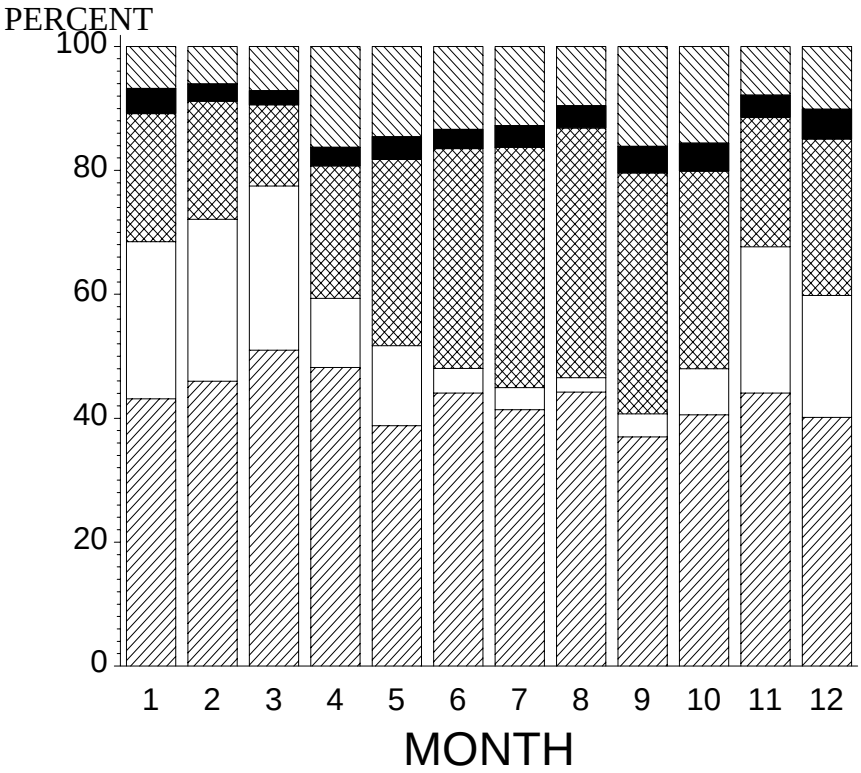

SULFATE NITRATE ORGANIC LAC SOIL

BANDELIER NM

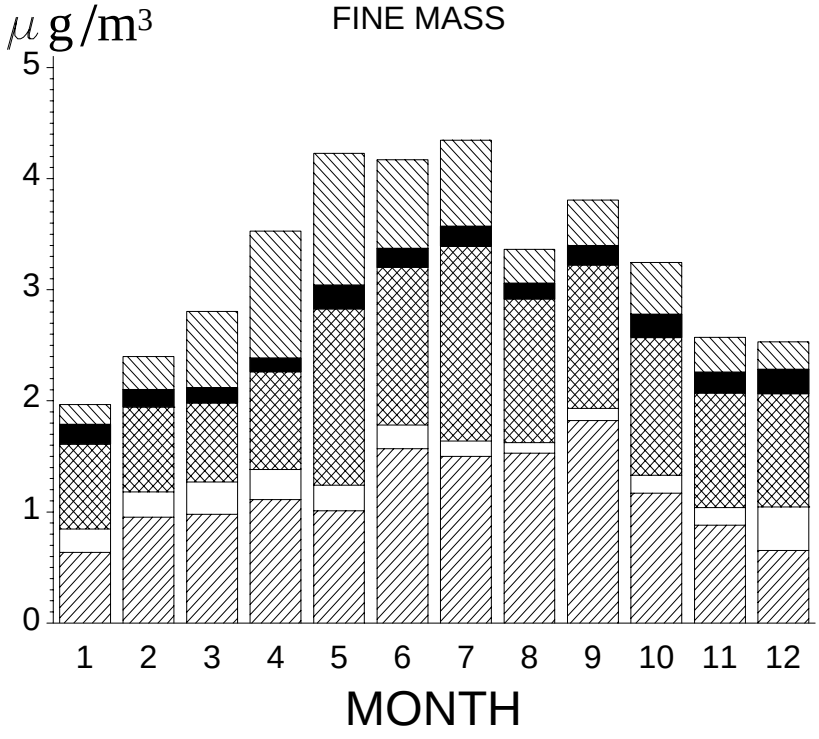

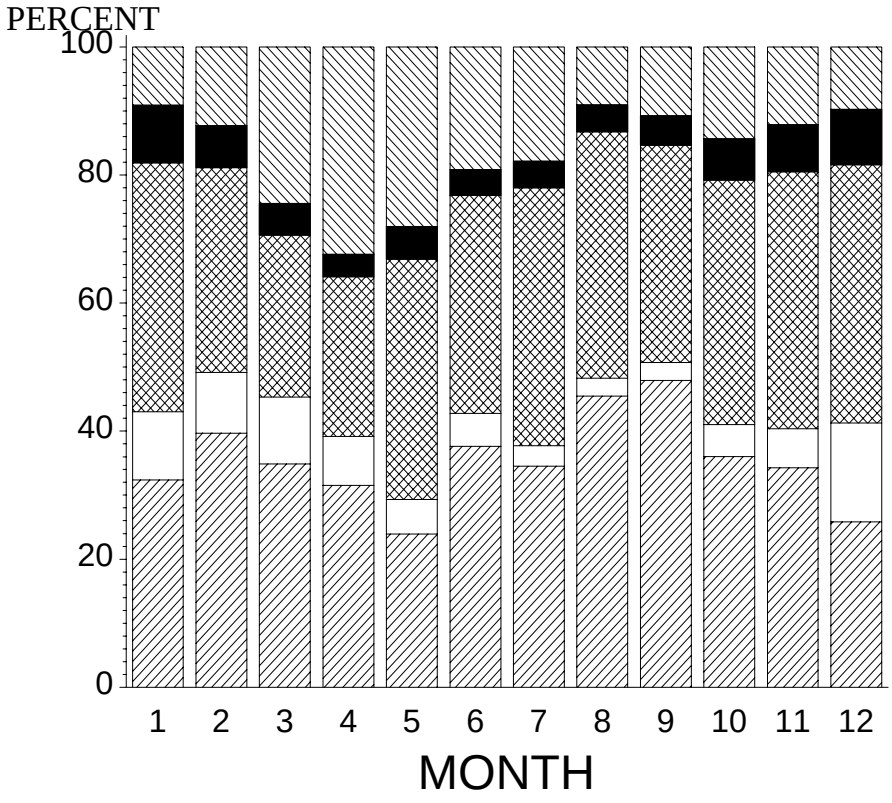

SULFATE NITRATE ORGANIC LAC SOIL

BIG BEND NP

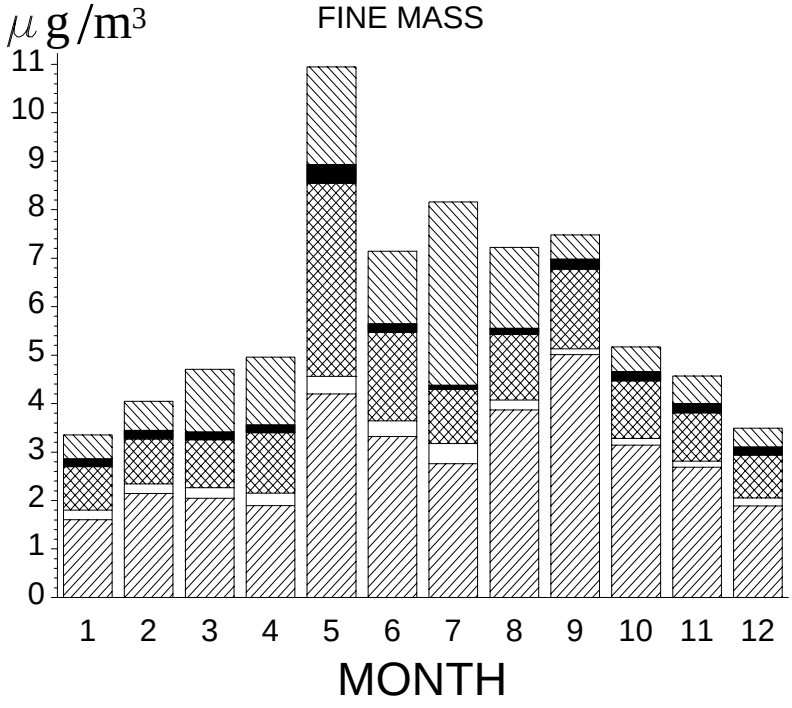
μg/m3
FINE MASS
0
1
2
3
4
5
6
7
8
9
10
11
1 2 3 4 5 6 7 8 9 10 11 12
MONTH

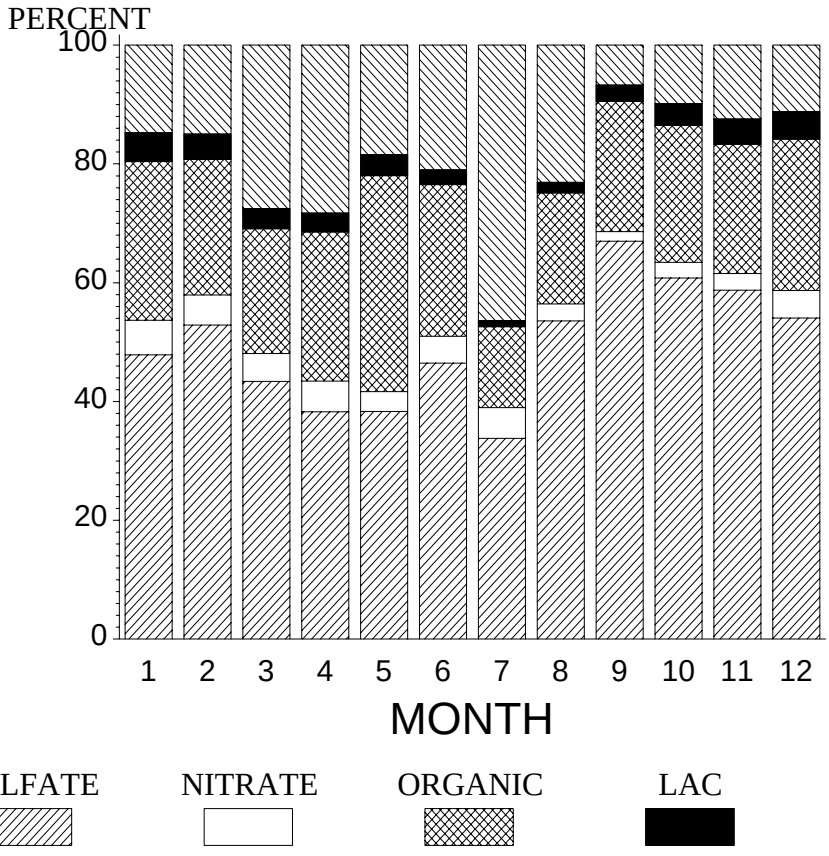
PERCENT
0
20
40
60
80
100
1 2 3 4 5 6 7 8 9 10 11 12
MONTH
SULFATE
NITRATE
ORGANIC
LAC
SOIL

BOUNDARY WATERS CA

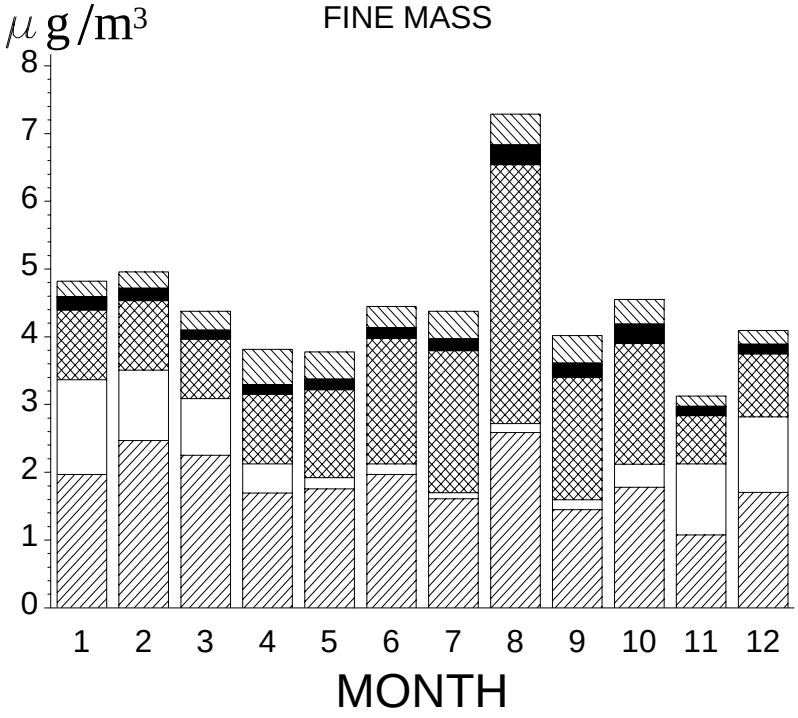

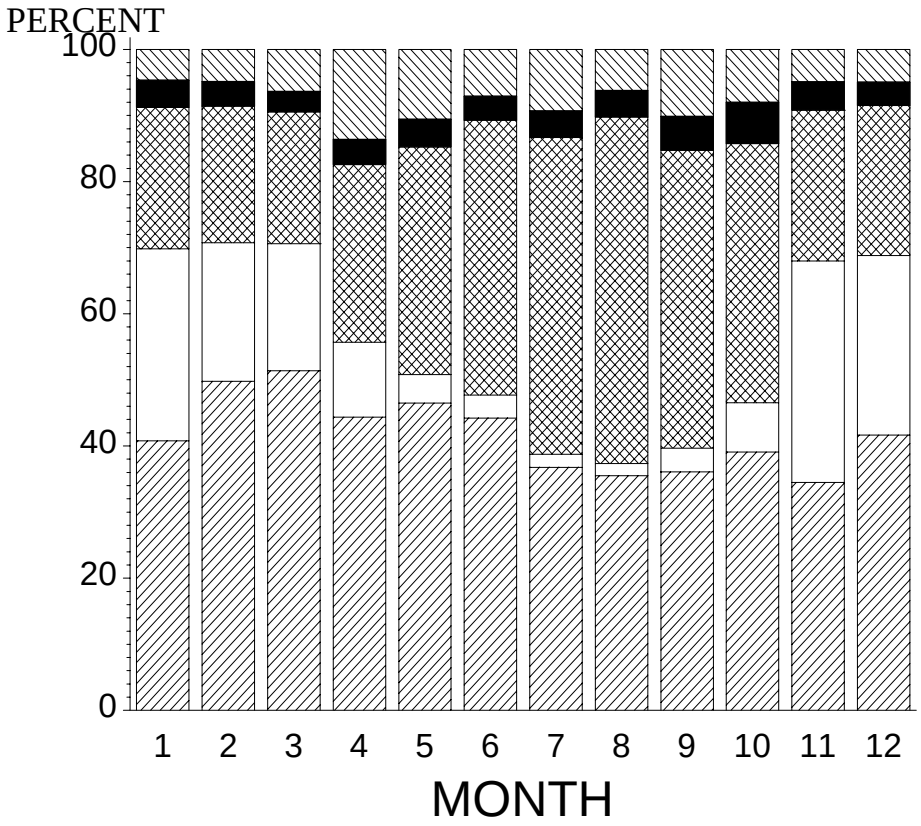

SULFATE NITRATE ORGANIC LAC SOIL

BRIDGER WA

FINE MASS

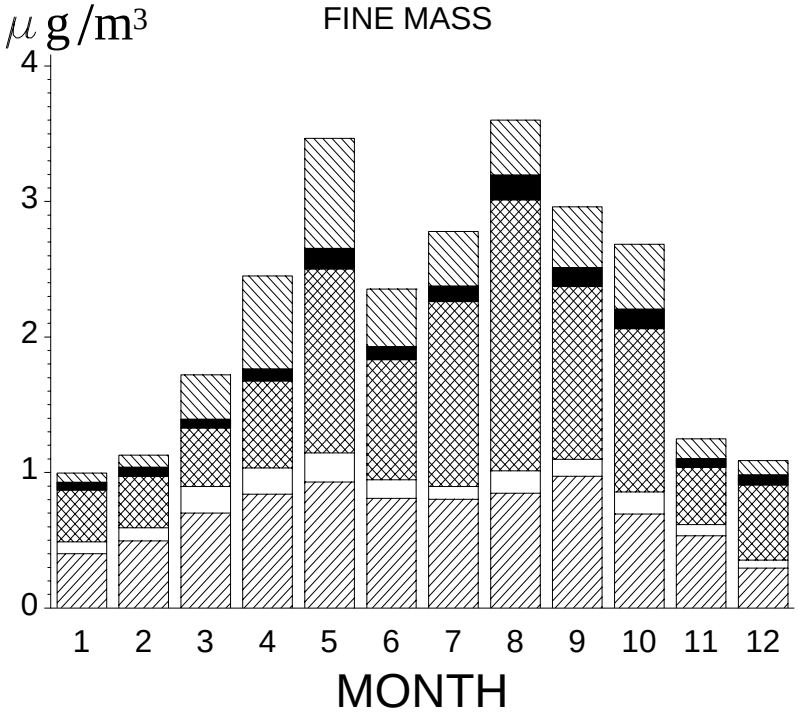

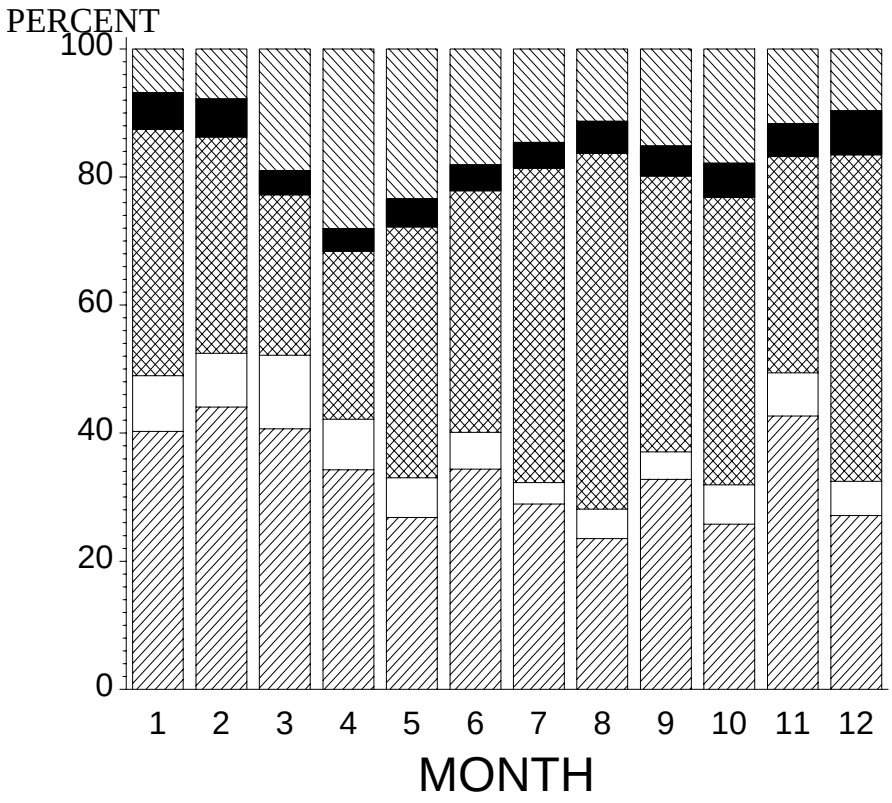

SULFATE NITRATE ORGANIC LAC SOIL

BRYCE CANYON NP

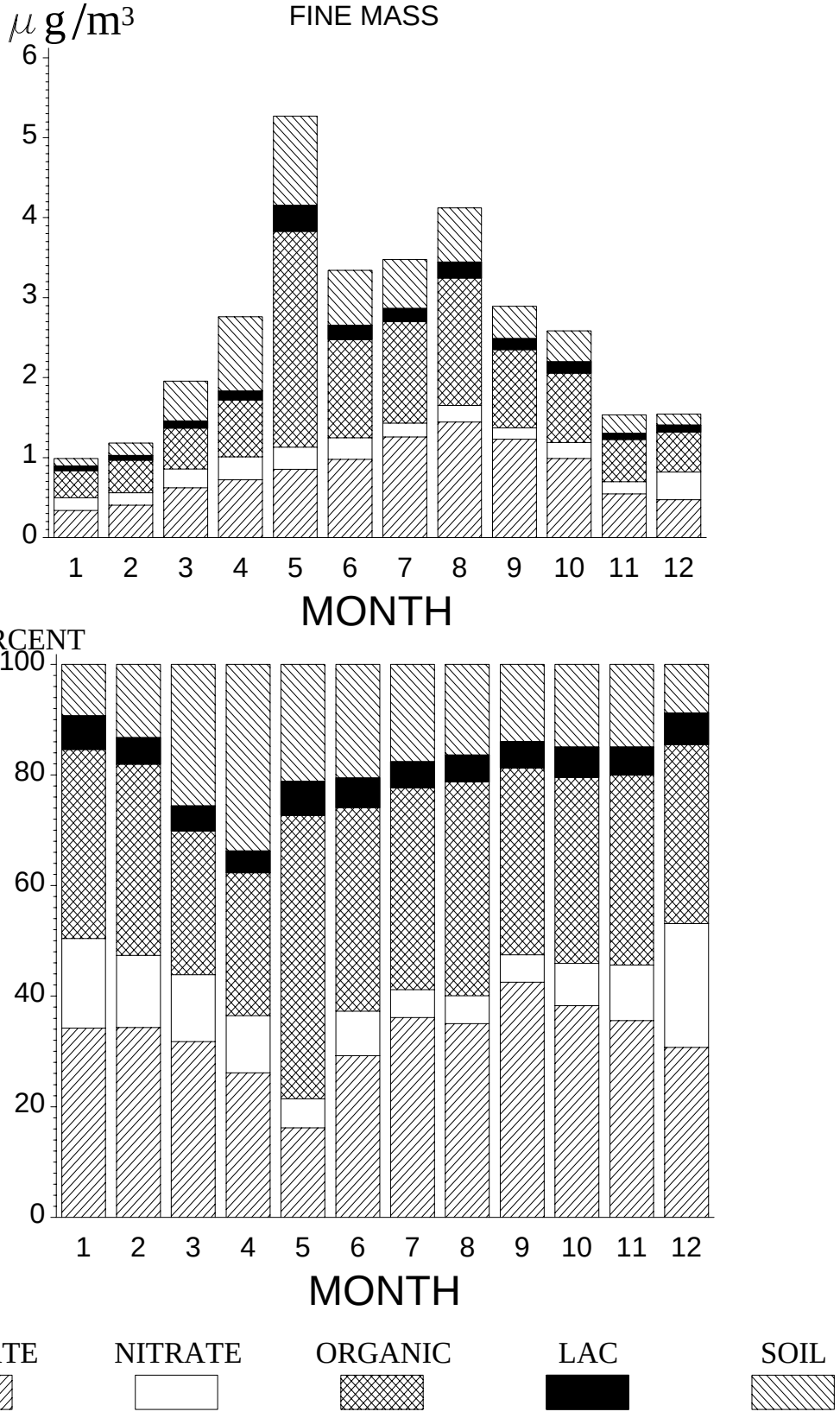

CANYONLANDS NP

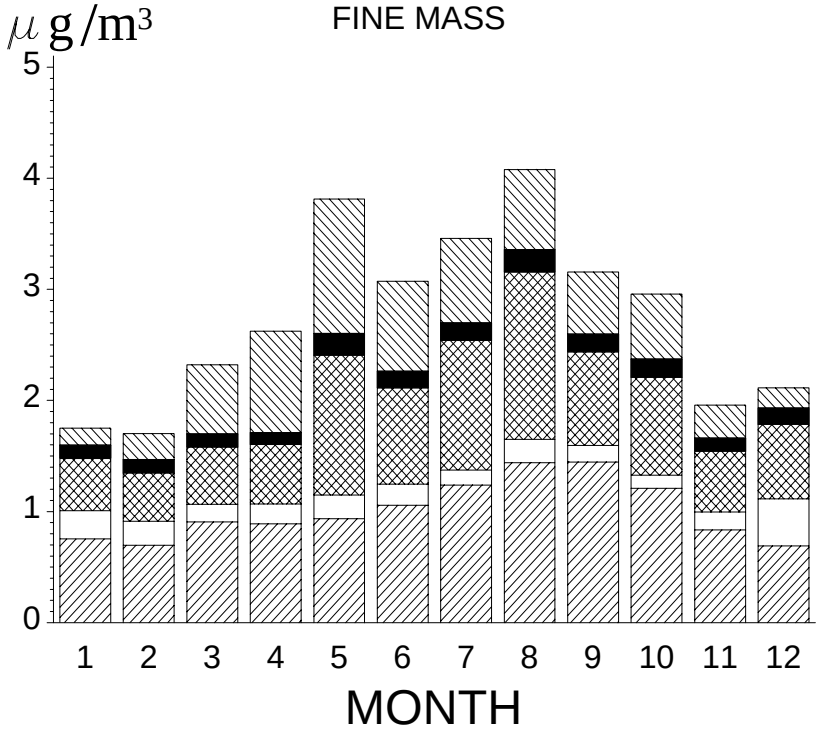

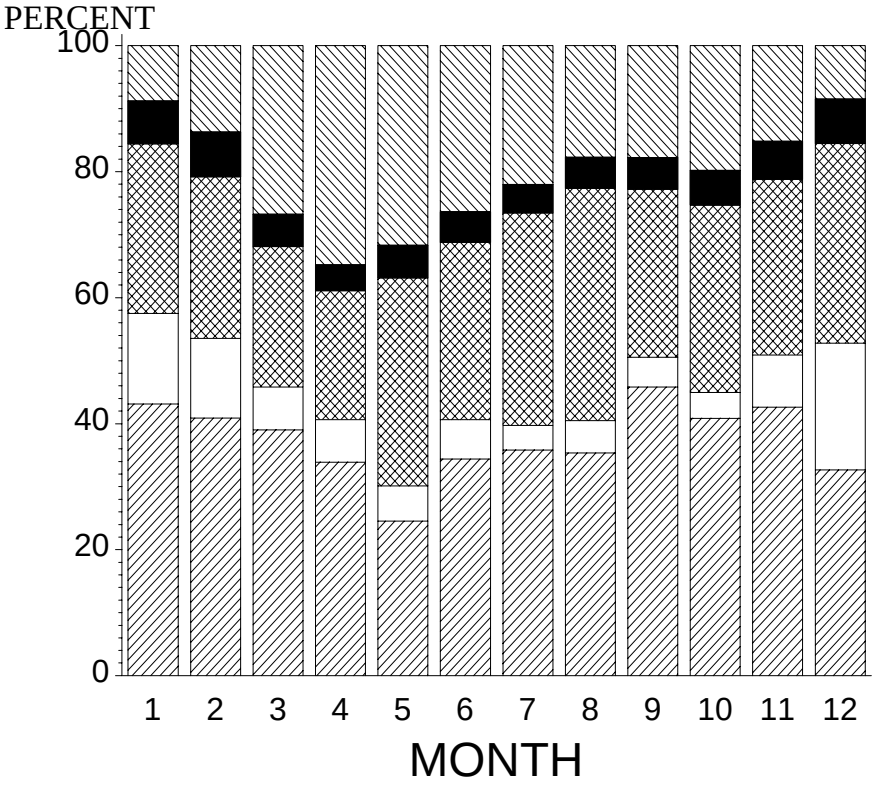

SULFATE NITRATE ORGANIC LAC SOIL

CAPE ROMAIN NWR

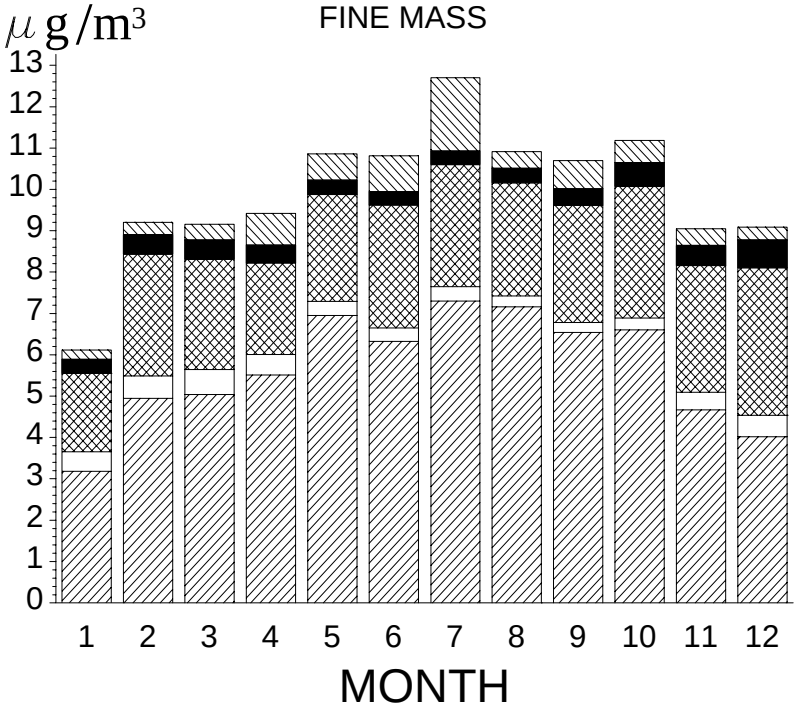

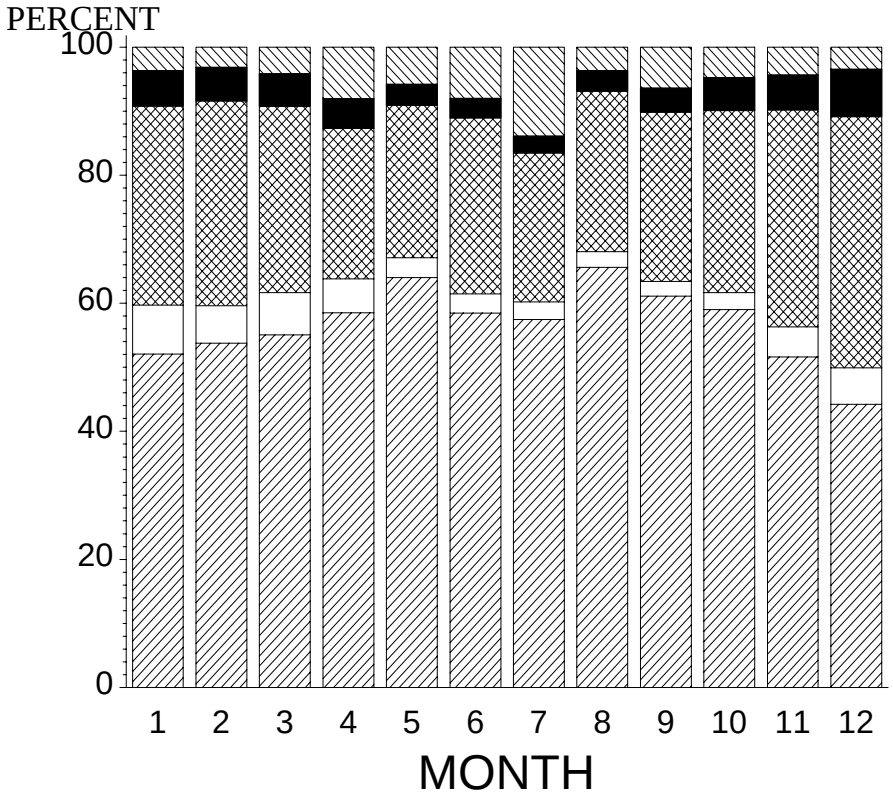

SULFATE NITRATE ORGANIC LAC SOIL

CHASSAHOWITZKA NWR

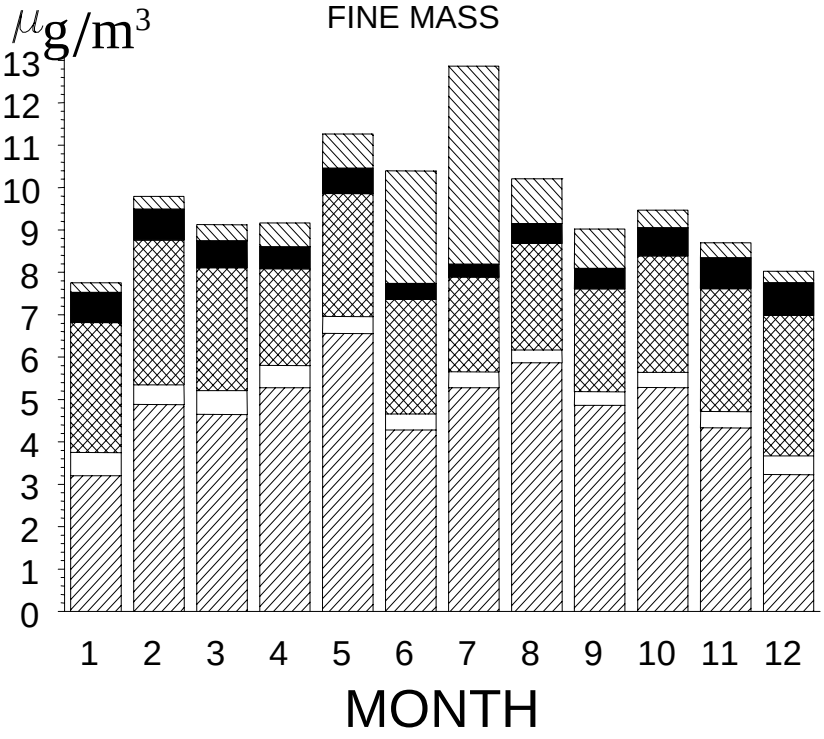

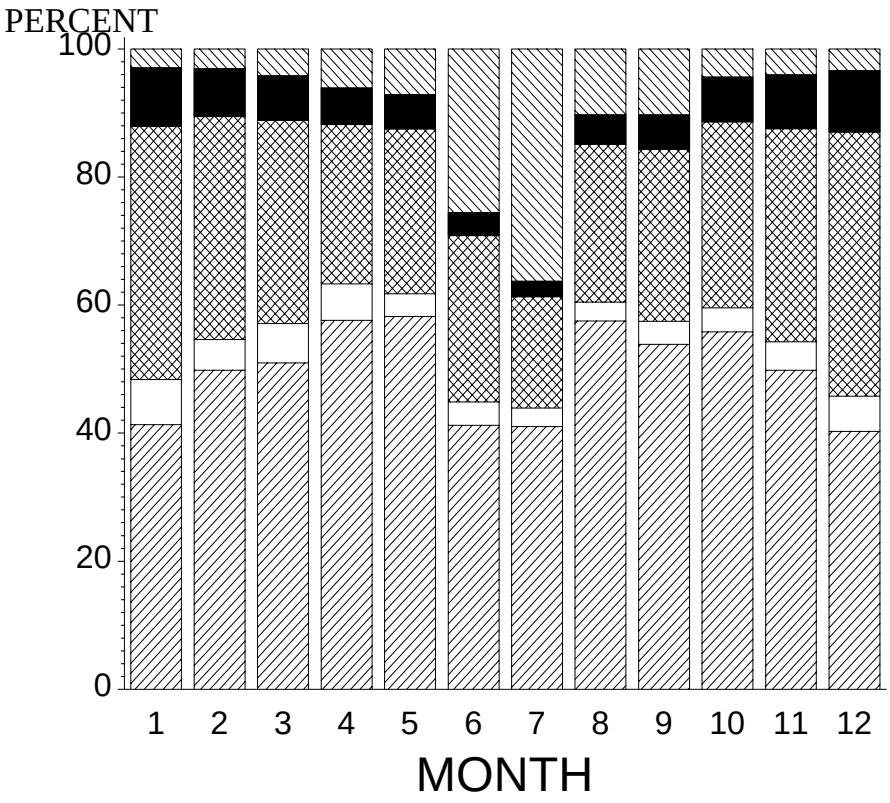

SULFATE NITRATE ORGANIC LAC SOIL

CHIRICAHUA NM

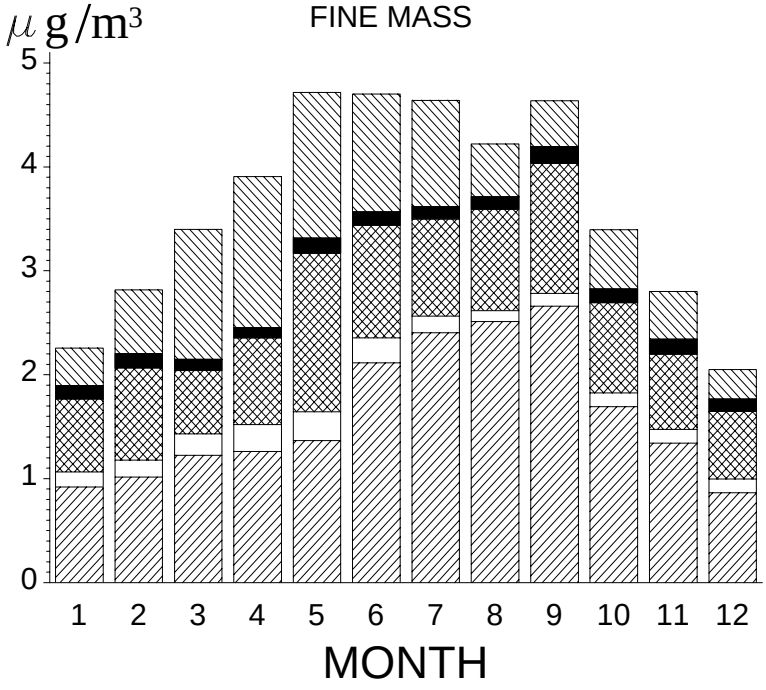

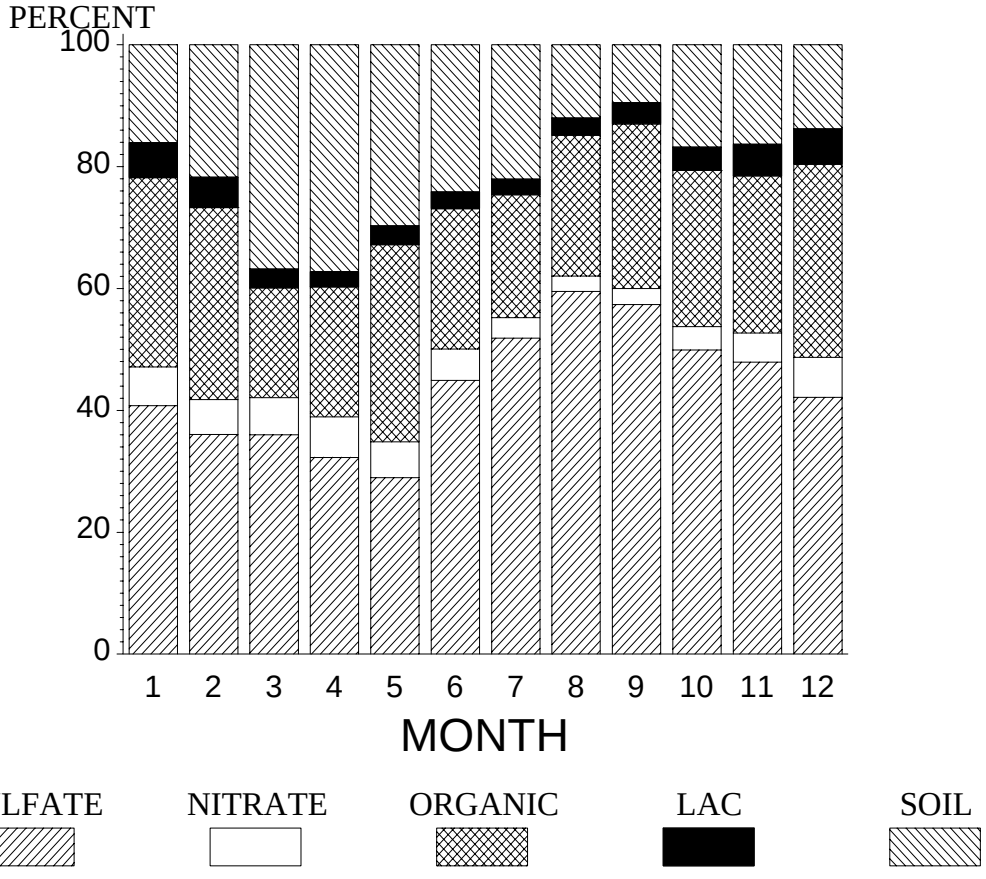

CRATER LAKE NP

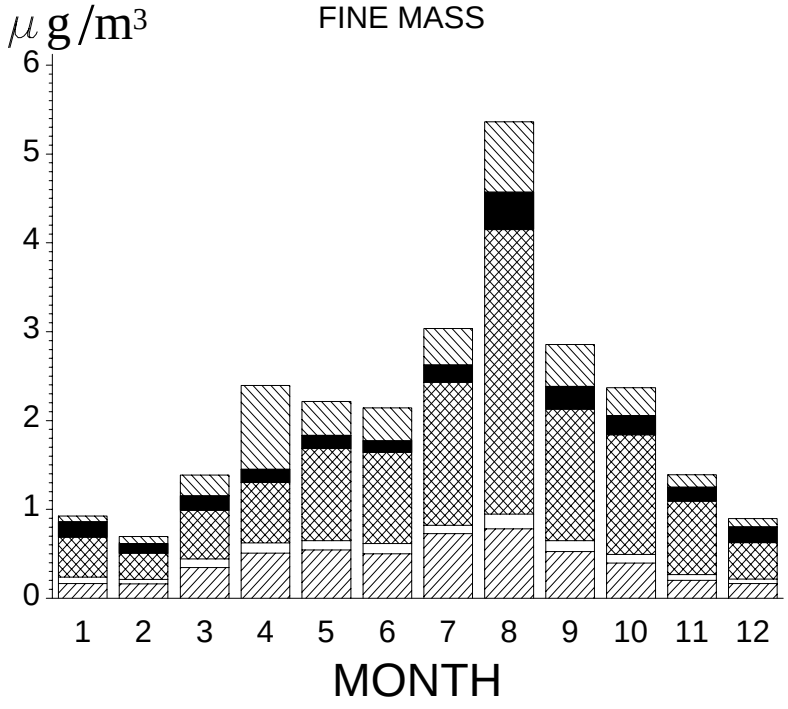

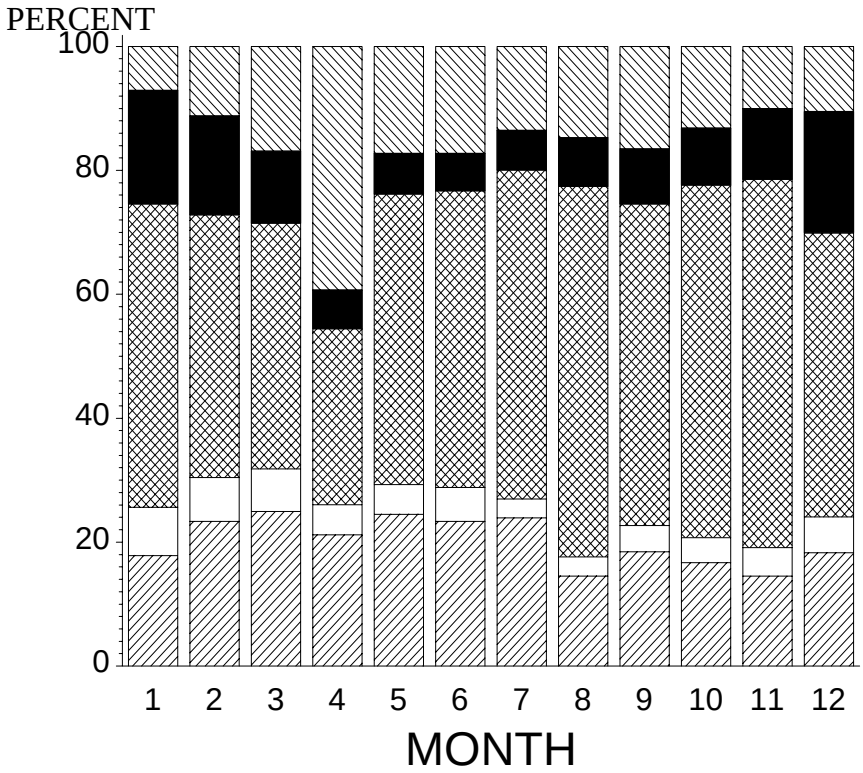

SULFATE NITRATE ORGANIC LAC SOIL

DENALI NP

FINE MASS

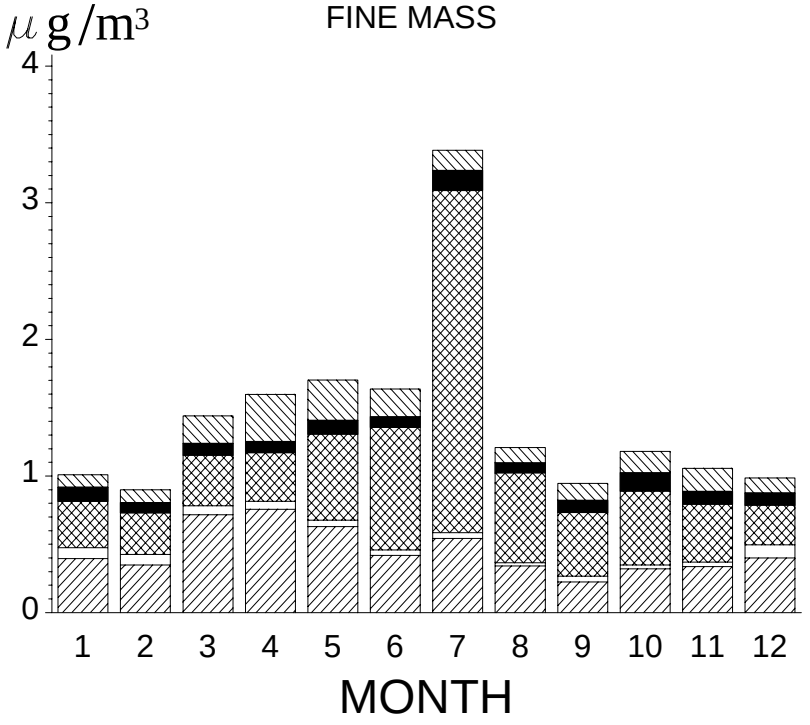

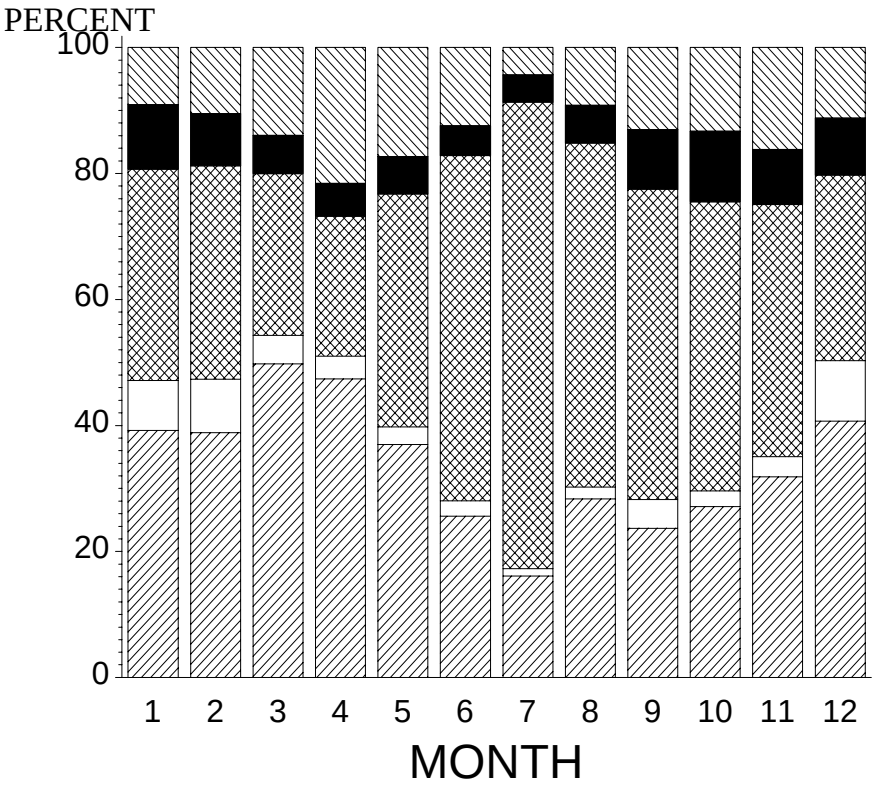

SULFATE NITRATE ORGANIC LAC SOIL

DOLLY SODS WA

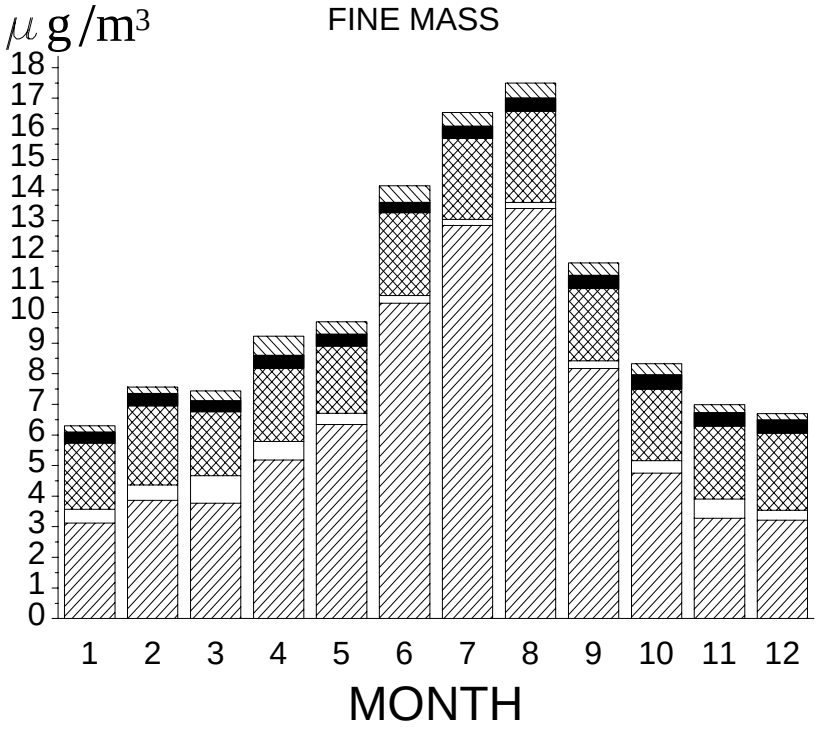

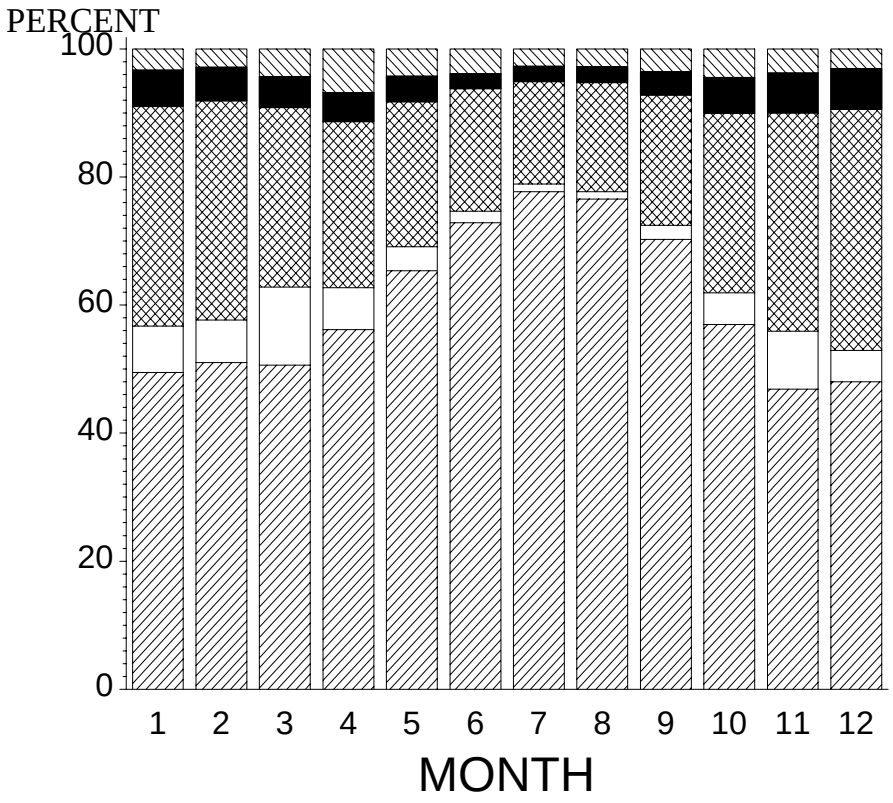

SULFATE NITRATE ORGANIC LAC SOIL

E B FORSYTHE NWR

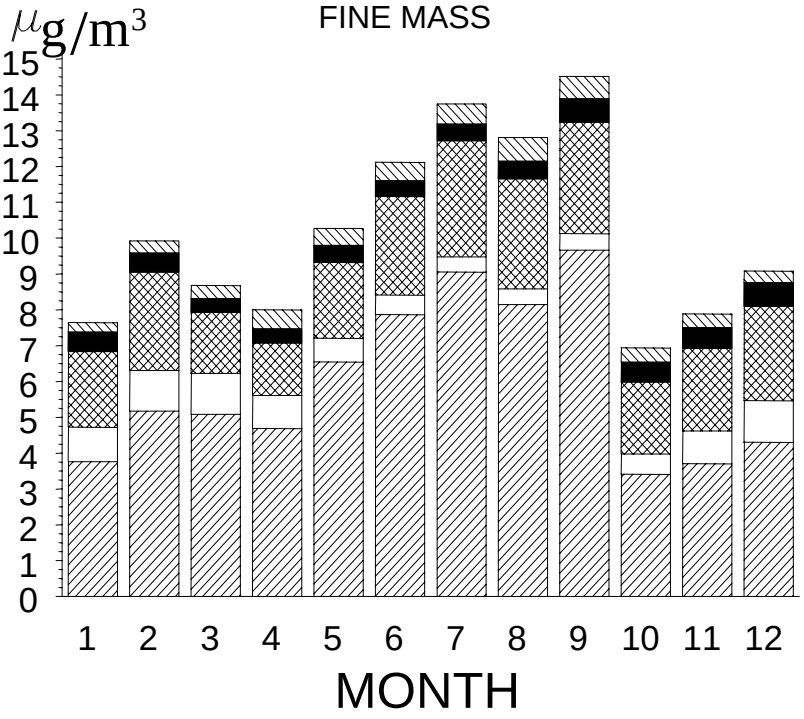

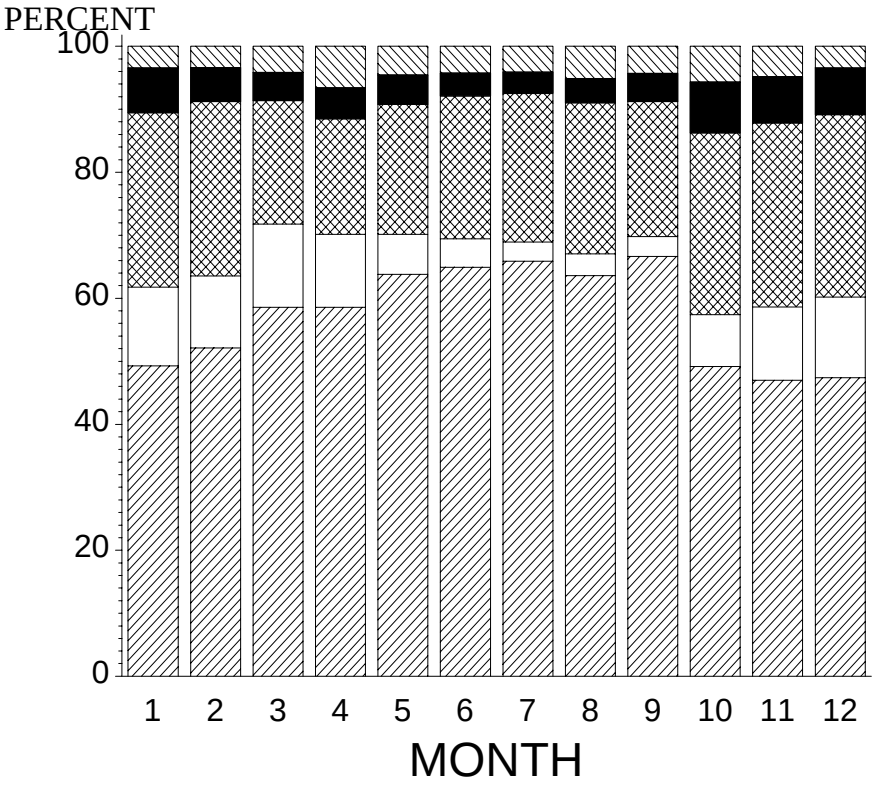

SULFATE NITRATE ORGANIC LAC SOIL

GLACIER NP

FINE MASS

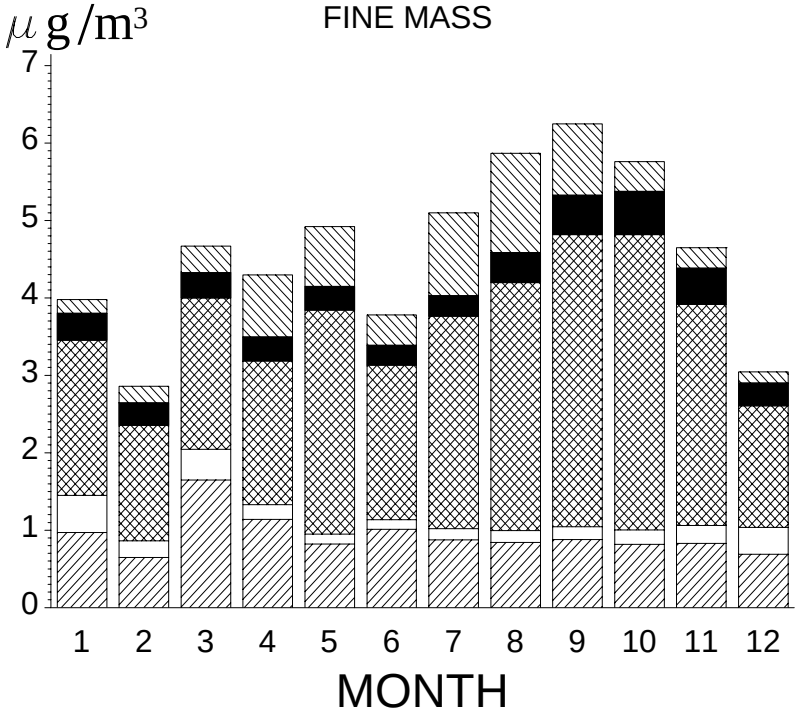

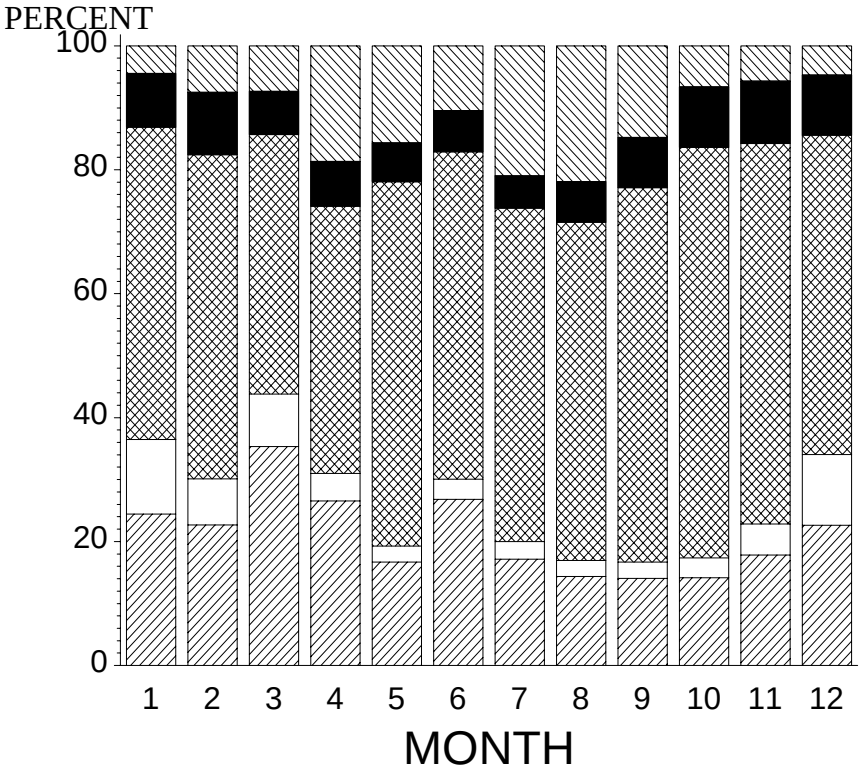

SULFATE NITRATE ORGANIC LAC SOIL

GRAND CANYON NP

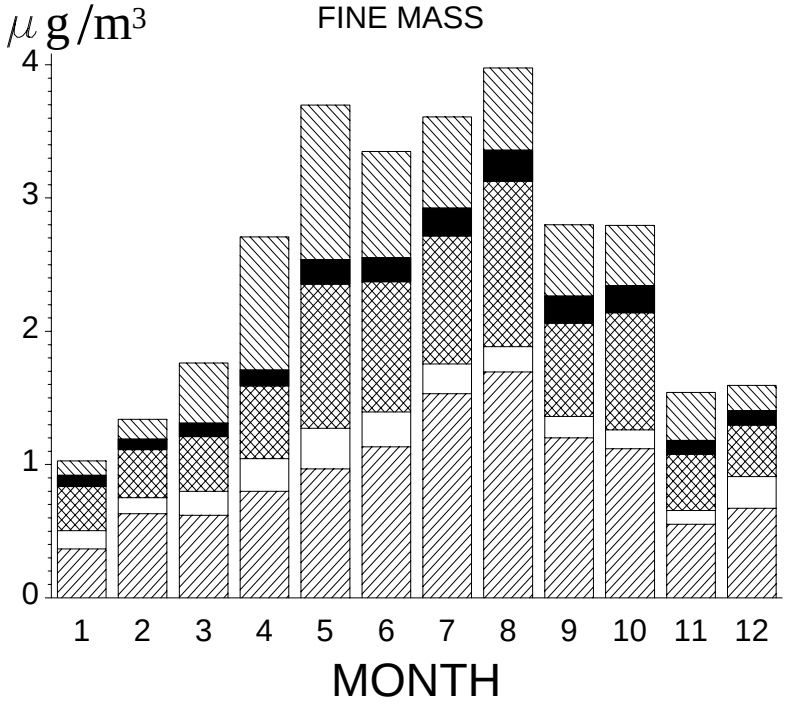

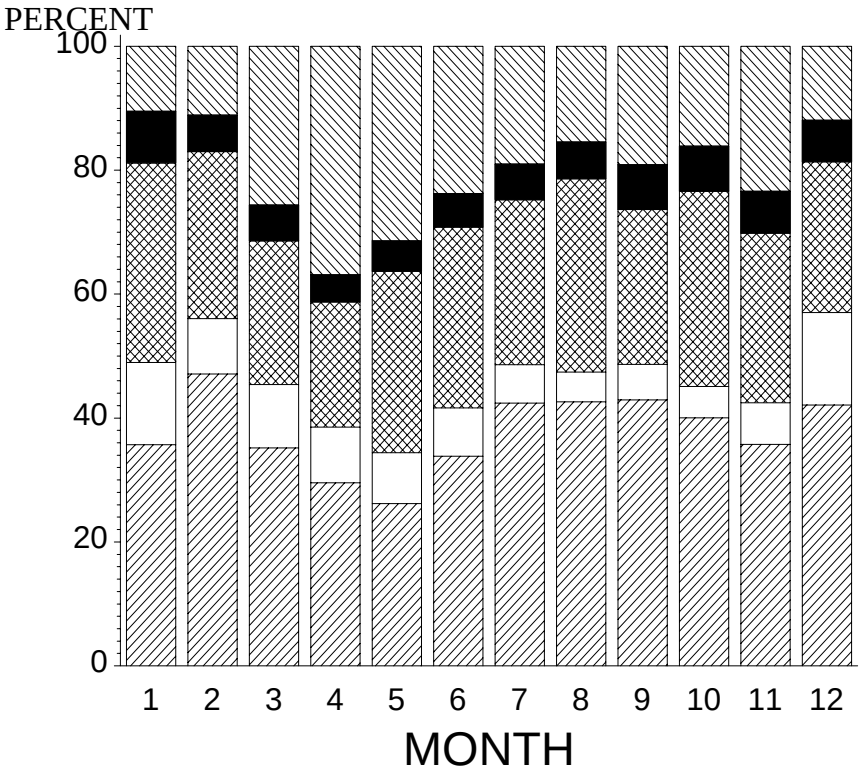

SULFATE NITRATE ORGANIC LAC SOIL

GREAT BASIN NP

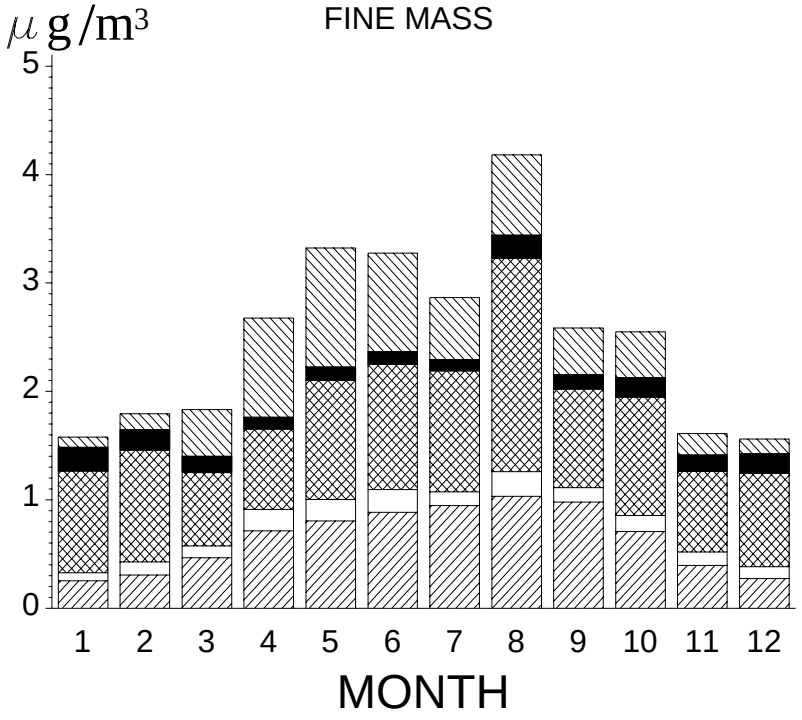

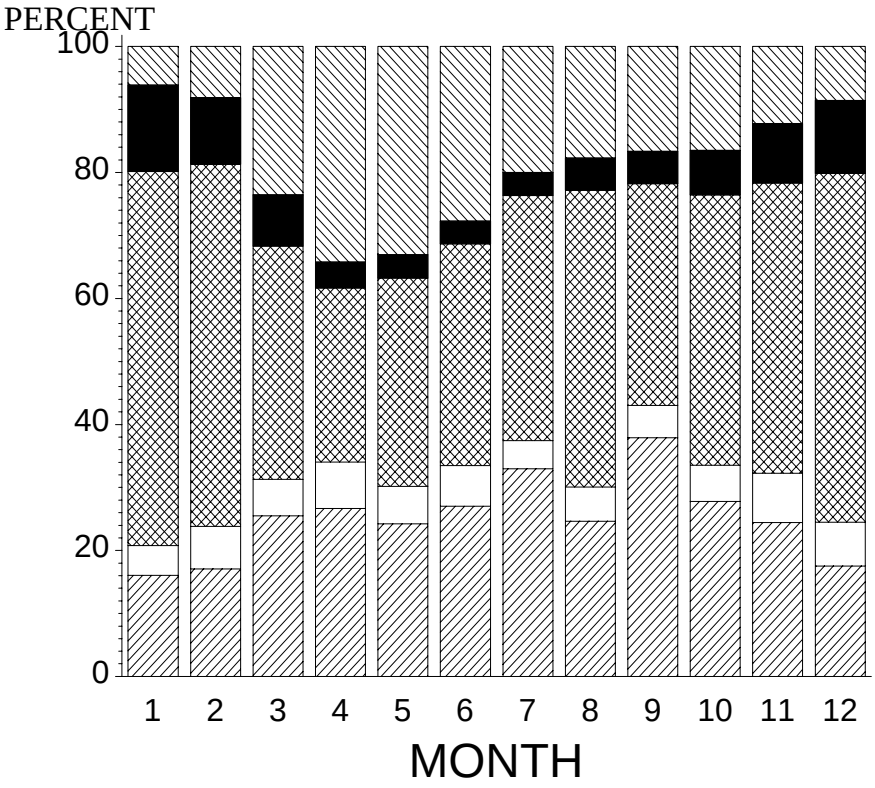

SULFATE NITRATE ORGANIC LAC SOIL

GREAT SAND DUNES NM

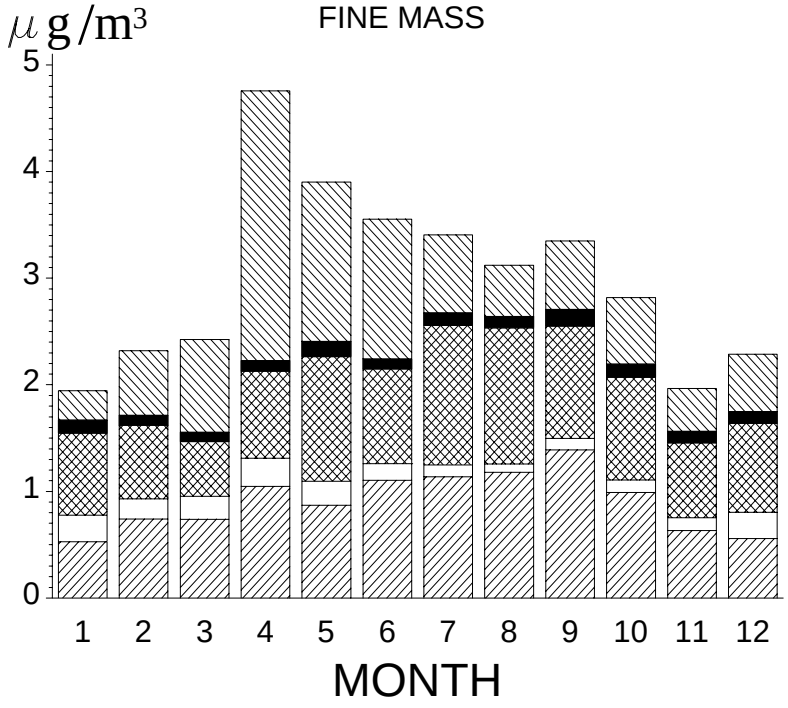

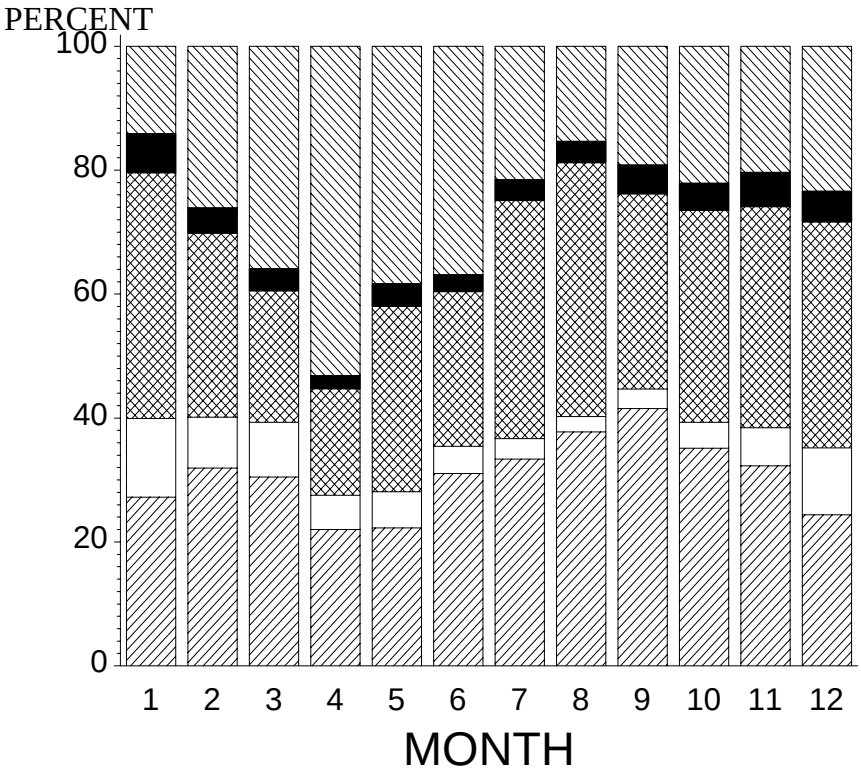

SULFATE NITRATE ORGANIC LAC SOIL

GREAT SMOKY MOUNTAINS NP

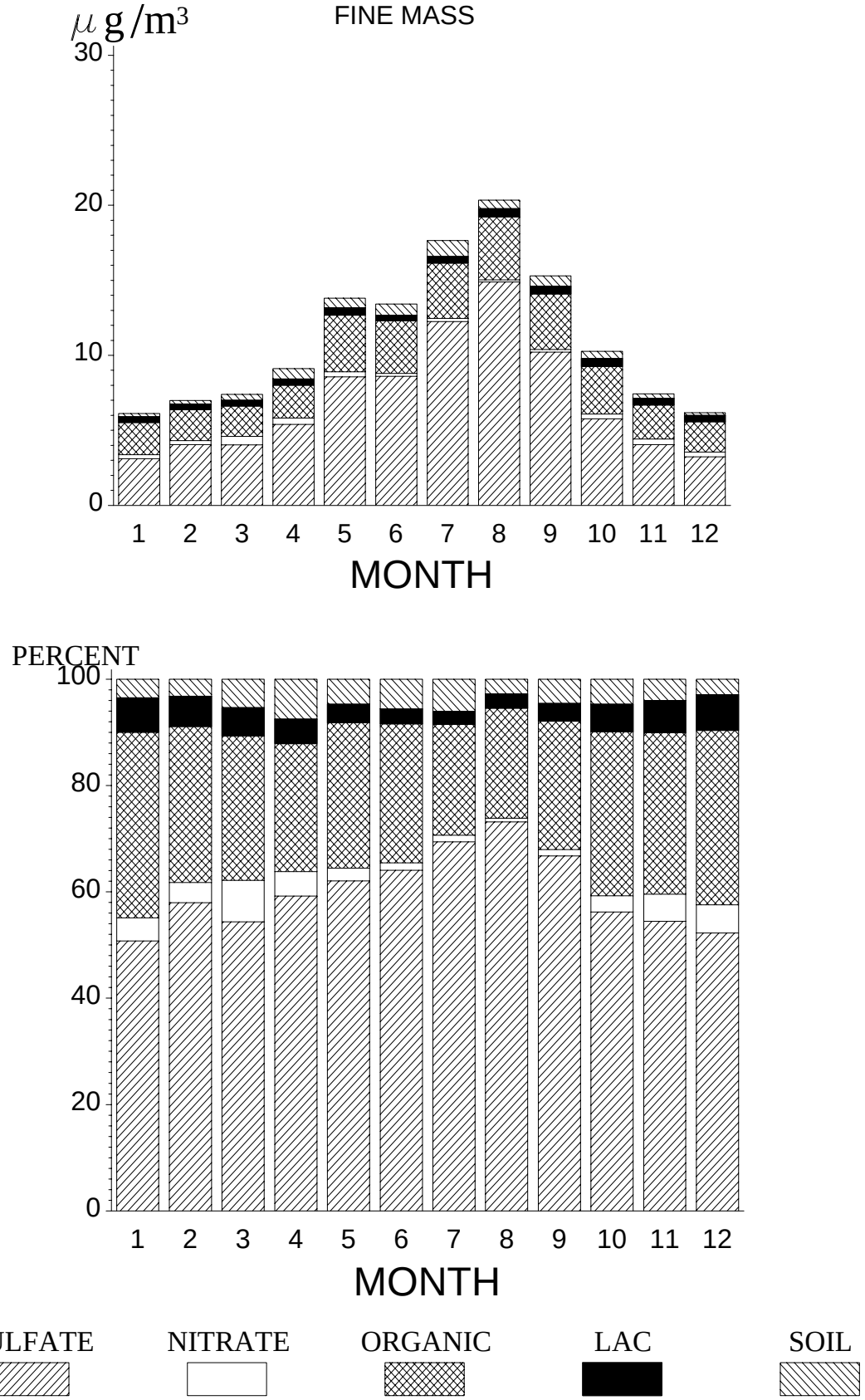

GUADALUPE MOUNTAIN NP

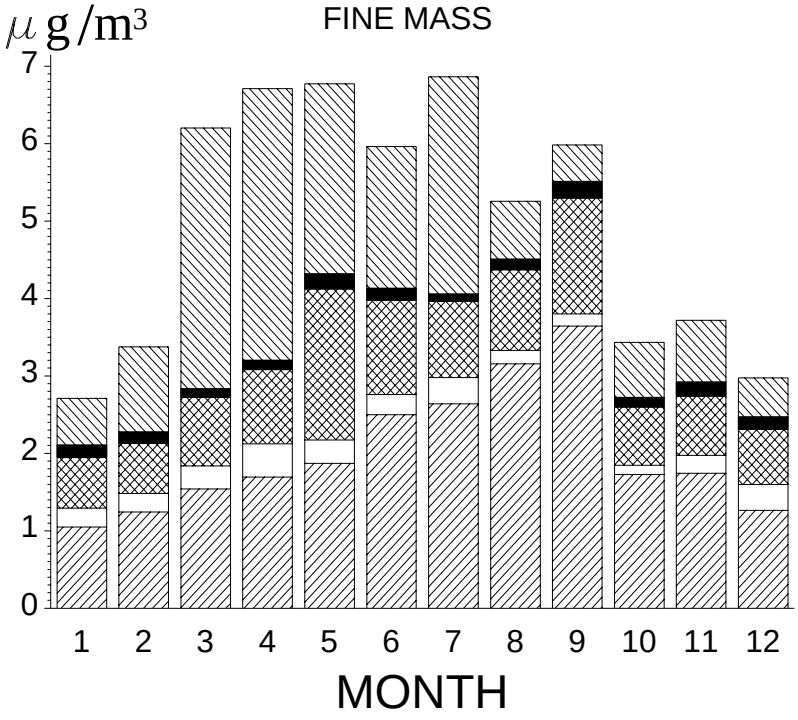

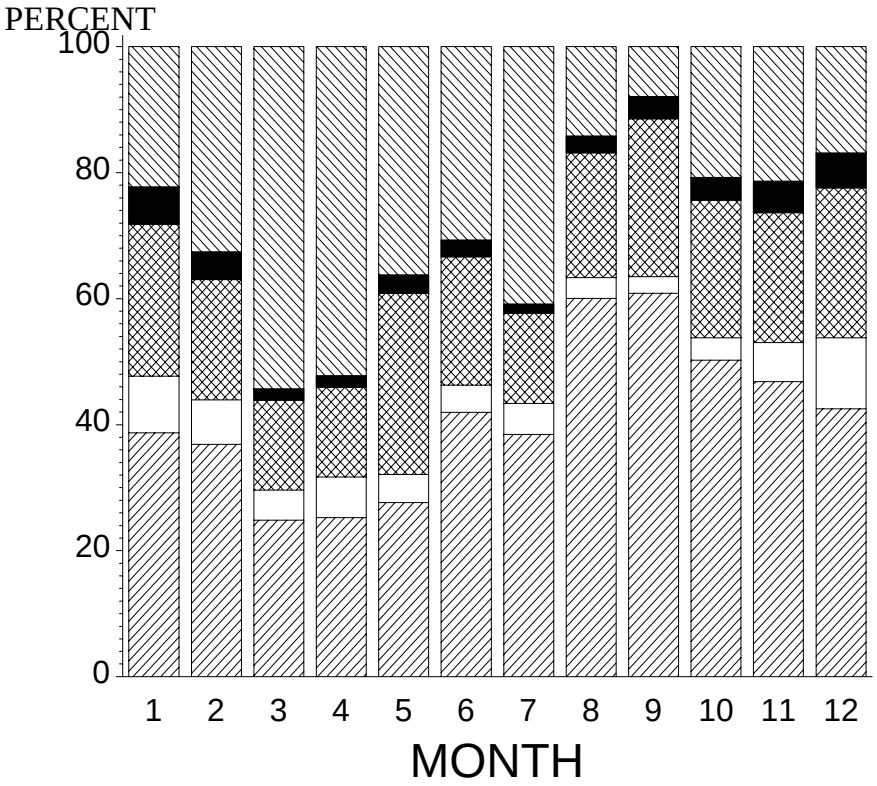

SULFATE NITRATE ORGANIC LAC SOIL

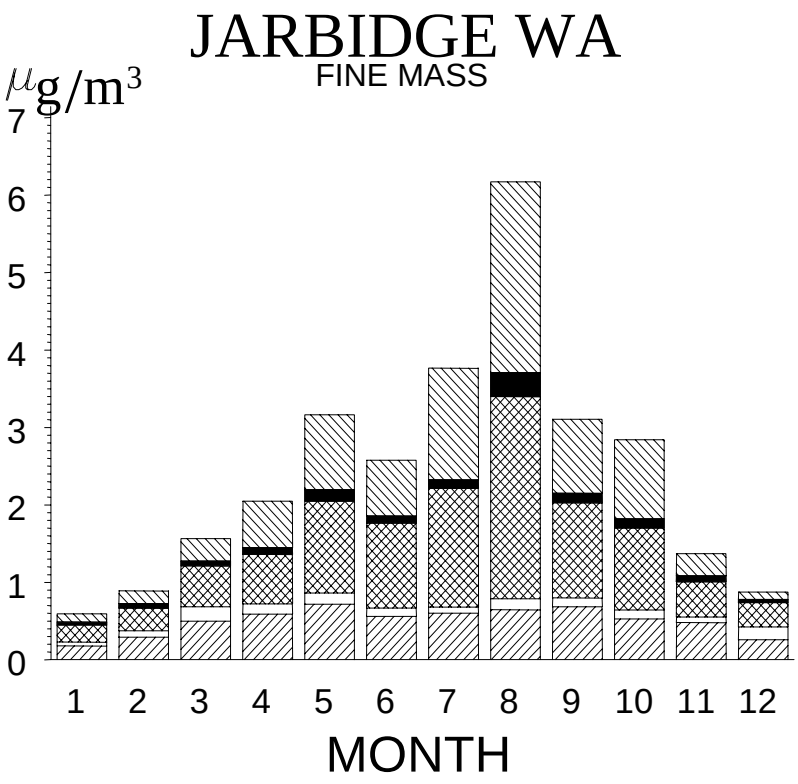
JARBIDGE WA
FINE MASS
μg/m3
7
6
5
4
3
2
1
0
1 2 3 4 5 6 7 8 9 10 11 12
MONTH

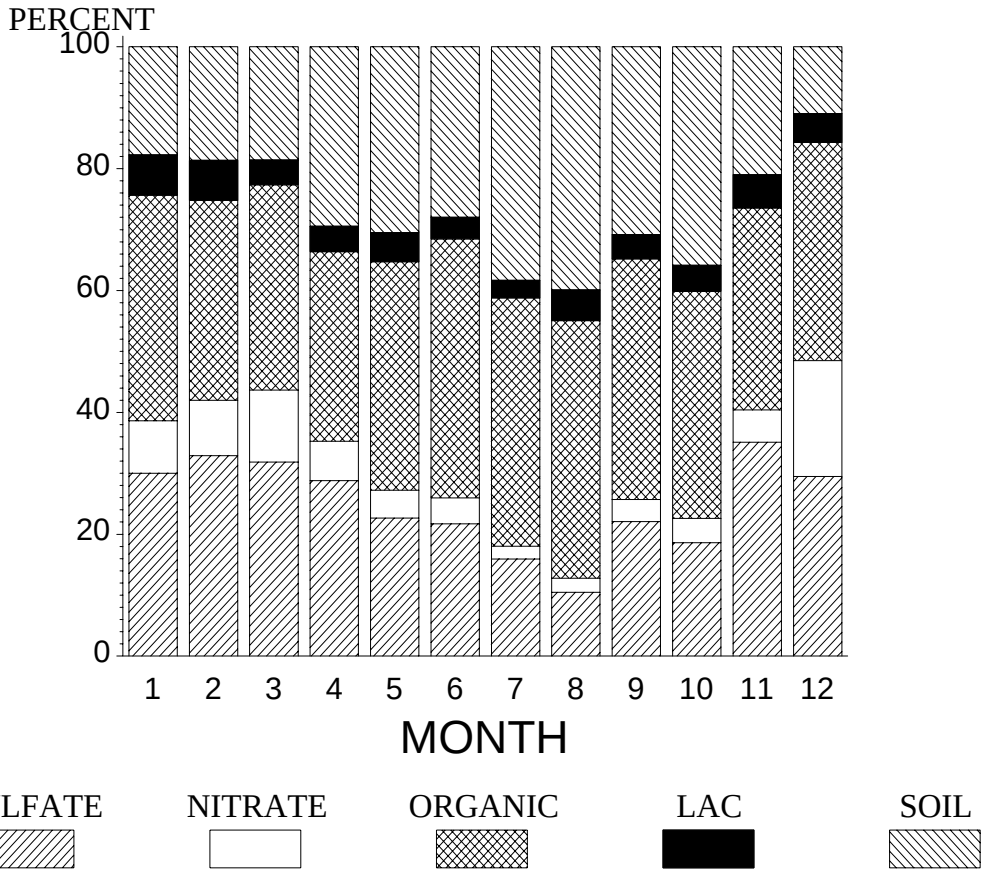
PERCENT
100
80
60
40
20
0
1 2 3 4 5 6 7 8 9 10 11 12
MONTH
SULFATE
NITRATE
ORGANIC
LAC
SOIL

LASSEN VOLCANIC NP

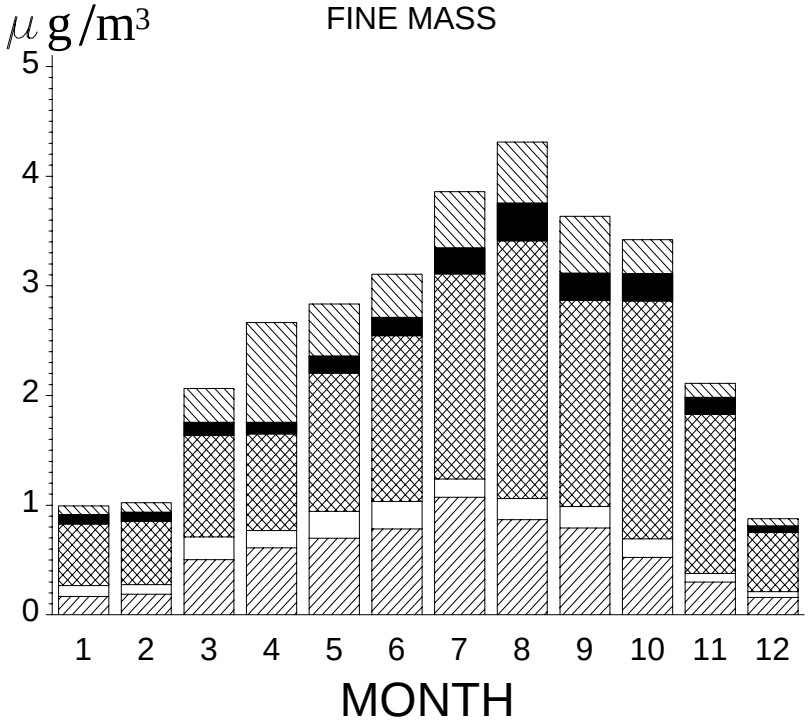

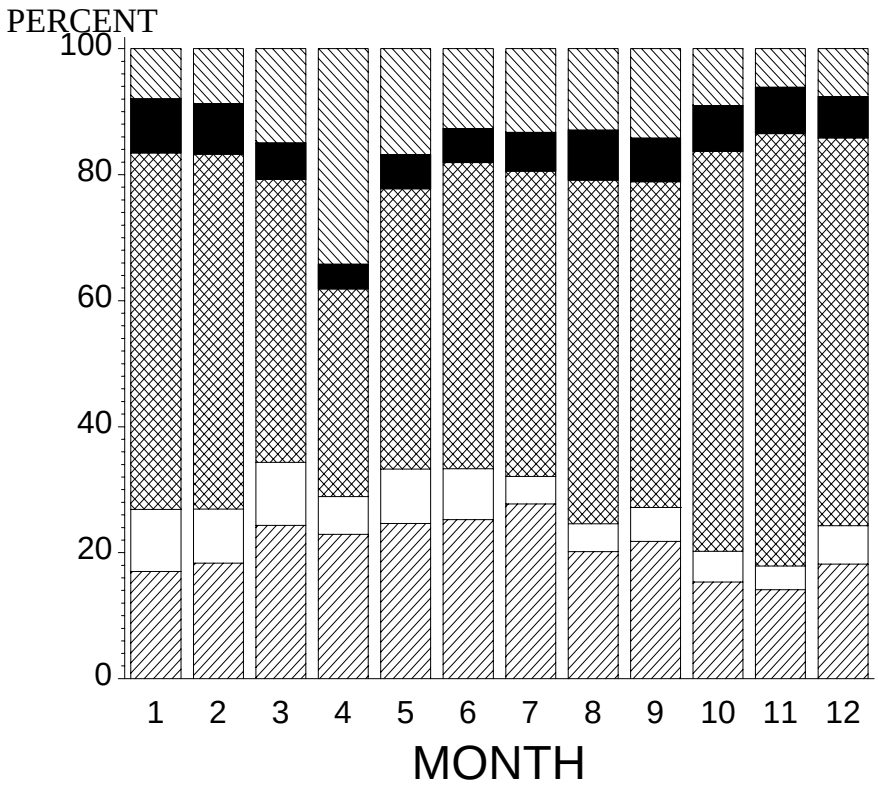

SULFATE NITRATE ORGANIC LAC SOIL

LONE PEAK WA

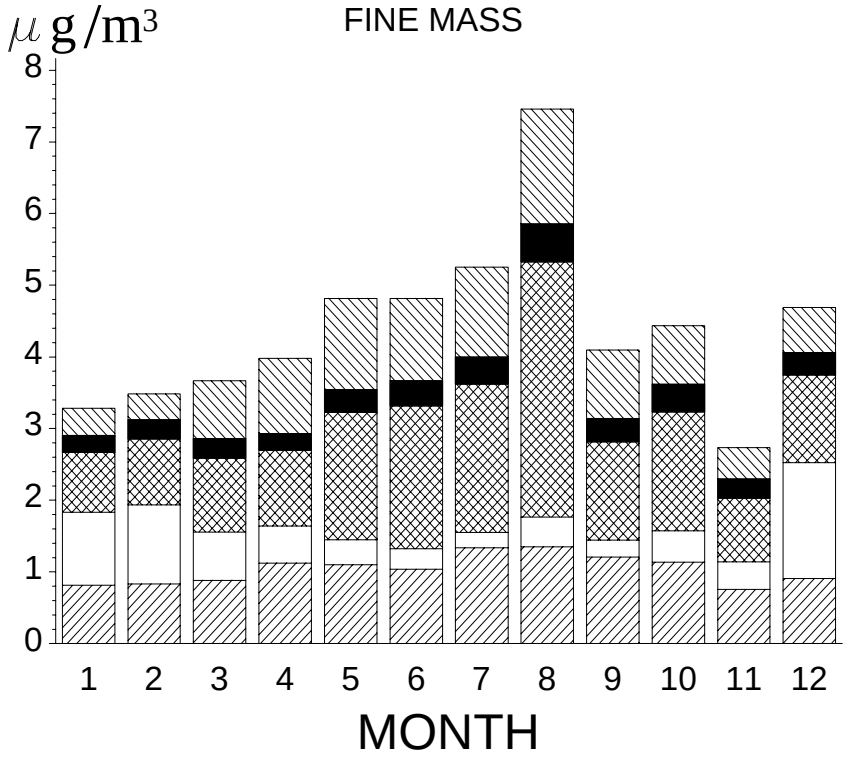

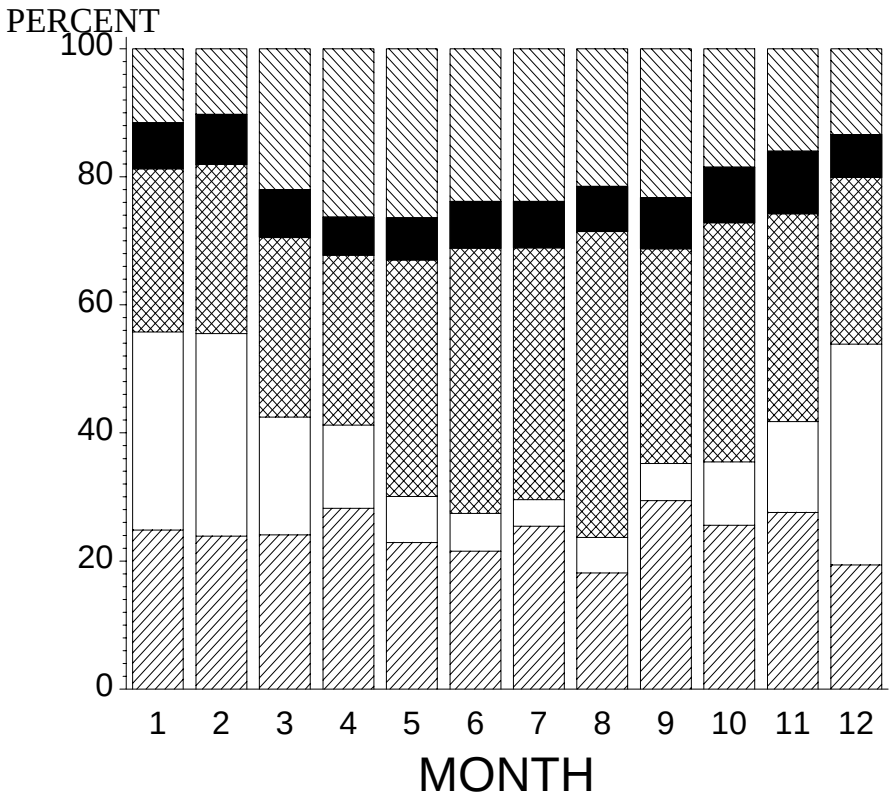

SULFATE NITRATE ORGANIC LAC SOIL

LYE BROOK WA

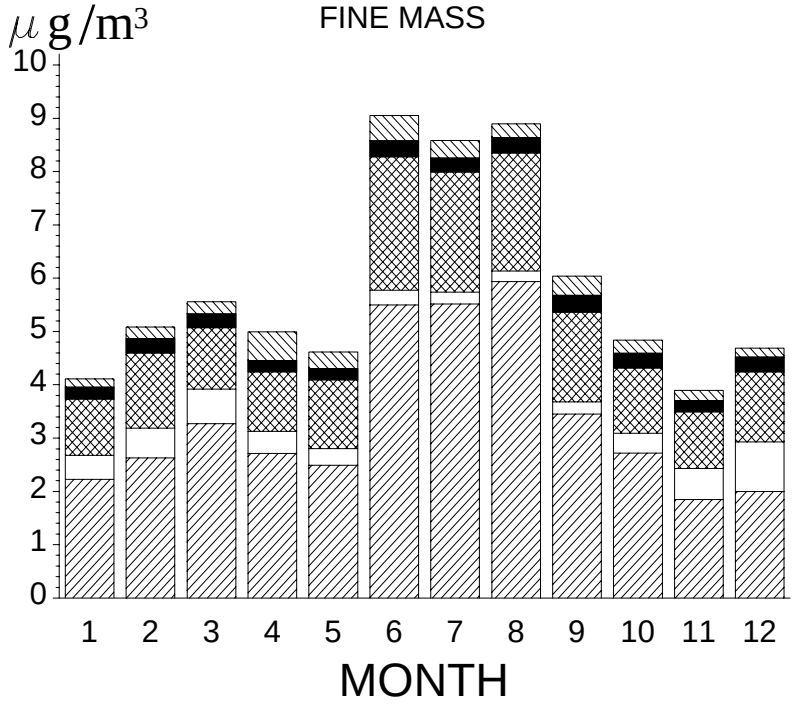
μg/m3
FINE MASS
10
9
8
7
6
5
4
3
2
1
0
1 2 3 4 5 6 7 8 9 10 11 12
MONTH

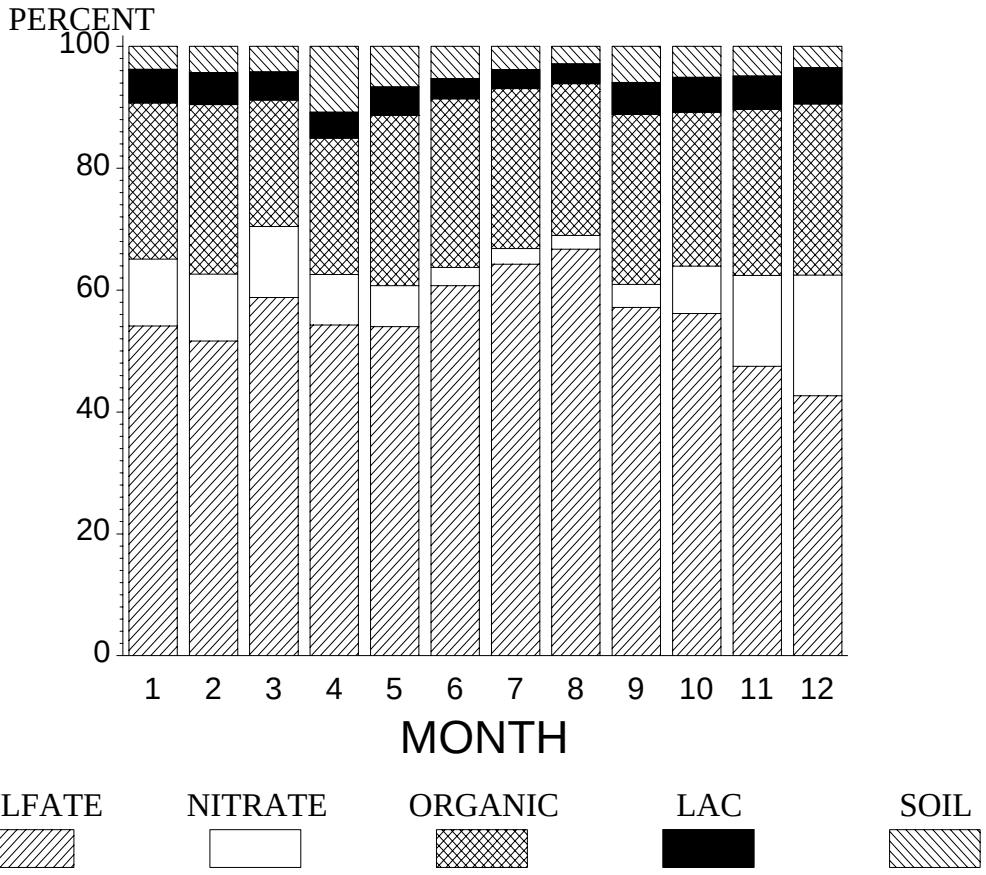
PERCENT
100
80
60
40
20
0
1 2 3 4 5 6 7 8 9 10 11 12
MONTH
SULFATE
NITRATE
ORGANIC
LAC
SOIL

MAMMOTH CAVE NP

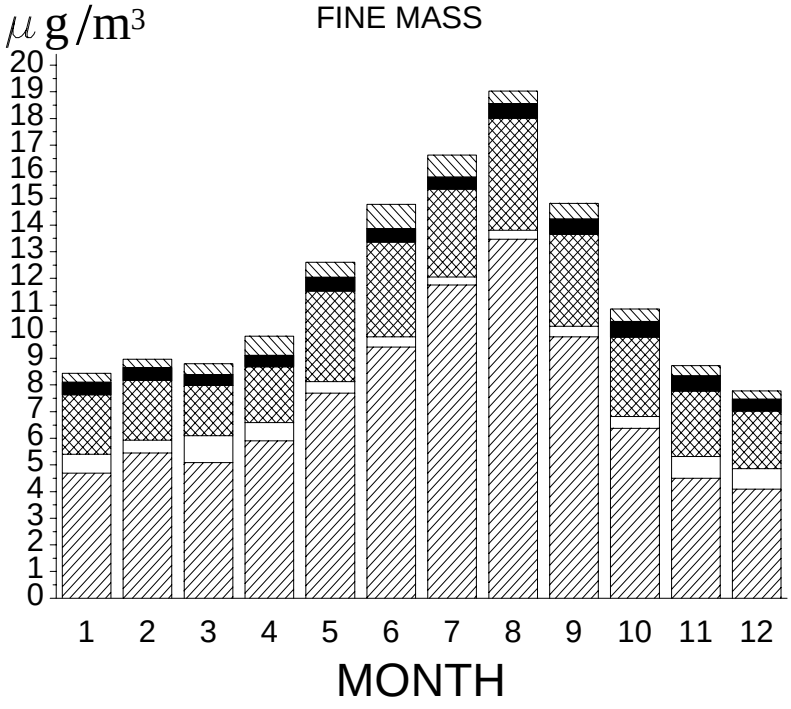

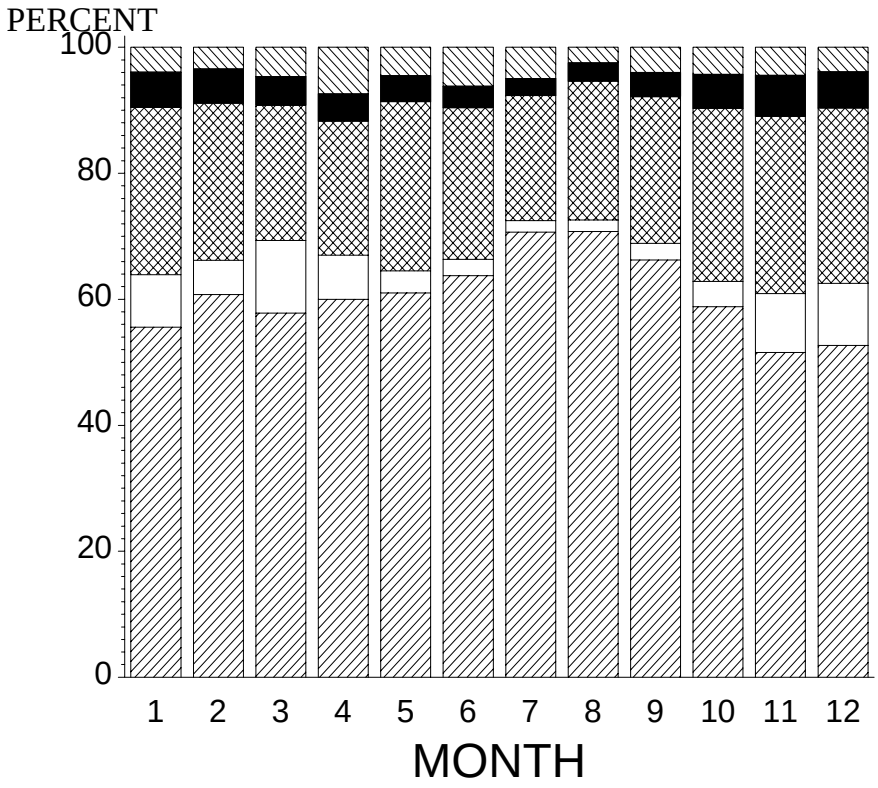

SULFATE NITRATE ORGANIC LAC SOIL

MESA VERDE NP

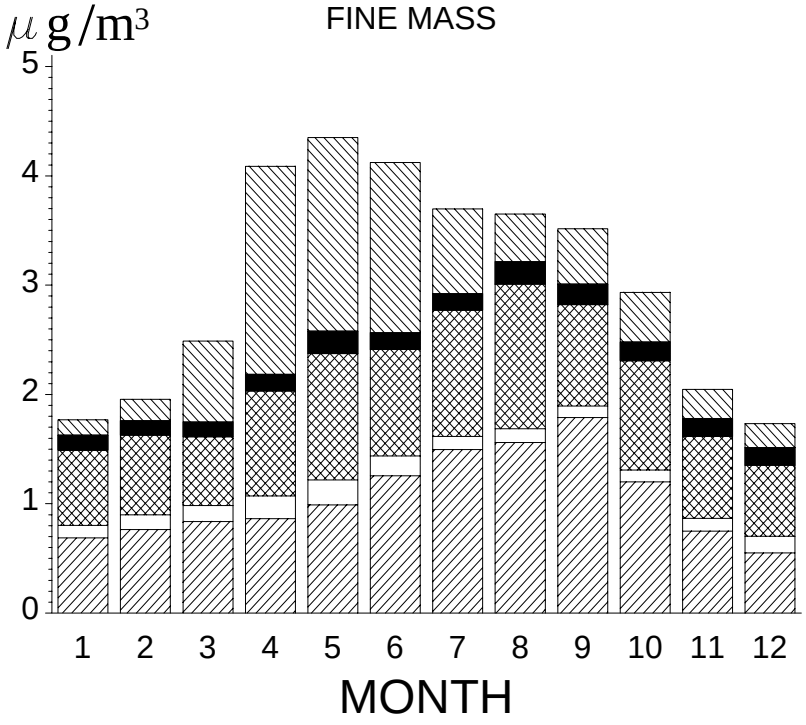

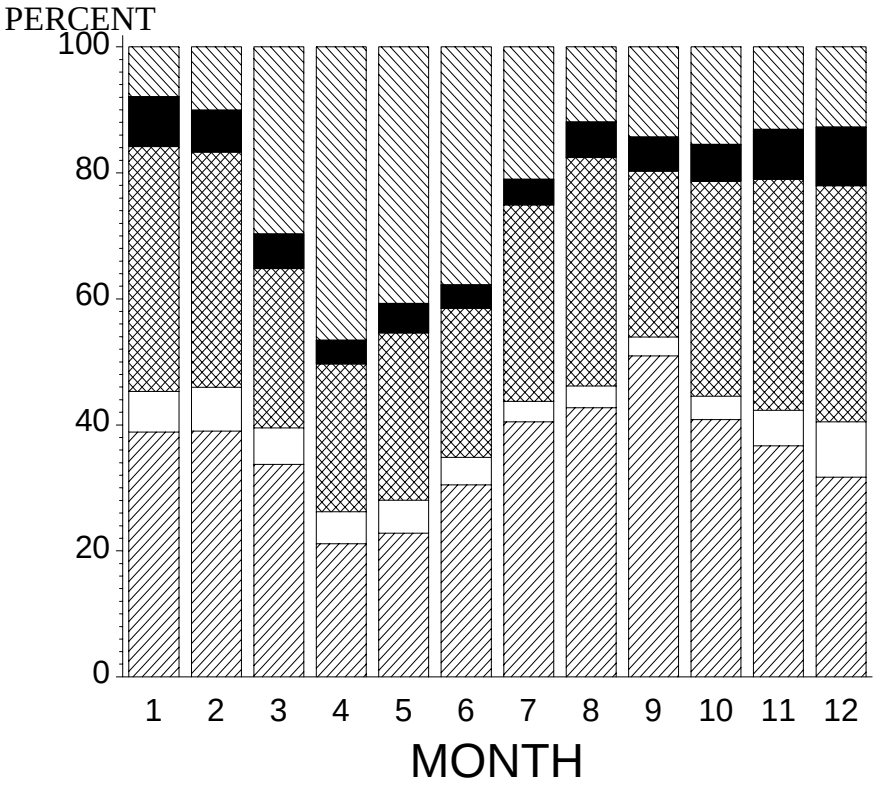

SULFATE NITRATE ORGANIC LAC SOIL

MOOSEHORN NWR

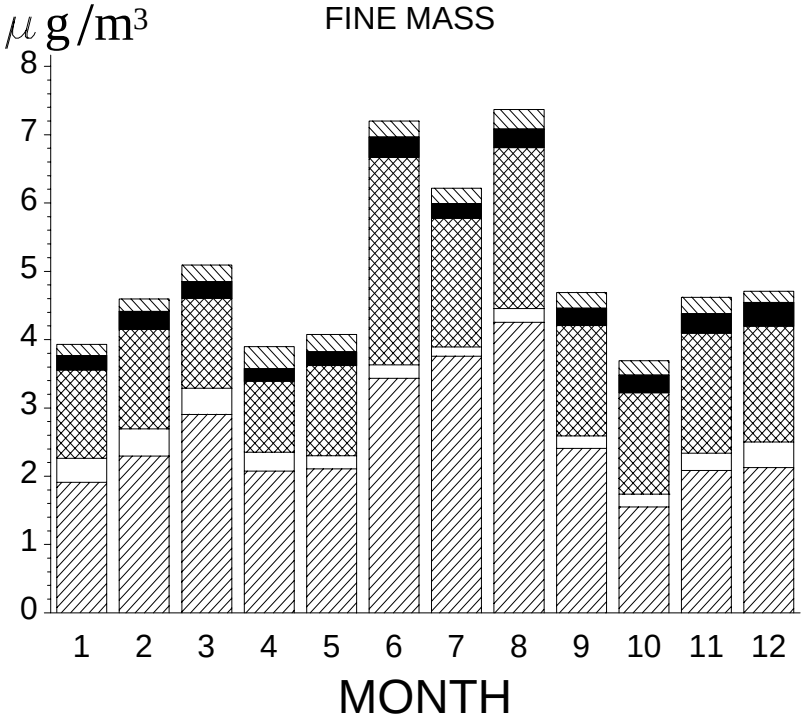

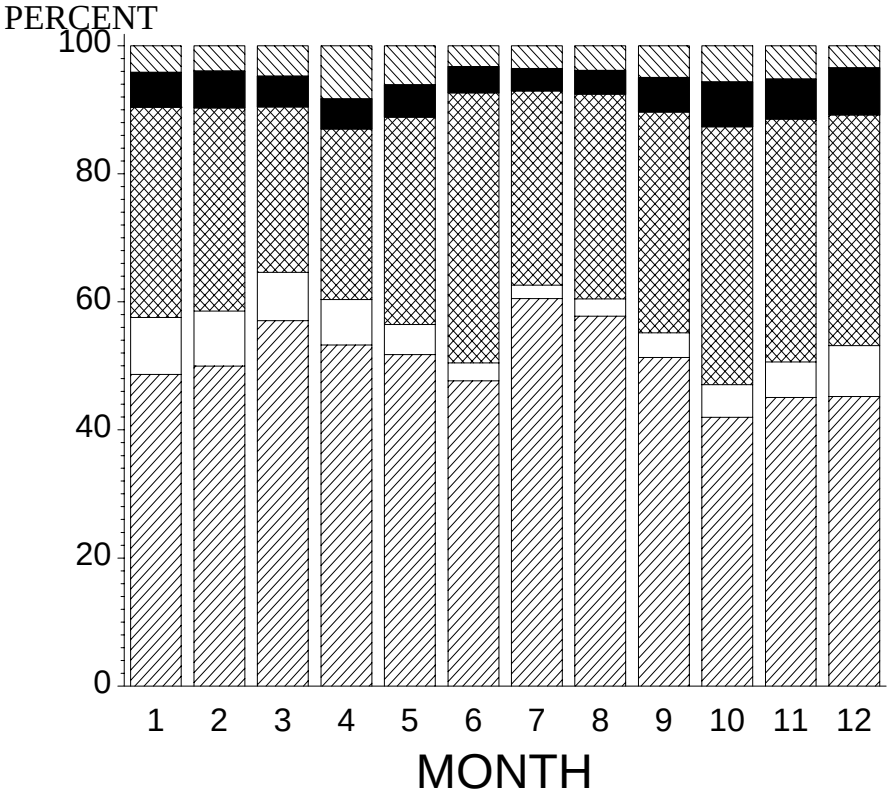

SULFATE NITRATE ORGANIC LAC SOIL

MOUNT RAINIER NP

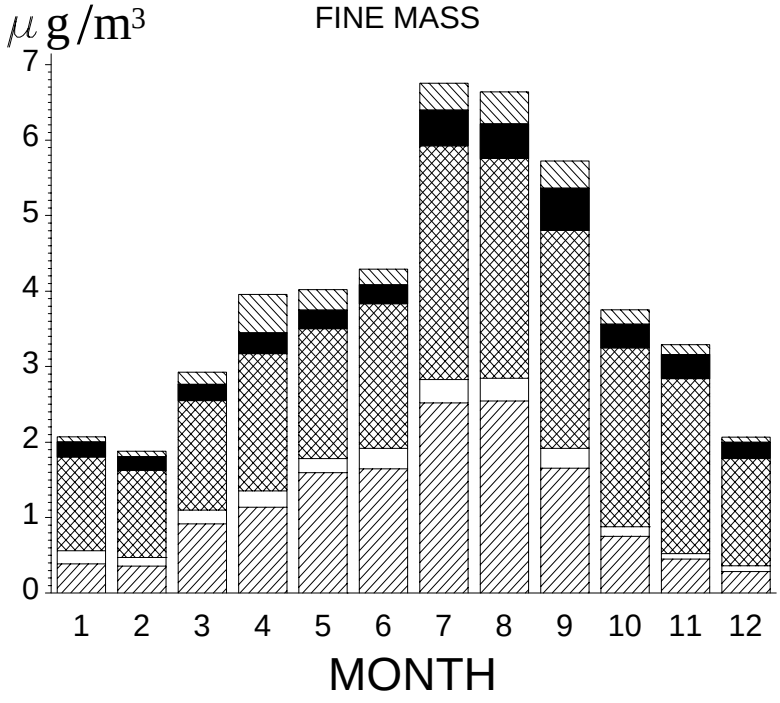

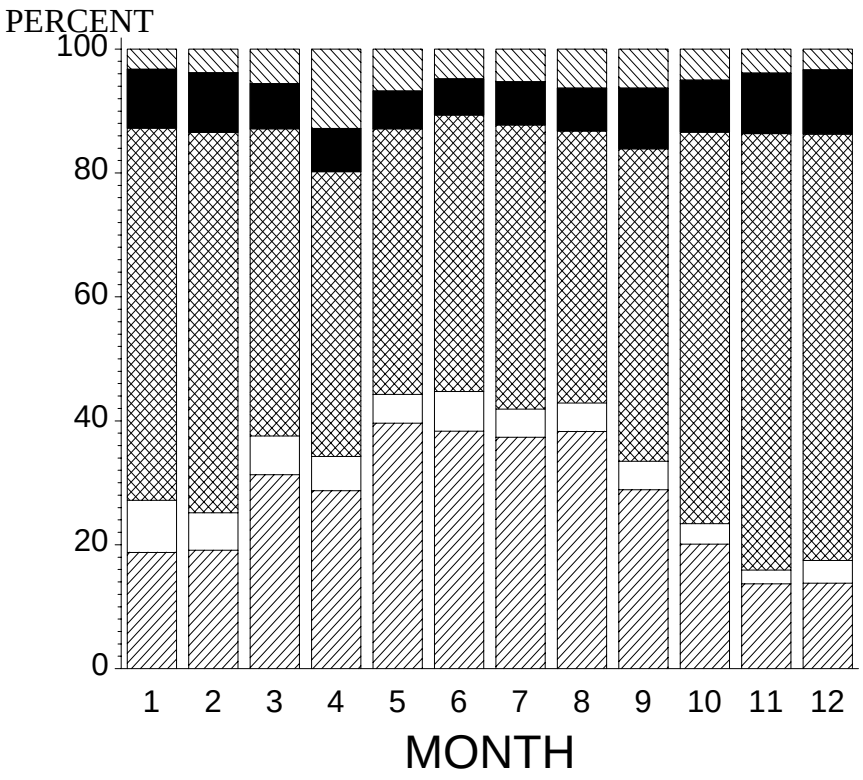

SULFATE NITRATE ORGANIC LAC SOIL

MOUNT ZIRKEL WA

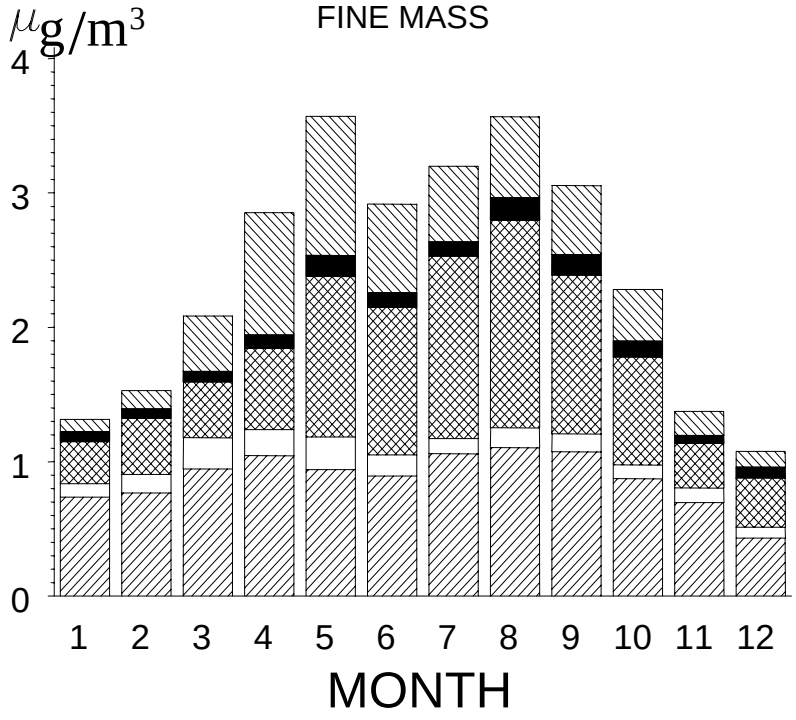

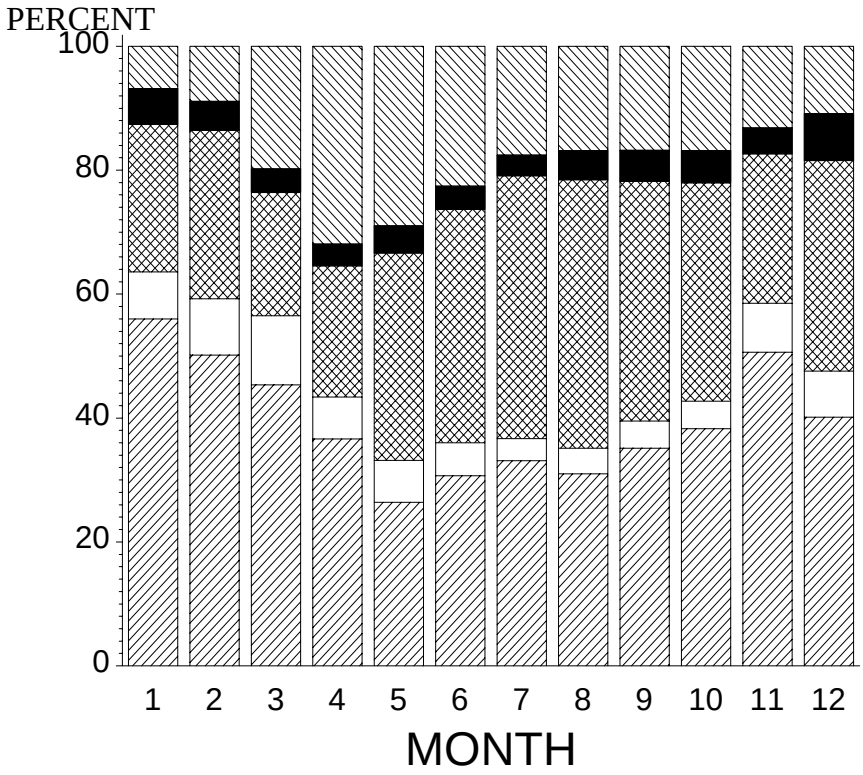

SULFATE NITRATE ORGANIC LAC SOIL

OKEFENOKEE NWR

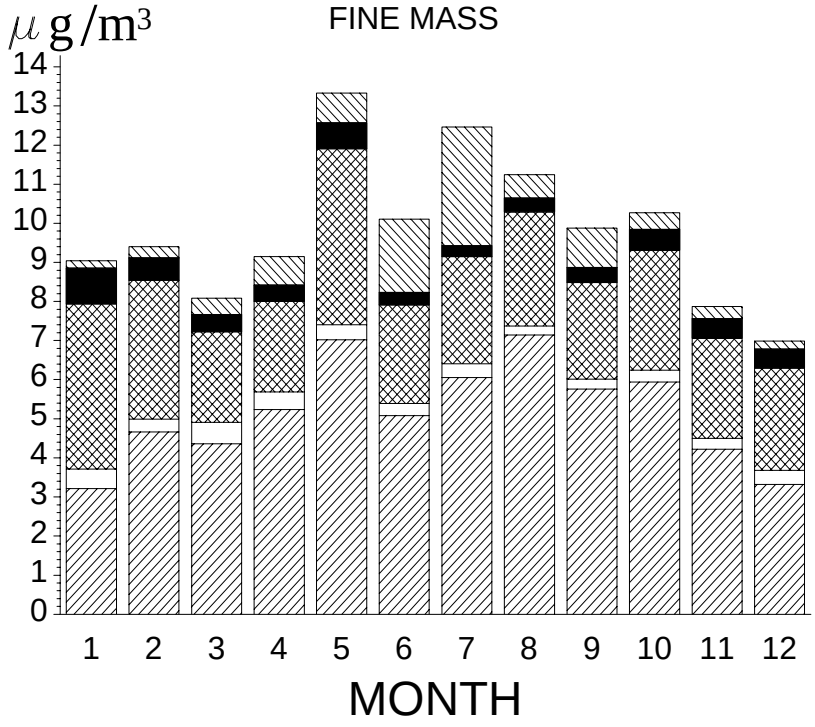

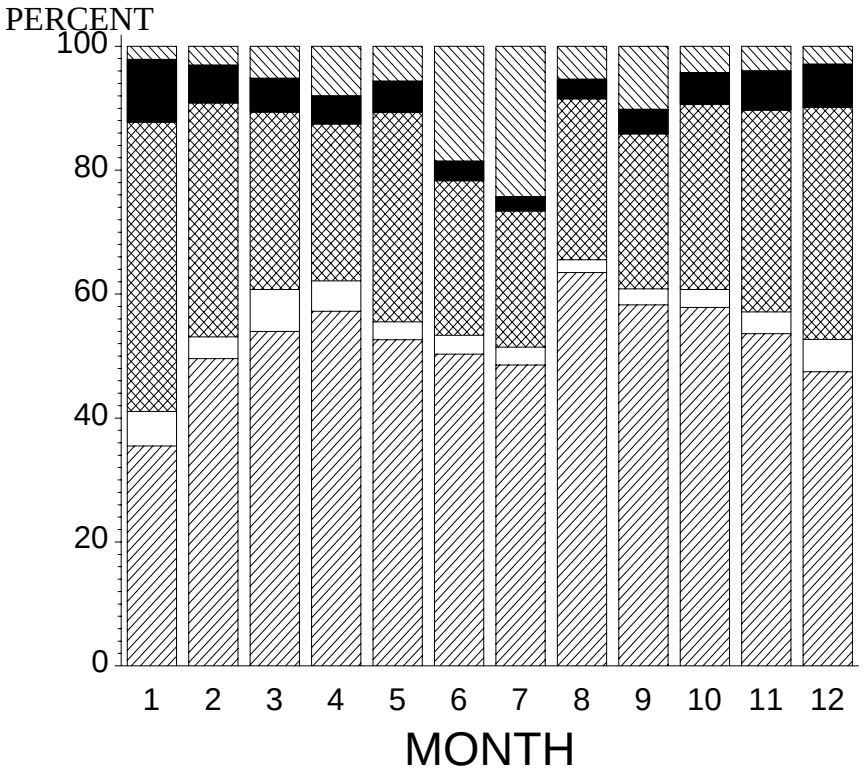

SULFATE NITRATE ORGANIC LAC SOIL

PETRIFIED FOREST NP

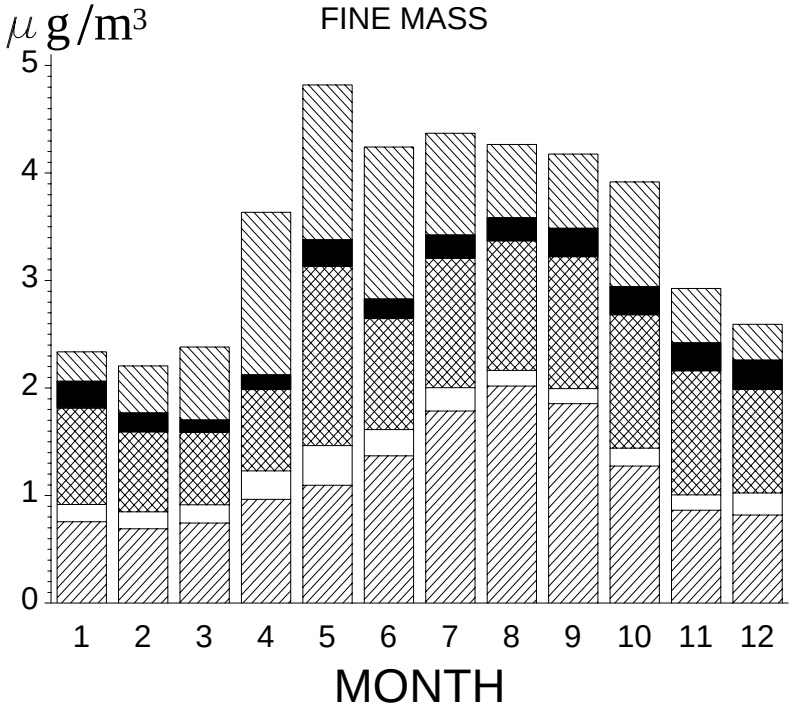

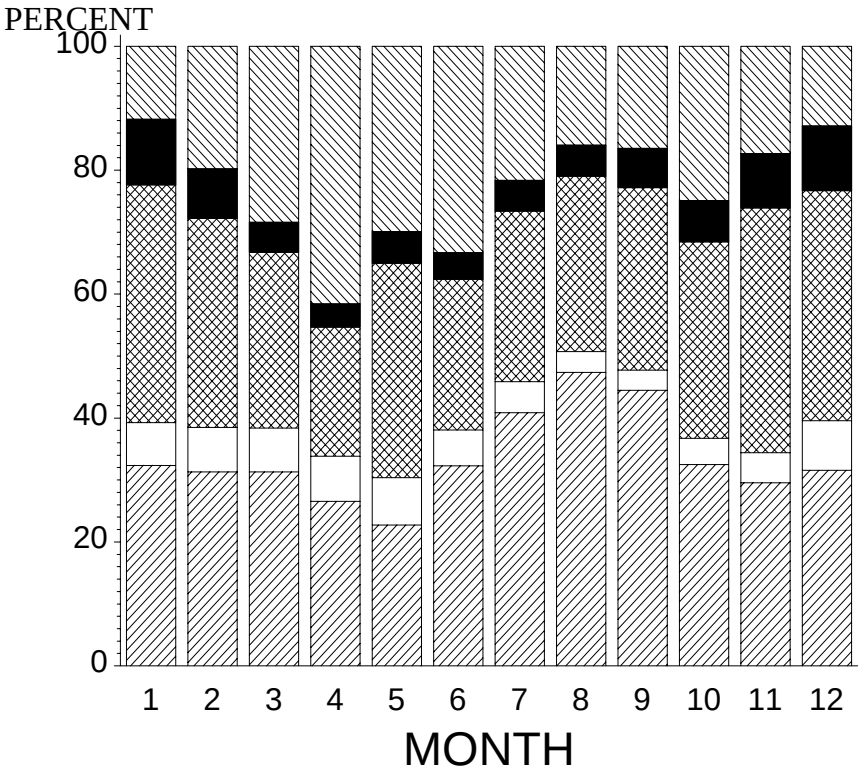

SULFATE NITRATE ORGANIC LAC SOIL

PINNACLES NM

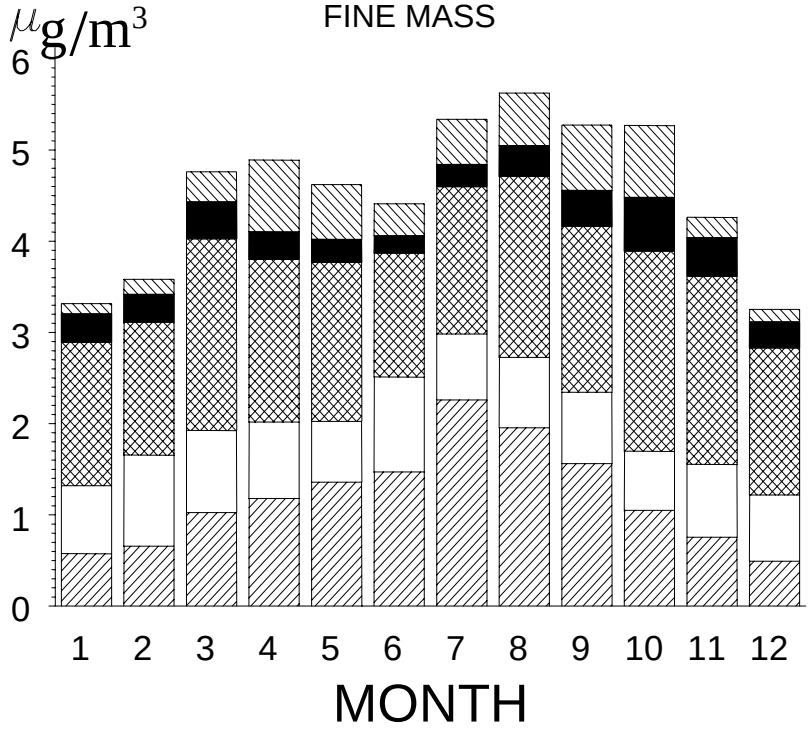

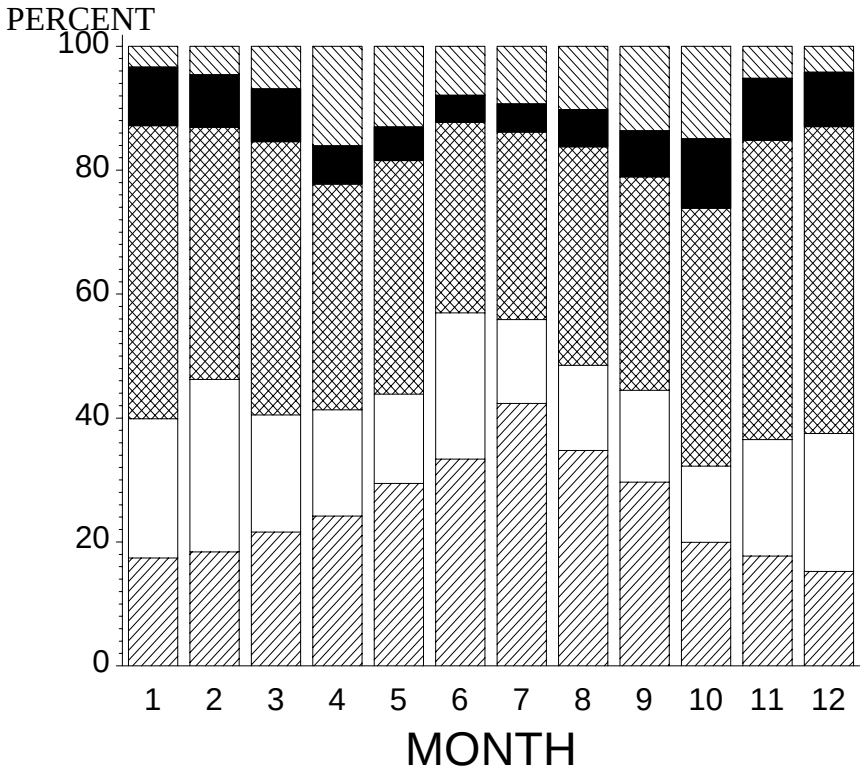

SULFATE NITRATE ORGANIC LAC SOIL

POINT REYES NS

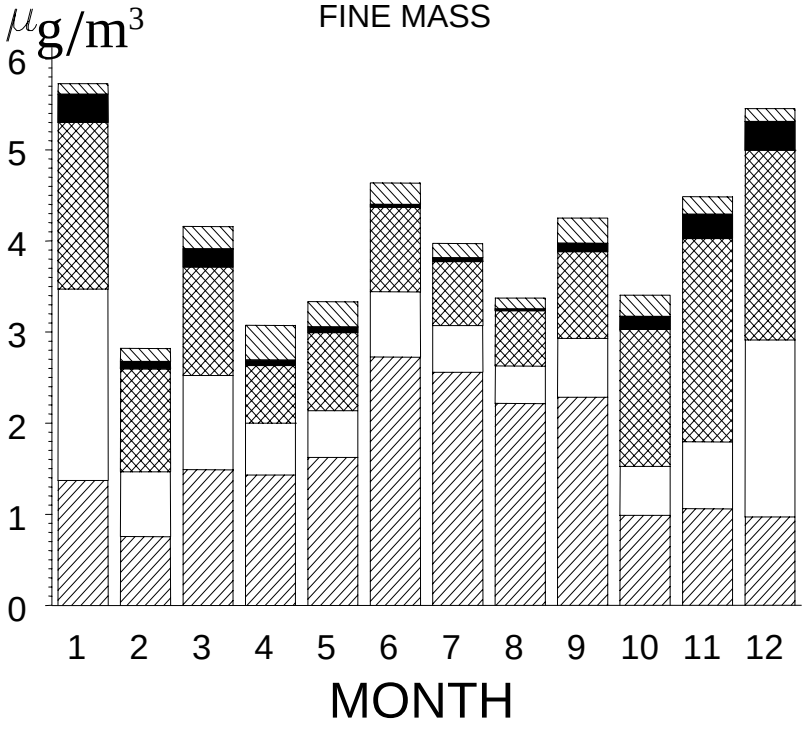

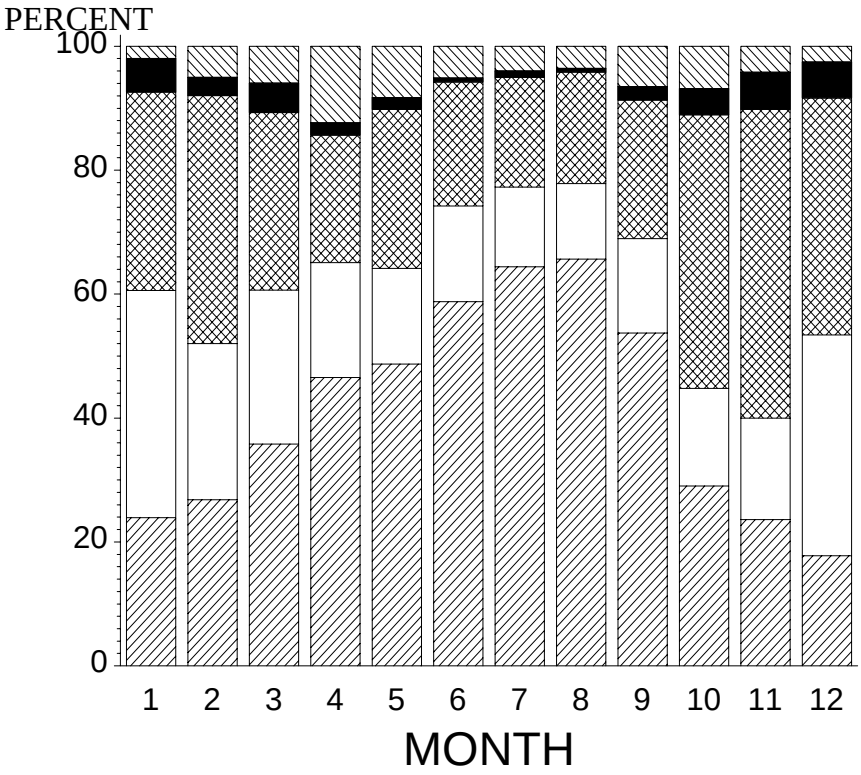

SULFATE NITRATE ORGANIC LAC SOIL

REDWOOD NP

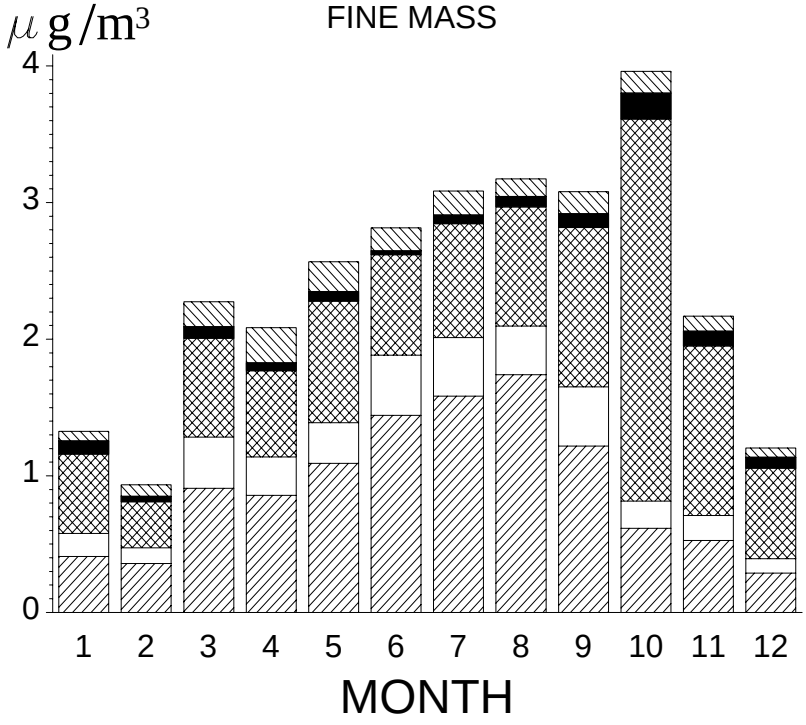

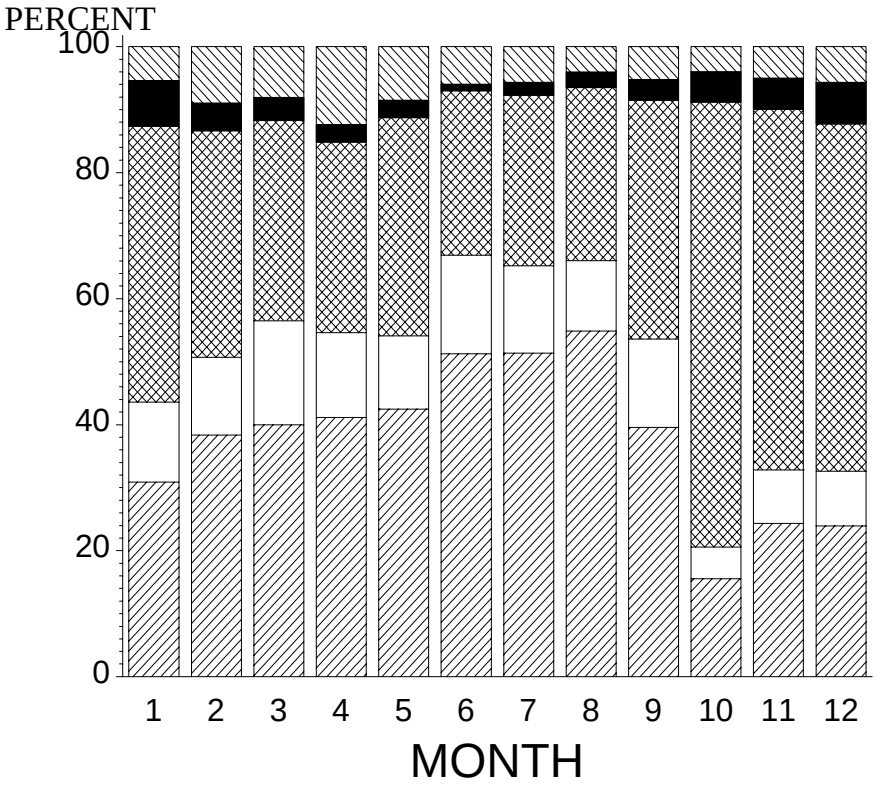

SULFATE NITRATE ORGANIC LAC SOIL

ROCKY MOUNTAIN NP

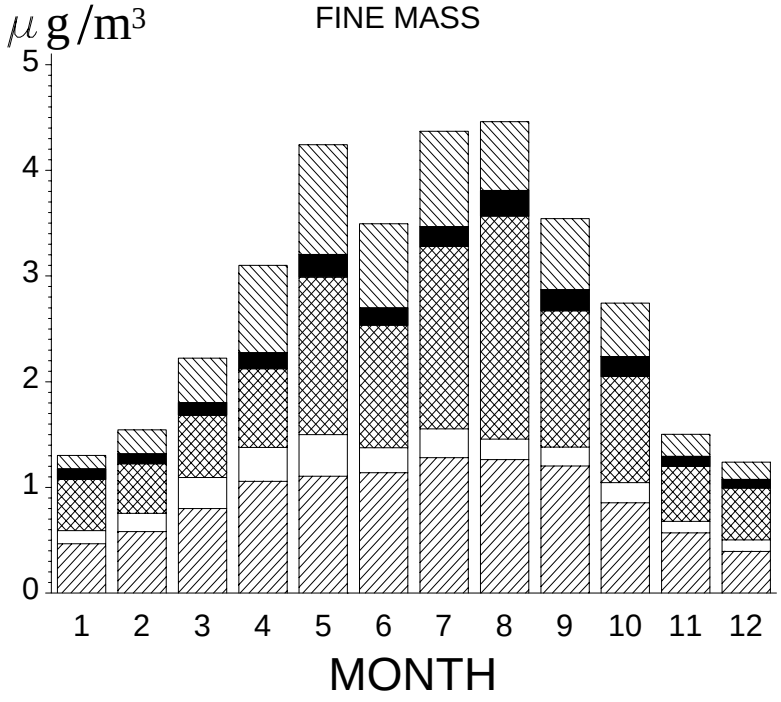

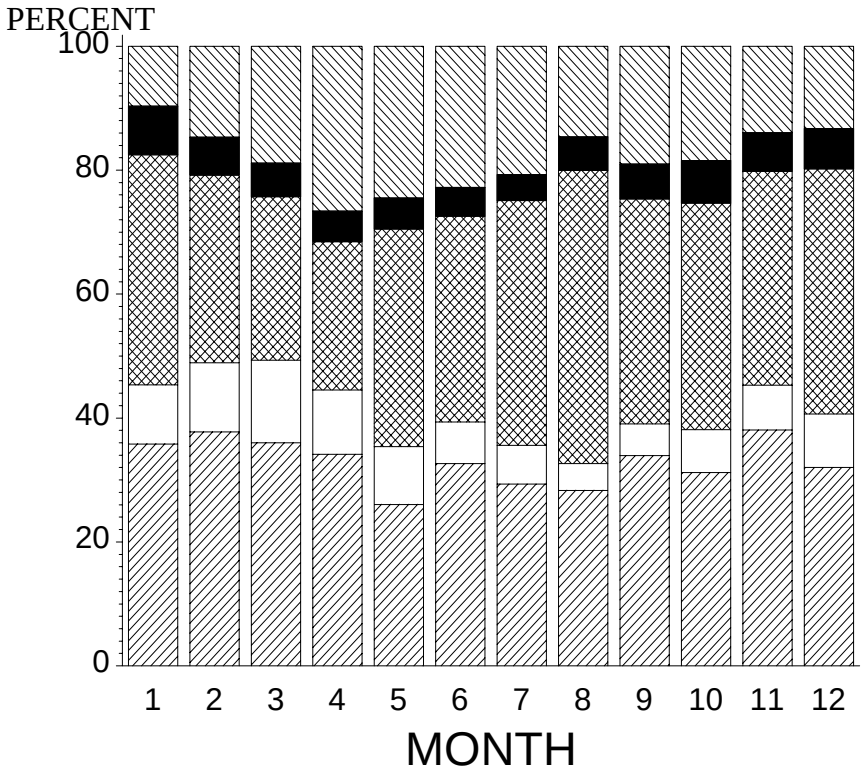

SULFATE NITRATE ORGANIC LAC SOIL

SAN GORGONIO WA

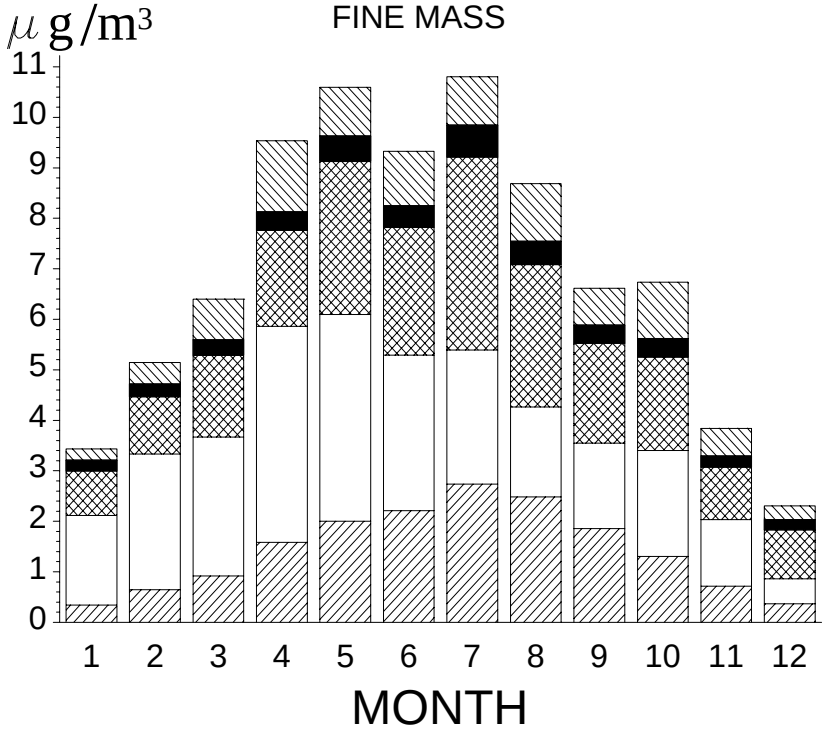

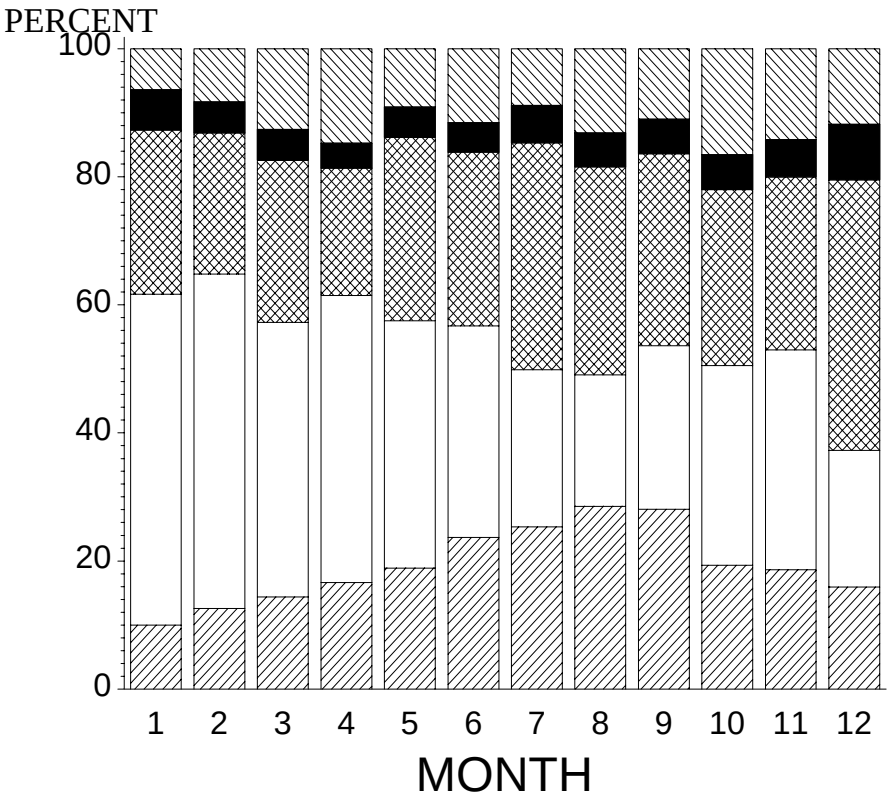

SULFATE NITRATE ORGANIC LAC SOIL

SEQUOIA NP

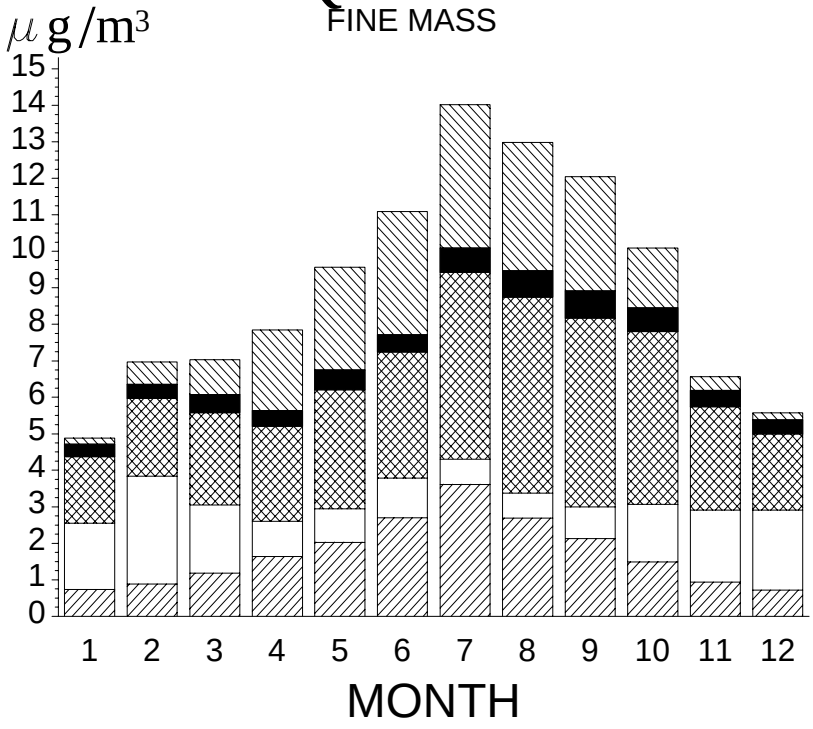

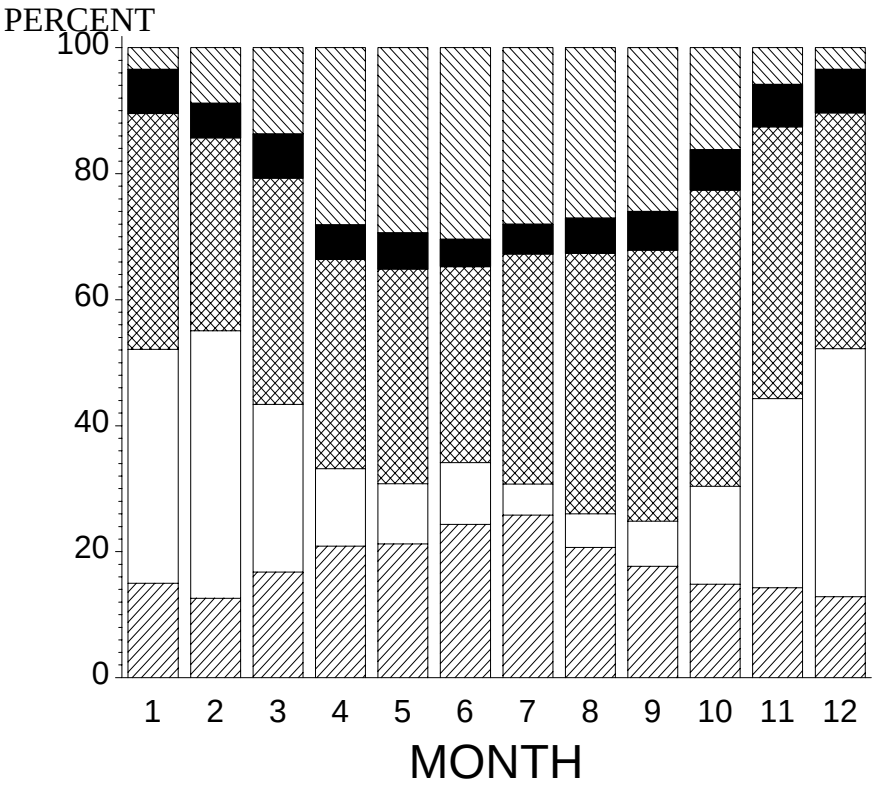

SULFATE NITRATE ORGANIC LAC SOIL

SHENANDOAH NP

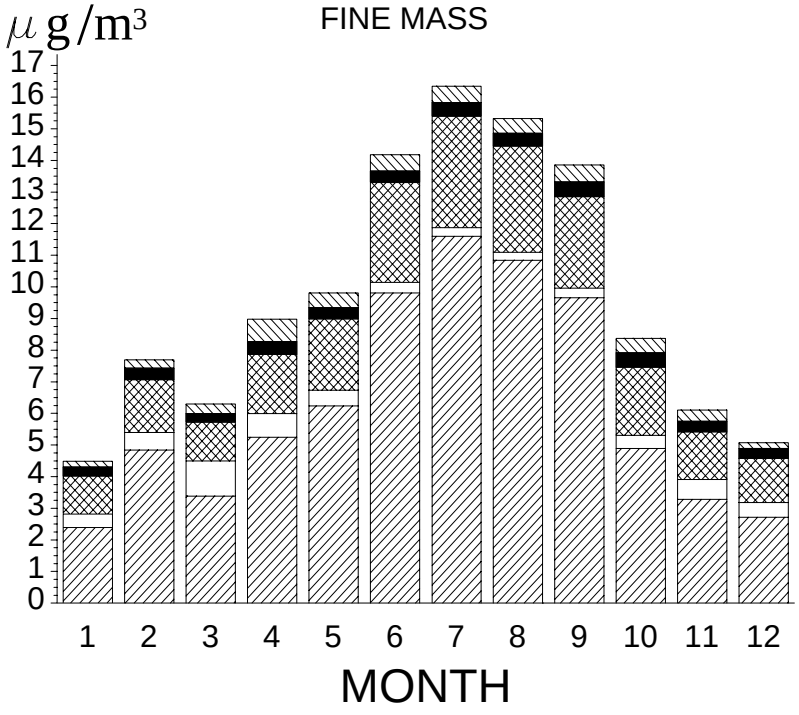

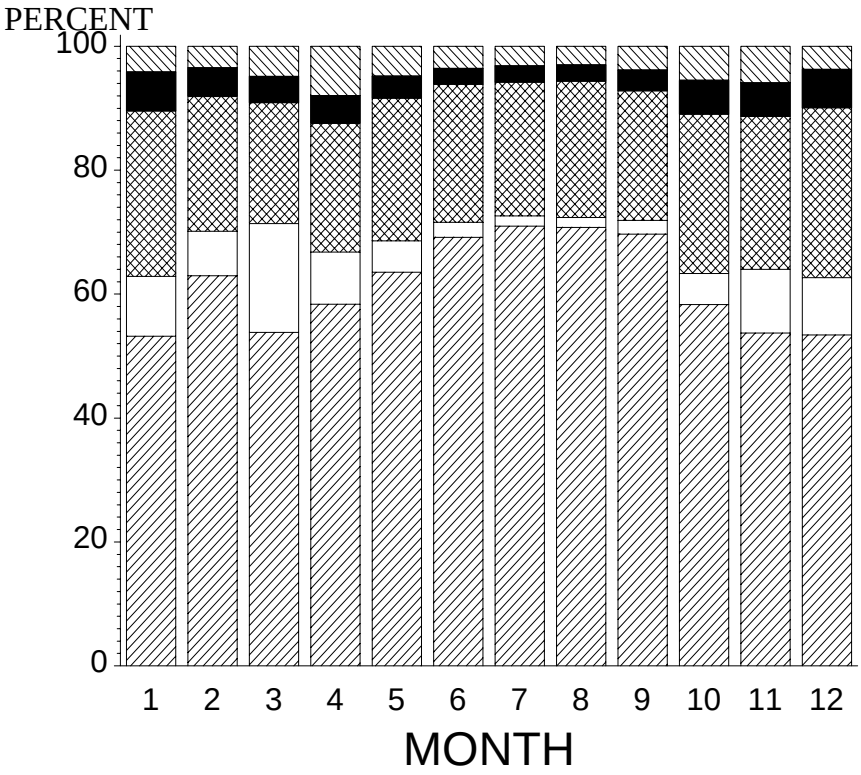

SULFATE NITRATE ORGANIC LAC SOIL

SHINING ROCK WA

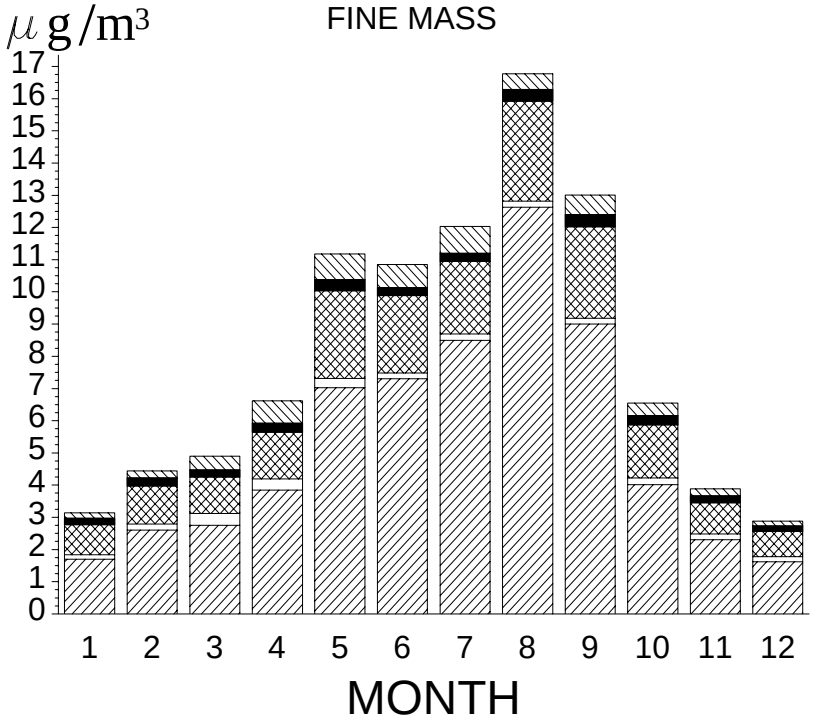

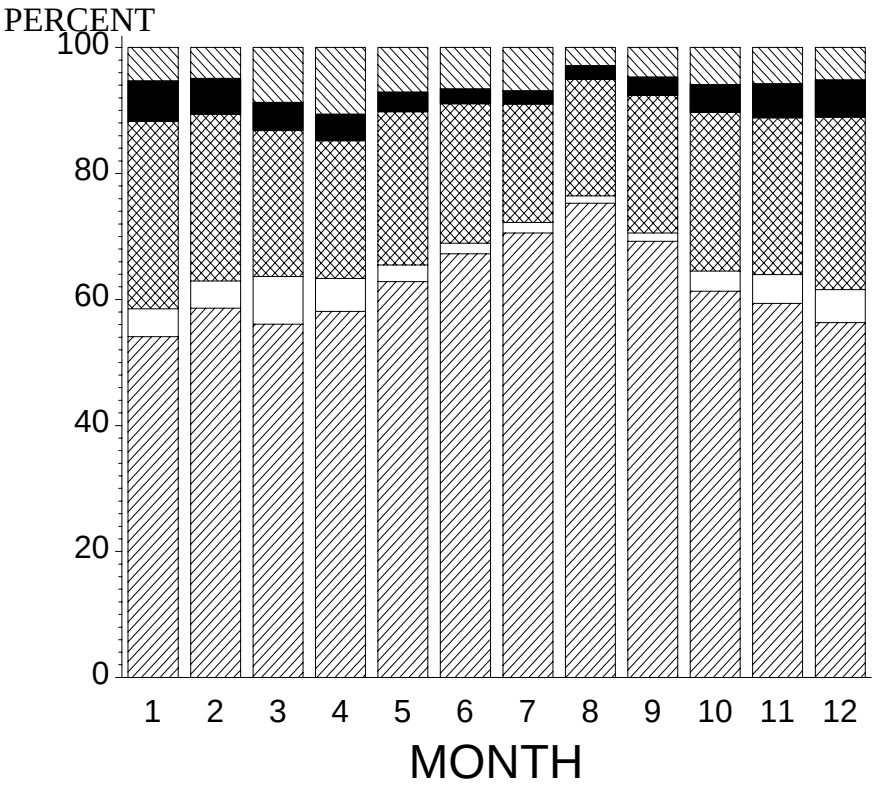

SULFATE NITRATE ORGANIC LAC SOIL

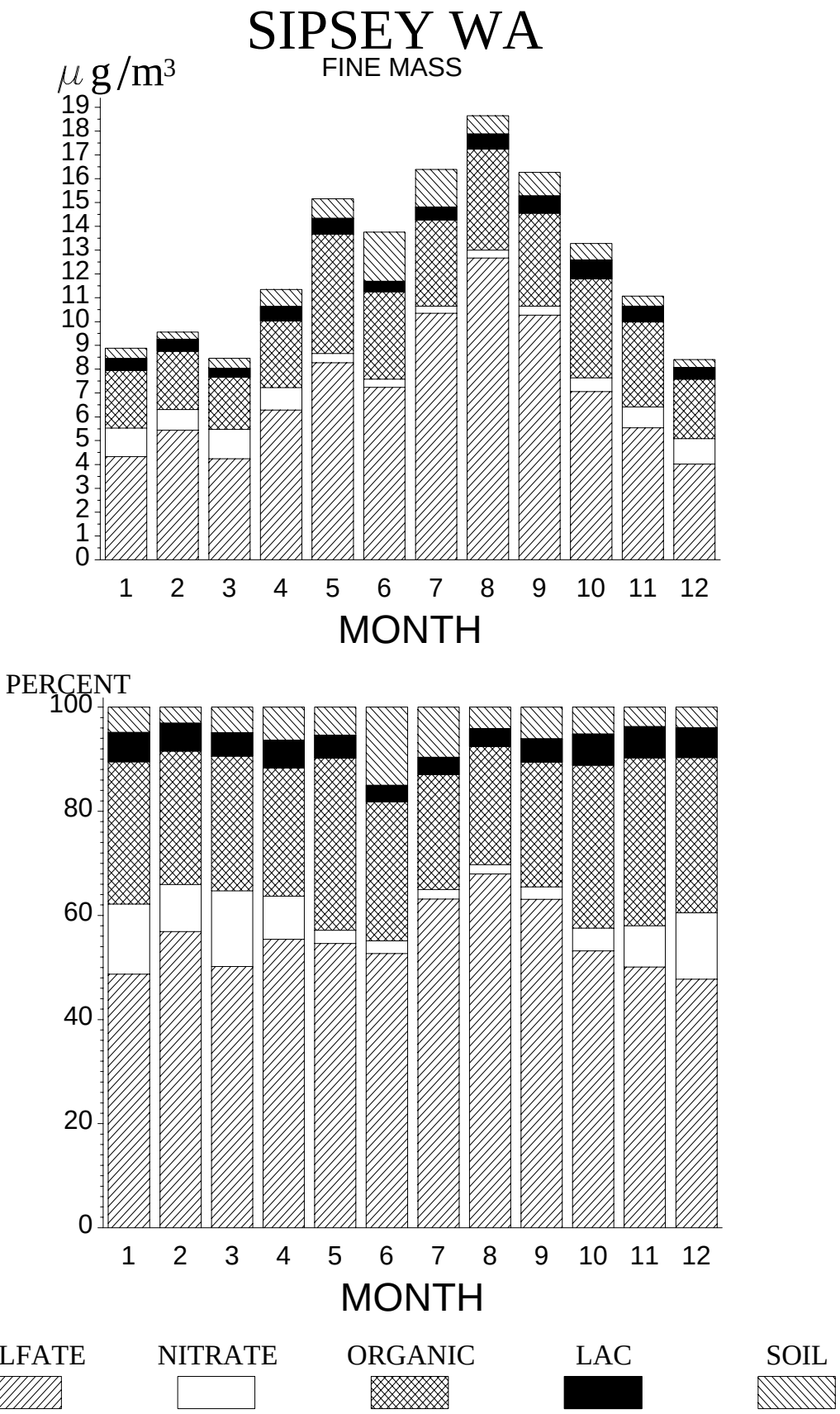
SIPSEY WA
FINE MASS
μg/m3
19
18
17
16
15
14
13
12
11
10
9
8
7
6
5
4
3
2
1
0
1 2 3 4 5 6 7 8 9 10 11 12
MONTH
PERCENT
100
80
60
40
20
0
1 2 3 4 5 6 7 8 9 10 11 12
MONTH
SULFATE
NITRATE
ORGANIC
LAC
SOIL

SNOQUALMIE PASS WA

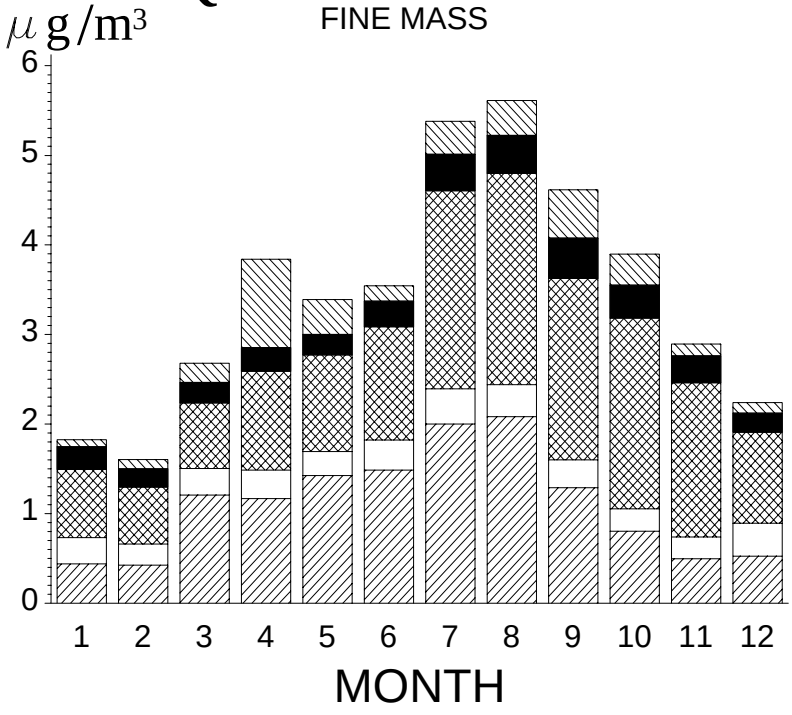

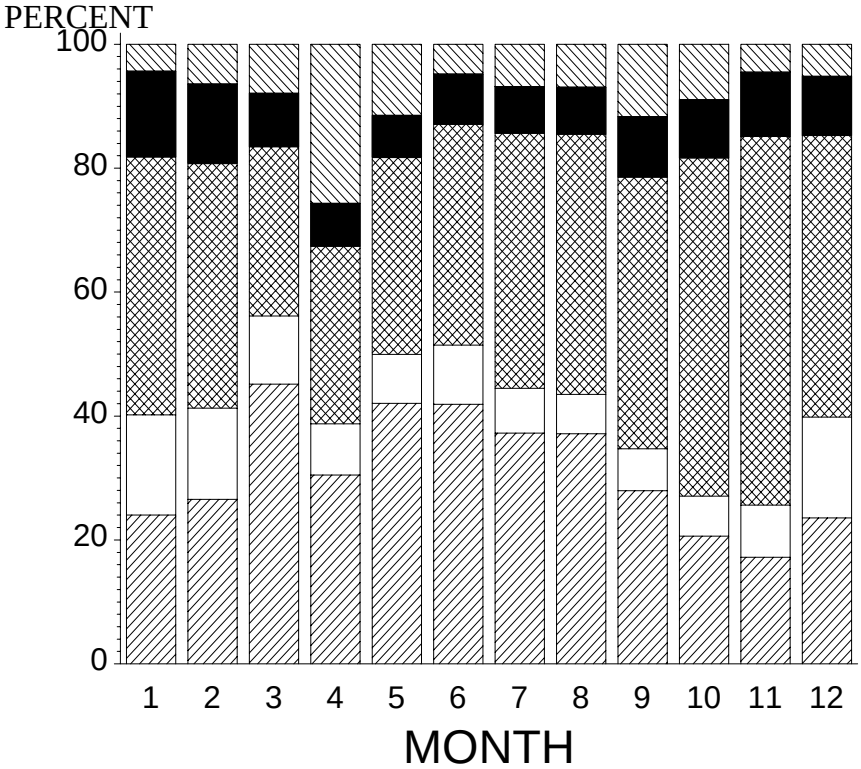

SULFATE NITRATE ORGANIC LAC SOIL

THREE SISTERS WA

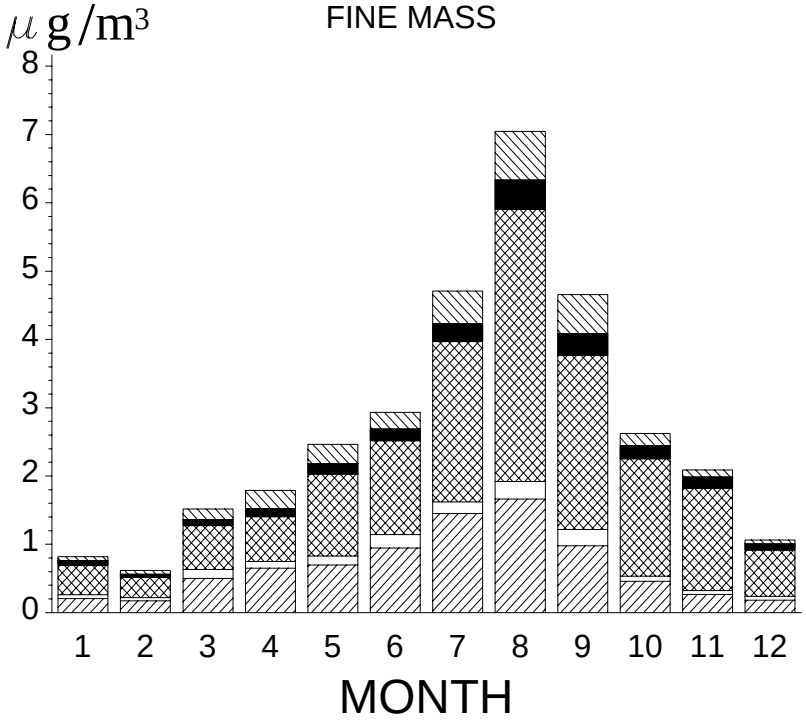

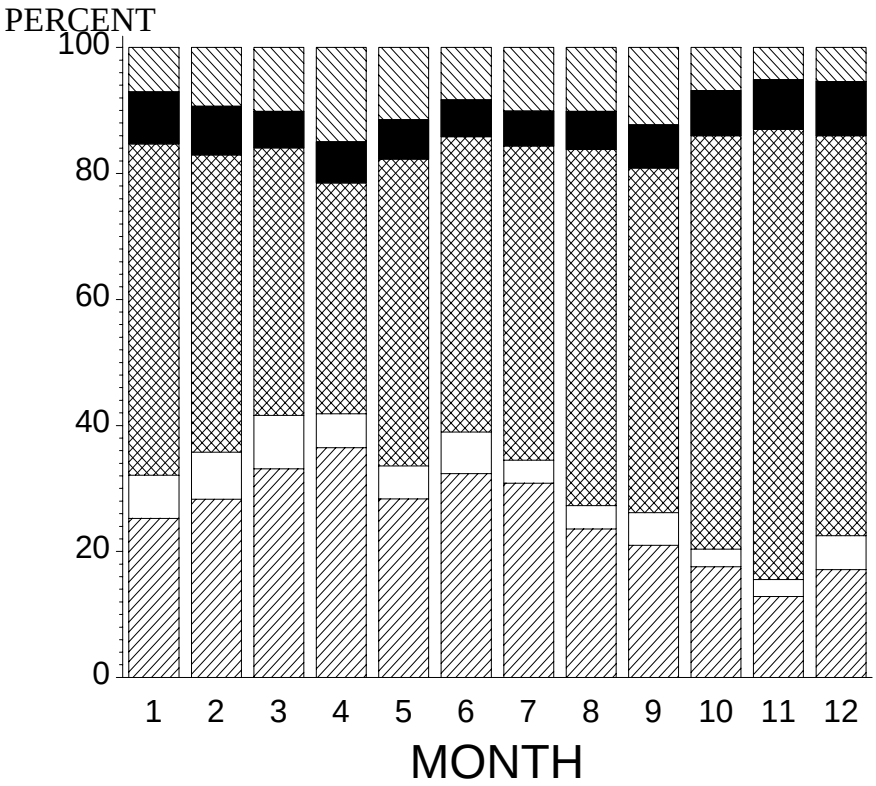

SULFATE NITRATE ORGANIC LAC SOIL

TONTO NM

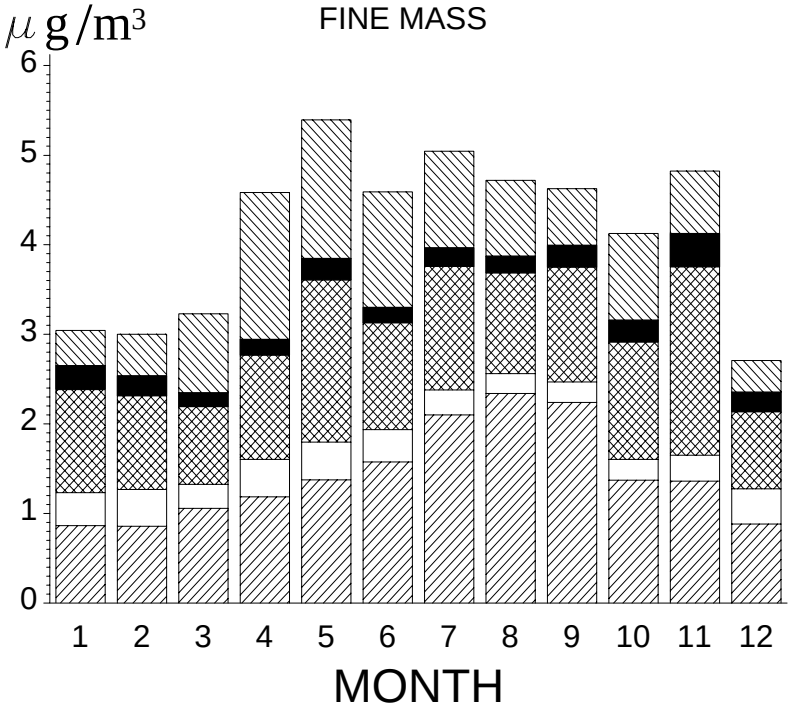

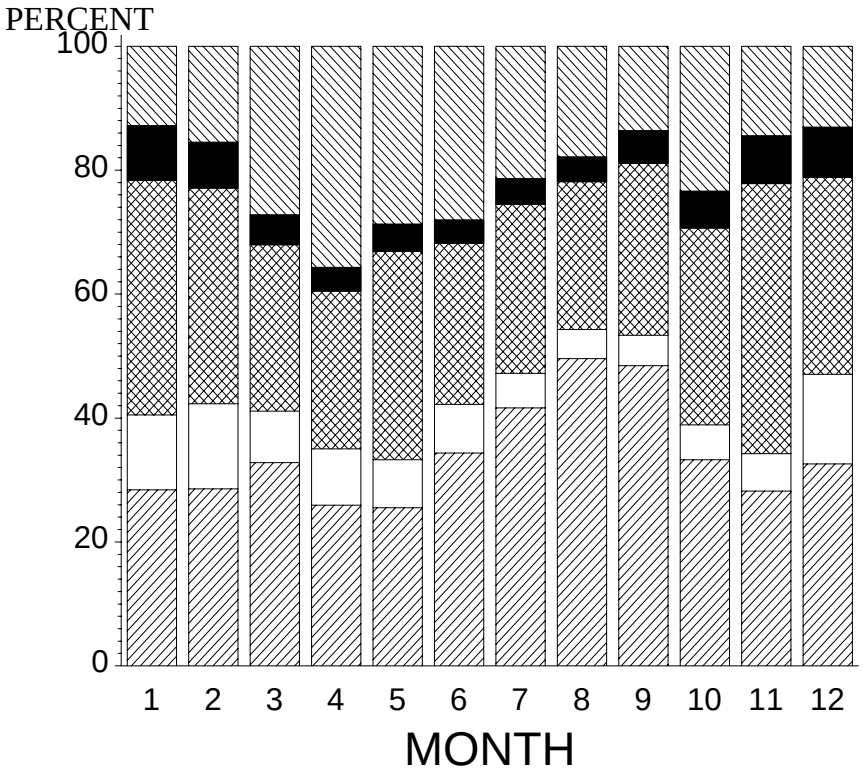

SULFATE NITRATE ORGANIC LAC SOIL

UPPER BUFFALO WA

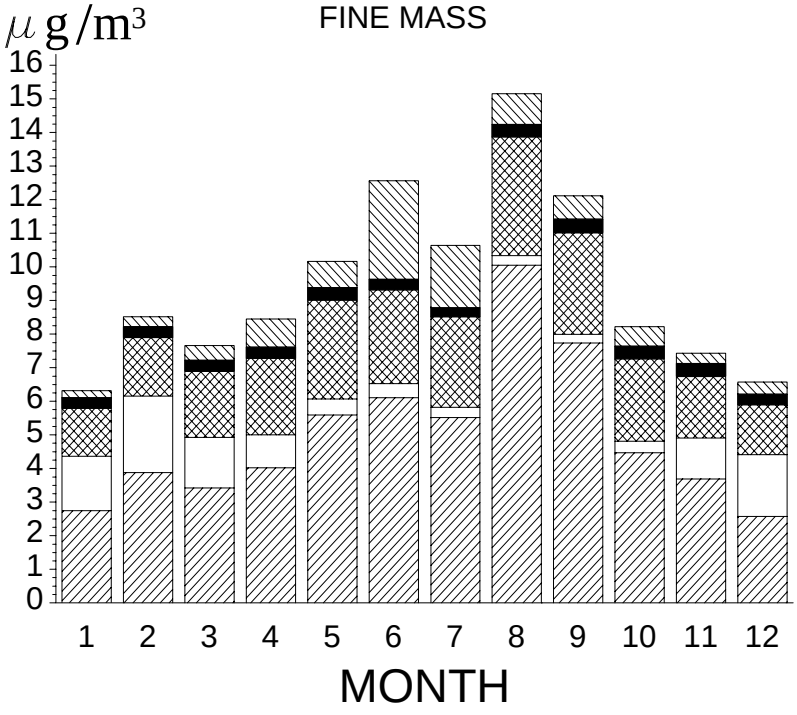

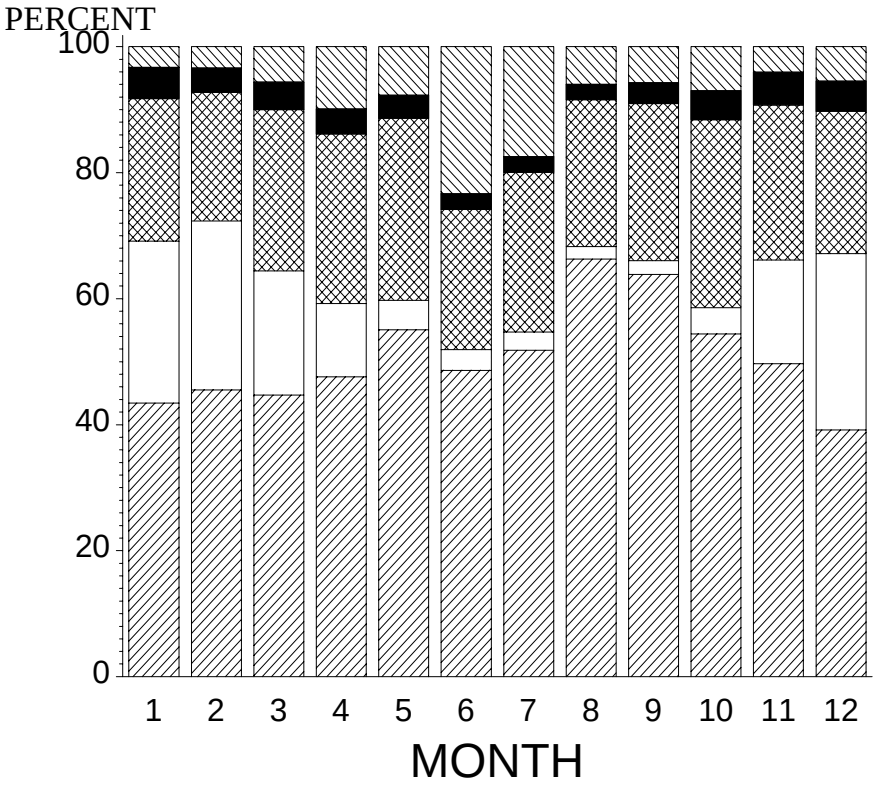

SULFATE NITRATE ORGANIC LAC SOIL

WASHINGTON DC

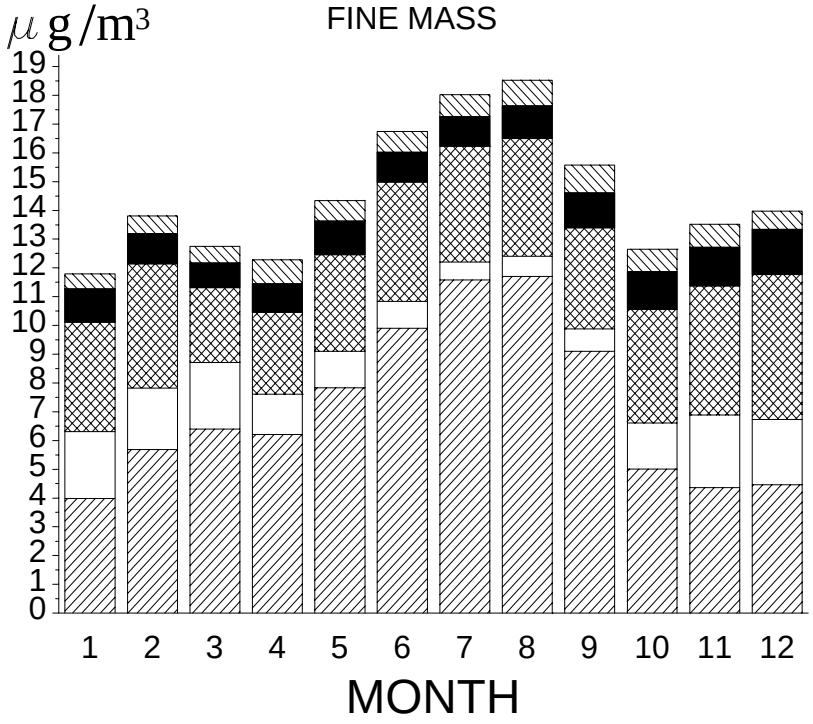

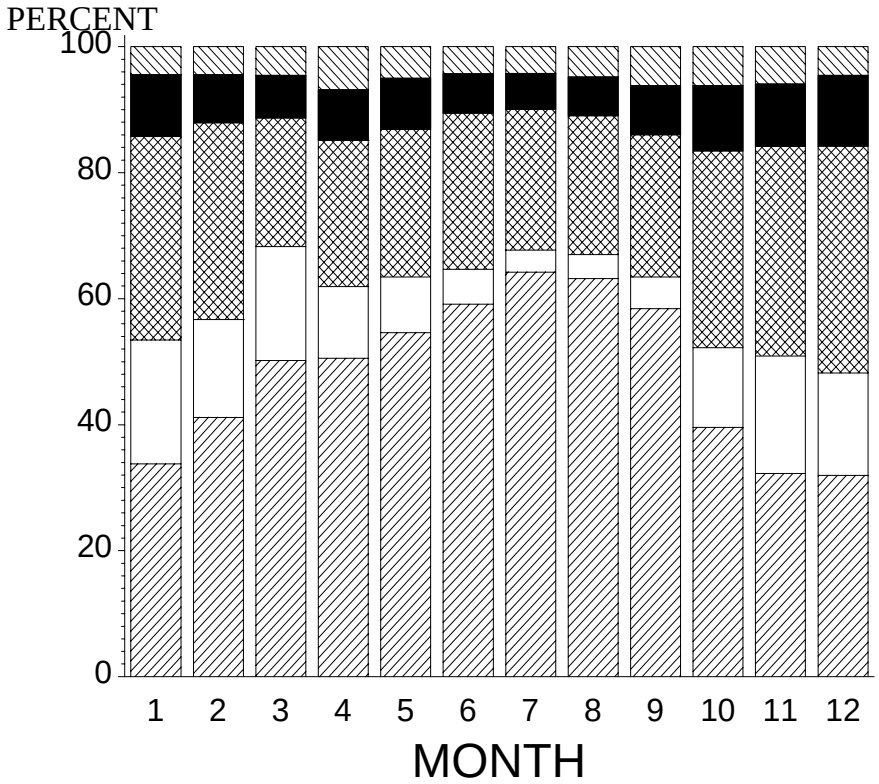

SULFATE NITRATE ORGANIC LAC SOIL

WEMINUCHE WA

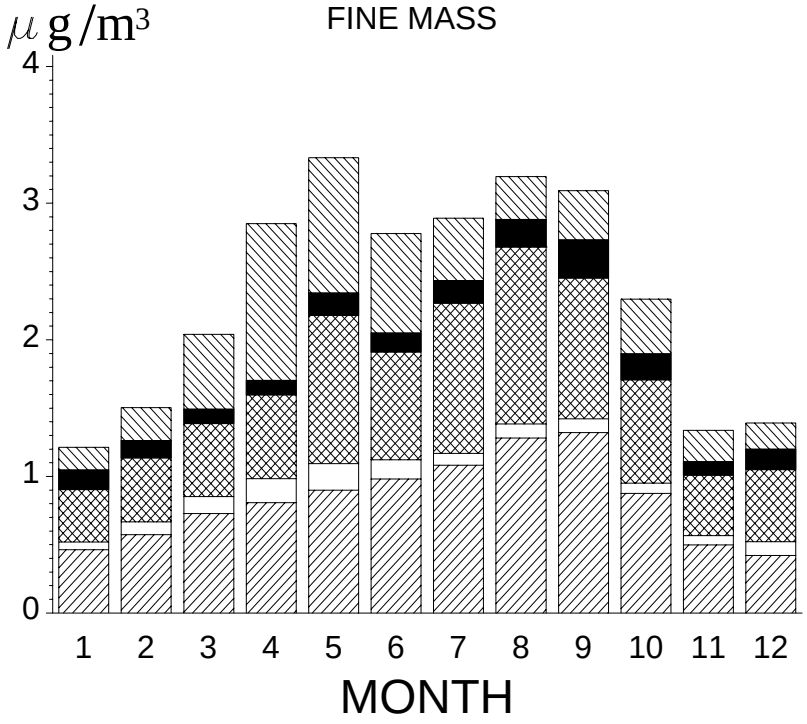

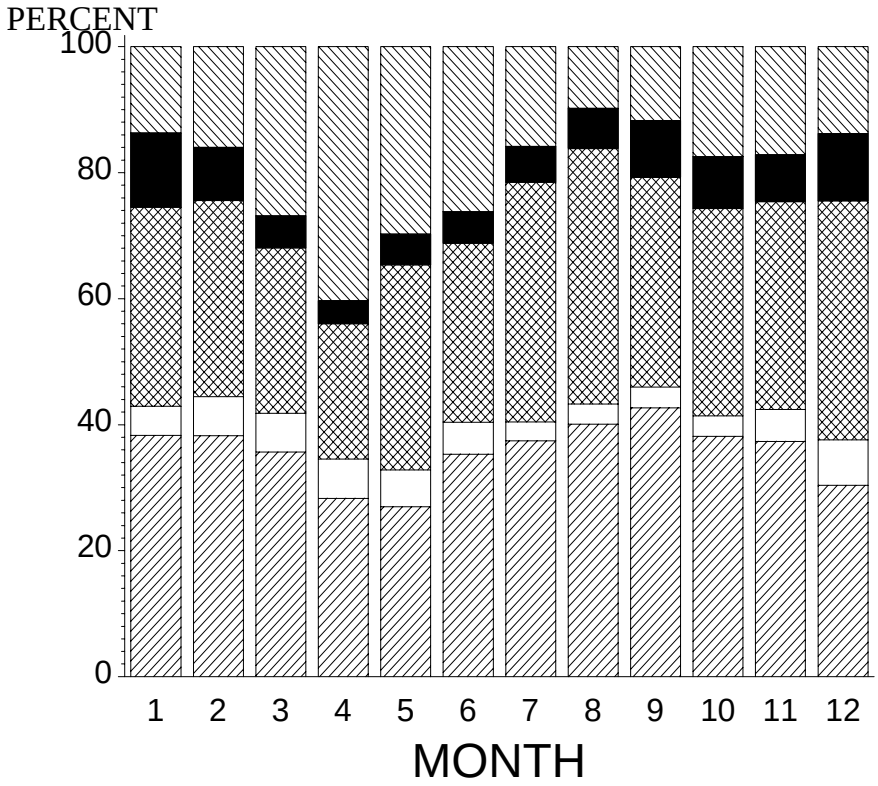

SULFATE NITRATE ORGANIC LAC SOIL

YELLOWSTONE NP

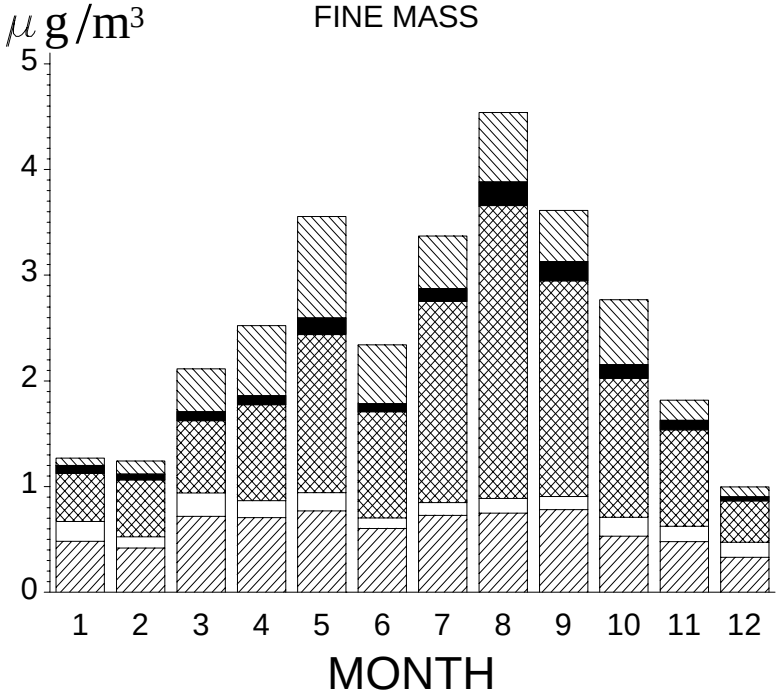

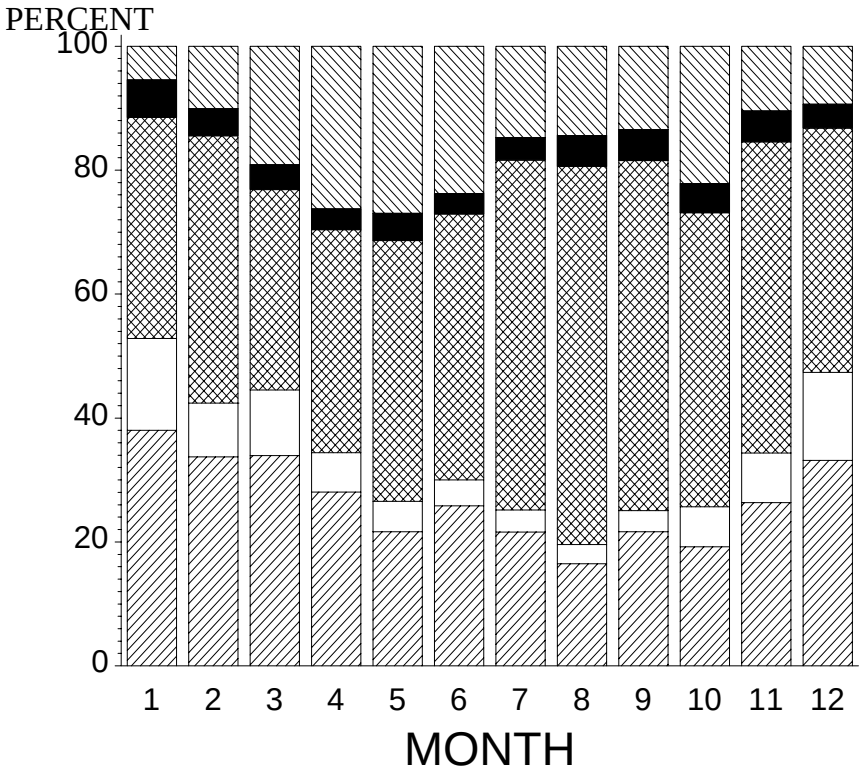

SULFATE NITRATE ORGANIC LAC SOIL

YOSEMITE NP

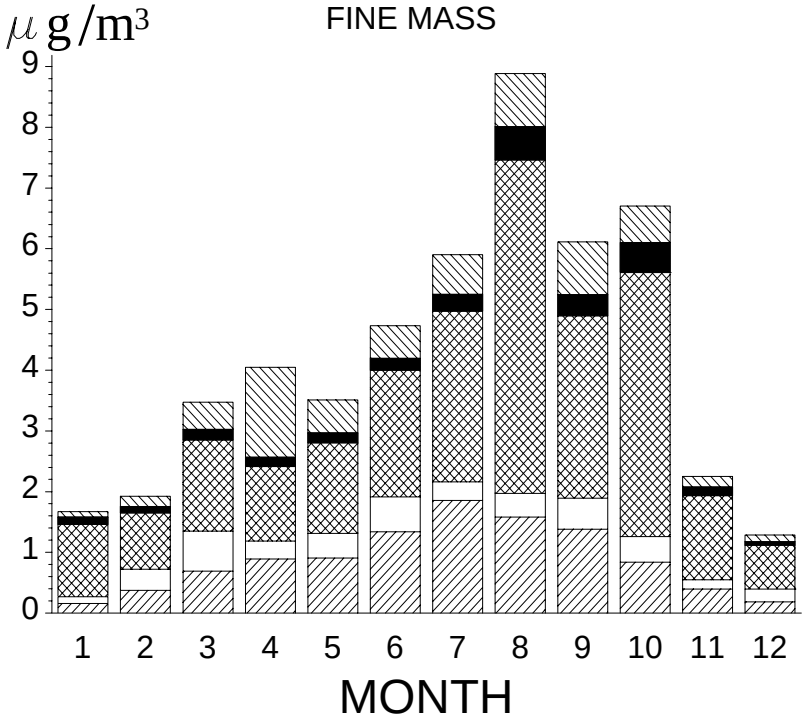

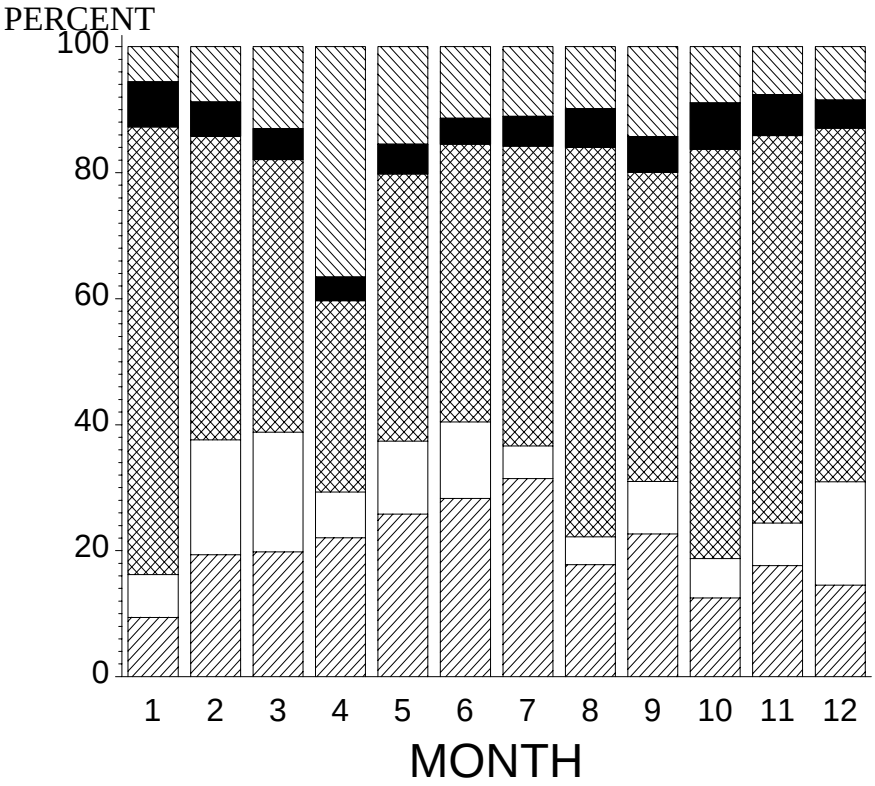

SULFATE NITRATE ORGANIC LAC SOIL

APPENDIX F

Diurnal patterns by season for RH, b_{ext}, and/or b_{scat} measured at IMPROVE monitoring sites across the United States. Start dates for the individual sites are listed in Table 1.1 in Chapter 1.

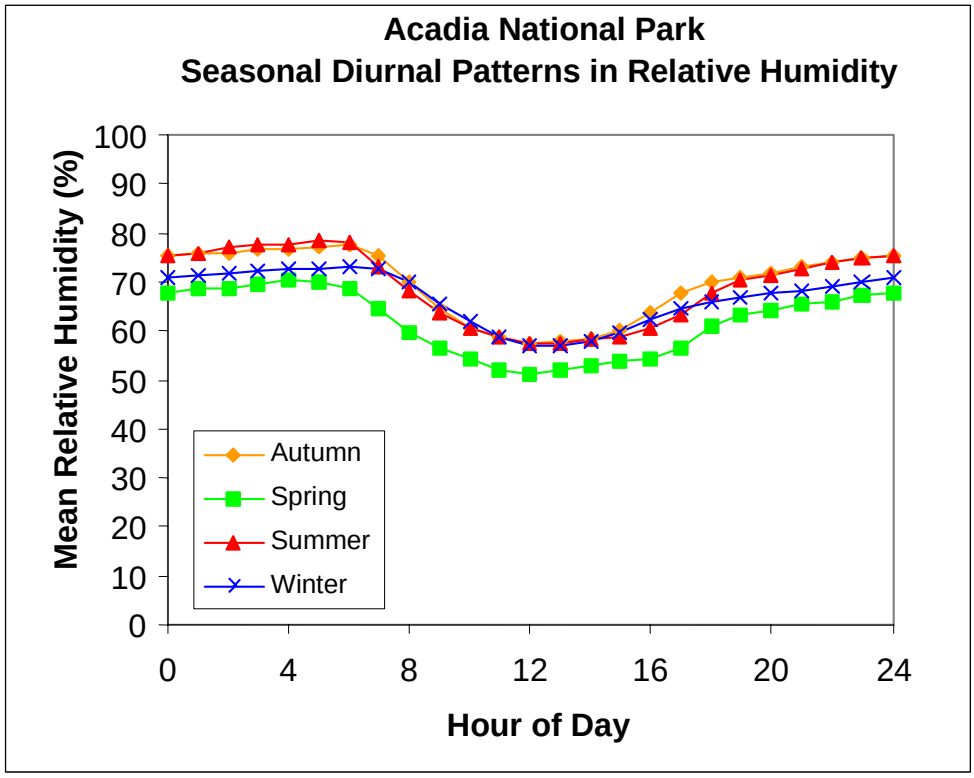
Acadia National Park
Seasonal Diurnal Patterns in Relative Humidity
Mean Relative Humidity (%)
100
90
80
70
60
50
40
30
20
10
0
0
4
8
12
16
20
24
Hour of Day
Autumn
Spring
Summer
Winter

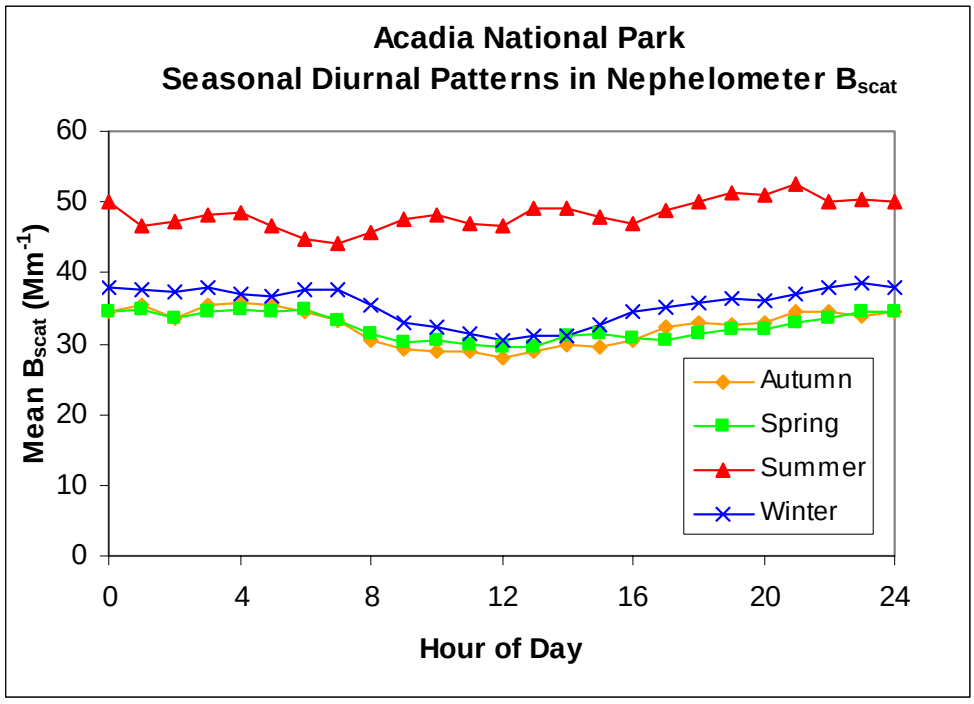
Acadia National Park
Seasonal Diurnal Patterns in Nephelometer Bscat
Mean Bscat (Mm-1)
60
50
40
30
20
10
0
0
4
8
12
16
20
24
Hour of Day
Autumn
Spring
Summer
Winter

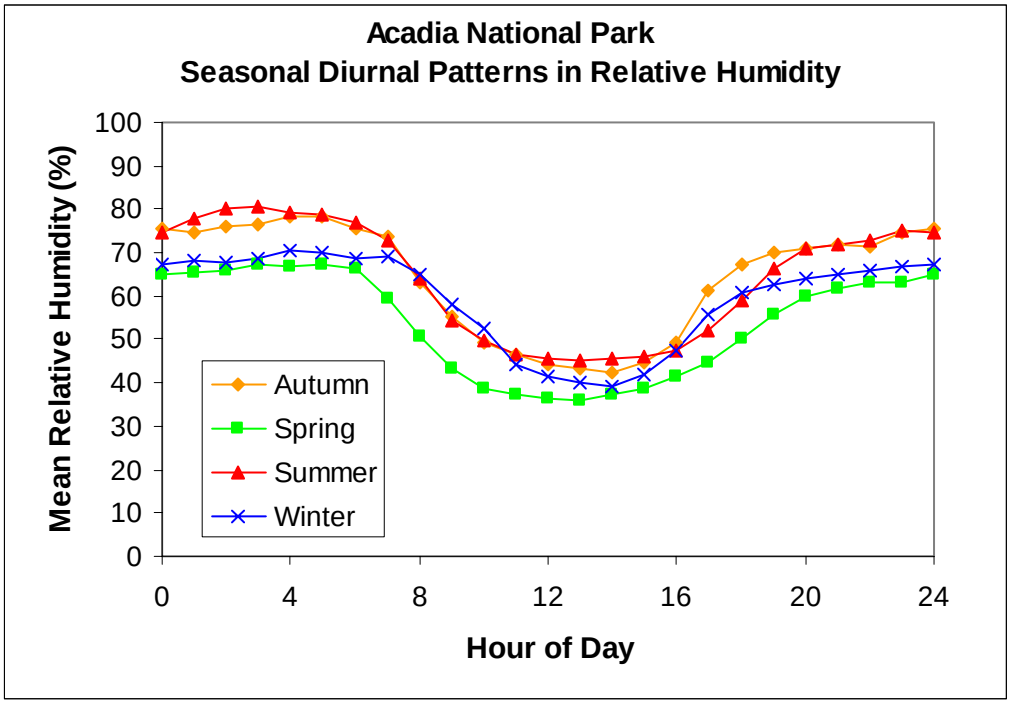
Acadia National Park
Seasonal Diurnal Patterns in Relative Humidity
Mean Relative Humidity (%)
100
90
80
70
60
50
40
30
20
10
0
0
4
8
12
16
20
24
Hour of Day
Autumn
Spring
Summer
Winter

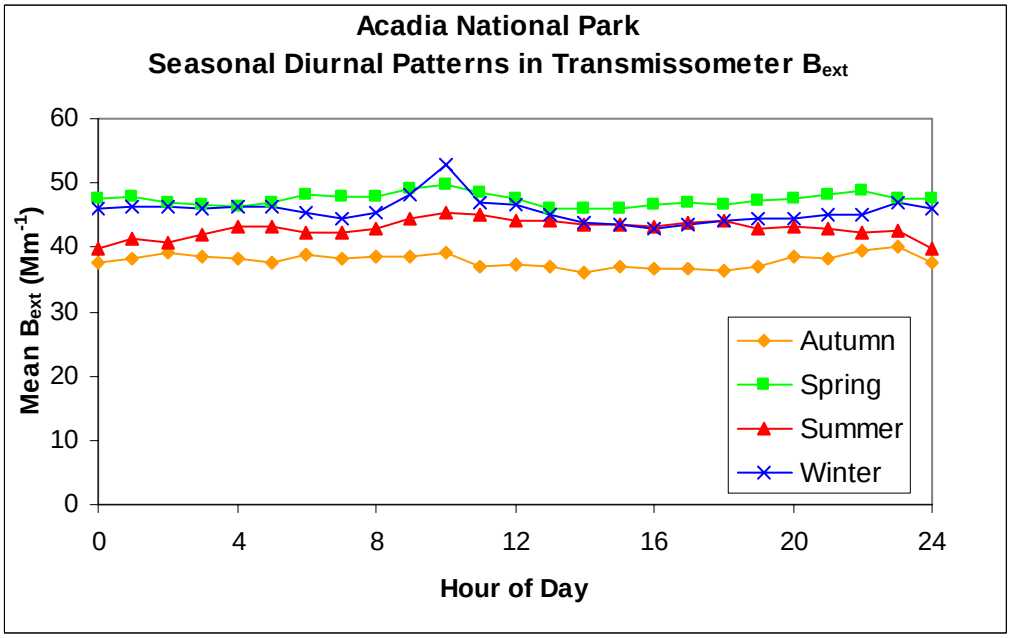
Acadia National Park
Seasonal Diurnal Patterns in Transmissometer Bext
Mean Bext (Mm-1)
60
50
40
30
20
10
0
0
4
8
12
16
20
24
Hour of Day
Autumn
Spring
Summer
Winter

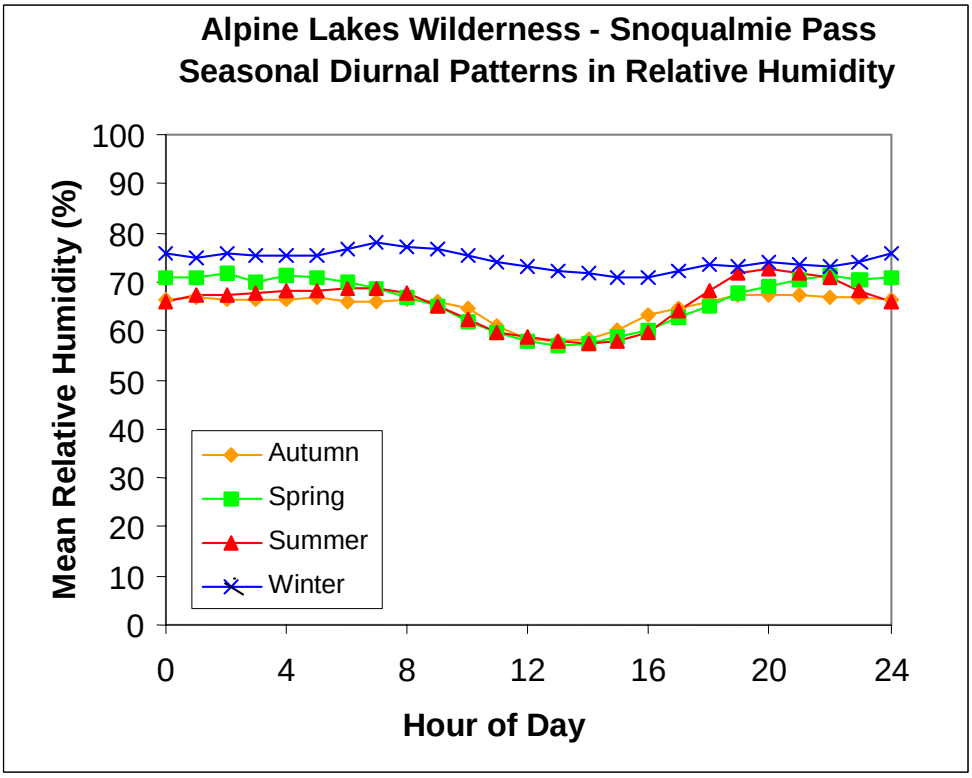
Alpine Lakes Wilderness - Snoqualmie Pass
Seasonal Diurnal Patterns in Relative Humidity
Mean Relative Humidity (%)
100
90
80
70
60
50
40
30
20
10
0
0
4
8
12
16
20
24
Hour of Day
Autumn
Spring
Summer
Winter

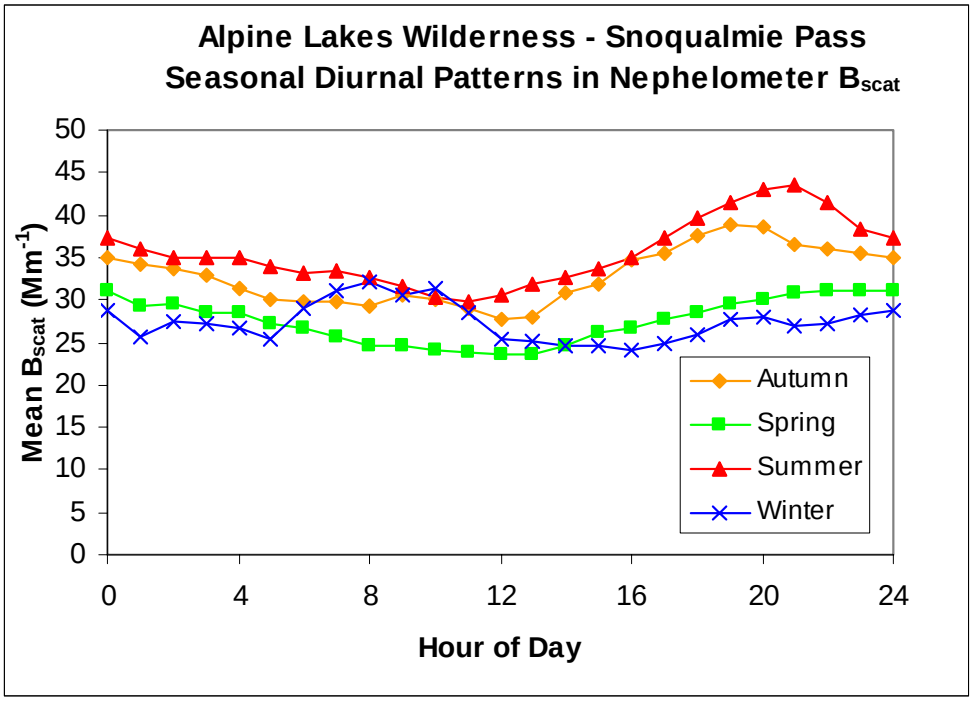
Alpine Lakes Wilderness - Snoqualmie Pass
Seasonal Diurnal Patterns in Nephelometer Bscat
Mean Bscat (Mm-1)
50
45
40
35
30
25
20
15
10
5
0
0
4
8
12
16
20
24
Hour of Day
Autumn
Spring
Summer
Winter

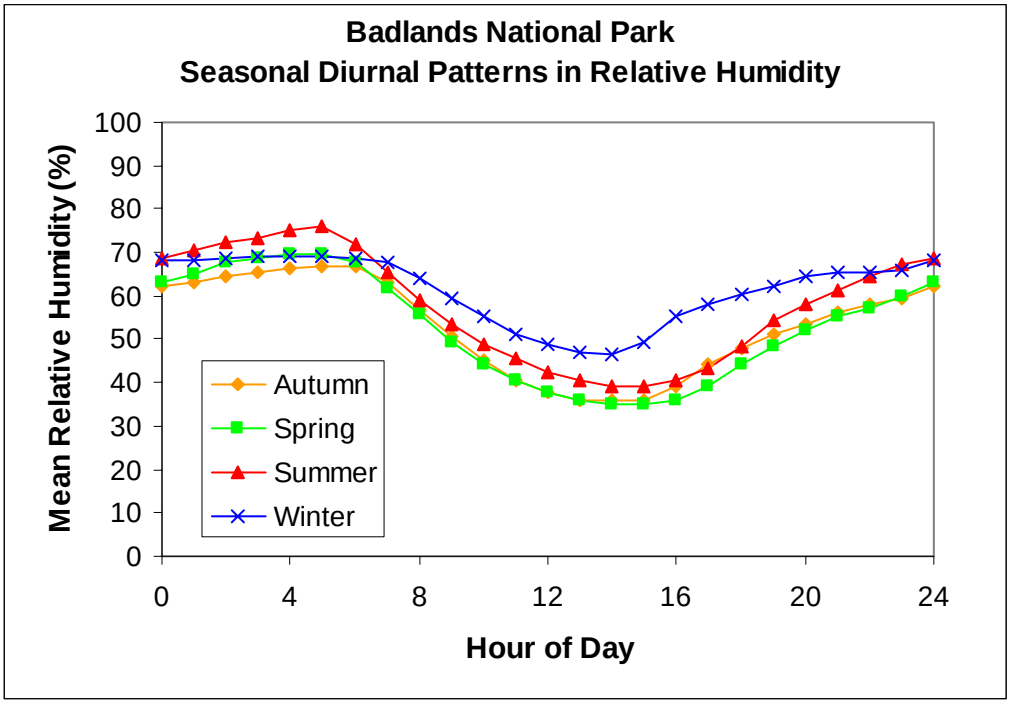
Badlands National Park
Seasonal Diurnal Patterns in Relative Humidity
Mean Relative Humidity (%)
100
90
80
70
60
50
40
30
20
10
0
0
4
8
12
16
20
24
Hour of Day
Autumn
Spring
Summer
Winter

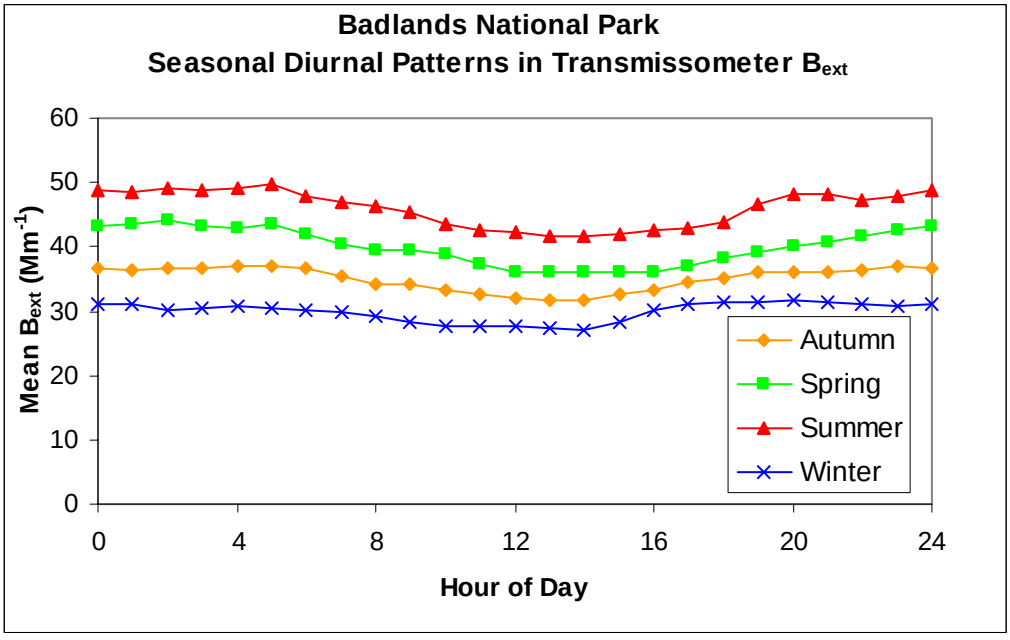
Badlands National Park
Seasonal Diurnal Patterns in Transmissometer Bext
Mean Bext (Mm-1)
60
50
40
30
20
10
0
0
4
8
12
16
20
24
Hour of Day
Autumn
Spring
Summer
Winter

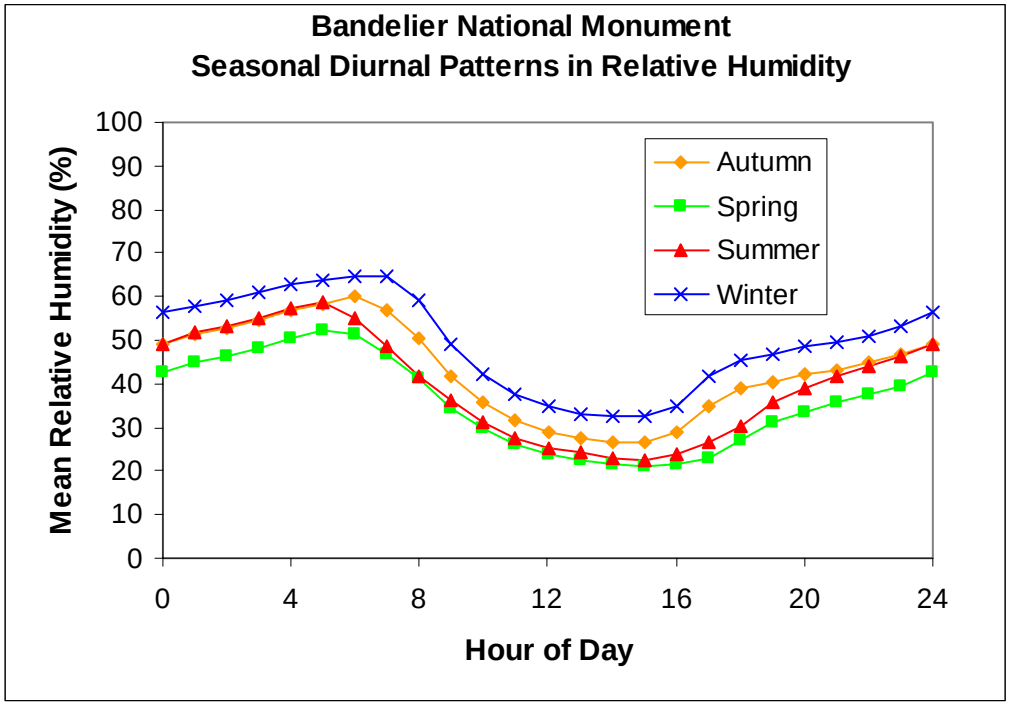
Bandelier National Monument
Seasonal Diurnal Patterns in Relative Humidity
Mean Relative Humidity (%)
100
90
80
70
60
50
40
30
20
10
0
0
4
8
12
16
20
24
Hour of Day
Autumn
Spring
Summer
Winter

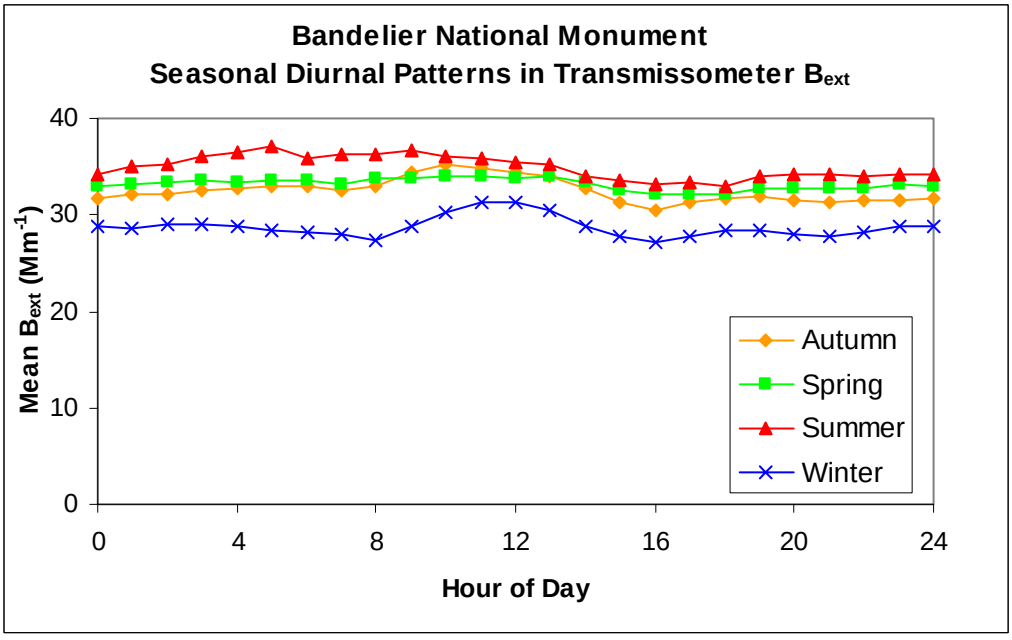
Bandelier National Monument
Seasonal Diurnal Patterns in Transmissometer Bext
Mean Bext (Mm-1)
40
30
20
10
0
0
4
8
12
16
20
24
Hour of Day
Autumn
Spring
Summer
Winter

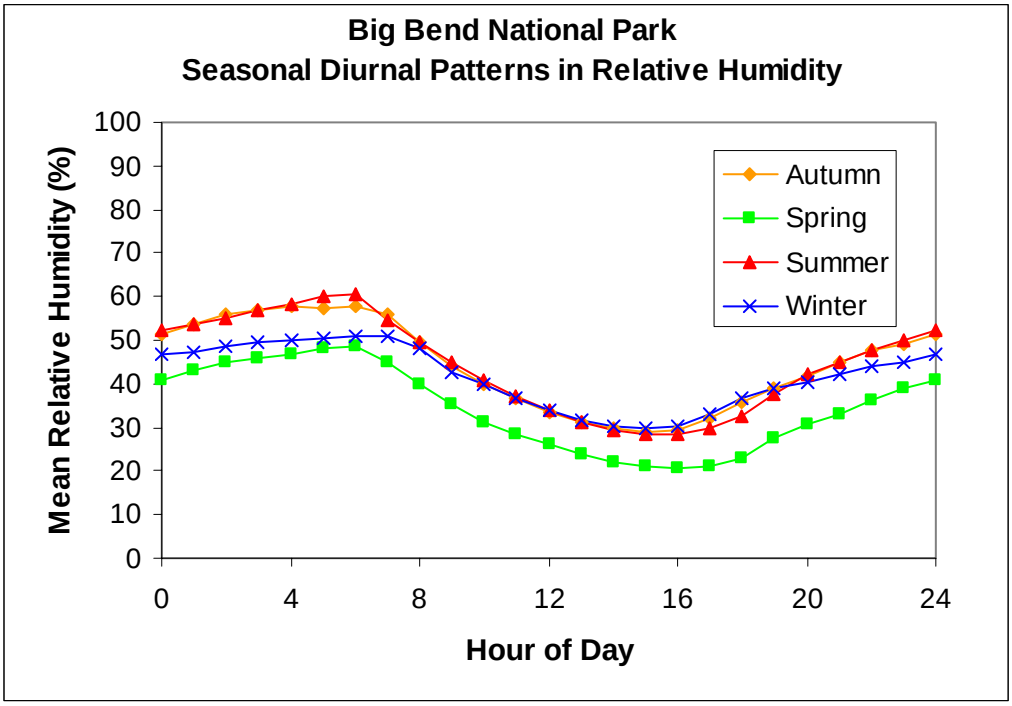
Big Bend National Park
Seasonal Diurnal Patterns in Relative Humidity
Mean Relative Humidity (%)
100
90
80
70
60
50
40
30
20
10
0
0
4
8
12
16
20
24
Hour of Day
Autumn
Spring
Summer
Winter

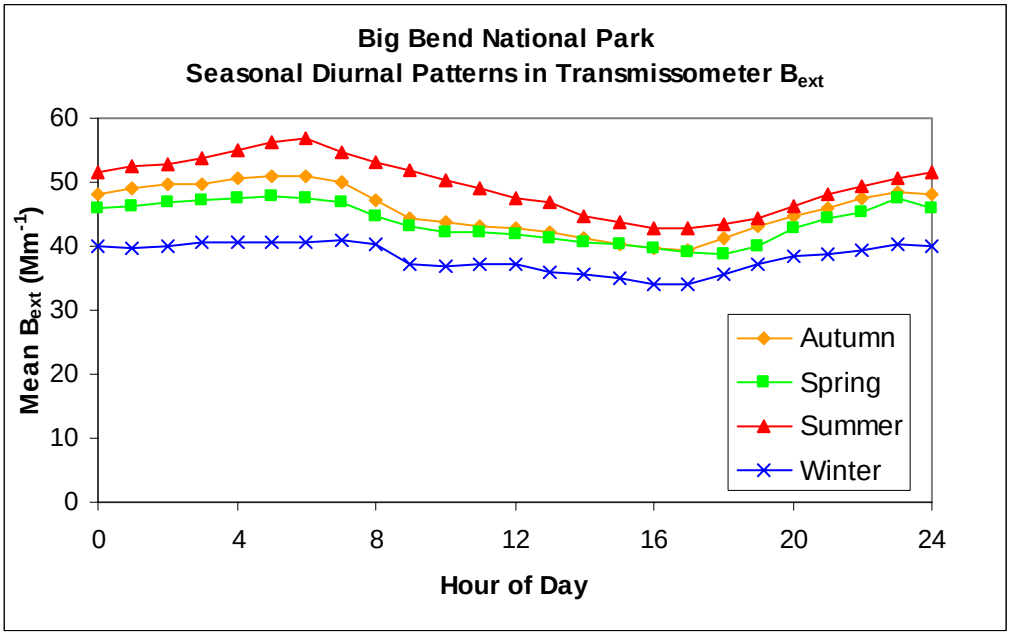
Big Bend National Park
Seasonal Diurnal Patterns in Transmissometer Bext
Mean Bext (Mm-1)
60
50
40
30
20
10
0
0
4
8
12
16
20
24
Hour of Day
Autumn
Spring
Summer
Winter

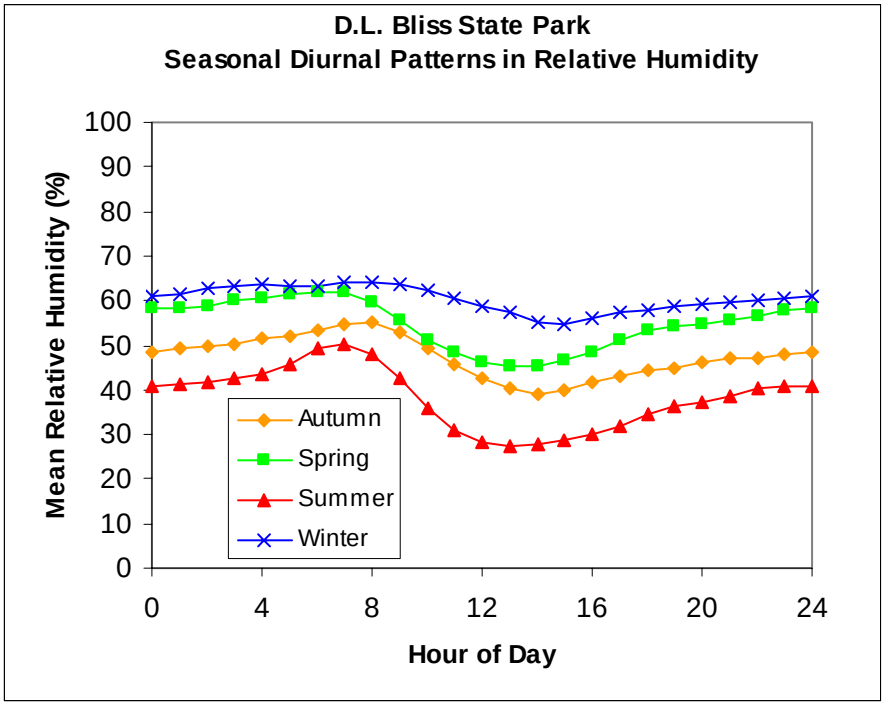
D.L. Bliss State Park
Seasonal Diurnal Patterns in Relative Humidity
Mean Relative Humidity (%)
100
90
80
70
60
50
40
30
20
10
0
0
4
8
12
16
20
24
Hour of Day
Autumn
Spring
Summer
Winter

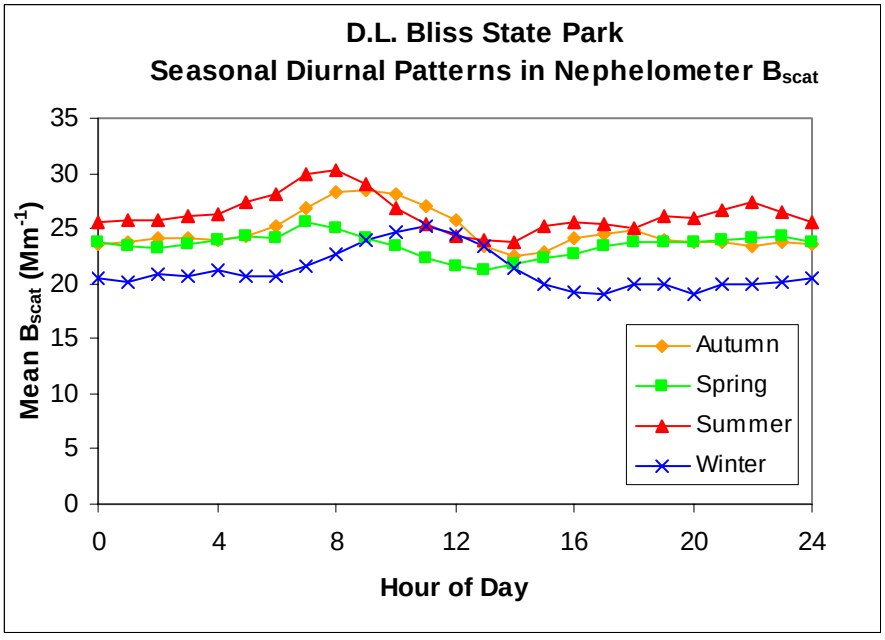
D.L. Bliss State Park
Seasonal Diurnal Patterns in Nephelometer Bscat
Mean Bscat (Mm-1)
35
30
25
20
15
10
5
0
0
4
8
12
16
20
24
Hour of Day
Autumn
Spring
Summer
Winter

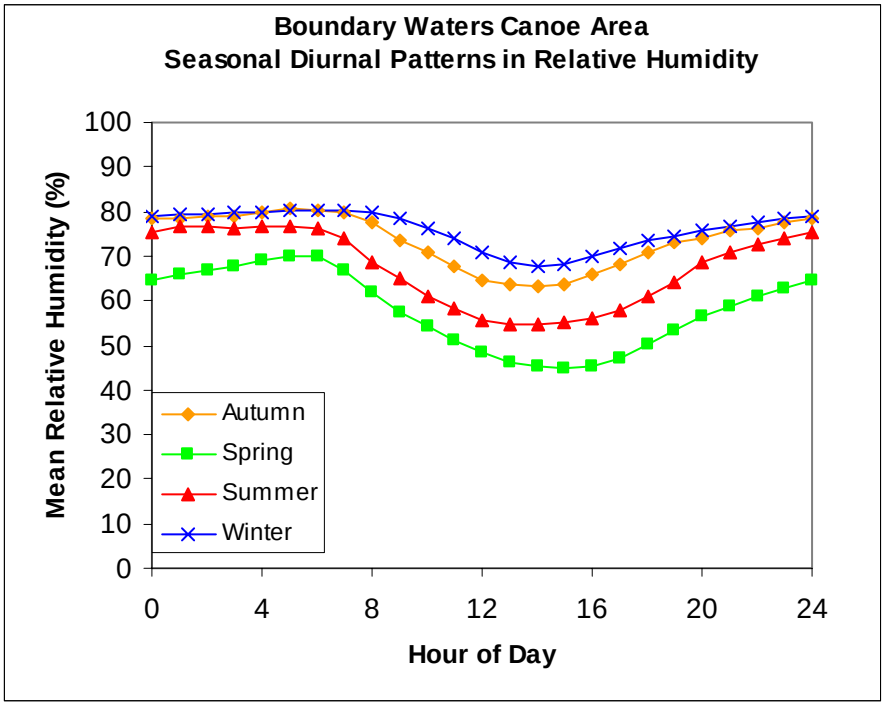
Boundary Waters Canoe Area
Seasonal Diurnal Patterns in Relative Humidity
Mean Relative Humidity (%)
100
90
80
70
60
50
40
30
20
10
0
0
4
8
12
16
20
24
Hour of Day
Autumn
Spring
Summer
Winter

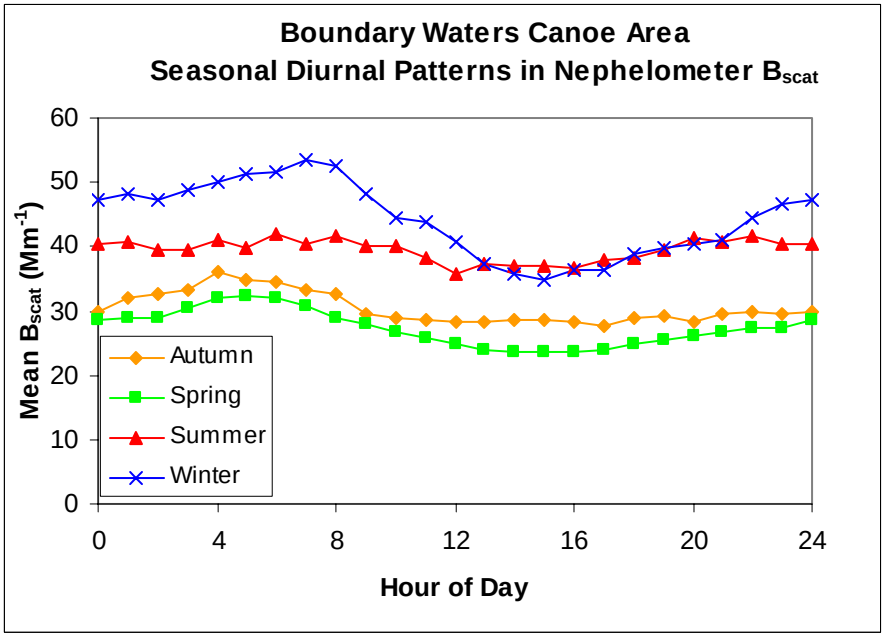
Boundary Waters Canoe Area
Seasonal Diurnal Patterns in Nephelometer Bscat
Mean Bscat (Mm-1)
60
50
40
30
20
10
0
0
4
8
12
16
20
24
Hour of Day
Autumn
Spring
Summer
Winter

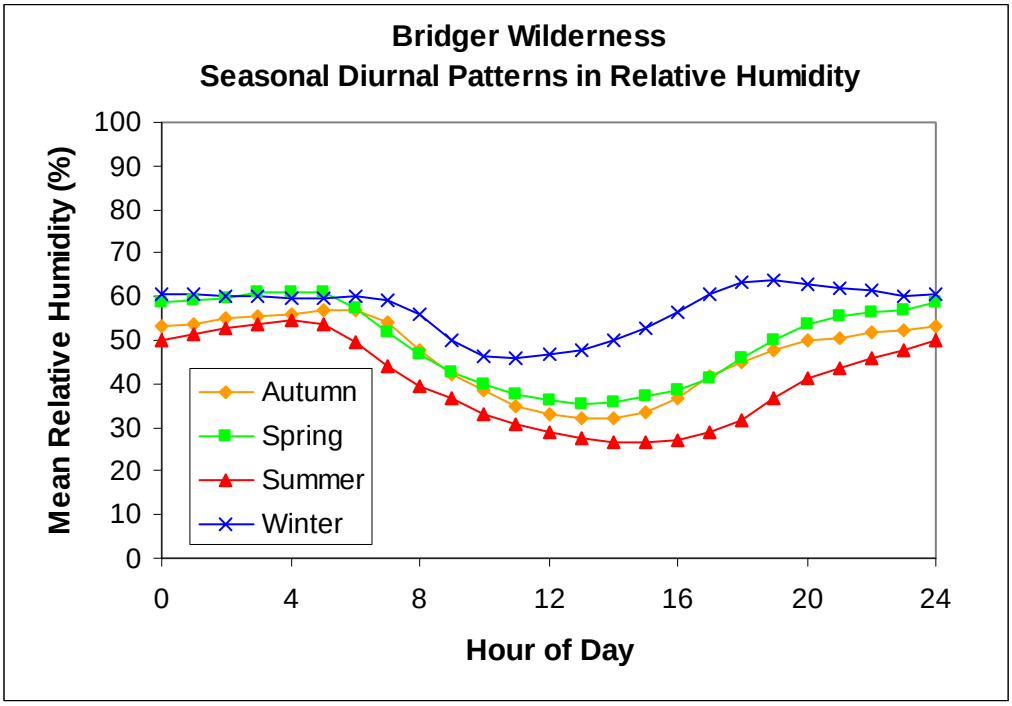
Bridger Wilderness
Seasonal Diurnal Patterns in Relative Humidity
Mean Relative Humidity (%)
100
90
80
70
60
50
40
30
20
10
0
0
4
8
12
16
20
24
Hour of Day
Autumn
Spring
Summer
Winter

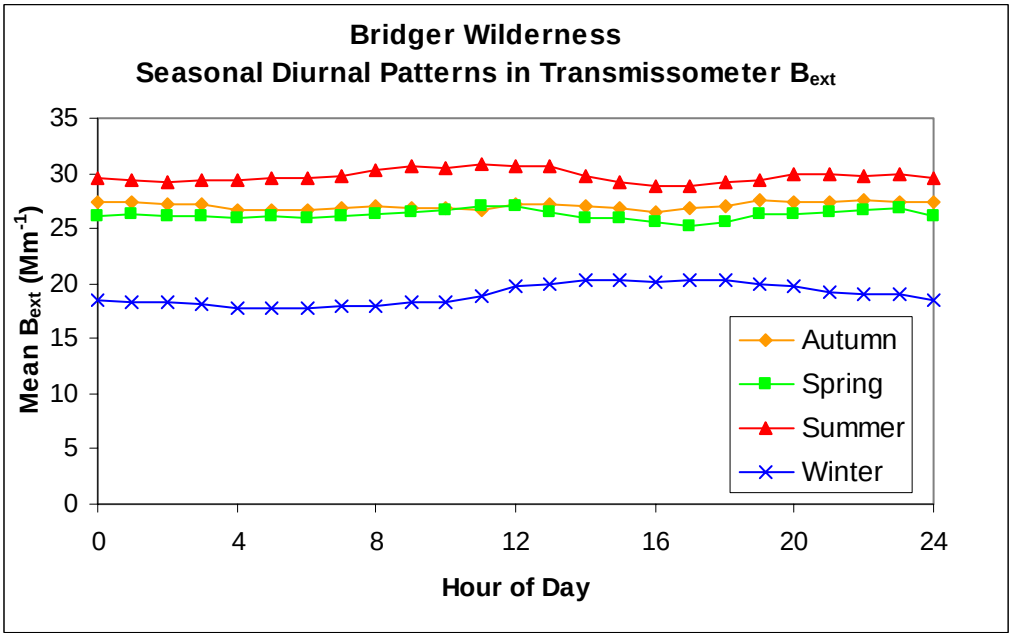
Bridger Wilderness
Seasonal Diurnal Patterns in Transmissometer Bext
Mean Bext (Mm-1)
35
30
25
20
15
10
5
0
0
4
8
12
16
20
24
Hour of Day
Autumn
Spring
Summer
Winter

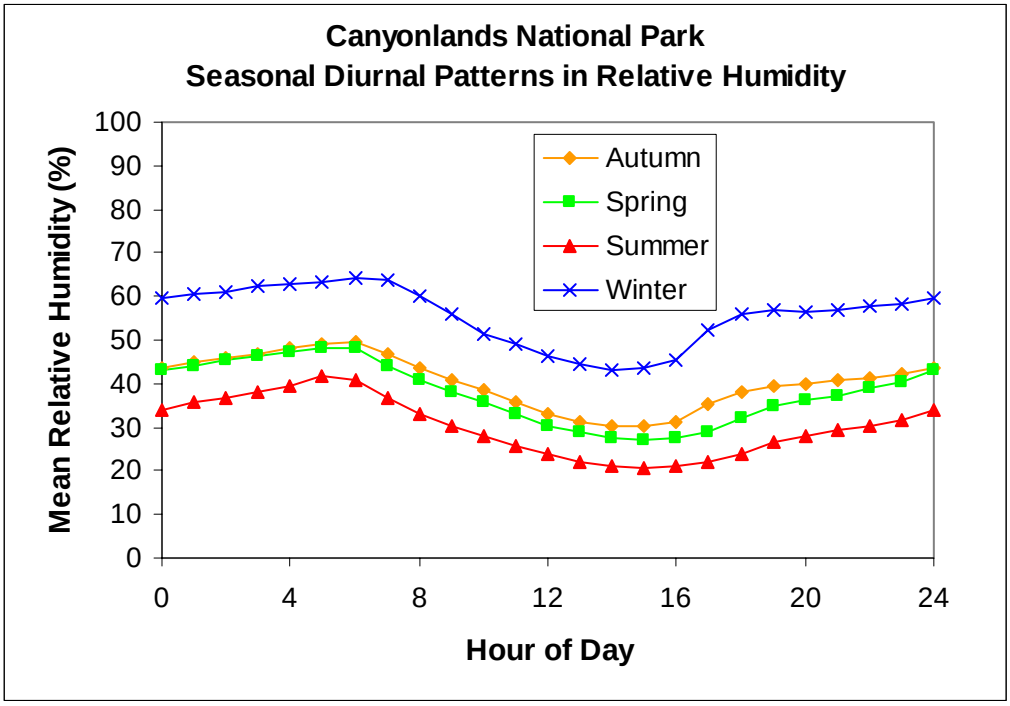
Canyonlands National Park
Seasonal Diurnal Patterns in Relative Humidity
Mean Relative Humidity (%)
100
90
80
70
60
50
40
30
20
10
0
0
4
8
12
16
20
24
Hour of Day
Autumn
Spring
Summer
Winter

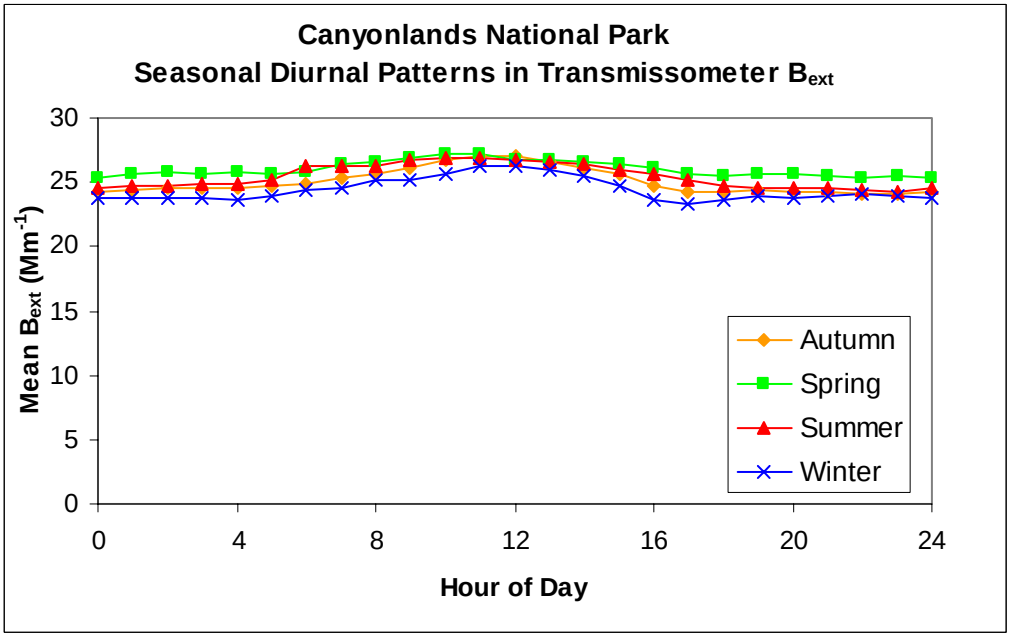
Canyonlands National Park
Seasonal Diurnal Patterns in Transmissometer Bext
Mean Bext (Mm-1)
30
25
20
15
10
5
0
0
4
8
12
16
20
24
Hour of Day
Autumn
Spring
Summer
Winter

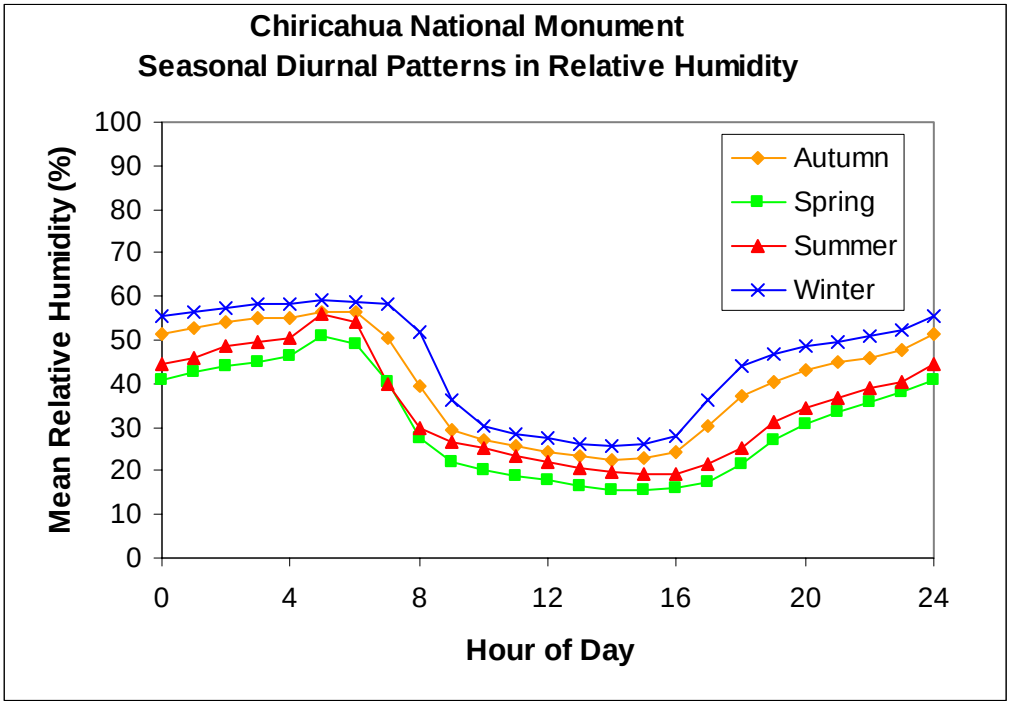
Chiricahua National Monument
Seasonal Diurnal Patterns in Relative Humidity
Mean Relative Humidity (%)
100
90
80
70
60
50
40
30
20
10
0
0
4
8
12
16
20
24
Hour of Day
Autumn
Spring
Summer
Winter

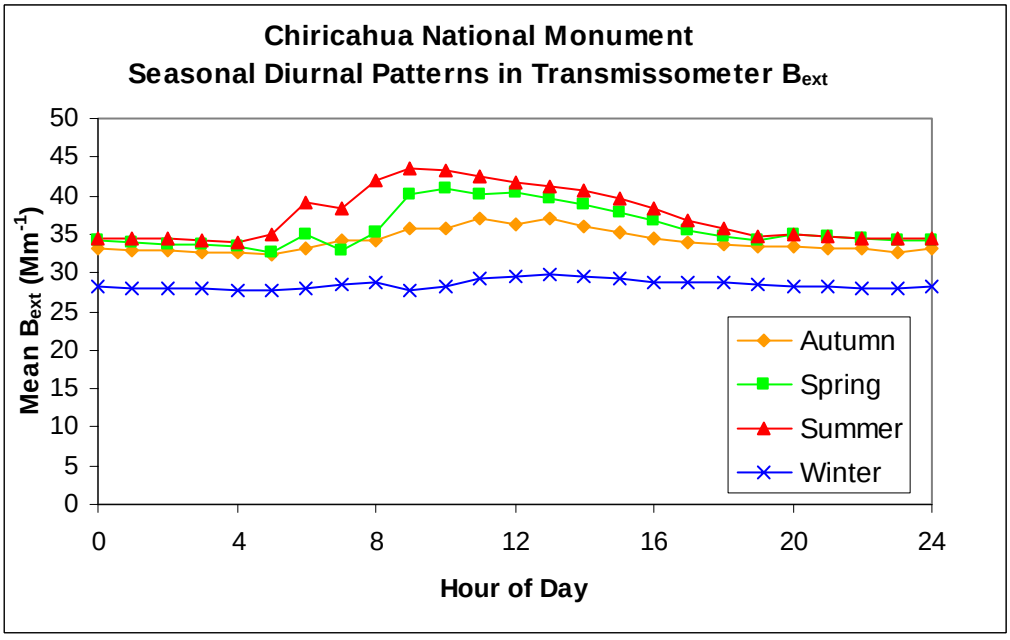
Chiricahua National Monument
Seasonal Diurnal Patterns in Transmissometer Bext
Mean Bext (Mm-1)
50
45
40
35
30
25
20
15
10
5
0
0
4
8
12
16
20
24
Hour of Day
Autumn
Spring
Summer
Winter

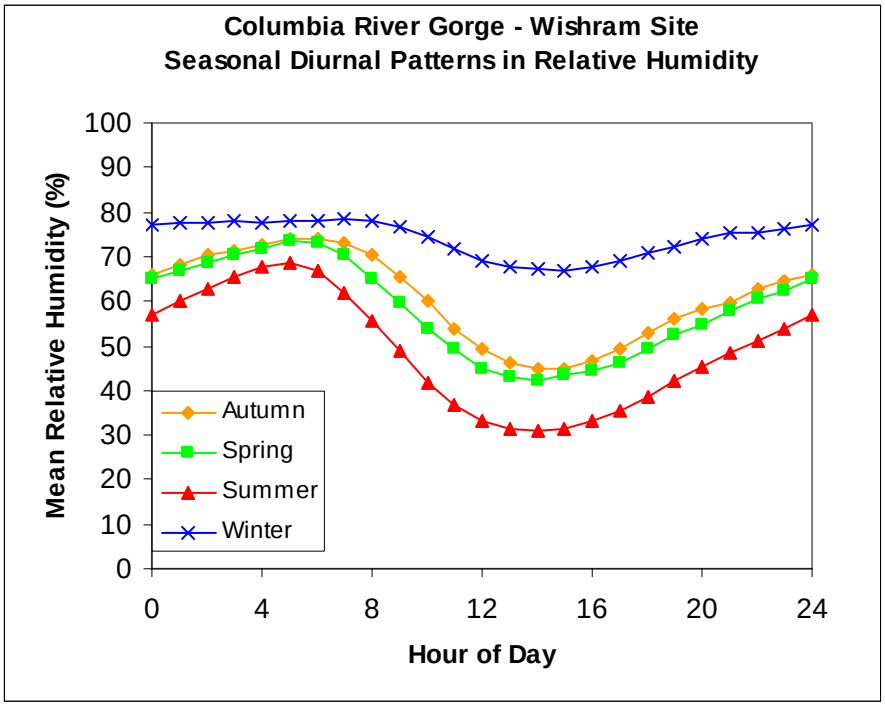
Columbia River Gorge - Wishram Site
Seasonal Diurnal Patterns in Relative Humidity
Mean Relative Humidity (%)
100
90
80
70
60
50
40
30
20
10
0
0
4
8
12
16
20
24
Hour of Day
Autumn
Spring
Summer
Winter

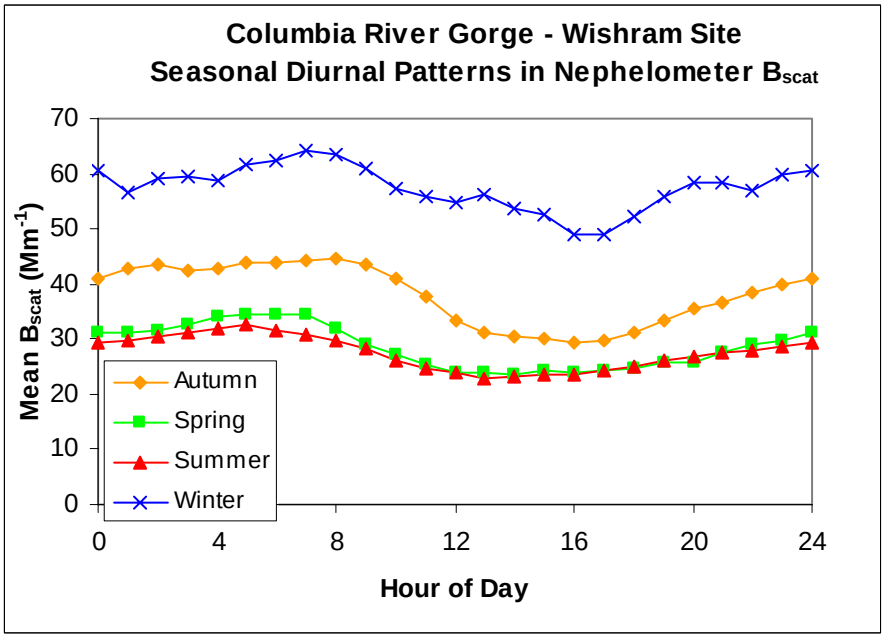
Columbia River Gorge - Wishram Site
Seasonal Diurnal Patterns in Nephelometer Bscat
Mean Bscat (Mm-1)
70
60
50
40
30
20
10
0
0
4
8
12
16
20
24
Hour of Day
Autumn
Spring
Summer
Winter

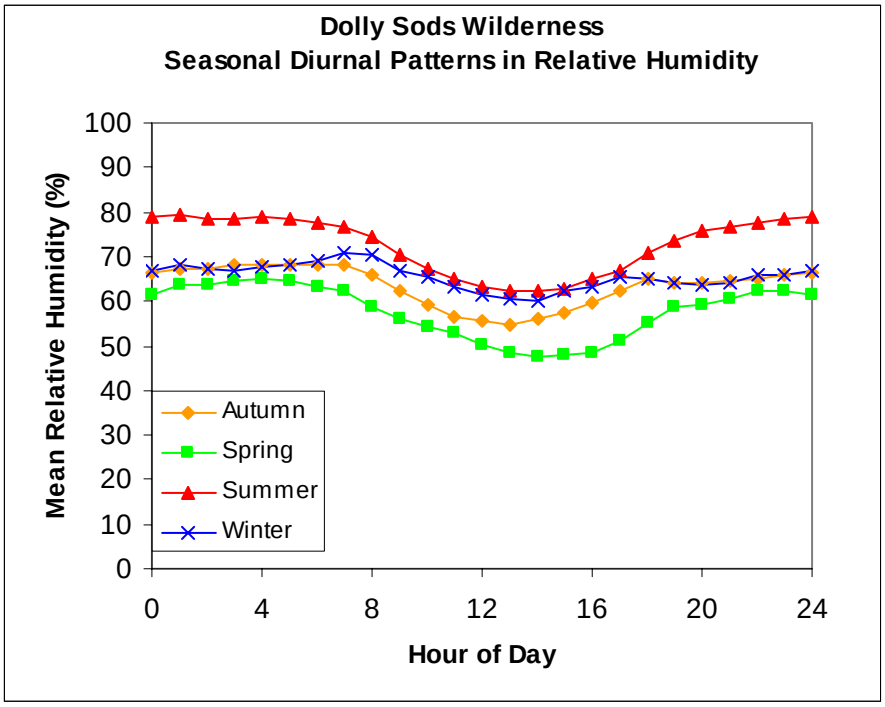
Dolly Sods Wilderness
Seasonal Diurnal Patterns in Relative Humidity
Mean Relative Humidity (%)
100
90
80
70
60
50
40
30
20
10
0
0
4
8
12
16
20
24
Hour of Day
Autumn
Spring
Summer
Winter

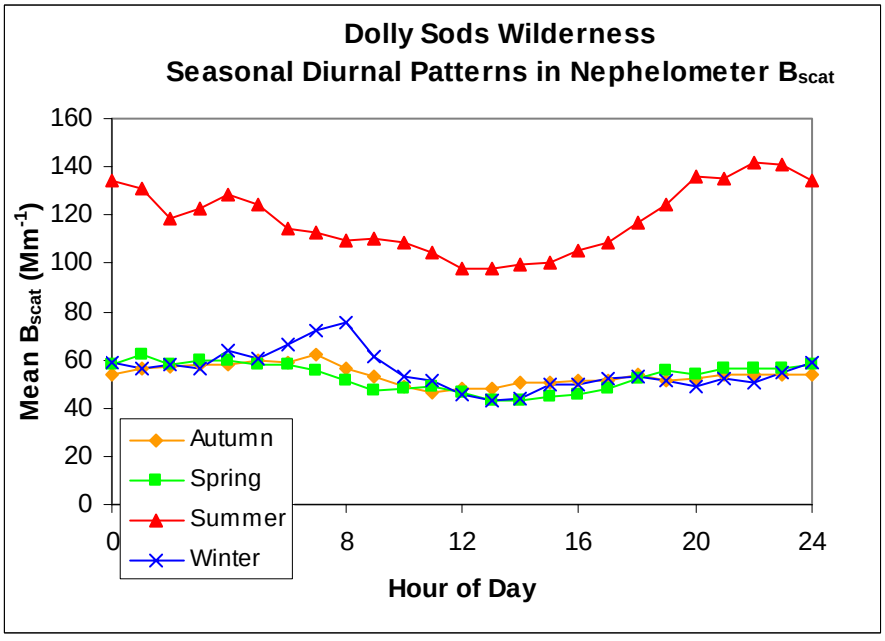
Dolly Sods Wilderness
Seasonal Diurnal Patterns in Nephelometer Bscat
Mean Bscat (Mm-1)
160
140
120
100
80
60
40
20
0
0
8
12
16
20
24
Hour of Day
Autumn
Spring
Summer
Winter

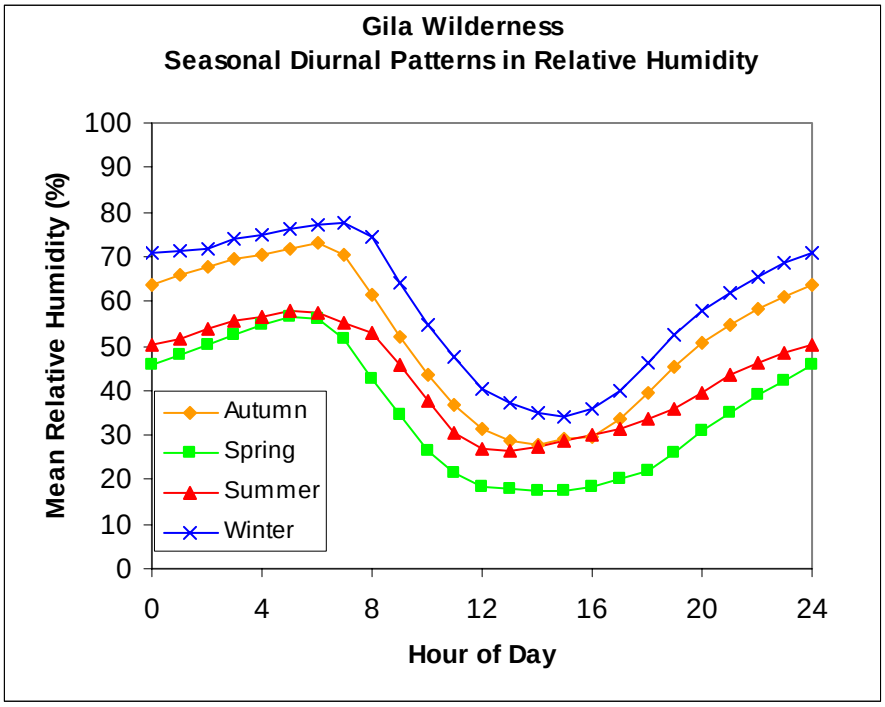
Gila Wilderness
Seasonal Diurnal Patterns in Relative Humidity
Mean Relative Humidity (%)
100
90
80
70
60
50
40
30
20
10
0
0
4
8
12
16
20
24
Hour of Day
Autumn
Spring
Summer
Winter

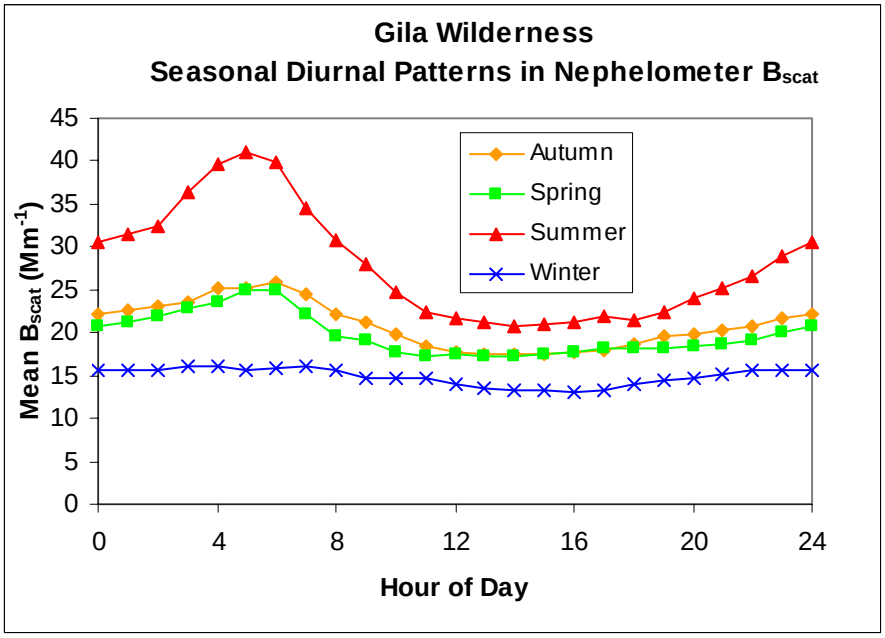
Gila Wilderness
Seasonal Diurnal Patterns in Nephelometer Bscat
Mean Bscat (Mm-1)
45
40
35
30
25
20
15
10
5
0
0
4
8
12
16
20
24
Hour of Day
Autumn
Spring
Summer
Winter

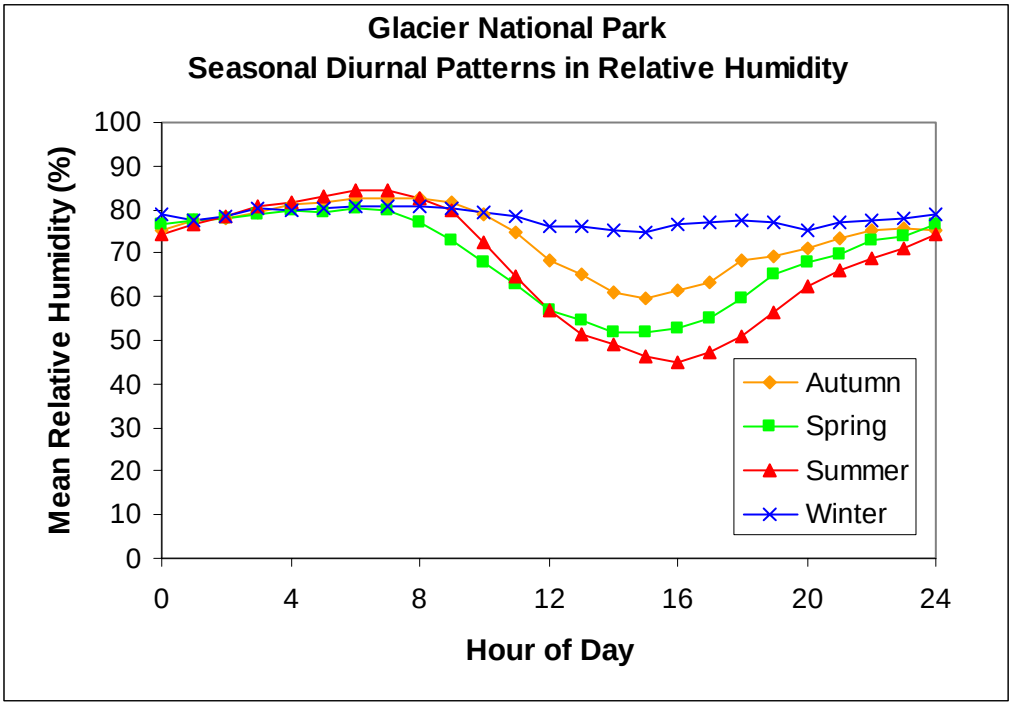
Glacier National Park
Seasonal Diurnal Patterns in Relative Humidity
Mean Relative Humidity (%)
100
90
80
70
60
50
40
30
20
10
0
0
4
8
12
16
20
24
Hour of Day
Autumn
Spring
Summer
Winter

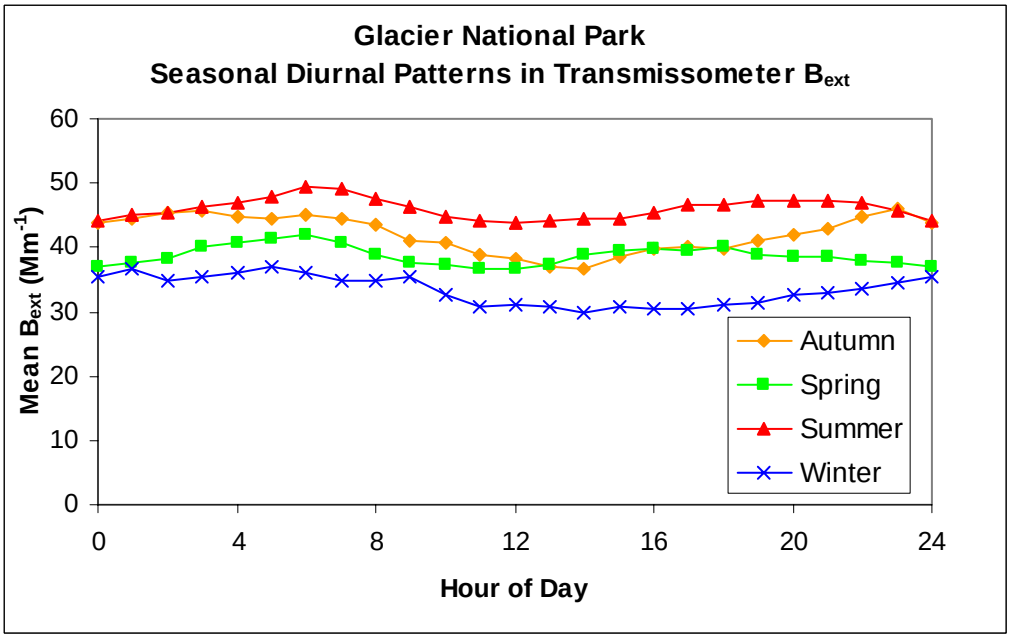
Glacier National Park
Seasonal Diurnal Patterns in Transmissometer Bext
Mean Bext (Mm-1)
60
50
40
30
20
10
0
0
4
8
12
16
20
24
Hour of Day
Autumn
Spring
Summer
Winter

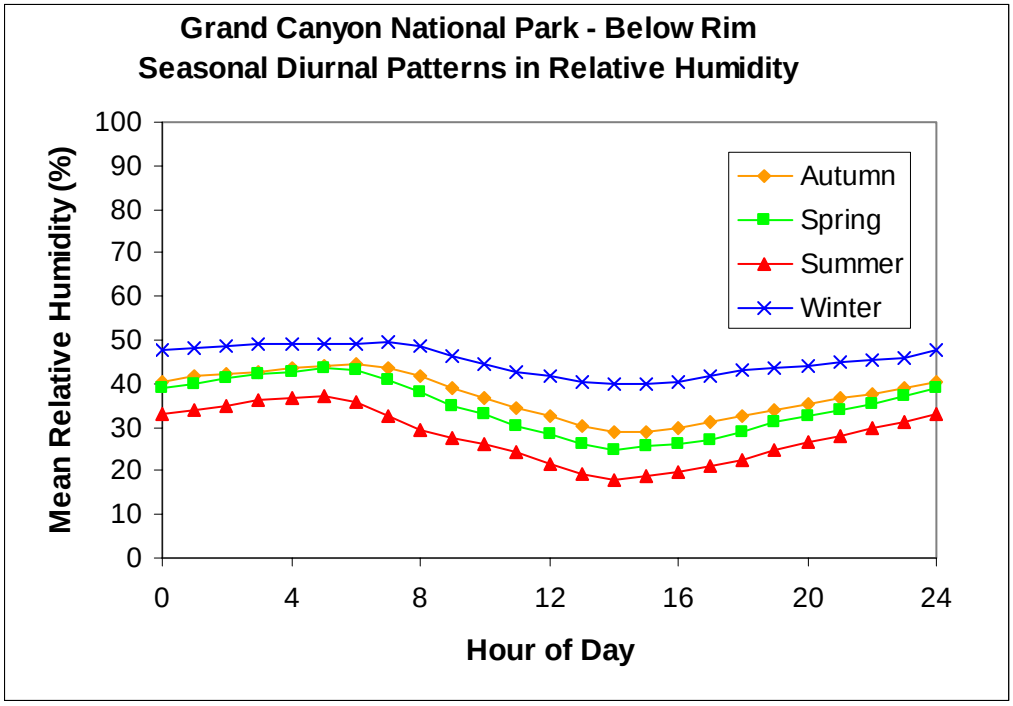
Grand Canyon National Park - Below Rim
Seasonal Diurnal Patterns in Relative Humidity
Mean Relative Humidity (%)
100
90
80
70
60
50
40
30
20
10
0
0
4
8
12
16
20
24
Hour of Day
Autumn
Spring
Summer
Winter

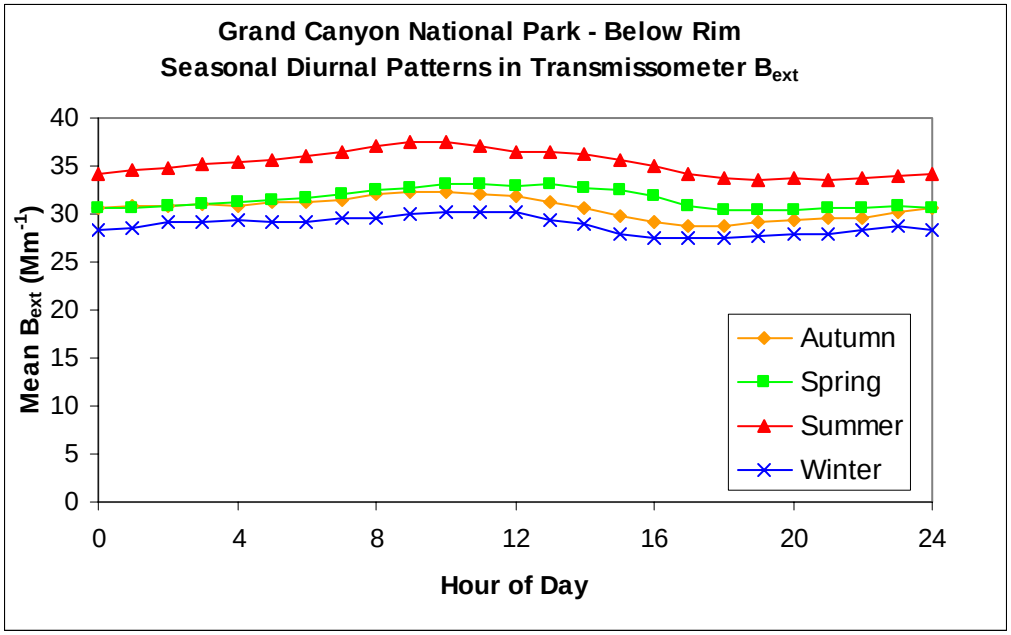
Grand Canyon National Park - Below Rim
Seasonal Diurnal Patterns in Transmissometer Bext
Mean Bext (Mm-1)
40
35
30
25
20
15
10
5
0
0
4
8
12
16
20
24
Hour of Day
Autumn
Spring
Summer
Winter

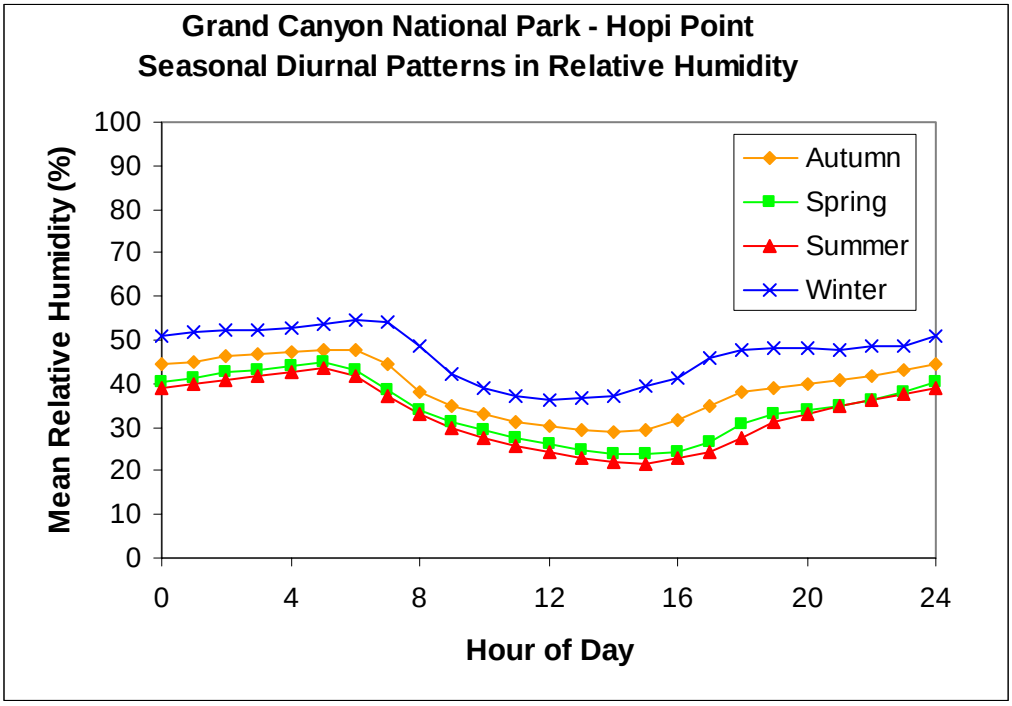
Grand Canyon National Park - Hopi Point
Seasonal Diurnal Patterns in Relative Humidity
Mean Relative Humidity (%)
100
90
80
70
60
50
40
30
20
10
0
0
4
8
12
16
20
24
Hour of Day
Autumn
Spring
Summer
Winter

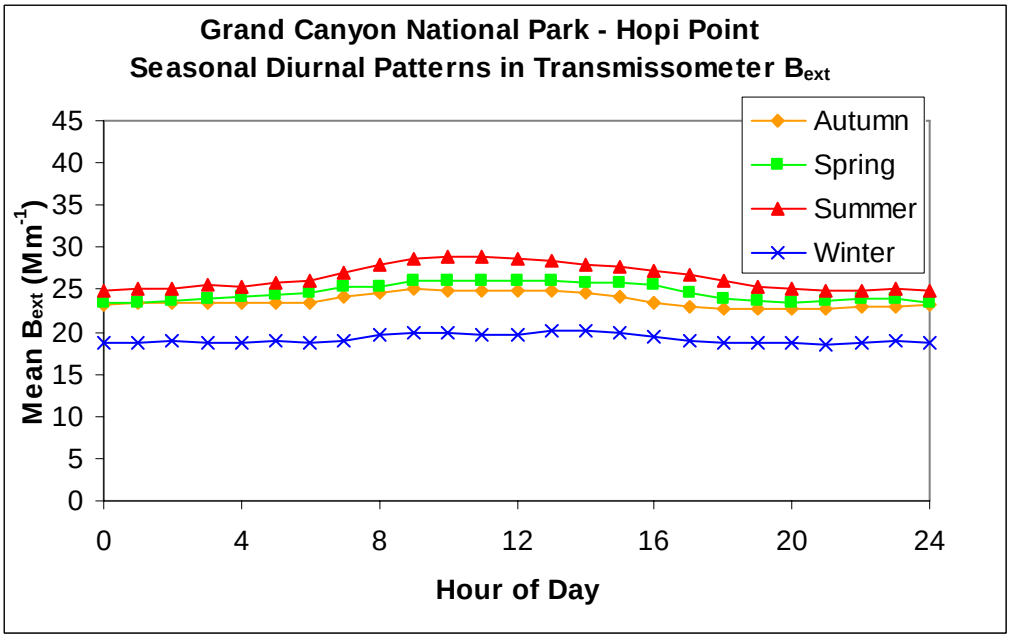
Grand Canyon National Park - Hopi Point
Seasonal Diurnal Patterns in Transmissometer Bext
Mean Bext (Mm-1)
45
40
35
30
25
20
15
10
5
0
0
4
8
12
16
20
24
Hour of Day
Autumn
Spring
Summer
Winter

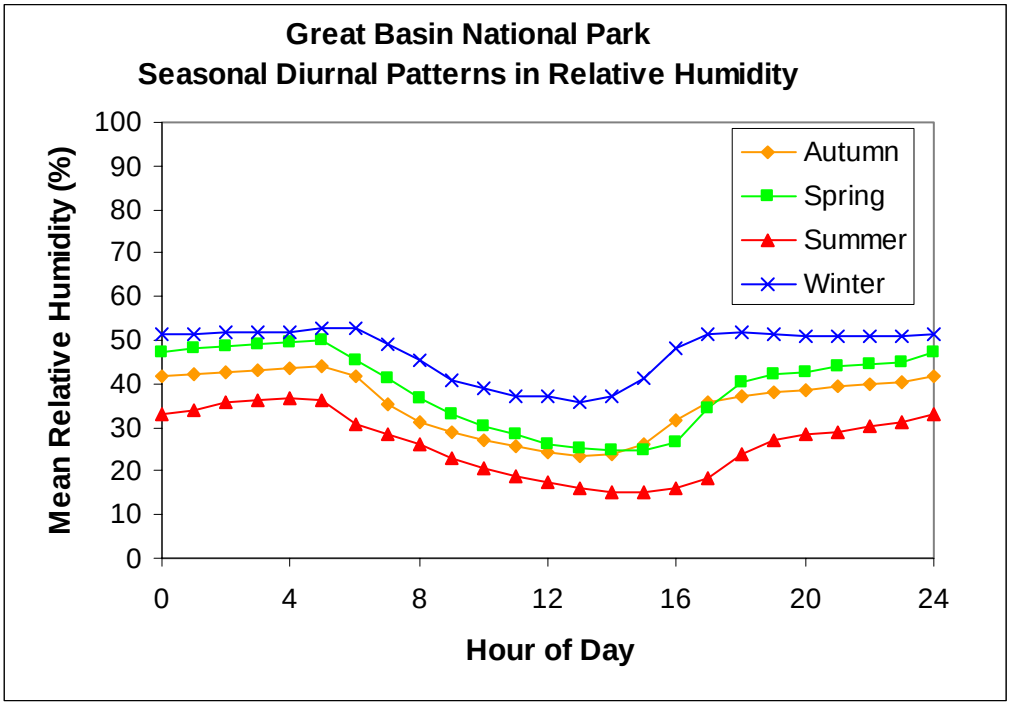
Great Basin National Park
Seasonal Diurnal Patterns in Relative Humidity
Mean Relative Humidity (%)
100
90
80
70
60
50
40
30
20
10
0
0
4
8
12
16
20
24
Hour of Day
Autumn
Spring
Summer
Winter

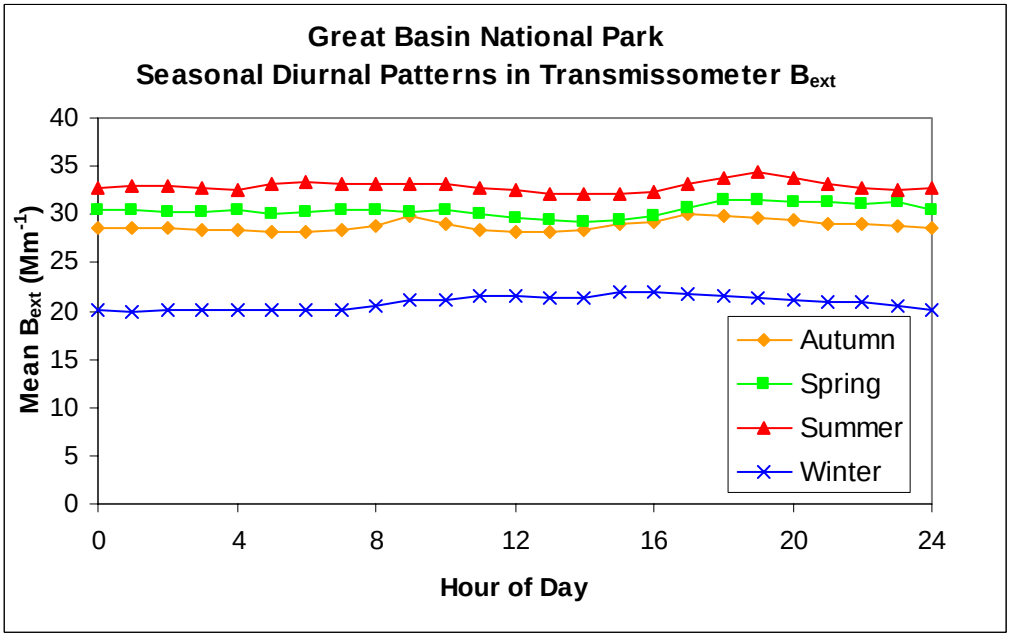
Great Basin National Park
Seasonal Diurnal Patterns in Transmissometer Bext
Mean Bext (Mm-1)
40
35
30
25
20
15
10
5
0
0
4
8
12
16
20
24
Hour of Day
Autumn
Spring
Summer
Winter

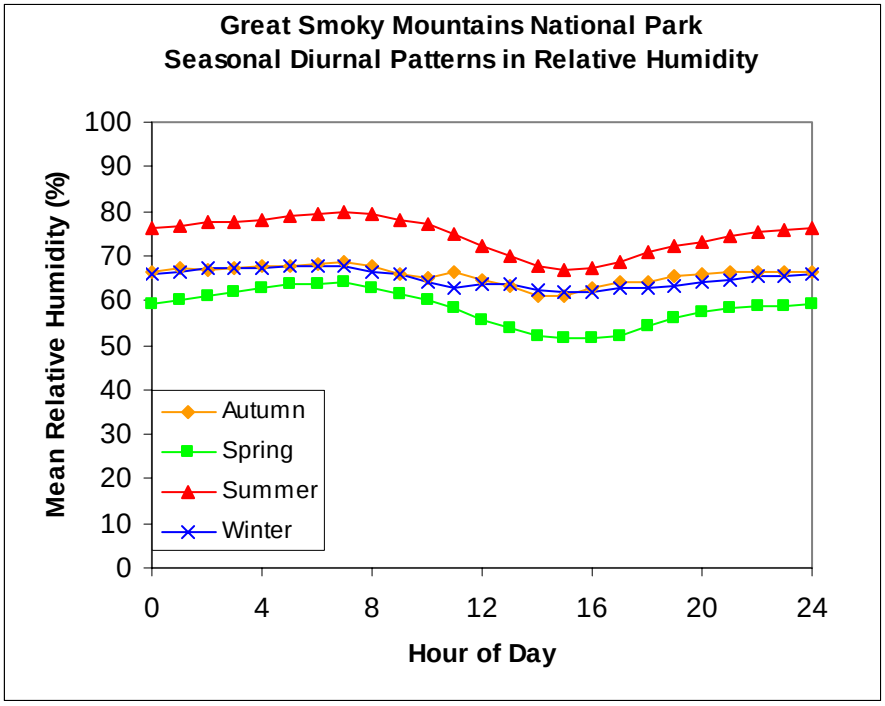
Great Smoky Mountains National Park
Seasonal Diurnal Patterns in Relative Humidity
Mean Relative Humidity (%)
100
90
80
70
60
50
40
30
20
10
0
0
4
8
12
16
20
24
Hour of Day
Autumn
Spring
Summer
Winter

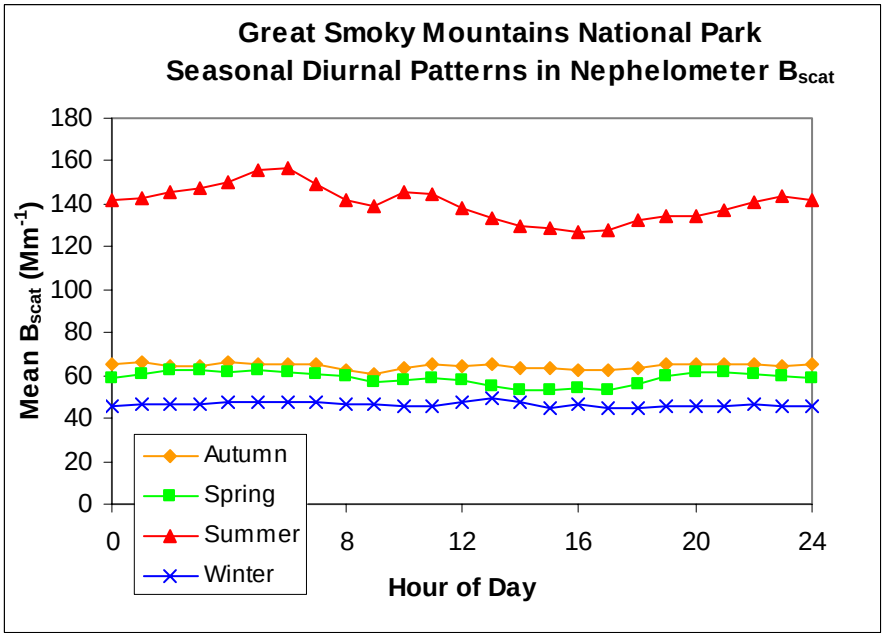
Great Smoky Mountains National Park
Seasonal Diurnal Patterns in Nephelometer Bscat
Mean Bscat (Mm-1)
180
160
140
120
100
80
60
40
20
0
0
8
12
16
20
24
Hour of Day
Autumn
Spring
Summer
Winter

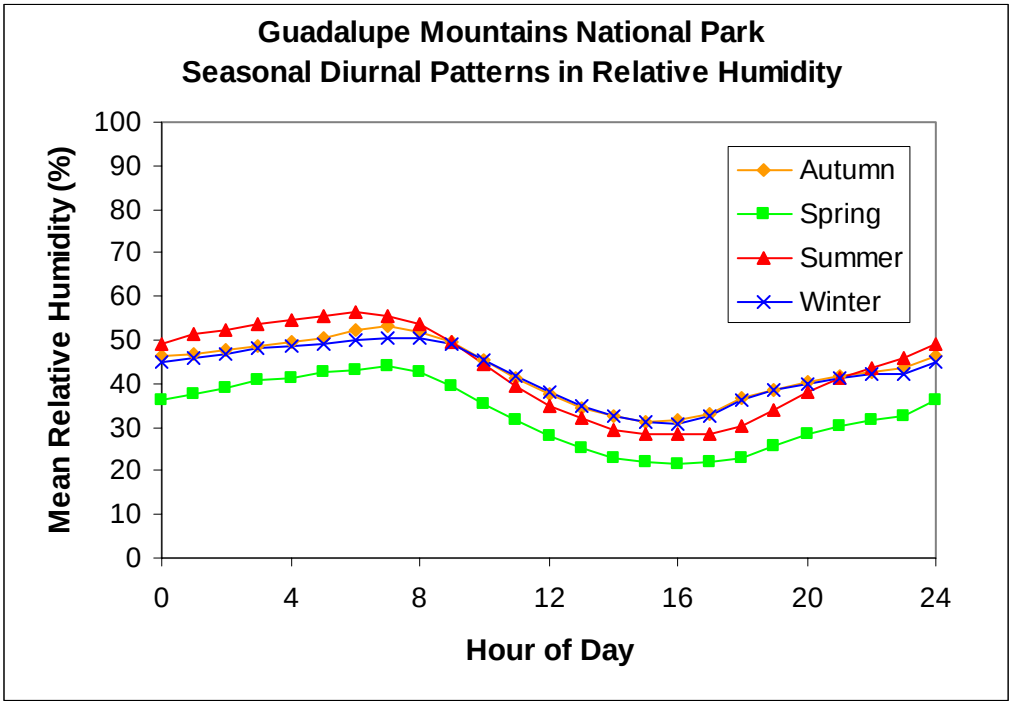
Guadalupe Mountains National Park
Seasonal Diurnal Patterns in Relative Humidity
Mean Relative Humidity (%)
100
90
80
70
60
50
40
30
20
10
0
0
4
8
12
16
20
24
Hour of Day
Autumn
Spring
Summer
Winter

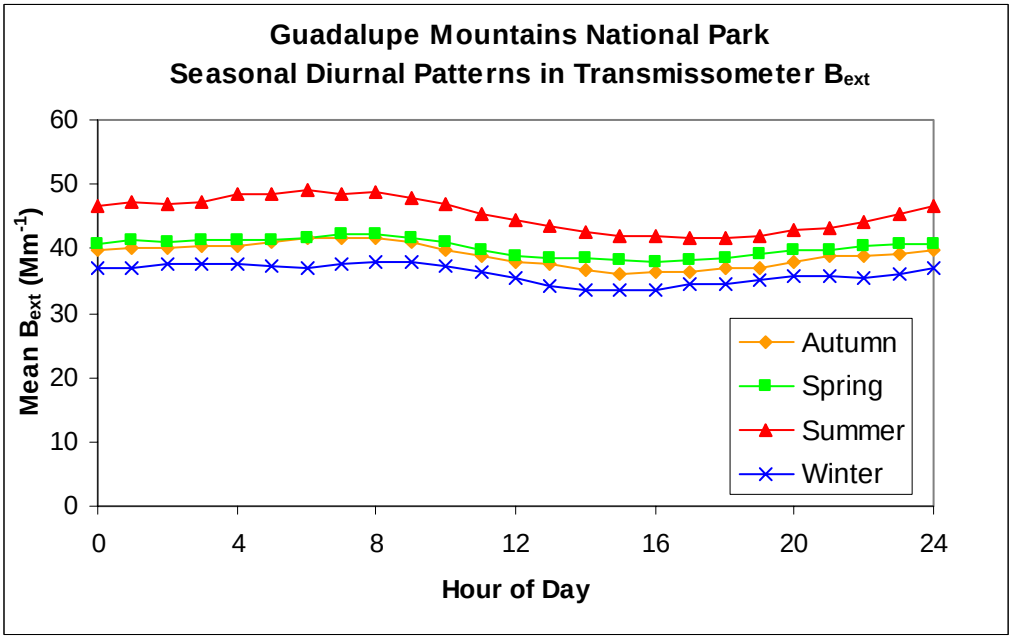
Guadalupe Mountains National Park
Seasonal Diurnal Patterns in Transmissometer Bext
Mean Bext (Mm-1)
60
50
40
30
20
10
0
0
4
8
12
16
20
24
Hour of Day
Autumn
Spring
Summer
Winter

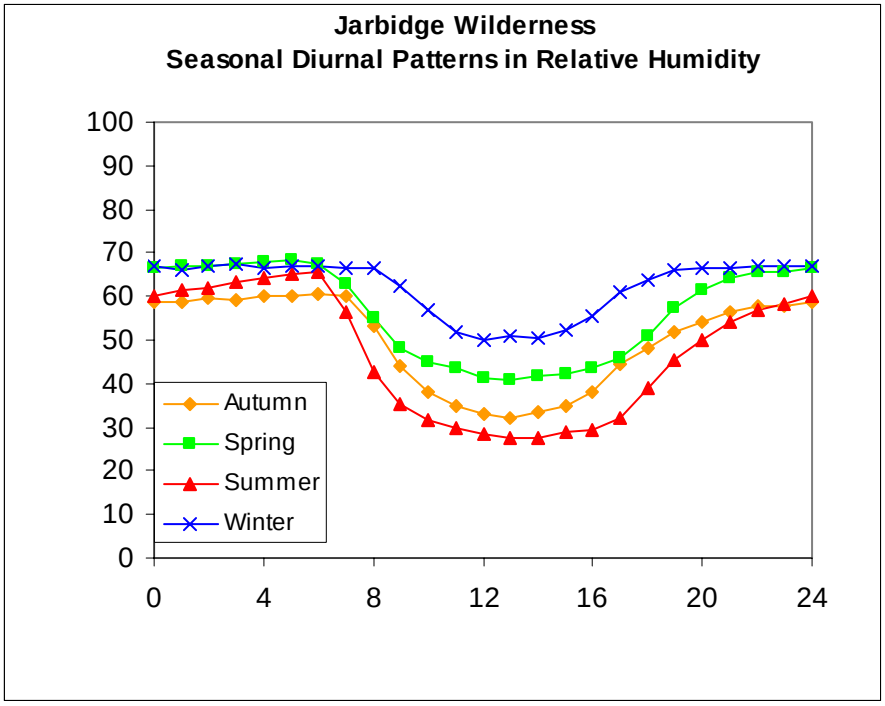
Jarbidge Wilderness
Seasonal Diurnal Patterns in Relative Humidity
100
90
80
70
60
50
40
30
20
10
0
0
4
8
12
16
20
24
Autumn
Spring
Summer
Winter

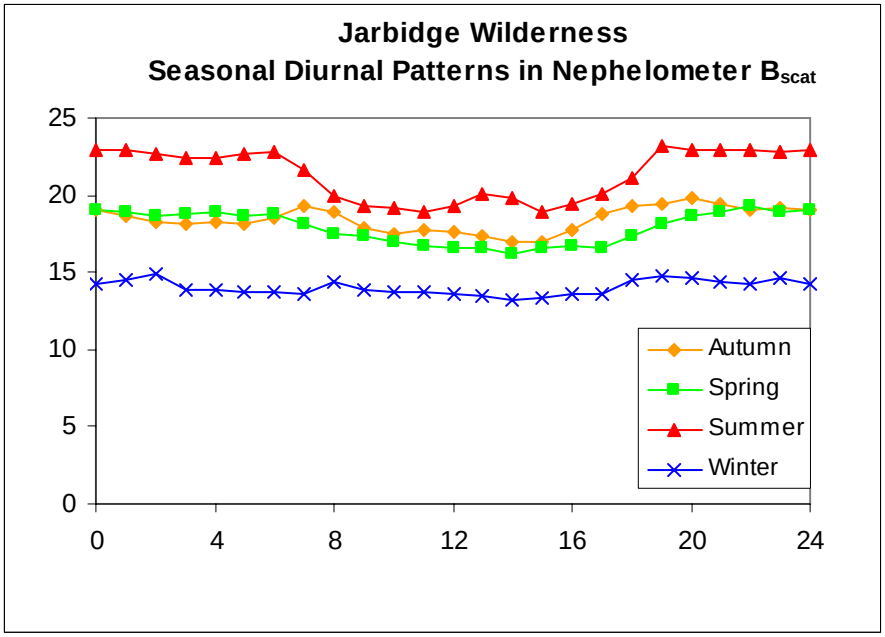
Jarbidge Wilderness
Seasonal Diurnal Patterns in Nephelometer Bscat
25
20
15
10
5
0
0
4
8
12
16
20
24
Autumn
Spring
Summer
Winter

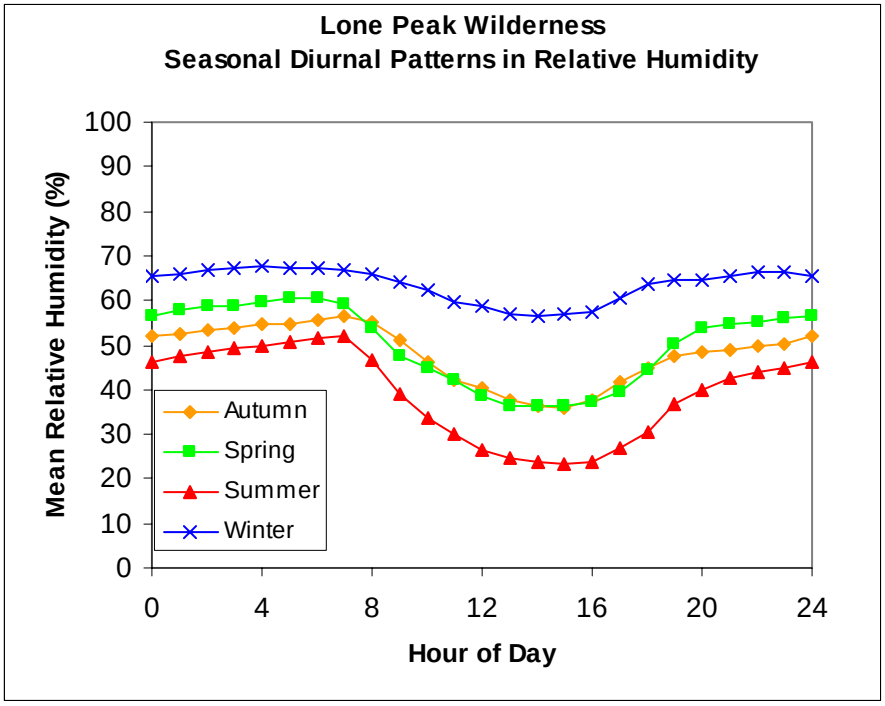
Lone Peak Wilderness
Seasonal Diurnal Patterns in Relative Humidity
Mean Relative Humidity (%)
100
90
80
70
60
50
40
30
20
10
0
0
4
8
12
16
20
24
Hour of Day
Autumn
Spring
Summer
Winter

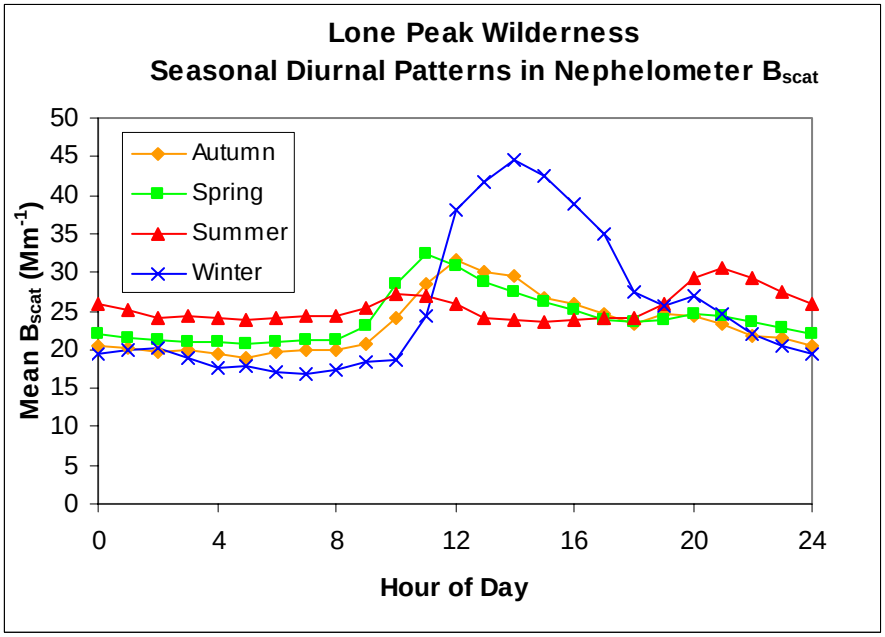
Lone Peak Wilderness
Seasonal Diurnal Patterns in Nephelometer Bscat
Mean Bscat (Mm-1)
50
45
40
35
30
25
20
15
10
5
0
0
4
8
12
16
20
24
Hour of Day
Autumn
Spring
Summer
Winter

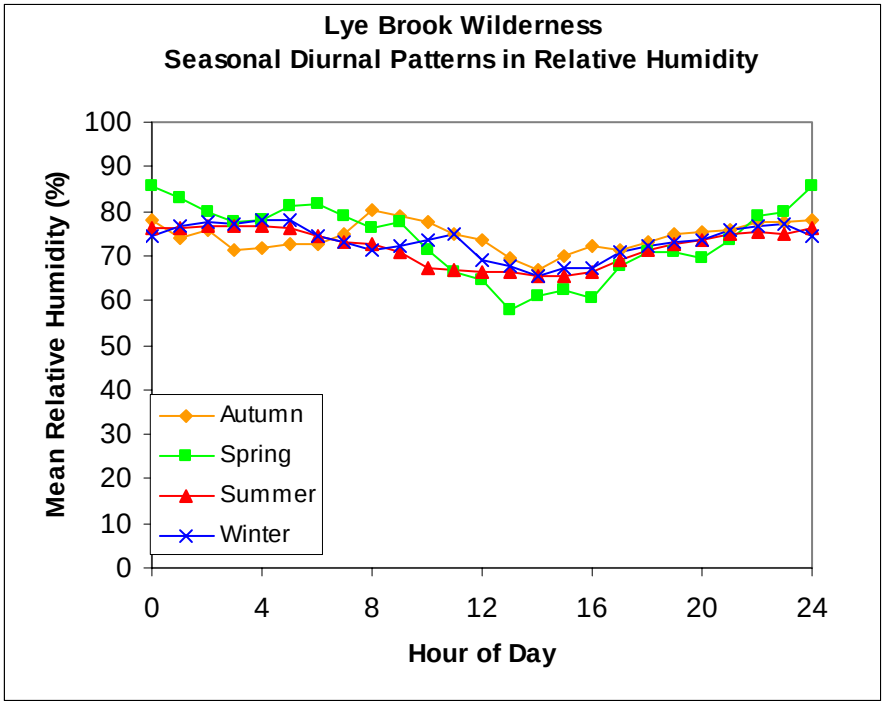
Lye Brook Wilderness
Seasonal Diurnal Patterns in Relative Humidity
Mean Relative Humidity (%)
100
90
80
70
60
50
40
30
20
10
0
0
4
8
12
16
20
24
Hour of Day
Autumn
Spring
Summer
Winter

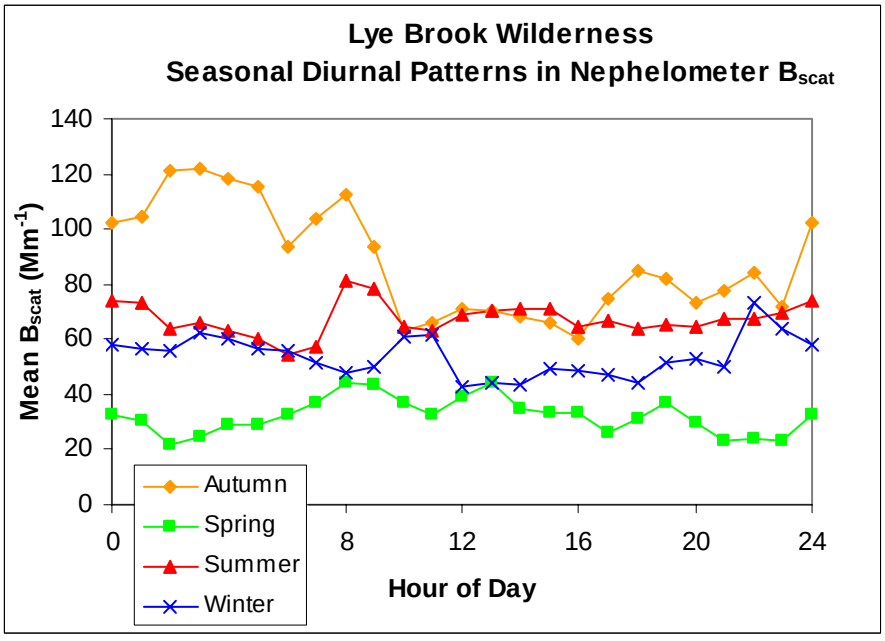
Lye Brook Wilderness
Seasonal Diurnal Patterns in Nephelometer Bscat
Mean Bscat (Mm-1)
140
120
100
80
60
40
20
0
0
8
12
16
20
24
Hour of Day
Autumn
Spring
Summer
Winter

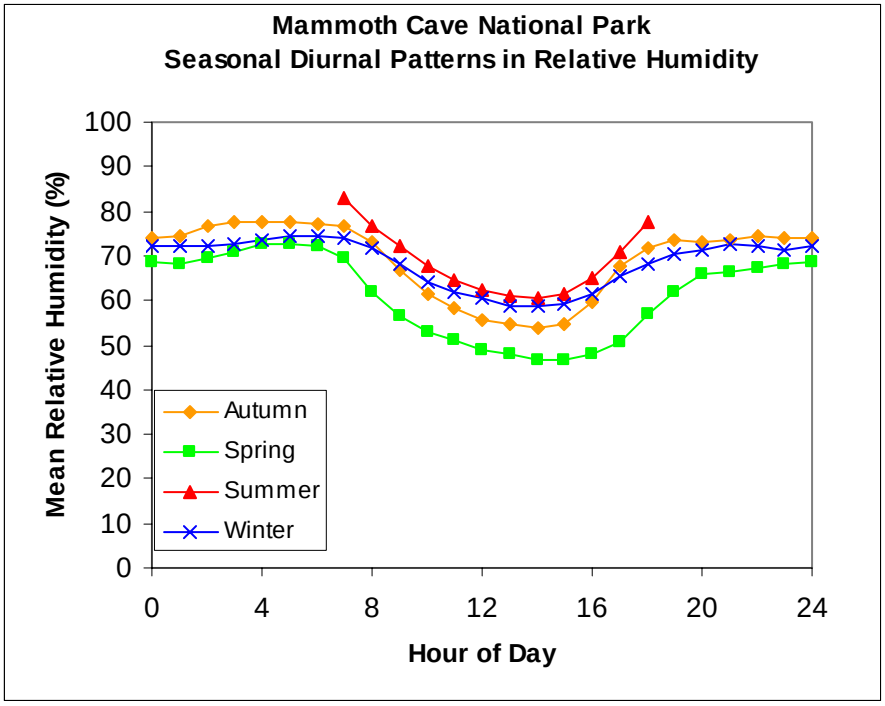
Mammoth Cave National Park
Seasonal Diurnal Patterns in Relative Humidity
Mean Relative Humidity (%)
100
90
80
70
60
50
40
30
20
10
0
0
4
8
12
16
20
24
Hour of Day
Autumn
Spring
Summer
Winter

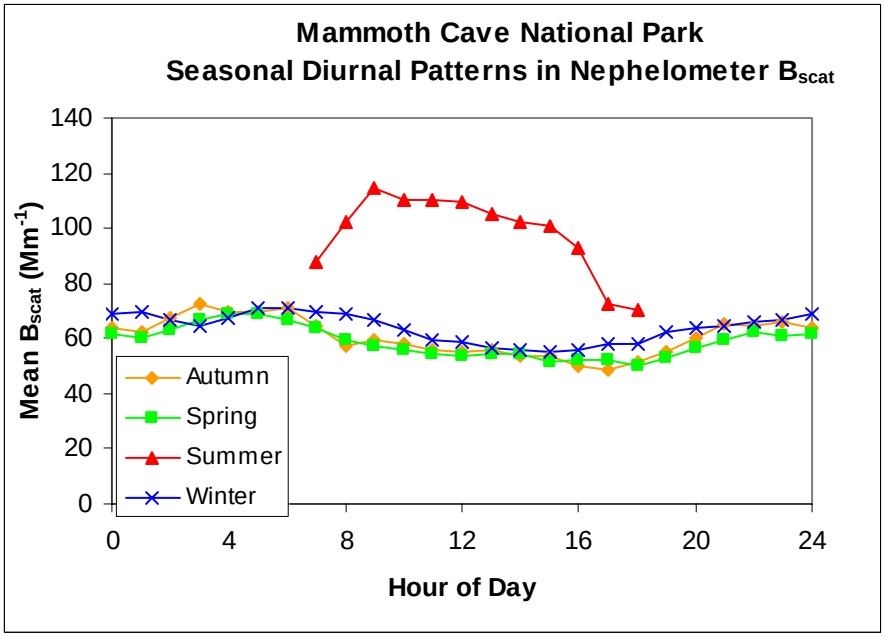
Mammoth Cave National Park
Seasonal Diurnal Patterns in Nephelometer Bscat
Mean Bscat (Mm-1)
140
120
100
80
60
40
20
0
0
4
8
12
16
20
24
Hour of Day
Autumn
Spring
Summer
Winter

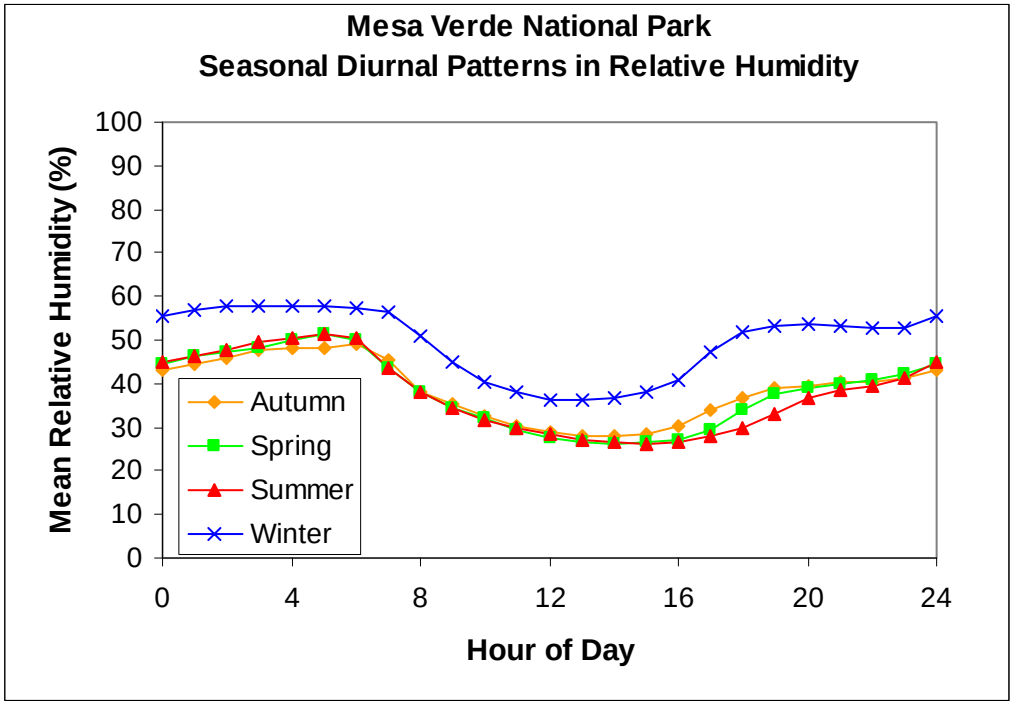
Mesa Verde National Park
Seasonal Diurnal Patterns in Relative Humidity
Mean Relative Humidity (%)
100
90
80
70
60
50
40
30
20
10
0
0
4
8
12
16
20
24
Hour of Day
Autumn
Spring
Summer
Winter

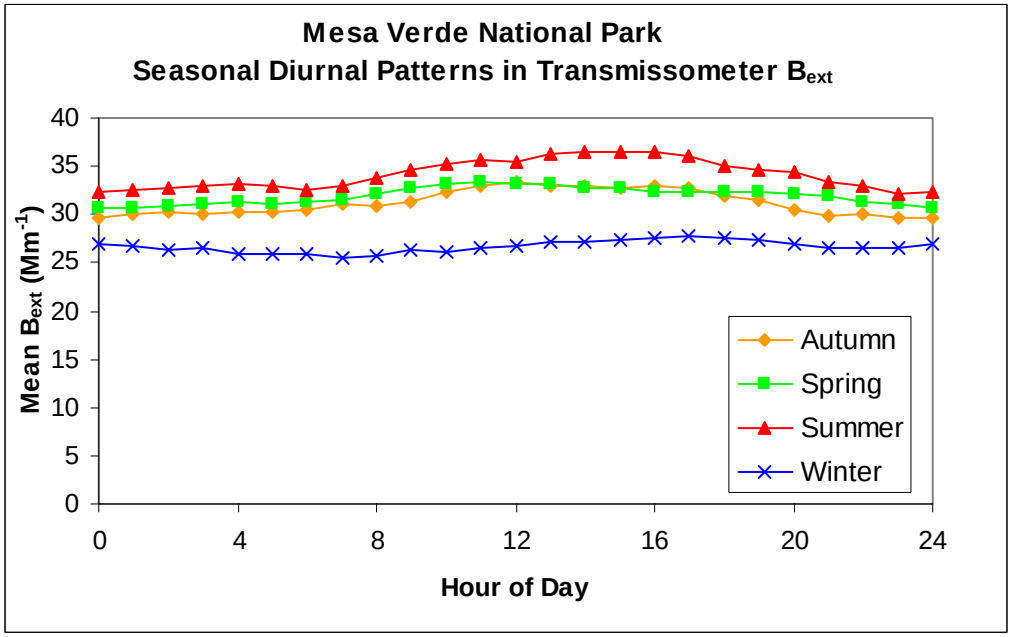
Mesa Verde National Park
Seasonal Diurnal Patterns in Transmissometer Bext
Mean Bext (Mm-1)
40
35
30
25
20
15
10
5
0
0
4
8
12
16
20
24
Hour of Day
Autumn
Spring
Summer
Winter

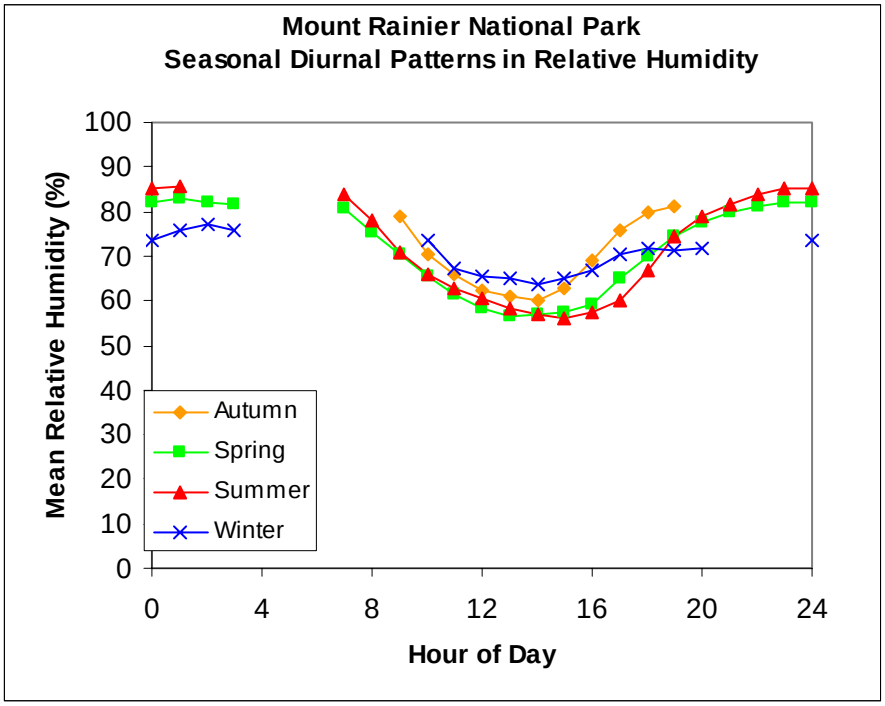
Mount Rainier National Park
Seasonal Diurnal Patterns in Relative Humidity
Mean Relative Humidity (%)
100
90
80
70
60
50
40
30
20
10
0
0
4
8
12
16
20
24
Hour of Day
Autumn
Spring
Summer
Winter

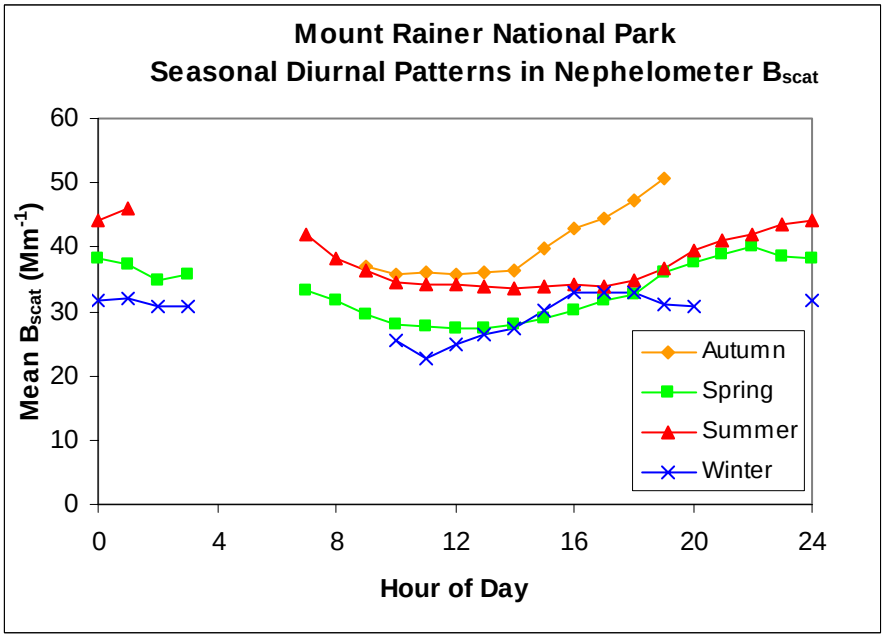
Mount Rainer National Park
Seasonal Diurnal Patterns in Nephelometer Bscat
Mean Bscat (Mm-1)
60
50
40
30
20
10
0
0
4
8
12
16
20
24
Hour of Day
Autumn
Spring
Summer
Winter

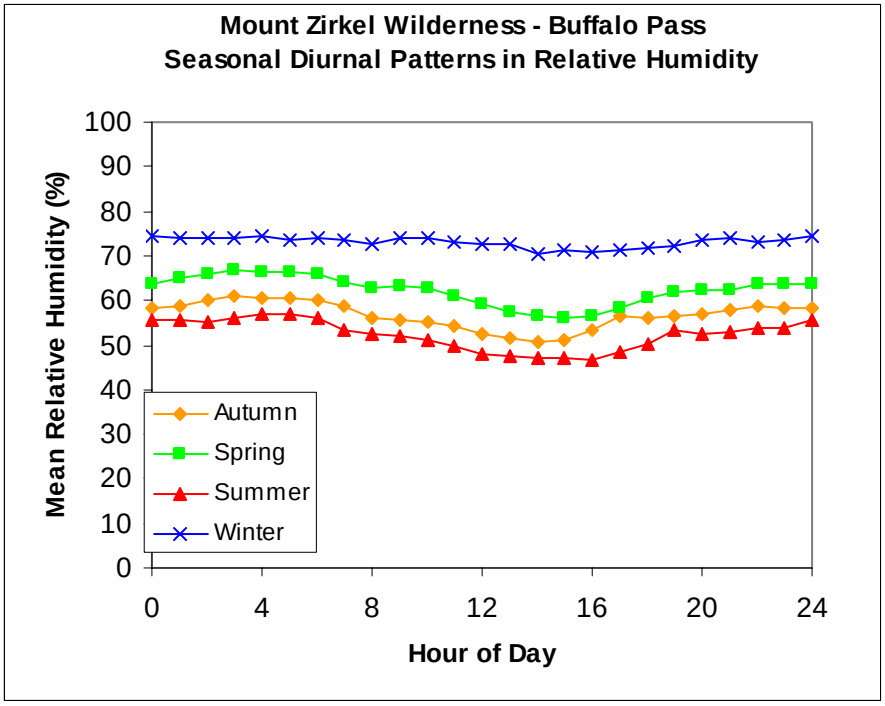
Mount Zirkel Wilderness - Buffalo Pass
Seasonal Diurnal Patterns in Relative Humidity
Mean Relative Humidity (%)
100
90
80
70
60
50
40
30
20
10
0
0
4
8
12
16
20
24
Hour of Day
Autumn
Spring
Summer
Winter

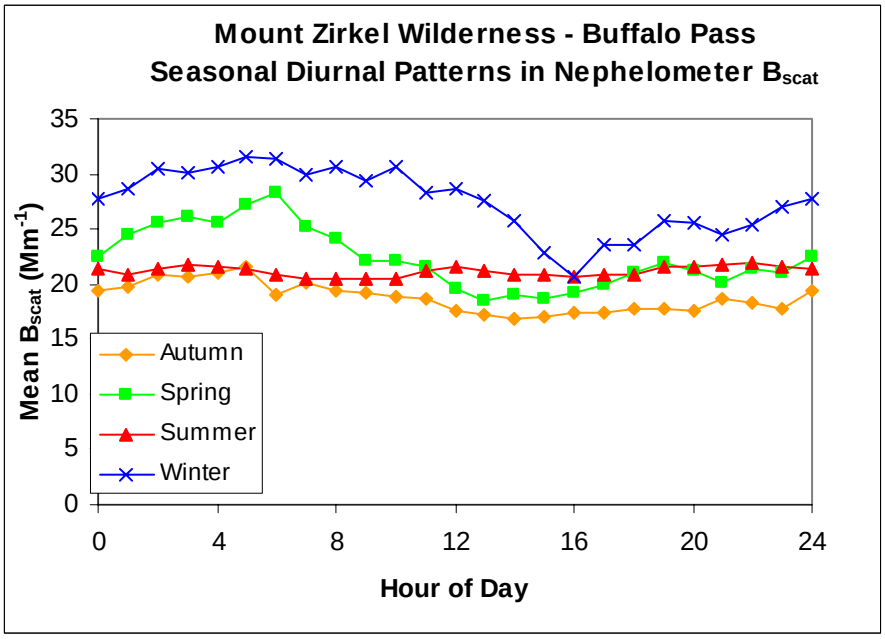
Mount Zirkel Wilderness - Buffalo Pass
Seasonal Diurnal Patterns in Nephelometer Bscat
Mean Bscat (Mm-1)
35
30
25
20
15
10
5
0
0
4
8
12
16
20
24
Hour of Day
Autumn
Spring
Summer
Winter

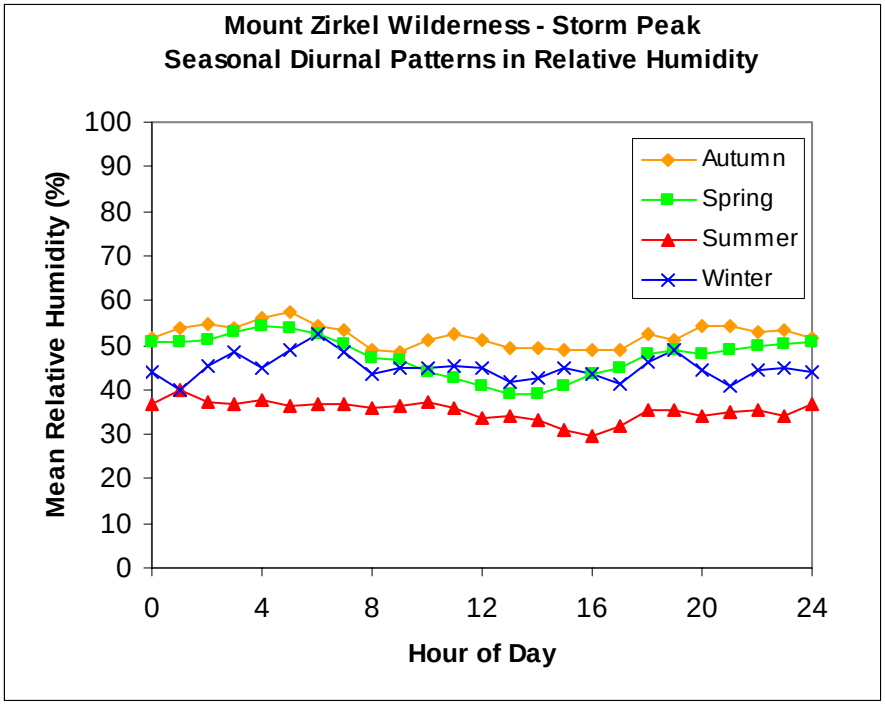
Mount Zirkel Wilderness - Storm Peak
Seasonal Diurnal Patterns in Relative Humidity
Mean Relative Humidity (%)
100
90
80
70
60
50
40
30
20
10
0
0
4
8
12
16
20
24
Hour of Day
Autumn
Spring
Summer
Winter

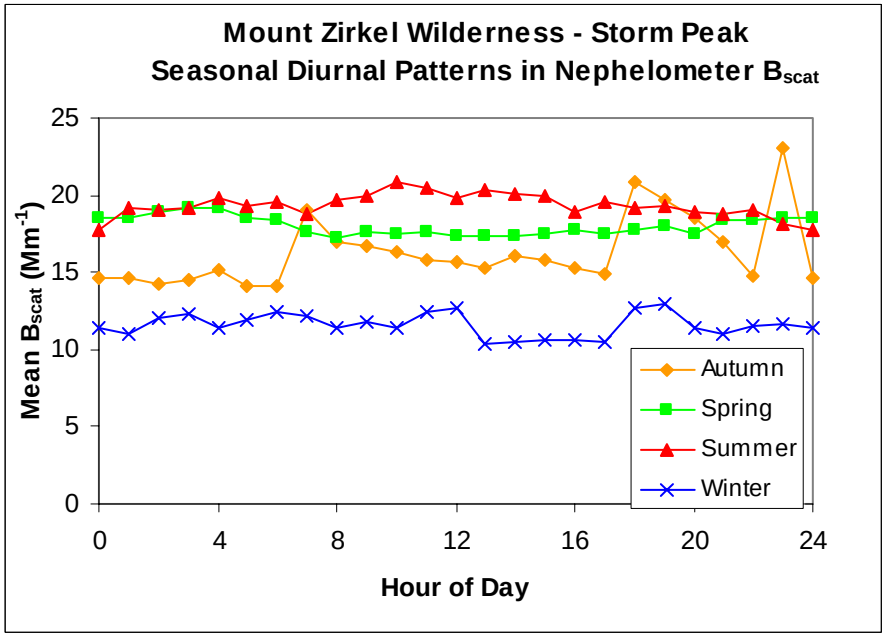
Mount Zirkel Wilderness - Storm Peak
Seasonal Diurnal Patterns in Nephelometer Bscat
Mean Bscat (Mm-1)
25
20
15
10
5
0
0
4
8
12
16
20
24
Hour of Day
Autumn
Spring
Summer
Winter

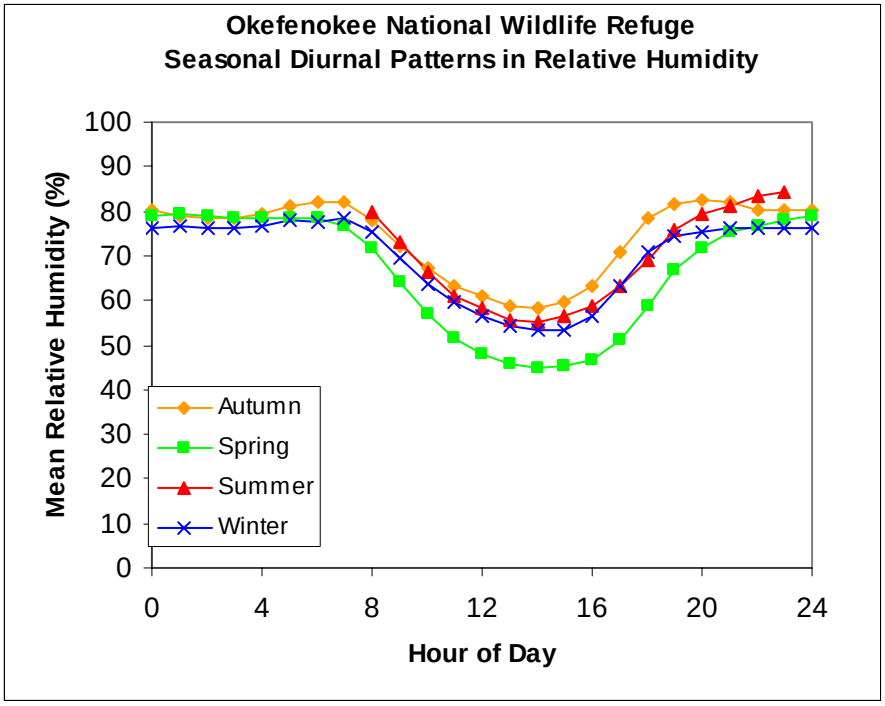
Okefenokee National Wildlife Refuge
Seasonal Diurnal Patterns in Relative Humidity
Mean Relative Humidity (%)
100
90
80
70
60
50
40
30
20
10
0
0
4
8
12
16
20
24
Hour of Day
Autumn
Spring
Summer
Winter

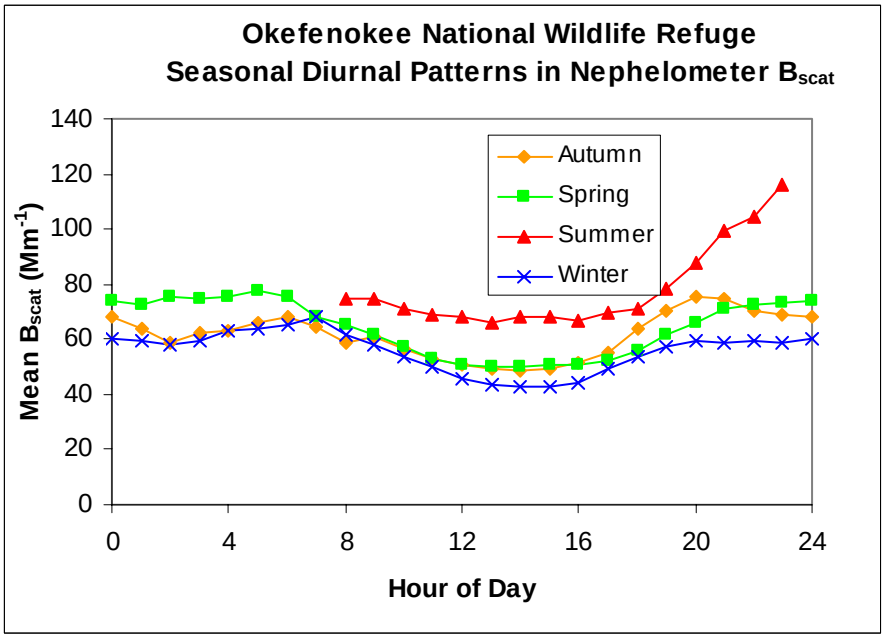
Okefenokee National Wildlife Refuge
Seasonal Diurnal Patterns in Nephelometer Bscat
Mean Bscat (Mm-1)
140
120
100
80
60
40
20
0
0
4
8
12
16
20
24
Hour of Day
Autumn
Spring
Summer
Winter

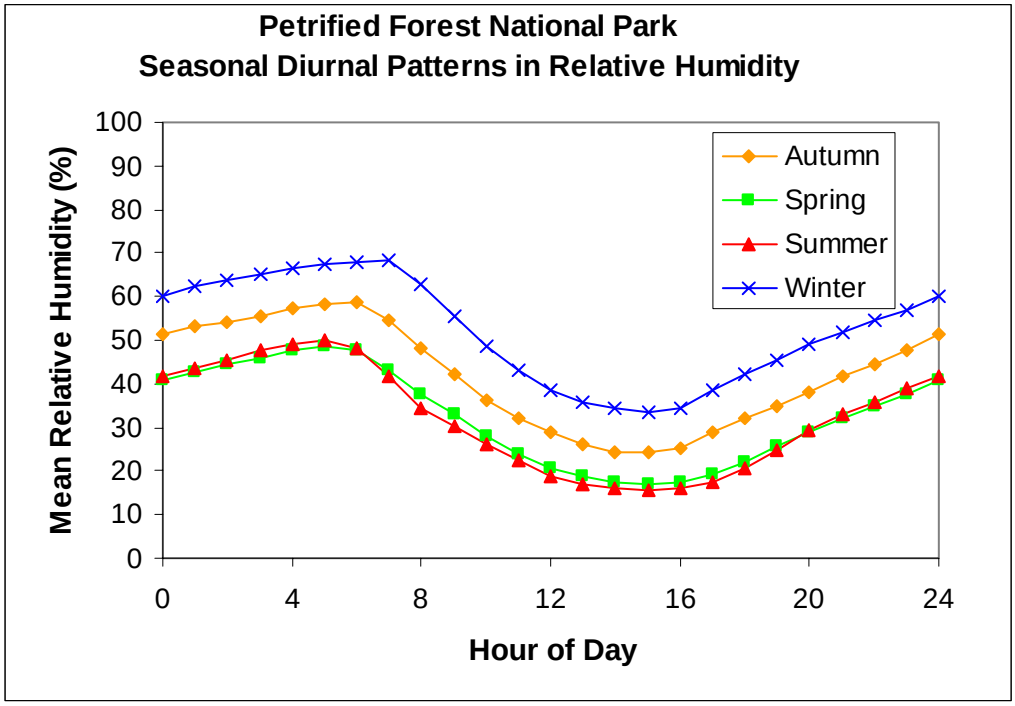
Petrified Forest National Park
Seasonal Diurnal Patterns in Relative Humidity
Mean Relative Humidity (%)
100
90
80
70
60
50
40
30
20
10
0
0
4
8
12
16
20
24
Hour of Day
Autumn
Spring
Summer
Winter

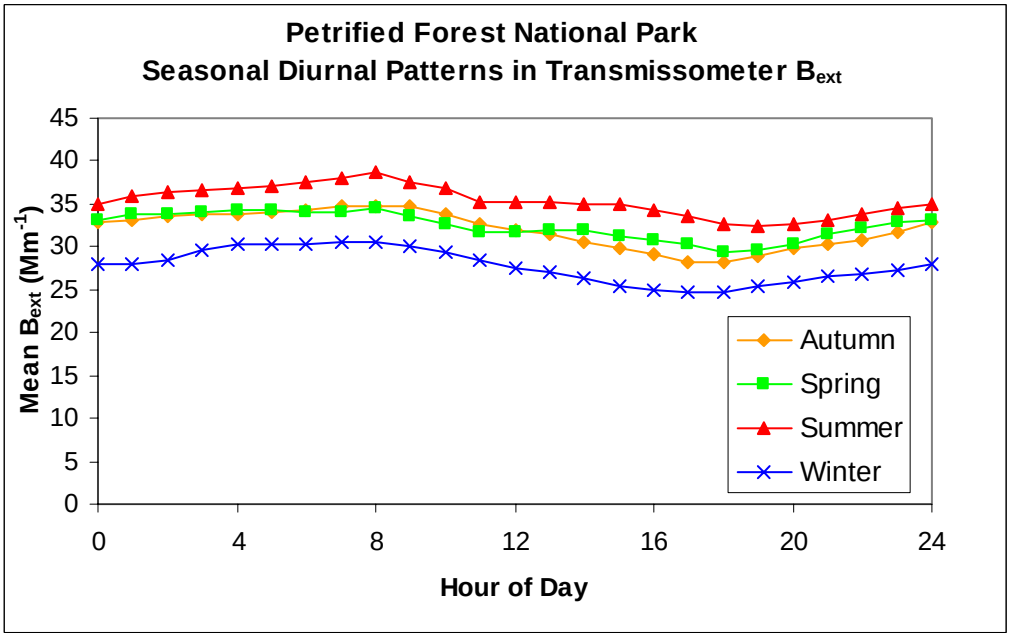
Petrified Forest National Park
Seasonal Diurnal Patterns in Transmissometer Bext
Mean Bext (Mm-1)
45
40
35
30
25
20
15
10
5
0
0
4
8
12
16
20
24
Hour of Day
Autumn
Spring
Summer
Winter

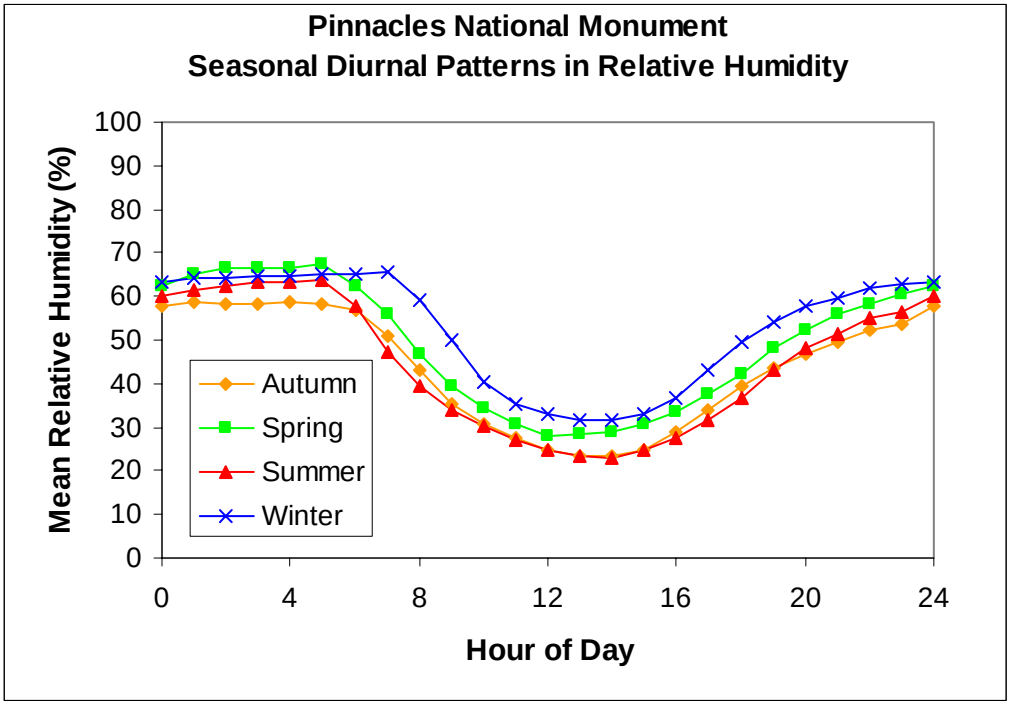
Pinnacles National Monument
Seasonal Diurnal Patterns in Relative Humidity
Mean Relative Humidity (%)
100
90
80
70
60
50
40
30
20
10
0
0
4
8
12
16
20
24
Hour of Day
Autumn
Spring
Summer
Winter

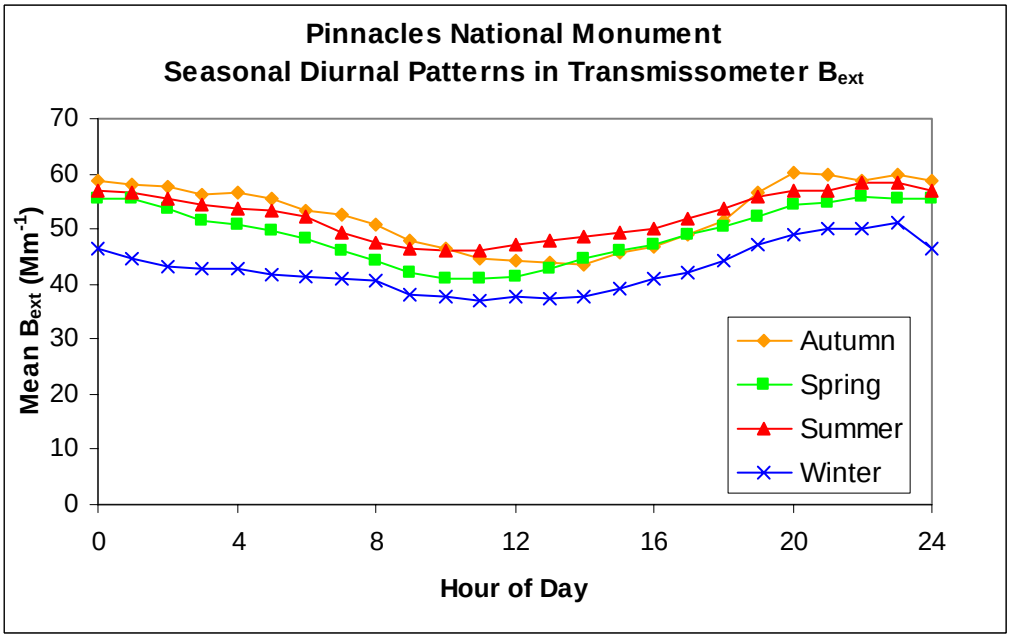
Pinnacles National Monument
Seasonal Diurnal Patterns in Transmissometer Bext
Mean Bext (Mm-1)
70
60
50
40
30
20
10
0
0
4
8
12
16
20
24
Hour of Day
Autumn
Spring
Summer
Winter

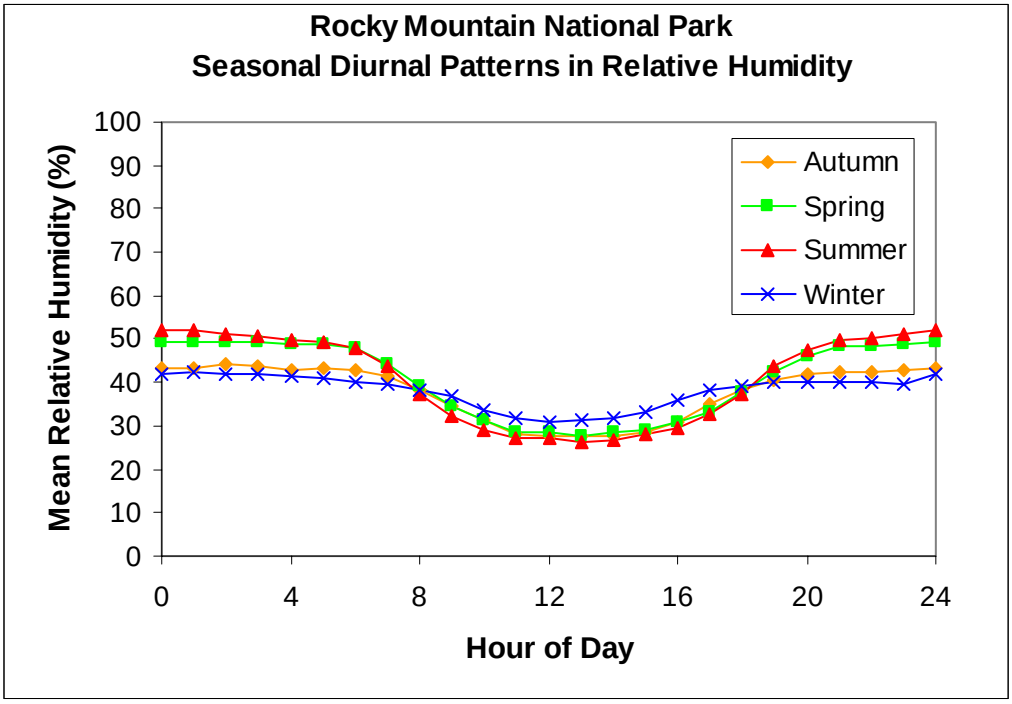
Rocky Mountain National Park
Seasonal Diurnal Patterns in Relative Humidity
Mean Relative Humidity (%)
100
90
80
70
60
50
40
30
20
10
0
0
4
8
12
16
20
24
Hour of Day
Autumn
Spring
Summer
Winter

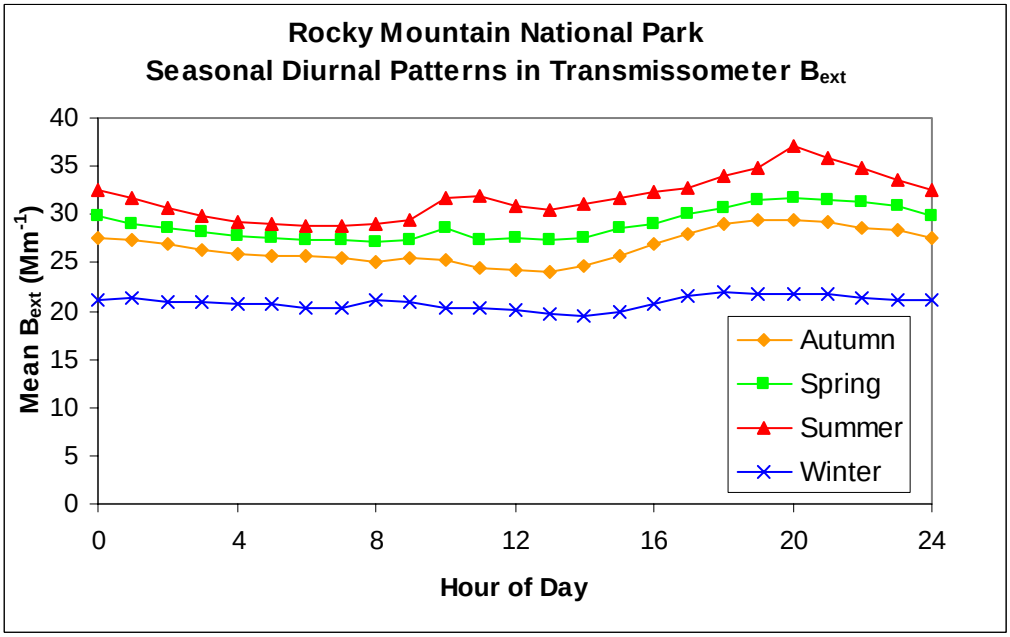
Rocky Mountain National Park
Seasonal Diurnal Patterns in Transmissometer Bext
Mean Bext (Mm-1)
40
35
30
25
20
15
10
5
0
0
4
8
12
16
20
24
Hour of Day
Autumn
Spring
Summer
Winter

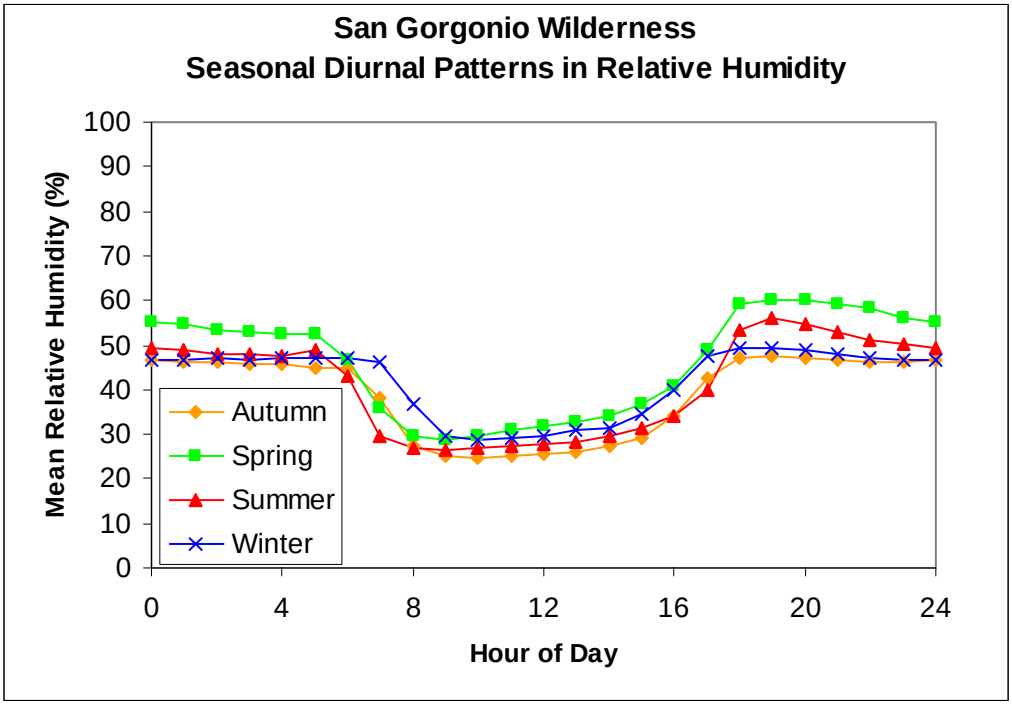
San Gorgonio Wilderness
Seasonal Diurnal Patterns in Relative Humidity
Mean Relative Humidity (%)
100
90
80
70
60
50
40
30
20
10
0
0
4
8
12
16
20
24
Hour of Day
Autumn
Spring
Summer
Winter

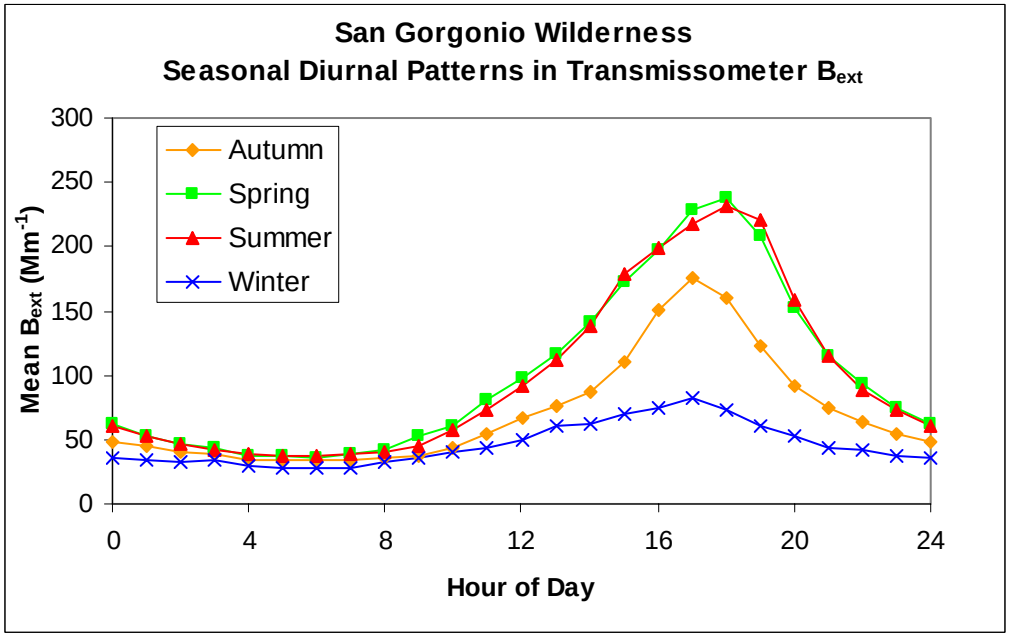
San Gorgonio Wilderness
Seasonal Diurnal Patterns in Transmissometer Bext
Mean Bext (Mm-1)
300
250
200
150
100
50
0
0
4
8
12
16
20
24
Hour of Day
Autumn
Spring
Summer
Winter

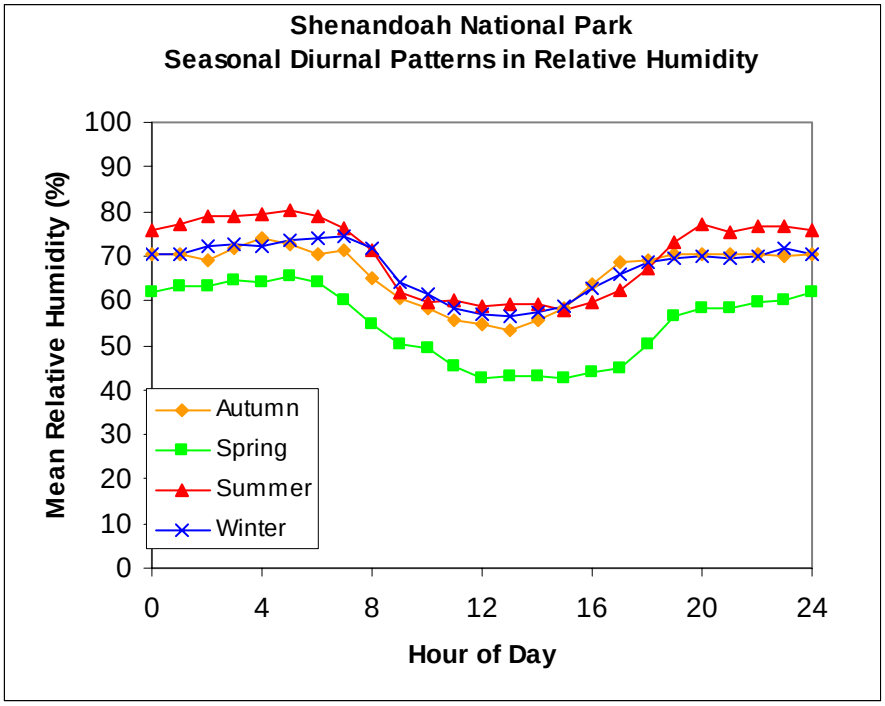
Shenandoah National Park
Seasonal Diurnal Patterns in Relative Humidity
Mean Relative Humidity (%)
100
90
80
70
60
50
40
30
20
10
0
0
4
8
12
16
20
24
Hour of Day
Autumn
Spring
Summer
Winter

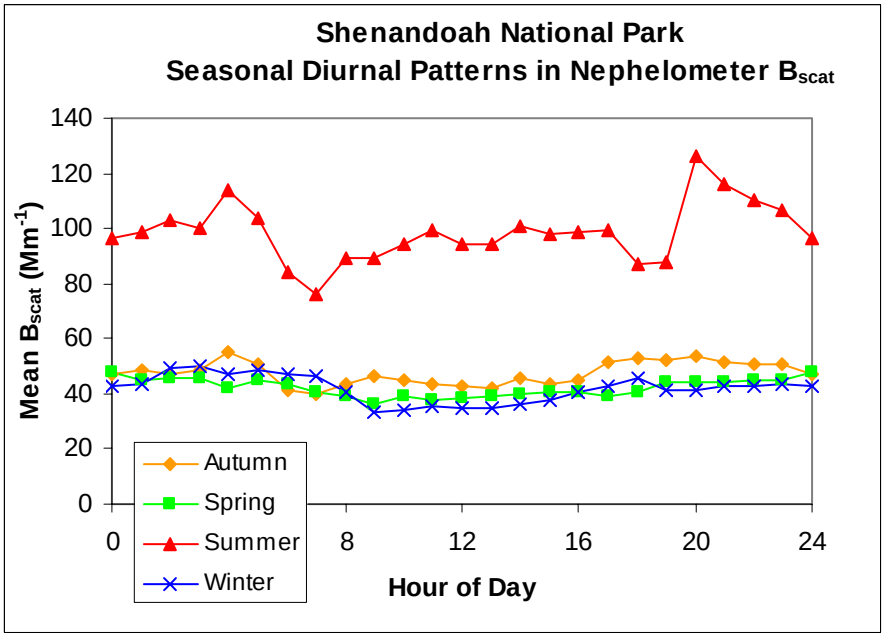
Shenandoah National Park
Seasonal Diurnal Patterns in Nephelometer Bscat
Mean Bscat (Mm-1)
140
120
100
80
60
40
20
0
0
8
12
16
20
24
Hour of Day
Autumn
Spring
Summer
Winter

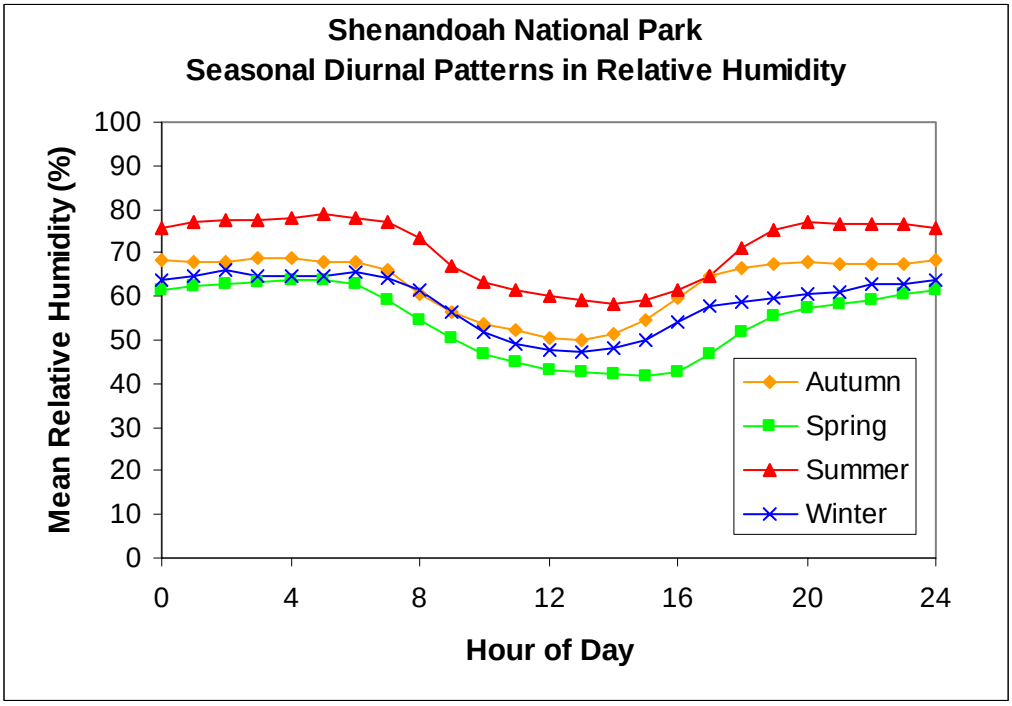
Shenandoah National Park
Seasonal Diurnal Patterns in Relative Humidity
Mean Relative Humidity (%)
100
90
80
70
60
50
40
30
20
10
0
0
4
8
12
16
20
24
Hour of Day
Autumn
Spring
Summer
Winter

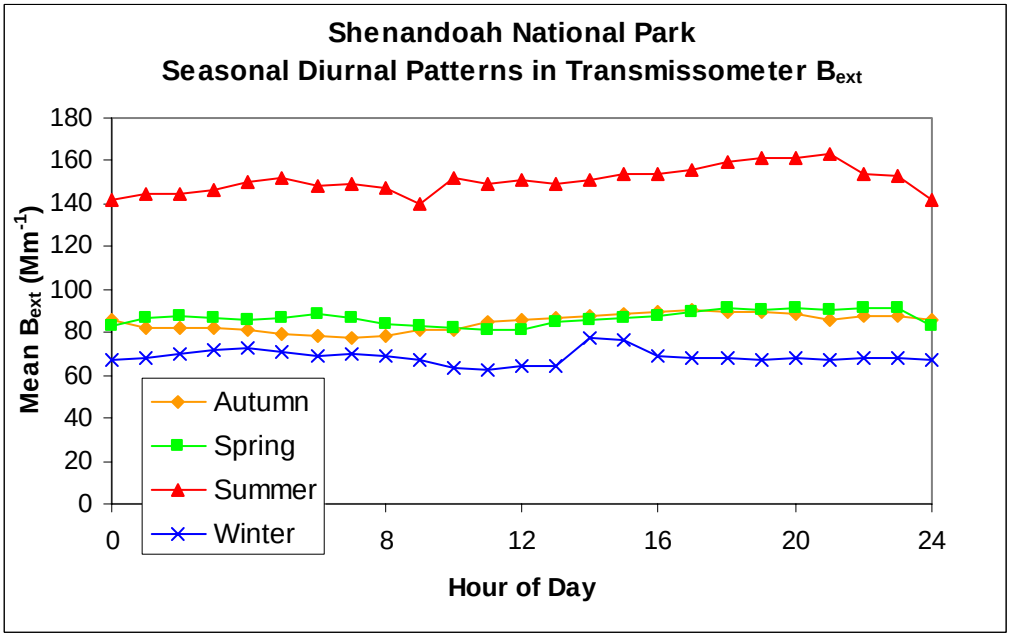
Shenandoah National Park
Seasonal Diurnal Patterns in Transmissometer Bext
Mean Bext (Mm-1)
180
160
140
120
100
80
60
40
20
0
0
8
12
16
20
24
Hour of Day
Autumn
Spring
Summer
Winter

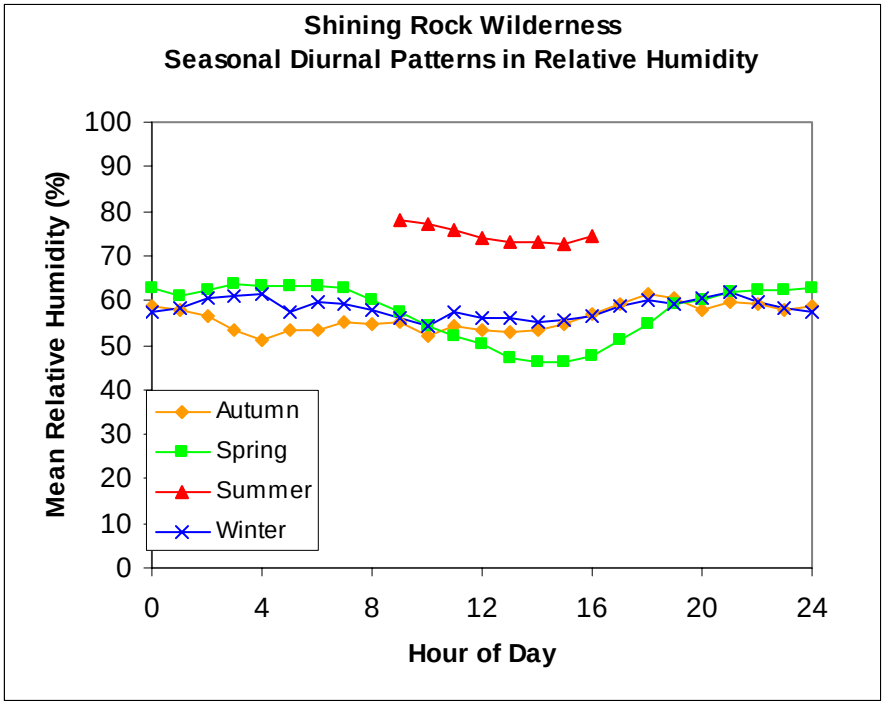
Shining Rock Wilderness
Seasonal Diurnal Patterns in Relative Humidity
Mean Relative Humidity (%)
100
90
80
70
60
50
40
30
20
10
0
0
4
8
12
16
20
24
Hour of Day
Autumn
Spring
Summer
Winter

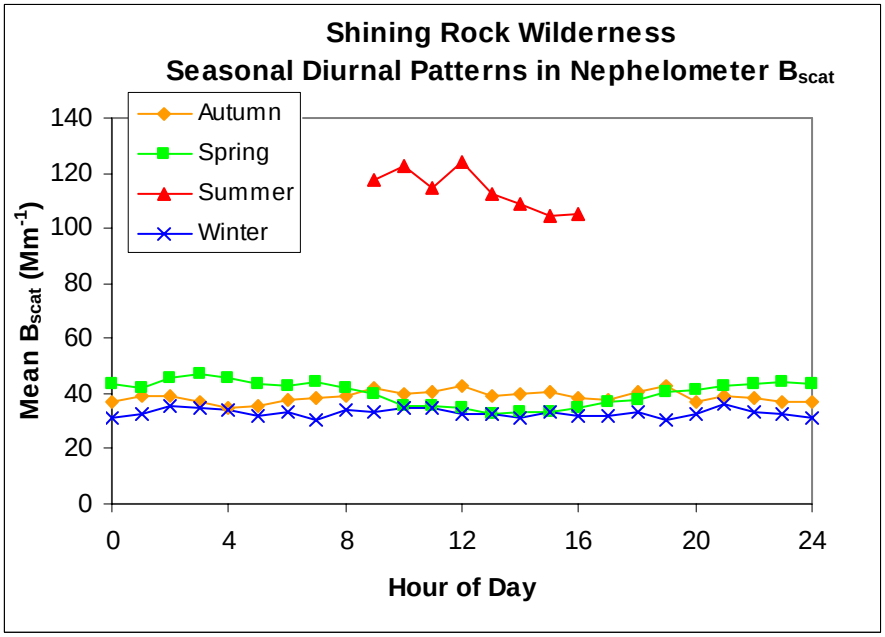
Shining Rock Wilderness
Seasonal Diurnal Patterns in Nephelometer Bscat
Mean Bscat (Mm-1)
140
120
100
80
60
40
20
0
0
4
8
12
16
20
24
Hour of Day
Autumn
Spring
Summer
Winter

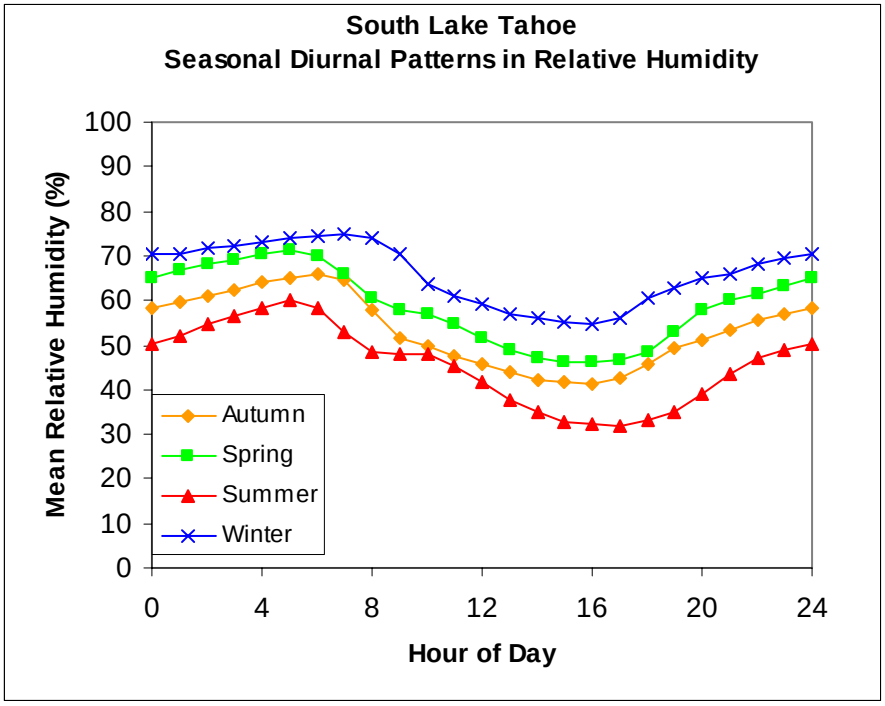
South Lake Tahoe
Seasonal Diurnal Patterns in Relative Humidity
Mean Relative Humidity (%)
100
90
80
70
60
50
40
30
20
10
0
0
4
8
12
16
20
24
Hour of Day
Autumn
Spring
Summer
Winter

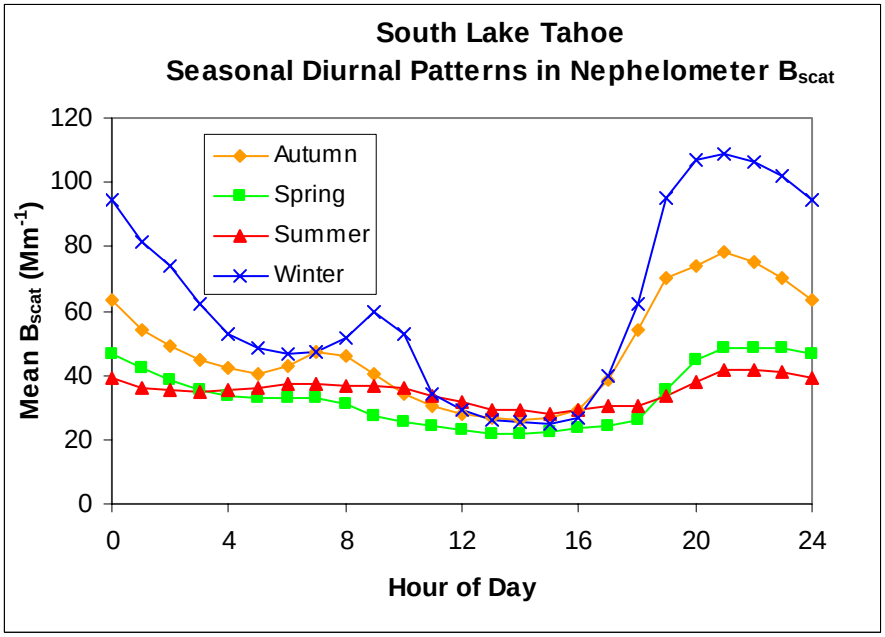
South Lake Tahoe
Seasonal Diurnal Patterns in Nephelometer Bscat
Mean Bscat (Mm-1)
120
100
80
60
40
20
0
0
4
8
12
16
20
24
Hour of Day
Autumn
Spring
Summer
Winter

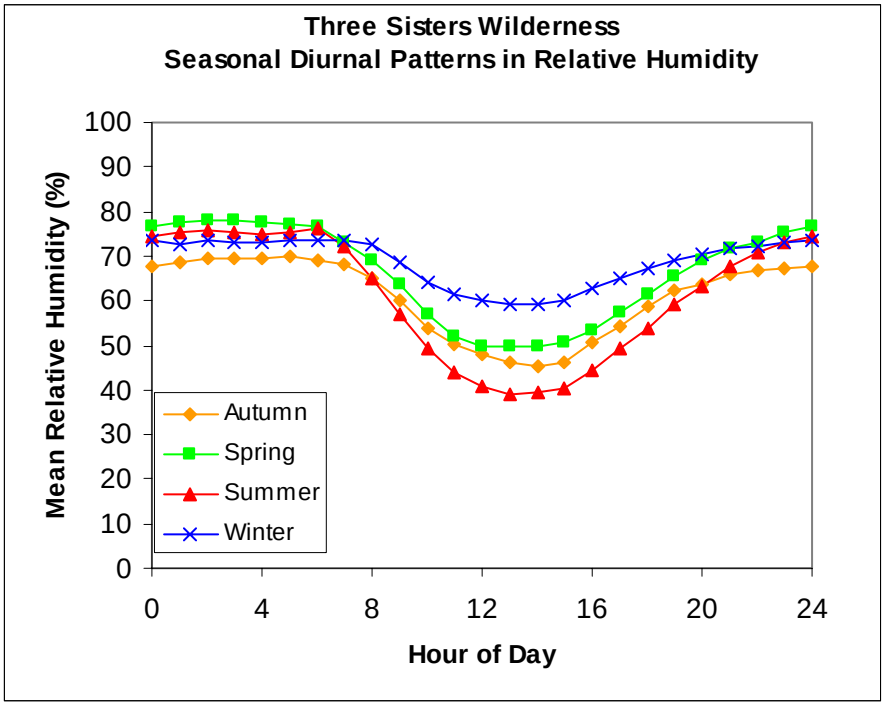
Three Sisters Wilderness
Seasonal Diurnal Patterns in Relative Humidity
Mean Relative Humidity (%)
100
90
80
70
60
50
40
30
20
10
0
0
4
8
12
16
20
24
Hour of Day
Autumn
Spring
Summer
Winter

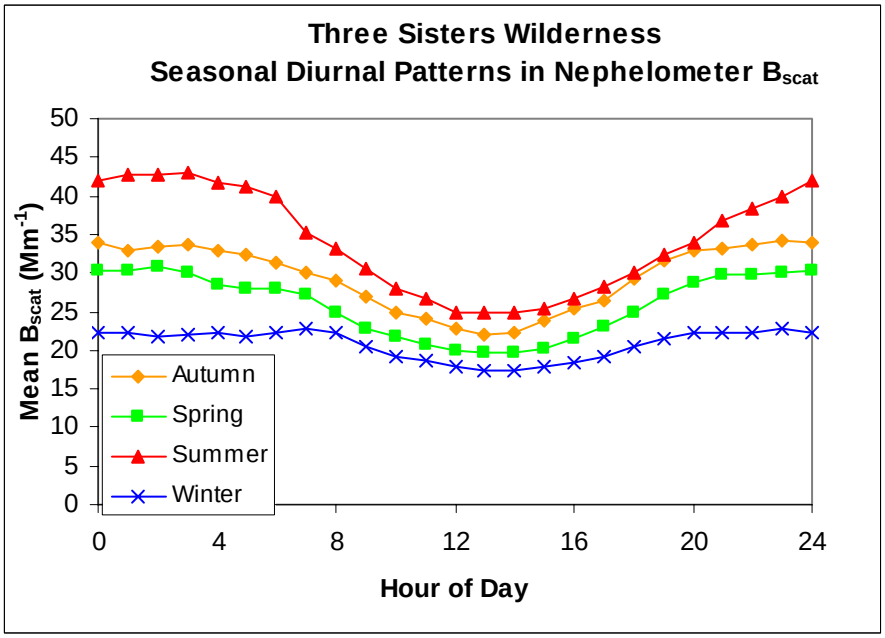
Three Sisters Wilderness
Seasonal Diurnal Patterns in Nephelometer Bscat
Mean Bscat (Mm-1)
50
45
40
35
30
25
20
15
10
5
0
0
4
8
12
16
20
24
Hour of Day
Autumn
Spring
Summer
Winter

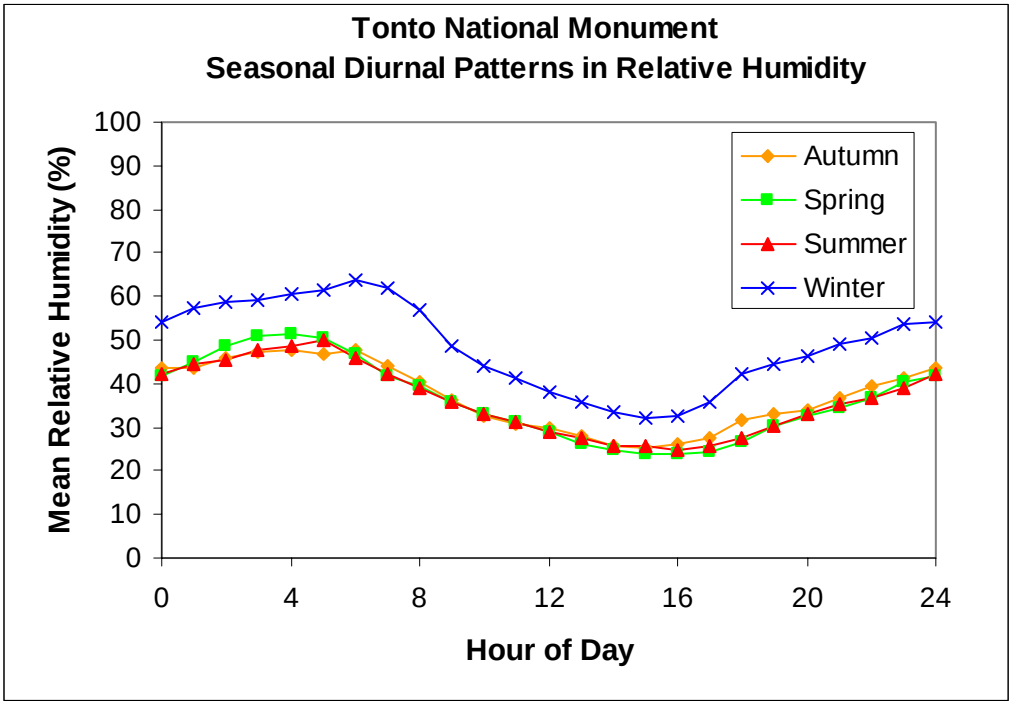
Tonto National Monument
Seasonal Diurnal Patterns in Relative Humidity
Mean Relative Humidity (%)
100
90
80
70
60
50
40
30
20
10
0
0
4
8
12
16
20
24
Hour of Day
Autumn
Spring
Summer
Winter

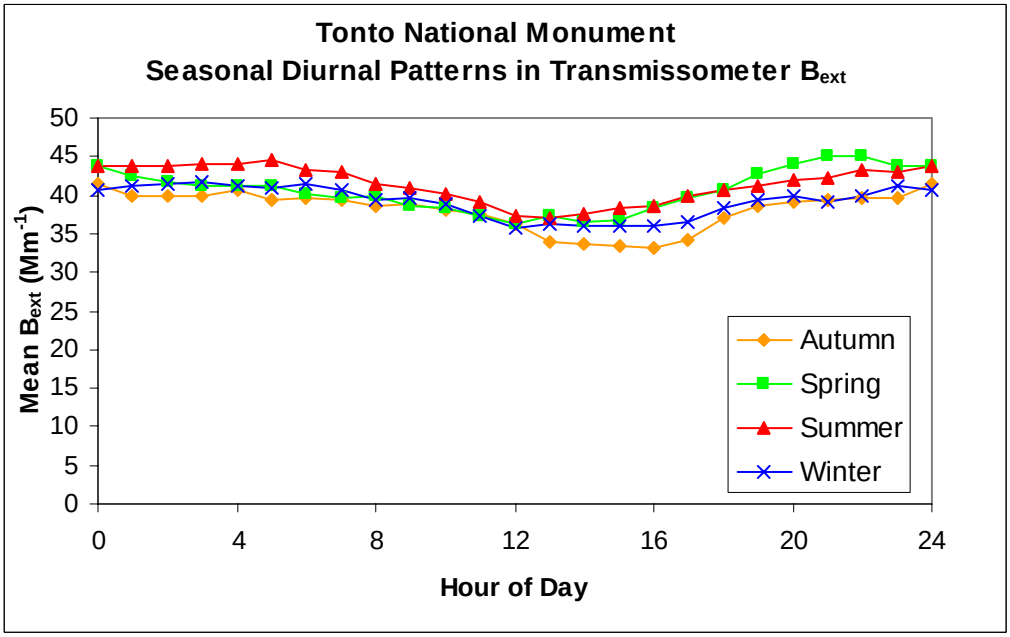
Tonto National Monument
Seasonal Diurnal Patterns in Transmissometer Bext
Mean Bext (Mm-1)
50
45
40
35
30
25
20
15
10
5
0
0
4
8
12
16
20
24
Hour of Day
Autumn
Spring
Summer
Winter

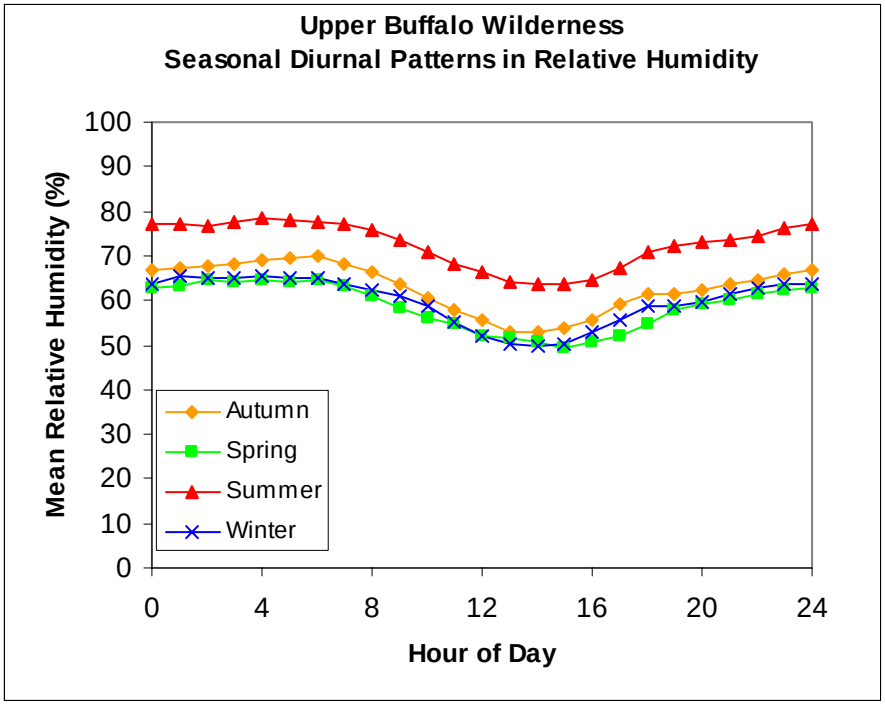
Upper Buffalo Wilderness
Seasonal Diurnal Patterns in Relative Humidity
Mean Relative Humidity (%)
100
90
80
70
60
50
40
30
20
10
0
0
4
8
12
16
20
24
Hour of Day
Autumn
Spring
Summer
Winter

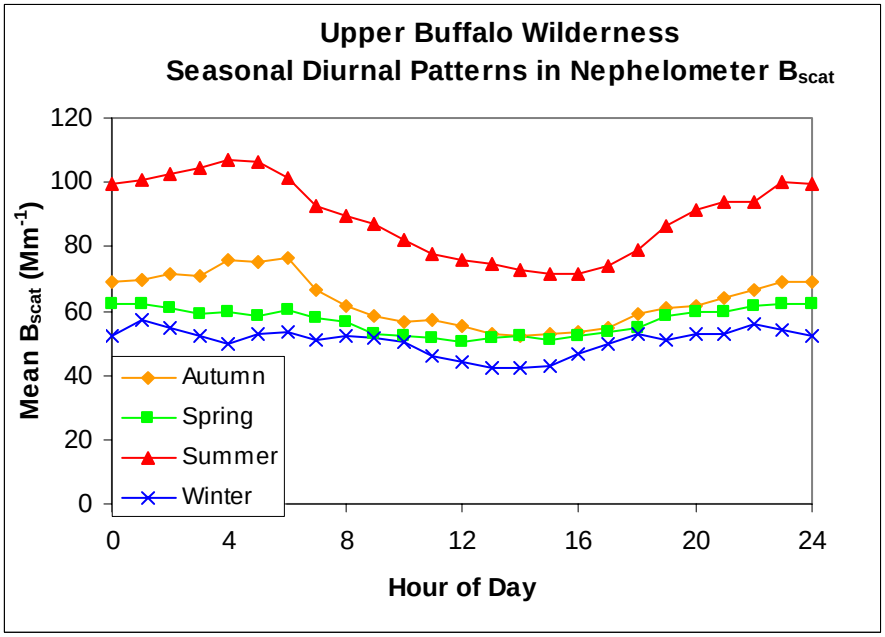
Upper Buffalo Wilderness
Seasonal Diurnal Patterns in Nephelometer Bscat
Mean Bscat (Mm-1)
120
100
80
60
40
20
0
0
4
8
12
16
20
24
Hour of Day
Autumn
Spring
Summer
Winter

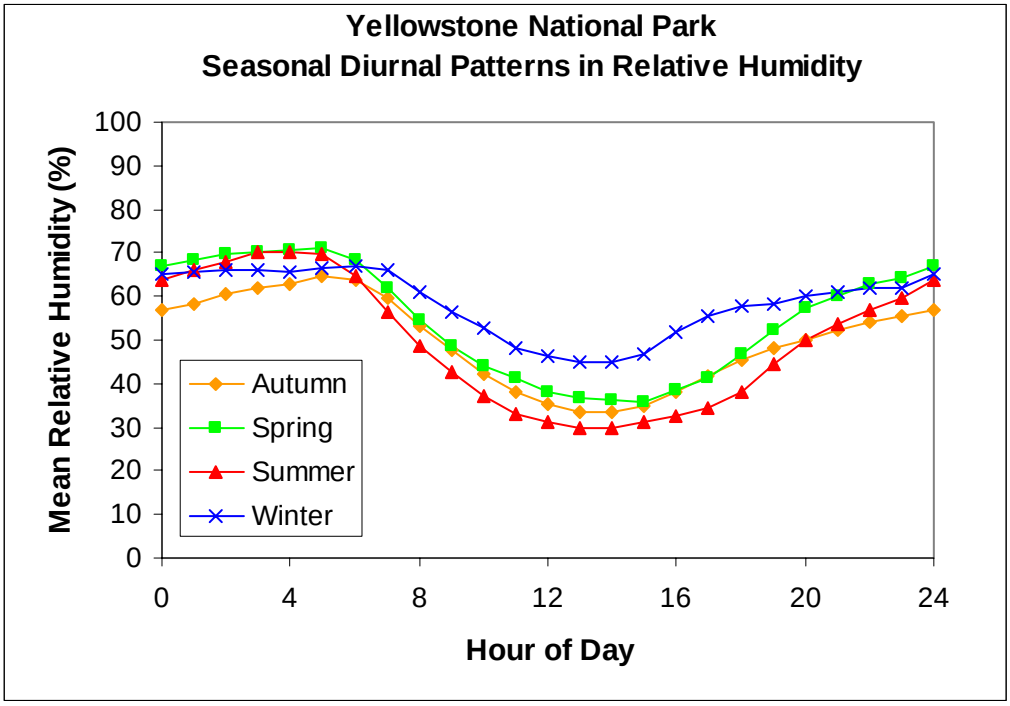
Yellowstone National Park
Seasonal Diurnal Patterns in Relative Humidity
Mean Relative Humidity (%)
100
90
80
70
60
50
40
30
20
10
0
0
4
8
12
16
20
24
Hour of Day
Autumn
Spring
Summer
Winter

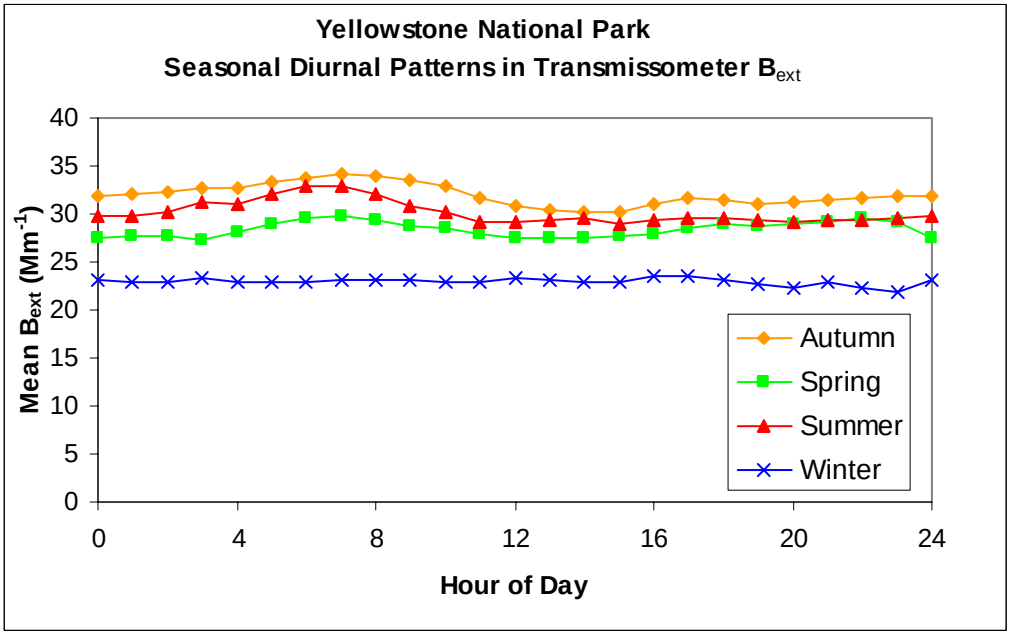
Yellowstone National Park
Seasonal Diurnal Patterns in Transmissometer Bext
Mean Bext (Mm-1)
40
35
30
25
20
15
10
5
0
0
4
8
12
16
20
24
Hour of Day
Autumn
Spring
Summer
Winter

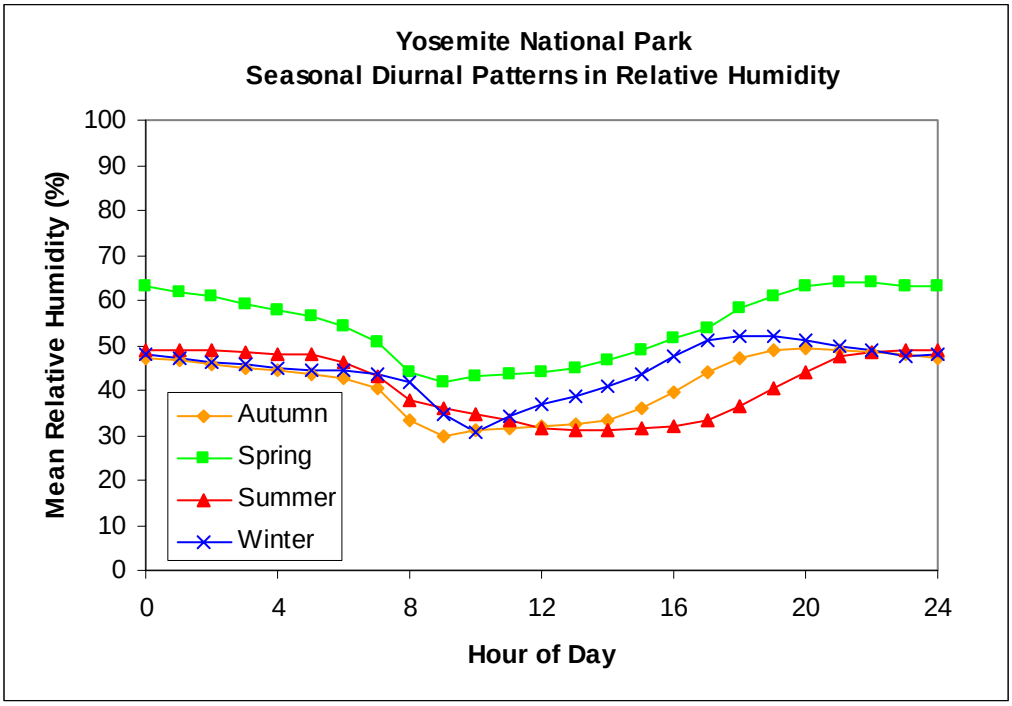
Yosemite National Park
Seasonal Diurnal Patterns in Relative Humidity
Mean Relative Humidity (%)
100
90
80
70
60
50
40
30
20
10
0
0
4
8
12
16
20
24
Hour of Day
Autumn
Spring
Summer
Winter

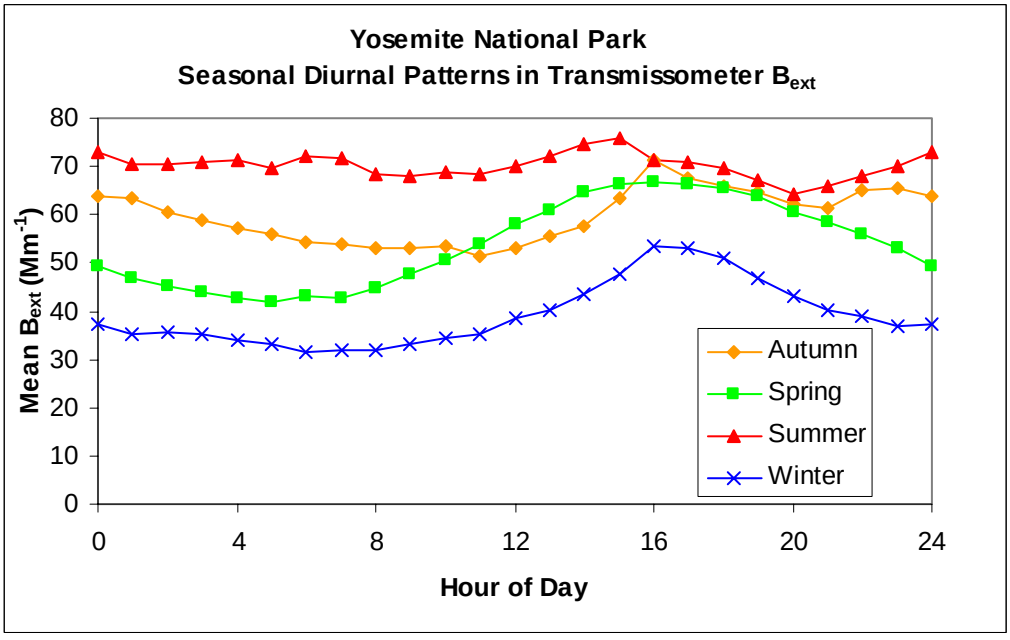
Yosemite National Park
Seasonal Diurnal Patterns in Transmissometer Bext
Mean Bext (Mm-1)
80
70
60
50
40
30
20
10
0
0
4
8
12
16
20
24
Hour of Day
Autumn
Spring
Summer
Winter

APPENDIX G

A COMPARISON OF SULFATE AND NITRATE PARTICLE MASS CONCENTRATIONS FROM IMPROVE AND THE CDN

G.1 INTRODUCTION

The Clean Air Status and Trends Network (CASTNet), or CASTNet Deposition Network (CDN) was established as a result of the 1990 Amendments to the Clean Air Act with the goal to determine the effect of emissions reductions mandated by the Act on air quality and deposition. Monitoring sites of the National Dry Deposition Network (NDDN), [CASTNet Report, 1998], itself established by the EPA in 1986, became a part of the CDN in 1992. Beginning in 1994, monitoring at 17 primarily western United States national parks began under the CDN, National Park Service (NPS), and EPA. The CDN monitoring program collects particle mass concentration data and meteorological parameters required to estimate dry particle deposition flux.

IMPROVE is primarily a visibility monitoring network, while the CDN was designed to estimate dry deposition. Each network has sampling protocols distinct from the other, although they both have a common interest in measurements of airborne species related to deposition and visibility related issues. If necessary data are available to initiate an inferential deposition model at IMPROVE sites, it would also be useful to use IMPROVE data to make estimates of dry particle deposition. Also, if necessary particle data, or estimates thereof, are available at CDN monitoring sites then one could use CDN data as a surrogate to estimate a visibility index (e.g., the particle light extinction coefficient) in regions where IMPROVE protocol data are not available. A first step is to see if concentrations from each respective network's sampling systems are comparable. We compare particle SO_4^{2-} and NO_3^- mass concentrations reported by the two networks using measurements from 23 locations where monitoring sites are within approximately 50 km.

Important differences between the samplers deployed by the CDN and IMPROVE networks should be kept in mind when comparing their respective data. For example, CDN protocol is to collect weekly integrated samples, while IMPROVE protocol is a twice a week 24-hour sampling schedule; CDN samplers are situated 10 m above ground level (agl), while IMPROVE sampler inlets are approximately 3 m agl; CDN samplers do not have size selective inlets, while IMPROVE samplers are fitted with either $PM_{2.5}$ or PM_{10} inlets; the CDN deploys filter pack

samplers to measure all reported chemical components, while IMPROVE uses separate modules, including a denuded inlet (intended to remove HNO_3) for particle NO_3^- sampling. CDN collects particle nitrate on Teflon, while IMPROVE uses a nylon substrate to collect fine particle nitrate. Any of these protocol differences, as well as spatial variability introduced from geographical separation of selected comparison sites, could lead to an observed measurement bias.

Particle SO_4^{2-} is measured accurately by a variety of sampler configurations [Benner et al., 1991], while the magnitude of particle NO_3^- loss from Teflon is often significant [Shaw et al., 1982; Benner et al., 1991; Ashbaugh et al., 1998; Hering and Cass, 1999 and references therein]. Denuded samplers using nylon collection substrates have been found to provide more accurate particle NO_3^- measurements than filter pack methods that collect particle NO_3^- on Teflon [Shaw et al., 1982; Hering, 1986; Benner et al., 1991]. Direct comparisons of particle mass measured by IMPROVE samplers to measurements made by other similarly configured samplers (e.g., denuded samplers operating with cyclones) show good agreement between particle SO_4^{2-} and NH_4^{2+} mass concentrations, although agreement among particle NO_3^- measurements can be poor [Chow et al., 1994; Turpin et al., 1997].

The mass of particle NO_3^- measured by filter pack samplers can underestimate ambient particle NO_3^- mass under certain conditions. Ammonium nitrate can be lost on the filter by volatilization or by reaction with strong acid under ammonia limited conditions [Appel et al., 1984]. Field studies have shown the magnitude of NO_3^- loss from Teflon due to volatilization is temperature dependent [Hering and Cass, 1999]. Particle NO_3^- volatilization is dependent on the ammonium nitrate equilibrium constant, *K*, which has a strong dependence on temperature and humidity [Mozurkewich, 1993]. Alternatively, it is possible particle NO_3^- measured by a denuded Nylasorb substrate, such as used for particle NO_3^- sampling under IMPROVE protocol, will be overestimated if gas phase NO_3^- is not efficiently removed from the sample stream and consequently interpreted as particle NO_3^-.

Sampler inlet particle size cut points can also affect particle mass measurements depending on partitioning of ambient particles between fine (particles < approximately 2.5 μm in aerodynamic diameter) and coarse (particles > approximately 2.5 μm in aerodynamic diameter) size modes. Field studies indicate particle SO_4^{2-} resides predominantly in the fine mode in air masses of continental origin, while coarse particle NO_3^- may be present in both maritime and continental regimes [Harrison and Pio, 1983; Wolff, 1984; Wall et al., 1988].

If one accounts for the particle NO_3^- volatilization artifact alone, they might anticipate the CDN filter pack sampler to measure less particle NO_3^- mass than the denuded IMPROVE sampler. However, this anticipated bias relies on several assumptions: 1) particle NO_3^- measured by both networks exists as fine particles, 2) no measurement biases result from elevation or siting differences, and 3) IMPROVE denuders efficiently remove ambient HNO_3 without disturbing the ambient equilibrium partitioning of particle ammonium nitrate during sampling.

We attempt to reconcile the different sampling frequencies of the two monitoring networks by averaging, and address the question of how many consecutive IMPROVE sample periods must be averaged to form a reliable estimator of the population mean for a specified time period. The CDN data provide a useful benchmark for this analysis because those data ideally are

continuous seven-day duration samples and should represent the population mean for a given sampling period. Averaging, of course, will not resolve bias due to spatial variability between comparison sites or non-random variability in the daily ambient mass concentrations. For example, if a monitoring site experiences a weekend pulse in particle mass concentration, the Wednesday Saturday sampling schedule may bias IMPROVE means over CDN means by preferential weighting of the weekend sample by IMPROVE.

We attempt to determine the magnitude, and multiplicative or additive nature, of observed biases between particle SO_4^{2-} and NO_3^- mass concentrations measured by the CDN and IMPROVE samplers. This analysis takes advantage of long-term monitoring data (up to ten years at some locations) that span all seasons and all observed meteorological conditions. Long-term data sets allow us to evaluate bias with greater statistical significance and to look for relationships between observed bias and external variables, such as aerosol composition and geographic region. Due to the many possible sources of bias between particle mass concentrations reported by the CDN and IMPROVE, including possible siting differences between respective comparison monitoring sites, this examination of the data does not constitute a controlled comparison study. Any inferred relationship to external factors is intended only as a clue to guide further investigations that may elucidate the mechanisms behind observed bias.

G.2 THE DATA

Detailed descriptions of the IMPROVE samplers are included in Chapter 1 and in related articles [Eldred et al., 1993; Malm et al., 1994]. For comparison to CDN data, IMPROVE particle mass concentrations are corrected to standard temperature of 25^{o}C and standard pressure of 1013 mb using daily averaged temperature from meteorological measurements at IMPROVE sites. If the IMPROVE sites do not have an adequate temperature record for the comparison period, then these data are taken from CDN temperature measurements at the CDN comparison site.

Ambient particle and some gas phase measurements reported by the CDN are one-week integrated samples that begin on Tuesday and continue through the following Tuesday. The weekly samples are made using filter packs situated on a pole 10 m above ground. The CDN filter packs have a non-size selective inlet followed by three filters in series. The first filter is Teflon and is intended to collect particles, the second filter is nylon (Nylasorb) designed to collect ambient HNO_3, and the third is a dual K_2CO_3 impregnated cellulose filter designed to collect SO_2. All filters are extracted and analyzed by ion chromatography to determine the mass concentrations of collected ionic constituents. The CDN sampler flow rates are 1.50 l/min in the eastern United States and 3.00 l/min at sites in the western United States. The CDN data are reported at the same reference temperature and pressure used to correct IMPROVE data. Required meteorological, groundcover, and observational data are collected at each site to parameterize the Big Leaf deposition model [CASTNet Summary Report, 1998].

G.3 COMPARISON SITES

To compare particle mass concentrations from CDN and IMPROVE we use data from 23 monitoring site pairs that are separated by less than approximately 50 km and have suitable

comparison data spanning approximately one year. The CDN and IMPROVE site names, horizontal separation in kilometers and vertical separation in meters, are listed in Table G.1. In Table G.1 the monitoring sites are separated into west, interior desert/mountain, and east regions of the United States. Figure G.1 is a map of the comparison sites labeled by their respective network site acronym.

Table G.1 *Horizontal and vertical distances between selected comparison sites from the CDN and IMPROVE network. Sites are shown sorted by geographic region. Elevation difference is the IMPROVE site elevation subtracted from the CDN site elevation.*

CDN Acronym	CDN Site Name	IMPROVE Acronym	IMPROVE Site Name	Δ Horizontal (km)	Δ Elevation (m)
West					
JOT	Joshua Tree NM	SAGO	San Gorgonio WA	80	-468
LAV	Lassen Volcanic NP	LAVO	Lassen Volcanic NP	41	-42
MOR	Mount Rainier NP	MORA	Mount Rainier NP	33	-1225
PIN	Pinnacles NM	PINN	Pinnacles NM	56	18
SEK	Sequoia NP	SEQU	Sequoia NP	52	676
YOS	Yosemite NP	YOSE	Yosemite NP	42	-10
Interior Desert/Mountain					
BBE	Big Bend NP	BIBE	Big Bend NP	1.5	-15
CAN	Canyonlands NP	CANY	Canyonlands NP	0.9	16
CHA	Chiricahua NM	CHIR	Chiricahua NM	16	-76
CNT	Centennial	BRLA	Brooklyn Lake	13	31
DEV	Death Valley NP	DEVA	Death Valley NP	2.0	3
GLR	Glacier NP	GLAC	Glacier NP	1.1	-396
GRB	Great Basin NP	GRBA	Great Basin NP	1.0	-13
GRC	Grand Canyon NP	GRCA	Grand Canyon NP	1.5	0
GTH	Gothic	WHRI	White River NF	25	-491
MEV	Mesa Verde NP	MEVE	Mesa Verde NP	0.9	-30
PND	Pinedale	BRID	Bridger WA	28	561
ROM	Rocky Mountain NP	ROMO	Rocky Mountain NP	3.1	20
YEL	Yellowstone NP	YELL	Yellowstone NP	39	549
East					
BEL	Beltsville	WASH	Washington, D.C.	55	43
LYE	Lye Brook	LYBR	Lye Brook	14	-261
PAR	Parsons	DOSO	Dolly Sods WA	20	-648
SHN	Shenandoah NP	SHEN	Shenandoah NP	8.6	-24

NP = National Park WA = Wilderness Area
NM = National Monument NF = National Forest

We recognize that the selected comparison sites are not collocated, and vertical as well as horizontal separation between some site pairs may introduce spatial bias. However, most of the selected monitoring sites are in remote areas where the mean particle SO_4^{2-} and NO_3^- mass concentrations are likely to be nearly uniform over areas larger than the distances that separate the respective comparison sites. Of course, the assumption of spatial homogeneity in mean ambient particle concentrations loses validity as the distance between monitoring site pairs increases and as the gradients in ambient particle concentration become steeper. For example, the majority of site pairs are within 100 m elevation, although respective monitoring sites

(MORA-MOR) have an elevation difference in excess of 1000 m. Elevation differences between sites can lead to diurnal and seasonal variability in measured particle mass. Similarly, the majority of site pairs are within 50 km, although the IMPROVE site at SAGO is approximately 80 km west of the CDN site at JOT. The distances between comparison sites are important to keep in mind when looking at results from this comparison analysis. Spatial bias cannot be separated from measurement bias related to particle sampler configuration by methods employed in this study.

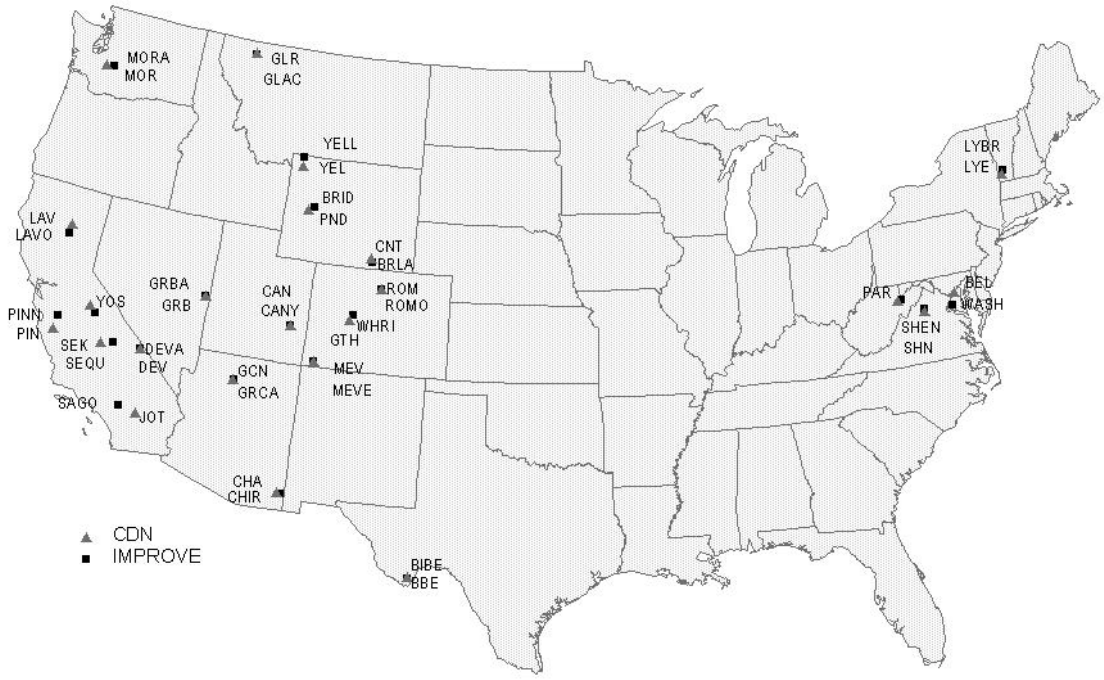

Figure G.1. *A map of comparison sites labeled by their respective network site acronym.*

G.4 RESULTS AND DISCUSSION

G.4.1 Averaging

We are interested in finding an optimal averaging time interval for IMPROVE data that is short enough to retain information about temporal variability in species mass concentrations, although long enough so that means from IMPROVE and the CDN would be indistinguishable, at a given confidence level, in the absence of a measurement bias for paired sites. This is relevant to a comparison of the respective network data because the networks sample with different frequencies. The IMPROVE protocol schedule introduces uncertainty in mean particle mass concentrations because only a fraction of the total days are sampled. This section examines the uncertainty in IMPROVE and CDN mean particle SO_4^{2-} and NO_3^- mass concentrations as a function of averaging time.

Paired CDN and IMPROVE data were selected for subsequent analysis using the criteria that CDN weekly samples had a duration of six to eight days and both 24-hour duration IMPROVE

samples per week were present. IMPROVE data were averaged beginning with the first Wednesday sample and continuing through the final Saturday sample in any given averaging time interval, so that the IMPROVE samples coincide in time to the CDN Tuesday through Tuesday samples. Thus, the highest time resolution for data pairs is weekly data. Data pairs used in this section have a duration from one to 52 weeks.

One approach to estimate the uncertainty associated with the respective network means, or data pairs, is adapted from Iyer et al. [1999]. Sampling variance, in the context of sampling a fraction of the entire population, as is done under IMPROVE protocol, can be estimated by,

$$sv = \frac{s^2}{n}\left(1 - n/N\right) \tag{G.1}$$

where *sv* is the estimated sampling variance associated with less than continuous sampling frequency, and *s* is the standard deviation of *n* measurements out of *N* possible measurements. In Equation (G.1), *s* is an estimate of the population standard deviation on the time scale of *n*, and is assumed to represent random variability. An estimate of measurement standard error (*se*) at a given averaging time interval is calculated from the combined sampling and analytical variance,

$$se = \sqrt{sv + av} \tag{G.2}$$

where *av* is the analytical variance. We estimate *av* using a polynomial fit to reported IMPROVE measurement precision (σ), as a function of the respective chemical species mass concentration. For consistency, we apply the polynomial to both CDN and IMPROVE mass concentration data,

$$\sigma_{SO_4} = 0.0349 + 50.2580\left[SO_4^{2-}\right]^{-1.3052} \tag{G.3}$$

$$\sigma_{NO_3} = 0.0484 + 26.9609\left[NO_3^{-}\right]^{-1.3244} \tag{G.4}$$

where $[SO_4^{2-}]$ and $[NO_3^-]$ are particle mass concentrations in ng/m^3, and the species measurement precision is expressed as a fraction of the respective chemical species mass concentration. Equations (G.3) and (G.4) asymptote to measurement precisions of approximately 4% of SO_4^{2-}, and 5% of NO_3^- mass concentrations in excess of 1 μg/m^3. The *av* of *n* measurements is calculated from the individual species measurement precision, σ_i, by:

$$av = \sum_{i=1}^{n} \sigma_i^2 \Big/ n^2 \tag{G.5}$$

Similarly, we calculate the square of the mean *se* associated with more than one data pair (i.e., the mean *se* associated with 52 means calculated at 1-week averaging intervals) by summing the squares of the individual *se's* from Equation (G.2).

The approach outlined in Equations (G.1) to (G.5) has the advantage of estimating *se* without knowledge of a population mean or standard deviation. However, it has the disadvantage in that *sv* (from Equation (G.1)) is calculated using an estimate of the population standard deviation. Another approach to estimate IMPROVE *sv* at a given averaging time interval is to use departures of IMPROVE means from the population, or true, mean averaged over the same time

interval. This approach requires knowledge of the population mean one seeks to represent by IMPROVE measurements.

We anticipate that means derived from the CDN data are essentially free of *sv* (in the absence of missing data). Therefore, we can then use means from the CDN to estimate the IMPROVE population mean, giving us another approach to estimate IMPROVE measurement uncertainty. To do so, we form data pairs from the respective networks at averaging time intervals ranging from one to 52-weeks. We denote the difference between individual data pairs as $d_{1..n}$, where n is the number of pairs, and we use D to denote the mean of $d_{1..n}$. This approach allows us to exclude much of the variability common to both networks, and thereby estimate the magnitude of *se* in IMPROVE means arising primarily from the IMPROVE sampling frequency, as a function of averaging time interval. The IMPROVE *se* in the difference approach is assumed to be represented by the standard deviation of $d_{1..n}$. Another assumption in this approach is that the respective network samplers are measuring the same quantity. That is, the respective network measurements are free of bias introduced by spatial and/or temporal variability between samplers.

Figure G.2 compares results from the two approaches. Figure G.2 shows the mean *se* associated with particle SO_4^{2-} mass concentrations from the CDN (diamonds) and IMPROVE (triangles), as calculated in Equations (G.1) to (G.5), and *se* associated with the difference (squares). Averaging time intervals shown in Figure G.2 range from one to 52-weeks and the mean *se's* shown incorporate the same number of samples regardless of averaging interval. We show data for five long-term sites, all of which have approximately 10 years of comparison data, so that the data include all seasons and ranges of expected particle mass concentrations.

Figure G.2 indicates the *se* associated with the CDN means is essentially constant as a function of averaging time interval. This is expected because the CDN data are continuous and *se* is determined by *av*, the mean of which is essentially constant for long-term data. The *se* associated with the IMPROVE means combines *sv* and *av*, and decreases with increasing averaging because *sv* (in Equation (G.1)) decreases as the number of samples incorporated in the averaging interval increases. Similarly, the IMPROVE *se* estimated from *D* decreases with increasing averaging time interval. Figure G.2 shows that for SO_4^{2-}, the *se* estimated from *D* is generally equivalent to or less than the IMPROVE *se* (from Equation (G.5)) at the same averaging time interval. It appears that at averaging time intervals of 1-week the IMPROVE *se* may be underestimated by using Equations (G.1) to (G.5). At longer averaging time intervals, the IMPROVE *se* may be overestimated by Equations (G.1) to (G.5) due to the incorporation of long-term variability of particle SO_4^{2-} mass concentration in the estimated population *s* in Equation (G.1). Long-term variability arises from the strong seasonal cycle in particle SO_4^{2-} mass concentrations, which is common to both networks and should not be included in the uncertainty estimates of IMPROVE means. This common variability is removed by estimating IMPROVE *se* by difference method. Based on the SO_4^{2-} data it appears that the difference approach gives a reasonable approximation of the uncertainty in means of IMPROVE measurements.

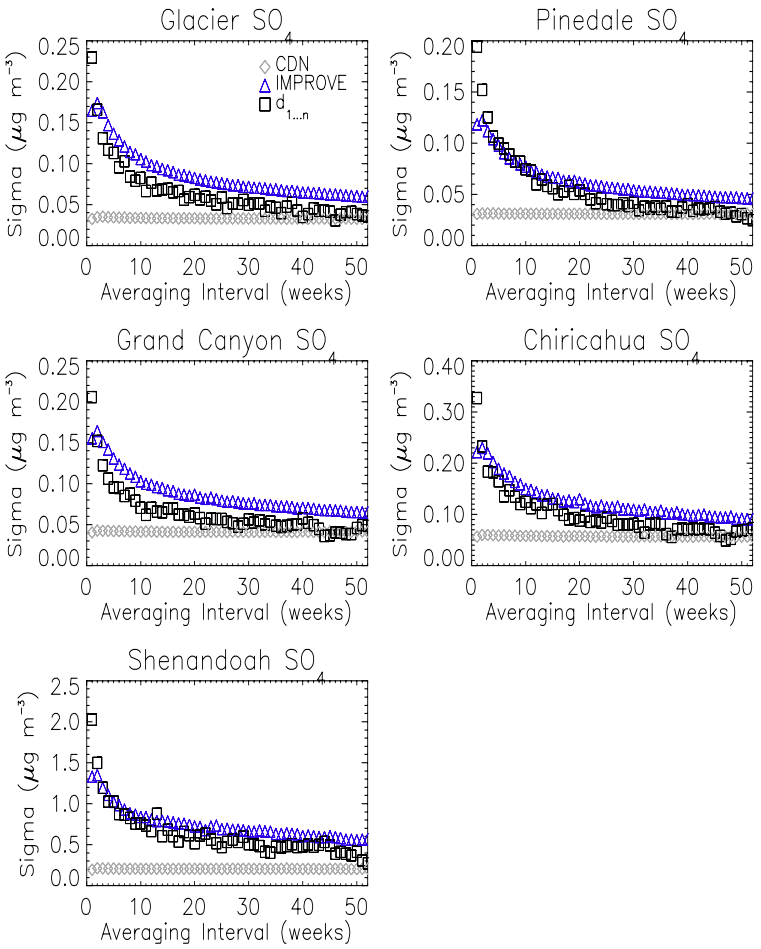

Figure G.2. *Particle SO_4^{2-} mass concentration se (sigma) for IMPROVE (triangles), CDN (diamonds) and the se for the difference between paired measurements, $d_{1..n}$ (squares), shown as a function of averaging time interval.*

Figure G.3 is analogous to Figure G.2, but shows the *se* associated with mean particle NO_3^- mass concentrations as a function of averaging time interval. From Figure G.3 we see that the *se* associated with CDN mean is again determined by *av*, and furthermore, that the *se* associated with the IMPROVE mean decreases with increasing averaging time interval. The main discrepancy between uncertainty estimates shown in Figures G.2 and G.3 is the relatively poor agreement between the two approaches used to estimate the *se* in IMPROVE mean. In almost all cases in Figure G.3 the IMPROVE *se* calculated using Equations (G.1) to (G.5) is less than the *se* estimated by the difference approach. This poor agreement could be explained by the fact that the CDN and IMPROVE samplers are not measuring the same quantity, suggesting a particle NO_3^- measurement bias between the two networks.

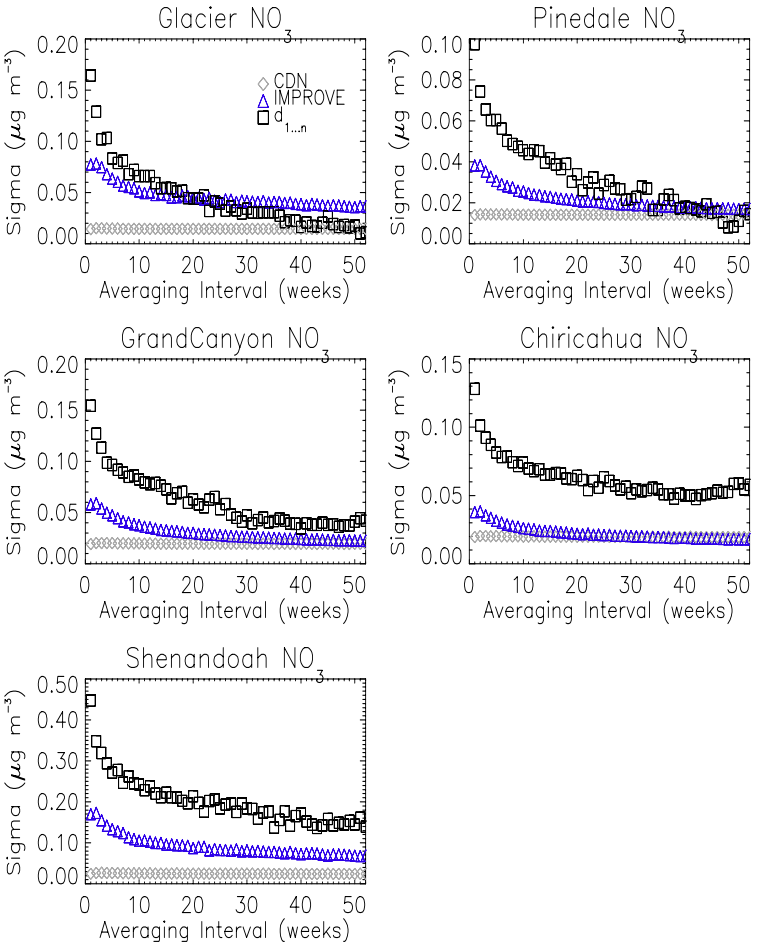

Figure G.3. *Particle NO_3^- mass concentration se (sigma) for IMPROVE (triangles), CDN (diamonds) and the se for the difference between paired measurements, $d_{1..n}$ (squares), shown as a function of averaging time interval..*

The *se* associated with the IMPROVE and CDN means is an estimate of the magnitude of uncertainty in the respective means at a given averaging time interval, where one *se* corresponds to an 84% confidence interval, based on a normal distribution. Values of the IMPROVE *se*, expressed as a percent of the mean IMPROVE particle SO_4^{2-} mass concentration, are shown in Table G.2 for selected averaging time intervals. Table G.2 compares values from the approach using Equations (G.1) to (G.5), denoted as *se(sv)*, and the approach using the *se* of *D*, denoted as *se(D)*. For SO_4^{2-}, the two approaches give similar results, with *se(D)* slightly lower than *se(sv)* at all but 1- to 2-week averaging intervals. Among the sites shown in Table G.2 the IMPROVE SO_4^{2-} *se* at a 1-week averaging time interval is as high as 30% and at 52 weeks the *se* is as low as 4%.

Values of the IMPROVE particle NO_3^- *se*, expressed as a percent of the mean IMPROVE mass concentration, are also shown in Table G.2. For particle NO_3^-, the two approaches do not

compare well, with *se(D)* generally higher than *se(sv)*, reflecting results shown in Figure G.3. Table G.2 shows that at 1-week averaging time intervals the IMPROVE particle NO_3^- *se(sv)* is as high as 30% and *se(D)* is as high as 90%. At 52-week averaging intervals, the *se* is as low as 4%. For reasons mentioned earlier, *se(D)* may not be a reasonable approximation of uncertainty associated with the IMPROVE mean. Also, *se(sv)* may underestimate IMPROVE measurement uncertainty at 1-week averaging intervals.

Table G.2. *Standard error (se) in IMPROVE particle SO_4^{2-} and NO_3^- mass concentration measurements as a function of averaging time interval at five long-term monitoring locations. The se is expressed as a percent of the respective IMPROVE chemical species mean particle mass concentration, and represents the mean se at the specified averaging interval for all available data at each site. Two methods are used to calculate se, se(sv) refers to the se obtained from Equations (G.1) to (G.5) in the text, while se(D) refers to the se associated with the difference between paired IMPROVE and CDN.*

Site	Averaging Interval (weeks)	SO_4^{2-} se(sv) (%)	SO_4^{2-} se(D) (%)	NO_3^- se(sv) (%)	NO_3^- se(D) (%)
Glacier	1	21	29	31	65
	2	22	21	31	51
	4	19	15	27	41
	13	12	8	19	23
	26	9	6	17	13
	52	7	4	14	4
Pinedale	1	19	31	30	76
	2	20	25	30	58
	4	17	17	26	47
	13	11	10	19	35
	26	9	6	15	24
	52	7	4	13	11
Grand Canyon	1	16	22	31	81
	2	17	16	31	67
	4	15	11	26	52
	13	10	7	18	41
	26	8	6	15	31
	52	7	5	12	22
Chiricahua	1	16	23	25	86
	2	16	17	26	68
	4	14	13	23	58
	13	10	7	16	46
	26	8	6	14	40
	52	7	5	12	38
Shenandoah	1	24	37	27	72
	2	24	27	28	56
	4	20	18	23	47
	13	14	16	16	35
	26	12	9	13	30
	52	10	5	10	21

Based on this analysis, we recommend using at least four weeks of IMPROVE particle SO_4^{2-} measurements to form a reliable estimate of the population mean. Variability in measured particle NO_3^-, relative to observed mean mass concentration, is greater than for particle SO_4^{2-},

and therefore we recommend that approximately 13-weeks of data from IMPROVE to estimate a population mean for particle NO_3^-. These suggested averaging time intervals correspond to the averaging required to reduce the uncertainty in the IMPROVE chemical species mean particle mass concentration to approximately 10 to 20%. Note that the analysis in this section is intended to estimate mean uncertainties in IMPROVE and CDN particle mass concentrations at specified averaging times, and is not necessarily intended to demonstrate uncertainties associated with long-term means. The latter is addressed in the following section using other statistical methods.

G.4.2 Regression Analysis and Comparison of Means

For the regression analysis and comparison of means, data from each network are paired and averaged to produce 4-week means, as described in the previous section. Averaging reduces sampling variance related to the twice a week IMPROVE sampling frequency, and is intended to give the comparison more physical significance related to differences between the respective network's sampler configurations. We explicitly look for multiplicative bias using the nonparametric Theil approach [Theil, 1950] and using a modified Theil approach to derive the slope intercept as an estimate of additive bias [Graybill and Iyer, 1994]. We chose a nonparametric regression because it is unbiased to extreme and outlying values. To determine the confidence level at which the difference in mean particle SO_4^{2-} and NO_3^- mass concentrations measured by the respective networks is significant we use a paired T-test, which is appropriate for data expected to have serial correlation.

G.4.2.1 Sulfate

Figure G.4 shows scatter plots of particle SO_4^{2-} mass concentrations data pairs from the CDN and IMPROVE at all 23 comparison sites, labeled by the CDN site name. Also shown in Figure G.4 are the 1:1 line and error bars representing one standard error (*se*) in the data pairs from each network. The *se* shown is calculated from Equation (G.2). Figure G.4 shows that the magnitude of *se* in the IMPROVE 4-week means is generally larger than in the CDN means, due to the contribution of sampling variance from IMPROVE sampling frequency, as discussed earlier. The mean *se* in 4-week averaged particle SO_4^{2-} mass concentrations shown in Figure G.4 is ±5% of the respective CDN means and ±19% of the IMPROVE means. Table G.3 lists the respective site pair acronyms (refer to Table G.1 for site names) and comparison statistics. Included in Table G.3 are the paired IMPROVE and CDN particle SO_4^{2-} mass concentration Theil regression intercepts (b_o) and slopes (b_1), with respective P-values. The P-value associated with b_o gives the lowest level at which we can reject the hypothesis that b_o is zero. The P-value associated with the regression slope gives the lowest level at which we can reject the hypothesis that b_1 is one. That is, if b_o P is less than 0.05 we can be 95% confident that the intercept is not equal to zero. N is the number of data pairs used in the regressions and to calculate means (X is CDN, Y is IMPROVE) shown in Table G.3. Means of X and Y and the P-value associated with the paired T-test are also shown in Table G.3, with start and stop dates corresponding to the initial and final month/year of the weekly comparison data, respectively.

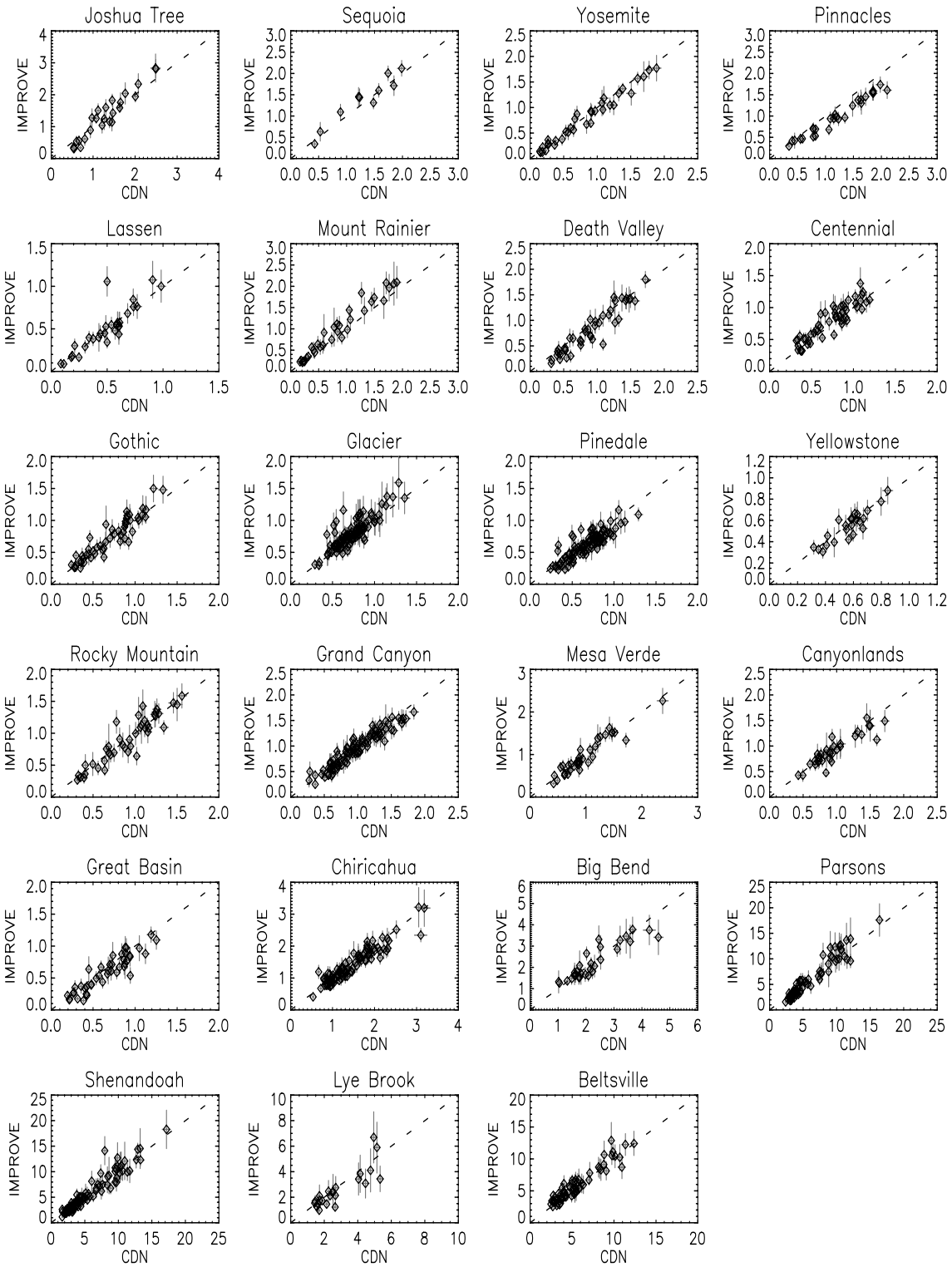

Figure G.4 *Comparison of IMPROVE and CDN particle SO_4^{2-} mass concentrations ($\mu g/m^3$) at 23 comparison sites. Scatter plots show 4-week means and error bars indicate ± one standard error in the respective network means.*

For the particle SO_4^{2-} comparison, Theil regression slopes are close to one and intercepts close to zero. Regression slopes are significant at the 95% confidence level at nine comparison sites, indicating multiplicative bias, and the regression intercepts are significant at two sites, indicating additive bias. Site pairs with significant slopes range in magnitude from 0.81 at BBE to 1.22 at JOT (site pairs are referred to in the text by their CDN acronym, as given in Table G.1).

Table G.3 *Particle SO_4^{2-} regression results from 23 CDN and IMPROVE comparison sites, separated by geographic region. Site acronyms are shown for each monitoring network. Statistics are described in the text.*

SITE ACRONYM		b_0	b_0 P	b_1	b_1 P	N	X_{ave}	Y_{ave}	X-Y P	Start	Stop
CDN	IMPROVE	µg/m^3					µg/m^3	µg/m^3			
West											
JOT	SAGO	0.14	0.387	1.22	0.013	24	1.32	1.35	0.506	2/95	12/98
LAV	LAVO	-0.03	0.212	1.01	0.809	29	0.50	0.50	0.747	7/95	12/98
MOR	MORA	0.01	0.598	1.12	0.011	32	0.86	1.00	0.000	11/95	12/98
PIN	PINN	0.03	0.500	0.83	0.000	27	1.19	0.98	0.000	5/95	11/98
SEK	SEQU	0.04	0.500	1.02	0.727	10	1.29	1.37	0.156	2/97	12/98
YOS	YOSE	-0.01	0.500	0.95	0.060	34	0.82	0.78	0.010	10/95	12/98
Interior Desert/ Mountain											
BBE	BIBE	0.48	0.212	0.81	0.025	29	2.30	2.25	0.497	8/95	12/98
CAN	CANY	0.00	0.598	0.85	0.010	33	0.97	0.92	0.046	3/95	12/98
CHA	CHIR	0.07	0.386	0.91	0.023	96	1.46	1.40	0.003	5/89	11/98
CNT	BRLA	0.19	0.115	0.94	0.269	51	0.73	0.79	0.001	9/93	12/98
DEV	DEVA	-0.03	0.500	1.05	0.363	43	0.90	0.80	0.000	2/95	12/98
GLR	GLAC	0.24	0.022	0.97	0.522	111	0.73	0.79	0.000	4/89	12/98
GRB	GRBA	0.03	0.500	0.91	0.143	43	0.66	0.59	0.000	5/95	12/98
GRC	GRCA	-0.02	0.443	0.94	0.042	99	0.97	0.94	0.003	6/89	8/98
GTH	WHRI	-0.08	0.347	1.05	0.312	52	0.70	0.73	0.105	7/93	12/98
MEV	MEVE	0.34	0.105	1.04	0.642	33	0.98	0.97	0.561	1/95	11/98
PND	BRID	0.07	0.198	0.86	0.001	100	0.67	0.62	0.000	1/89	12/98
ROM	ROMO	0.19	0.095	1.04	0.481	42	0.91	0.90	0.757	1/95	12/98
YEL	YELL	-0.08	0.500	0.99	0.958	23	0.57	0.55	0.134	7/96	12/98
East											
BEL	WASH	-0.42	0.569	0.96	0.350	66	5.51	5.86	0.001	1/90	10/98
LYE	LYBR	0.19	0.500	0.82	0.248	23	2.86	2.61	0.126	5/94	11/98
PAR	DOSO	-1.23	0.001	1.15	0.004	77	5.79	5.72	0.535	9/91	11/98
SHN	SHEN	-0.12	0.286	1.03	0.520	100	5.47	5.57	0.307	1/89	12/98

Twelve site pairs indicate significant differences in mean particle SO_4^{2-} mass by paired T-test. The magnitude of significant difference (the IMPROVE mean subtracted from the CDN mean, expressed as a percent of the IMPROVE mean) ranges from 22% at PIN to –14% at MOR. The mean relative difference in SO_4^{2-} is 0% for each of the three regions shown in Table G.4, and the root mean square (RMS) relative difference among all 23 comparison sites is 8%. Bearing in mind that spatial variability may account for some observed bias, this result indicates surprisingly good comparability for the respective particle SO_4^{2-} measurements.

Comparison site pairs with significant differences in mean particle SO_4^{2-} mass concentrations are not necessarily the same comparison sites that show significance in one or both regression terms. A possible explanation is that the paired difference test removes variability common to both data sets, while regression analysis relies on a linear model to account for common variability, which may not be appropriate to explain differences in particle mass concentrations observed at all comparison sites during all seasons.

G.4.2.2 Nitrate

Figure G.5 shows scatter plots of paired particle NO_3^- mass concentration data for the CDN and IMPROVE at the 20 comparison sites with particle NO_3^- data, with the 1:1 line and error bars representing one *se* in the data pairs from each network, analogous to Figure G.4 for SO_4^{2-}. The mean *se* in 4-week averaged particle NO_3^- mass concentrations shown in Figure G.5 is ±7% for the CDN data and ±26% for the IMPROVE data. Table G.4 lists regression statistics and means for the CDN and IMPROVE particle NO_3^- mass concentration data, analogous to Table G.3 for SO_4^{2-}. We use 4-week NO_3^- means so that all sites have sufficient comparison data pairs for the regression and paired T-test. While this is a shorter time period than the 13-week averaging time recommended in Section G.4.1 to estimate the population mean at a given confidence level, the regression and paired T-test analysis in this section make use of a minimum of ten 4-week means.

Table G.4 shows the particle NO_3^- regression slope at six comparison sites is indistinguishable from one, while the remaining sites have slopes significantly less than one at the 95% confidence level. The magnitude of significant regression slopes ranges from 0.68 at LAV to 0.34 at BBE. A slope less than one indicates particle NO_3^- measured by the CDN is multiplicatively biased higher than the corresponding IMPROVE data. The particle NO_3^- regression intercepts at all comparison sites are either indistinguishable from or greater than zero at the same confidence level. The largest magnitude particle NO_3^- regression intercepts are at the BEL and JOT comparison sites.

The paired T-test indicates differences in mean particle NO_3^- mass are significant at the 95% confidence level at all but three comparison site pairs, with means from CDN predominantly greater than means from IMPROVE, or a positive CDN bias, in all geographic regions indicated in Table G.4, except in the East. The magnitude of relative difference in particle NO_3^- mass concentrations (the IMPROVE mean subtracted from the CDN mean (X_{ave}-Y_{ave}) from Table G.4), expressed as a percent of the IMPROVE mean, or ΔNO_3^-%) ranges from 151% at BBE to -29% at SHN. The minimum relative difference among non-eastern sites is –28% at GLR. The average ΔNO_3^-% by region is 40% in the West, 56% in the interior desert/mountain region, and -9% in the East. The RMS mass concentrations difference, among 18 of 20 particle NO_3^- comparison sites, is 59%, when expressed as a percent of the IMPROVE means, or 35% when expressed as a percent of the CDN means.

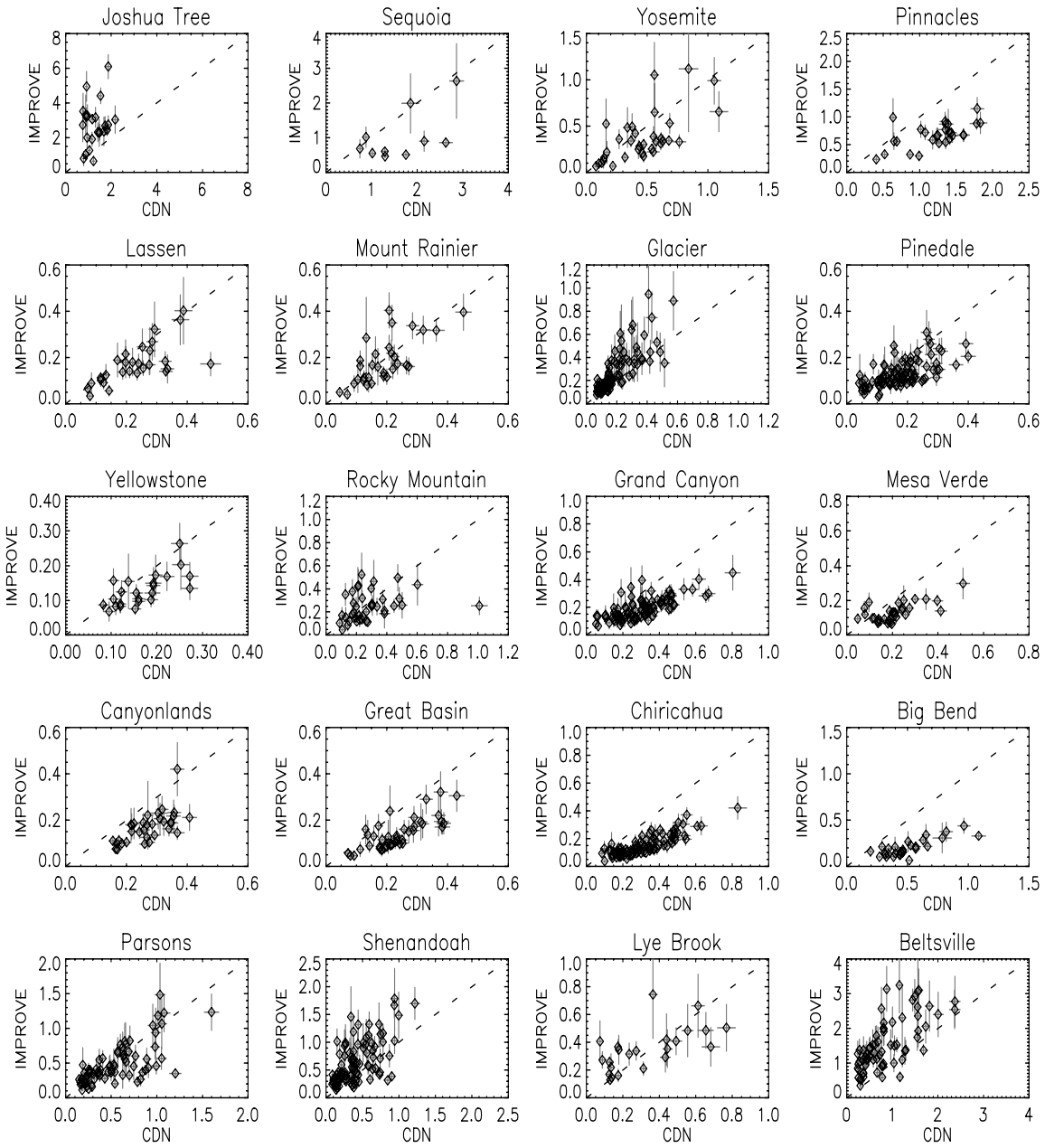

Figure G.5 *Comparison of IMPROVE and CDN particle NO_3^- mass concentrations ($\mu g/m^3$) at 20 comparison sites. Scatter plots show 4-week means and error bars indicate ± one standard error in the respective network means.*

Table G.4 *Particle NO_3^- regression results, mean mass concentrations, and comparison time periods for the 20 CDN and IMPROVE sites pairs, analogous to Table G.3. Site acronyms are shown for each monitoring network. Statistics are described in the text*

SITE ACRONYM		b_0	b_0 P	b_1	b_1 P	N	X_{ave}	Y_{ave}	X-Y P	Start	Stop
CDN	IMPROVE	μg/m^3					μg/m^3	μg/m^3			
West											
JOT	SAGO	2.21	0.073	0.67	0.476	24	1.28	2.73	0.000	2/95	12/98
LAV	LAVO	-0.01	0.605	0.68	0.025	28	0.23	0.17	0.001	7/95	11/98
MOR	MORA	0.00	0.500	0.78	0.114	31	0.19	0.19	0.728	11/95	11/98
PIN	PINN	0.10	0.133	0.37	0.000	27	1.22	0.67	0.000	5/95	11/98
SEK	SEQU	0.24	0.500	0.19	0.073	10	1.65	1.02	0.014	2/97	12/98
YOS	YOSE	0.06	0.072	0.53	0.002	34	0.46	0.37	0.020	10/95	12/98
Interior Desert/ Mountain											
BBE	BIBE	0.05	0.605	0.34	0.000	29	0.50	0.20	0.000	8/95	12/98
CAN	CANY	-0.07	0.105	0.56	0.001	33	0.27	0.17	0.000	3/95	12/98
CHA	CHIR	0.05	0.042	0.39	0.000	97	0.31	0.15	0.000	5/89	12/98
GLR	GLAC	0.06	0.091	1.11	0.165	112	0.18	0.25	0.000	2/89	11/98
GRB	GRBA	-0.02	0.500	0.54	0.000	43	0.23	0.14	0.000	5/95	12/98
GRC	GRCA	0.06	0.012	0.39	0.000	101	0.30	0.19	0.000	7/89	8/98
MEV	MEVE	0.04	0.105	0.37	0.000	33	0.21	0.13	0.000	1/95	11/98
PND	BRID	0.05	0.045	0.39	0.000	101	0.18	0.13	0.000	1/89	12/98
ROM	ROMO	0.26	0.058	0.40	0.000	41	0.28	0.25	0.203	1/95	12/98
YEL	YELL	0.01	0.500	0.57	0.006	23	0.17	0.13	0.000	7/96	12/98
East											
BEL	WASH	0.82	0.000	1.02	0.947	70	0.86	1.53	0.000	1/90	10/98
LYE	LYBR	0.23	0.113	0.43	0.000	23	0.33	0.35	0.583	5/94	11/98
PAR	DOSO	0.16	0.026	0.64	0.000	77	0.54	0.48	0.018	9/91	11/98
SHN	SHEN	0.21	0.000	0.96	0.716	102	0.41	0.63	0.000	1/89	12/98

Spatial variability in ambient particle NO_3^- between site pairs may cause some of the observed bias in particle NO_3^- measurements. For example, the IMPROVE site SAGO is about 50 km closer to the Los Angeles basin, and has a two-fold higher mean particle NO_3^- mass concentration than the CDN site JOT. Also, a large magnitude difference is observed between mean particle NO_3^- at the IMPROVE site WASH, which is in an urban setting, and the CDN site BEL, 20 km to the north. The observed differences between means at these site pairs may be related to spatial variability. Both site pairs have large magnitude regression intercepts, which may account for much of the observed bias between mean particle mass concentration. However, we do not imply that spatial variability will necessarily be manifest in the regression intercept. Based on their geographic separation alone, spatial variability may account for some of the observed bias at the JOT and BEL site pairs, and comparison data from these two sites are excluded from the summary in the preceding paragraph, and from any subsequent discussion.

A cursory examination of the data shows that the further south the sampling location, the larger the relative magnitude of particle NO_3^- bias. Figure G.6 is a plot of site latitude vs. relative particle NO_3^- mass concentration difference (ΔNO_3^-%) for 15 comparison sites in the West and interior desert/mountain regions, with the CDN site acronyms shown for each site pair. Figure G.6 demonstrates an increasing positive CDN particle NO_3^- bias with decreasing site

latitude, suggesting factors related to site geography influence the observed bias. An analogous geographic trend is observed in the particle NO_3^- regression slope, although not in the regression intercept. Comparison sites in the eastern United States are not shown in Figure G.6 because the small number of comparison sites in this region make any geographic trends difficult to resolve.

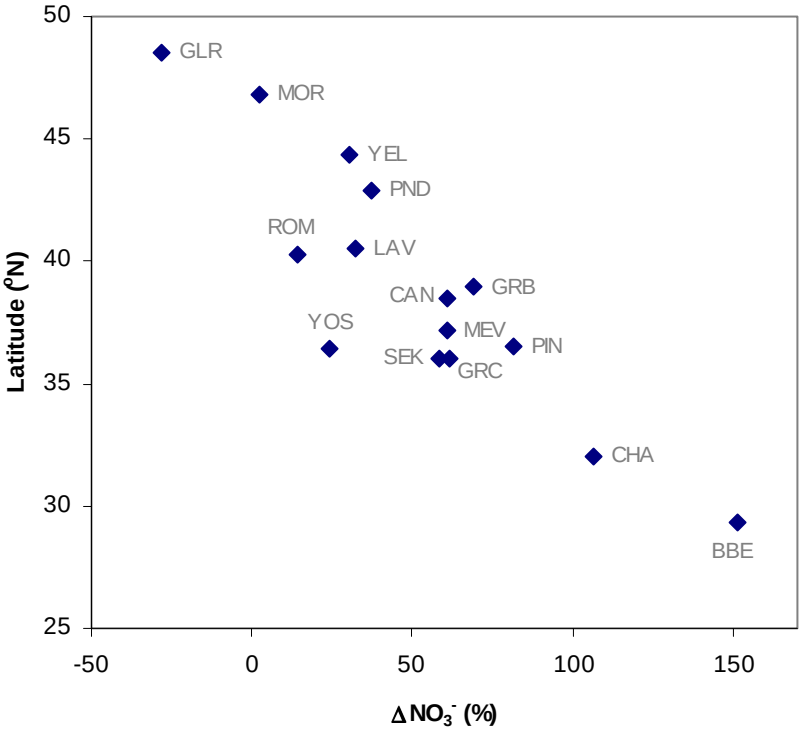

Figure G.6 *Site latitude vs. relative difference in mean particle NO_3^- mass concentration (expressed as the IMPROVE mean subtracted from the CDN mean as a percent of the IMPROVE mean) for 16 comparison sites in the western and interior desert/mountain regions.*

G.4.3 Comparison of Seasonal Means

G.4.3.1 Sulfate

Figure G.7a shows the absolute difference (IMPROVE subtracted from CDN as a percent of the IMPROVE mean) in mean particle SO_4^{2-} mass concentration for the winter (DJF), spring (MAM), summer (JJA), and autumn (SON) seasons. The IMPROVE site acronyms are shown to identify the respective site pairs. Figure G.7b shows the same difference expressed as a percent of the IMPROVE means. In Figure G.7a and G.7b, wintertime data at SEK-SEQU are not shown due to lack of sufficient comparison data during this season. Large differences in absolute SO_4^{2-} mass concentration are observed at comparison sites in the East, particularly during the summer when ambient SO_4^{2-} concentrations are high, however on a relative basis differences in the East are comparable to relative differences observed in other regions. Large relative differences in SO_4^{2-} mass concentrations (on the order of 20% or more) are observed at a number of comparison sites. Frequently, the relative differences are greatest during the winter, when low level inversions are likely to cause spatial sampling variability between sites with large

vertical separation. For example, the IMPROVE site at DOSO is 648 m higher than the CDN site at PAR, which could explain higher particle mass concentrations at the lower elevation CDN site.

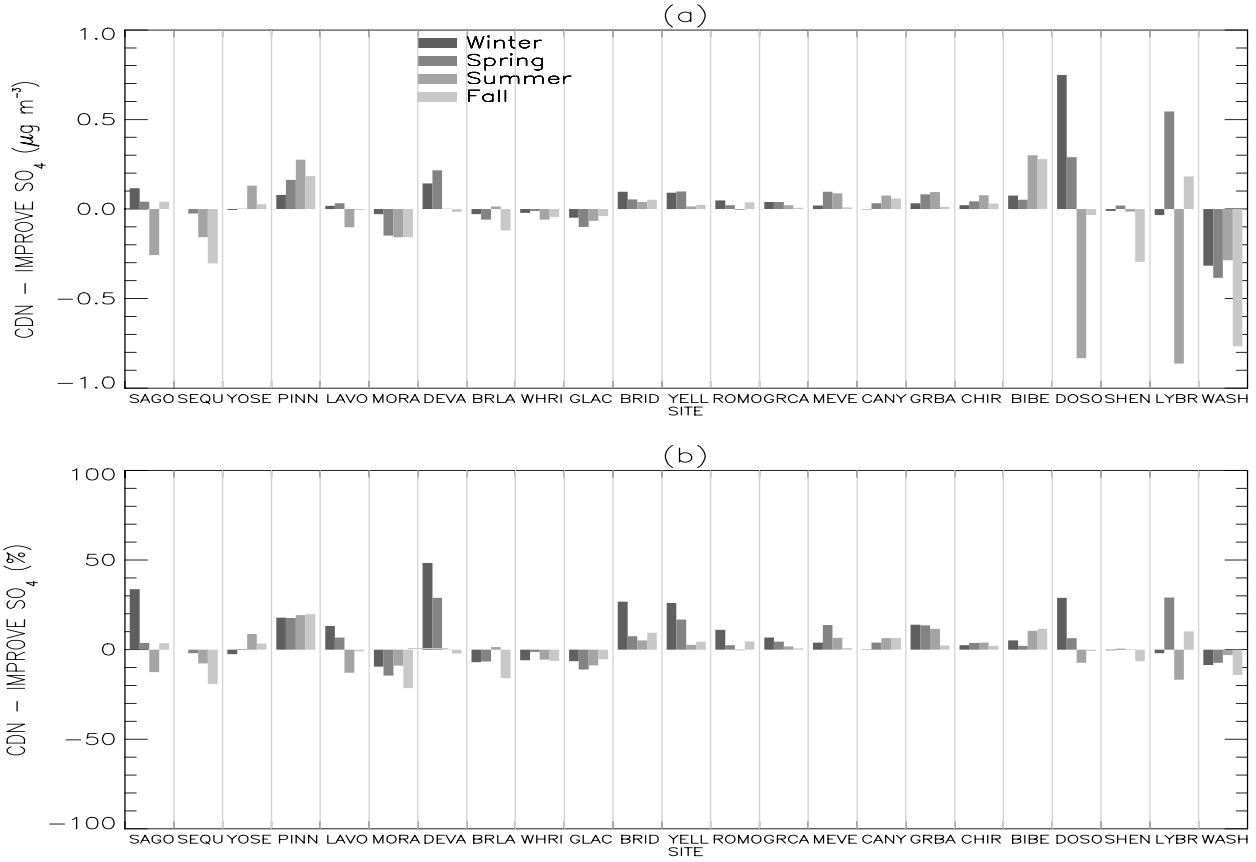

Figure G.7 *(a) Absolute difference in particle SO_4^{2-} mass by season. (b) Relative difference in particle SO_4^{2-} mass by season.*

G.4.3.2 Nitrate

Figures G.8a and G.8b show analogous plots to those in Figure G.7, but for the seasonal comparison of particle NO_3^-. Note the relative scale in Figure G.8b is from –100 to +300%. In Figure G.8a and G.8b, wintertime data at SEK-SEQU are not shown due to lack of sufficient comparison data. Most comparison sites shown in Figure G.8 have higher particle NO_3^- mass concentrations from the CDN than IMPROVE. Exceptions are found among most eastern sites and the JOT-SAGO and GLR-GLAC comparison sites. It is perhaps noteworthy that Glacier National Park and sites in the eastern United States are the only comparison sites among those considered that exhibit a strong wintertime maximum in ambient particle NO_3^- mass concentration. Among comparison sites in the western and interior desert/mountain regions the magnitude of particle NO_3^- mass concentration differences are generally lowest during the winter.

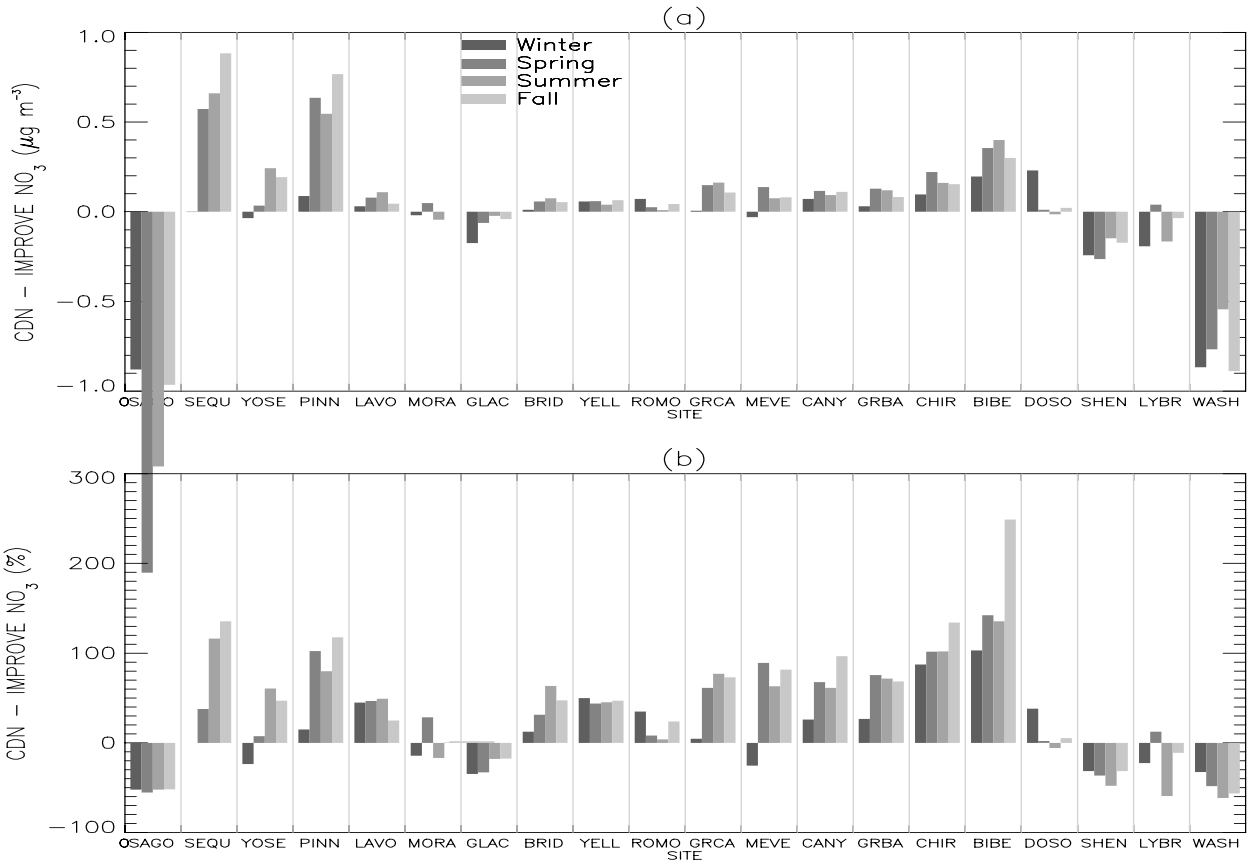

Figure G.8 *(a) Absolute difference in particle NO_3^- mass by season. (b) Relative difference in particle NO_3^- mass by season.*

G.4.4 Possible Explanations for Observed Particle NO_3^- Bias Related to Sampler Configuration

Because the observed relationship between ΔNO_3^-% and latitude elucidates no physical mechanisms that may explain ΔNO_3^-%, we look for relationships to other quantities having latitude dependence, which may also serve as indicators of mechanisms that cause the observed bias. Figure G.9 shows ΔNO_3^-% plotted against mean site temperature and the absolute particle NO_3^- mass concentration difference (ΔNO_3^-) expressed as a percent of coarse mass (CM) concentration for the 15 comparison sites shown in Figure G.6. The latitude dependence of temperature is intuitive, and CM concentrations are generally lower in the northern United States than in southern regions (Chapter 2.5.2). Figure G.9 indicates the mean site temperature increases proportionally to ΔNO_3^-%, suggesting a temperature dependent mechanism, such as the ammonium nitrate equilibrium, may play a role in the observed bias. Figure G.9 also shows the magnitude of ΔNO_3^- relative to CM increases as ΔNO_3^-% increases, suggesting particle NO_3^- associated with CM may explain some of the observed bias.

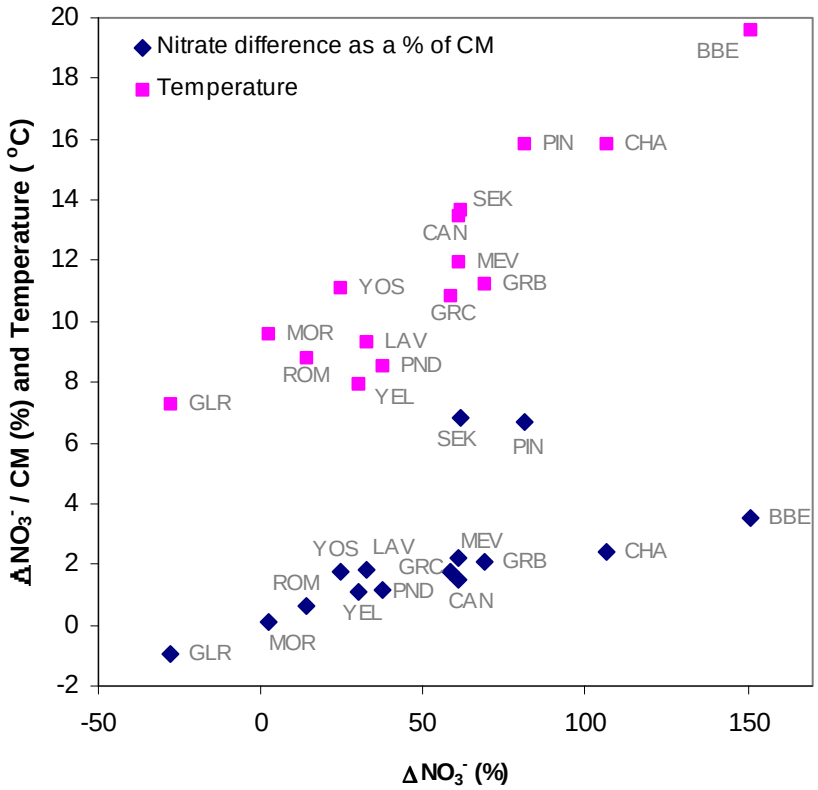

Figure G.9 *Two variables, $\Delta NO_3^-/CM$ and temperature, plotted against $\Delta NO_3^-(\%)$ for 15 comparison sites in the western and interior desert/mountain regions. CDN site acronyms are shown at each data point.*

Two outlying CM values in Figure G.9 are the PIN and SEK site pairs, which may be due to particle NO_3^- sampling characteristics at these sites indicative of urban, rather than rural, conditions. Linear correlation coefficients for $\Delta NO_3^-\%$ to site latitude, temperature and CM (the latter excluding the PIN and SEK site pairs) are 0.9 or greater, and highly significant (P-values less than 0.001).

We use ordinary least-squares multiple regression to form a simple model of the observed particle NO_3^- bias is the interior desert/mountain region. We chose this region because it contains the greatest number of comparison sites, and particle NO_3^- data from some sites in this region display the largest magnitude relative bias among all comparison sites. In the regression, the absolute nitrate bias (ΔNO_3^-) is the dependent variable and temperature (T) and a CM tracer in the fine particle mode (CM_f) are independent variables. CM_f is defined as elements characteristic of soil and sea salt, where soil is the sum of common oxides of crustal elements (2.2*Al + 2.49*Si + 1.63*Ca + 2.42*Fe + 1.94*Ti) and sea salt is NaCl (2.5*Na) from IMPROVE Module A [Malm et al., 1994]. CM_f is used as a surrogate for CM because it is measured with more precision and accuracy than gravimetrically determined CM, and it has been shown to be the "tail" of the coarse particle distribution [Perry et al., 1997]. The multiple regression R^2, using means from the nine comparison sites in the interior desert/mountain region where $\Delta NO_3^->0$, is 0.96. Apportionment of ΔNO_3^- to CM_f and T in the regression is approximately 35:65, respectively. The results from the multiple regression are:

$$\Delta NO_3^- = -0.157 \ \ + 0.013^{\pm 0.004}[T(^oC)] + 0.109^{\pm 0.043}[CM_f\,(\mu g\, m^{-3})] \qquad \text{(G.6)}$$

Equation (G.6) indicates that ΔNO_3^- increases as both mean site temperature and CM concentration increase for comparison sites in the interior desert/mountain region.

The positive correlation between ΔNO_3^- and temperature shown in Figure G.9 and indicated by Equation (G.6) is opposite to what would be expected if ammonium nitrate volatilization from Teflon in the CDN filter packs is responsible for the observed particle NO_3^- bias. However, this mechanism is consistent with higher particle NO_3^- mass concentrations from IMPROVE protocol measurements than from the CDN (as seen at GLR and some eastern comparison sites), if ammonium nitrate is volatilized from Teflon in the CDN filter packs. A study sponsored by the CDN found HNO_3 measured by its filter pack sampler is 11 to 12% higher than HNO_3 recovered from a collocated annular denuder sampler at a site in Indiana [CDN Deposition Summary Report, 1998]. Particle NO_3^- biases, with magnitudes up to 60% and attributed to ammonium nitrate volatilization from Teflon, have been observed during summer months [Chow et al., 1994; Hering and Cass, 1999].

The majority of comparison sites in the west and interior desert/mountain regions indicate particle NO_3^- mass concentrations measured using CDN sampling protocol are higher than those measured by IMPROVE protocol. If particle ammonium nitrate volatilization occurs in the IMPROVE denuder prior to collection on the Nylasorb substrate, then CDN particle NO_3^- could be higher than IMPROVE measurements (see Durham et al., [1986] for a discussion of HNO_3 release from particle NO_3^- in diffusion denuders). However, this mechanism is unlikely because the particle residence time in the IMPROVE denuder (about one second) is much less than the ammonium nitrate gas phase equilibration time scale which, although highly uncertain, is about 1 to 15 minutes [Wexler and Seinfeld, 1992]. Another mechanism that may explain a positive CDN bias is enhanced coarse particle NO_3^- collection efficiency for the non-size selective CDN sampler over that of the IMPROVE module fitted with a $PM_{2.5}$ cyclone. During the Subregional Cooperative Electric Utility, Department of Defense, National Park Service and Environmental Protection Agency (SCENES) Study [Benner et al., 1991], conducted in Arizona, filter packs operating without a cyclone (AeroVironment Filter Packs) measured higher particle NO_3^- mass concentrations than denuded samplers operating with cyclones under certain conditions. Zhang and McMurry [1992] suggest this bias may have resulted from collection of coarse particle nitrate by the filter pack samplers.

The magnitude of ΔNO_3^- relative to observed CM concentration is consistent with laboratory studies that indicate heterogeneous reactions between soil and/or sea salt particles and oxides of nitrogen and/or HNO_3 can form particle NO_3^- in amounts up to approximately 3% of coarse particle mass [Mamane and Gottlieb, 1992]. We do not interpret ΔNO_3^- as a direct measurement of coarse particle NO_3^- mass, although it is of interest to point out that while ΔNO_3^-% is in some cases large, the absolute particle NO_3^- bias expressed as a percent of CM is generally small. The positive correlation between ΔNO_3^- and temperature and CM shown in Figure G.9 and indicated by Equation (G.6) is consistent with a coarse particle NO_3^- mechanism explaining some of the observed bias.

G.5 SUMMARY

Particle SO_4^{2-} and NO_3^- mass concentrations reported by the CDN and IMPROVE network at nearby monitoring locations are compared with the intent to quantify biases that may be introduced from differences in the respective network's sampling protocols. Particle sampling following CDN protocol employs a filter pack with non-size selective inlet, while sampling under IMPROVE protocol employs separate modules fit with either $PM_{2.5}$ or PM_{10} inlets, as well as a denuded inlet on the particle NO_3^- module. The two networks also use different sampling frequencies, the CDN on a weekly schedule and IMPROVE on a 24-hour twice a week schedule.

An averaging time analysis was performed to estimate the magnitude of uncertainty in IMPROVE twice a week samples as a function of averaging time. Based on this analysis, we recommend using at least four weeks of IMPROVE particle SO_4^{2-} measurements to form a reliable estimate of the population mean. Variability in measured particle NO_3^-, relative to mass concentration observed at selected comparison sites used in this study, is greater than observed particle SO_4^{2-} variability and therefore we recommend that approximately 13 weeks of IMPROVE data be used to estimate a population mean for particle NO_3^-. At these recommended averaging times, the uncertainty in the respective species particle mass concentrations is about 10 to 20%.

The nonparametric Theil regression was used to discriminate additive from multiplicative bias between particle mass measurements from the two monitoring networks. In the Theil regressions, the CDN data are used as the independent variable. The regression slopes for the particle SO_4^{2-} comparison are generally close to one and intercepts close to zero. For the particle NO_3^- comparison, regression slopes are indistinguishable from one at six comparison sites and significantly less than one at 14 comparison sites. Among comparison sites in the west and interior desert/mountain regions the magnitude of particle NO_3^- regression slopes tend to decrease as the monitoring site latitude became more southerly, indicating CDN is multiplicatively biased higher than IMPROVE in these regions. All comparison sites have particle NO_3^- regression intercepts either significantly greater than, or indistinguishable from, zero.

Differences between mean particle SO_4^{2-} mass concentrations reported by the two monitoring networks are small (mean difference of 0% among all comparison sites, by geographic region). On the other hand, differences between mean particle NO_3- mass concentrations are substantial, with measurements from the CDN higher than those from IMPROVE among 14 of 16 sites in the west and interior desert/mountain regions. CDN particle NO_3^- mass concentrations are biased progressively higher than IMPROVE measurements as site latitude becomes more southerly, consistent with the north-south trend observed in the Theil regression slope magnitude. Among comparison sites in the east, mean particle NO_3^- mass concentrations from IMPROVE protocol measurements are generally higher than those from the CDN. Mean differences in particle nitrate are 40% in the west, 56% in the interior desert/mountain region, and –9% in the east, excluding locations with likely spatial variability between comparison sites.

Because the CDN filter pack sampler collects particles on a Teflon substrate, we anticipate loss of fine particle NO_3^- from the CDN samplers due to ammonium nitrate volatilization. In

addition, we anticipate ammonium nitrate volatilization will not produce a significant sampling artifact in particle NO_3^- mass concentrations measured by the IMPROVE module operating with a denuded inlet and nylon collection substrate. Particle NO_3^- loss from the CDN filter packs may explain the observed bias at some comparison sites (e.g., some eastern United States sites) where particle NO_3^- mass concentrations measured using IMPROVE protocol are greater than those from the CDN. On the other hand, other mechanisms must be considered for cases where particle NO_3^- measured by the CDN is greater than that from IMPROVE. Coarse particle NO_3^- could produce a positive CDN bias if the cyclone on the IMPROVE NO_3^- module removes NO_3^- associated with coarse particles more efficiently than the non-size selective CDN inlet. However, our ability to accurately estimate the magnitude of the particle NO_3^- measurement bias related to one mechanism, such as coarse particle NO_3^-, may be confounded by the presence of an opposite bias related to a different mechanism, such as fine particle NO_3^- volatilization from Teflon in the CDN filter packs.

This study indicates particle SO_4^{2-} sampled using IMPROVE protocol can be used as a surrogate for similar measurement from the CDN, although particle NO_3^- measurements cannot. Bias between CDN and IMPROVE particle NO_3^- measurements is widespread and not easily explained due to the large number of sampling protocol differences between the two monitoring networks. Because most comparison sites used in this study are located in the western United States some conclusions reached herein may not be representative of areas with dissimilar ambient sampling conditions. This study points to a need for continued in depth and regionally specific comparisons of particle NO_3^- measurements from distinct sampler configurations either currently in use or intended for future air quality monitoring programs.

G.6 REFERENCES

Appel B. R., Tokiwa, Y., Haik M., and Kothny, E. L., Artifact particulate sulfate and nitrate formation on filter media, *Atmos. Environ.* 18(2):409-416, 1984.

Ashbaugh L. L., Eldred R. A., Hering S., Loss of particle nitrate from Teflon sampling filters: effects on measured gravimetric mass, California Air Resources Board, Final Report, Contract No. 96-305, September, 1998.

Benner C. L., Eatough D. J., Eatough N. L., and Bhardwaja P., Comparison of annular denuder and filter pack collection of HNO_3(g), HNO_2(g), SO_2(g), and particulate-phase nitrate, nitrite and sulfate in the south-west desert, *Atmos. Environ.* 25A(8):1537-1545, 1991.

Chow, J. C.; Fujita, E. M.; Watson, J. G. ; Lu, Z., Lawson, D. R., Ashbaugh, L. L., Evaluation of filter-based aerosol measurements during the 1987 Southern California Air Quality Study, Environmental Monitoring and Assessment, *Environ. Monit. Assess.*, 30(1):49-80, 1994.

Clean Air Status and Trends Network (CASTNet) Deposition Summary Report (1987-1995), EPA/600/R-98-207, July, 1998.

Durham J. L., Spiller L. L., and Ellestad T. G., Nitric acid-nitrate aerosol measurements by a diffusion denuder: a performance evaluation, *Atmos. Environ.*, 21(3):589-598, 1986.

Eldred, R. A., Cahill, T. A., Feeney, P., Comparison of independent measurements of sulfur and sulfate in the IMPROVE network, *Proceedings of the 86th Annual Meeting of the Air and Waste Management Association, paper # 93-RA-110.02*, Pittsburgh, PA, 1993.

Environmental Science and Engineering, Inc. (ESE), Comparison of CASTNet filter pack and annular denuder samplers – Interim data report (October 1996 – February 1997), Gainesville FL, 1997.

Graybill F. A. and Iyer, H. K., Regression Analysis: Concepts and Applications, Duxbury Press, Belmont California, 1994.

Harrison R. M. and Pio C. A., Size differentiated composition of inorganic atmospheric aerosols of both marine and polluted continental origin, *Atmos. Environ.* 17(9):1737-1738, 1983.

Hering S. V., Field comparisons of sampling methods for aerosol nitrate, In Aerosols: Formation and Reactivity, 2nd Int. Aerosol Conf. Berlin, Pergamon Journals Ltd., 1986.

Hering S. and Cass G., The magnitude of bias in the measurement of $PM_{2.5}$ arising form volatilization of particulate nitrate from Teflon filters, *J. Air and Waste Management Association*, 49(6):725-733, 1999.

Iyer H., Malm W., and Patterson P., Sampling duration calculations, Accepted for publication in *J. Air and Waste Management Association*, 2000.

Malm W. C., Sisler J. F., Huffman D., Eldred R. A., and Cahill T. C., Spatial and seasonal trends in particle concentration and optical extinction in the U.S. *J. Geophys. Res*. 99(D1):1347-1370, 1994.

Mamane, M. and Gottlieb J., Nitrate formation on sea-salt and mineral particles - a single particle approach, *Atmos. Environ.* 26A(9):1763-1769, 1992.

Mozurkewich, M., The dissociation constant of ammonium nitrate and its dependence on temperature, relative humidity and particle size, *Atmos. Environ.* 27A(2): 261-270, 1993.

Perry K. D., Cahill T. A., Eldred R. A., Dutcher D. D., and Gill T. E., Long-range transport of North African dust to the eastern United States, *J. Geophys. Res.* 102(D10):11,225-11,238, 1997.

Shaw R. W., Stevens R. K, Bowermaster J., Tesch J. W., and Tew E., Measurements of atmospheric nitrate and nitric acid: the denuder difference experiment, *Atmos.Environ.* 16(4):845-853, 1982.

Theil, H., A rank-invariant method of linear and polynomial regression analysis (I-III), *Proc. Kon. Ned. Akad. v. Wetensch. A.*, (53), 1950.

Turpin B.J., Saxena P., Allen G., Koutrakis P., McMurry P. and Hildemann L., Characterization of the southwestern desert aerosol, Meadview, AZ, *J. Air and Waste Management Association*, 47(3):344-356, 1997.

Wall S. M., John W., Ondo J. L., Measurement of aerosol size distributions for nitrate and major ionic species, *Atmos. Environ.* 22(8):1649-1656, 1988.

Wexler A. S. and Seinfeld J. H., Analysis of ammonium nitrate: departures from equilibrium during SCAQS, *Atmos. Environ.* 26A(4):579-591, 1992.

Wolff, G. T., On the nature of coarse continental aerosols, *Atmos. Environ.* 18(5):977-981, 1984.

Zhang X. and McMurry P. H., Evaporative losses of fine particulate nitrates during sampling, *Atmos. Environ.* 26A(18):3305-3312, 1992.